University of Southampton

Faculty of Medicine

Human Development and Health

Characterisation of Induced Mesenchymal Stem Cells and Human Foetal Bone Cells

–

Implications for Disease Physiology and Regenerative Medicine

by

Susanne Maria Renz

Thesis for the degree of Doctor of Philosophy

April 2019

University of Southampton

Abstract

Faculty of Medicine

Human Development and Health

Thesis for the degree of Doctor of Philosophy

Characterisation of Induced Mesenchymal Stem Cells and Human Foetal Bone Cells – Implications for Disease Physiology and Regenerative Medicine

by

Susanne Maria Renz

The paucity of skeletal stem cell (SSC) progenitors, commonly referred to as mesenchymal stem cells (MSCs), makes the determination of a new source for SSCs necessary. MSCs derived from induced pluripotent stem cells (iPSC-MSCs) are regarded as such a potential new source. The presented work looked to generate iPSC-MSCs and to characterise iPSC-MSCs alongside human foetal bone cells (HFBCs) isolated from human foetal femurs 7 – 17 weeks post conception (wpc).

A fully characterised control iPSC line was differentiated into iPSC-MSCs using a protocol published by Chen et al., (2012). After initial culture in small molecule SB431542 supplemented medium for 10 days, *in vitro* culture aimed to mature iPSC-MSCs for six passages did not succeed in the generation of mature iPSC-MSCs with elongated fibroblastic morphology and increased cell proliferation.

In order to provide a base for future comparison of iPSC-MSC with HFBCs, human foetal femurs and HFBCs were characterised. Histological staining of human foetal femurs demonstrated a cartilage template for future bone with a thin bone collar surrounding the diaphysis at 8 wpc and, with ongoing development, a transition from a cartilage template toward a bone matrix with invading blood vessels (17 wpc). HFBCs isolated from 7 – 17 wpc human foetal femurs did not show any differences in morphology or proliferation capacity between developmental weeks. A temporal increase in chondrogenic gene expression was observed in HFBCs between 7 – 17 wpc with type IX collagen (*COL9A1*, $p < 0.001$) and aggrecan (*ACAN*, $p < 0.001$) demonstrating significantly enhanced expression. Osteogenic gene expression for *OCN*, *OPN*, *COL1A1* and *ALPL* did not show a significant increase or decrease in HFBCs between 7 – 17 wpc. Two osteogenic media were tested on HFBCs isolated from 8 and 14 wpc human foetal femurs as well as iPSC-MSCs: i) standard osteogenic differentiation medium containing dexamethasone, ascorbate-2-phosphate, 1,25-$(OH)_2$-vitamin D_3 (referred to as osteogenic background medium, oBG) and, ii) oBG supplemented with small molecules smoothened agonist (SAG) and (4-(4-methoxyphenyl)pyrido[4′,3′:4,5]thieno[2,3-b]pyridine-2-carboxamide) (TH). Comparison of the osteogenic potential of HFBCs isolated from 8 and 14 wpc human foetal femurs using both osteogenic differentiation media showed an advantage of HFBCs isolated from 8 wpc human foetal femurs cultured in oBG + TH + SAG for 19 days.

Global DNA methylation showed no major significant decrease in HFBCs between 7 and 17 wpc. Bisulfite pyrosequencing demonstrated significant demethylation in proximal *COL9A1* promoter at CpGs within SOX/Sry-binding sites correlating significantly with increase *COL9A1* gene expression. CpG sites within the vitamin D_3 response element in the *OCN* promoter were found to be strongly demethylated. Analysis of the regulatory function of miRNAs associated with chondrogenesis and osteogenesis was not successful.

The current studies demonstrated a regulatory role of DNA methylation on *COL9A1* expression in HFBCs isolated from a unique and developmentally relevant skeletal tissue, human foetal femurs from 7 - 17 wpc, thus providing an overview of foetal bone development during the first two trimesters. Although comparison between iPSC-MSCs and HFBCs was ultimately not possible, the acquired characterised sample set of HFBCs will prove advantageous in future comparison of generated iPSC-MSCs and HFBCs isolated from different developmental stages.

Table of Contents

Table of Tables

Table of Figures

Research Thesis: Declaration of Authorship

Print name:	Susanne Maria Renz

Title of thesis:	Characterisation of Induced Mesenchymal Stem Cells and Human Foetal Bone Cells – Implications for Disease Physiology and Regenerative Medicine

I declare that this thesis and the work presented in it are my own and has been generated by me as the result of my own original research.

I confirm that:

1. This work was done wholly or mainly while in candidature for a research degree at this University;
2. Where any part of this thesis has previously been submitted for a degree or any other qualification at this University or any other institution, this has been clearly stated;
3. Where I have consulted the published work of others, this is always clearly attributed;
4. Where I have quoted from the work of others, the source is always given. With the exception of such quotations, this thesis is entirely my own work;
5. I have acknowledged all main sources of help;
6. Where the thesis is based on work done by myself jointly with others, I have made clear exactly what was done by others and what I have contributed myself;
7. Part of this work has been published as:

Abstracts

"Differentiation protocols for osteoblasts and adipocyte formation from human bone marrow stromal cells (HBMCs)", Future Investigators of Regenerative Medicine 2016, Griona, Spain

"Differentiation protocol for osteoblast formation from human foetal femur skeletal stromal cells (SSCs), Future Investigators of Regenerative Medicine 2017, Girona, Spain

"Differentiation protocol for osteoblast formation from human foetal femur skeletal stromal cells (SSCs), Faculty of Medicine Research Conference 2017, Southampton General Hospital, Southampton UK

"Regulation of human foetal femur development by epigenetics", Faculty of Medicine Research Conference 2018, Southampton General Hospital, Southampton, UK

Contributions

All experiments and data analysis were performed by the author in the Bone and Joint Research Group laboratory, Academic Unit of Human Development and Health, Faculty of Medicine, Southampton, Southampton University Hospital, University of Southampton, with the following exception:

Section 5.3.1

Digested DNA (with DNA Degradase Plus™ Kit) of HFBCs isolated from 7 – 17 wpc human foetal femurs were sent to Esteban Guitián Fernández, Campus Vida, University of Santiago de Compostela, Spain who performed the analysis by HPLC-ESI-MS/MS-SRM to determine the ratio of 5mC to total cytosine content (5mC/5mC+C).

Signature:		Date:	

Acknowledgements

First and foremost, I would like to thank my supervisors Prof Richard Oreffo and Dr Maria De Andres Gonzalez for giving me the opportunity to undertake my doctoral research at the University of Southampton and broaden my knowledge in the many aspects of stem cells and epigenetic regulation. I am immensely grateful for your support and constructive criticism during my time in the lab and the writing of this thesis.

My sincere thanks to Julia Wells, Stef Inglis, Kate White and Janos Kanczler for the training given at the beginning of my PhD and organising the day-to-day laboratory routines. Thank you Julia for sharing her expertise in histology and taking beautiful images on the dotSlide microscope. Thanks to Kate Wright, for coated plates, running the ES lab and sharing her experience in culturing pluripotent stem cells. Special thanks to Dr May de Andres Gonzalez for sharing much of her knowledge on molecular biology, especially DNA methylation and pyrosequencing. Thanks to the Bone and Joint Research Group for making my PhD journey a rather pleasant one with weekly cake feasts and countless socials.

I would like to thank my family for their support over the past three years.

Finally, a very special thanks goes to Jay. Thank you for your patience, encouragement and for taking care of me during the process of putting three years of lab work into one big document. I would not have made it without you.

Definitions and Abbreviations

%	percent
°C	degree celcius
µCT	micro-computed tomography
5'AZA	5'azacitidine
5hmC	5-hydroxymethylcytosine
5mA	5-methyl-adenosine
5mC	5-methyl-cytosine
5mC/5mC+C	ratio of 5mC to total cytosine content
8-Br-cAMP	8-bromoadenosine 3',5'-cyclic monophosphate
A2P	ascorbate-2-phosphate
ACTB	β-actin
ADSCs	multipotent adult stem cells
AER	apical ectodermal ridge
AGO	argonaute
AKT	AKT Serine/Threonine Kinase 1
ALK	activin-receptor kinase
ALP	alkaline phosphatase
ALPL	alkaline phosphatase gene
APLNR	aplein receptor
ATF4	activating transcription factor 4
BAMBI	BMP and activin membrane bound inhibitor
bFGF	basic fibroblast growth factor
BGLAP	bone gamma-carboxyglutamate (Gla) protein
BIO	6-bromoindirubin-3'-oxime
BMMNCs	human bone marrow mononuclear cells
BMP	bone morphogenetic protein
BMP2k	bone morphogenetic protein 2 kinase
BSP	bone sialoprotein
C	cytosine
CaPs	calcium phosphate ceramics
Cat. No.	catalogue number

CCND	cyclin D
CCND1	cyclin D1
CD10	neprilysin
CD92	choline transporter-like protein 1
CDC	cell division cycle
CDH1	E-Cadherin
CDH2	N-Cadherin
CDK	cyclin dependent kinase
CDK complex	cyclin dependent kinase complex
CDKN	cyclin-dependent kinase inhibitor
CH_3	methyl-
CLDN1	claudin 1
cm^2	square centimeter
c-MYC	MYC proto-oncogene, bHLH transcription factor
COL1A1	collagen type 1 alpha 1
COL2A1	collagen type II alpha 1
COX7A	cytochrome c oxidase polypeptide 7A1
CpG	5'-C-phosphate-G-3'
CRB3	crumbs3
Crim1	cysteine-rich motor neuron 1 protein
CRYaB	alpha-crystallin B chain
C_t	threshold cycle
CXADR	coxsackie virus and adenovirus receptor
Cyc	cyclopamine
DAPI	4′,6-diamidino-2-phenylindole
DAZAP	DAZ-associated protein
Dex	dexamethasone
DGCR8	DiGeorge syndrome critical region gene 8
dH_2O	distilled water
DKK	dickkopf
DMR	differentially methylated regions
DNA	deoxyribonucleic acid
DNMT	DNA methyltransferase

dNTPs	deoxyribonucleotide triphosphate
dpc	days post conception
ds	double stranded
E8	Essential 8 Flex medium
EB	elusion buffer
EBs	embryoid bodies
ECM	extracellular matrix
EDTA	ethylenediaminetetraacetic acid
EGF	epidermal growth factor
EGFR	epidermal growth factor receptor
EGR2	early growth response protein 2
EMT	epithelial-to-mesenchymal transition
EPCAM	epithelial cell adhesion molecule
EPHA1	erythropoietin-rroducing hepatoma receptor
EpiSC	epiblast stem cell
E-RAS	embryonic stem cell-expressed ras
ERBB	Erb-B2 receptor tyrosine kinase
ESCs	embryonic stem cells
EtOH	ethanol
EZA2	Histone-lysine N-methyltransferase
FACIT	fibril-associated protein with an interrupted triple-helix
FAK	focal adhesion kinase
FBS	foetal bovine serum
FGF	fibroblast growth factor
FMR	fusion mediated reprogramming
FOXO	forkhead box
g	gram
GAPDH	glyceraldehyde 3-phosphate dehydrogenase
GBP3	guanylate-binidng protein 3
gDNA	genomic DNA
h	hour(s)
H3	histone 3
H3K27me3	histone methylation occurring on the amino (N) terminal tail of the core histone H3

H3K36me3	histone H3 lysine 36 methylation
H3K4me2	addition of two methyl groups to the lysine 4 on the histone H3
H3K4me3	addition of three methyl groups to the lysine 4 on the histone H3
H4	histone 4
HAT	histone acetyl transferases
HBM	human bone marrow
HBMMNCs	human bone marrow mononuclear cells
HBMSCs	human bone marrow stromal cells
HCBMNCs	human cord blood mononuclear cells
HCL	hydrochloric acid
HDAC	histone deacetylases
HDF	human dermal fibroblast
hESCs	human embryonic stem cells
HFBCs	human foetal bone cells
HFF	human foreskin fibroblast
HGS	hepatocyte growth factor-regulated tyrosine kinase substrate
HH	hedgehog
hiPSCs	human induced pluripotent stem cells
HNFF	human neonatal foreskin fibroblasts
HOX	homeobox
HPLC	high performance liquid chromatography
HPLC-ESI-MS/MS-SRM	high-performance liquid chromatography-electrospray ionization-tandem mass spectrometry-selected reaction monitoring
hsa	homo sapiens
hSSC	human skeletal stem cell
ICM	inner cell mass
IGF	insulin like growth factor
IgG	immunoglobulin G
IGSF3	immunoglobulin Superfamily Member 3
IHH	indian Hedgehog
Ikki	IκB kinase inhibitor

IL-6	interleukin 6
iPSC-MSCs	iPSC-derived MSCs
iPSCs	induced pluripotent stem cells
JAG	Jagged
KLF4	Kruppel-like factor 4
KO-DMEM	Knock out™-DMEM/F12
KOSR	knockout serum replacement
LYST	Lysosomal Trafficking Regulator
MAPCs	multipotent adult progenitor cells
MBDs	methyl-CpG- binding domain proteins
MCA	mesenchym-angioblast
MCL1	induced myeloid leukemia cell differentiation protein
MECP	methyl CpG binding protein 2
MEFs	mouse feeder cells
MEM NEAA	MEM Non-essential amino acids
MEPE	matrix extracellular phosphoglycoprotein
MET	mesenchymal-to-epithelial-transition
MFLC	mouse foetal liver cells
mg	milli gram
$MgCl_2$	magnesium chloride
MHC	major histocompatibility complex
microRNAs	miRNAs
MIF1	macrophage migration inhibitory factor
min	minutes
miR-	microRNA
miRNA	microRNA
MKI67 (Ki67)	marker of proliferation Ki-67
ml	milli liter
mM	milli molar
MMPs	matrix metalloproteinases
mmu	mus musculus
MNF	mouse neonatal fibroblasts
MP	mesenchymal passage

mRNA	messenger RNA
ms	mouse
MSCs	mesenchymal stem cells
MSX1/2	msh homeobox 1
NaB	sodium butyrate
NANOG	homeobox transcription factor NANOG
N-CAM	neural cell adhesion molecule
NCCs	neural crest cells
ng	nano gram
NIBSC	National Institute for Biological Standards and Control
nM	nano molar
nm	nanometer
NOTCH	Notch homolog 1, translocation-associated
OA	osteoarthritis
oBG	osteogenic background medium
oBG + TH + SAG	oBG supplemented with TH and SAG
OCLN	occludin
OCN	osteocalcin
OCT4	octamer-binding transcription factor 4
ON	osteonectin
OP	osteoporosis
OPN	osteopontin
OSX	osterix
P	passage
P/S	penicillin/streptomycin
PBS	phosphate buffer saline without calcium and magnesium
PCNA	proliferating cell nuclear antigen
PDCD4	programmed cell death protein 4
PDGF	platelet-derived growth factor
PFA	paraformaldehyde
PI3K	phosphoinositide 3-kinases
PICMI	post-ICM intermediate
PPARγ	peroxisome-proliferator activator protein gamma (gene)

PPAR	peroxisome-proliferator activator protein gamma (protein)
pre-miRNA	precursor-miRNA
pri-miRNA	primary miRNA
PS48	activator of 3'-phosphoinositide-dependent kinase (PDK-1)
PSCs	pluripotent stem cells
PTPN6	protein tyrosine phosphatase, non-receptor type 6
PZ	progress zone
qRT-PCR	quantitative real-time RT-PCR
R^2	Spearman's correlation coefficient
RA	retinoic acid
RAB25	Ras-Related Protein Rab-25
RALA	Ras-related protein Ral-A
RANK	receptor activator of nuclear κB
RANK-L	recptor activator of nuclear κB ligand
rb	rabbit
RBL	retinoblastoma-like protein 2
REDOX	oxidation/reduction
RFU	realtive fluoresence units
RISC	RNA-induced silencing
RN18S1	18S ribosomal RNA
RNA	ribonucleic acid
RT	room temperature
RUNX2	runt-related transcription factor 2
SAG	smoothened agonist
SALL4	sal-like protein 4
SAM	S-adenosyl-L-methionine
SATB2	special AT-rich sequence-binding protein 2
SCRIB	Scribble
SD	standard deviation
SLAIN	SLAIN motif family
SMAD	SMAD family member
SNAIL	snail family transcriptional repressor

SOST	sclerotin
SOX	Sry-related HMG box
SP100	SP100 Nuclear Antigen
ss	single stranded
SSCs	skeletal stem cells
STAT	signal transducer and activator of transcription
T	brachyury
TAE	Tris-acetate-EDTA
TCP	tissue culture plastic
TERT	Telomerase reverse transcriptase
TET	ten-eleven translocation
TF	transcription factor
TFAP2C	transcription factor AP-2 gamma
TGFβ	transforming growth factor beta
TH	4-(4-methoxyphenyl)pyrido[4',3':4,5] thieno[2,3-b]pyridine-2-carboxamide
TMEM119	transmembrane protein 119
TMEM64	transmembrane protein 64
TSS	transcription start site
TWIST	twist basic helix-loop-helix transcription factor
UBE1L	ubiquitin-like modifier-activating enzyme 7
UK	United Kingdom
UTR	untranslated region
UV	ultra violett
VIM	vimentin
viPSCs	iPSCs generated with viral reprogramming approach
VitD3	1,25-$(OH)_2$ -vitamin D_3
vitronectin	VN
VPA	valproic acid
w/v	weight/volume
WNT	wingless
wpc	weeks post conception
wpc	weeks post conception
ZEB	Zinc finger E-Box Binding Homeobox

αMEM	Minimum Essential Medium Eagle - Alpha modification
β-GP	β-glycerophosphate
Δ	delta
µl	microliter
µm	micro meter
µM	micro molar

Chapter 1 Introduction

1.1 Development of Novel Technologies for Bone Tissue Repair and Replacement

Advances in technology, nutrition and medicine have led to a welcome increase in world population demographics and life expectancy. However, the increased frequency of age-associated diseases, especially osteoporosis (OP), osteoarthritis (OA) and cardiovascular diseases, negatively affected by obesity, represents a growing socio-economic burden for healthcare systems in the European Union and across the world [1, 2]. Given the estimated growth of the world's population (people aged > 60 years will have doubled by 2050), the estimated financial costs on the treatment of OP will increase to $131.50 billion with 6.3 million hip fractures per year by 2050 [3, 4]. The need for improved treatments for tissue repair/replacement for age related degenerative diseases remains, to date, a significant unmet need.

1.1.1 Osteoporosis (OP) and obesity

The effects of a dietary shift during the 1970s toward an increased intake of sugar and fat accompanied with reduced physical activity began to manifest in the middle 1990s with a global increase in diabetes, hypertension or obesity [5]. Around 1.5 billion adults were overweight or obese in 2008 and, estimations predict there will be 2.16 billion overweight and 1.12 billion obese people in 2030 [6]. Furthermore, diseases negatively triggered by obesity (cardiovascular diseases, type 2 diabetes, liver/kidney damage as well as certain types of cancer) are predicted to be more prevalent. Preferred subcutaneous or visceral/abdominal fat accumulation has been shown to be determined by genetic predisposition, early-life influences alongside lifestyle during adult life, therefore contributing to the varying individual obesity risk [7, 8].

Obesity and OP were long regarded as two separate disorders with a protective effect from fractures in obese individuals, particularly in postmenopausal women [9]. This view was subsequently revisited in the years after the Global Longitudinal Study of Osteoporosis in Women (GLOW) study in 2011 showing no significant difference of fracture incidences between obese and non-obese postmenopausal women [10]. Bone acquisition is known to

peak at approximately 35 years (in both men and women) before slowing down as a consequence of an imbalance between bone resorption (osteoclast activity) and bone formation (osteoblast production). This time point coincides with adipocytes beginning to infiltrate the bone marrow cavity and an increase in key adipocyte regulator peroxisome-proliferator activator protein gamma (PPARγ) expression which continues with age [11, 12]. After this peak in bone mass acquisition, bones gradually become less dense, display enhanced fragility and, as a consequence, are prone to fractures. Arguments for and against the hypothesis of obesity being protective for the skeleton are summed up in Table 1.1.

Table 1.1 Hypothesis: "fat is protective for skeleton". Adapted from [13].

pro	**contra**
Increased loading on the cortical skeleton	Inflammatory cytokines impact bone formation by recruitment of osteoclasts
Increased protection against falls and fractures	Fatty acids stimulate bone resorption
Leptin directly stimulated bone formation	Leptin inhibits bone formation via sympathetic system
Increase in estradiol which results in decreased bone resorption	Hyperglycemia impairs bone formation
	PPARG activation ➔ Inhibition of bone formation ➔ Stimulation of bone resorption

Life style (e.g. smoking), diseases or medication are regarded as risk factors and responsible for accelerated, excessive bone resorption [14]. In addition, low testosterone levels in men, hyperthyroidism, calcium as well as vitamin D_3 deficiency or low estrogen levels in women prior/during menopause can shift the balance towards increased bone resorption [15]. Fractures due to OP are more frequent in postmenopausal women (44 % in female patients, 25 % in male patients of 60 years of age), however, fracture outcome is more severe in men due to limited knowledge concerning the course of OP in men and hence fewer treatment options. Additional to environmental and hormonal cues, the gap in the fracture risk between males and females is partially due to differences in bone size, ~ length, ~ strength and ~ density [16].

OP, one of the most common diseases in elderly people, itself is not defined by any specific symptoms, therefore is typically discovered only at fracture (predominantly at the spine, hip or wrist). Given the lack of symptoms prior to fracture, prevention has centered on the use of bisphosphonates, hormone supplementation, administration of minerals or exercise, but, approaches to treat the cause of the disease, specifically focused on bone formation are limited. People with OP fractures (fragility fractures), undergo surgery where the bone is either fixed or the hip joint entirely replaced. To date, commonly used prosthetics last approximately 10 years before a follow-up surgery may be required [17]. In addition, further bone loss due to inflammation, triggered by implant particles, in the area between implant and bone surface have recently emerged as issues in the conventional treatment of osteoporotic fractures [17].

1.1.2 Stem cells in bone fracture healing

There is, as indicated, a significant unmet need for strategies to augment bone. The application of stem cell based therapies to promote healing of the skeleton after a fracture has been heralded as a promising approach to address these clinical problems. Research over the last two to three decades has focussed on the isolation and differentiation along the stromal lineage of skeletal stem cells (SSCs). However, a significant limitation for improvements in fracture healing remains the paucity of SSC populations required for bone tissue repair. The bone marrow is the most common source for skeletal progenitors although their number is small (1 in 10,000-100,000) [18, 19]. The extraction of SSCs is associated with risks for the patient's health (e.g. an infection during the wound healing process), is painful and the fraction of progenitor cells further decreases with increasing patient age or in functionality/potency and is impaired by other diseases of the patient [20].

The idea of patient-specific induced pluripotent stem cells (iPSCs) has galvanised the research community in recent years. Knowledge of the pluripotency network (key for successful generation and maintenance of iPSCs), as well as the signalling pathways involved in the differentiation process has improved together with our understanding of events involved in embryonic development and cell fate decisions over the past few years. This highly regulated network is responsible for the constant self-renewal and expansion in *in vitro* cultures. Minimal changes can weaken the network and potentially initiate the differentiation process. Patient/disease-specific iPSCs can be generated from any somatic cells source and used for disease mechanism studies ("disease-in-a-dish" platform) [21-23],

investigation of pathophysiological pathways [24-26], or drug screening platforms [27] for the treatment of human diseases. To translate the application of iPSCs as disease modelling platforms ever closer to conditions in the human body, organoid-cultures have been applied in various studies, to form so called “organs-in-a-dish”. Studies have shown that such cells in organoid cultures resemble the “natural” state of cells in the tissue and appear advantageous over conventional 2D cultures [28]. Furthermore, previous studies have shown the possibility to generate iPSC-derived MSCs (iPSC-MSCs) which would offer a new cell source for the generation of patient specific osteoblasts (see chapter 1.6) which in turn could potentially be applied in the clinic.

1.1.3 Clinical trials and stem cell banking

A plethora of clinical trial studies using iPSC- or ESC-derived cells to treat a variety of diseases (e.g. spinal cord injuries, age-related macular degeneration, type 1 diabetes or Parkinson’s disease) was launched since 2014 with trials in Japan and China using customised iPSC-derived retina cells to treat age-related macular degeneration [29]. Major concerns regarding cell transplantation have included (i) heterogeneity of the transplanted iPSC- or ESC-derived cells due to contamination of the iPSC-/ESC-derived cells with undifferentiated cells and therefore development of benign teratoma or malignant teratocarcinoma, (ii) occurrence of genetic variations affecting gene expression or cell behaviour and, (iii) rejection of the transplant due to immune reaction of the recipient [29].

In a recent study, genetic aberrations were found in patient-specific iPSCs prior to the trial resulting in postponement and later termination of the study [30]. However, genetic variations can be found in all pluripotent stem cell lines due to long term culture. Hence, a framework determining what makes a mutation unacceptable depending on cell type, patient and transplantation site is required. This issue has triggered an international discussion already and will require an international consensus in the future. Reported transplantation of ESC-derived cells and the rejection of the transplant by the recipient’s immune system resulted in the concern the same could apply to iPSC-derived cells and would make lifelong treatment with immunosuppressives a necessity. Studies have shown that iPSCs as well as ESCs lack major histocompatibility complex (MHC) class I and II, therefore are immune privileged. Moreover, iPSC-derived cells lost their immunogenicity in contrast to ESC-derived cells which were repeatedly shown to trigger the host’s immune response [29, 31].

In conclusion, iPSCs are currently considered as a novel source for the generation of different cell types.

To date there are three possible iPSC sources for transplantation studies: (i) autologous iPSCs, i.e. customised iPSC lines for each patient, (ii) allogenic iPSCs, i.e. limited number of banked iPSC lines, (iii) human leukocyte antigen (HLA)-matched allogenic iPSC, i.e. restricted number of matching iPSC lines. Use of customised iPSC lines for each patient may avoid transplant rejection although this is a slow and expensive approach. Therefore, the latter option is considered to be the most economical and practical solution for future stem cell based treatments. Importantly, the number of the iPSC lines required would depend on the genetic heterogeneity of a population. Japan and the UK would require less iPSC lines (50 cell lines in Japan to match ~91 % of the population, 150 iPSC lines to match 93 % of the population in the UK) than Northern America, which holds a more heterogenic population [31].

1.2 Bone – Development, Structure, Composition and Function

Two weeks after fertilisation (weeks post conception, wpc) human development continues in two consecutive stages: the embryonic period (3-8 wpc) followed by the foetal period (9 wpc until birth). Major cell fate determinations, establishment of body axes and patterning and development of rudimental organs occur during the embryonic period. The foetal period is characterised by a gain in size of the embryo and maturation of the organs [32]. An overview of the major events during prenatal development is displayed in Figure 1.1.

The skeletal system consisting of bones, muscles, cartilage, ligaments and tendons helps maintaining the shape of the body as well as protecting several organs like lungs or heart. Furthermore, the skeletal system is involved in essential functions of the human body: red blood cells are generated from hematopoietic stem cells residing in the bone marrow, regulation of calcium and phosphate homeostasis or shock absorbance during exercise. In addition, bone tissue is highly dynamic and constantly triggered/influenced by differing hormone levels or mechanical stresses from the environment [33]. The skeletal system can be divided into the axial (cranium, neck, trunk) and the appendicular (limbs) skeleton [32].

1.2.1 Germ layer development

After fertilization, the developing zygote undergoes several morphological changes as well as ongoing cell division with distinct development potential. Around the 8-cell stage, first lineage segregation occurs and the zygote loses its totipotency that is the ability to give rise to a complete organism and all cell types. At the 8-cell stage, blastomers become polarized and the blastocyst together with the outer trophoblast and an inner cell mass (ICM), also called embryoblast, develops. The ICM contains the sole natural and limited source for pluripotent stem cells – embryonic stem cells (ESCs). Pluripotent stem cells can give rise to any cell type but are unable to form an entire embryo as compared to totipotent cells [34, 35]. Further on in human development, cell potency and differentiation potential become more restricted and the stem cells therein can only give rise to cells of their specific tissue (multipotent cells, e.g. hematopoietic cells give rise to the different blood cells or SSCs give rise to bone, cartilage, fat). Figure 1.1 displays the early developmental stages of a human embryo as well as the different stages of potency during early embryogenesis. At the end of the first week after fertilization (1 wpc), the blastocyst is implemented in the uterus and during the second wpc the ICM divides into the epiblast, giving rise to amnioblasts lining the amniotic cavity, and the hypoblast which gives rise to cells surrounding the primitive yolk sac [32].

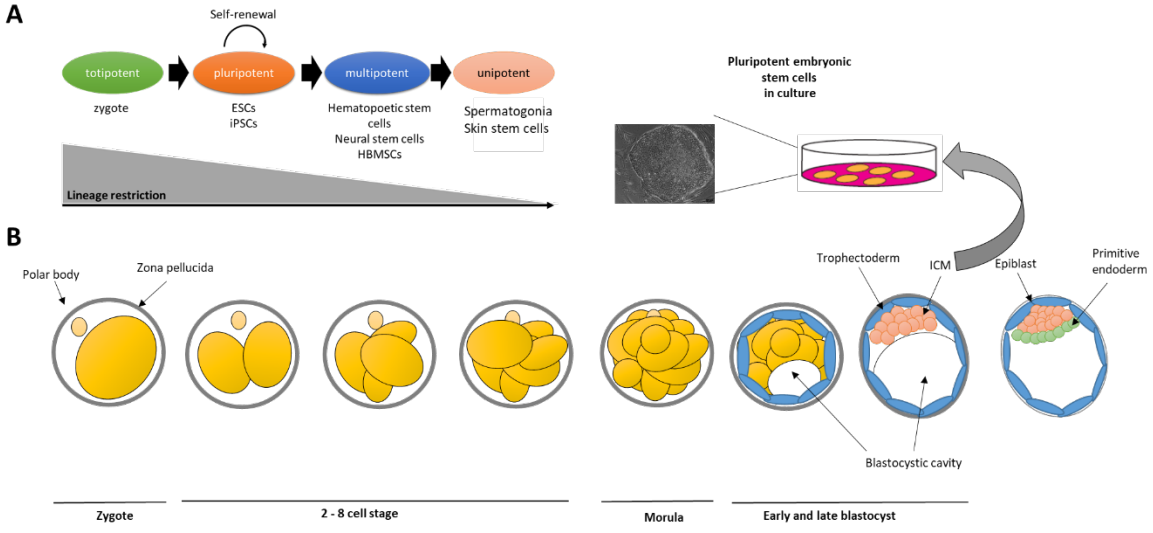

Figure 1.1. Embryonic developmental stages and cell potency. A: With ongoing development the cells in the embryo lose their potency, the ability for self-renewal. Multipotent stem cells can give rise to more specialised (restrictive) cell types, while unipotent cells are so restricted in their potency, only give rise to one cell type while a totipotent cell can form an entire organism. **B:** After fertilization, the zygote (fertilized egg) undergoes several cell divisions and morphological

changes until blastocyst is formed. Until this stage, cells are totipotent which describes the ability to form an entire embryo. Cells in the blastocyst either belong to the inner cell mass (ICM) or the trophoblast. Only cells of the ICM are pluripotent, can be cultured *in vitro* and give rise to all types of tissue. Based on [36, 37].

After ~15 days post conception (dpc), the primitive streak develops on top of the epiblast, indicating the start of the gastrulation process with cells of the epiblast migrating toward the primitive streak and slipping underneath in a process referred to as invagination [32]. The ectoderm germ layer is involved in the formation of the outer layer (skin, hair, nails, teeth), neural tube (giving rise to brain, motor neurons, spinal cord) and neural crest cells (NCCs), located on the dorsal side of the neural tube between the epidermis and the neural plate border of the embryo [38, 39]. Originally, NCCs were associated with the neural development, however, it was later shown that these cells possess the capability to give rise to visceral cartilage and teeth (summarised in [40]). NCCs possess the ability to migrate through the embryo, and give rise to different cell type of several tissues (osteoblasts, chondrocytes, MSCs, melanocytes, myoblasts, connective tissues, teeth and neurons), thus proving their multipotent character [40]. Furthermore, NCCs were shown to be of significant importance in the development of craniofacial connective tissues by giving rise to the ectomesenchyme, a specialised form of mesenchymal tissue, which in turn is involved in the formation of various craniofacial structures such as bones, tongue, muscles or teeth [38]. Given their ability to migrate through the embryo, their multipotency and the capacity to generate a large amount of differentiated cells from various tissues, the neural crest is now regarded as the fourth germ layer in addition to ectoderm, mesoderm and endoderm [38]. Cells of the endoderm line the inside of the digestive system (pharynx, stomach, colon, liver, pancreas, glands) and the lungs. Mesoderm, arising from cells underneath the primitive streak, is further divided into paraxial, intermediate and lateral plate mesoderm with on-going prenatal development shown in Figure 1.2. [39]. The paraxial mesoderm is organised in segments (somitomeres) starting from the head to tail region of the embryo. Establishment of somites is regulated by expression of specific genes (*WNT* and *NOTCH*) as well as signals from surrounding notochord, neural tube and lateral plate mesoderm. The intermediate mesoderm links the other two mesoderm types, paraxial and lateral plate mesoderm, and gives rise to urogenital and reproductive systems [32]. Cells from the ventral sclerotome migrate to different locations to give rise to the axial skeleton following epithelial-to-mesenchymal transition (EMT). Sclerotomal cells reaching the lateral plate mesoderm are

able to give rise to costal hyaline cartilage while parietal cells of the lateral plate mesoderm migrate to form the future limb bud of the appendicular skeleton. Cells having undergone EMT reverse to epithelial cells during development by mesenchymal. The lateral plate mesoderm is further divided into somatic and visceral mesoderm [32]. The somatic mesoderm forms the dermis as well as muscles of body and limbs as well as bones and connective tissues. Visceral mesoderm along with the endoderm form the gut tube [32].

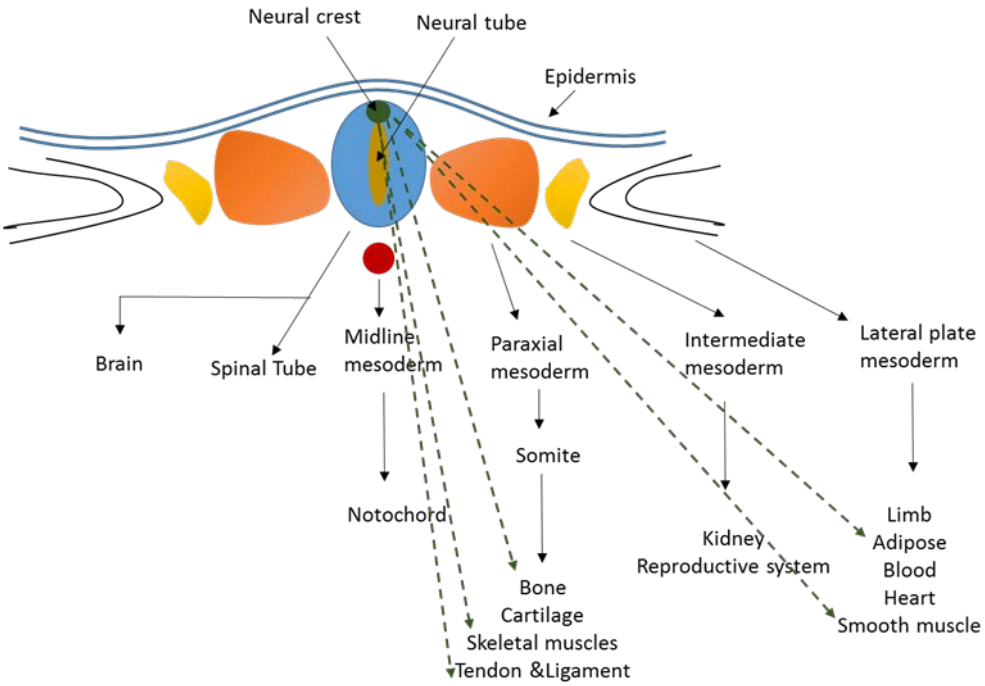

Figure 1.2. Mesoderm types and neural crest give rise to various types of tissues. Based on [38-40].

1.2.2 Limb development during the embryonic period

Limb buds of both, upper and lower limb, become visible toward the end of the fourth week; the lower limb bud 1-2 days later than the upper limb bud. Positioning as well as shape and location of future bones are initially determined by the expression pattern of *HOX* genes (*HOX-A* and *HOX-D* gene clusters) [41]. The limb bud consists of a mesenchymal core covered by the ectoderm layer. The area at the distal end of the limb bud thickens and is further referred to as the apical ectodermal ridge (AER). Beneath the AER lies the progress zone (PZ) and a positive feedback loop between FGF4 and FGF8 secreted by AER and PZ results in rapid proliferation of the mesenchymal stem cells in the bud's core [42]. With ongoing growth, the cells further from the AER will begin to differentiate into muscle and cartilage as they are beyond the influence of the AER. After six weeks post conception,

hand- or footplates develop by flattening of the limb bud and by constriction extremity structures are formed. Digit primordia (to become fingers and toes) are formed by cell death dividing the AER into five parts. After rotation of the upper limb and establishment of the external shape, the mesenchymal cells in the limb bud begin to differentiate into chondrocytes and form a hyaline cartilage template for future bone development by the end of sixth wpc [41].

1.2.3 Long bone formation by endochondral ossification

Bone formation involves two different processes depending on the type of developing bone: endochondral ossification (cartilage serving as a template for all prospective bones except clavicle and craniofacial bones) or intramembranous ossification (direct differentiation into bones of skull and clavicle without intermediate step) [43]. Development of long bones in the foetus occurs by endochondral ossification. This process is divided into the following steps: i) mesenchymal condensation, ii) chondrocyte proliferation and condensation, iii) hypotrophy of chondrocytes, iv) invasion of blood vessels and secretion of osteoblasts by primary ossification centre in diaphysis, and v) secondary ossification centre in epiphyses for long bone growth. Key events of endochondral bone formation during foetal development are illustrated in Figure 1.3.

Aggregation of mesenchymal cells and maintenance of this state (known as mesenchymal condensation) results in the generation of a cartilage anlage [43-46] and is mediated by cell-cell interactions through adhesion molecules N-CAM and N-Cadherin (promoted by TGFβ - signalling) as well as interaction of the cells with surrounding ECM [47] proteins hyaluronan, tencasin and fibronectin [48-51]. Hyaluronan is essential for initiation of condensation as it inhibits differentiation and facilitates proliferation of mesenchymal cells; cease of hyaluronan results in initiation of chondrogenic differentiation. Fibronectin promotes attachment and spreading of cells [52-54]. SOX9 is not necessarily required for the initiation but for the maintenance of the condensation. Cells in the centre of the cartilage anlage, that will become the primary ossification centre, begin to undergo chondrogenic differentiation while peripheral cells differentiating into cells of the perichondrium [43]. Chondrocytes in the centre secrete characteristic ECM proteins: collagen type II, type IX, type XI, aggrecan. Collagen type I is expressed in perichondrium only [55, 56]. Expression of SOX5 and SOX6 together with SOX9 is required for production of mentioned ECM proteins [57, 58]. With ongoing development chondrocytes in the centre of the shaft

(diaphysis) increase in size, a process referred to as hypertrophy, and levels of collagen type X increase [59, 60]. Hypertrophic chondrocytes eventually undergo apoptosis, leaving cavities within the cartilaginous shaft. The bone collar forms from perichondral cells due to Indian Hedgehog (IHH) signalling from hypertrophic chondrocytes. Osteoprogenitor cells from the perichondrium will migrate into the centre of the diaphysis in invading blood vessels resulting in mineralisation of the matrix and form woven bone. Due to the activity of invading osteoclasts, bone will be reabsorbed and hence generate an enlarged cavity for bone marrow. The bone collar will become thicker and stronger with time. Elongation of long bones occurs by interstitial growth with different types of chondrocytes in distinct zones along the longitudinal axis (see Figure 1.3) [43].

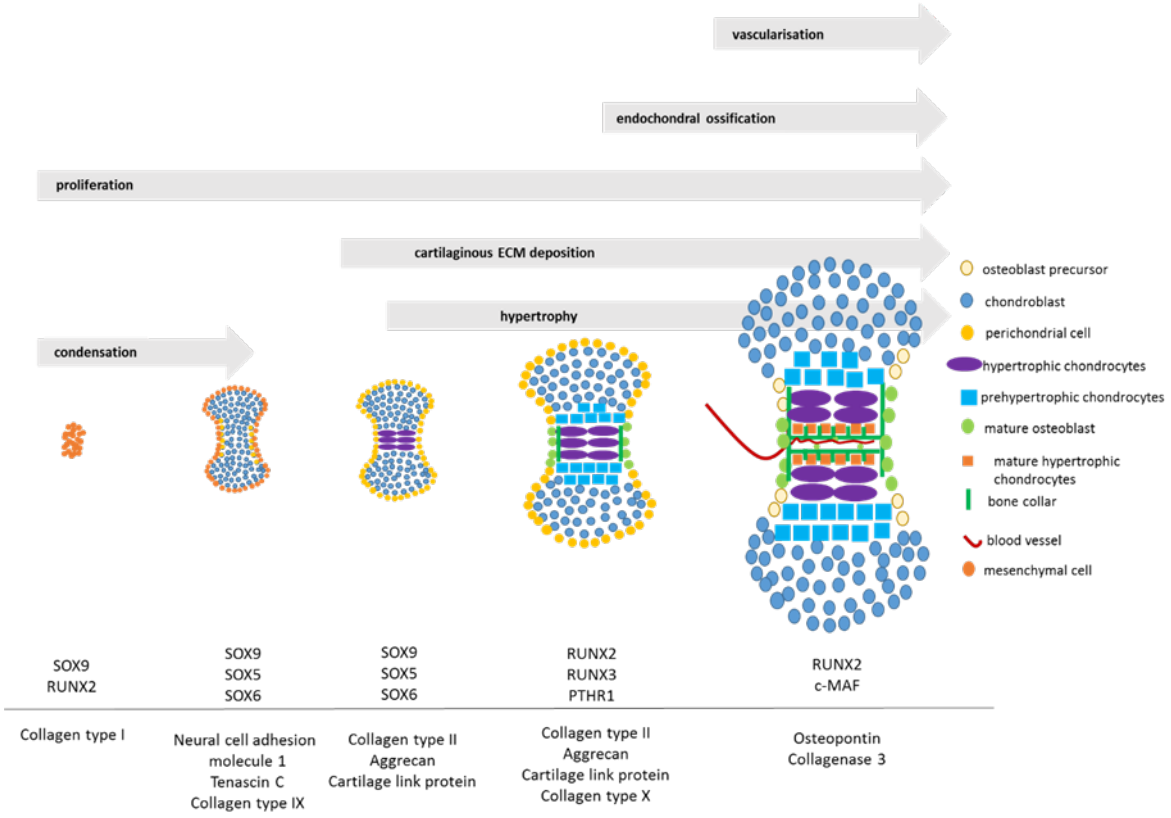

Figure 1.3 Foetal development of long bones. Formation of long bones in the foetus occurs by endochondral ossification. Mesenchymal stem cells condensate and form a cartilage anlage serving as a model for the future long bone. Chondrogenic differentiation gives rise to pre-hypertrophic and hypertrophic chondrocytes and surrounding matrix becomes calcified by osteoblasts migration in invading blood vessels, forming the primary ossification centre. Interstitial growth of the bone is due to distinct zones with different types of chondrocytes: reserve chondrocytes toward the epiphyseal end of the shaft, proliferating chondrocytes followed by pre-hypertrophic and hypertrophic chondrocytes toward the centre of the shaft (purple). TF: transcription factor. Based on [43].

1.2.4 Human foetal bone cells (HFBCs)

Human foetal bone cells (HFBCs) were characterised for their proliferative capacity, multipotency and differentiation potential by Montjovent et al. [61] and Mirmalek et al. [62]. Montjovent et al. [61] isolated HFBCs from human foetal femurs between 13 and 16 wpc while Mirmalek et al. [62] isolated HFBCs from human foetal femurs from 8 – 11 wpc.

HFBCs isolated from 8 – 11 wpc human foetal femurs, predominantly comprised of chondrocytes in the epiphyses with the diaphysis being surrounded by perichondrium/periosteum, demonstrated the ablilty to differentiate into bone, cartilage and fat, with reduced culture periods compared to adult mesenchymal populations. These findings suggest that HFBCs isolated from 8 -11 wpc human foetal femurs possess a higher proliferation potential alongside a multipotent differentiation potential compared to STRO-1^+ adult bone marrow-derived skeletal stem cells isolated from elderly patients [62]. The majority of human foetal femurs used in this study were from 8 wpc while only one human foetal femur at 11 wpc was used. This study demonstrated that HFBCs and STRO-1^+ adult bone marrow-derived skeletal stem cells shared similar osteogenic and chondrogenic differentiation potentials while enhanced adipogenesis was showm in differentiated HFBCs compared to unselected and STRO-1^+ adult bone marrow-derived skeletal stem cells [62].

HFBCs isolated from 13 – 16 wpc human foetal femurs demonstrated a similar proliferation potential compared to adult-derived mesenchymal cells, however, shorter than for adult bone cells [61]. Mean doubling time in the three HFBCs populations (isolated from 13, 14 and 16 wpc human foetal femurs) was 7.2 x lower compared to the three adult bone cell populations (isolated from human trabecular bone from adult donors at 31, 50 and 60 years. Mean doubling times in HFBCs and mesenchymal stem cells (isolated from 26 year old adult donor) was ~ 1 day while adult bone cells required ~8 days to double in number. Doubling times of HFBCs did not change significantly within three passages. Only differentiation of HFBCs toward the osteogenic lineage was studied with increased expression of RUNX2, ALP and COL1A1 in HFBCs compared to adult bone cells and mesenchymal stem cells [61]. Selection with specifc surface markers was not studied in either of the cell types in this study [61].

Taken together these two studies provided a first overview of the characteristics of HFBCs isolated from human foetal femurs covering the first two trimesters. To date a full panel of human foetal femurs covering the first two trimesters has not been published.

Gothard et al. reported that HFBCs isolated from different regions in the human foetal femur (epiphysis and diaphysis) possess different characteristics influencing differentiation outcomes with epiphyseal HFBCs being more chondrogenic while diaphyseal cells are more osteogenic [63]. However, each of the two HFBCs populations exhibited trilineage differentiation potential, suggesting a shared cell population. This shared sub-population was found to comprise STRO-1^+ cells suggesting the presence of a skeletal stem cell population [63] .

The identification of suitable surface markers is hampered by controversy regarding the nomenclature of MSCs and SSCs (see chapter 1.3). A plethora of work has gone into the identification of a true skeletal stem cell with CD90, CD105, CD73, CD44, CD146 and CD271 having previously been identified to improve enrichment for skeletogenic activity in mesenchymal cultures [64-68]. In 2018, Chan et al. have discovered the surface marker combination of $PDPN^+$, $CD73^+$, $CD164^+$, $CD146^-$ by using single-cell RNA sequencing of seven different zones of a 17 wpc human foetal femur [64]. Multilineage differentiation of cells expressing this surface marker combination resulted in successful osteogenic and chondrogenic differentiation, however, no adipogenesis could be detected [64]. *In vivo* transplantation showed the formation of multilineage ossicles containing bone, cartilage and stroma. Differences in skeletogenic capacity of hSSCs (human skeletal stem cell) with identified surface marker expression isolated from different tissue sources (foetal, adult, iPSC) demonstrated that foetal and iPSC-derived SSCs predominantly form cartilage compared to adult-derived SSCs [64]. Further cluster gene analysis showed that compared to foetal and iPSC-derived hSSCs, adult-derived hSSCs are more heterogenous while iPSC-derived hSSCs clustered closer to foetal-derived hSSCs [64].

1.2.5 Structure of long bones

In the early human embryo, woven bone which consists of irregular arranged collagen fibrils provides a degree of flexibility to the bones in the embryo as well as in the initial stage of fracture healing. This immature bone is later replaced by lamellar bone comprised of trabecular (spongy) and cortical (compact) bone [33, 69]. Trabecular and cortical bone share a similar composition but differ in structure and function. The trabecular (spongy) bone is responsible for absorption of loads and the cortical (compact) bone for stability (Figure 1.4 A). Cortical bone surrounds the medullary cavity (diaphysis) containing the bone marrow while trabecular bone is present in the metaphysis (below the growth plate) and the

epiphysis (above the growth plate) surrounded by thin layer of cortical bone [33, 69, 70]. Cortical bone consists of an outer (periosteal) and an inner (endosteal) layer. The outer layer is attached to the thin layer of vascularised, fibrous connective tissue by Sharpey's fibers while the inner layer is a membrane covering the inner surface of cortical bone and blood vessel canals (Volkman's canals) in the bone and is in touch with the medullary cavity [70]. Cortical and trabecular bone are both composed of osteons. Osteons in the cortical bone are lamellae with a central canal named harversian canal and harbouring blood vessels and nerves. Embedded osteocytes (osteoblasts surrounded by organic matrix) are responsible for the regulation of calcium homeostasis. Trabecular bone is the major bone type in the proximal and distal epiphysis. There is high percentage of vasculature running through and, sinusoids are responsible for the contact between bone and bone marrow (Figure 1.4 B). Compared to cortical bone, the rate of bone remodelling is higher in trabecular bone given that the osteoblasts localised at the surface and, therefore more exposed to cytokines and growth factors [33, 69].

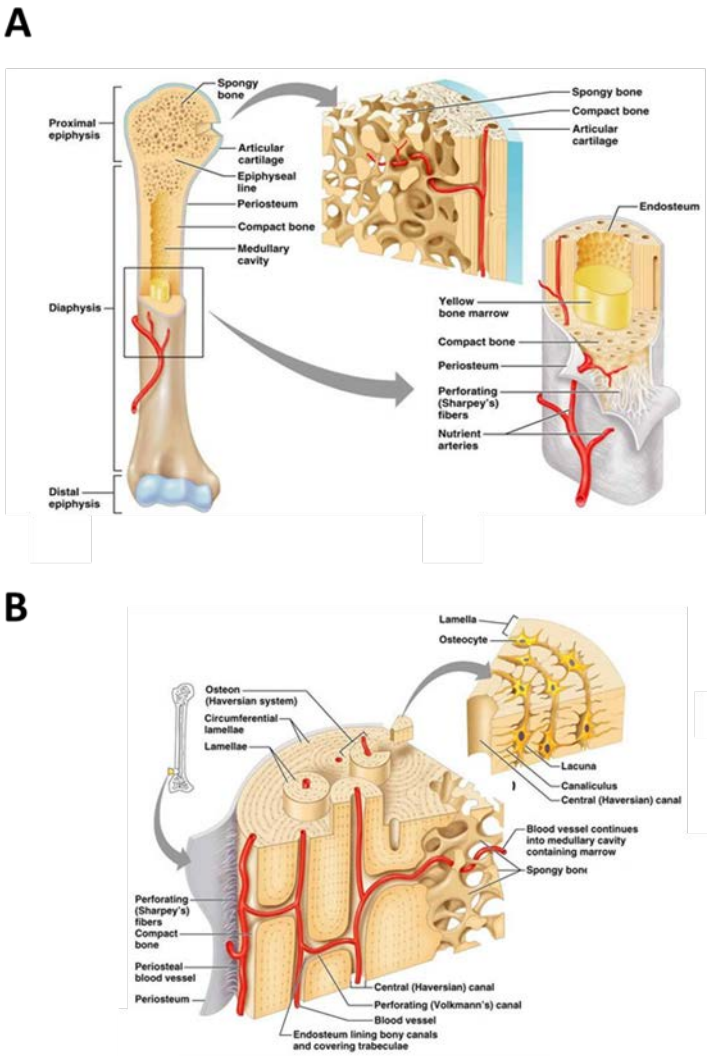

Figure 1.4. Structure of long bones. (Images: http://veterinary-online.blogspot.co.uk/2012/11/veterinary-online-bones.html (accessed 29.01.2017) and http://anatomybody101.com/human-long-bone-anatomy/ (accessed 29.01.2017)).

Bone Remodelling

In both men and women, bone acquisition peaks at approximately 35 years and then slows down [33]. An imbalance between bone resorption (osteoclast activity, hematopoietic origin) and bone formation (osteoblast production, mesenchymal origin) can subsequently lead to increased risk for fractures and indeed diseases like OP [71]. Bone remodelling is a process that occurs throughout life, maintaining a stable calcium homeostasis and aiding the repair of microfractures in bone. Osteocytes residing in the bone signal to bone lining cells, resulting in an increased release of receptor activator of nuclear κB ligand (RANKL) [71]. RANKL in turn binds to receptor activator of nuclear κB (RANK) on pre-osteoclasts triggering their maturation into committed osteoclasts. Osteoclasts can adhere to the bone and secrete proteolytic enzymes and hydrogen ions to resorb the mineralized bone. Ions,

minerals as well as growth factors embedded in the bone are released and can recruit osteoblasts which in turn invade the resorption pits generated by osteoclasts to lay down new bone matrix. Bone matrix is later mineralised by deposition of hydroxyapatites again to seal the holes in the bone. Osteoblasts release insulin like growth factor 1 (IGF-1) and interleukin 6 (IL-6), amongst other cytokines, to recruit osteoclasts and therefore to restart the cycle of resorption and mineralisation again. Bone can be resorbed in 2-3 weeks while the bone formation process requires 2-3 months [71].

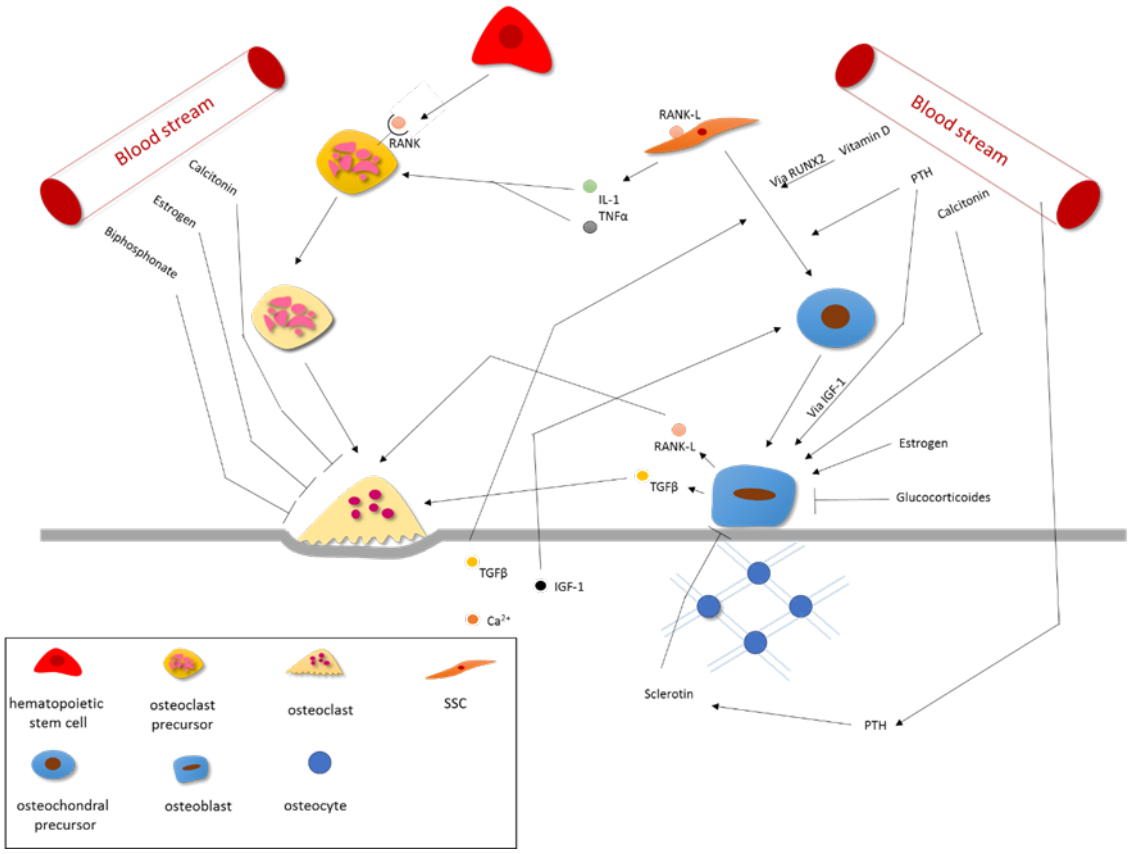

Figure 1.5 Factors influencing the balance between bone resorption and bone formation. IGF-1: insulin like growth factor 1; TGFβ: transforming growth factor beta; Ca^{2+}: calcium ion; PTH: parathyroid hormone; RANK: receptor activator of nuclear factor κ B; RANKL: receptor activator of nuclear factor κ B ligand; RUNX2: runt-related transcription factor 2. Based on [72, 73].

1.3 Skeletal stem cells (SSCs) *versus* mesenchymal stem cells (MSCs)

Human bone marrow (HBM) has long been known to harbour the source of progenitor cells of all blood cells, the hematopoietic stem cells [74]. The seminal work of Friedenstein and

colleagues showed a second entity, much rarer in cell numbers and first unidentified, with the ability to give rise to bone tissue. This osteogenic potential was ascribed first to adherent, non-hematopoietic cells and later to clonogenic stromal cells. These cells that gave rise to single cell-derived colonies, isolated from HBM samples and Friedenstein formulated the idea of a second class of stem cells in the bone marrow (summarised by Bianco et al. in [75]). Differentiation of these cells into osteoblasts, chondrocytes and adipocytes demonstrated the multipotent potential of this cell type. Friedenstein's idea had distinct boundaries: the newly described stem cell was to be found in the bone marrow and able to give rise to skeletal tissues only, not to all mesoderm-derived tissues as suggested later on [18, 76]. Based on this concept cells isolated from bone marrow are referred to as SSCs or human bone marrow stromal cells (HBMSCs). The concept of MSCs is based on the work of Friedenstein but proposed these MSCs to be progenitors for non-hematopoietic "mesenchymal tissues", not skeletal tissues exclusively. The idea of a new class of stem cells in all postnatal tissues gained rapid acceptance given their potential therapeutic application in regenerative medicine.

The Mesenchymal and Tissue Stem Cell Committee from the International Society for Cellular Therapy (ISCT) defined three criteria to identify/characterise MSCs: i) adherence to plastic, ii) expression of specific surface markers (CD105, CD73, CD90) while lacking the expression of CD45, CD34, CD14 and, iii) potential of multipotential (osteogenic, adipogenic, chondrogenic) differentiation [77]. However, these are inconsistent in the scientific community, on one hand as a consequence of different culture protocols and, on the other the tissue of origin, resulting in extensive variation in accepted and published criterion. Moreover, certain aspects of the idea are inconsistent with developmental aspects (e.g. different types of mesodermal tissues that do not share a common progenitor since they are developmentally distinct as soon as specification took place). Despite the observed differences between MSCs and BMSCs, thousands of studies detail the concept of MSCs as an established fact and this has resulted in confusion of a definition, characteristics and true identity of the cells isolated from HBM.

This inconsistence is further evidence for an existing difference between bone marrow stromal cells (BMSCs), also called stromal precursors, SSCs and "MSCs". The work of Sacchetti et al. [78] showed "MSCs" isolated from different tissues differ in the transcriptomic signature as well as *in vivo* differentiation potential. Hence, a clear separation

of the terms describing cells giving rise to skeletal tissues only (SSCs) and other mesodermal tissues (MSCs) is needed [75].

1.4 Generation of pluripotent stem cells *in vitro*

1.4.1 Sources of pluripotent stem cells

Human embryonic stem cells (hESCs), obtained from human embryos, are the only natural occurring source of pluripotent stem cells, but due to ethical concerns regarding their application, as well as low cell numbers in the ICM, are limited in supply [79]. Furthermore, hESCs are less suitable for clinical patient-specific cell therapies as their application may trigger the patient's immune response, resulting in the rejection of the ESC-derived transplant (see section 1.1.3). Indeed, allogenic transplantation of ESCs in mice has been shown to trigger the host's immune system and resulted in the rejection of the cells and repeated transplantation led to an accelerated secondary reaction of the immune system, suggesting an immunologic memory [80]. Therefore, techniques enabling scientists to obtain 'artificial' pluripotent stem cells resembling the same features of the natural occurring ESCs in high quantities *in vitro* have come to the fore in an attempt to replace the use of ESCs. Three key techniques to obtain such an alternative source of pluripotent stem cells *in vitro* have been developed over the past two decades:

1. The first method was developed by John Gordon in 1962 called **somatic cell nuclear transfer (SSCT)**. Gordon exchanged the nucleus of a *Xenopus* oocyte with the nucleus of a somatic cell, resulting in a totipotent blastocyst from which ESCs could be derived. The nuclei contained all genetic information necessary to generate zygote and ICM. However, as the technique involves generation of a totipotent blastocyst, ethical concerns surrounding clinical applications made this a reduced improvement compared to the use of 'natural' ESCs [81, 82].

2. Fusion mediated reprogramming (FMR) generates pluripotent cells by fusion of a somatic cell with an embryonic stem cell. The somatic characteristics and properties are rewound and a pluripotent phenotype generated. However, given the use of embryonic material, FMR does not provide an improvement or replacement for 'natural' pluripotent stem cells [83].

3. The seminal work of Shinya Yamanaka in 2007 demonstrated that forced expression of four transcription factors (OCT4, SOX2, KLF4, c-MYC, abbreviated OSKM) led to the conversion of human somatic cells into a pluripotent state, a process referred to as "**direct reprogramming**" and the resulting cell type as iPSCs [84]. To date, this discovery remains the method of choice to obtain 'artificially' generated pluripotent stem cells. Ten years on, a raft of systems have been proposed for the delivery of reprogramming factors (including the application of lenti-/retro-/Sendai virus, modified RNAs, plasmids and small molecules) in order refine the original method and increase the efficiency. All the various reprogramming strategies, their dis-/advantages as well as the process itself will be discussed in the following.

1.4.2 Generation of iPSCs – the process of reprogramming

The idea for direct reprogramming is based on Waddington's model of the epigenetic landscape (Figure 1.6), a concept proposed by Conrad Waddington in 1956 (reviewed in [85]). The image of a carved valley with marbles (to resemble a single pluripotent stem cell, blue marble) rolling downhill, undergoing developmental restriction in potency (red marbles) and coming to rest at different locations (different somatic cell types, yellow marbles) due to selection of different/alternative grooves. As all the different cell types originated from the same cell type in the beginning (pluripotent), scientists wondered whether it would be possible to reverse the different cell types into the original cell ('to roll the marbles uphill to the starting point again') [85].

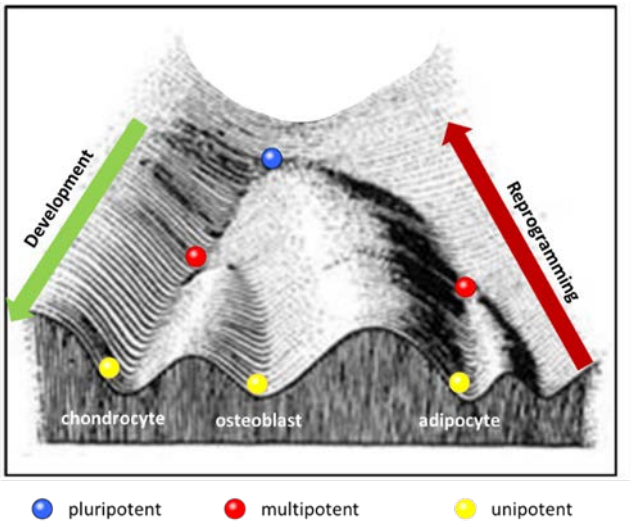

Figure 1.6. Adaptation of Waddington's model of the epigenetic landscape during embryonic development. Conrad Waddington suggested a marble rolling downhill in a carved valley

resembling the different possible cell fates during development. Blue marble: pluripotent cell; red marble: multipotent cell; yellow marble: unipotent cell. Modified from [85]. Several genes (*SOX2*, *NANOG*, *OCT3/4*, *c-MYC*, *KLF4*, *E-RAS*, *STAT*) [86-91] had already been proven to be involved in the maintenance of pluripotency prior to the seminal work of Shinya Yamanaka and colleagues in 2006 [88]. Yamanaka proposed that a shift from a differentiated somatic cell into a pluripotent stem cell could be triggered by over-expression of specific pluripotency genes. By screening 24 genes previously being reported to be related to ES-cell pluripotency, four factors were identified to be sufficient for direct reprogramming adult fibroblasts into iPSCs: *OCT*4, *SOX*2, *KLF*4, *c-MYC* ('Yamanaka factors') [84, 88]. To date, there are thousands of publications focusing on reprogramming and differentiation of generated iPSCs. The fact that the starting donor material consists of cells in different development stages and different, refined reprogramming approaches in the different institutions have made comparison across laboratories challenging. In the beginning only an approximate idea surrounding the suppression of EMT signals and the promotion of pro-mesenchymal-to-epithelial-transition (MET) was known in mice [92]. Figure 1.7 displays these basic events of the reprogramming process. SOX2, OCT4 and c-MYC are responsible for suppression of EMT (SOX2/OCT4 impair SNAIL, c-MYC suppresses TGFβ receptors) while KLF4 supports activity of E-Cadherin and therefore MET. Figure 1.7 illustrates the EMT process and the function/targets are summed up in Table 1.6.

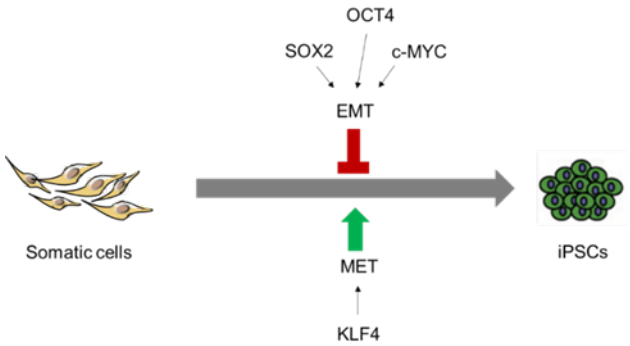

Figure 1.7. Schematic of basic events during the reprogramming process. SOX2, OCT4 and c-MYC suppress EMT (epithelial-to-mesenchymal transition) by impairment of *SNAIL* expression by SOX2 and OCT4 as well as suppression of TGFβ receptors by c-MYC; KLF4 promotes MET (mesenchymal-to-epithelial transition) by promotion of E-Cadherin activity. Modified from [92].

A more detailed summary of events in chronological order during direct

reprogramming with regards to cellular, molecular and epigenetic events is displayed in section 1.7.1.1 in Figure 1.12. OCT4, SOX2 and NANOG were known to be the key regulators of the pluripotency state with NANOG described as the core pluripotency factor. Investigation of the pluripotency network in mice and human iPSCs in recent years demonstrated that OCT4, SOX2 and NANOG together co-regulate the pluripotent state by controlling other genes and regulatory elements generating feedback loops and recruitment of activators, repressors, regulatory RNAs as well as epigenetic mechanisms. However, research has also shown that OCT4 and SOX2 act as heterodimer and expression is upregulated consistently across pluripotent population while NANOG acted separately and was expressed in high or low levels in a uniform population. NANOG was suggested to be a safeguard for pluripotency as PSCs lacking its expression were able to maintain an undifferentiated state and self-renew. In the OCT4-SOX2 relationship, SOX2 primes binding sites on the chromatin for OCT4 and binding of the OCT4-SOX2 dimer is stabilised by OCT4 itself.

1.4.3 Refinement of Yamanaka's reprogramming approach

Understanding the reprogramming process is key in optimisation and refinement of reprogramming approaches to increase reprogramming efficiency. Following Yamanaka's original publications [84, 88], the technique - delivery of the reprogramming factors, culture conditions, media composition, small molecules - was refined in follow-up studies and finally applied to any type of somatic cells of mouse and human origin [93-96] (Table 1.2). Either in substitution or in addition of the Yamanaka factors, various studies demonstrated the promoting and facilitating effect of small molecules on the reprogramming process (Table 1.3). Culture under hypoxic conditions during and after reprogramming resulted in improved stemness and stability of the generated iPSCs with increased levels of metabolic genes and higher expression of *NANOG* [97].

However, a variety of issues including i) efficiency of the process, ii) application of tumour-causing genes (pre-oncogenes *OCT*4, *c-MYC*), iii) modulation of epigenetic donor memory and iv) variation between hiPSC lines, remain to be resolved in advance of clinical application of iPSCs [98]. A number of studies indicate reprogramming efficiency is dependent on the mode of delivery, cell type and mechanistic pathways at play (e.g. p53-p21 pathway, chromatin regulation, Wnt (wingless)/β-catenin, TGFβ pathways, innate

immune response) [99-105]. Approaches to generate iPSCs suitable for clinical application have included: i) substitution with small molecules, ii) removal of critical pre-oncogenes (*OCT*4, *c-MYC*) which may produce genomic aberrations and, iii) determination of the absence of any transfection load following iPSCs generation. Bhutani and co-workers recently demonstrated that iPSC lines, generated using either retrovirus, Sendai virus or mRNAs, contained minimal tumour formation risk and only limited benign tumours introduced by the reprogramming process following iPSC transplantation were observed [106]. However, comparison of reprogramming efficiencies is complicated by variations in the set-ups of the different approaches (e.g. seeding cell density, different proliferation behaviour of the different starting cell populations, passaging methods).

Non-viral delivery systems such as episomal plasmids, protein, mRNA and microRNAs are better suited for clinical translational approaches as these systems harbour no risk of viral induced mutations. Efficiencies of mRNA and microRNA generated iPSCs during recent years are higher compared to older viral and also non-viral approaches.

Thus iPSC technology has, to date, resulted in several advantages: i) the generation of specific cell types from human iPSCs instead of mouse cells aided research [107-109], ii) *in vitro* results have translated to clinical applications, iii) human disease studies with iPSCs could overcome limitations in disease studies with mouse cells, iv) disease models using human cells instead of mouse best reflect the epi-/genetic landscape of a diseased donor. No visible immune reaction after transplantation of iPSC-derived cells compared to ESC-derived cell types generates high expectations for future clinical applications of these cells [110]. Other studies have shown a moderate frequency (10-20 %) of rejection of the transplanted hiPSC- and hESC-derived cells. However, comparison proved difficult due to variations in experimental set up, studied cell type and transplantation site. Potential causes for immunogenicity include: i) immature iPSC-derived cells *in vitro* with expression of proteins characteristic for embryonic or foetal cells to which the adult immune system has never developed antibodies, ii) culture of iPSCs on MEFs as these secrete *N*-glycolneuramic acid to which humans possess antibodies, iii) changes in epi-/genome during reprogramming process (summarised in [111]).

Table 1.2. Comparison of different delivery methods for the reprogramming factors. VPA: valproic acid; miRNA: microRNA; MEFs: mouse embryonic fibroblasts; HFF: human foreskin fibroblasts; HDF: human dermal fibroblasts; HNF: human new born fibroblasts; HBMMNC: human bone marrow mononuclear cells; HCBMNC: human cord blood mononuclear cells; MFLC: mouse foetal liver cells; MNF: mouse neonatal fibroblasts; HNFF: human neonatal foreskin fibroblasts.

	Efficiency	**Integration into genome**	**Karyotype**	**Species & Cell type**	**Advantages/Disadvantages**	**References**
Lenti-/Retrovirus	Retrovirus: 0.001% Lentivirus: 0.027%, 0.5%	yes	Retrovirus: Aneuploidy 13.5% Lentivirus: Aneuploidy 4.5%	HDF	Lentivirus: genome integrating but infection of non-dividing cells as well vectors with antibiotic cassettes available. Retrovirus: silencing of transgenes during process.	[84, 112, 113]
Adenovirus	0.0001%-0.001%	no	N/A	HFF IMR90 MFLC MNF	Non-integrating, lower reprogramming efficiencies compared to lenti-/retroviral approaches.	[114, 115]
Sendai virus	0.1%-1.5% 0.077%	no	Aneuploidy: 4.6%	HDF HNFF	Unable to enter the nucleus (non-integrating), viral particles are eliminated from transfected cells over the course of several passages (8-10), more efficient than other viral approaches.	[100, 106, 112, 116-120]
Episomal plasmids	0.006%, 0.035%, 0.013%	yes	Aneuploidy: 11.5%	HDF HBMMNCs HCBMNCs	High amount of partially reprogrammed colonies, development of new plasmids (e.g. Yamanaka, Thomson) and addition of small molecules significantly enhanced the efficiency, larger starting number of cells, high amount of aneuploidy, after > 10 passages cells are clear of plasmids.	[93, 119, 121]

	Efficiency	Integration into genome	Karyotype	Species & Cell type	Advantages/Disadvantages	References
Protein	0.001%	no	N/A	HNF	Low efficiency, high amount of pure protein required, recombinant protein of reprogramming factors stoichiometry/concentration can be regulated easily so protein can be distributed in a directed way, innate immune reaction is avoided. Several technical issues: expression system, design of the recombinant protein is of great importance, problems with release of proteins form endosomes.	[122, 123]
mRNA	1.4-2.1%	no	Aneuploidy: 2.3%	MEFs HFF HDF	High efficiency, integration free, delivery more efficient due to small size, daily delivery, triggers strong immune response in human cells (but not in mice), which decreases efficiency.	[123, 124]
microRNA	miR302/367: 2-5% miR302/367+VPA: 10%	no	N/A	Mouse fibroblasts HDF	No need for oncogenic transcription factors, addition of small molecules increases efficiency.	[123-125]

Table 1.3 Small molecules promoting/facilitating the reprogramming process. 8-Br-cAMP: 8-bromoadenosine 3',5'-cyclic monophosphate; NaB: sodium butyrate; PS48: activator of 3'-phosphoinositide-dependent kinase (PDK-1); PSC: pluripotent stem cell; EpiSC: epiblast stem cell; VPA: valproic acid.

Compound	Effect & advantages/disadvantages	Reference
VPA NaB	Histone deacetylase inhibition by deacetylation of lysine residue and histone hyperacetylation resulting in remodelled chromatin and gene expression; the positive effect of VPA on reprogramming is supposed to be due to other mechanisms in addition. Sodium butyrate was found to be more reliable than VPA (20-fold increase compared to 3-fold in VPA treated cultures).	[126, 127]
5'azacitidine (5'AZA)	DNA methyltransferase inhibitor Inhibition of DNA methylation (mainly in CpG dinucleotides).	[126, 128, 129]
PD0325901 SB43152	Blockade of the TGFβ and MAPK/ERK pathways.	[130]
Vitamin C	10-fold increase in efficiency in treated cultures.	[131]
Thiazovivin	ROCK signalling inhibition; supports survival of pluripotent cells and only used in combination with other small molecules.	[132]
8-Br-cAMP VPA	Downregulation of p53 pathway in early reprogramming stages; 8-BR-cAMP alone increased efficiency by 2-fold, in combination with VPA by 6.5-fold in cultures transduced with the four reprogramming factors.	[133]
MM-401	Histone H3K4 methyltransferase MLL1 inhibitor; highly efficient and rapid reprogramming (50% naïve PSCs after 3 days of treatment) in mouse EpiSCs.	[134]
A-83-01	TGFβ kinase/activin receptor-like kinase inhibitor can replace *SOX*2 by inducing *NANOG* and *c-MYC* expression.	[130, 135]
A-83-01 PD0325901	Transduction with *OCT*4 only resulted in iPSCs but with low efficiency.	[136]
CHIR99021 Parnate	Transduction with only *OCT*4 and *KLF*4.	[137]
PS48 NaB	Enhancement of reprogramming efficiency over 25-fold in cells transduced with *OCT*4 only.	[136]

1.4.4 Differences between human and mouse ESCs/iPSCs

Pluripotent stem cells of mice represent the “naïve” state of pluripotency, compared to the “primed” state of human pluripotent stem cells, which are able to differentiate in response to cytokines [138-142]. Several studies have tried to reveal the differences between these two pluripotency states [143, 144]. Cells of the epiblast were shown to be advanced in the development compared to naïve cells from the ICM, but despite their more limited potential in development, compared to naïve pluripotent stem cells, cells of the epiblast are regarded as pluripotent [34]. While hESC lines are derived from the ICM of plated blastocyst-stage embryos, little is known regarding the molecular/cellular events proceeding the ESC state *in vitro*. ESCs and cells of the ICM differ in gene expression and requirement of media supplementation in *in vitro* culture. It was speculated and later shown that the human ICM first develops into an epiblast-like stage (called ‘post-ICM intermediate’, PICMI) with inactive X chromosome in cells from females. ESC can be derived from this PICMI state and subsequently cultured *in vitro* [145]. Table 1.4 summarises features of naiive and primed state.

Table 1.4 Comparison of naive and primed pluripotent states.

Naïve state = ground state	**Primed state**
expression of NANOG upregulated	expression of NANOG and KLF4 decreased
requirement of LIF in culture media	requirement of Activin A and bFGF in culture media
pre-implantation embryo	post transplantation embryo
TFs bind to enhancers marked with H3K4me1 and H3K27ac at histone tails	NANOG alone can induce cell fate
global DNA hypomethylation	

A number of studies have also compared various generated hiPSCs with hESCs, with evidence of only subtle differences in cell morphology, surface marker expression and pluripotency of hESCs [84, 93, 146-148], summary see Table 1.5. These alterations could be connected to: i) the reprogramming methodology, ii) the origin, differentiation state and endogenous expression level of reprogramming factors in the somatic cell, and iii) the epigenetic donor memory of the somatic cells or disease-related mutations [149]. Daley’s group reported alterations in CpG methylation patterns specific for different tissues between different types of pluripotent cells and that this is inherited from the parental cell

causing the preferential commitment to the original lineage [150]. hiPSCs display the key characteristics of hESCs, thus, in the context of this thesis, hiPSCs could be used as a potential new source for bone precursor cells to study bone development and related diseases.

Table 1.5 Comparison of dis-/advantages of iPSCs and ESCs [151-153].

	advantage	**disadvantage**
ESCs	• Established and characterised cell lines • No risk of viral load in ESC-derived cells • Lack of MHC class I and II resulting in immunopriviledged cells • Unlimited proliferative capacity • Drug and toxicity testing possible • Allows for gene targeting and gene editing • Any cell type can be generated from ESCs	• Destruction of an embryo in order to obtain ESCs from preimplantation blastocysts is necessary as initial step to generate ESC line • Different genetic background to host increasing risk of rejection of transplanted ESC-derived cells • Formation of teratomas • Genetic mutations during longterm *in vitro* culture • During isolation from blastocysts, ESCs are selected based on proliferation and *in vitro* survival, not based on the differentiaton potential for specifc lineage • Heterogeneity of cell lines due to culture conditions/variations between research labs
iPSCs	• Only few standardised and established iPSC lines, however, number slowly increasing • Disease modelling is possible with investigation of disease casusing mutations • Avoiding use of embryonic tissue derived cells • Gene targeting and gene editing to correct mutations is possible • Drug and toxicity testing possible • Lack of MHC class I and II resulting in immunopriviledged cells • Any cell type can be generated	• Formation of teratomas • Potential viral load (depending on delivery method of reprogramming factors) in iPSC-derived cells • Donor memory (depending on age/environmental factors of donor) • Only few standardised and established iPSC lines so far (however number is slowly increasing) • Differences in gene expression and epigenome compared to ESCs • Heterogeneity of cell lines due to culture conditions/variations between research labs • Generally low reprogramming rates

	advantage	**disadvantage**
	• Personalised medicine • Unlimited proliferative capacity • Elimination of religious/ethical concerns associated with ESCs use as no embryo had to be destroyed to generate the cell line • Donor cells are generally obtained non-invasive and relatively esay	• Genetic mutations can occur during longterm *in vitro* culture • Risk of mutations due to virus-based delivery of reprogramming factors (only applies if viral delivery system was chosen initially) • High costs for production and characterisation for each line (depending on delivery method and subsequent culture)

1.5 Induction of Mesoderm Differentiation of IPSCs *In Vitro*

New sources for MSCs are urgently required given: i) the low occurrence of these cells in bone marrow [18, 19], ii) the decline of the stemness of HBMSCs with age characterized by limited proliferation capacity [20], and, iii) differentiation potential and the limited availability of foetal tissue derived MSCs, resembling a young phenotype [154, 155]. Moreover, it has been wondered in the community whether iPSC-derived MSCs (iPSC-MSCs) can be regarded as equivalent to either aged MSCs or rather foetal tissue derived MSCs and if iPSC-MSCs resemble a better source for clinical applicable MSCs. It is reasoned that iPSC-MSCs may offer enhanced differentiation potential compared to the parental MSCs. Comparison of telomerase activity as an indicator for level of self-renewal of HBMSCs, iPSC-MSC and fibroblasts revealed greater telomerase levels in iPSC-MSCs (10x compared to HBMSCs, 100x compared to fibroblasts) [156-158]. In addition, differentiation experiments revealed that generated iPSC-MSC displayed greater osteo-/chondrogenic potential in comparison to adipogenic differentiation [159].

Epithelial-to-mesenchymal transition (EMT) is a key event during differentiation and has a conserved programme with characteristic hallmarks throughout the process: i) upon onset of EMT intercellular junctions (tight~, adherence ~, gap ~, desomosomes) are disrupted and the associated proteins degraded (e.g. tight junctions - claudin and occludin, adherence junctions – E-Cadherin, gap junctions - connexin) [160-162], ii) the cytoskeleton is reorganised and acquires enrichment in actin allowing cell elongation and greater mobility [163-166], iii) loss of apical-basal polarity (due to repression of polarity complex genes *CRB*3 (Crumbs3) and *SCRIB* (Scribble)) also allowing enhanced motility and ability to

invade into tissue [160], iv) 'cadherin-switch' (E-Cadherin repression, N-Cadherin upregulation) promotes migrative and invasive character of developing mesenchymal cells [161, 167, 168]. Genes encoding transcription factors snail family transcriptional repressor 1 (*SNAI*1), snail family transcriptional repressor 2 (*SNAI*2), Zinc finger E-Box Binding Homeobox 1 (*ZEB*1), Zinc finger E-Box Binding Homeobox 2 (*ZEB*2) and proteins vimentin (*VIM*), E-Cadherin (*CDH*1), N-Cadherin (*CDH*2), occludin (*OCLN*), claudin 1 (*CLDN*1), crumbs 3 (*CRB*3), epithelial cell adhesion molecule (*EPCAM*) positively or negatively regulated during EMT and the function/targets are summed up in Table 1.6 and events of EMT are illustrated in Figure 1.8.

Table 1.6. Genes positively or negatively expressed during epithelial-to-mesenchymal transition (EMT). Summarised in [167].

Ref	Gene	Name	Function/Target	Effect on EMT
[169-171]	*SNAI*1	Snail family transcriptional repressor 1	repression of E-Cadherin	positive
	*SNAI*2	Snail family transcriptional repressor 2		
[172, 173]	*VIM*	Vimentin	type III intermediate filament protein (interacts with motor proteins)	
[168]	*CDH*2	N-Cadherin	cellular adhesion protein facilitating motility and invasion	
[169, 174, 175]	*ZEB*1	Zinc finger E-Box Binding Homeobox 1	master regulators of cellular plasticity	
	*ZEB*2	Zinc finger E-Box Binding Homeobox 2		
[163, 167]	*CRB*3	Crumbs 3	cell polarity complex component	negative
[163, 167]	*EPCAM*	Epithelial cell adhesion molecule	exclusively expressed in epithelial cells	
[163, 167]	*OCLN*	Occludin	protein located in tight junctions	
[168]	*CDH*1	E-Cadherin	transmembrane protein	

Ref	Gene	Name	Function/Target	Effect on EMT
[163, 167]	*CLDN*1	Claudin1	membrane protein in tight junctions	

During the differentiation process cells lose the ability to self-renew and develop into specialised cells with specific functions. Various intrinsic and extrinsic factors (e.g. growth factors, mechanical tension) can stimulate the onset of the differentiation process. Differentiation protocols can be divided into three different types: i) direct differentiation as monolayer on extracellular matrix proteins (one step/multiple steps), ii) co-culture with cells of the desired lineage and, iii) culture as embryoid bodies (EBs) followed by adherence culture. However, step wise differentiation results in a heterogeneous progenitor population which makes time consuming MSC-specific surface antigen sorting a fair necessary intermediate step. Hence, the current aim is to establish a differentiation protocol that will allow the generation of an efficient amount of MSCs with the specific antigen profiles in a short time frame. Studies on the generation of MSCs arising from different germ layers have been published over the past few years (summarised in Table 1.7), and are already under investigation in clinical trials. Characterisation and comparison of MSCs derived from different mesodermal sub-tissues like craniofacial, paraxial mesoderm, lateral ~, intermediate ~ and neural crest would allow to determine the influence on future differentiation behaviour [38, 39, 176]. However, efficiencies of the various protocols are difficult to compare due to inconsistency in analysed surface markers. Two major findings may aid development of less heterogeneous populations: i) Graneli et al. identified two surface (CD10 (MME, neprilysin), CD92 (SLC44A1, choline transporter-like protein 1)) and one intracellular (CRYaB (alpha-crystallin B chain)) proteins that displayed a correlation in expression with the osteogenic/adipogenic differentiation potential [177]. Thus, the intracellular marker *CRYaB* could present a novel SSC identification marker. ii) Twist Basic Helix-Loop-Helix Transcription Factor 1 (*TWIST*1) has been reported to maintain the MSC state but with varying expression levels between different MSC populations from different tissue sources. Furthermore, *TWIST*1 expression was shown to promote adipogenic while repressing osteogenic/chondrogenic differentiation [178].

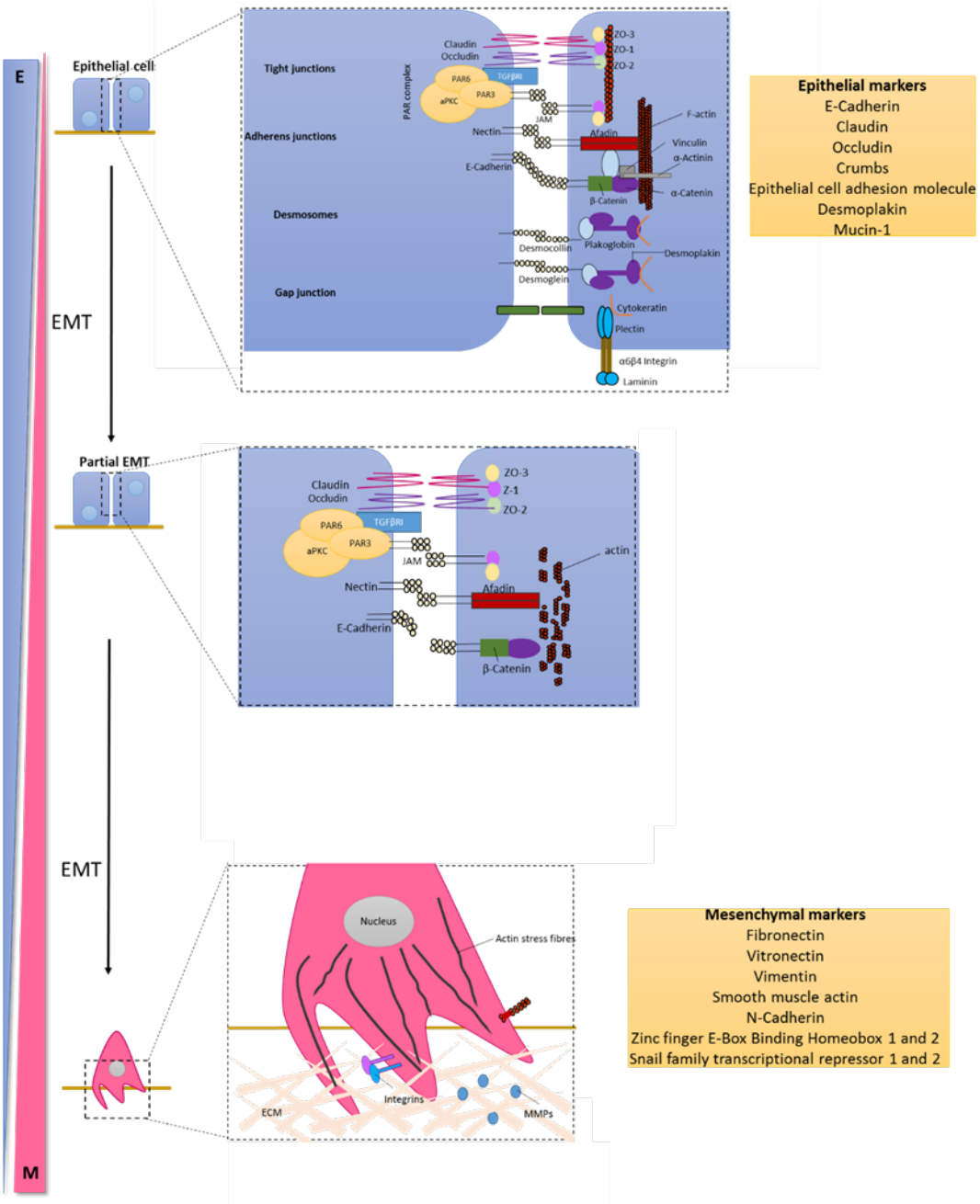

Figure 1.8 Epithelial-to-mesenchymal transition (EMT). During the early steps of EMT the cell-cell contacts such as tight junctions, adherens ~, gap ~ and desmosomes are disassembled. EMT characteristic genes are repressed and mesenchymal genes are transcribed. The actin structure within the cells is reorganised and cells become more motile and acquire invasive capacities and by expression of matrix metalloproteinases (MMPs) are able to degrade the surrounding matrix. Based on [163, 167].

Table 1.7. Protocols for the generation of iPSC-MSCs as monolayers with current limitations. MCA: mesenchym-angioblast; bFGF: basic fibroblast growth factor; PDGF: platelet derived growth factor; T: brachyury; APLNR: aplein receptor; BIO: 6-bromoindirubin-3'-oxime; BMP: bone morphogenetic protein; Cyc: Cyclopamine; Ikki: IκB kinase inhibitor

Cell type & species	Progenitor stage	Final stage	Components	Duration [days]	Animal model	Characteristics of generated MSCs/ efficiency of protocol	Ref
hESCs	MCA	MSC	bFGF bFGF + PDGF-BB	3 9	mouse	$CD146^+$ $CD31^-$ $CD43^-$ $CD45^-$ 7% $CD31^+$/$CD144^+CD43^-$ endothelial cells.	[179] [180]
hiPSCs	mesoderm	MSC	Activin A + BMP4 + BIO (ABB) EGF + bFGF	3 10	no	only 20% $CD105^+$ cells; no enhancement of endo- or ectodermal genes after 3 day treatment with ABB.	[181]
hiPSCs miPSCs	mesoderm	MSC	SB431542	10	no	96% mesodermal progenitor cells (EpCAM-, NCAM+); CD73, CD105, CD90 < 50% of cells before passaging into MSC medium (containing FBS); after ~ 2 passages in MSC medium MSC-like morphology.	[182]
hiPSCs	mesoderm	MSC	CHIR99021 + Cyc	5	no	no quantification performed; cell types identified by gene expression; therefore no evidence on efficiency given	[183]
hESC	mesoderm	MSC	Ikki no Ikki	4 3	yes	Spontaneous differentiation: sorting after 7 days resulted in 3.6% $CD73^+CD90^+CD146^+CD45^-$ MSCs of the total differentiated cells; IKKi treated cultures: CD73 and Cd146 upregulated at day 4 and sorting after 7 days resulted in a 3-fold increase in the proportion of	[184]

Cell type & species	Progenitor stage	Final stage	Components	Duration [days]	Animal model	Characteristics of generated MSCs/ efficiency of protocol	Ref
						$CD73^{+}CD90^{+}CD146^{+}CD45^{-}$ MSCs in the total differentiated population; subsequent differentiation toward osteoblasts osteogenic genes were 3.5-4x upregulated in MSCs generated with Ikki;	
hESCs	mesoderm	MSC	SB431542	28	no	After 28 days ~ 42% MSCs ($CD73^{+}/CD90^{+}/CD105^{+}/CD44^{+}/CD166^{+}/CD45^{-}/CD14-/CD19^{-}$); subsequent sorting for $CD73^{+}$ $CD90^{+}$ cells; displayed MSC morphology and phenotype with faster growth than MSCs derived from somatic tissues;	[185]

1.6 Generation of Osteoblasts *In Vitro*

1.6.1 Osteogenic differentiation *in vitro* from primary cell sources

Over the years, osteogenic differentiation media have been standardised, especially for lineage committed cells and typically contain a distinct set of small molecules: Ascorbate-2-phosphate (A2P), supports matrix formation and later upregulated *ALPL* expression; β-glycerophosphate (GP), serves as phosphate source for mineralization of matrix; 1,25-$(OH)_2$-vitamin D_3, showed increase in *OCN* expression; BMP2 (bone morphogenetic protein 2), stimulation of SMAD signalling pathway followed by transcription of osteogenic genes; and dexamethasone (Dex), enhanced proliferation but also support of adipogenesis. However, the concentrations of the different components vary in the literature (Table 1.8) and, lately, 3D culture conditions (spheroids/pellets, micromass, gels, scaffolds, sponges) are reported to be more efficient for osteoblast generation rather than 2D monolayer approaches [186-189].

Table 1.8. Concentrations of osteogenic media components in the literature for BMSC differentiation. Dex: dexamethasone; A2P: Ascorbate-2-phosphate; GP: β-glycerophosphate; BMP: bone morphogenetic protein.

Medium + FBS	Dex	A2P	GP	BMP2	Reference
DMEM	0.1 µM	50 µg/ml	10 mM	-	[190]
αMEM	10^{-8}M	0.05 mM	10 mM	300 ng/ml	[191]
αMEM	10 nM	50 µg/ml	2 mM	-	[192]
DMEM	10^{-8}M	50 µg/ml	10 mM	-	[193]
αMEM	10^{-8}M	200 µM	1.8 mM	-	[194]

Local identity is acquired during pattern formation in embryogenesis and is controlled by a number of signalling pathways [195]. Based on previously gained knowledge, the initial step is the generation of osteochondral progenitors by activation of runt-related transcription factor 2 (*RUNX*2), followed by subsequent expression of osterix (*OSX*) and other osteogenic genes such as alkaline phosphatase (*ALPL*), collagen type 1 alpha 1 (*COL1A1*), osteocalcin (*OCN*), osteonectin (ON), osteopontin (*OPN*), also known as bone sialoprotein (*BSP-1*) [196, 197]. *Runx*2-null mice did not express the direct downstream target *Osx* which resulted

in the absence of osteoblasts and the production of a cartilaginous skeleton lacking mineralisation *in vitro,* whereas *Runx*2 was still expressed in *Osx*-null mice but led to the formation of cartilage [198, 199]. Consequently, *Runx*2 and *Osx* function as fate-switch regulators at distinct time points during osteogenic differentiation *in vitro* and *in vivo* in mice and humans.

1.6.2 Generation of iPSC-derived osteoblasts

Recent studies have used classic osteogenic differentiation media as backbone medium but supplemented with various small molecules, growth factors, chemicals (either alone or in combination) (see Figure 1.9 for the effects/targets of the different components and Table 1.9 for osteogenic differentiation protocols) to enhance the efficiency and the extent of calcification in those cultures. These small molecules were selected based on the signalling pathways involved (between MSC state, osteogenic commitment, mature osteoblast) (Figure 1.9 and Figure 1.10); however, subsequent tailoring as well as fine tuning of these osteogenic differentiation cocktails is still required [18, 200-202]. Based on the knowledge of the involved signalling pathways, differentiation protocols for several tissues (e.g. pancreas, intestine, retina) derived from human PSCs have been published already [203-205].

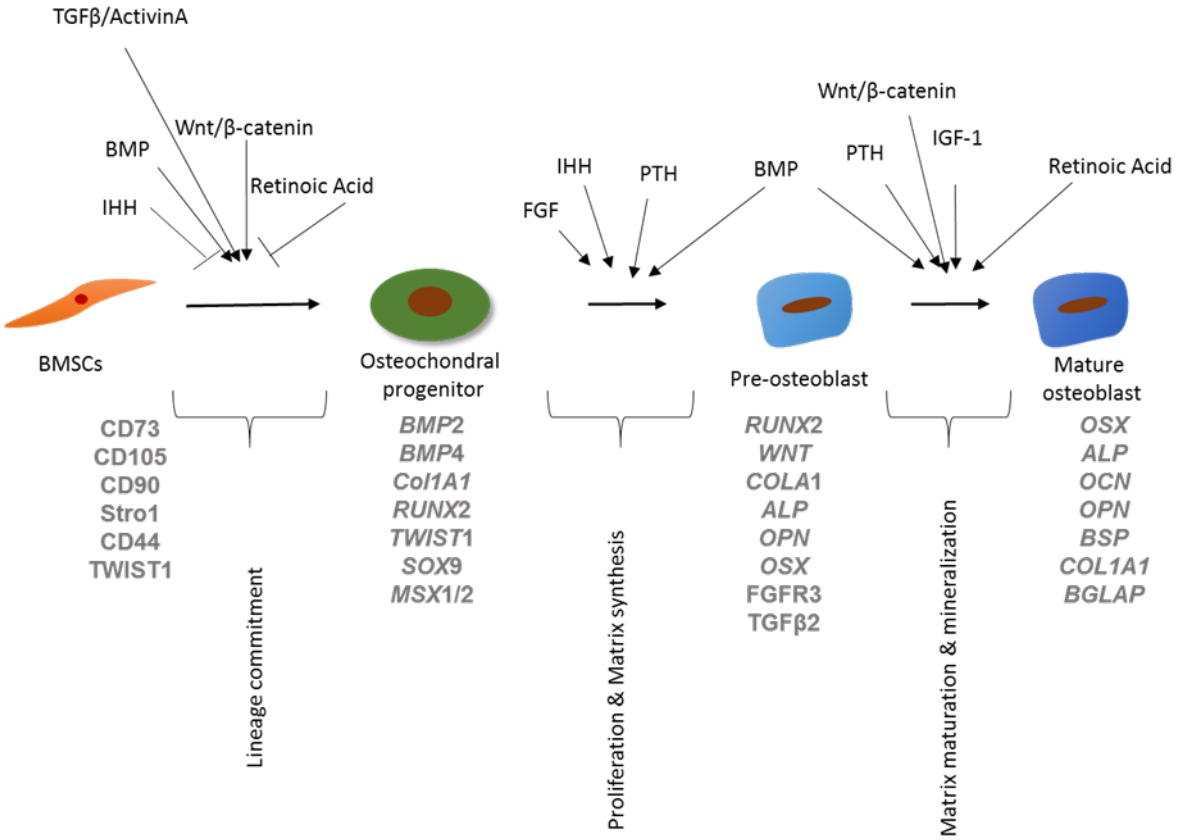

Figure 1.9. Schematic of signalling pathways during osteogenic differentiation of MSCs. The process consists of different stages: lineage commitment resulting in the generation of osteochondral progenitors, further proliferation generates pre-osteoblasts being able to produce matrix proteins. This matrix then starts to mineralize and consequently matures into the osteoblasts. After maturation, the osteoblasts can become osteocytes when getting trapped in the osteoid or bone lining cells covering and thus protecting the entire bone. Several signalling pathways are involved in this process during the different stages and the cells express stage-specific markers as indicated. RUNX: Runt-related transcription factor 2; OSX: osterix; BMP: bone morphogenetic protein; WNT: wingless; ALPL: alkaline phosphatase; COL1A1: collagen type 1; SOX9: Sry-related HMG box 9; MSX1/2: msh homeobox 1; OPN: osteopontin; FGF: fibroblast growth factor; TGFβ2: transforming growth factor beta 2; OCN: osteocalcin; BSP: bone sialoprotein. Based on references [136, 206-213].Canonical Wnt signalling results in the expression of *RUNX2* and subsequently *OSX* while inhibiting adipogenesis [206]. Fate decision toward the osteogenic lineage in hiPSCs is due to Indian Hedgehog (IHH) pathway, block of IHH signalling in non-committed cells resulted in a reduction of *RUNX*2 expression levels, which led to a chondrogenic fate; inhibition of IHH in committed osteogenic progenitor cells did not affect the expression of *RUNX*2 [206]. This suggests that IHH signalling is the key factor involved in lineage commitment, although the time point and the duration

of IHH treatment is critical, as a delayed activation of this pathway might be not able to compensate the shift towards chondrogenesis. TGFβ-signalling (MAPK and Smad2/3 pathways) interacts with WNT- (resulting in enhancing or inhibiting effect), FGF- as wells as BMP- (significant increase in bone volume of BMP2 induced bone formation) pathways and was shown to be important for ossification [207]. Early stage stimulation of the epidermal growth factor receptor (EGFR) resulted in an increased amount of MSCs and consequently the pool of osteochondral progenitors by the expression of the anti-apoptotic protein *MCL*1 and *EGR*2, responsible for proliferation [136]. IGF-1 signalling (via the P13K/AKT) interacts with mTORC in MSCs and is important for cell proliferation, differentiation, matrix secretion and mineralization of osteoblasts, although the extent of its involvement in early MSC differentiation has to be further elucidated [208]. Platelet-derived growth factor (PDGF) plays a role in the regulation of proliferation of MSCs and was shown to support the function of TGFβ but alone was not observed to modulate of osteogenic differentiation of human MSCs [209].

The two key requirements for an efficient osteogenic step-wise differentiation protocol are i) the activation of the master regulator *RUNX*2 (to promote osteogenesis) and ii) suppression of adipogenic/chondrogenic lineage. The modulation of involved signalling pathways could offer an elegant method for this purpose.

Table 1.9. Growth factors/small molecules and their specific functional mechanisms/effects on osteogenic differentiation of primary MSCs, MSC-like cells (iPSC-MSCs), ESCs and mESCs.

Substance	Effect & Mechanism	Reference
Activin A/Nodal	TGFβ-pathway ligand Activin together with BMP4, FGF and WNT signalling is essential for mesoderm induction and its dose is critical for the fate decisions between mesoderm and endoderm.	[214, 215]
TH (4-(4-methoxyphenyl)pyrido[4',3':4,5] thieno[2,3-b]pyridine-2-carboxamide)	helioxanthin-derivative optimal concentration for mouse pre-osteoblastic cell line: 10^{-6} M; but treatment of HBMSCs did not show osteogenic differentiation; TH alone only supports osteogenesis in already committed cells and acts via the BMP/SMAD signalling pathway; TH was shown to	[216]

Substance	Effect & Mechanism	Reference
	require extracellular BMP for function and in combination with BMP2 osteocalcin was higher expressed at day 5 and further increased until day 10; involved during maturation and mineralisation stage.	
EGF (epidermal growth factor)	EGF treatment resulted in an enhancement of the function of BMP9. Thus, the expression of early (*ALPL*) as well as late (*OCN*, *OPN*) osteogenic genes and matrix mineralization was observed to act in a dose-dependent manner. Treatment with EGF alone did not show any supportive effect on differentiation. Treatment with EGF receptor inhibitors (Gefitinib, Erlotinib) inhibited the BMP9-induced activity of ALP.	[217]
Vitamin D_3	Treatment with 1,25-$(OH)_2$-vitamin D_3 over 6 days resulted in the expression of *COL1A1* and *OCN* in a dose-dependent manner (50 nM optimal).	[202]
Dorsomorphin	BMP signalling inhibitor; no effect on osteogenesis but inhibition of chondrogenesis.	[218, 219]
SAG (smoothened agonist)	Activator of HH signalling; involved in early stage of osteoblast formation; combination of SAG and TH resulted in differentiation of osteoblasts.	[220]
Litium Chloride	GSK3 inhibitor; support of cartilage mineralization	[218]
Cyclopamine	Inhibition of HH-ligand smoothened. Increased formation of cartilage; sufficient to induce the expression of *COL2A1* on its own.	[218]
Resveratrol	Pretreatment resulted in the prevention of cell apoptosis induced by dexamethasone cytotoxicity.	[221]
BMP4 (bone morphogenetic protein 4)	Impairment of expression of adipogenic genes while supported expression of genes for osteoblast maturation; use of 100 ng/ml ([222]) in mouse cells was more efficient compared to 50 ng/ml.	[222] [223]
LY294002	PI3K inhibitor Impairs maturation of osteoblasts by inhibition of expression of collagen type I expression.	[224]

Substance	Effect & Mechanism	Reference
Retinoic Acid (RA)	Studies suggest responsibility in induction and formation of neuroectoderm and mesoderm as wells as anterior to posterior change in mesoderm. High dose promotes neural crest development while intermediate dose (at an early stage) resulted in adipocyte generation. Normal osteogenic differentiation was characterized by an increased expression of an RA degradation enzyme (Cyp26b1). RA was shown to reduce the levels of *RUNX*2 and *OSX*, thus decreased expression of *ALPL*, *BGLAP* and *OCN*. Treatment for 2-5 days was shown to be necessary for the expression of *OCN*.	[210-213]
Compactin	Inhibitor of HMG-CoA reductase. Treatment with 2.5 – 5 μM compactin resulted in large mineralized deposits but the shape of the nodules itself was not as dense compared to the nodules resulting from BMP2 treatment in monolayer culture, no further effects on expression of other osteogenic markers were observed.	[225]
Insulin like growth factor (IGF)	Not required in normal development of bone and cartilage, but supportive effect on IGF downstream targets osterix (*OSX*) and osteocalcin (*OCN*) was observed.	[222]
Rapamycin (mTORC1 inhibitor)	Serine/threonine kinase, exists in two different complexes: mTORC1 + Raptor: controlling size of chondrocytes and matrix production; mTORC2 + Rictor: enhances formation of bone. mTORC1 inhibition resulted in increased expression of mTORC2, subsequently increased Akt phosphorylation, decreased production of matrix and mineralization.	[226, 227]
Sclerostin	Activation of PDGFR (platelet-derived growth factor receptor) and the downstream targets PLCγ, PKC, Akt, ERK1/2, therefore inhibition of bone formation.	[228]
BMP2	Loss of BMP2 resulted in the impaired bone formation (and enhanced adipogenesis) while BMP2 (high	[229-231]

Substance	Effect & Mechanism	Reference
	concentrations) treated cells showed an increase in the *OCN* levels.	
Fucoidan	BMP2 expression was induced (signalling via ERK and JNK pathways) in dose dependent manner although under high concentration (10 µg/ml); *ALPL* was less expressed whereas calcium accumulation did increase.	[232]
6-bromoindirubin-3–oxim (BIO)	BIO is able to block adipogenesis.	[218, 219]
Narginin	Upregulation of FOCX22 via IHH pathway resulted in increased mineralisation of BMSCs while decreasing adipocyte specific marker *PPARG*. It is able to promote MSC proliferation and upregulation of BMPs in osteoblast.	[233]

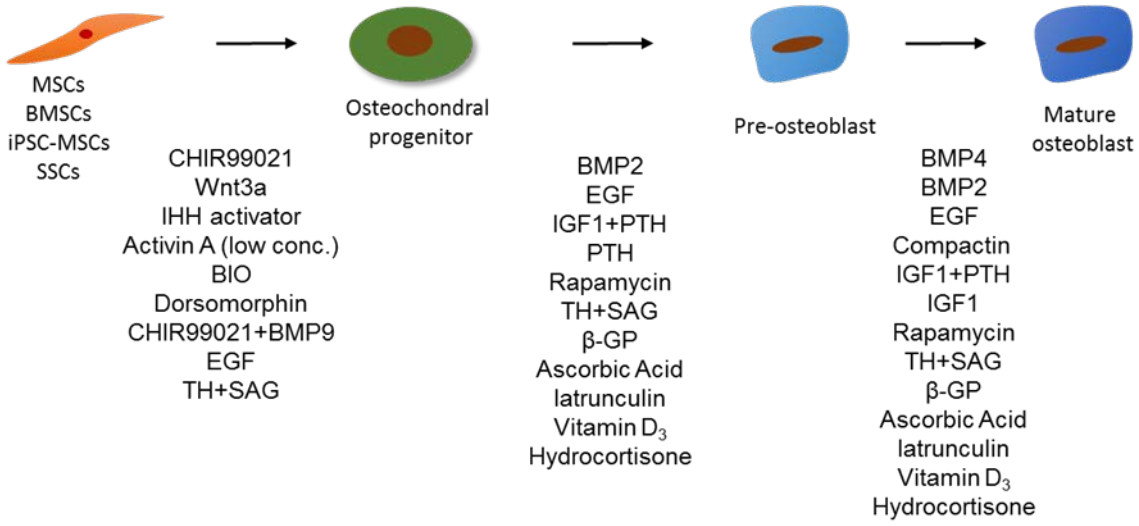

Figure 1.10. Schematic of compounds involved during step-wise osteogenic differentiation of iPSC-derived MSCs. BMP: bone morphogenetic protein; IHH: indian hedgehog; WNT: wingless; FGF: fibroblast growth factor; TGFβ: transforming growth factor beta; PTH: parathyroid hormone; IGF: insulin-like growth factor; OCT: octamer-binding transcription factor; SOX: SRY (sex determining region Y)-box; COL1A1: collagen type 1 alpha 1; RUNX2: Runt-related transcription factor 2; TWIST1: Twist Family BHLH Transcription Factor 1; MSX: Msh homeobox 1; BGLAP: bone gamma-carboxyglutamate (Gla) protein; BSP: integrin-binding sialoprotein; OPN: osteopontin; OSX: osterix; OCN: osteocalcin; ALPL: alkaline phosphatase. TH: 4-(4-methoxyphenyl)pyrido[4',3':4,5]thieno[2,3-b]pyridine-2-carboxamide; SAG: smoothened agonist; BIO: 6-bromoindirubin-3'-oxime; β-GP: β-glycerophosphate; SSC: skeletal stem cell; MSC: mesenchymal stem cell; iPSC-MSCs: iPSC-derived MSCs; BMSC: bone marrow stromal cell. Based on references [202, 210-233].**Table 1.10. Protocols for the**

generation of human iPSC-, hESC- and miPSC-derived osteoblasts. SAG: smoothened agonist; bFGF: basic fibroblast growth factor; IGF: insulin like growth factor; TGF: transforming growth factor; TH: 4-(4-methoxyphenyl)pyrido[4',3':4,5]thieno[2,3-b]pyridine-2-carboxamide; Dex: dexamethasone; A2P: Ascorbate-2-phosphate; GP: β-glycerophosphate; EB: embryonic body; RA; retinoic acid; KOSR; knockout serum replacement.

Cell type & Species	**Components**	**Duration [days]**	**Details of differentiation protocol**	**Ref**
miPSCs hiPSCs	Cyclopamine + CHIR99021 TH + SAG	5 23	Multi-step process which involved more work and is more costly compared to more simple strategies.	[183]
hiPSCs	bFGF + IGF-1 + TGFβ 1,25-$(OH)_2$-vitaminD_3	14 12	Generation of EBs for 6 days, followed by switch to adherence culture and incubation with osteogenic medium for 14 days (generation of late phase osteoblasts), incubation with 1,25-$(OH)_2$-vitaminD_3 for additional 12 days for mineralisation. Components of standard osteogenic differentiation cocktail included (Dex, GP, A2P).	[202]
hiPSCs	Culture as EBs Osteogenic medium + cultured on scaffold	7 7	Generation of EBs with subsequent culture in MSC medium (containing FBS, Glutamax, bFGF) for 7 days; osteogenic medium contained the standard osteogenic components; osteoclasts were generated by co-culture of lineage-committed mesenchymal cells with macrophages	[234]
miPSCs	RA dexamethasone, ascorbic acid, glycerol-phosphate	2 8-12 weeks	EBs were cultured in RA supplemented medium for 2 days and culture on geltrex coated wells for 3 days; Osteogenic differentiation medium consisted of low glucose DMEM, FBS, dexamethasone, ascrobic acid, glycerol-2-phosphate; Culture of EBs in differentiation medium for 8 or 12 weeks; after 12 weeks differentiated cells were seeded in gelfoam matrix and implanted in mice for 12 weeks;	[235]

Cell type & Species	Components	Duration [days]	Details of differentiation protocol	Ref
miPSCs	ascorbic acid 2-phosphate, β-glycerolphosphate, dexamethasone	15	Transduction of *Runx*2 gene into mouse iPSCs with adenovirus vector system at days 0, 2, and 5; culture on gelatin coated wells prior to treatment with osteogenic medium consisting of ascorbic acid 2-phosphate, β-glycerolphosphate and dexamethasone;	[236]
hESCs	Coating with lysate of hESC-derived osteoblasts followed by incubation with osteogenic medium containing ascorbic acid 2-phosphate, β-glycerolphosphate, dexamethasone	21	hESCs were treated with osteogenic differentiation medium consisting of DMEM, KOSR, l L-glutamine, β-mercaptoethanol, nonessential amino acids, ascrobic acid, β-glycerophosphate and dexamethasone; prior to differentiation hESCs were seeded on cell culture wells coated with gelatine and lysate of hESC-derived osteoblasts; the autologous cell lysate resulted in the formation of nodule-like structures;	[237]

1.7 Epigenetic Involvement in Maintenance of Cell Identity and Differentiation

Gene expression during development is not only directly controlled by growth factors and transcription factors via signalling pathways but also by heritable changes that do not alter the DNA sequence itself. Such changes include chromatin remodelling, histone modifications, DNA methylation of CpG dinucleotides and microRNAs (miRNAs), altogether referred to as 'epigenetics'. Modifications of histone and chromatin result in the tighter or looser packaging of the DNA strand resulting in improved or impaired accessibility of genes by RNA polymerases.

The role of epigenetic modifications in gene expression has come to the fore in recent years. Epigenetic modifications have been shown to be involved in fundamental developmental events and often are tightly correlated with each other influencing gene expression regulation [238]. Thus analysis of the epigenetic landscape of a certain cell type can lead to a better understanding of underlying mechanisms and reveal new potential targets for therapeutic approaches.

1.7.1 DNA methylation and histone modifications

During the DNA methylation process, a methyl (CH_3) group is covalently attached to a cytosine (in mammals) or an adenosine (in plants or bacteria) nucleotide by a DNA methyltransferase (DNMT) resulting in a 5-methyl-cytosine (5mC) or a 5-methyl-adenosine (5mA). An increase of the methylation level of DNA is referred to as hypermethylation, whereas hypomethylation describes a decrease in the DNA methylation level. This mechanism is involved in genomic silencing, aging, carcinogenesis and X-chromosome inactivation during development/reprogramming [239]. The majority of methylation occurs on cytosines within CpG dinucleotides in somatic cells whereas non-CpG cytosines are methylated in ESCs (~ 25 %) [240]. CpG islands, region with high CpG frequency, can be found within the promoter of a gene or the gene body itself. CpG dinucleotides in the promoters are usually protected from the methylation process. DNMTs can be divided into two categories: maintenance DNMTs and *de novo* DNMTs [241]. Maintenance DNMT (DNMT1) is responsible for the addition of the methyl group to the DNA strand after replication opposite the methyl groups on the parental strand, therefore methylation of a hemi-methylated DNA strand. *De novo* DNMTs (DNMT3A, DNMT3B) add the methyl

group to unmethylated CpG dinucleotides during development. These *de novo* DNMTs are assisted by DNMT3L which increases the binding ability to the methyl-group donor S-adenosyl-L-methionine (SAM). Similarly as methyl groups can be attached, they can be removed again due to the activity of demethylases such as ten-eleven translocation (TET) enzyme oxidising 5mC [242, 243].

The methylation of DNA is an important regulatory mechanism of gene expression during development. Gene transcription is affected in different ways: i) impairment of transcription factors by the methylated DNA itself or ii) DNA is bound by other proteins such as, methyl-CpG- binding domain proteins (MBDs), which in turn recruit more proteins such as histone deacetylases (HDAC), chromatin remodelling proteins, resulting in deacetylation of histones and, therefore inactive chromatin in some specific regions due to tight wrapping of DNA to histones (heterochromatin) (Figure 1.11) [242].

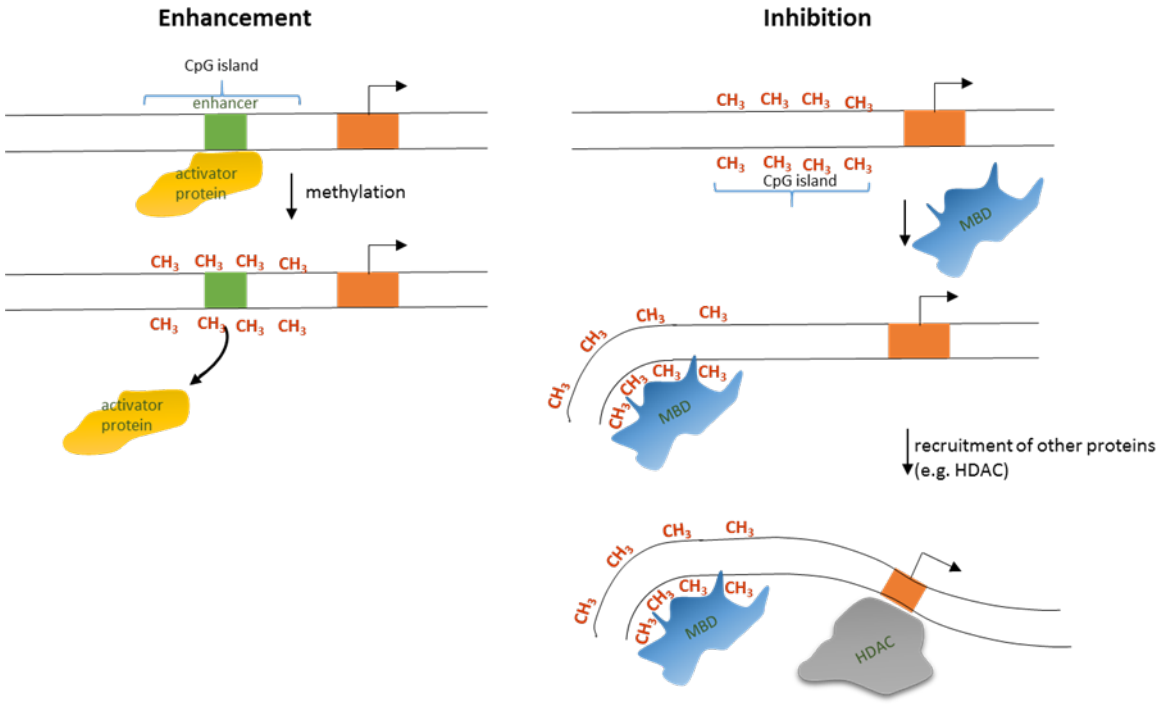

Figure 1.11. Schematic of effects of DNA methylation on gene transcription. Methylation of DNA can have different effects on gene transcription. Left: an activator protein that blocks a gene can be released due to methylation of the DNA, leading to transcription of the gene. Right: the DNA is methylated leading to the recruitment of MBDs (methyl-CpG-binding domain proteins) resulting in a change of the chromatin structure which in turn recruits HDAC (histone deacetylases), blocking transcription the gene. Based on literature [242-244].Similarly, histones can be chemically modified through methylation, acetylation, phosphorylation or

ubiquitination; the following will only focus on methylation and acetylation processes.

Acetylation (usually occurring at histone 4 (H4)) is catalysed by histone acetyl transferases (HAT) which results in the unwinding of the DNA from the histone allowing for RNA polymerases to transcribe a gene in a region usually tightly packed to the histone. Through the activity of histone deacetylases (HDAC), the DNA is wrapped tight to the histones again, preventing transcription of genes as RNA polymerases are unable to bind to the DNA. Histone methylation (usually occurring at histone 3 (H3)) occurs at the carboxyl groups of glutamate, lysine, cysteine, arginine or histidine and can either promote or inhibit gene transcription depending on which amino acids are methylated as well as the number of methyl groups attached to the amino acids [244].

1.7.1.1 Histone and DNA methylation state during reprogramming and in maintenance of pluripotent cells

Despite the widespread application of the reprogramming technology since its discovery, knowledge of the underlying molecular events and responsible regulatory networks still remains largely unresolved. The remaining low efficiency in iPSC generation despite improved delivery systems or small molecule supplementation is regarded as proof for several epigenetic barriers - 'roadblocks' - still to be overcome. Expression of characteristic genes accompanying the morphological changes during the process has been reported before with focus on different aspects of the process [107, 245-248], but no exact timing or order of the events during the process have been elucidated to date. Muraro et al. described for the first time a timeline of events chronologically taking place during the reprogramming process showing that histone and DNA methylation are key mediators of the ongoing events [249]. After administration of the reprogramming factors, transcripts of these exogenous transgenes, which will start to be silenced around day 4 until the end of reprogramming, trigger the induction of the reprogramming process. In this early first phase, histone modifications (e.g. H3K4me2, H3K27me3) occur in promoters associated with both, pluripotency as well as differentiation, marking the shift from a somatic cell to an ES cell programme. Accumulation of RNA polymerase as well as H3K36me3 proved at the same time the priming of the endogenous pluripotency genes for their transcription later during the reprogramming process. Downregulation of lineage-specific markers and upregulation of early pluripotency factors (e.g. ALP, SSEA1 or SSEA4) as part of mesenchymal-to-

epithelial transition (MET) proceeds the activation of the endogenous pluripotency genes like *NANOG* and *OCT*4. Therefore, genes involved in cell cycle and DNA replication are upregulated after the first few days (~ day 3) after the administration of the reprogramming cocktail, resulting in a decrease in cell size which develop into ES-like looking colonies (~ day 10). Independence of cells from the exogenous transcription factors marks the end of the early stage of reprogramming. Long telomeres are a key characteristic of pluripotent cells. The late stage of reprogramming is characterised by several epigenetic changes: telomere elongation, X chromosome reactivation and DNA methylation of promoters of pluripotency genes. Telomerase reverse transcriptase (TERT), the enzyme being responsible for the elongation process, is activated in the early phase but the actual elongation takes place over the entire reprogramming. Around one week after administration of the exogenous transgenes, telomeres already demonstrate an intermediate telomere length with continuing lengthening with further passaging of the iPSC colonies. Epigenetic changes including histone and DNA methylation take place during the late phase in a gradual manner. Developmental genes show bivalent chromatin domains, these are domains that contain two antagonizing epigenetic marks, for example repressive H3K27me3 and activating H3K4me3 in one place, which is supposed to promote the silencing of these genes until differentiation of ESCs or iPSCs is initiated again. Changes of the DNA methylation pattern in differentially methylated regions (DMR) are responsible for the hypomethylation of pluripotency gene promoters as well as the somatic donor cell memory [250]. Figure 1.12 illustrates the described events during the reprogramming process in a chronological manner. There remains an ongoing debate whether or not the epigenetic memory is erased entirely during reprogramming and has to be investigated further by examination of genome-wide H3K4/H3K27 methylation pattern [249]. Overall, genes in pluripotent cells showed a higher rate of hypermethylation compared to cells undergoing differentiation. Genes highly expressed in pluripotent cells (*EPHA1*, *PTPN6*, *RAB25*, *SALL4*) show hypomethylation while other genes (*GBP3*, *LYST*, *SP100*, *UBE1L*) are hypermethylated, therefore repressed [251].

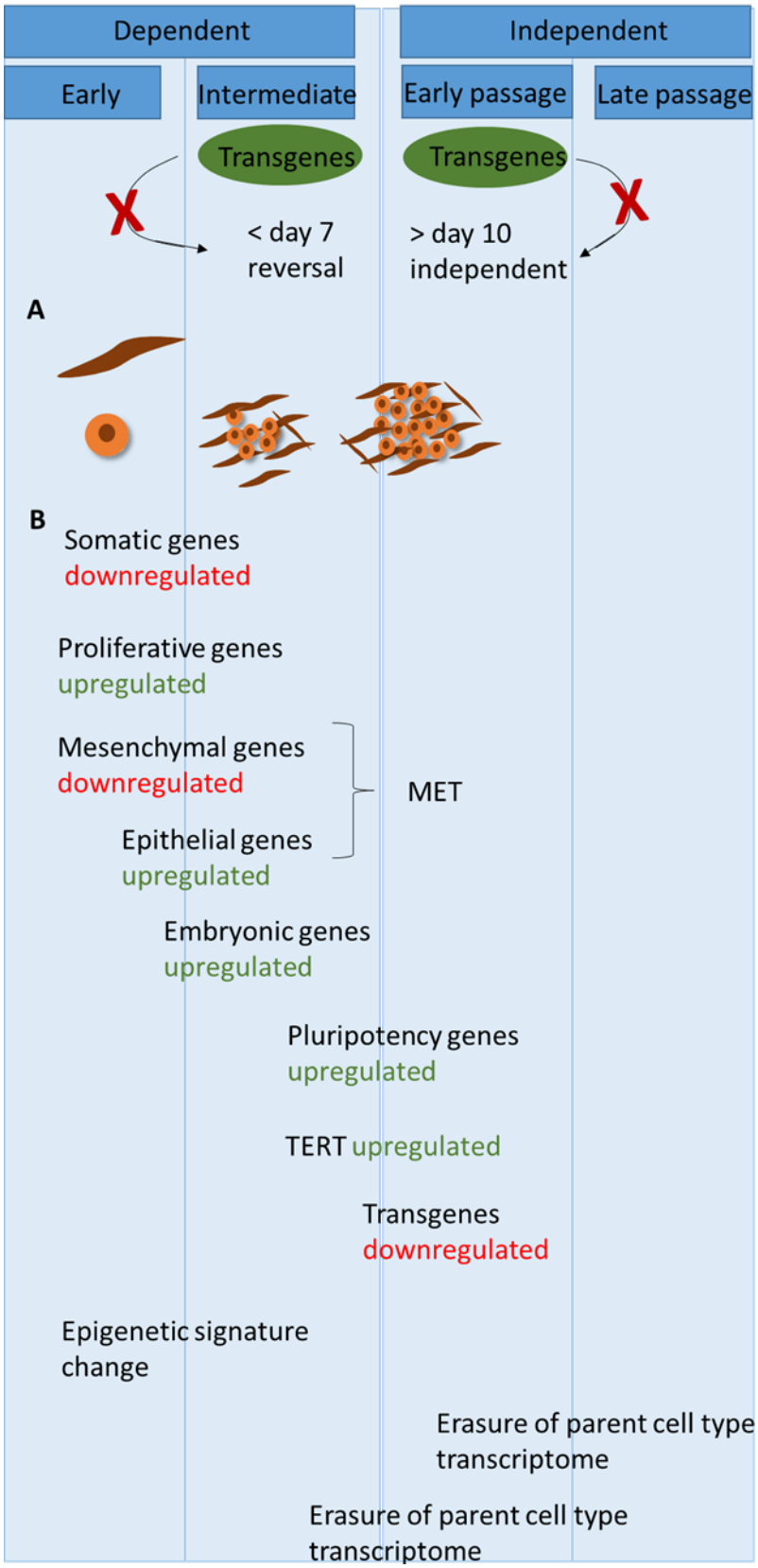

Figure 1.12 Schematic overview of morphological, molecular and epigenetic events during the reprogramming process. A: Morphological changes occur in two stages with the first one being dependent on the transgenes (day 0-7) while the second stage is independent of transgenes (> day 10). During the first stage somatic cells first change into small, round cells which then

aggregate into loose micro colonies. These become denser and show ESC-like morphology surrounded by fibroblast-like looking cells between day 7 and 10. **B:** Administration of the transgenes is followed by increased proliferation, upregulation of epithelial and embryonic specific genes, an event referred to as mesenchymal-to-epithelial transition (MET). Genes encoding the somatic and mesenchymal programme are downregulated during the first days of the reprogramming process. Endogenous pluripotency genes along with TERT are starting to be transcribed around day 7. Transgenes start being silenced during the shift from the dependent to independent phase. Chromatin is remodelled over the entire reprogramming process. Change of the histone methylation pattern in enhancer and promoters of pluripotency genes (H3K27me3 is removed and replaced by H3K4me2) take place during the transgene dependent phase. Several more gradual remodelling events such as elongation of the telomeres and decrease of DMRs occur during the transgene-independent stage. Adapted from [249].

1.7.1.2 DNA methylation in MSCs and during osteogenic differentiation *in vitro*

Changes in DNA methylation were found to not always correlate with changes in gene expression but rather to be a part of pre-patterning mechanism proceeding the activation or repression of respective genes later during differentiation/development [252]. Therefore, DNA methylation can be regarded as the initiating event of changes in the genome which then leads to the recruitment of histone deacetylation and subsequent silencing of a gene. Analysis of the methylome of MSCs from different human tissue sources showed 1,755 hypermethylated genes shared between all the analysed MSCs independent of their source. These hypermethylated genes were associated with an early developmental stage of MSCs and were shown to be regulated with ongoing differentiation [253, 254]. Also, most cell type specific promoters were revealed to be hypomethylated independent of their lineage specification [255]. Comparison of the epigenome of pluripotency and genes associated with differentiation in ESCs, MSCs, multipotent adult progenitor cells (MAPCs) and multipotent adult stem cells (ADSCs) revealed that these genes in ESCs are more epigenetically repressed by DNA methylation and histone modifications than in cells with more restricted differentiation potential [256]. Expression of osteogenic specific genes (e.g. *RUNX*2, *OSX*, *OCN*) was shown to correlate with the methylation status of their specific promoters. This suggests that the expression of these genes is highly dependent of the activity of DNMTs as it was shown that demethylated promoters of osteogenic genes correlated with the expression of these genes; therefore, methylation impairs differentiation into osteoblasts [253]. One example is the *OCN* gene (upregulated later during osteogenic differentiation); the locus was hypermethylated in undifferentiated genes, whereas methylation level decreased during

differentiation into osteoblasts [257]. WNT and BMPs are the two most important signalling pathways during *in vitro* osteogenic differentiation. Interestingly, inhibitors of these pathways, *SOST, DKK1, MEPE* and *MIF1,* were shown to be highly methylated [258].

1.7.2 MicroRNAs

The first microRNA (miRNA) lin-4 was discovered in 1993 followed by the second miRNA, let-7, in 2000 (both in *Caenorhabditis elegans*). These findings (reviewed in [259]), suggesting the greater importance of miRNAs in fundamental developmental events, paved the way for the investigation of the regulatory function of these small RNAs in differentiation and maintenance of stem cells.

1.7.2.1 Biogenesis and nomenclature of (miRNAs)

MicroRNAs belong to the group of small non-coding RNAs and are 20-25 nucleotides long with a 5' poly A cap. Genes encoding miRNAs can be independent with their own promoter (intergenic regions) or under the control of another gene's promoter (intragenic regions). In addition, several genes encoding for miRNAs can be transcribed at the same time, resulting in one single miRNA transcript subsequently cropped down into smaller individual miRNA fragments; such regions are called miRNA clusters [260].

The first discovered miRNAs were named after the phenotype the miRNAs generated. All later discovered miRNAs were numbered and a general nomenclature as well as species-specific prefixes for human (*homo sapiens*) hsa and for mouse (*mus musculus*) mmu introduced. MiRNAs with identical seed sequences belong to the same "miRNA family" while "miRNA sisters" are labelled with a lettered suffix (e.g. miR-125a, miR-125b). If the same mature miRNA is transcribed and generated by multiple separate miRNA loci, then a numeric suffix is added (e.g. miR-125b-1). The miRNA duplex (miRNA - miRNA*) during miRNA biogenesis consists of a guide strand (miRNA) and a passenger strand (miRNA*) with the miRNA strand usually being more active. [260].

Biogenesis of miRNAs and regulatory levels are displayed in Figure 1.13 below. The miRNA gene is transcribed by RNA polymerase II and folds into a hairpin structure, the primary miRNA (pri-miRNA) transcript. This pri-mRNA is processed by the microprocessor complex Drosha-DGR8 (two RNA Polymerase III enzymes) by cleaving the single stranded RNA fragments at the 5' and 3' end at the bottom of the loop stem. The

remaining fragment (~ 65nt in length) is called precursor-miRNA (pre-miRNA) and is transported from the nucleus into the cytoplasm by the protein Exportin 5 where the loop of the pre-miRNA is cropped off by Dicer (RNase III endonuclease). Helicase unwinds the double stranded (ds) miRNA-miRNA* duplex, leading to the single stranded (ss) miRNA and ssmiRNA*, latter degraded during the further process [260]. The ssmiRNA is bound by RNA-induced silencing (RISC)-Argonaute (AGO) complex. The "seed sequence" at the 5' end of the ssmiRNA bound targets the complementary sequence at the 3'UTR (untranslated region) of the mRNA (messenger RNA). The level of compatibility of target mRNA and ssmiRNA determines the post-transcriptional repression of the mRNA. Complete complementary binding results in the degradation of the mRNA into smaller fragments by deadenylation (= 'de-capping'). Incomplete complementary binding of miRNA to mRNA results in inhibition of translation process [260]. Due to the short seed sequence there is a large number of target sequences, which is the reason that one miRNA can target more genes. [260]. Biogenesis of miRNAs can be regulated at several stages and miRNA production be impaired: the microprocessor Drosha-DGCR8, the RNase III Dicer and AGO/RISC complex.

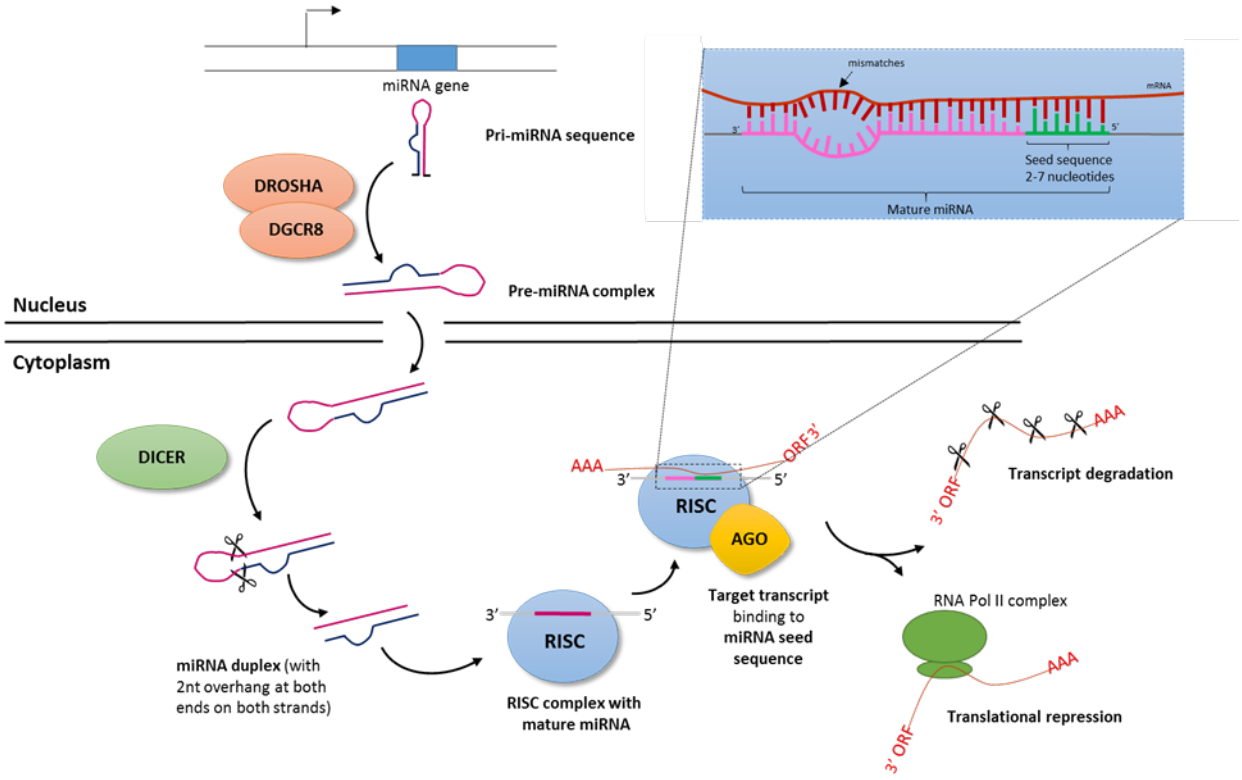

Figure 1.13. Biogenesis of microRNAs. After transcription and formation of the primary (pri-) miRNA transcript, the microprocessor complex consisting of Drosha/DGGR8 cleaves off the single stranded RNA fragments at the 5' and 3' end at the bottom of the loop stem loop on pri-miRNA,

creating precursor (pre-) miRNA. After translocation into the cytoplasm, the loop is cleaved off from the pre-miRNA transcript by Dicer, the dsmiRNA (miRNA – miRNA*) duplex is unwound by helicase into ssmiRNA (pink) and ssmiRNA* (black). ssmiRNA is bound by RISC/AGO complex (blue/yellow) where the seed sequence (green) binds the complementary sequence on the mRNA transcript. The mRNA transcript is then either degraded into smaller fragments or translation is repressed. mRNA: messenger RNA; miRNA: microRNA; AGO: Argonaute; RISC: RNA-induced silencing complex; ss: single stranded; ds: double stranded [260].

MiRNAs during reprogramming and pluripotency maintenance

Self-renewal and the potential for differentiation are key features of PSCs. Understanding the involvement and role of regulators of these features will help improve reprogramming efficiencies, differentiation into different cell types and potential therapeutic approaches. Only a few miRNA families specific to PSCs have been identified in humans: hsa-miR-302, miR-106, miR-372, miR-17, miR-520, miR-195 and miR-200 families [261-264] (summary see Table 1.11 and Figure 1.14). Seed sequences of these few miRNA families are quite similar, suggesting the same for mRNA targets for the maintenance of the pluripotent state. Some studies indicate that the four Yamanaka factors contribute to the activation of pluripotency-related miRNAs and in turn are regulated by these miRNAs. OCT4 and SOX2 were shown to have a positive effect on the hsa-miR-302/367 cluster while hsa-miR-302 together with OCT4 levels decreased during differentiation [265, 266]. c-MYC activated the hsa-miR-17 cluster and was able to repress hsa-miR-34 and hsa-miR-29 [266-268]. Overall, repression of miRNAs that are expressed at lower levels in PSCs compared to differentiated cells may contribute to successful reprogramming. Transfection of somatic cells with lenti- or retroviral constructs carrying pluripotency associated miRNAs (e.g. mmu/hsa-miR-302/367, mmu-miR-17/92, mmu-miR-290/hsa-miR-372) resulted in a slight increase of reprogramming efficiency that the original Yamanaka factor approach [261, 269]. Research has started to identify the role of miRNAs in the different pathways/events taking place during reprogramming for example epigenetic changes, decreased apoptosis rate, EMT or increased proliferation.

PSCs have a shortened G1 phase due to the absence of a G1/S phase checkpoint leading to an increased level of proliferation compared to differentiated cells [270]. Cells lacking cell cycle associated miRNAs (e.g. hsa-miR-372, hsa-miR-195, mmu-miR-290, hsa-miR-302 cluster) resulted in defects in the cell cycle. These miRNAs have different targets of the cell cycle: hsa-miR-372 targets cyclin D1 (CCND1), retinoblastoma-like 2 (RBL2), cyclin-dependent kinase inhibitor 1A (CDKN1A) and 1C (CDKN1C); hsa-miR-302 cluster inhibits

cyclin D1 translation directly, although the majority of the cell cycle associated miRNAs is supposed to be involved in the transition to an accelerated G1 to S phase transition [261, 265, 271]. Members of the TGFβ/Nodal signalling pathway (Lefty 1 and 2) were found to regulated by miR-302-367 family in a negative way, while the same miRNA family acted upstream regulators of TGFβ/Nodal signalling pathway via Smad2/3, preventing differentiation of PSCs [272, 273]. p53 has been regarded as one of the major roadblocks in the reprogramming process [274, 275]. Several miRNAs were identified to be involved in the regulation of p53: miR-21, miR-29b, miR-92, miR-141 and miR-138 [276-279]. Thus, it was shown that after p53 induction miR-34 cluster is activated, in human as well as in murine cells, resulting in increased cell death [280]. In turn, administration of inhibitors of the p53 target resulted in enhancement of reprogramming.

The main process during reprogramming is the transition from a mesenchymal to an epithelial state (MET) with several microRNAs (hsa/mmu-miR-205 and the hsa/mmu-miR-200, hsa/ mmu-miR-302 and hsa/mmu-miR-372 clusters) being involved as well [261]. miR-200 and miR-205 are more widely expressed in different cell types whereas miR-302 and miR-372 are more specific to the pluripotent state. By targeting ZEB1 and ZEB2 (zinc finger E-box binding homeobox) by miR-200, -205 families, E-Cadherin is de-repressed [281]. MET is thought to be driven by response to BMP signalling promoted by hsa-miR-302/367 targeting BMP inhibitors such as transducer of ERBB2, 2 (TOB2), DAZ-associated protein 2 (DAZAP2) and SLAIN motif family, member 1 (SLAIN1) that results in the expression of miR-200, 205 clusters in murine cells. Additionally, hsa-miR-302/367 repress TGFβ2R and decreased levels of the mesenchymal markers ZEB1, ZEB2, fibronectin 1 (FN1), and snail homologue 2 (SNAI2) leading to MET [261, 269].

Table 1.11. miRNAs in reprogramming and pluripotency of human cells. Summarised in [269].

miRNA	Effect	Target	Ref
miR-200s	Stimulation	ZEB2, LIN7c, TOX, BPTF, CPSF6, DNAJ13	[282]
miR-181	Stimulation	NOL8, CDYL, MARCKS, IGH2BH2, YWHAG, BCLAF1, NLR2C2	[283]
miR-29b	Stimulation	DNMT3a, DNMT3b	[276, 277]

miRNA	Effect	Target	Ref
miR-17-92 miR-106b-25 miR-106a-364	Stimulation	TGFRB2, p21	[284, 285]
miR-138	Stimulation	p53	[278]
mir-291, -294, -295, -296 miR-302a,b,c,d miR-367	Stimulation	DDHD1, DPYSL2, HIVEP2 Lefty, MBD2, NR2F2, PTEN, RHOC, TGFRB2, CyclinD1	[286-289]
miR-766	Inhibition	SIRT6	[290]
miR-21	Inhibition	p85α, SPRY1	[277]
miR-34a	Inhibition	NANOG, SOX2, N-MYC	[280]

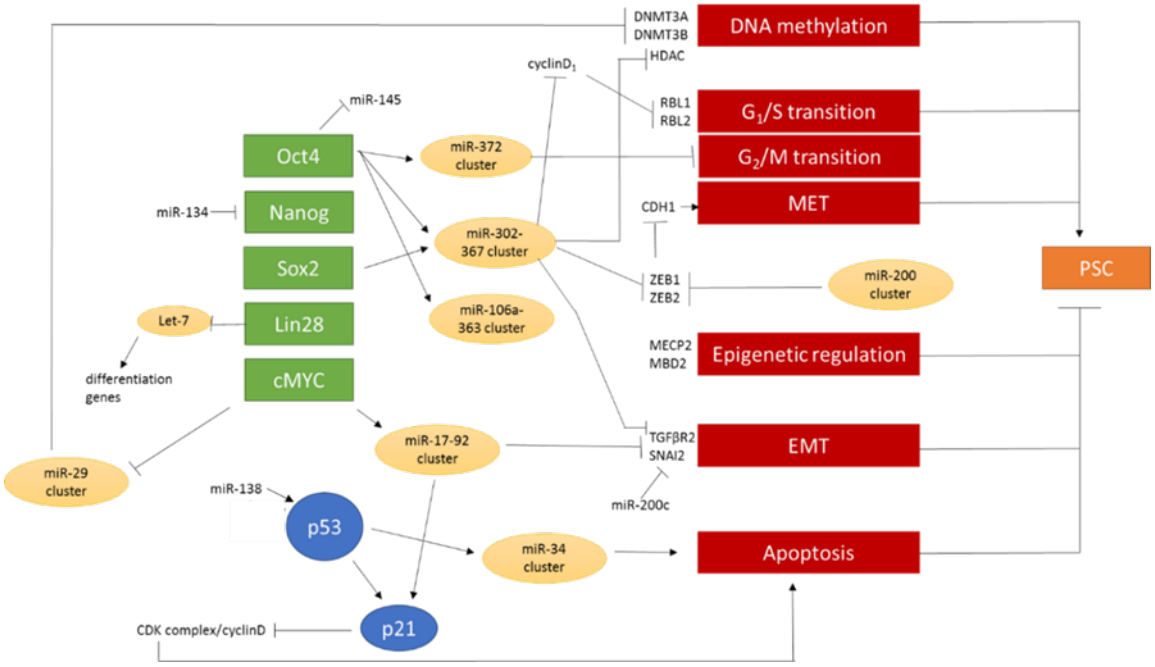

Figure 1.14. miRNAs involved in maintenance of human pluripotent state. Oct4: octamer-binding transcription factor 4; Sox2: (sex determining region Y)-box 2; miR: microRNA; DNMT: DNA methyltransferase; HDAC: histone deacetylase; PSC: pluripotent stem cell; EMT: epithelial-mesenchymal transition; RBL: retinoblastoma-like protein 2; CDH: cadherin-1; ZEB: zinc finger E-box-binding homeobox; MECP: methyl CpG binding protein 2; MBD2: methyl-CpG-binding domain protein 2; TGFβ: transforming growth factor beta; SNAI: snail family transcriptional repressor 2; CDK complex: cyclin dependent kinase complex. Modified from [261].

MiRNAs in bone and cartilage development

Bone is formed either by endochondral ossification (cartilage serving as a template for all prospective bones except clavicle and craniofacial bones) or intramembranous ossification (direct differentiation into bones of skull and clavicle without a cartilage intermediate step) [291]. Different miRNAs can act at different stages of osteogenic and chondrogenic differentiation and the bone formation process with roles in fate decision between chondrocytes and osteoblasts through targeting components of signalling pathways, transcription factors involved in skeletogenesis or regulators of matrix production. By targeting positive regulators of chondrogenesis or osteogenesis, differentiation into one of the two cell types will be inhibited whereas by targeting of negative regulators miRNAs involved in either chondrocyte or osteoblasts formation will be upregulated. miRNAs are also involved in the osteoclast generation and can regulate their function. Thus, miRNAs play a crucial role in bone remodelling as well as differentiation into osteoblasts and chondrocytes. Osteoblast specific miRNAs, their effects and targets are summarised in Figure 1.15 and Table 1.12.

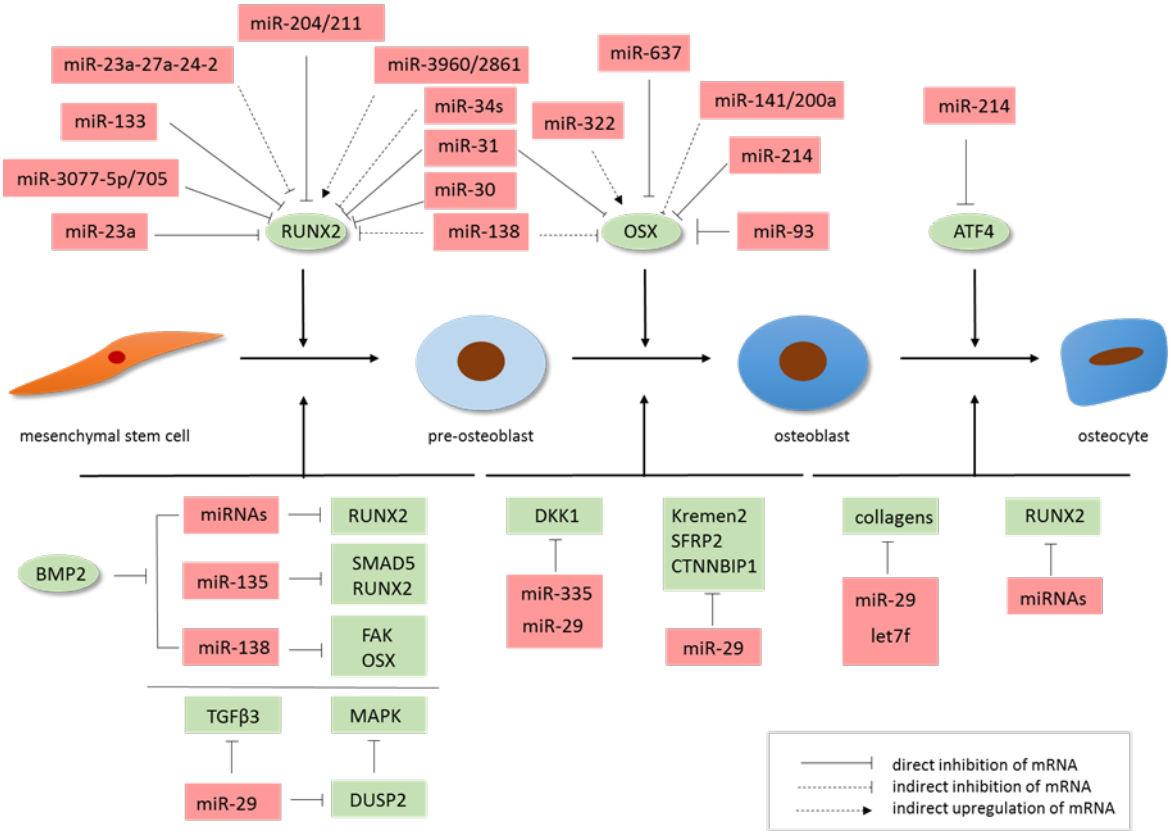

Figure 1.15. microRNAs in human osteoblast differentiation. pink: selected miRNAs; green: targets of miRNAs; miR: microRNA; RUNX2: runt-related transcription factor 2; OSX: osterix; ATF4: activating transcription factor 4; SATB2: special AT-rich sequence-binding protein 2. BMP2: bone morphogenetic protein. Modified from [292, 293].

Table 1.12. microRNAs in human osteoblast regulation and bone formation. PPARγ: Peroxisome proliferator-activated receptor gamma; Bambi: BMP and activin membrane bound inhibitor; Crim1: Cysteine-rich motor neuron 1 protein; TMEM64: transmembrane protein 64; PDCD4: programmed cell death protein 4; FAK: focal adhesion kinase; Runx2: runt-related transcription factor 2; DKK1: dickkopf Wnt signalling pathway inhibitor 1; ON: osteonectin; BMP2k: bone morphogenetic protein 2 kinase; summarised in [292, 294].

miRNA	**Target**	**Effect**	**Ref**
Let-7	Axin2	Axin2 inhibits Wnt signalling	[295]
miR-15b	SMURF1	Protection of RUNX2 from degradation	[296]
miR-17~92 cluster (miR-17, miR-18a, miR-19a, miR-20a, miR-19b-1, miR- 92a)	BMP2 TGFβ pathway	Cluster is expressed in osteoprogenitors but decreases upon osteogenic differentiation	[297]
miR-20a	PPARγ BAMBI CRIM1	Repression of PPARγ (→ inhibition of adipogenesis) Repression of Bambi and Crim1 (= inhibitors of BMP signalling) ➔ Activation of BMP/RUNX2 signalling	[294, 298]
miR-20b	PPARγ BAMBI CRIM1	Repression of PPARγ (→ inhibition of adipogenesis) Repression of Bambi and Crim1 (= inhibitors of BMP signalling) ➔ Activation of BMP/RUNX2 signalling	[294, 298]
miR-23a	RUNX2	Repression in osteocytes → attenuation of osteoblast maturation	[299]
miR-23a/27a/24-2	FAK RUNX2 SATB2	Suppression of SATB2; RUNX2 impairs expression of miRNAs;	[299, 300]
miR-29a,c	DKK1 ON	miR-29 binding sites on ON ➔ Repression of ON upon maturation and mineralisation miR-29a: suppression of Wnt inhibitors (DKK1) ➔ Stimulation of Wnt signalling pathway	[301]
miR-30c	RUNX2	Downregulation	[300]

miRNA	Target	Effect	Ref
miR-34a	JAG1 (ligand of Notch pathway) CCND1 CDK4,6 CDC25a	Downregulation of targets	[302]
miR-34c	RUNX2 SATB2 Notch pathway	Downregulation of targets	[300, 303, 304]
miR-133a	RUNX2 OSX	Downregulation of targets	[300]
miR-135a	RUNX2	Downregulation of targets	[300]
miR-137	RUNX2	Downregulation of targets	[305]
miR-138	FAK	FAK stimulates RUNX2 & OSX transcription → induction of osteogenesis; miR-138 downregulated during osteoblast differentiation in vitro in hMSCs	[305]
miR-141, miR-200a	DLX5	Inhibition of osteoblast differentiation	[306]
miR-146a	SMAD2/3	Downregulation of targets → Upregulation of RUNX2 and downregulation of SOX9	[307]
miR-148b	WNT1	Promotion of osteogenesis	[308, 309]
miR-181 (a,b,c,d)	TGFβ signalling pathway	Downregulation of TGFβ signalling (= negatively regulates osteogenic differentiation)	[310]
miR-182	FOXO1	Suppression of FOXO1 → Negative effect on osteogenic differentiation	[311]
miR-204/211	RUNX2 SOST	Downregulation Promotion of Wnt pathway	[300]
miR-205	RUNX2	Downregulation of target	[300]

miRNA	Target	Effect	Ref
miR-217	RUNX2	Downregulation of target	[300]
miR-218	SOST DKK2 SFRP2	downregulation of Wnt pathway inhibitors (SOST, DKK2, SFRP2) ➔ Promotion of Wnt signalling pathway	[312]
miR-322	OSX RUNX2 MSX2 IBSP	Increased expression of target genes ➔ Promotive effect on osteogenic differentiation	[313]
miR-335-5p	DKK1	Suppression ➔ Enhanced Wnt signalling and therefore promotion of osteogenesis	[314]
miR-338	RUNX2	Downregulation of target	[300]
miR-637	COL1a1 BMP2k OSX	Upregulated upon vitaminD3 treatment miR-637 suppresses osteoblast differentiation	[315, 316]

Table 1.13 microRNAs in chondrogenic differentiation. SOX9: SRY-Box9; FOXO: Forkhead Box; RALA: Ras-related protein Ral-A. Summarised in [317].

miRNA	Target	Effect	Ref
miR-140-3p	unknown	Upregulate during chondrogenic differentiation	[317, 318]
miR-145	SOX9 SMAD3	Downregulated during chondrogenic differentiation enabling de-repression of *SOX9* resulting in expression of chondrogenic genes	[319]
miR-221	MDM2	Upregulated during chondrogenesis	[320]
miR-29a	FOXA3A	Downregulated in chondrogenic differentiation enabling de-repression of *FOXO3A* resulting in transcription expression of *SOX*9, *COL2A1*, *ACAN*	[301]
miR-140-5p	RALA	Upregulated during chondrogenic differentiation, Knockdown of RALA resulted in upregulation of SOX9	[321, 322]
miR-146a	SMAD2 SMAD3	Downregulated during chondrogenesis enabling de-repression of *SMAD2* and *SMAD3*	[307]

miRNA	**Target**	**Effect**	**Ref**
miR-146b	SOX5	Downregulate during chondrogenesis enabling de-repression of SOX5 which is co-expressed with SOX6 and SOX9 resulting in enhanced *COL2A1* expression and binding of SOX9 to *ACAN* enhancer	[323, 324]
miR-193b	TGFB2 TGFBR3	Upregulated during chondrogenesis	[325, 326]
miR-194	SOX5	Downregulate during chondrogenesis enabling de-repression of SOX5 which is co-expressed with SOX6 and SOX9 resulting in enhanced *COL2A1* expression and binding of SOX9 to *ACAN* enhancer	[327]
miR-495	SOX9	Downregulated during chondrogenic differentiation enabling de-repression of *SOX9* resulting in expression of chondrogenic genes	[328]

1.8 Hypothesis and Aims

Research hypothesis

The overall hypothesis of this thesis is that HFBCs isolated from human foetal femurs and iPSC-MSCs are able to differentiate towards the osteogenic lineage

Specifically this hypothesis will be broken down into:

I. The use of the small molecule SB431542 can give rise to iPSC-MSCs and iPSC-MSC-derived osteoblasts can be subsequently generated in small molecules TH and SAG supplemented osteogenic differentiation media *in vitro.*

II. Human foetal femurs display a cartilaginous phenotype and the expression of genes required for skeletal development arise with increasing foetal femur age.

III. HFBCs isolated from 14 wpc human foetal femurs result in better osteogenic differentiation outcome than HFBCs isolated from 8 wpc human foetal femurs

IV. Epigenetic mechanisms are involved in the regulation of gene expression during human foetal femur development and *in vitro* osteogenic differentiation of theses cells

Aims:

The overarching aim is to understand the characteristics of iPSC-MSCs as well as HFBCs for their phenotype and skeletal regenerative potential as well as for their molecular and epigenetic profiles.

This aim will be broken down into:

I. To examine the generation of iPSC-MSCs from a standardised iPSC control line, NIBSC-8, and subsequent differentiation into osteoblasts *in vitro* using the small molecule SB431542

II. To characterise human foetal femurs and HFBCs isolated from human foetal femurs during the first two trimesters (7 - 17 wpc)

III. To compare *in vitro* osteogenic differentiation potential of HFBCs isolated from 8 and 14 wpc human foetal femurs using two osteogenic differentiation media

IV. To investigate the influence of epigenetic regulatory mechanisms during early human foetal femur development (7 - 17 wpc) and during *in vitro* osteogenic differentiation

Chapter 2 Methodology

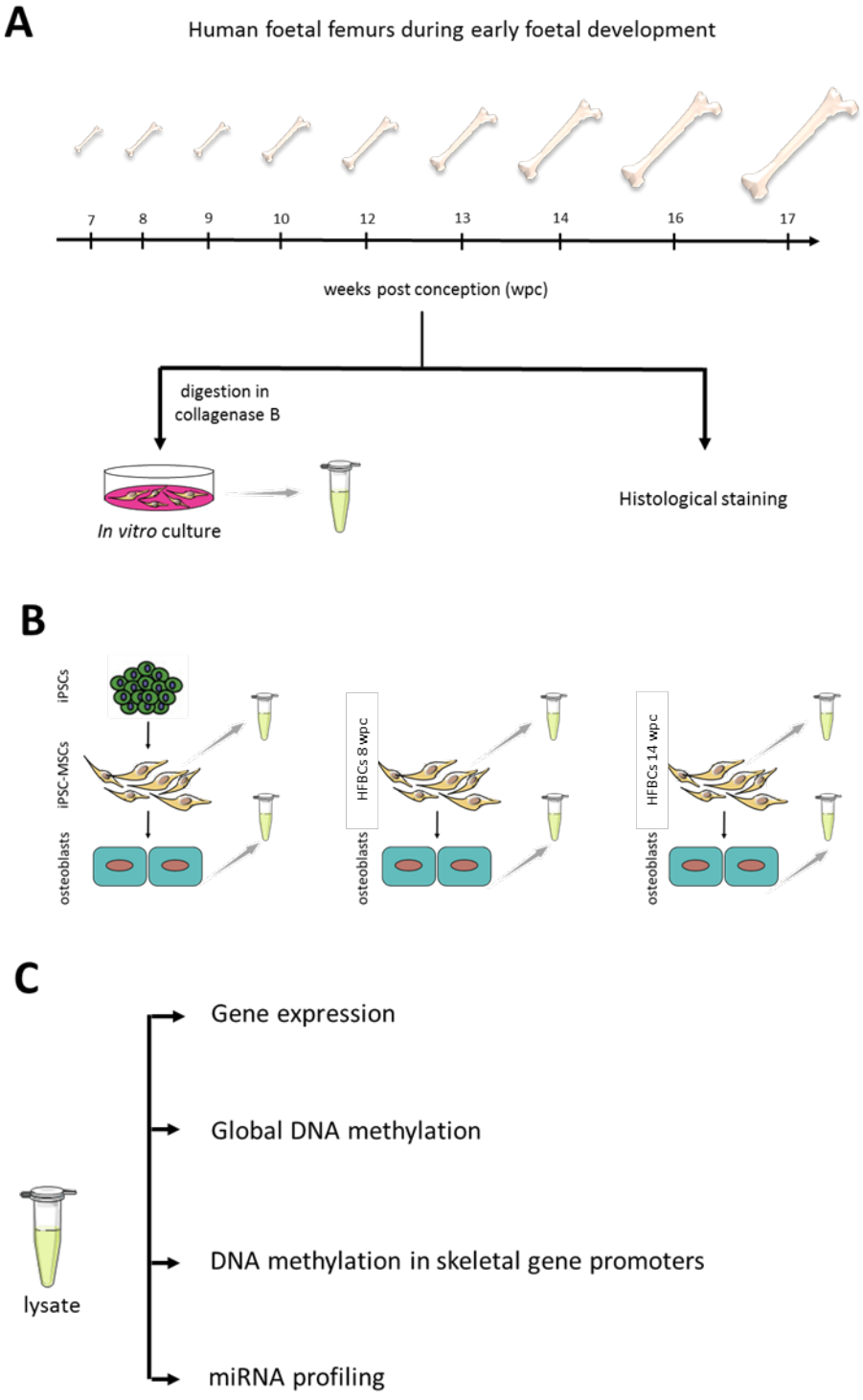

Figure 2.1 Overview of experimental design of study. A: Human foetal femurs (7 - 17 weeks post conception (wpc)) were digested in collagenase B overnight and human foetal bone cells (HFBCs) cultured on tissue culture plastic (TCP) for two passages. Cell lysates were subsequently harvested. **B:** iPSCs were differentiated into iPSC-derived mesenchymal stem cells (iPSC-MSCs) and subsequently towards the osteogenic lineage together with HFBCs isolated from human foetal

femurs (8 wpc and 14 wpc). **C:** Isolated genomic DNA (gDNA) and RNA from cell lysates were used for analysis of DNA methylation (global methylation profiling), DNA methylation in promoters of genes implicated in skeletal development (bisulfite pyrosequencing), gene expression (quantitative real-time RT-PCR (qRT-PCR) and microRNA expression (miRNA profiling).

Figure 2.1 summarises the experimental design of the studies undertaken in this thesis. Methods and details are provided in full to avoid repetition and redundancy in the description of protocols within chapters 3 - 5 as well as the appendices. Methods detail: i) cell culture techniques employed, ii) *in vitro* cell differentiation protocols, iii) media/buffer compositions, iv) histological staining procedures, v) molecular methods, vi) microscopy and, vii) statistical tests employed.

2.1 Cell Culture Methods and Media Composition

2.1.1 Isolation and culture of human bone marrow mononuclear cells (BMMNCs)

Bone marrow samples were obtained from patients undergoing total hip replacement surgery at the University Hospital Southampton, UK. All patients gave informed consent and the use of the human material was approved by the local ethics committee (LREC number: 194/99/1; R&D number: T&O/079). Bone marrow aspirate was transferred into a universal tube under sterile conditions and washed three times with Minimum Essential Medium Eagle - Alpha modification (αMEM) (Lonza, UK, Cat. No. BE02-002F) containing 1 % Penicillin/Streptomycin (P/S, Lonza, Cat. No. 17-603E). Trabecular bone pieces were isolated using a cell strainer and BMMNCs obtained following centrifugation in a density gradient separation solution (Lymphoprep, Axis-Shield) for 40 minutes (min) at 800 x g. Cells were stained with trypan blue solution (Sigma-Aldrich, Gillingham, UK, Cat. No. T8154) to aid cell count and seeded in αMEM supplemented with 10 % foetal bovine serum (FBS, Lonza, UK, Cat. No. 10270-106) and 1 % P/S (referred to as MSC medium) into 175 cm^2 flasks to select adherent cells (referred to as human bone marrow stromal cells (HBMSCs)).

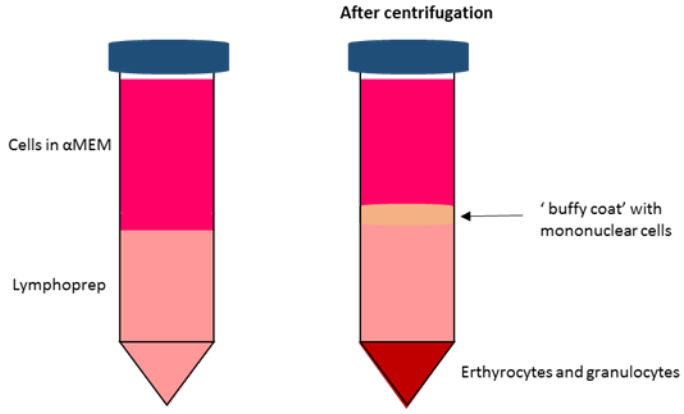

Figure 2.2. Lymphoprep separation of bone marrow samples. Lymphoprep enables separation of different cell types by density gradient separation. Red blood cells form a pellet at the bottom of the universal while mononuclear cells accumulate in the interphase between the lymphoprep and media. **Isolation and culture of human foetal bone cells (HFBCs)**

Human foetal samples were obtained from women undergoing termination of pregnancy, with informed consent. Use of human foetal material was approved by the local ethics committee (LREC number: 296100). Foetal age was determined by foot length measurement and expressed as weeks post conception (wpc). Experiments were performed using femurs from 7 - 17 wpc. The foetal femur was separated from surrounding skeletal muscle and connective tissue, cut into fine pieces and digested in 5 mg/ml collagenase B (Roche Diagnostics, Cat. No. 11088815001) in α-MEM overnight. Cells were centrifuged (302 x g, 5 min) and the pellet resuspended in MSC medium and cultured in 75 cm^2 cell culture flasks.

2.1.3 Generation and culture of human induced pluripotent stem cells (hiPSCs)

hiPSC lines from parental (somatic) cells were generated by collaborators in the Molecular Embryology and Aging Group led by Prof Dr James Adjaye, now at the Institute for Stem Cell Research and Regenerative Medicine, University Hospital of Dusseldorf, Germany or purchased from the National Institute for Biological Standards and Control (NIBSC), UK. Details of the hiPSC lines, corresponding somatic parental cell type and the applied reprogramming method, as well as iPSC media employed are detailed in Table 2.1.

Table 2.1. iPSC lines, reprogramming method and corresponding parental lines. viPSCs: iPSCs generated with viral reprogramming approach; HBMSCs: human bone marrow stromal cells; dpc: days post conception.

parental	**female, 74 years HBMSCs**	iPSC line was generated by Matthias Megges, PhD student in Molecular Embryology and Aging Group, Max Planck Institute for Molecular Genomics, Berlin, Germany, under Prof Dr James Adjaye. Prof Adjaye moved his group to the Institute for Stem Cell Research and Regenerative Medicine, University Hospital of Dusseldorf, Germany in 2012.	**female, MRC-9**	Stem cell line was purchased from National Institute for Biological Standards and Control (NIBSC), UK in 2016.
reprogramming method	pMX vector based retroviral delivery +SB431542 +PD325901 +Pifithrin α		mRNA	
generated by	Matthias Megges, Charite, Berlin		National Institute for Biological Standards and Control (NIBSC)	
iPSCs	**viPSCs**		**NIBSC-8 iPSCs**	
culture media	StemMACS XF Brew iPSC medium		Essential 8 Flex medium	
coating	matrigel		vitronectin	

viPSCs were generated from HBMSCs (74 year old female) as previously described [329]. Briefly, cells were transduced with retroviruses containing pMX-vectors expressing *OCT*4, *SOX*2, *KLF*4 and c*MYC* (Addgene, Cat. No. 17217, 17218, 17219, 17220) and cultured in cell culture dishes coated with matrigel and inactivated MEFs in iPSC medium containing Knock out™-DMEM/F12 (KO-DMEM) with 20 % knockout serum replacement (KOSR), L-glutamine, non-essential amino acids, sodium pyruvate, P/S, 0.1 ml β-mercaptoethanol (all from Life technologies) and 8 ng/ml bFGF (Peprotech, Cat. No. 100-18B). After seven days, the medium was switched to conditioned medium supplemented with 2 μM SB431542 (Sigma-Aldrich, Gillingham, UK, Cat. No. S4317), 0.5 μM PD325901 and 10 μM Pifithrin α (both Stemgent, Cambridge, USA, Cat. No. 04–0006, 04–0038). Colonies displaying the characteristic iPSC round morphology were mechanically detached and transferred to a new culture vessel coated with matrigel and MEF culture vessel. viPSCs were routinely passaged using collagenase IV. Cells were incubated with collagenase IV for 5 min at 37 °C after washing with phosphate buffer saline without calcium and magnesium (PBS, Lonza, Cat. No. LZBE17-512F), collagenase IV was discarded and the cells were covered with desired volume corresponding iPSC medium depending on split ratio. Cells were then carefully detached with a cell scraper until small fragments could be observed in the medium and subsequently transferred to new wells previously coated with matrigel. Medium was supplemented with 0.5 μM Thiazovivin for 24 h to aid cell attachment. Cells were routinely incubated at 37 °C, 5 % CO_2/20 % O_2 and the medium changed daily.

NIBSC-8 was purchased from the National Institute for Biological Standards and Control (NIBSC), UK. Donor cells were reprogrammed by using mRNA and cultured in Essential 8 Flex medium (Life technologies, Cat. No. A2858501). For passaging, colonies were washed with PBS, incubated in 0.5 mM EDTA/PBS (Sigma-Aldrich, Cat. No. E1644-100G) for 4 min at 37 °C and gently detached using a cell scrapper. Fragments were transferred to new wells coated with vitronectin (VN, Life technologies, Paisley, UK, Cat. No. A14700) and fresh iPSC medium and incubated in 0.5 μM Thiazovivin for 24 h to aid cell attachment. Cells were routinely incubated at 37 °C, 5 % CO_2/20 % O_2 and the medium changed daily.

2.1.4 Generation of hiPSC-MSCs

hiPSCs-MSCs were generated using the protocol of Chen *et al*. [182]. Colonies were incubated with the TGFβ-pathway inhibitor SB431542 (10 μM, abcam, Cat. No. ab120163) in DMEM/F12, 20 % KOSR, 10 mM MEM NEAA (Gibco, Cat. No. 11140-035) and

1 % P/S for 10 days with daily media changes. Cells were then passaged to produce single cells using TrypLE Select (Life technologies, Paisley, UK, Cat. No. 12604013) and further cultured in MSC medium for approximately 6 passages (using 1x Trypsin/EDTA in PBS) for maturation of the iPSC-MSCs (Figure 2.3).

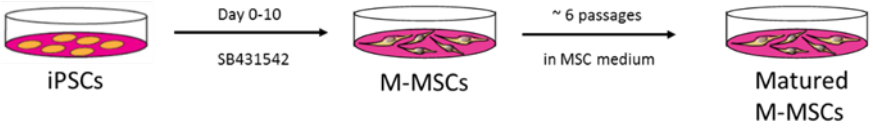

Figure 2.3. Schematic of the generation of mesoderm-MSCs (M-MSCs) derived from iPSCs following treatment with the TGFβ-pathway inhibitor SB431542 for 10 days. iPSCs were seeded as large fragments on to a matrix coated culture vessel and incubated with SB431542 for 10 days followed by repeated passaging, as single cells, to allow maturation into MSCs.

Osteogenic differentiation

Cells were washed with PBS, incubated with collagenase IV for 30 min followed by 1 x Trypsin/EDTA in PBS for 5 min at 37 °C and the reaction stopped using MSC medium. The cell suspension was transferred into a 50 ml falcon tube and centrifuged (5 min, 302 x g). The cell pellet was resuspended in MSC medium and cells seeded for osteogenic differentiation as a monolayer (50,000 cells per 24-well, 300,000 cells per 6-well) and differentiation initiated upon cell confluence. A combination of published osteogenic differentiation protocols were applied for 21 days with media changes twice a week [183] as detailed in Table 2.2. Media supplements and small molecules included: ascorbate-2-phosphate, dexamethasone and 1,25-$(OH)_2$-vitamin D_3 (all Sigma-Aldrich, Gillingham, UK, Cat. No. D4902, A8960, D1530-10 µg); smoothened agonist (SAG), Calbiochem Cat. No. 566660-1MG; 4-(4-methoxyphenyl)pyrido[4′,3′:4,5]thieno[2,3-b]pyridine-2-carboxamide (referred to as TH) was obtained from Shinuke Ohba, Tokyo, Japan [183].

Table 2.2. Small molecule supplemented osteogenic differentiation protocol. MSC medium: αMEM containing 1 % Penicillin/Streptomycin (P/S); A2P: ascorbate-2-phosphate; Dex: dexamethasone; $VitD_3$: 1,25-$(OH)_2$-vitamin D_3; SAG: smoothened agonist; TH: 4-(4-methoxyphenyl)pyrido[4′,3′:4,5]thieno[2,3-b]pyridine-2-carboxamide.

Medium	**Medium**	**TH**	**SAG**	**A2P**	**Dex**	**$VitD_3$**
Small molecule supplemented standard osteogenic medium [183]	MSC medium	1 µM	1 µM	100 µM	10 nM	10 nM
Standard osteogenic medium (osteogenic background medium)	MSC medium	/	/	100 µM	10 nM	10 nM

2.2 Histological Staining and Biochemistry

2.2.1 alamarBlue® cell viability assay

Cells were seeded into 96-well black clear bottom plates (Corning, Cat. No. 3603) and incubated for 24 h at 37 °C. alamarBlue® reagent (ThermoFisher, Cat. No. DAL1025) was diluted 1:10 in MSC culture medium, directly added to the cells (100 µl/well) and incubated for 4 h at 37 °C. Diluted alamarBlue® reagent was added to wells without cells as negative control. After 4 h, fluorescence intensity was measured at GloMax® Discover Multimode Reader (Promega) using a fluorescence excitation wave length of 540 - 570 nm (peak excitation is 570 nm) and fluorescence emission at 580 - 610 nm (peak emission is 585 nm). The reagent acts as oxidation/reduction (REDOX) indicator by acting as intermediate electron acceptor, thus, detecting the metabolic activity by a colour change of the reagent from blue, non - fluorescent (oxidised) to red, fluorescent (reduced). The reduced environment in the cell is maintained with ongoing cell growth, thus, the intensity of the colour shift from blue to red increases over time. The greatest advantage of this assay compared to other cell viability assays (such as MTT) is that the respiratory chain is not impaired by the REDOX indicator while tetrazolium salts used in MTT assays trap electrons, in turn, shutting down the respiratory chain and impairing cell viability.

2.2.2 Alkaline phosphatase (ALP) staining on cell culture plates

Cells were washed twice in 1x PBS and fixed in 100 % ethanol for 10 min. Meanwhile, 9.6 ml dH_2O with 400 µl Naphtol AS-MX Phosphatase Staining Solution and 0.0024 g Fast Violet B Salt (both Sigma-Aldrich, Gillingham, UK, Cat. No. F1631) were prepared

separately. Fixed cells were washed twice with 1 x PBS. The prepared Naphtol AS-MX Phosphatase Staining Solution was substituted with Fast Violet Salt and added to each well and samples were incubated at 37 °C in the dark. The reaction was stopped after 1 h by rinsing the wells with dH_2O. Stained cells were stored at 4 °C in 1 x PBS and imaged within 2 - 3 days.

2.2.3 Alcian Blue Staining on cell culture plates

1.5 g Alcian Blue 8GX (Acros organics, Cat. No. 400460100) was dissolved in 300 ml dH_2O and mixed with 3 ml acetic acid. The solution was filtered before use. PBS was removed from cells previously fixed in 4 % paraformaldehyde (PFA) and cells were washed with dH_2O. 300 µl per 24-well Alcian Blue staining solution was added to the cells and samples incubated for 10 min. Samples were subsequently washed 3 x with dH_2O and stored at 4 °C in PBS.

2.2.4 Alizarin red staining on cell culture plates

1 g Alizarin Red powder (Sigma-Aldrich, Gillingham, UK, Cat. No. A5533) was dissolved in 50 ml dH_2O and mixed for 3 h. 0.5 % ammonium hydroxide was used to adjust the pH to 4.2. The solution was freshly prepared for each stain analysis. Cells previously fixed in 100 % ethanol were washed twice in 1 x PBS and incubated using filtered Alizarin red solution for 20 min on a rocker (Gant-Bio Orbital Shaker PSU-10i), followed by rinsing with excess dH_2O. Calcium deposits appear orange-red.

2.2.5 Alcian Blue/Sirius Red staining on paraffin sections of rapid decalcified human foetal femurs

Paraffin sections of human foetal femurs (6 µm) were de-waxed/cleared and rehydrated as follows: Histoclear - 1 (7 min), Histoclear - 2 (7 min), 100 % - 1 ethanol (2 min), 100 % - 2 ethanol (2 min), 90 % ethanol (2 min) and 50 % ethanol (2 min). Haematoxylin working solution (50:50 mix of Haematoxylin Weigert's solutions A (alcoholic haematoxylin, Cat. No. 640494) and B (acidified ferric chloride, Cat. No. 640504, Clin Tech) was prepared and left to mature (colour change from orange-brown to black-violet) for ~ 3 min in the dark. Slides were placed in a running water bath (tap water) for 10 min until the glass surface was clear and slides then laid out on a metal tray and stained with

haematoxylin for 10 min in the dark. The staining solution was washed off in a running water bath (tap water) for 10 min. Slides were subsequently dipped into a glass jar containing 1 % HCL in 70 % ethanol to remove excess haematoxylin from the slides. Slides were placed in a running water bath (tap water) for 5 - 10 min to enable development of the colour back to black. Alcian Blue staining solution (1.5 g Alcian Blue 8GX (Acros organics, Cat. No. 400460100) mixed with 3 ml acetic acid in 300 ml dH_2O) was added to slides laid out on a metal tray and stained for 10 min, followed by a short wash (< 1 min) to remove any excess staining solution and directly placed in a glass jar containing freshly made molybdophosphoric acid (Acros organics, Cat. No. 206381000) for 10 min. Slides were rinsed in tap water (< 1 min) and placed in Sirius Red staining solution (Clin Tech, Cat. No. 640745) for 45 - 60 min. Excess staining solution was washed off by placing the rack with slides in glass jar with tap water. Slides were then dehydrated through graded alcohols as follows: 50 % ethanol (30 sec), 90 % ethanol (30 sec), 100 % - 1 ethanol (30 sec), 100 % - 2 ethanol (30 sec), histoclear - 1 (30 sec), and histoclear - 2 (30 sec). Stained sections were mounted using DPX (Fisher, Cat. No. D/5330/05).

2.2.6 Goldner's Trichrome staining on paraffin sections of decalcified human foetal femurs

Paraffin sections of human foetal femurs (6 μm) were de-waxed, cleared and rehydrated as described in section 2.2.5. Staining with Haematoxylin was performed as described in section 2.2.5. Ponceau-fuchsin-azophloxin working solution (10 ml Ponceau-fuchin solution mixed with 2 ml Azophloxin in 88 ml 0.2 % Acetic acid solution, see Table 2.3 for stock solutions) was added on slides laid out on metal tray and incubated for 5 min in the dark. Slides were transferred back on to the metal staining rack and rinsed in 1 % acetic acid for 15 sec and drained. Slides were placed in a glass jar containing phosphomolybdic acid/orange G (3 g phosphomolybidc acid (Acros organics, Cat. No. 206381000) with 2 g Orange G (Acros organics, Cat. No. 229820250) in 500 ml dH_2O) for 20 min. After rinsing in 1 % acetic acid for 15 sec the slides were drained and stained with light green (1 g light green (Acros organics, Cat. No. 229770100) mixed in 1 ml acetic acid in 500 ml dH_2O) for 5 min and rinsed in 1 % acetic acid for 15 sec again. Slides were then dehydrated by going through the following steps: 90 % ethanol (30 sec), 100 % - 1 ethanol (30 sec), 100 % - 2 ethanol (30 sec), histoclear - 1 (30 sec), histoclear - 2 (30 sec). Stained sections were mounted using DPX (Fisher, Cat. No. D/5330/05).

Table 2.3 Ponceau-Fuchsin-Azophloxin stock solutions.

Ponceau-fuchsin stock solution	**Mass/volume**
Ponceau de xylidine (Sigma-Aldrich, Cat. No. P2395-25G)	0.75 g
Acid fuchsin (Sigma-Adlrich, Cat. No F8129-25G)	0.25 g
	Add to 100 ml dH2O
Acetic acid	1 ml
Azophloxin stock solution	**Mass/volume**
Azophloxin (Raymond A. Lamb, Cat. No. 18050)	0.5 g
	Add to 100 ml dH2O
Acetic acid	0.6 ml

2.2.7 Immunofluorescence staining on cell culture plates

Cells fixed in 4 % PFA were washed with PBS and incubated with 100 mM glycine/PBS (0.375 g glycine in 50 ml PBS) for 10 min at room temperature. After removal of the glycine, cells were permeabilised in 0.2 % Triton-X/PBS (200 µl of 10 % Triton-X to 9800 µl PBS) for 10 min and wash in PBS for 10 min. Cells were blocked in 10 % FBS/PBS for 30 min and incubated with the appropriate primary antibody dilution (E-Cadherin: abcam, ab40772, 1:50; vimentin: abcam, ab92547, 1:50; OCT4: Santa Cruz, sc5279, 1:100; SOX2: Cell Signalling, D6D9XP, 1:200; NANOG: abcam, ab109250, 1:100), see Table 2.4, in 0.6 % BSA/PBS (0.3 g BSA in 50 ml PBS) for 90 min at room temperature. After washing twice in PBS, cells were incubated with secondary antibody (1:200) in 0.6 % BSA/PBS for 60 min in the dark. After additional washes in PBS (2 x 10 min) and one wash step with dH_2O (10 min) vectashield mounting medium containing DAPI (Vector Laboratories, Cat. No. H-1200) was added to each well (2 - 3 drops/well) and placed on an orbital shaker to allow equal distribution of the solution.

Table 2.4. Primary antibodies for immunofluorescence staining. ms: mouse; gt: goat; rb: rabbit.

Primary antibody	Species	Epitope	Manufacturer	Cat. No.	Dilution	Surface marker	Intracellular marker
hOCT4	ms	IgG2b	Santa Cruz	sc5279	1:100		X
hSOX2	rb	monoclonal	Cell Signalling	D6D9XP	1:200		X
hNANOG	rb	monoclonal	abcam	ab109250	1:100		X
E-Cadherin	rb	monoclonal	abcam	ab40772	1:50		X
vimentin	rb	monoclonal	abcam	ab92547	1:50		X
CD45	rb	polyclonal	abcam	ab10559	1:100	X	
CD44	rb	monoclonal	abcam	ab6124	1:100	X	
CD90	ms	monoclonal	abcam	ab23894	1:100	X	
CD105	ms	monoclonal	abcam	ab44967	1:100	X	
CD73	ms	monoclonal	abcam	ab81720	1:100	X	
CD34	rb	monoclonal	abcam	ab81289	1:100	X	

Table 2.5. Secondary antibodies for immunofluorescence staining. ms: mouse; gt: goat; rb: rabbit.

Secondary antibody	Species	Epitope	Manufacturer	Cat. No.	dilution
Alexa Fluor 488	ms	IgG	Invitrogen	A11017	1:100
Alexa Fluor 488	rb	IgG	Invitrogen	A11008	1:100

2.3 Molecular Biology Techniques

2.3.1 Cell lysis

Cells were washed with PBS and lysed in 600 µl RLT Plus lysis buffer (part of Qiagen, Cat. No. 80224) and harvested with a filtered pipette tip. The cell lysate was transferred to a nuclease - free 1.5 ml Eppendorf tube and kept at - 80 °C for storage prior to DNA/RNA/miRNA isolation.

2.3.2 Isolation of Genomic DNA (gDNA), RNA and miRNAs

Genomic DNA (gDNA) and RNA (containing mRNA as well as small RNAs) of cells lysed with 600 µl RLT lysis buffer were purified using the AllPREP® DNA/RNA/miRNA Universal Kit (Qiagen, Cat. No. 80224) according to the manufacturer's instructions. In brief, cell lysates were vortexed (1 min), and transferred to an AllPrep® DNA spin column in a 2 ml collection tube and centrifuged (1 min, 8000 x g). The AllPrep® DNA spin column was placed in a new 2 ml collection tube and stored at 4 °C until processing. Flow through from the AllPrep® DNA spin column was mixed with 80 µl Proteinase K together with 350 µl 100 % ethanol and incubated for 10 min at room temperature. 400 µl 100 % ethanol were added, mixed and 700 µl of sample transferred to an RNeasy spin column placed in a 2 ml collection tube and centrifuged (1 min, 8000 x g). This step was repeated with the remaining sample volume. The column was washed with 500 µl RPE buffer, centrifuged (1 min, 8000 x g), incubated with 80 µl DNase I for 15 min at room temperature and washed twice with 500 µl FRN buffer and once with 500 µl RPE buffer. Thereafter, the filter column was washed with 100 % ethanol, followed by 2 min centrifugation (8000 x g) to dry the membrane. RNA was eluted in 80 µl RNase-free dH_2O. 350 µl AW1 buffer was added to AllPrep® DNA spin column in 2 ml collection tube, centrifuged (1 min, 8000 x g) and incubated with 20 µl Proteinase K for 5 min at room temperature. The filter column was washed once with 350 µl AW1 and once with 350 µl AW2 buffer and centrifuged (2 min, 8000 x g). DNA was eluted with 100 µl EB buffer. RNA and DNA concentrations were measured using a NanoDrop 100 V3.8.1 from Thermo Scientific (see Appendix B) and samples stored at - 80 °C (RNA) or - 20 °C (gDNA).

2.3.3 Reverse transcription for complementary DNA (cDNA) synthesis

Isolated RNA (500 ng) was transcribed into cDNA using TaqMan Reverse Transcription Kit (Applied Biosystems, Foster City, CA) in a 20 µl total reaction volume per sample (2 µl TaqMan RT Buffer (10x), 4.4 µl $MgCl_2$ (25mM), 4 µl dNTPs (2.5 mM), 1 µl random hexamer primers (50 µM), 0.4 µl RNase inhibitor and 0.5 µl Reverse Transcriptase) and incubated for 10 min at 25 °C followed by 30 min at 48 °C and 5 min at 95 °C. Samples were diluted 1:5 in RNase free H_2O for use in quantitative RT-PCR (qRT-PCR) analysis and stored at - 20 °C.

2.3.4 Quantitative real-time PCR (qRT-PCR)

Gene expression was analysed using quantitative reverse trancriptase PCR (qRT-PCR) using 10 µl GoTaq Master Mix (Promega, Cat. No. A6002), 1 µl of forward and reverse primer (5 µM each) combined together and 8 µl RNase free H_2O in a 20 µl reaction volume. qRT-PCR was performed in a 96-well plate using a 7500 Real Time PCR system (Applied Biosystems) with the following cycling conditions: two holding stages with each 50 °C for 2 min and 95 °C for 10 min, 40 cycles at 95 °C for 15 s and 60 °C for 1 min, holding stage at 4 °C. Data were analysed with Applied Biosystems 7500 System SDS Software, version 2.0.5 programme. Threshold for calculation of cross over threshold (C_t) was set to 0.2 and all samples normalised to chosen housekeeping gene. The $\Delta\Delta C_t$ method was used to calculate relative expression levels for each gene of interest.

Table 2.6. Primer sequences used for gene expression analysis. Primers designed in house by Rahul Tare, María C de Andrés and Michael Glinka of the Bone and Joint Research Group, Southampton, and ordered from Sigma-Aldrich, Gillingham, UK. EMT: epithelial-to mesenchymal transition.

	Target	**Species**	**Forward 5'-3'**	**Reverse 5'-3'**
Housekeeping genes	*ACTB*	human	ggcatcctcaccctgaagta	aggtgtggtgccagattttc
	GAPDH	human	gacagtcagccgcatcttctt	tccgttgactccgaccttca
	RN18S	human	gccgctagaggtgaaattct	tcggaactacgacggtatct
Osteogenic genes	*RUNX2*	human	gtagatggacctcgggaacc	gaggcggtcagagaacaaac
	ALPL	human	ggaactcctgacccttgacc	tcctgttcagctcgtactgc
	COL1A1	human	gagtgctgtcccgtctgc	tttcttggtcggtgggtg
	OCN	human	ggcagcgaggtagtgaagag	ctcacacacctccctcct
	OPN	human	gtttcgcagacctgacatcc	cattcaactcctcgctttcc
Chondrogenic genes	*SOX9*	human	cccttcaacctcccacacta	tggtggtcggtgtagtcgta
	COL2A1	human	cctggtccccctggtcttgg	catcaaatcctccagccatc
	COL9A1	human	cctggtgctcttggtttga	cacgctcccccttttctc
	ACAN	human	gacggcttccaccagtgt	gtctccatagcagccttcc
Adipogenic genes	*TFAP2C*	human	tagatgggggtgtcctggta	cgcattccaccaccagtt
	PPARG	human	gggcgatcttgacaggaaag	ggggggtgatgtgtttgaacttg

	Target	Species	Forward 5'-3'	Reverse 5'-3'
Pluripotency genes	*NANOG*	human	ggtggcagaaaaacaactgg	tccctggtggtaggaagagtaa
	*OCT*4	human	ctcaccctgggggttctatt	agctaagctgcagagcctca
	*SOX*2	human	caagatgcacaactcggaga	gcttagcctcgtcgatgaac
	MYC	human	caccaccagcagcgactc	gcctgcctcttttccaca
EMT marker genes	*SNAI*1	human	ttaccttccagcagccctac	gacagagtcccagatgagca
	*SNAI*2	human	cccatgccattgaagctgaa	tttctagactgggcatcgca
	*CDH*1	human	gaagctggctgacatgtacg	tttctagactgggcatcga
	*CDH*2	human	agggatcaaagcctggaaca	ttggagcctgagacacgatt
	*ZEB*1	human	aggcagatgaagcaggatgt	ctcttcaggtgcctcaggaa
	*ZEB*2	human	caagcaccaccttatcgagc	tgtgattcatgtgctgcgag
	EPCAM	human	cctccagaacaatgatgggc	tgttcacacaccagcacatg
	VIM	human	aataagatcctgctggccga	ggctttgtcgttggttagct
	*CRB*3	human	cctgcatctgtctcccttca	ctcaggggcagagtctttga
	*CLDN*1	human	ttcttcttgcaggtctggct	cagtgaagagagcctgacca
	OCLN	human	gagctgagatcgcgacattg	gagctgagatcgcgacattg
DNA methyltransferases	*DNMT*1A	Human	caggcccaatgagactgaca	gtgggtgttctcaggcctgta
	*DNMT*3A	Human	gcctaatgttaccctggaa	cagcagatggtgcagtagga
	*DNMT*3B	human	atctttccccacacgagg	aacagcatcggcaggaac

2.3.5 MicroRNA (miRNA) profiling

Expression levels of miRNAs associated with osteogenesis and chondrogenesis (Table 2.7) were analysed in two steps: first each miRNA was amplified in a single reverse transcriptase PCR (RT-PCR) step using Taqman® MicroRNA Reverse Transcription Kit (Applied Biosystems, Cat. No. 4366596) and miRNA primers from Taqman® MicroRNA Assays (Applied Biosystems, Table 2.7). For one reaction 0.500 µl MultiScribe™ RT enzyme (50 U/µl), 0.750 RT Buffer (10x), 0.075 µl dNTPs (100 M), 1.500 µl miRNA primer (see Table 2.7), 0.094 µl RNAse Inhibitor (20 U/µl) and 3.581 µl nuclease-free water were

mixed with 10 ng RNA sample and 6.5 µl master mix (Table 2.7). Quantification of the miRNAs with quantitative PCR (qPCR) was performed using 12 µl Taqman® Universal PCR Master Mix No AmpErase® UNG (Applied Biosystems, Cat. No. 4324018), 7.7 µl RNase free H_2O and 1.2 µl of microRNA primers with 1.4 µl reverse transcriptase product for one reaction. The reaction mixture was distributed between two 96-wells. qRT-PCR was performed in a 96-well plate using a 7500 Real Time PCR system (Applied Biosystems) with the following cycling conditions: two holding stages of 50 °C for 2 min and 95 °C for 10 min, 40 cycles at 95 °C for 15s and 60 °C for 1 min, holding stage at 4 °C. Data were analysed using the Applied Biosystems 7500 System SDS Software, version 2.0.5 programme. Threshold for calculation of cross over threshold (C_t) was set to 0.2 and all samples normalised to the selected housekeeping gene Mamm U6 (Applied Biosystems, Cat. No. 001973). The $\Delta\Delta C_t$ method was used to calculate relative expression levels for each gene of interest.

Table 2.7. MicroRNA primers obtained from Applied Biosystems.

Osteogenic miRNA	**Species**	**Cat. No.**	**Chondrogenic miRNA**	**Species**	**Cat. No.**
miR-138	Human	002284	miR-140-3p	Human	002234
miR-R23a	Human	000399	miR-145	Human	002278
miR-20a	Human	000580	miR-146a	Human	000468
miR-20b	Human	001014	miR-146b	Human	001097
miR-133a	Human	002246	miR-34a	Human	000426
miR-218	Human	000521			
miR-296	Human	000527			
miR-148b	Human	000471			
miR-29a	Human	002112			
let-7f	Human	000382			

2.3.6 Global DNA methylation profiling using high-performance liquid chromatography-electrospray ionization-tandem mass spectrometry-selected reaction monitoring (HPLC-ESI-MS/MS-SRM)

For global DNA methylation profiling, 100 ng of genomic DNA (gDNA) was incubated with DNA Degradase Plus Kit (ZymoResearch, Cambridge Bioscience, UK, Cat. No. E2020) for 2 h at 37 °C in a PCR cycler to digest the gDNA (set-up of reaction mix detailed in Table 2.8). The enzymatic reaction was stopped with 175 µl 0.1 % (w/v) formic acid. The digested samples and prepared cytosine (C) and 5-methylcytosine (5mC) standards (both 1 µg each) were separated using high-performance liquid chromatography-electrospray ionization-tandem mass spectrometry-selected reaction monitoring (HPLC-ESI-MS/MS-SRM) as previously described and methylation was quantified as ratio of 5mC to total cytosine content (5mC/5mC+C) [330, 331]. The principle of HPLC-ESI-MS/MS-SRM is described in Appendix A and Appendix B.

Table 2.8. Composition reaction for digestion of genomic DNA with DNA Degradase™ Plus Kit.

Component	Volume [µl]
gDNA (500 ng/µl)	2
DNA Degradase™ Reaction Buffer 10x	2.5
DNA Degradase Plus™ (5 units/µl)	1
dH_2O	19.5
Total volume	25

2.3.7 DNA methylation analysis of genes implicated in skeletal development using bisulfite pyrosequencing

2.3.7.1 Bisulfite conversion

gDNA was treated with sodium bisulfite to convert unmethylated cytosine in CpG dinucleotides into uracil using EZ DNA Methylation-Gold™ Kit (Zymo Research, Cat. No. E1644-100G) according to the manufacturer's instructions. Briefly, CT conversion reagent was prepared (900 µl nuclease-free water, 300 µl M-Dilution Buffer and 50 µl M-Dissolving Buffer to one tube of CT conversion reagent) and wrapped in foil to protect from light. 500 ng DNA from each sample were prepared in nuclease-free water (total volume 20 µl) and 130 µl prepared CT conversion reagent were added, mixed and incubated in a

thermocycler as follows: 98 °C for 10 min, 64 °C for 2.5 h, 4 °C storage up to 20 h. 600 µl M-Binding Buffer were added to a Zymo-Spin™ IC Column with collection tube, sample loaded and mixed by inverting. After centrifugation (10,000 x g, 30 sec), flow through was discarded and 100 µl M-Wash Buffer was added, centrifuged (10,000 x g, 30 sec). 200 µl M-Desulphonation Buffer was added to the column, incubated for 20 min at room temperature and centrifuged (10,000 x g, 30 sec) followed by two wash steps with 200 µl M-Wash Buffer. The column was centrifuged to dry the membrane and bisulfite converted DNA was eluted using 10 µl EB buffer (part of Qiagen, Cat. No. 80224) and stored at - 20 °C.

2.3.7.2 Pyrosequencing primer validation using PCR and 1 % agarose gels

Pyrosequencing primers for *RUNX2*, *COL9A1* and *OCN* used in this study were previously described in [332, 333]. Primers were validated for non-specific binding and optimisation of annealing temperature (T_a) and cycle number by PCR. 7.5 µl Platinum™ Hot Start PCR 2x Master Mix (Invitrogen, Cat. No. 13000-013 for 200 reactions), 0.3 µl forward primer (10 µM) and 0.3 µl reverse primer (10 µM), and 5.9 µl nuclease-free water were mixed with 1 µl nuclease-free water (as non-template control, NTC) or 1 µl bisulfite converted DNA and amplified in a thermocycler with the following cycling conditions: 95 °C for 5 min, respective number of cycles as indicated in Table 2.9 with 95 °C for 15 sec, 56 °C for 30 sec, 72 °C for 30 sec, and holding stage at 4 °C. Primer sequences, product size, annealing temperature, cycle number as well as target CpGs for each of the primer sets after optimisation are displayed in Table 2.9. PCR product (8 µl) was mixed with 2 µl Loading Dye (30 % glycerol, 0.3 % Brom Blue, 0.3 % Xylene Cyan) and pipetted into 1 % agarose gel (1 g agarose (Fisher Scientific, Cat. No. BP1356-500) in 100 ml 1x TAE buffer (20 ml 50x TAE buffer (Fisher Scientific, Cat. No. BP1332-1) in 980 ml dH_2O) with 10 µl GelRed™ Nucleic Acid Gel Stain (Biotium, Cat. No. 41003). 5 µl O'GeneRuler 1kb (Thermo Fisher, Cat. No. SM1343) were added in one gel pocket for product size indication. The agarose gel was run for 50 min at 100 V and imaged using a gel documentation system (InGenius) under UV light.

Table 2.9 pyrosequencing primer. F: forward; R: reverse; T_a: annealing temperature.

gene	primer	sequences (5' – 3')	T_a, cycle number	target CpG
RUNX2	RUNX2_Pryro 0	(F) GTTTTTGTTTTTTTGGATTGTGTGA (R-Biotin) CCAAAAACTTCTTACTATCCTCCTAA	56°C 45 cycles	+17
	RUNX2_Pyro 1	(F) AGAGGAGGTAAAAAGGTAGAGG (R-Biotin) TCTACAATTAAAAACTTTCCTTTCTACTCCC	56°C 45 cycles	-336
	RUNX2_Pyro 2	(F) TGGTTGTTATGAAAGTGTTAGTT (R-Biotin) CCCTATCATTCATTTTTTTAAAATCTTC	56°C 45 cycles	-686, -720
COL9A1	COL9A1_Pyro 1	(F) GTTGTTGTGAGAATTAAATGGTATTAAG (R-Biotin) ACACCCAACAATCATTATTTATCA	56°C 45 cycles	-599, -614, -632
	COL9A1_Pyro 2	(F) AGGGATTGAAATTTAGGTTGAT (R-Biotin) AAATTCCAATAAAAATATACCCACTAA	56°C 45 cycles	-400, -382
	COL9A1_Pyro 3	(F) TGAGGGTTAAAAGTAAAGGGAGAG (R-Biotin) TGAGGGTTAAAAGATAAGGGAGAG	56°C 45 cycles	-49, -95
OCN	OCN_Pyro 1	(F) AGTAGGTTGTTTTTGGTGATTTAT (R-Biotin) CCAACTATCTCACAACCTATAATTTC	58°C 45 cycles	-572, -559, -541, -536, -517
	OCN_Pyro 2	(F) AGGTAGTTTGTTGTGGGTGTAGTT (R-Biotin) CCCCACCTCCATTAACTTTAA	58°C 45 cycles	-514, -476, -468, -457, -422

2.3.7.3 Pyrosequencing

PCR was performed as previously described and the presence of a single clean product confirmed by electrophoresis on a 1 % agarose gel (section 2.3.7.2.). All solutions required for pyrosequencing were warmed to room temperature before application. Optimised amount of PCR product was added into 96-wells and made up to 40 µl with high-purity water. 2 µl Streptavidin beads (GE Healthcare, Cat. No. 17-5113-01) were mixed with 38 µl Pyro Mark Binding buffer (Cat. No. 979006) and dispensed into 96-wells (40 µl per well). The plate was sealed and placed on a shaker for 5 min the master mix for each sequencing primer was prepared (0.5 µl 10 µM sequencing primer in 11.5 µl annealing buffer) and 12 µl of the sequencing primer master mix dispensed into each well of a PSQ HS 96-well plate and placed in the holding bay of the Vacuum Prep Workstation. The five troughs in the worktable were filled with approximately 180 ml of the respective solution except for denaturation solution (filled with approximately with 120 ml). The 96-well PCR plate with the PCR product and the beads was placed in the holders of the worktable as indicated. The Vacuum Prep Tool was washed for approximately 20 sec. The beads were captured by slowly lowering the Vacuum Prep Tool into the 96-well PCR plate. This step was performed within 3 min after removing the PCR plate from the shaker. The Vacuum Prep Tool was moved to 70 % ethanol and flushed through for 5 sec, followed by denaturation solution for 5 sec and washing buffer for 5 sec. Beads were released into the PSQ HS 96-well plate by shaking the vacuum Prep Tool while allowing the probes to rest on the bottom of the well. The Vacuum Prep Tool was moved to the water trough, vacuum turned on and agitated for 10 sec before returning to parking station. The PSQ HS 96- well plate with the beads and the samples was heated at 80°C for 2 min with the “iron” on top. The plate was removed after exactly two minutes and allowed to cool down at room temperature before pyrosequencing (~ 5 min before running pyrosequencing). Whilst the plate was cooling, instrument parameters were selected (CDT005) and run file set up with correct sequencing primer files. Recommended amount of nucleotides, enzyme and substrate stated by pyrosequencing software was added to each tip and the tips were placed in the tip holder and placed in the pyrosequencer and a tip test was performed assuring the correct dispensation of each solution. After successful testing of the tips, the chamber lid was opened and plate placed into the holding area, compartment closed and the run initiated. The principle of pyrosequencing is described in Appendix D.

2.4 Microscopy and Imaging Setups

2.4.1 Bright field and fluorescence microscopy

For bright field and fluorescence imaging a Carl Zeiss AxioVert 200 microscope with AxioCam HR (colour) and AxioCam MR3 (monochrome) digital cameras and software AxioVision version 4.7 (Carl Zeiss Ltd, Cambridge, UK) was used. Image analysis software, ImageJ 1.50f, was used for false colouring and superimposition of acquired images.

2.4.2 Photography

Plates were imaged using a Canon G10 digital Camera (Canon Europe Ltd., Uxbridge, UK) and a Carl Zeiss KL1500 LCD light-source (Carl Zeiss Ltd, Cambridge, UK). The light-source was set to a colour temperature of 3300K corresponding to the aperture size setting E of the KL1500 LCD light-source.

2.5 Statistics

Statistical analysis was carried out using the statistics software GraphPad Prism software version 7. Specific tests for individual experiments are indicated in the respective figure legend alongside the number of patient samples, the number of experimental repeats and the significance values in relation to p-values. Shapiro-Wilk normality test was performed to determine normal distribution of data values. Appropriate non-parametric and parametric tests including unpaired t-test with Welch’s correction, One-way ANOVA and Two-way ANOVA (both with Dunnett’s post-hoc test) were performed.

Chapter 3 Generation of iPSC-derived mesenchymal stem cells

3.1 Introduction

The transplantation of mesenchymal stem cells (MSCs) to aid skeletal repair has been widely studied in different model platforms [334]. Autologous MSCs hold a number of requisite advantages for the application in bone healing in regenerative medicine: i) the ability to migrate to the fracture site, ii) patient specificity and, iii) recruitment of additional factors for bone regeneration [335, 336]. Therefore, administration of MSCs to the fracture site is an attractive tool for treatment of bone fractures, especially given the increase in osteoporotic fractures as a consequence of an ageing population [3]. However, a limitation of MSCs from aged patients is the potential limited stem cell number, decreased proliferation rate and efficiency in osteoblast formation [154, 155]. Therefore, a new source for stromal progenitor cells with high proliferation rate is an important clinical need.

Induced pluripotent stem cells (iPSCs) have galvanised the research community for the past decade given their ability to differentiate into any somatic cell and their potential use as an *in vitro* disease model platform. IPSC-derived MSCs (iPSC-MSCs) have been generated [179-182, 184, 185, 337] and, were reported to possess i) enhanced proliferation capacity [157, 158], and ii) increased efficiency in the generation of cells of the stromal lineage [159]. Importantly, iPSC-MSC are already under evaluation in clinical trials [338]. Recently, the molecular and epigenetic differences or similarities between iPSC-MSCs, and donor cells (parental cells) have been reported [339].

During human development, the primitive streak in the epiblast layer undergoes invagination, giving rise to the mesendoderm which then separates into endoderm and mesoderm by epithelial-to-mesenchymal transition (EMT). The mesoderm formed during this process eventually gives rise to the primary mesenchyme with axial, paraxial, intermediate and lateral plate mesoderm [340]. Furthermore, EMT is involved in the development of migratory neural crest cells which can then separate from the neural folds, migrate through the body and give rise to craniofacial structure or parts of the nervous system [340]. Type I EMT occurs during implantation, embryogenesis and development of organs. Cells undergoing this type of EMTs, transform into mesenchymal cells (primary

mesenchyme) with the potential to generate secondary epithelia (e.g. notochord, somites) by undergoing mesenchymal-to-epithelial transition (MET). Type II EMT is involved in tissue regeneration and type III EMT associated in cell growth and development of tumours [340].

The process of EMT consists of characteristic hallmarks: i) acquisition of a fibroblast-like morphology, ii) production of extracellular matrix (ECM), iii) intercellular junctions (tight~, adherence ~, gap ~, desomosomes) are disrupted and associated proteins degraded (e.g. tight junctions - claudin and occludin, adherence junctions - E-Cadherin, gap junctions - connexin), vi) the cytoskeleton is reorganised and acquires enrichment in actin allowing cell elongation and greater mobility, v) loss of apical-basal polarity (due to repression of polarity complex genes *CRB*3 (Crumbs3) and *SCRIB* (Scribble) also allowing enhanced motility and the ability to invade into tissue, vi) 'cadherin-switch' (E-Cadherin repression, N-Cadherin upregulation) promotes migration and the invasive character of developing mesenchymal cells [167], (Figure 1.8 in chapter 1). Genes encoding transcription factors including: snail family transcriptional repressor 1 (*SNAI*1), snail family transcriptional repressor 2 (*SNAI*2), Zinc finger E-Box Binding Homeobox 1 (*ZEB*1), Zinc finger E-Box Binding Homeobox 2 (*ZEB*2) as well as proteins vimentin (*VIM*), E-Cadherin (*CDH*1), N-Cadherin (*CDH*2), occludin (*OCLN*), claudin 1 (*CLDN*1), crumbs 3 (*CRB*3), epithelial cell adhesion molecule (*EPCAM*) are known to be positively or negatively regulated during EMT and the function/targets are summarised in Table 3.1.

Table 3.1 Genes positively or negatively expressed during epithelial-to-mesenchymal transition (EMT). Summarised in [167].

Ref	Gene	Name	Function/Target	Effect on EMT
[169-171]	*SNAI*1	Snail family transcriptional repressor 1	repression of E-Cadherin	positive
	*SNAI*2	Snail family transcriptional repressor 2	promotion of Vimentin	
[172, 173]	*VIM*	Vimentin	type III intermediate filament protein (interacts with motor proteins)	
[168]	*CDH*2	N-Cadherin	cellular adhesion protein facilitating motility and invasion	

Ref	Gene	Name	Function/Target	Effect on EMT
[169, 174, 175]	*ZEB*1	Zinc finger E-Box Binding Homeobox 1	master regulators of cellular plasticity	
	*ZEB*2	Zinc finger E-Box Binding Homeobox 2		
[163, 167]	*CRB*3	Crumbs 3	cell polarity complex component	negative
[163, 167]	*EPCAM*	Epithelial cell adhesion molecule	exclusively expressed in epithelial cells	
[163, 167]	*OCLN*	Occludin	protein located in tight junctions	
[168]	*CDH*1	E-Cadherin	transmembrane protein	
[163, 167]	*CLDN*1	Claudin1	membrane protein in tight junctions	

Several studies have reported the generation of MSC-like cells from pluripotent stem cells (ESCs, iPSCs) (Table 1.7 in chapter 1), and have been partly tested in clinical trials. Here, the small molecule **SB431542**, a TGFβ-pathway inhibitor, was used to generate iPSC-MSCs from a characterised iPSC control line using a published protocol [182]. The TGFβ-pathway is involved in pluripotency maintenance [272, 341, 342] and SB431542 inhibits the activation of activin-receptor kinase (ALK) receptors 4, 5, 7, in turn, resulting in the inhibition of SMAD2/3 phosphorylation which in turn decreases the ability of SMAD2/3 to bind to the SMAD-responsive element in the *NANOG* promoter, thus, inducing a shift from pluripotent state toward differentiation [343, 344].

3.2 Hypothesis and Aims

Hypothesis:

The use of the small molecule SB431542 can give rise to iPSC-MSCs and iPSC-MSC-derived osteoblasts can be subsequently generated in small molecules TH and SAG supplemented osteogenic differentiation media *in vitro.*

Aims:

I. To examine *in vitro* generation of iPSC-MSCs from a standardised iPSC control line, NIBSC-8, using the small molecule SB431542

Specifically:

a. The morphological and immunocytochemical characterisation of NIBSC-8 iPSCs
b. The generation of iPSC-MSCs following treatment of NIBSC-8 iPSCs with SB431542 supplemented differentiation medium for 10 days
c. To image changes in cell morphology following 10 days treatment with SB431542 supplemented medium using bright field microscopy
d. The use of qRT-PCR for quantification of expression of pluripotency genes and genes involved in regulation of EMT after 10 days treatment with SB431542 supplemented differentiation medium and subsequent *in vitro* culture in MSC medium on tissue culture plastic (TCP)
e. The analysis of immunocytochemistry for E-Cadherin and vimentin following 10 days treatment with SB431542 supplemented differentiation medium.

II. To differentiate generated iPSC-MSCs into osteoblasts *in vitro* using two different osteogenic media

Specifically:

a. Osteogenic differentiation of iPSC-MSCs in standard osteogenic differentiation medium (oBG) and in oBG supplemented with small molecules SAG and TH for 19 days
b. Histological staining for ALP, proteoglycans and mineralised nodules at two time points (day 7 & 19) during *in vitro* osteogenic differentiation of iPSC-MSCs
c. The application of qRT-PCR for quantification of osteogenic and chondrogenic gene expression at two time points (day 7 & 19) during *in vitro* osteogenic differentiation of iPSC-MSCs

Material and Methods

The methodology used in this chapter can be found in chapter 2 with the following techniques detailed in respective subchapters: immunofluorescence staining in section 2.2.7, culture conditions and media composition for the differentiation of NIBSC-8 iPSCs into NIBSC-8 MSCs in section 2.1.4, capturing of cell morphology using bright field microscopy or capturing of immunofluorescence staining in section 2.4.1, molecular methods in chapter 2.3 with analysis of mRNA expression using qRT-PCR in section 2.3.4, composition of the different tested osteogenic media compositions and culture conditions in section 2.1.5 and histological stainings (ALP, Alcian Blue, Alizarin Red) of NIBSC-8 MSCs at two different time points during osteogenic differentiation in sections 2.2.2, 2.2.3 and 2.2.4.

Statistics

Differentiation experiments in this results chapter were performed in three independent experiments (n = 3). Unpaired t-test with Welch's correction was used for analysis of day 0 and day 10 of the generation of NIBSC-8 MSCs. One-way ANOVA with Dunnett's post-hoc test was used to analyse proliferation of NIBSC-8 MSCs between increasing passages; this test was also used for the comparison of gene expression between day 0 and MP6 during generation and maturation of NIBSC-8 MSCs. Gene expression of osteogenic differentiation was analysed with a Two-way ANOVA test with Dunnett's post-hoc test.

3.3 Results

3.3.1 Characterisation of NIBSC-8 iPSCs

NIBSC-8 iPSCs were acquired from the National Institute for Biological Standards and Control (NIBSC) and iPSC colonies were cultured on vitronectin in Essential 8 Flex medium (Life technologies, Cat. No. A2858501) (Figure 3.1). This control iPSC line was fully characterised by the NIBSC and displayed the typical characteristic tightly packed colonies with distinct borders. Immunofluorescence staining of NIBSC-8 iPSCs for expression of pluripotency markers OCT4, NANOG and SOX2 confirmed the pluripotent nature of the cell line (Figure 3.2 and Figure 3.3).

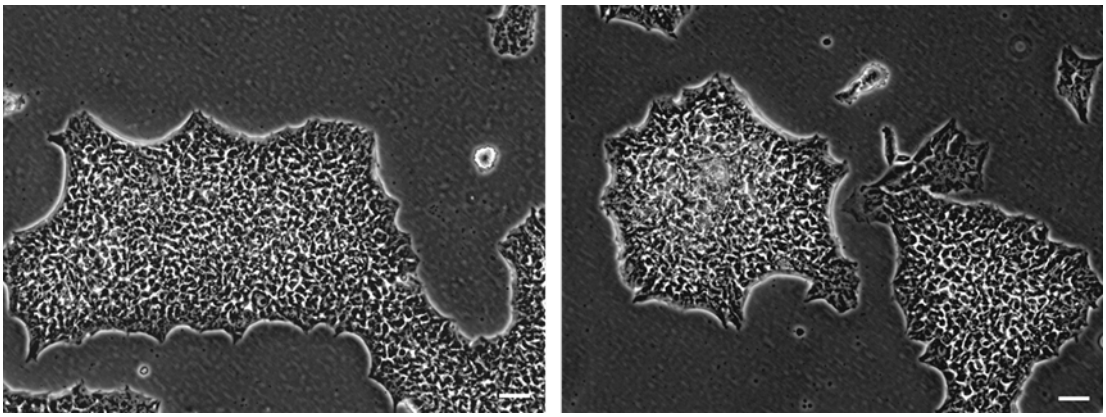

Figure 3.1 NIBSC-8 iPSC colonies (passage 22) cultured on vitronectin (VN) in Essential 8 Flex iPSC medium. Scale bars: 50 μm.

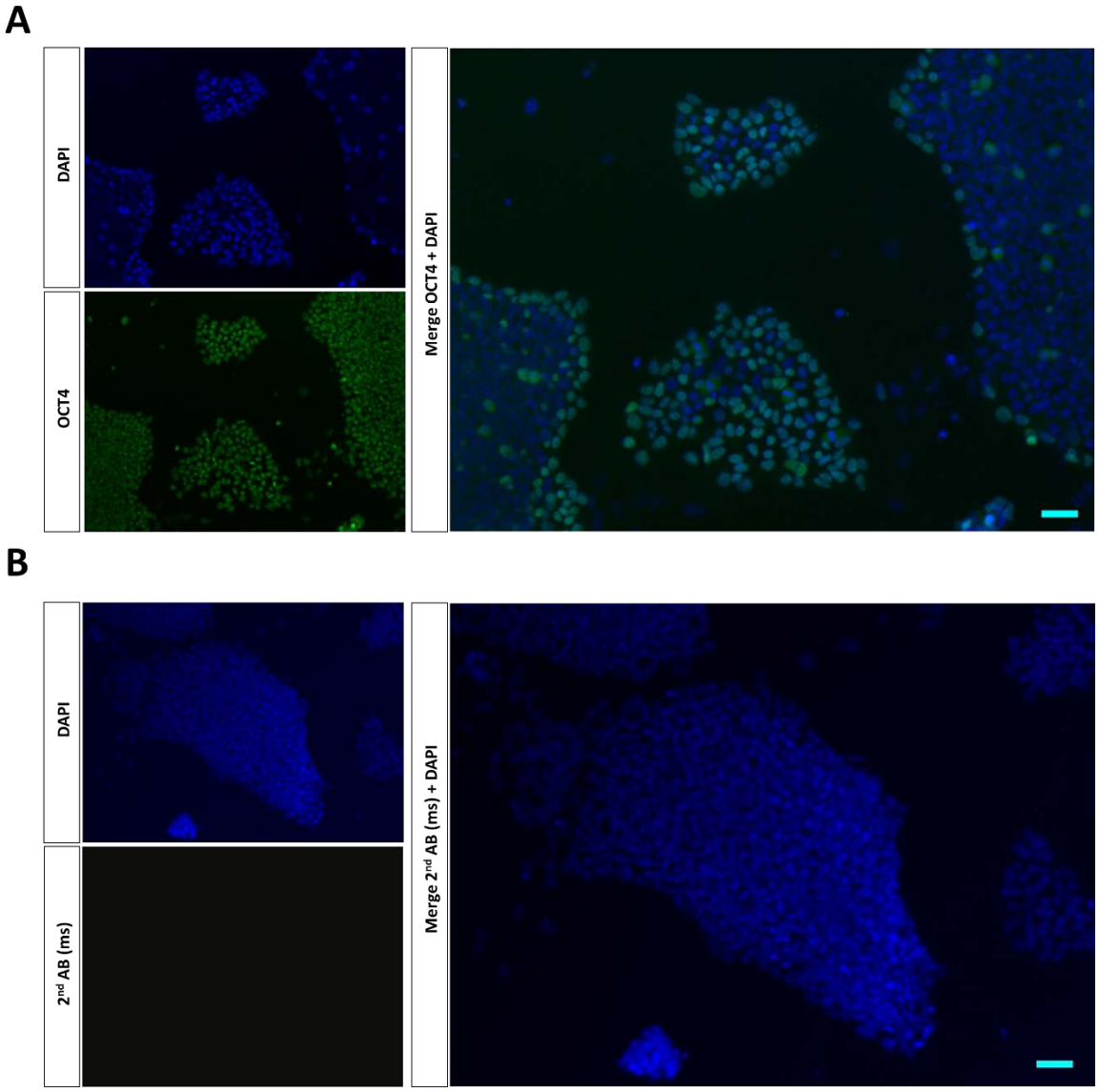

Figure 3.2 Immunocytochemistry for pluripotency marker OCT4 (A) and secondary antibody (B) in NIBSC-8 iPSCs cultured on vitronectin in Essential 8 Flex iPSC medium. Secondary antibody only (Alexa Flour 488 anti-mouse IgG, Cat. No. A11017) was used as negative control. OCT4: octamer-binding transcription factor 4.Scale bar: 50 μm.

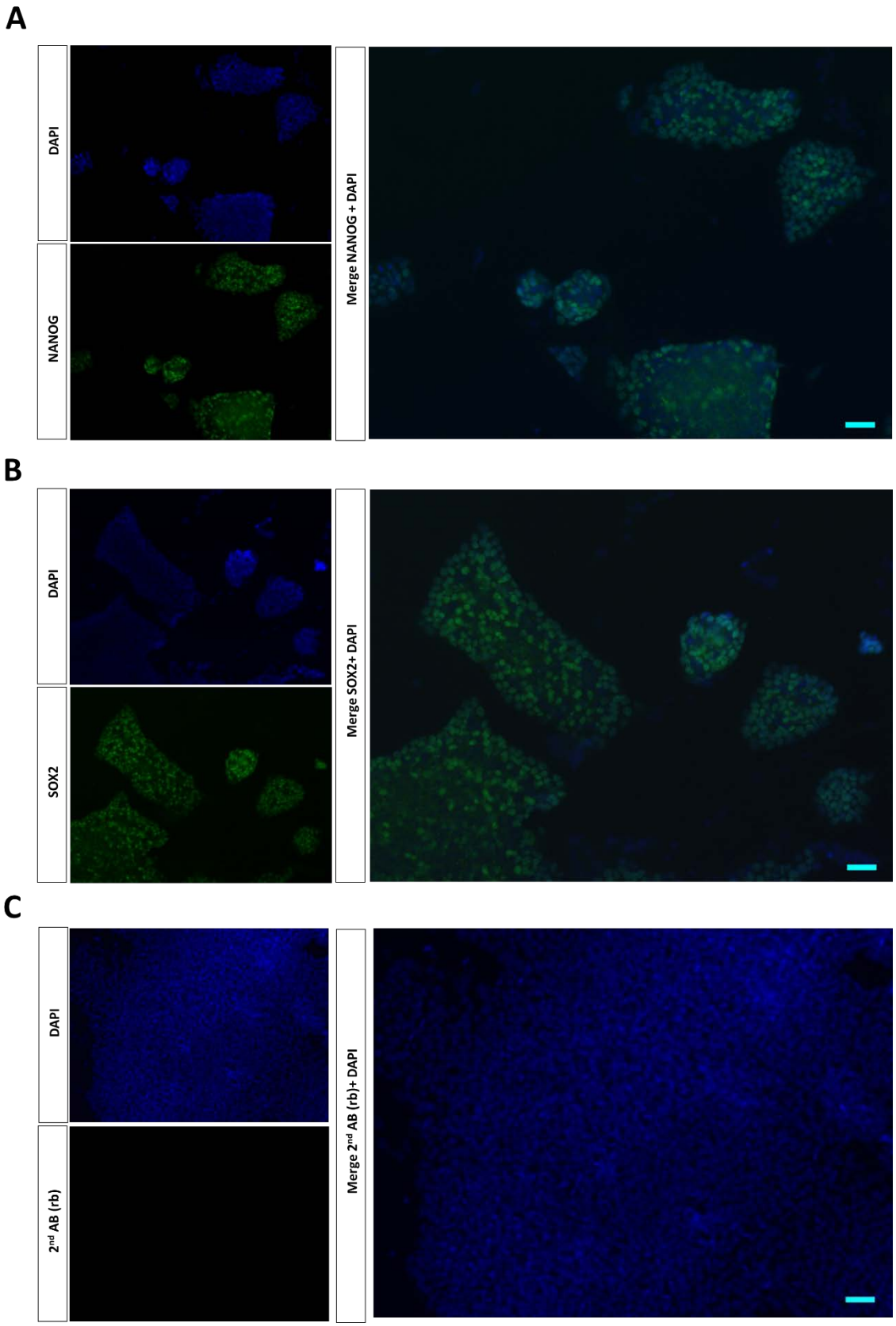

Figure 3.3 Immunocytochemistry for pluripotency markers NANOG (A) and SOX2 (B) and secondary antibody (C) in NIBSC-8 iPSCs cultured on vitronectin in Essential 8 Flex iPSC medium. Secondary antibody only (Alexa Fluor 488 anti-rabbit IgG, Cat. No. A11008) was used as

negative control. NANOG: homeobox transcription factor NANOG; SOX2: Sry-related HMG box 2. Scale bar: 50 μm.

3.3.2 Generation of NIBSC-8 MSCs using TGFβ-pathway inhibitor SB431542

In order to generate NIBSC-8-MSCs, NIBSC-8 iPSCs were seeded as large fragments onto vitronectin-coated 6-well plates and cultured in Essential 8 Flex iPSC medium until 50 % confluence. Colonies were subsequently cultured in differentiation medium containing TGFβ-pathway inhibitor SB431542 for 10 days with daily media change (full composition of differentiation medium see chapter 2). Cell morphology over the 10 day period was captured using bright field microscopy. After 1 day of treatment with SB431542, NIBSC-8 iPSC colonies displayed elongated cells along the colony borders (Figure 3.4) with cells in the colonies less tightly packed compared to NIBSC-8 iPSCs (Figure 3.1). Transition area of iPSC colony and elongated cells is indicated by the dotted line with arrows indicating elongating cells undergoing differentiation at the outer edge of the cell colony. Over the remaining 9 days of culture, the NIBSC-8 iPSC colonies lost their tightly packed structure and cells transitioned from a round to elongated, fibroblastic morphology. By day 3, differentiating cells formed a monolayer consisting of areas of cells with enlarged cytoplasm (indicated by arrows) as well as iPSC colony-like areas (indicated by dotted line and asterisk). By day 10, continued cell proliferation resulted in areas of cells with elongated morphology (within dotted circle) as well as cells appearing more rounded (indicated by asterisk) due to limited growth area. The amount of elongated cells resembling a fibroblast-like morphology increased until day 10 to approximately 80 % of the monolayer (Figure 3.4).

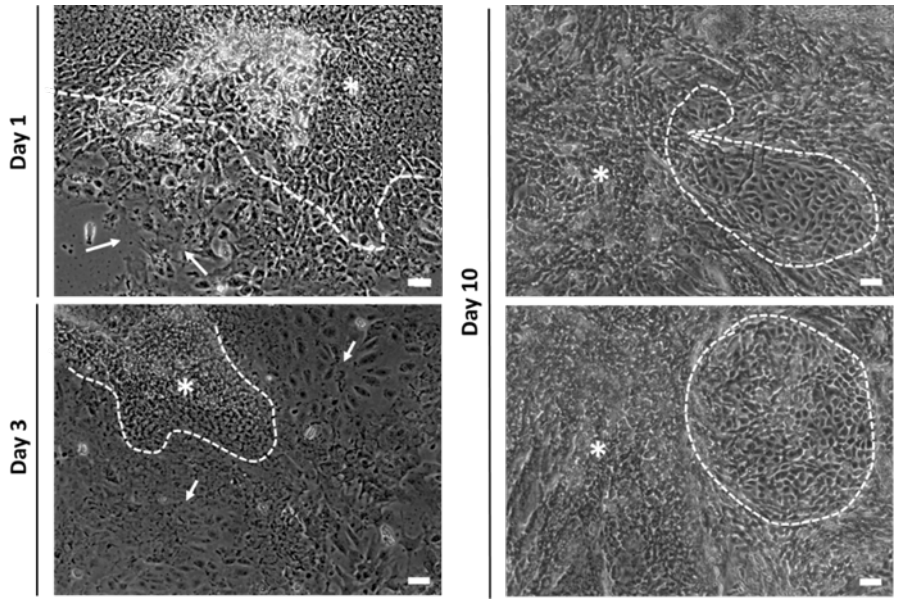

Figure 3.4 Change in cell morphology of NIBSC-8 iPSCs during the treatment with TGFβ-pathway inhibitor SB431542 supplemented differentiation medium for 10 days. After 1 day of treatment, NIBSC-8 iPSCs showed less tightly packed colonies with elongated cells on the borders of the colonies. Monolayer of cells with enlarged cytoplasm and areas of elongated, fibroblastic cells was present by day 3. Areas with elongated, fibroblastic cells increased until day 10 of culture. Representative images shown for each day. Scale bar: 50 μm.

Gene expression was analysed in order to investigate the process of EMT on a molecular level. Firstly, expression of pluripotency genes was analysed in order to ensure the downregulation of the pluripotency genes *OCT*4, *NANOG*, *cMYC* and *SOX*2 after 10 days of culture in SB4315242 supplemented culture medium (Figure 3.5). Secondly, genes with a positive or negative effect on EMT (see Table 3.1) were analysed in order to assess the success of the induction of EMT after 10 days of culture in SB431542 supplemented culture medium (Figure 3.6 and Figure 3.7). Data were normalised to day 0 (Figure 3.5 - Figure 3.7, Table 3.3).

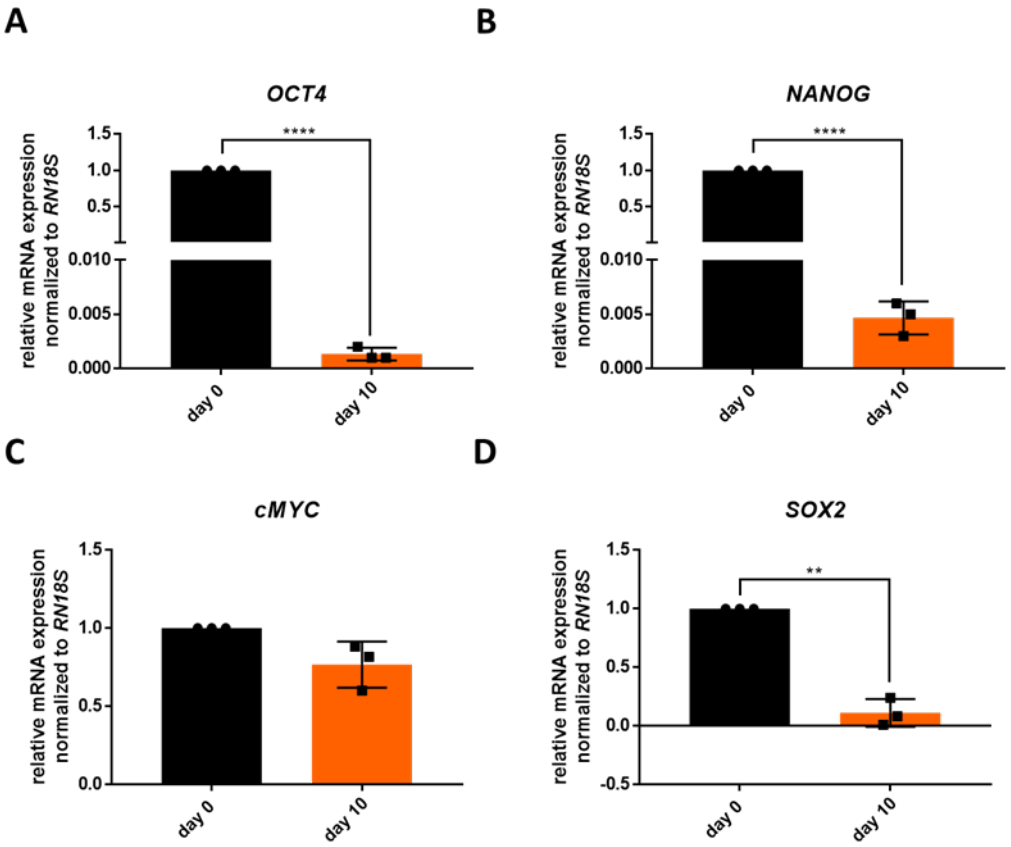

Figure 3.5 Expression of core pluripotency genes *OCT4* (A), *NANOG* (B), *cMYC* (C) and *SOX2* (D) after treatment with TGFβ-pathway inhibitor SB431542 supplemented differentiation medium for 10 days. Gene expression is displayed as mean +/- SD and normalised to *RN18S* at day 0. Differentiation experiments were performed three times (n = 3) and unpaired t-test with Welch's correction was performed to compare SB431542 treated NIBSC-8 iPSCs at day 10 with untreated NIBSC-8 iPSCs at day 0. OCT4: octamer-binding transcription factor 4; cMYC: MYC proto-oncogene; SOX2: SRY (sex determining region Y)-box 2; NANOG: Homeobox transcription factor NANOG; RN18S: subunit of 18S ribosomal RNA; ** $p < 0.01$; **** $p < 0.0001$.

Pluripotency factors *OCT4* and *NANOG* showed significantly ($p < 0.0001$) decreased mRNA expression levels at day 10 following treatment with SB431542 supplemented differentiation medium (*OCT4*: 0.00-fold change; *NANOG*: 0.00-fold change) (Figure 3.5 A-B). *c-MYC* showed 0.77-fold change compared to day 0 (Figure 3.5 C), however was not significantly lower expressed at day 10 compared to day 0. *SOX2* expression showed a significantly ($p < 0.01$) decreased mRNA expression level (0.11-fold change) (Figure 3.5 D).

Genes positively involved in EMT were not significantly differently expressed following 10 days treatment with SB431542 supplemented differentiation medium compared to day 0

except *SNAI1* which was significantly decreased at day 10 (0.46-fold change, $p < 0.001$) (Figure 3.6 A).

Expression levels at day 10 of *ZEB1* and *ZEB2* were 17.62-fold change compared to day 0 (*ZEB1)* and 41.98-fold change compared to day 0 *(ZEB2*). *CDH2* showed 5.87-fold change compared to day 0 while *VIM* demonstrated 8.75-fold change compared to day 0 (Figure 3.7 B - E). *CRB3* and *EpCAM*, genes negatively regulated during EMT, showed 0.83-fold change compared to day 0 at day 10 (*CRB3*) while EpCAM gene expression was 0.76-fold change compared to day 0 (Figure 3.7 A and C). *CDH1*, another gene negatively regulated during EMT, showed 0.10-fold change at day 10 (Figure 3.7 B). However, due to the high standard deviation no significant difference in gene expression between day 10 and day 0 could be detected. S*NAI2* could not be detected by qRT-PCR at day 0.

Analysis of gene expression of pluripotency factors demonstrated a significant downregulation in expression of *OCT*4, *NANOG* and *SOX*2 suggesting loss of the pluripotent molcular character after 10 days in SB431542 supplemented culture medium. *cMYC* did not show significant downregulation after 10 days. This could be due to *cMYC* potentially being downregulated later once loss of the pluripotent character of a cell is initiated.
Of the analysed genes with positive or negative effect on EMT, only *SNAI1* showed a significant downregulation in expression after 10 days of culture in SB431542 supplemented medium compared to day 0. Reason for this could be that *SNAI1* was downregulated earlier than other EMT regulating genes as the effect of this gene is the repression of E-Cadherin. Loss of E-Cadherin is one of the first hallmarks of the EMT process, the downreglation of *SNAI1* could therefore indicate the successful downregulation of E-Cadherin after 10 days culture in SB431542 supplemented medium. In order for a decrease in *CDH1* expression after 10 days, *SNAI1* expression was expected to show increased expression after 10 days of culture in SB431542 supplemented medium compared to day 0. *CDH1* did not show a significant difference after 10 days culture with SB431542 supplemented medium compared to day 0. Therefore, no conclusion regarding the effect of decreased *SNAI1* expression on *CDH1* expression after 10 days culture in SB431542 supplemented medium can be made based on gene expression results alone. In order to come to conclusion of E-Cadherin expression at day 0 (in NIBSC-8 iPSCs) and after 10 days of SB431542 supplemened medium immunocytochemistry staining for E-Cadherin was performed.

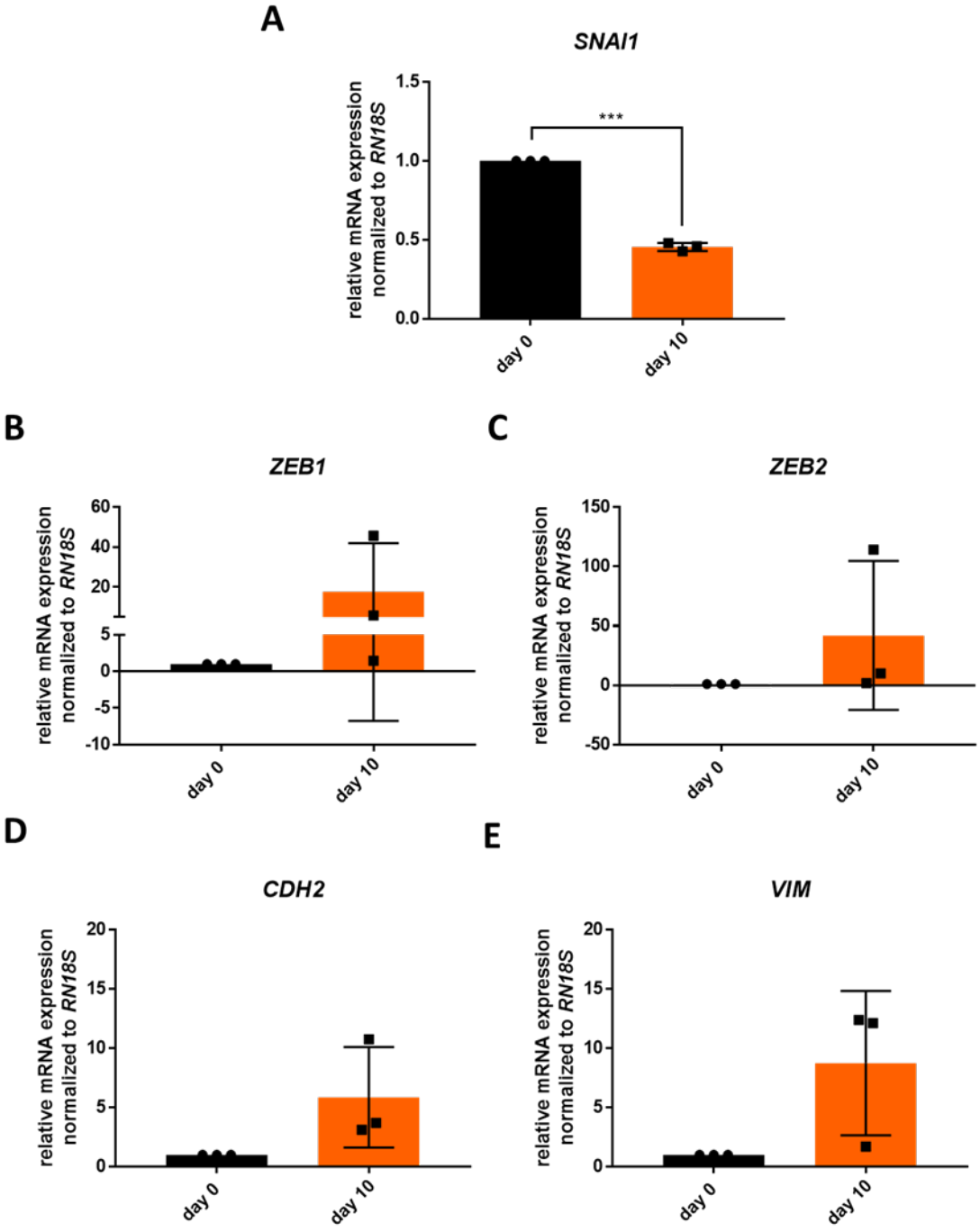

Figure 3.6 Expression of genes with a positive effect on epithelial-to-mesenchymal transition (EMT) *SNAI*1 (A), *ZEB*1 (B), *ZEB*2 (C), *CDH*2 (D) and *VIM* (*E*) following treatment with SB431542 supplemented differentiation medium for 10 days. Gene expression displayed as mean +/- SD normalised to *RN18S* at day 0. Differentiation experiments were performed three times (n = 3) and unpaired t-test with Welch's correction was performed to compare SB431542 treated NIBSC-8 iPSCs at day 10 with untreated NIBSC-8 iPSCs at day 0. SNAI1: snail family transcriptional repressor 1; ZEB1: Zinc finger E-Box Binding Homeobox 1; ZEB2: Zinc finger E-Box Binding Homeobox 2; VIM: vimentin; CDH2: N-Cadherin; RN18S: subunit of 18S ribosomal RNA; *** $p < 0.001$.

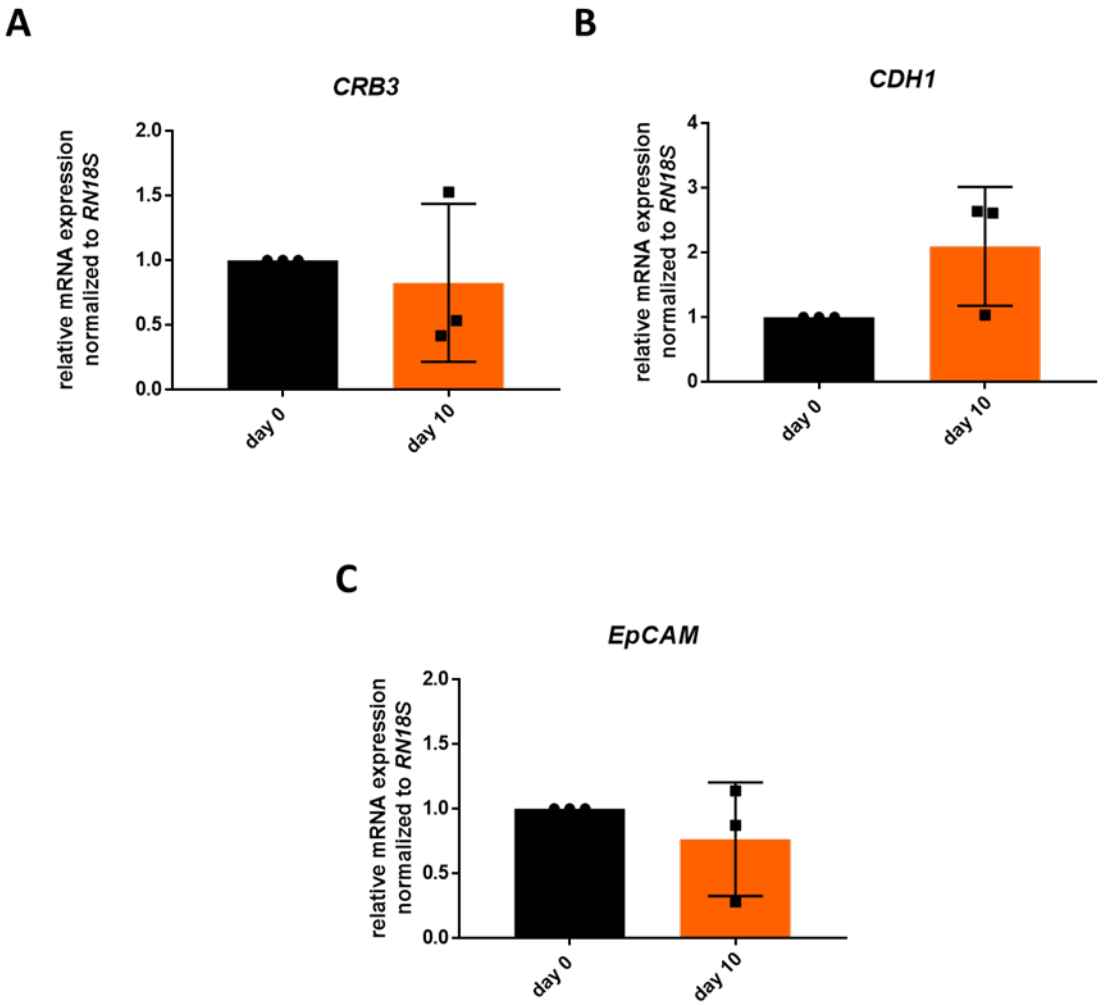

Figure 3.7 Expression of genes with a negative effect on epithelial-to mesenchymal transition (EMT) *CRB3* (A), *CDH*1 (B) and *EpCAM* (C) after treatment with SB431542 supplemented differentiation medium for 10 days. Gene expression displayed as mean +/- SD and normalised to *RN18S* at day 0. Differentiation experiments were performed three times (n = 3) and unpaired t-test with Welch's correction was performed to compare SB431542 treated NIBSC-8 iPSCs at day 10 with untreated NIBSC-8 iPSCs at day 0. CRB3: crumbs 3; CDH1: E-Cadherin; EpCAM: epithelial cell adhesion molecule; RN18S: subunit of 18S ribosomal RNA.

Immunofluorescence staining was performed after 10 days of culture in SB41542 supplemented culture medium in order to confirm the findings of EMT markers E-Cadherin and vimentin on the protein level. NIBSC-8 iPSCs were used as day 0 control.

Immunofluorescence staining for E-Cadherin (expressed in epithelial cells and negatively regulated during EMT) and VIM (expressed in mesenchymal cells and positively regulated during EMT) was performed on NIBSC-8 iPSCs following 10 days treatment with

SB431542 supplemented differentiation medium and on NIBSC-8 iPSCs at day 0 (Figure 3.8 and Figure 3.10).

NIBSC-8 iPSCs failed to express E-Cadherin protein following 10 days of treatment with SB431542 supplemented differentiation medium (Figure 3.8) while NIBSC-8 iPSCs at day 0 showed E-Cadherin expression in the membrane (Figure 3.8). VIM was expressed in elongated, fibroblastic cells, in monolayer, after 10 days treatment with SB431542 supplemented differentiation medium (Figure 3.10). NIBSC-8 iPSCs showed positive expression of VIM at day 0 (Figure 3.11).

Loss of E-Cadherin indicates the loss of the epithelial phenotype of the NIBSC-8 iPSCs after 10 days of culure in SB431542 supplemented medium. In combination with the expression of vimentin in NIBSC-iPSCs after 10 days of culture in SB431542, these findings could suggest the loss of the epithelial character in NIBSC-iPSCs and the initiation of a mesenchymal programme after 10 days of culture in SB431542 supplemented culture medium. However, vimentin expression was not exclusively detected in NIBSC-8 iPSCs after 10 days of culture in SB431542 but also in NIBSC-iPSCs.

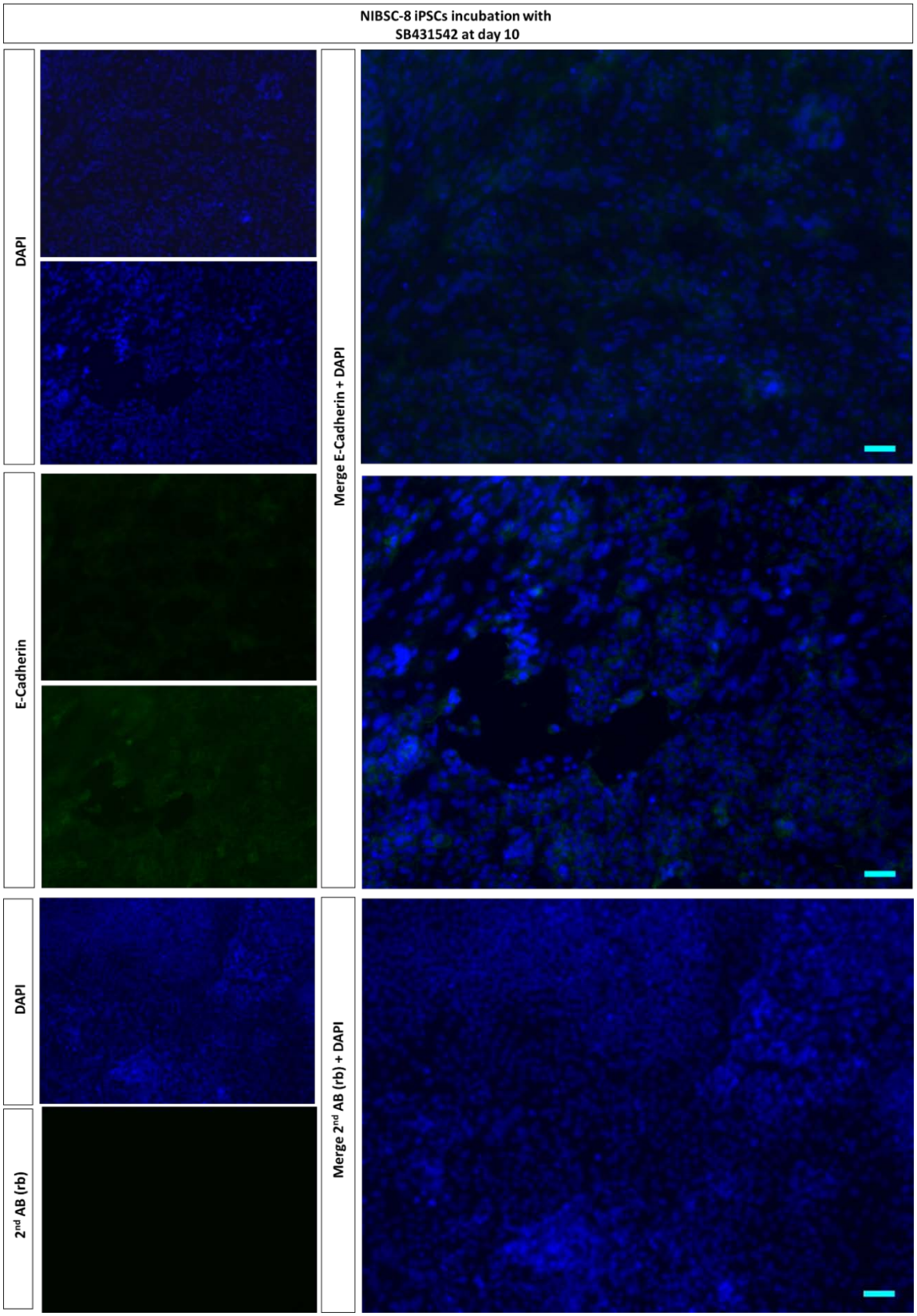

Figure 3.8 Immunocytochemistry for E-Cadherin in NIBSC-8 iPSCs following treatment with SB431542 supplemented differentiation medium for 10 days. Secondary antibody only (Alexa Fluor 488 anti-rabbit IgG, Cat. No. A11008) was used as negative control. Scale bar: 50 μm.

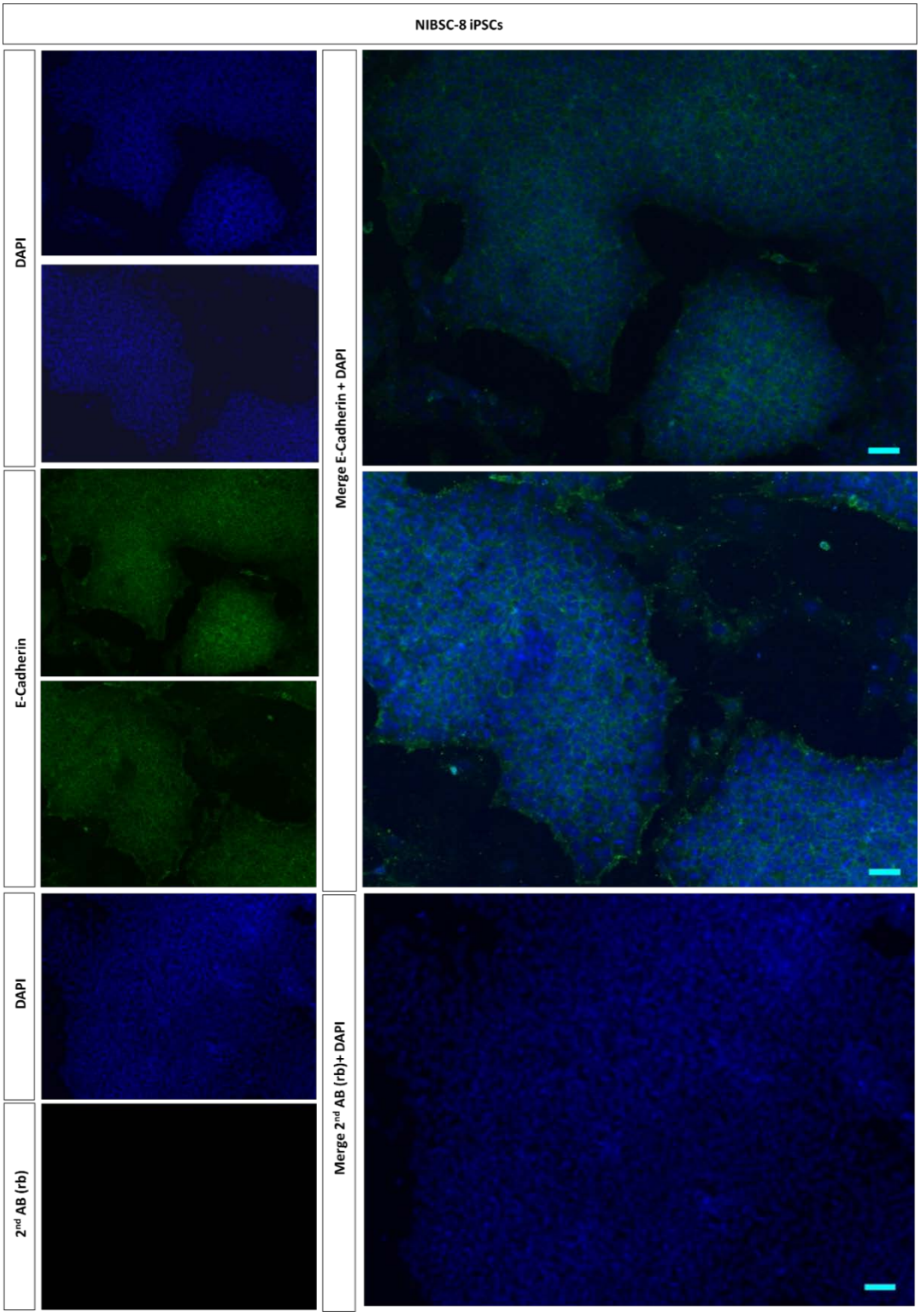

Figure 3.9 Immunocytochemistry for E-Cadherin in NIBSC-8 iPSCs prior to treatment with SB431542 supplemented differentiation medium for 10 days. Secondary antibody only (Alexa Fluor 488 anti-rabbit IgG, Cat. No. A11008) was used as negative control.Scale bar: 50 μm.

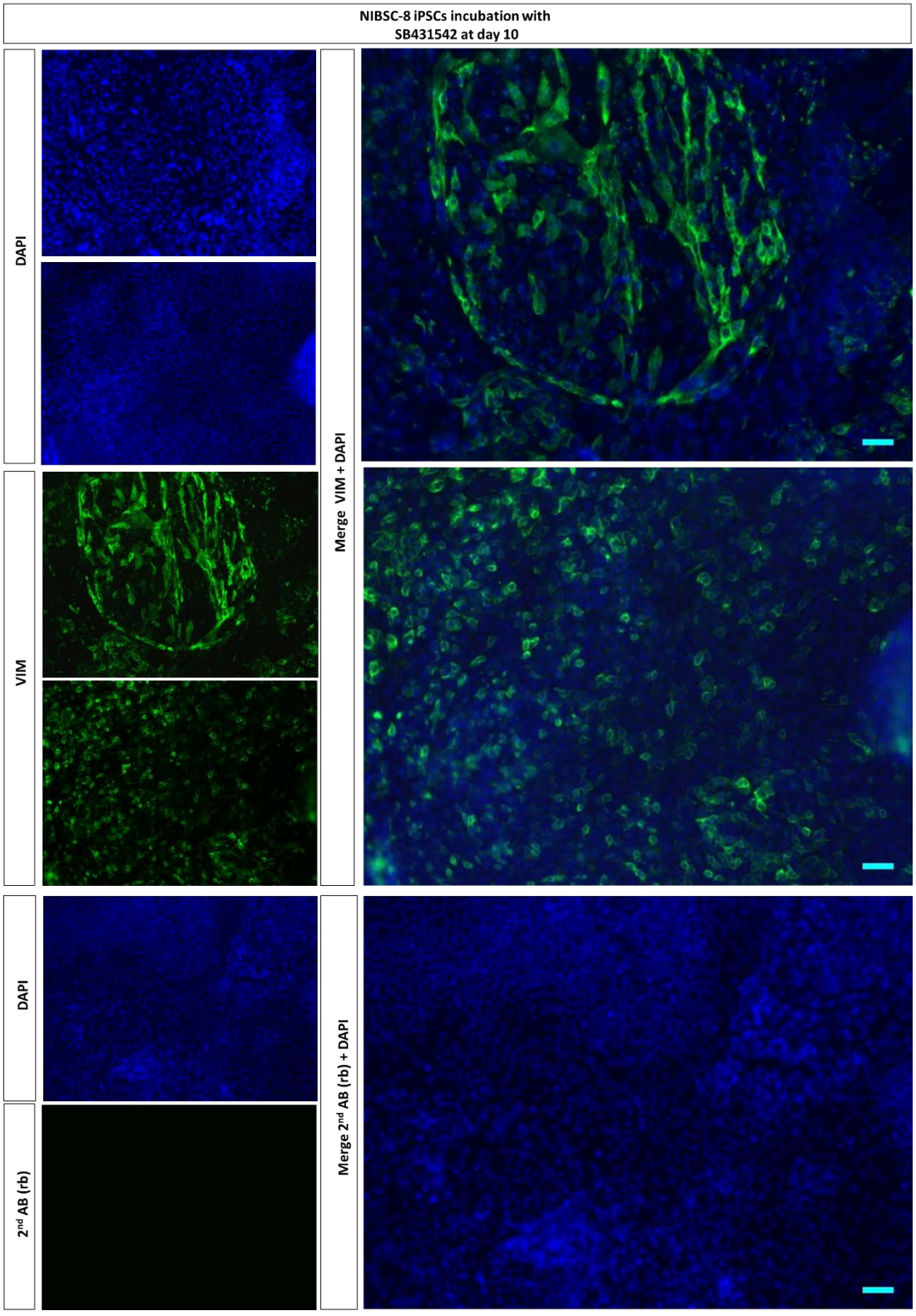

Figure 3.10 Immunocytochemistry for vimentin (VIM) in NIBSC-8 iPSCs after treatment with SB431542 supplemented differentiation medium for 10 days. Secondary antibody only (Alexa Fluor 488 anti-rabbit IgG, Cat. No. A11008) was used as negative control. Scale bar: 50 μm.

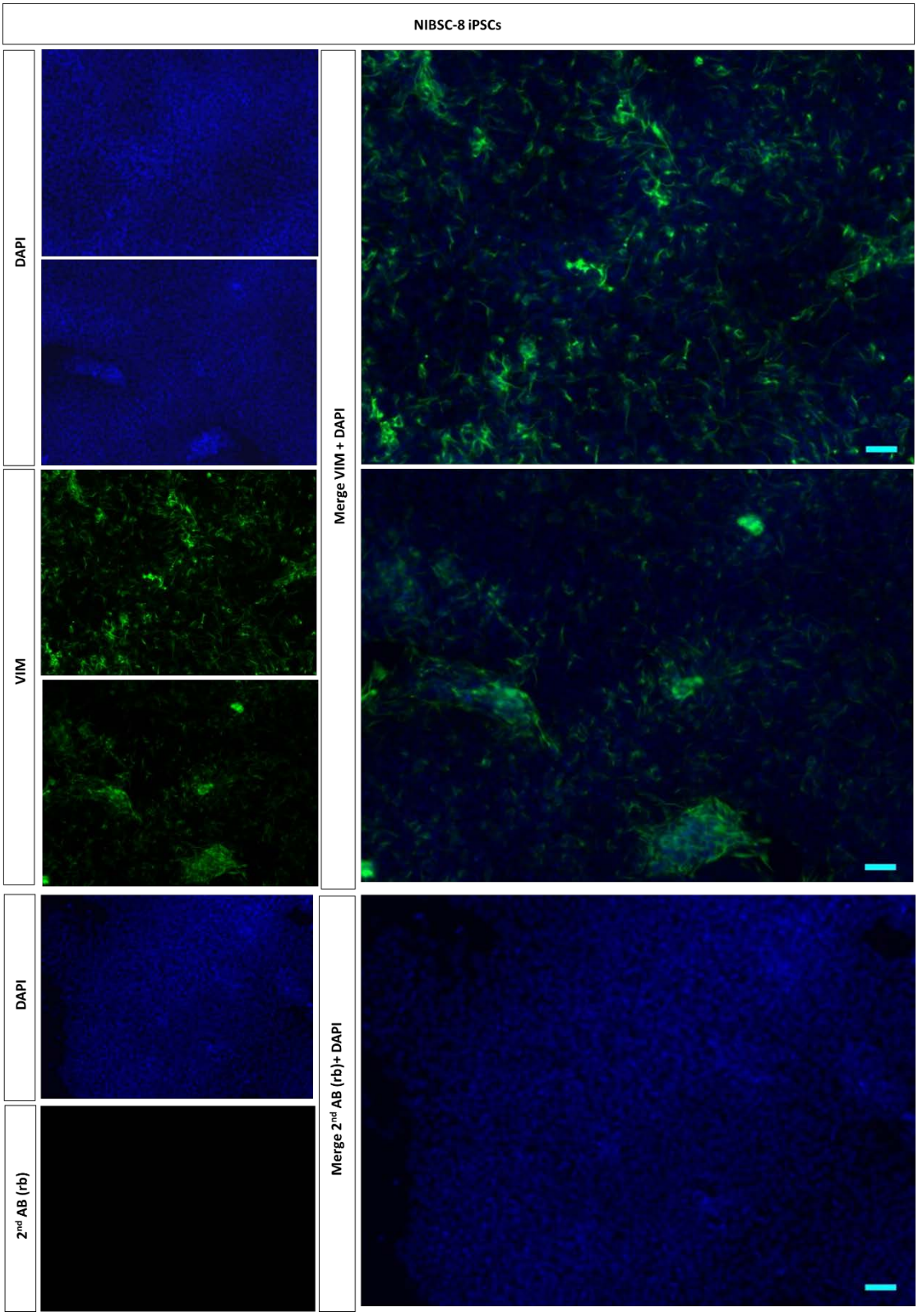

Figure 3.11 Immunocytochemistry for vimentin (VIM) in NIBSC-8 iPSCs prior to treatment with SB431542 supplemented differentiation medium for 10 days. Secondary antibody only (Alexa Fluor 488 anti-rabbit IgG, Cat. No. A11008) was used as negative control. Scale bar: 50 μm.

In order to allow for cells to mature into NIBSC-8 MSCs after the initial 10 days of culture in SB431542 supplemented medium, cells were continuously cultured in standard MSC culture medium containing FBS (composition see section 2.1.4) on TCP. The first passage on TCP is referred to as mesenchymal passage 0 (MP0) from here on. Double the number of cells as stated in [182] were seeded onto TCP at MP0 (80,000 cells/cm^2 instead of 40,000 cells/cm^2) to aid adaptation and proliferation of the cells through cell-cell contacts. With increasing passage number, seeding density was reduced (40,000 cells/cm^2 at MP1 and 20,000 cells/cm^2 for all subsequent passages) in accordance with the published protocol [182]. Morphology was monitored over six passages by bright field microscopy (Figure 3.12).

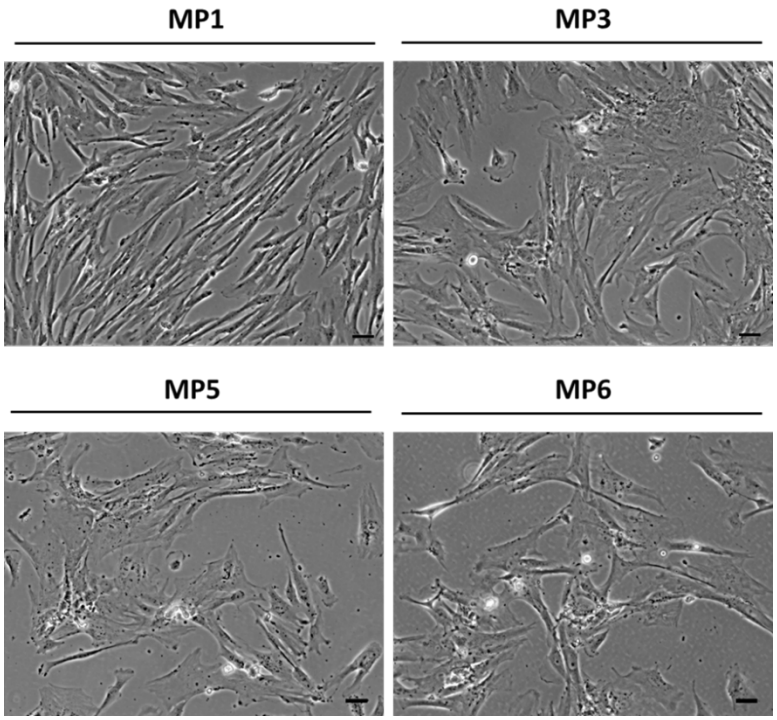

Figure 3.12 Change of morphology of NIBSC-8 iPSCs treated with SB431542 supplemented differentiation medium for 10 days over several passages (MP1, MP3, MP6) on TCP in MSC medium MP: mesenchymal passage; scale bar: 50 μm.

Cells seeded in T175cm^2 flasks for *in vitro* expansion showed rapid attachment to TCP and fibroblast-like morphology. Reduced cell growth was observed during culture, from MP3 and further declined until MP6. Additionally, cells at MP5 and MP6 showed initial cluster formation after seeding followed by a slow increase in cell number. Cell growth was investigated by using alamarBlue® cell viability assay (see section 2.2.1). Analysis of cell viability of NIBSC-8 MSC generation during *in vitro* expansion showed no significant difference in fluorescence intensity from MP1 to MP6 (Figure 3.13, Table 3.2).

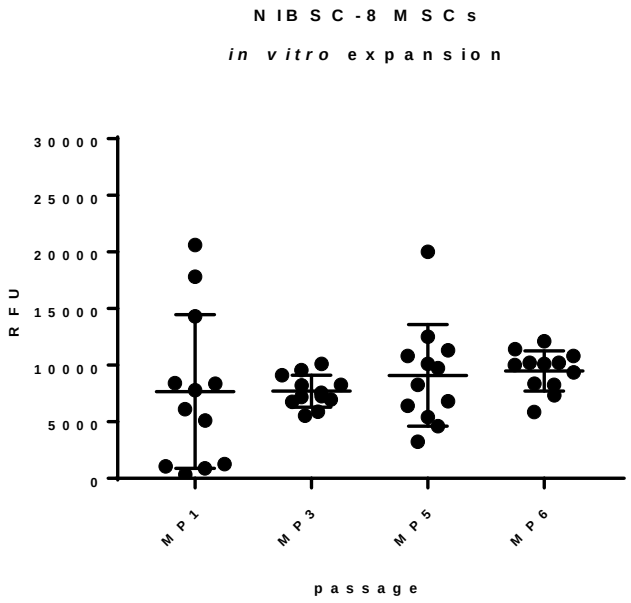

Figure 3.13 Analysis of cell viability and proliferation in NIBSC-8 MSCs during *in vitro* expansion using alamarBlue® cell viability assay. Cells were seeded in 96-wells (20,000 cells/cm^2) as four replicates (n = 4) and cultured in MSC medium for 24 h. MSC medium was mixed with 1:10 of alamarBlue® reagent, incubated for 4 h at 37°C and fluorescence emission measured at 580-610 nm (peak emission 585 nm) in a plate reader. Measured fluorescence of cells without cells was subtracted from values obtained. Mean +/- SD displayed from 4 replicates (N = 4) from n = 3 for each mesenchymal passage (MP). One-way ANOVA with Dunnett's post-hoc test was used to compare statistical significance between passage MP1 and higher passages for all replicates.

Table 3.2 Mean values of cell viability and proliferation in NIBSC-8 MSCs during *in vitro* expansion using alamarBlue® cell viability assay. Cells were seeded in 96-wells (20,000 cells/cm^2) as four replicates (n = 4) and cultured in MSC medium for 24 h. MSC medium was mixed with 1:10 of alamarBlue® reagent, incubated for 4 h at 37°C and fluorescence emission measured at 580-610 nm (peak emission 585 nm) in a plate reader. Measured fluorescence of cells without cells was subtracted from values obtained from wells with seeded cells. One-way ANOVA with Dunnett's post-hoc test was used to compare statistical significance between passage MP1 and higher passages for all replicates. n = 3 experiments.

passage	**MP1**	**MP3**	**MP5**	**MP6**
mean +/- SD	15336.88 +/- 14270	15409.89 +/- 2137	18205.67 +/- 5246	18979.09 +/- 2934

Analysis of gene expression of *OCT*4, *NANOG*, *cMYC* and *SOX*2 as well as genes with positive and negative effect on EMT, as already analysed for day 10, was performed for cells undergoing maturation on TCP in standard MSC medium at MP0 – MP6 in order to assess expression levels of those genes at higher passages.

Expression of core pluripotency genes (*OCT*4, *NANOG*, *cMYC*, *SOX*2), genes positive (*SNAI*1, *SNAI*2, *VIM*, *CDH*2, *ZEB*1, *ZEB*2) and negatively (*CDH*1, *CRB*3, *EpCAM*, *OCLN*, *CLDN*1) regulated genes during epithelial-to-mesenchymal transition were analysed at passages MP0, MP1, MP3, MP6 and normalised to day 0 (Figure 3.14 - Figure 3.16, Table 3.3). Gene expression data from day 10 (Figure 3.5 - Figure 3.7, Table 3.3) were included for comparison.

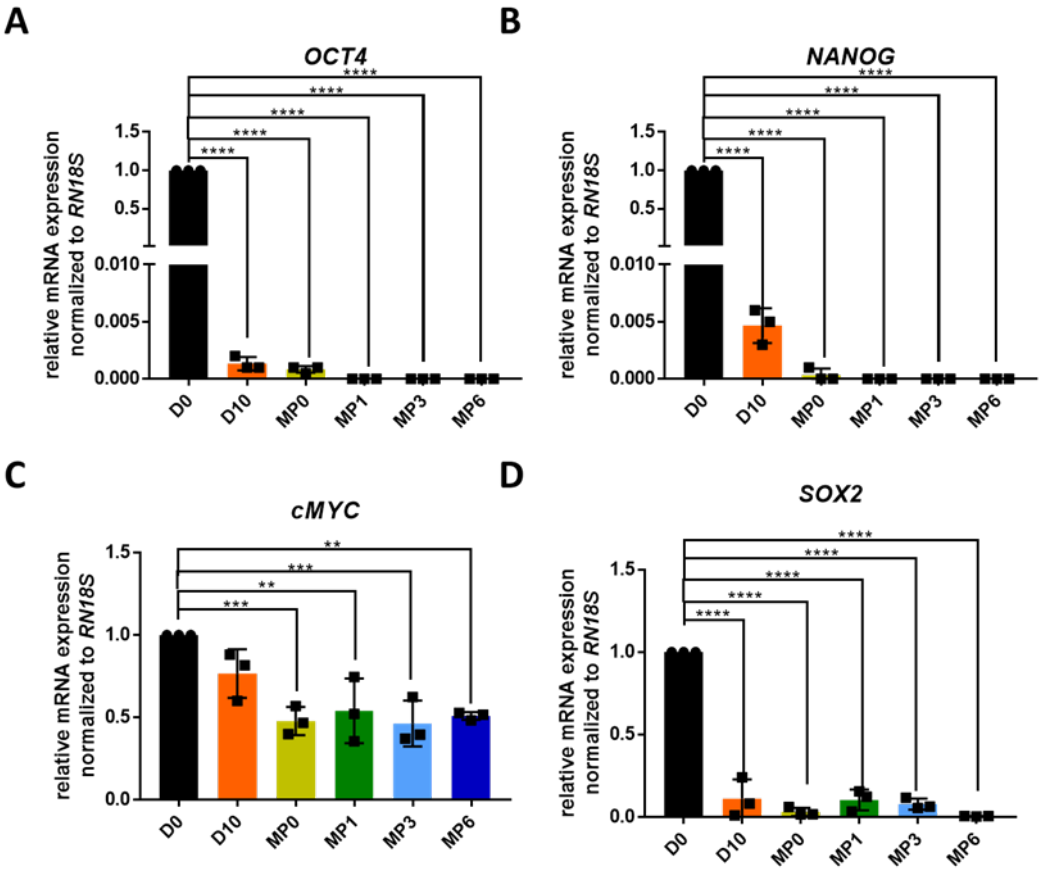

Figure 3.14 Expression of core pluripotency genes *OCT*4 (A), *NANOG* (B), *SOX*2 (C) and *cMYC* (D) after 10 days of treatment with SB431542 supplemented differentiation medium and at mesenchymal passages (MP) 0, 1, 3, 6. Gene expression displayed as mean +/- SD and normalised to *RN18S* (subunit of 18S ribosomal RNA) at day 0. Differentiation into NIBSC-8 MSCs with subsequent passaging was performed three times (n = 3). One-way ANOVA with Dunnett's post-hoc test was performed to compare SB431542 treated NIBSC-8 iPSCs at day 10 and passaged NIBSC-8 MSCs with untreated NIBSC-8 iPSCs at day 0. OCT4: octamer-binding

transcription factor 4; cMYC: MYC proto-oncogene; SOX2: SRY (sex determining region Y)-box 2; NANOG: Homeobox transcription factor NANOG. Differentiation into NIBSC-8 MSCs with subsequent passaging was performed three times (n = 3). ** $p < 0.01$; *** $p < 0.001$; **** $p < 0.0001$.

Expression of pluripotency genes *OCT4*, *NANOG*, *cMYC* and *SOX*2 decreased with passage of NIBSC-8 MSCs on TCP (Figure 3.14, Table 3.3). *OCT*4 and *NANOG* showed a significant ($p < 0.0001$) decrease in expression at day 10 (*OCT*4: 0.001-fold change expression; *NANOG*: 0.001-fold change expression) and a further decrease at MP0 (*OCT4*: 0.001-fold change expression, *NANOG*: 0.001-fold change; $p < 0.0001$). Expression could not be detected at MP1, MP3 and MP6 by qRT-PCR (Figure 3.14 A and B, Table 3.3) for *OCT4* and *NANOG*. *cMYC* mRNA levels at day 10 did not show a significant change compared to day 0. However, *cMYC* expression decreased in all subsequent passages following day 10 (MP0: 0.48-fold change expression; MP1: 0.54-fold change expression; MP3: 0.46-fold change expression), $p < 0.001$ (Figure 3.14 C, Table 3.3). *SOX2* showed a similarly significant ($p < 0.0001$) decreased expression as for *OCT4* and *NANOG* (day 10: 0.11-fold change expression; MP0: 0.03-fold change expression; MP1: 0.10-fold change expression; MP3: 0.08-fold change expression) compared to day 0 (Figure 3.14 D, Table 3.3). Pluripotency genes *OCT4* and *NANOG* showed no expression at MP6 while *SOX2* and *cMYC* showed a modest expression (*SOX2*: 0.005-fold change expression, $p < 0.0001$; *cMYC*: 0.51-fold change expression, $p < 0.0001$), (Figure 3.14 C and D, Table 3.3).

SNAI1 expression at day 10 showed 0.46-fold change compared to day 0, 1.55-fold change at MP0 compared to day 0 followed by an increase to 3.37-fold change compared to day at MP1 ($p < 0.05$). Expression in MP3 and MP6 was similar with 1.45-fold change compared to day 0 at MP3 and 1.66-fold change compared to day 0 (Figure 3.15 A, Table 3.3), yet insignificantly different in either D10, MP0, MP3 and MP6 compared to day. *SNAI2* could not be detected at day 0, therefore gene expression was normalised to day 10. *SNAI2* expression showed 4.56-fold change expression at MP0, 4.12-fold change expression at MP1, 2.38-fold change expression at MP3 and 4.43-fold change expression at MP6 (all compared to day 0) (Figure 3.15 B, Table 3.3). Due to the great standard deviation in all tested passages, *SNAI2* expression was not significantly different in either passage compared to day 10. *ZEB1* expression demonstrated 17.62-fold change expression at day 10, then fluctuated slightly with little change observed with increasing passage (MP0: 12.33-fold change expression; MP1: 15.71-fold change expression; MP3: 16.50-fold change

expression). Gene expression at MP6 showed 29.43-fold change compared to day 0 (Figure 3.15 C, Table 3.3). Increased standard deviation in all tested passaged resulted in insignificant ZEB1 expression in all passages compared to day 0. *ZEB2* expression showed 41.98-fold change at day 10 compared to day 0, 91.05-fold change at MP0, 137.22-fold change at MP1, 126.10-fold change at MP3 and 85.38-fold change at MP6 (Figure 3.15 D, Table 3.3). Due to the great standard deviation in all tested passages, *SNAI2* expression was not significantly different in either passage compared to day 10.

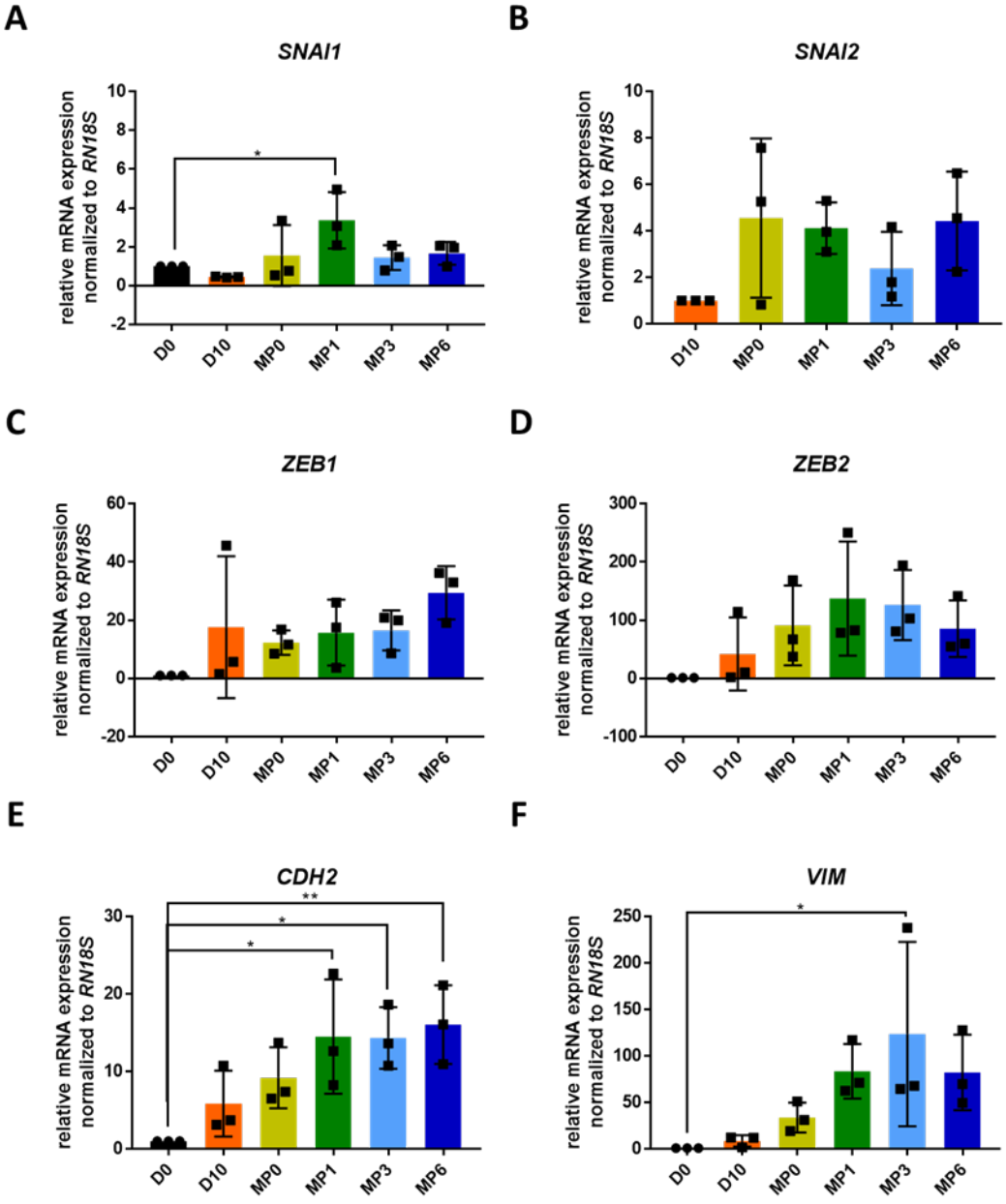

Figure 3.15 Expression of genes with a positive effect on epithelial-to-mesenchymal transition (EMT). *SNAI*1 (A), *SNAI*2 (B), *ZEB*1 (C), *ZEB*2 (D), *CDH*2 (E) and *VIM* (F) 10 days of treatment with SB431542 supplemented differentiation medium and at mesenchymal passages (MP)

0, 1, 3, 6. Gene expression displayed as mean +/- SD and was normalised to *RN18S* (subunit of 18S ribosomal RNA) at day 0. Differentiation into NIBSC-8 MSCs with subsequent passaging was performed three times (n = 3). One-way ANOVA with Dunnett's post-hoc test was performed to compare SB431542 treated NIBSC-8 iPSCs at day 10 and passaged NIBSC-8 MSCs with untreated NIBSC-8 iPSCs at day 0. SNAI1: snail family transcriptional repressor 1; ZEB1: Zinc finger E-Box Binding Homeobox 1; ZEB2: Zinc finger E-Box Binding Homeobox 2; VIM: vimentin; CDH2: N-Cadherin. Differentiation into NIBSC-8-MSCs with subsequent passaging was performed three times (n = 3). * $p < 0.05$; ** $p < 0.01$

CDH2 demonstrated 5.87-fold change at day 10 compared to day 0 and 9.20-fold change at MP0 compared to day 0. However, there was no significant difference in *CDH2* expression at day 10 and MP0 compared to day 0. Gene expression increased to 14.51-fold change expression ($p < 0.05$) at MP1 (Figure 3.15 D, Table 3.3). Gene expression plateaued between MP1 and MP3 (14.34-fold change expression) with a significant increase at MP3 (13.30-fold change change compared to day 0) ($p < 0.05$). *CDH2* mRNA showed further an increase in expression at MP6 (16.06-fold change expression compared to day 0, $p < 0.01$) (Figure 3.15 D, Table 3.3). Relative to day 0 as control, *VIM* expression at day 10 showed 7.75-fold change, 33.92-fold change at MP0 and 83.70-fold change at MP1, however no significant difference in gene expression between day 0 and either day 10, MP0 and MP1 was detected. Gene expression at MP3 showed increase in expression compared to day 0 (123.640-fold change expression, $p < 0.05$). MP6 demonstrated 82.39-fold change compared to day 0 (Figure 3.15 E, Table 3.3), yet without demonstrating a significant difference to day 0.

Genes negatively regulated during EMT were significantly downregulated with passage number (*EpCAM* and *CDH1*) or could not be detected by qRT-PCR (*CRB3*), (Figure 3.16, Table 3.3).

CRB3 showed 0.83-fold change compared to day 0 at day 10, however no significant difference. *CRB3* expression could not be detected in passages MP0 – MP6 ($p < 0.001$, Figure 3.16 A, Table 3.3). *EpCAM* at day 10 showed no significant change in expression between day 0 and day 10 (0.76-fold change compared to day 0). A significant decrease with almost undetectable mRNA expression at MP0 (0.03-fold change, $p < 0.001$) and at MP1 (0.04-fold change expression, $p < 0.001$) compared to day 0 was detected. Expression could not be detected in MP3 and MP6 by qRT-PCR ($p < 0.0001$), (Figure 3.16 B, Table 3.3).

CDH1 mRNA demonstrated no significant difference in expression between day 0 and day 10 (2.10-fold change expression at day 10 compared to day 0). A significant decrease until MP1 (MP0: 0.05-fold change expression, $p < 0.01$; MP1: 0.02-fold change expression, $p < 0.01$). *CDH1* expression could not be detected in MP3 and MP6. Decrease in mRNA expression at MP3 and MP6 compared to day 0 was statistically significant (MP3: $p < 0.01$; MP6: $p < 0.01$), (Figure 3.16 C, Table 3.3).

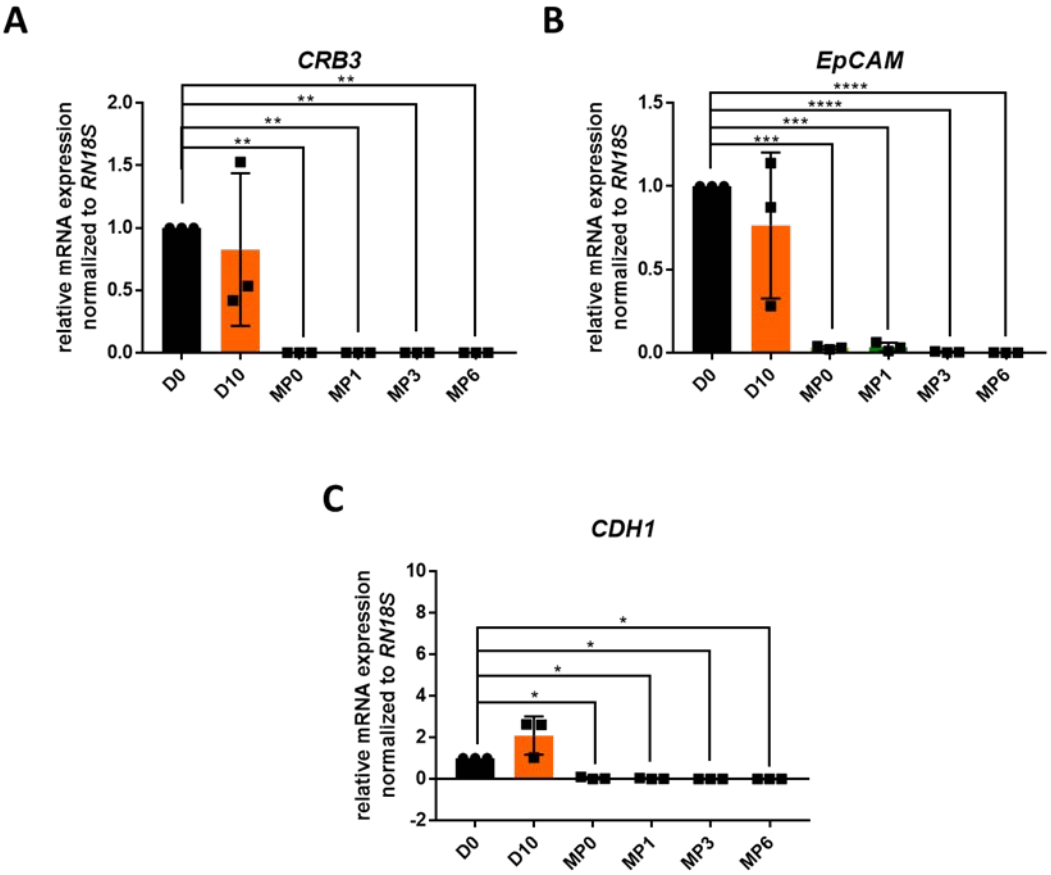

Figure 3.16 Expression of genes with a negative effect on epithelial-to mesenchymal transition (EMT) *CRB3* (A), *CDH*1 (B) and *EpCAM* (C) after 10 days of treatment with SB431542 supplemented differentiation medium and at mesenchymal passages (MP) 0, 1, 3, 6. Gene expression is displayed as mean +/- SD and was normalised to *RN18S* (subunit of 18S ribosomal RNA) at day 0. Differentiation into NIBSC-8 MSCs with subsequent passaging was performed three times (n = 3). One-way ANOVA with Dunnett's post-hoc test was performed to compare SB431542 treated NIBSC-8 iPSCs at day 10 and passaged NIBSC-8 MSCs with untreated NIBSC-8 iPSCs at day 0. CRB3: crumbs 3; CDH1: E-Cadherin; EpCAM: epithelial cell adhesion molecule. Differentiation into NIBSC-8 MSCs with subsequent passaging was performed three times (n = 3). ** $p < 0.01$; *** $p < 0.001$; **** $p < 0.0001$.

Table 3.3 Summary of gene expression characteristic for epithelial-to-mesenchymal transition (EMT) following treatment with SB431542 supplemented medium for 10 days and subsequent passage in MSC medium. Gene expression was normalised to *RN18S* (subunit of 18S ribosomal RNA) at day 0. Differentiation into NIBSC-8 MSCs with subsequent passaging was performed three times (n = 3). OCT4: octamer-binding transcription factor 4; c-MYC: MYC proto-oncogene, EMT: epithelial-to-mesenchymal transition, SNAI1: snail family transcriptional repressor 1; SNAI2: snail family transcriptional repressor 2; ZEB1: Zinc finger E-Box Binding Homeobox 1; ZEB2: Zinc finger E-Box Binding Homeobox 2; VIM: vimentin, CDH1: E-Cadherin; CDH2: N-Cadherin, CRB3: crumbs 3, EpCAM: epithelial cell adhesion molecule.

Gene	Day 10	MP0	MP1	MP3	MP6
OCT4	0.001 +/- 0.0006	0.001 +/- 0.0003	0.000 +/- 0.0000	0.000 +/- 0.0000	0.000 +/- 0.0000
NANOG	0.005 +/- 0.002	0.001 +/- 0.0006	0.000 +/- 0.0000	0.000 +/- 0.0000	0.000 +/- 0.0000
c-MYC	0.77 +/- 0.15	0.48 +/- 0.09	0.54 +/- 0.20	0.46 +/- 0.14	0.51 +/- 0.02
SOX2	0.11 +/- 0.12	0.03 +/- 0.03	0.10 +/- 0.06	0.08 +/- 0.03	0.00 +/- 0.00
SNAI1	0.46 +/- 0.03	1.55 +/- 1.57	3.37 +/- 1.46	1.45 +/- 0.64	1.66 +/- 0.59
SNAI2	1.00 +/- 0.00	4.56 +/- 3.43	4.12 +/- 1.11	2.38 +/- 1.58	4.43 +/- 2.13
ZEB1	17.62 +/- 24.37	12.33 +/- 4.21	15.71 +/- 11.30	16.50 +/- 6.85	29.43 +/- 9.12
ZEB2	41.98 +/- 62.68	91.05 +/- 68.56	137.22 +/- 98.09	126.10 +/- 60.14	85.38 +/- 48.61
CDH1	2.10 +/- 0.92	0.05 +/- 0.05	0.02 +/- 0.02	0.00 +/- 0.00	0.00 +/- 0.00
CDH2	5.87 +/- 4.25	9.20 +/- 3.93	14.51 +/- 7.36	14.34 +/- 3.98	16.06 +/- 5.08
EpCAM	0.76 +/- 0.44	0.03 +/- 0.01	0.04 +/- 0.03	0.00 +/- 0.00	0.00 +/- 0.00
CRB3	0.83 +/- 0.61	0.00	0.00	0.00	0.00

Gene	Day 10	MP0	MP1	MP3	MP6
		+/- 0.00	+/- 0.00	+/- 0.00	+/- 0.00
VIM	8.75 +/- 6.09	33.92 +/- 16.08	83.70 +/- 29.41	123.64 +/- 99.12	82.40 +/- 40.54

All pluripotency genes were significantly downregulated at day 10 as well as all mesenchymal passages MP0 – MP6 compared to NIBSC-iPSCs at day 0. *SNAI1*, *CDH2* and *VIM*, genes with a positive effect on EMT, were significantly upregulated in one or more mesenchymal passages. *CRB3*, *EpCAM* and *CDH1*, genes negatively affected during EMT, were significantly decreased in all mesenchymal passages.

3.3.3 Osteogenic differentiation of NIBSC-8 MSCs

After 6 passages on TCP, NIBSC-8 MSCs were tested for osteogenic differentiation potential using standard osteogenic medium (oBG) as well as standard osteogenic medium supplemented with two small moledcules (oBG + TH + SAG) in order to determine whether the additon of small molecules promotes the differentiation outcome compared to the standard osteogenic medium.

NIBSC-8 MSCs were treated with a combination of 1 µM TH and 1 µM SAG (each supplemented with osteogenic background medium (oBG) consisting of 10 nM dexamethasone, 10 nM 1,25-$(OH)_2$-vitamin D_3 and 100 µM ascorbic-2-phosphate) for 19 days as monolayer. Cells were analysed using histological methods (alkaline phosphatase (ALP) staining, alcian blue staining, alizarin red staining) and expression of genes characteristic for osteogenesis (*RUNX*2, *ALPL*, *COL1A1*, *OCN*, *OPN*) as well as chondrogenesis (*COL2A1*, *ACAN*) was compared between the different media combinations using qRT-PCR.

ALP staining (Figure 3.17) showed an increase in intensity over the time course of differentiation in osteogenic and basal medium conditions, with equally intense staining at day 19 in both osteogenic culture conditions in all three independent studies. oBG supplemented with TH and SAG in differentiation experiment 1 resulted in the strongest staining after 19 days. ALP staining was less intense in experiment 3 compared to the other two differentiation experiments. The negative control (NIBSC-8 MSCs cultured under basal medium in absence of osteogenic differentiation components) showed negligible staining after 7 days of differentiation in any of the three individual differentiation experiments.

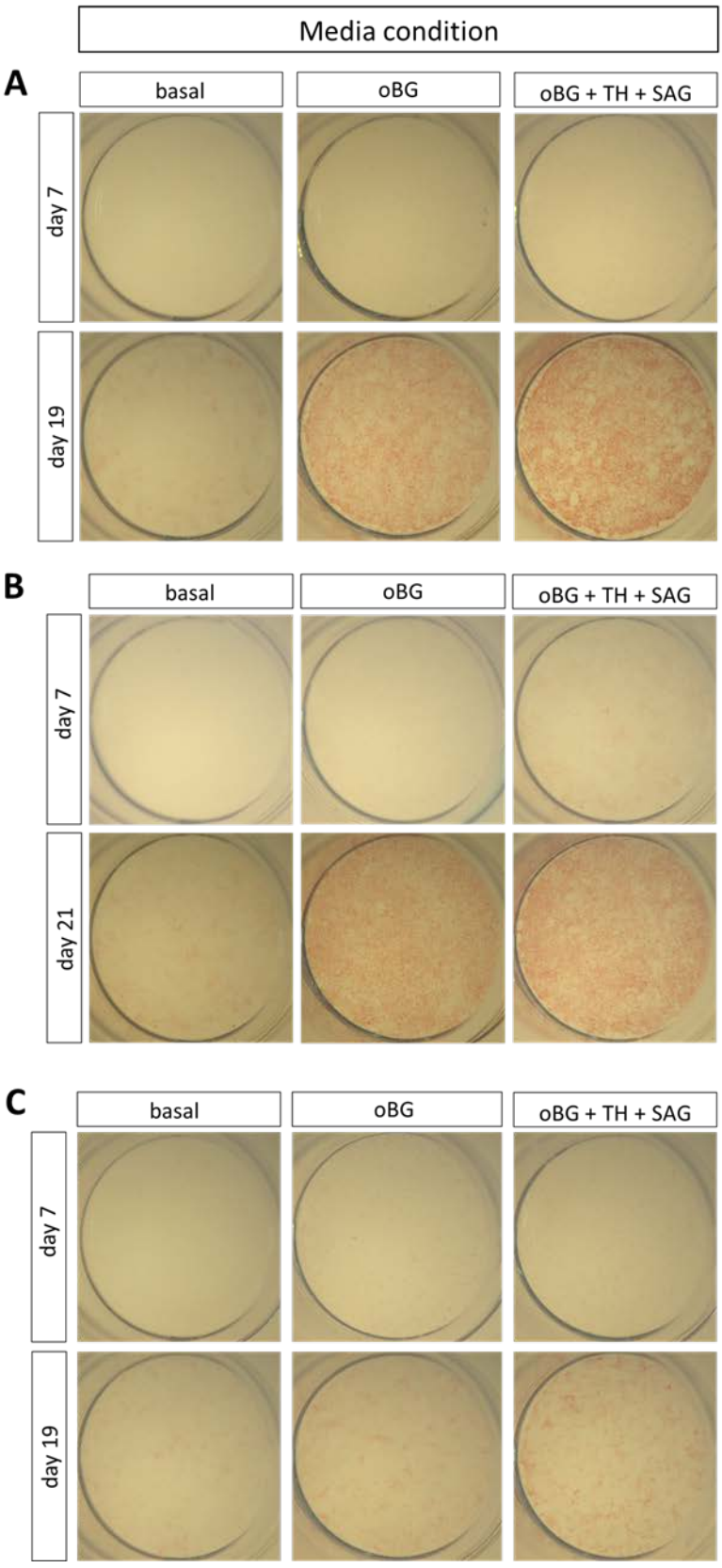

Figure 3.17 Alkaline phosphatase (ALP) staining in NIBSC-8 MSCs treated with basal medium, osteogenic background medium (oBG, 10 nM dexamethasone, 10 nM 1,25-$(OH)_2$-vitamin D_3 and 100 µM ascorbic-2-phosphate) and osteo background (oBG) medium supplemented

with small molecules SAG (smoothened agonist) and TH (4-(4-methoxyphenyl)pyrido[4′,3′:4,5]thieno[2,3-b]pyridine-2-carboxamide). Results of three individual differentiation experiments in 24-wells are displayed in **A**: experiment 1, **B**: experiment 2 and **C**: experiment 3. Images display entire 24-well.

Alcian blue staining, commonly used to stain polysaccharides (e.g. glycosaminoglycans (GAGs) in cartilage), was widely distributed in all three differentiation experiments with NIBSC-8 MSCs (Figure 3.18). Alcian Blue staining showed temporal continuous increase in intensity in NIBSC-8 MSCs under osteogenic media conditions (oBG and oBG + TH + SAG) over the time course of differentiation. NIBSC-8 MSCs under basal culture conditions also demonstrated faint staining at day 7 and day 19 of culture, however, with less intensity compared to NIBSC-8 MSCs cultured under osteogenic media conditions. NIBSC-8 MSCs after 7 days showed faint staining in all three culture conditions. No difference in staining intensity were observed in the three independent differentiation experiments in any of the two time points.

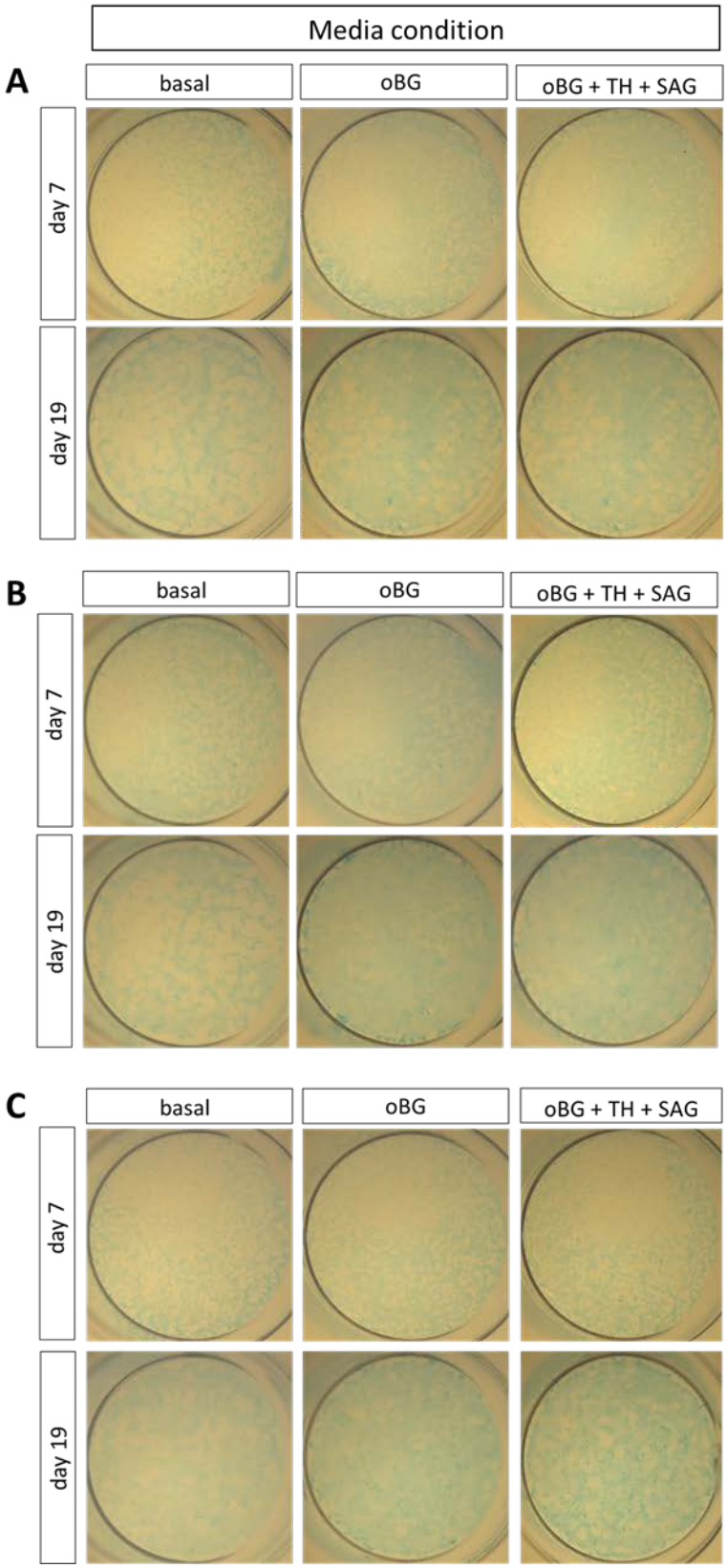

Figure 3.18 Alcian Blue staining in NIBSC-8 MSCs treated with basal medium, osteogenic background medium (oBG, 10 nM dexamethasone, 10nM 1,25-$(OH)_2$-vitamin D_3 and 100 µM ascorbic-2-phosphate) and osteo background (oBG) medium supplemented with small molecules SAG (smoothened agonist) and TH (4-(4-methoxyphenyl)pyrido[4′,3′:4,5]thieno[2,3-

b]pyridine-2-carboxamide). Results of three individual differentiation experiments in 24-wells are displayed in **A**: experiment 1, **B**: experiment 2 and **C**: experiment 3. Images display entire 24-well.

To determine the efficiency of mineralisation, alizarin red staining (Figure 3.19) was performed. Alizarin red staining was widely distributed in the NIBSC-8 MSCs monolayer cultures as opposed to the demonstration of compact nodule-like structures [345]. Treatment with basal or osteogenic medium did not result in measurable differences in alizarin red staining after 7 and 19 days in all three performed differentiation experiments.

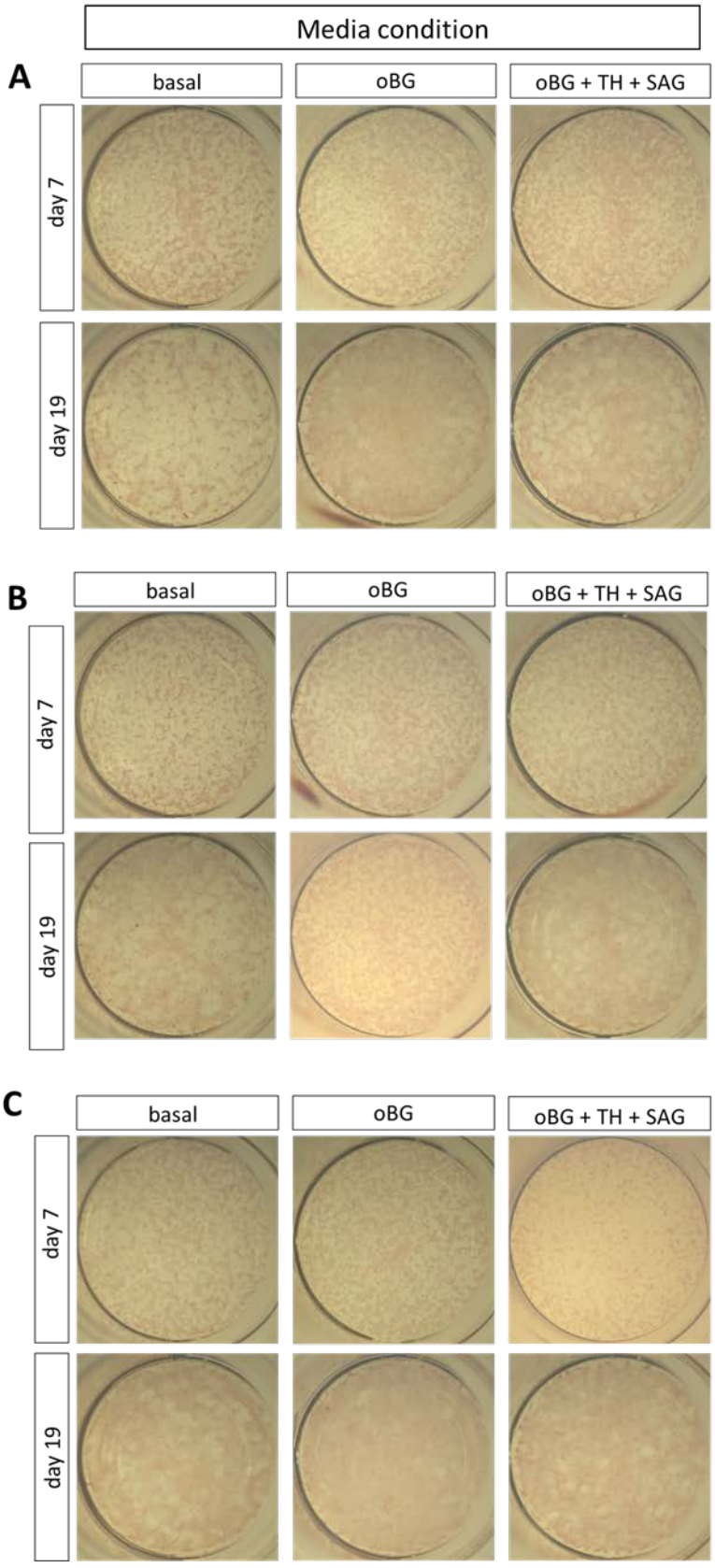

Figure 3.19 Alizarin Red staining in NIBSC-8 MSCs treated with basal medium, osteogenic background medium (oBG, 10 nM dexamethasone, 10 nM 1,25-$(OH)_2$-vitamin D_3 and 100 µM ascorbic-2-phosphate) and osteo background (oBG) medium supplemented with small molecules

SAG (smoothened agonist) and TH (4-(4-methoxyphenyl)pyrido[4′,3′:4,5]thieno[2,3-b]pyridine-2-carboxamide). Results of three individual differentiation experiments in 24-wells are displayed in **A**: experiment 1, **B**: experiment 2 and **C**: experiment 3. Images display entire 24-well.

NIBSC-8 MSCs demonstrated overall faint ALP, Alcian Blue and Alizarin Red staining in all tested conditions and timepoints. Staining intensity of ALP and Alican Blue was arguably slightly higher in NIBSC-8 MSCs after 19 days of culture in oBG + TH + SAG compared to oBG and basal culture conditions. Alizarin Red staining did not show any difference in staining intensity in any of the tested conditions or timepoints. Due to ALP reportedly being secreted by osteoblasts during the mineralisation process [346] and Alizarin Red indicating sites of mineralisation, the findings suggest a low outcome of osteogenesis in generated NIBSC-8 MSCs after 19 days culture in oBG + TH + SAG.

Gene expression profile of marker genes in both osteogenic differentiation (*RUNX*2, *ALPL*, *OCN*, *OPN*, *COL1A1*) and chondrogenesis (*COL2A1*, *ACAN*) was analysed using qRT-PCR in order to investigate the success of the osteogenic differentiaton of the generated NIBSC-8 MSCs.

Osteogenic genes

A key regulator for osteogenesis, ***RUNX2***, showed no significant increase between day 7 and day 19 in all three conditions (Figure 3.20A, Table 3.4, Appendix G). Cells cultured under basal conditions demonstrated 0.58-fold change expression after 7 days and 0.63-fold change expression after 19 days. *RUNX2* mRNA was found to be 1.16-fold change expressed in NIBSC-8 MSCs treated with oBG medium for 7 days and 1.04-fold change after 19 days. NIBSC-8 MSCs cultured in oBG + TH + SAG showed 0.83-fold change expression after 7 days of culture and 0.94-fold change expression after 19 days (Figure 3.20 A, Table 3.4, Appendix G).

ALPL mRNA expression under basal culture conditions was1.54-fold change expression after 7 days of culture followed by 1.47-fold change expression after 19 days of culture (Figure 3.20 B, Table 3.4, Appendix G), thus demonstrating an insignificant difference in *ALPL* expression under basal culture conditions at day 7 and day 19 compared to day 0. Treatment of NIBSC-8 MSCs with oBG resulted in 4.71-fold change expression after 7 days and 4.19-fold change expression after 19 days, however due to high standard deviation at both timepoints (day 7 and day 19) no significant difference in gene expression compared to

day 0 could be detected. *ALPL* expression in NIBSC-8 MSCs cultured in oBG + TH + SAG ostegenic medium showed 4.65-fold change expression after 7 days (without a significant difference in gene expression compared to day 0) and a significant increase in gene expression after 19 days (6.58-fold change compared to day 0, $p < 0.05$, 1.93-fold change increase compared to day 7) (Figure 3.20 B, Table 3.4, Appendix G).

COL1A1 expression under basal culture conditions demonstrated no significant difference between either day 7 or day 19 compared to day 0 with 1.04-fold change expression after 7 days of culture and 0.79-fold change expression after 19 days of culture (Figure 3.20 C, Table 3.4, Appendix G). In oBG treated NIBSC-8 MSCs, expression was significantly increased between day 0 and day 7 (2.10-fold change expression compared to day 0, $p < 0.05$). Gene expression in NIBSC-8 MSCs cultured in oBG for 19 days was significantly different compared to day 0 (0.83-fold change expression). Cells treated with oBG + TH + SAG medium did not demonstrate a significant difference in *COL1A1* expression after either 7 days or 19 days of culture (1.30-fold change expression after 7 days of culture and 0.76-fold change expression after 19 days) (Figure 3.20 C, Table 3.4, Appendix G).

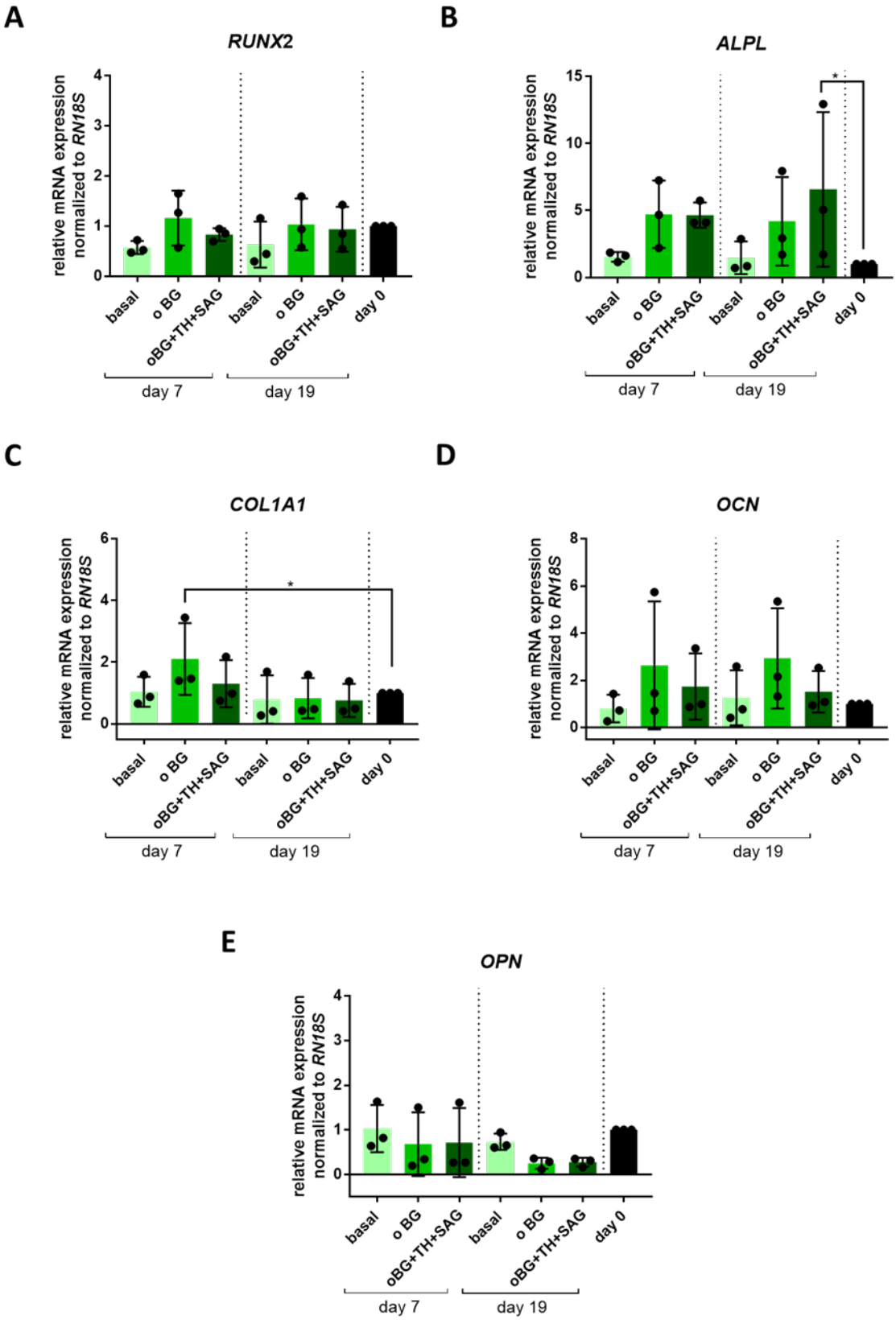

Figure 3.20 Expression of genes characteristic for osteogenic differentiation in NIBSC-8 MSCs treated with basal medium, osteogenic background medium (oBG, 10 nM dexamethasone, 10 nM 1,25-$(OH)_2$-vitamin D_3 and 100 µM ascorbic-2-phosphate) and osteo background (oBG)

medium supplemented with small molecules SAG (smoothened agonist) and TH (4-(4-methoxyphenyl)pyrido[4′,3′:4,5]thieno[2,3-b]pyridine-2-carboxamide). Gene expression is displayed as mean +/- SD and was normalised to *RN18S* at day 0 in basal medium. Two-way ANOVA with Dunnett's post-hoc test for multiple comparisons was performed to compare different culture conditions of n = 3 differentiation experiments. * $p < 0.05$. RUNX2: runt-related transcription factor 2; ALPL: alkaline phosphatase; COL1A1: collagen type 1; OCN: osteocalcin; OPN: osteopontin, RN18S: subunit 18S ribosomal RNA.

.

OCN mRNA showed no significant difference between day 7 and day 19 in all three conditions compared to day 0 (Figure 3.20 D, Table 3.4, Appendix G). *OCN* expression under basal culture conditions in NIBSC-8 MSCs was observed to be 0.80-fold change expression after 7 days of culture and 1.26-fold change expression after 19 days NIBSC-8 MSCs cultured in oBG medium for 7 days showed 2.63-fold change expression and NIBSC-8 MSCs cultured for 19 days showed 2.93-fold change after 19 days. Cells cultured in oBG + TH + SAG for 7 days demonstrated 1.74-fold change expression and 1.52-fold change expression after 19 days.

Culture of NIBSC-8 MSCs showed no significant difference in ***OPN*** expression between day 7 and day 19 in all three conditions compared to day 0 (Figure 3.20 E, Table 3.4, Appendix G). In basal culture medium for 7 days showed 1.03-fold change in *OPN* expression and 0.73-fold change in *OPN* expression after 19 days of culture Treatment with oBG medium resulted in 0.68-fold change expression after 7 days of culture and 0.25-fold change expression afer 19 days of culture. oBG + TH + SAG medium demonstrated 0.72-fold change expression in NIBSC-8 MSCs after 7 days of culture and 0.28-fold change after 19 days of culture.

Table 3.4 Summary of respective gene expression characteristic for osteogenesis in NIBSC-8 MSCs treated with basal medium, osteogenic background medium (oBG, 10 nM dexamethasone, 10 nM 1,25-$(OH)_2$-vitamin D_3 and 100 µM ascorbic-2-phosphate) and osteo background (oBG) medium supplemented with small molecules SAG (smoothened agonist) and TH (4-(4-methoxyphenyl)pyrido[4′,3′:4,5]thieno[2,3-b]pyridine-2-carboxamide). Gene expression displayed as mean +/- SD and was normalised to *RN18S* at day 0 in basal medium. Osteogenic differentiation was performed three times (n = 3). RUNX2: runt-related transcription factor 2; ALPL: alkaline phosphatase; COL1A1: collagen type 1; OCN: osteocalcin; OPN: osteopontin.

	condition	*RUNX2*	*ALPL*	*COL1A1*	*OCN*	*OPN*
Day 7	basal	0.58 +/- 0.13	1.54 +/- 0.36	1.04 +/- 0.49	0.80 +/- 0.58	1.03 +/- 0.53
	oBG	1.16 +/- 0.55	4.71 +/- 2.52	2.10 +/- 1.16	2.63 +/- 2.71	0.68 +/- 0.71
	oBG + TH + SAG	0.83 +/- 0.13	4.65 +/- 0.94	1.30 +/- 0.76	1.74 +/- 1.40	0.72 +/- 0.77
Day 19	basal	0.63 +/- 0.46	1.47 +/- 1.21	0.79 +/- 0.78	1.26 +/- 1.17	0.73 +/- 0.18
	oBG	1.04 +/- 0.51	4.19 +/- 3.30	0.83 +/- 0.65	2.93 +/- 2.12	0.25 +/- 0.12
	oBG + TH + SAG	0.94 +/- 0.45	6.58 +/- 5.77	0.76 +/- 0.54	1.52 +/- 0.88	0.28 +/- 0.10

Chondrogenic genes

Culture of NIBSC-8 MSCs showed no significant difference in ***COL2A1*** expression between day 7 and day 19 in all three conditions compared to day 0 (Figure 3.21A, Table 3.5, Appendix G). In basal culture medium for 7 days resulted in 0.78-fold change *COL2A1* expression while culture for 19 days resulted in 0.81-fold change expression. Treatment with oBG medium demonstrated 0.52-fold change expression after 7 days of culture and 0.81-fold change expression after 19 days. oBG + TH + SAG showed 0.75-fold change expression in NIBSC-8 MSCs after 7 days and 1.40-fold change expression after 19 days. ***ACAN*** showed no significant difference in expression between day 7 and day 19 in all three conditions compared to day 0 except under oBG + TH + SAG after 7 days (2.13-fold change expression, $p < 0.05$) (Figure 3.21 B, Table 3.5, Appendix G). *ACAN* expression under basal culture conditions was observed to be 0.95-fold change expression after 7 days and 0.52-fold change expression after 19 days After 7 days under oBG culture conditions, NIBSC-8 MSCs showed 1.79-fold change expression and 0.40-fold change expression. *ACAN*

expression after 19 days of culture in oBG + TH + SAG medium resulted in 0.54-fold change expression.

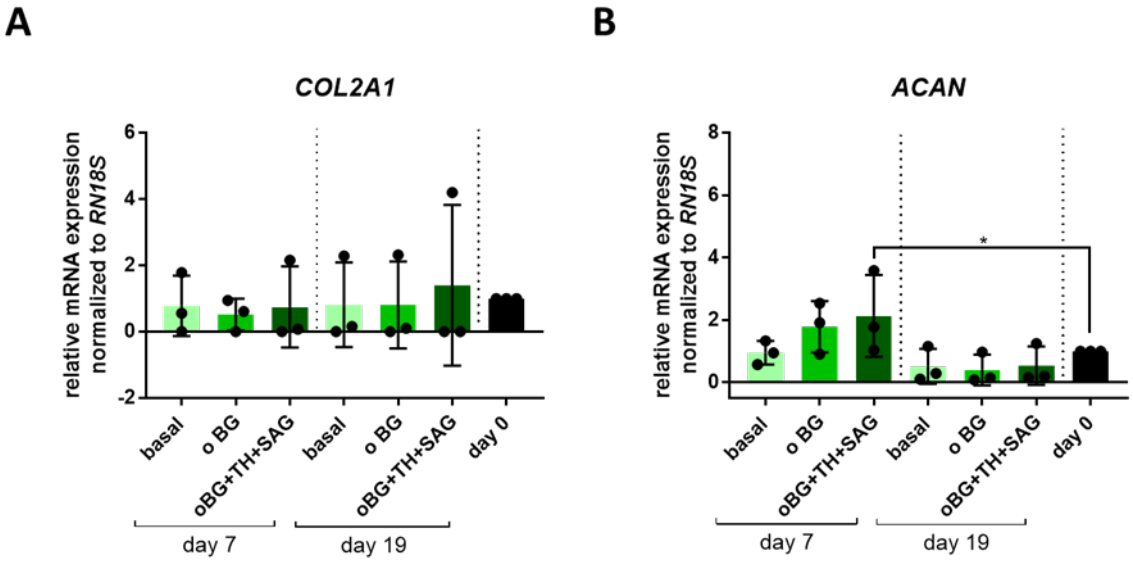

Figure 3.21 Expression of genes characteristic for chondrogenic differentiation in NIBSC-8 MSCs treated with basal medium, osteogenic background medium (oBG, 10 nM dexamethasone, 10 nM 1,25-(OH)$_2$-vitamin D$_3$ and 100 µM ascorbic-2-phosphate) and osteo background (oBG) medium supplemented with small molecules SAG (smoothened agonist) and TH (4-(4-methoxyphenyl)pyrido[4′,3′:4,5]thieno[2,3-b]pyridine-2-carboxamide). Gene expression is displayed as mean +/- SD and was normalised to *RN18S* at day 0 in basal medium. Two-way ANOVA with Dunnett's post-hoc test for multiple comparisons was performed to compare different culture conditions of n = 3 differentiation experiments. * $p < 0.05$. COL2A1: collagen type II; ACAN: aggrecan; RN18S: subunit 18S ribosomal RNA.

Table 3.5 Summary of respective gene expression characteristic for chondrogenesis in NIBSC-8 MSCs treated with basal medium, osteogenic background medium (oBG, 10 nM dexamethasone, 10 nM 1,25-$(OH)_2$-vitamin D_3 and 100 µM ascorbic-2-phosphate) and osteo background (oBG) medium supplemented with small molecules SAG (smoothened agonist) and TH (4-(4-methoxyphenyl)pyrido[4′,3′:4,5]thieno[2,3-b]pyridine-2-carboxamide). Gene expression displayed as mean +/- SD and was normalised to *RN18S* at day 0 in basal medium. Osteogenic differentiation was performed three times (n = 3). COL2A1: collagen type II; ACAN: aggrecan; RN18S: subunit 18S ribosomal RNA.

	condition	***COL2A1***	***ACAN***
Day 7	basal	0.78 +/- 0.91	0.95 +/- 0.38
	oBG	0.52 +/- 0.48	1.79 +/- 0.82
	oBG + TH + SAG	0.75 +/- 1.23	2.13 +/- 1.31
Day 19	basal	0.81 +/- 1.28	0.52 +/- 0.56
	oBG	0.81 +/- 1.31	0.40 +/- 0.49
	oBG + TH + SAG	1.40 +/- 2.42	0.54 +/- 0.62

Gene expression analysis for osteogenic as well as chondrogenic genes after performed osteogenic differentiation of NIBSC-8 MSCs was not significant except for i) *ALPL* being upregulated after 19 days in oBG + TH + SAG medium, ii) *COL1A1* being upregulated in oBG after 7 days of culture and iii) *ACAN* being increased after 7 days under oBG + TH + SAG culture conditions. Due to the lack of significance in gene expression analysis, it is not possible to determine the success or the advantage of any of the two tested osteogenic differentiation media based on gene expression only. However, in combination with the previously gathered histological staining, it can be concluded that generated NIBSC-8 MSCs were able to differentiate towards the osteogenic lineage although with low efficiency.

3.4 Discussion

Generation of iPSC-MSCs has been described in several studies and initial attempts of pluripotent stem cell differentiation into MSC-like cells included embryoid body (EB) formation, sorting for selected surface antigens, co-culture or viral transduction [347-352]. The protocol published by Chen et al. [182] reported a simple one-step, small molecule based method for the generation of iPSC-derived MSCs that did not require expensive and time consuming antibody sorting protocols. The authors claimed that cells developed into mature MSCs within 6 passages after initial 10 days treatment with SB431542 supplemented differentiation medium. The total culture period from iPSCs to mature MSCs was claimed to be less than 30 days. This protocol was chosen in this thesis as established by our collaboration partners in Dusseldorf (Germany), who generated iPSCs from HFBCs as well as aged HBMSCs as donor populations and subsequently used the small molecule based approach [182] to generate iPSC-MSCs.

A standardised control iPSC line (NIBSC-8), reprogrammed from human foetal lung tissue cells (MRC-9), purchased from the NIBSC was used to generate iPSC-derived MSCs by applying the protocol published by Chen et al. [182]. The morphological shift from the round tightly packed iPSC colonies into elongated cells and the significant downregulation of key pluripotency genes confirmed the loss the epithelial and pluripotent character of NIBSC-8 iPSCs after 10 days of culture in SB431542 suplemented medium. During culture on TCP, the cells demonstrated an elongated, fibroblast-like morphology and remaining/further downregulation of pluripotency genes initially (MP0 and MP1). It was observed that *cMYC* showed slower decrease with continuous passaging compared to *OCT4*, *NANOG* and *SOX2*.

CDH2, encoding for N-Cadherin, and *VIM* (both mesodermal markers) were upregulated at MP1 - MP6 and at MP3 respectively. These findings in combination with the significant downregulation of *CDH1*, *CRB3* and *EpCAM* (all characteristic for epithelial cells) indicate the occurance of EMT and adoption of a mesenchymal cell character during culture on TCP in standard MSC medium. Proliferative capacity (measured by alamarBlue® assay) showed only slight increase over the expansion period between MP0 and MP6. alamarBlue® assay was used as the active ingredient, reazuirn, is soluble in cell culture medium, non-toxic and permeable through cell membranes. Therefore, this assay possess considerable advantages over other cell viability assays such as MTT or XTT which employ cytotoxic tetrazolium salts in order to measure cell viability [353]. NIBSC-8 MSCs showed fibroblastic cell

morphology during the expansion process on TCP, however, the maturation process required longer than described in the publication (12 weeks instead of ~3 weeks) and cell number was slightly reduced between passages MP3 and MP5 which limited expansion of cells for subsequent osteogenic differentiation experiments.

Performance of immunocytochemistry staining for E-Cadherin and VIM protein expression in NIBSC-8 iPSCs as well as in NIBSC-8 iPSCs treated with SB431542 for 10 days showed expression of E-Cadherin only in NIBSC-8 iPSCs. VIM expression was not only detected in NIBSC-8 iPSCs treated with SB431542 for 10 days but also in untreated NIBSC-8 iPSCs. This could suggest that the starting population of NIBSC-8 iPSCs is not entirely pure, i.e. does not exclusively contain pluripotent stem cells. The presence of differentiated cells within a supposedly pluripotent cell population is not uncommon in practical handling and culture of iPSCs. In turn, this does pose a certain difficulty with regards to the assessment of the efficiency of the chosen differentiation protocol toward the mesenchymal lineage as cells primed for differentiation toward mesenchymal lineage may release small molecules into the cell culture medium, thus, inducting/facilitating mesenchymal differentiation of pure iPSCs. This observation in turn raises the question if, and to what extent, donor memory influences iPSC-MSC generation. With the donor cell population prior to reprogramming comprising mesenchymal origin, the generation of iPSC-MSCs would be facilitated as a consequence of traits of the mesenchymal donor cells still present in the iPSCs and therefore facilitating the (re-) activation of the mesenchymal genes. The use of a non-mesenchymal donor cell population (human foetal lung tissue cells (MRC-9) in the case of NIBSC-8 iPSCs; fibroblasts in the case of the iPSC lines used in [182]) could result in the generated iPSCs being less receptive to the cues of the mesenchymal differentiation protocol, thus, it would be more difficult to drive the iPSCs toward the mesenchymal lineage. The use of an iPSC line reporgrammed from non-mesenchymal donor cells would prove the efficiency and the ability of the chosen differentiation protocol togenerate iPSC-MSCs from different donor cell types, not MSCs only. Various studies have reported the generation of iPSC-MSCs employing different differentiation media compositions, culture techniques, cell types and starting cell populations (see Table 1.7 in chapter 1.5). Generation of iPSC-MSCs from a control line approved by the NIBSC might potentially have been more successful if a different differentiation protocol would have been chosen in the first instance. However, in order of experimental consistency with our collaboration partners and planned comparison of DNA methylation status in skeletal promoters in different iPSC lines, corresponding

donor populations and generated iPSC-MSCs, the study published by Chen et al. was used [182]. The results of the published study could not be successfully replicated with the standardised NIBSC-8 iPSC line. This could be due to several factors: i) cell number during the maturation process not being high enough or too high, or ii) the practicality of the chosen protocol and the generated cells is questionable as expansion/maturation period was considerably longer than described in the publication. However, in the preliminary data for this differentiation protocol using a different cell line showed a similar decreasing trend in cell number with lower starting cell number used at MP0 compared to NIBSC-8 iPSCs treated with SB431542 for 10 days, which made performance of planned osteogenic differentiation experiments impossible (see Appendix F).

Continuous culture of the generated cells in MSC medium resulted in maturation and expansion, however, the published study by Chen et al. [182] failed to provide an explanation for the chosen endpoint of the maturation period at MP6. Following the published protocol in this regard, it was observed that NIBSC-8 MSCs at MP1 during the maturation/expansion process appeared to grow more rapidly and to display a closer resemblance to a fibroblastic morphology compared to NIBSC-8 MSCs at MP6. Therefore, the necessity to culture iPSC-derived MSCs until MP6 is questionable and could potentially be rendered unnecessary. Instead another measure of the maturation status of the iPSC-derived MSCs should be chosen. Furthermore, it was reasoned that iPSC-MSCs resembled the phenotypic characteristics of primary cells isolated from young/foetal donors as opposed to cells isolated from elderly patients, however, evidence is scarce due to multitude of variations in differentiation protocol, culture procedures [339, 354, 355]. Optimisation of the differentiation approach published by Chen et al [182] could occur at several steps during the differentiation process: i) culture of iPSCs in T175 flasks rather than 6-well plates in order to increase the starting cell population before applying the SB431542 supplemented differentiation medium for 10 days, ii) assessment of the required starting cell number at MP0, iii) addition of a higher percentage of FBS to the standard MSC medium in order to encourage improved growth rate during expansion and maturation on TCP, iv) reduce the time of maturation culture (e.g. culture only up to MP3). Furthermore, further characterisation of the generated iPSC-MSCs should be performed in order to confirm the multipotent character (trilineage differentiation into osteoblasts, chondrocytes and adipocytes) as well as flow cytometry for established mesenchymal cell surface markers (e.g.

CD105, 73, 90, 44, 146, STRO-1) in order to quantify the success of the mesenchymal differentiation process on the protein level as well [77].

In order to test the ability of the generated NIBSC-8 MSCs to form bone or cartilage cells, NIBSC-8 MSCs were treated with different osteogenic differentiation media compositions. The majority of osteogenic media contain dexamethasone, ascorbate-2-phosphate and vitamin D3 or β-glycerophosphate (see section 1.6.1 for details). This media composition is considered as the standard medium for osteogenic differentiation. In recent years, supplementation of the standard osteogenic medium with additional chemicals or small molecules was investigated (see Table 1.9 in section 1.6.2). After review of different studies and techniques (see Table 1.7 in section 1.6.2), a protocol using osteogenic medium supplemented with the small molecules TH and SAG [183] was chosen for the osteogenic differentiation experiments throughout this thesis. This protocol was chosen for several reasons: i) no EB formation, transformation or special coating of TCP was required, ii) sorting of the generated iPSC-MSCs was not necessary, and, iii) iPSCs were used as a starting cell population with iPSC-MSC generated in a previous step. In order to investigate the advantage of the small molecule supplemented medium over the standard osteogenic differentiation medium, the two media were tested on NIBSC-8 MSCs simultaneously and basal culture condition used as a negative control.

No clear advantage of TH + SAG supplemented osteogenic medium over standard osteogenic medium was observed. This is most likely due the n-number (n = 3) being not high enough. Overall faint ALP, Alcian Blue and Alizrin Red staining of NIBSC-8 MSCs in any of the tested culture conditons at both time points indicated that the generated donor cells (NIBSC-8 MSCs) are unable to undergo osteogenesis.

Conclusion

The use of a standardised iPSC line (NIBSC-8) for the generation of iPSC-MSCs with the published protocol by Chen et al. [182] and the subsequent osteogenic differentiation of the generated cells in standard osteogenic medium as well as small molecule (TH + SAG) supplemented standard osteogenic differentiation medium [183] has never been reported before.

It is unclear whether the differentiation protocol used for the generation of NIBSC-8 MSCs resulted in equivalent success as reported in the published protocol and if NIBSC-8 iPSCs

were successfully differentiated into NIBSC-8 MSCs. Elevated gene expression of N-Cadherin and vimentin in combination with decreased E-Cadherin (gene and protein expression) are indicators of the successful inititation of EMT in NIBSC-8 iPSC cultured in SB431542 supplemented culture medium. Transfer and culture on TCP in standard MSC culture medium resulted in elongated, fibroblast-like cells initially (MP0 and MP1), however, further culture on TCP resulted in loss of the elongated, fibroblast-like morphology and the acquisition of a morphologhy found in BMSCs isolated from bone marrow of elderly patients. In order to produce mature iPSC-MSCs, the next steps should be i) further optimisation of the SB431542 supplemented differentiation approach using the NIBSC-8 iPSC line, or ii) a different differentiation protocol which has provided substantial proof of its efficacy (e.g. the protocol used for generating iPSC-MSCs currently tested in a phase I clinical trial in Australia [179]).

The comparison of standard osteogenic differentiation medium (oBG) and oBG supplemented with two small molecules TH and SAG did not result in a clear advantage of one differentiation medium over the other. Overall faint staining of ALP, Alcian Blue and Alizarin Red suggested that the generated NIBSC-8 MSCs were unable to differentiated toward the osteogenic lineage or only to a very low extent.

Due to the unsuccessful generation of NIBSC-8 MSCscomparison of NIBSC-8MSCs with HFBCs isolated from human foetal femurs on molecular and epigenetic level as well as for osteogenic differentiation potential was not possible. However, in order to lay the groundwork for a future comparative study between these two cell types HFBCs isolated from 7-17 wpc human foetal femurs were investigated further in this thesis.

Chapter 4 Characterisation of Human Foetal Bone Cells (HFBCs) during human foetal femur development

4.1 Introduction

Long bone formation occurs by the process of endochondral ossification with cartilage serving as a template. Endochondral ossification is comprised of five stages: i) mesenchymal condensation within the core of the limb bud, ii) proliferation of the chondrocytes, iii) hypertrophy of chondrocytes, iv) formation of the primary ossification centre in the diaphysis, and, v) formation of the secondary ossification centres in the epiphysis. Interstitial growth across the chondrocyte zones is responsible for growth in length [43].

Limb development in humans starts at around week 4 (post conception) with the limb bud becoming visible. The limb bud consists of a mesenchymal core surrounded by an ectodermal layer and, outgrowth is regulated by feedback loops between the apical ectodermal ridge (AER) and the progress zone (PZ) [41]. With ongoing outgrowth of the limb bud from the core of the embryo, cells at a greater distance to the influence of the AER and PZ increase their proliferative capacity and undergo chondrogenic differentiation. A hyaline cartilage model is formed which serves as a template for future long bones with hand- and foot plates visible by the end of week 6 [41]. During weeks 7 and 8 of development, the limb increases in size and length with fingers and toes becoming more distinct. The end of the developmental embryonic period is indicated by the initiation of bone formation between weeks 8 and 9, with deposition of collagen matrix. Chondrocytes in the centre of the diaphysis undergo hypertrophy and eventually apoptosis, leaving cavities in the cartilaginous shaft for future bone marrow. Blood vessels invade the primary ossification centre in the diaphysis (~ week 12), penetrating the collagenous model [356]. Osteoprogenitors from the perichondrium, surrounding the cartilaginous core in the diaphysis, are transported into the centre of the diaphysis along with the invading blood vessels resulting in the mineralisation of the matrix (endochondral ossification) and formation of woven bone. The foetus increases rapidly in size during week 13-16 followed by a reduction in growth between weeks 17-20. Growth continues and mineralisation becomes visible around week 16 [356] (Figure 4.1). The secondary ossification centre in

the epiphyses was reported to be detectable from 32 wpc [357]. For more detailed display of events during foetal femur development refer to section 1.2.3.

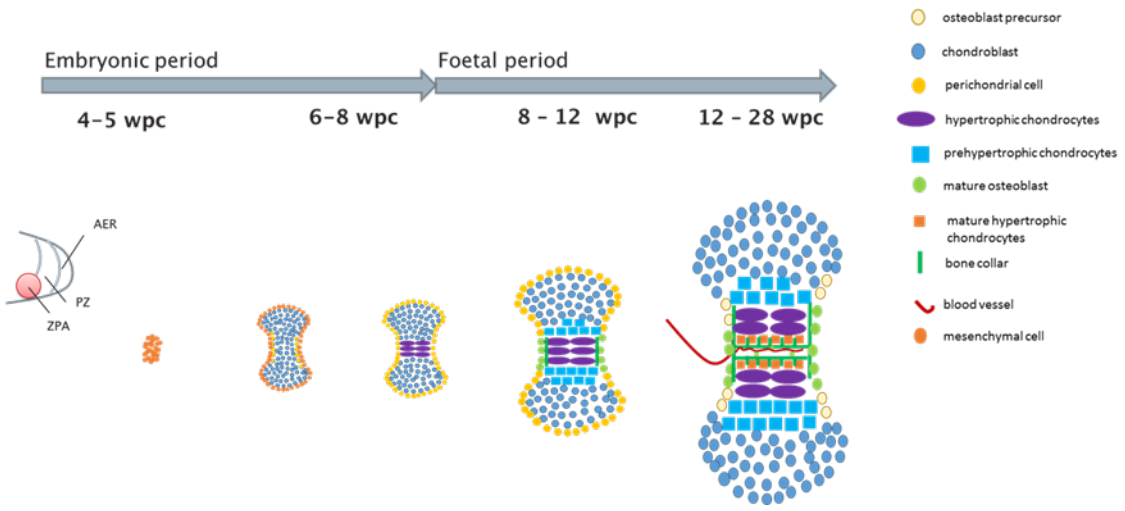

Figure 4.1 Foetal development of long bones in humans. Mesenchymal stem cells (MSCs) in the limb bud undergo condensation resulting in the formation of a cartilage anlage serving as a model for the future bone. Continuous chondrogenic differentiation results in the formation of pre-hypertrophic and hypertrophic chondrocytes. With time and ongoing development, the matrix slowly becomes mineralised due to the presence of osteoblasts being transported into the centre of the developing bone template by invading blood vessels, subsequently forming the primary ossification centre. Interstitial growth is due to distinct zones of different chondrocyte types: reserve chondrocytes toward the epiphyseal end of the shaft, proliferating chondrocytes followed by pre-hypertrophic and hypertrophic chondrocytes toward the centre of the shaft (purple). TF: transcription factor; wpc: weeks post conception. Based and adapted from [43].

Skeletal repair following transplantation of mesenchymal stem cells (MSCs) has been widely studied over the past decades [334]. Primary MSCs hold several advantages including specificity for each patient (autologous transplantation) or the recruitment of other factors for bone regeneration [335, 336]. However, identification of the appropriate mesenchymal progenitor populations for the promotion of bone formation is a critical step in the field of skeletal tissue engineering. Such cell populations, and their potential to differentiate into bone alongside cartilage and fat, have been identified in various tissues including bone marrow and fat tissue. Issues surrounding the definition of MSCs and current sources are outlined in more detail in chapter 1.3.

Typically, MSCs isolated from older patients hold several limitations in their application in bone regeneration: i) limited cell number, ii) decreased proliferation rate or, iii) efficiency in osteoblast formation [154, 155]. A significant limitation in skeletal regeneration remains

the paucity of stem cells and the necessity for *in vitro* expansion before potential clinical application. Cells isolated from foetal tissues, such as femoral tissue or umbilical cord, showed greater proliferation potential which would limit the time required for *in vitro* culture [355]. Human foetal femurs 8 - 11 wpc have been characterised and their multipotency reported [62]. However, characterisation of developmentally advanced samples (until 14 wpc) has not been studied before due to the limited availability and accessibility of older foetal samples. Furthermore, the *in vitro* osteogenic potential between HFBCs isolated from early developmental foetal femurs to developmentally advanced femurs remains unknown.

4.2 Hypothesis and Aims

Hypotheses

I. Human foetal femurs display a cartilaginous phenotype and the expression of genes required for skeletal development arise with increasing foetal femur age

II. HFBCs isolated from 14 wpc human foetal femurs result in better osteogenic differentiation outcome than HFBCs isolated from 8 wpc human foetal femurs

Aims

I. To characterise human foetal femurs during the first two trimesters (7 - 17 wpc)

Specifically:

a. The histological staining of paraffin embedded human foetal femurs using Alcian Blue/Sirius Red staining
b. The histological staining of paraffin embedded human foetal femurs using Goldner's Trichrome staining

II. To characterise HFBCs isolated from human foetal femurs

Specifically:

a. The imaging of cell morphology using bright field microscopy during *in vitro* culture of HFBCs isolated of 7 – 17 wpc human foetal femurs
b. The cell proliferation using alamarBlue® assay
c. qRT-PCR for quantification of expression of genes implicated in skeletal development and proliferation

III. To compare *in vitro* osteogenic differentiation potential of HFBCs isolated from 8 and 14 wpc human foetal femurs using two osteogenic differentiation media

Specifically:

a. *In vitro* osteogenic differentiation of HFBCs isolated from human foetal femurs in standard osteogenic differentiation medium (oBG) and in oBG supplemented with small molecules SAG and TH for 19 days.
b. The histological staining for ALP, proteoglycans and mineralised nodules at two time points (day 7 & 19) during *in vitro* osteogenic differentiation of HFBCs isolated from human foetal femurs
c. qRT-PCR for quantification of osteogenic and chondrogenic gene expression at two time points (day 7 & 19) during *in vitro* osteogenic differentiation of HFBCs isolated from human foetal femurs

Material and Methods

Methodology used in this chapter can be found in Chapter 2 with the following techniques detailed in respective subchapters: histological staining of human foetal femurs with Alcian Blue in section 2.2.5 and Goldner's Trichrome staining in section 2.2.6, capturing of cell morphology using bright field microscopy or capturing of immunofluorescence staining in section 2.4.1, molecular methods in chapter 2.3 with analysis of mRNA expression using qRT-PCR in section 2.3.4, composition of the different tested osteogenic media compositions and culture conditions in section 2.1.5 and histological stainings (ALP, Alcian Blue, Alizarin Red) of HFBCs at two different time points during osteogenic differentiation in sections 2.2.2, 2.2.3 and 2.2.4.

Statistics

Comparison of cell proliferation of HFBCs isolated from 7 – 17 wpc human foetal femurs using alamar® Blue assay was analysed using Kruskal-Wallis test with Dunn's post-hoc test for multiple comparisons within one passage and, Mann-Whitney U test was performed to compare between two passages individually for HFBCs isolated from one human foetal femur. Gene expression in HFBCs isolated from 7 – 17 wpc human foetal femurs were analysed using non-linear regression test. Osteogenic differentiation experiments in this results chapter were performed three times (n = 3). Gene expression of osteogenic differentiation was analysed with a Two-way ANOVA test with Dunnett's post-hoc test.

4.3 Results

4.3.1 Histological characterisation of human foetal femurs during the first two trimesters of pregnancy

The human foetal femur develops by endochondral ossification through an interplay of a mixed population of different cell types including stem cells, (pre-) chondrocytes and osteoblasts (see section 1.2.3). The amount of each cell type present in the developing human foetal femur is dependent on the age of the foetus. Histological staining of human foetal femur sections at different developmental stages (Table 4.1), was performed to provide an overview of the development of the different tissues in the human femur.

Decalcification (where necessary), embedding and sectioning was carried out by Janos Kanczler and/or Julia Wells from the Bone and Joint Research Group, Southampton, UK. Sections were stained for cartilage matrix, proteoglycans and collagens in matrix using Alcian Blue/Sirius Red in order to show the development of the hyaline cartilage model (~7 wpc) toward bone matrix. Goldner's Trichrome staining was performed on human foetal femur sections as described in section 2.2.6 to visualise the blood vessels and collagen matrix during femur development. Individual femurs are displayed in separate figures in order to allow for more detailed illustration of epi- and diaphysis.

Table 4.1 Human foetal femur samples used for Alcian Blue/Sirius Red and Goldner's Trichrome staining. wpc: weeks post conception.

Sample ID	Age [wpc]
14033	8
13786	12
13850	15
13842	17

Table 4.2 summarises the components of the two histological stainings used, the targeted tissues and colour of the stained tissue/cell type.

Table 4.2 Components of developing human foetal femur stained by Alcian Blue/Sirius Red staining and Goldner's Trichrome staining. In Goldner's Trichrome staining, Poncheau-fuchsin-azophloxin is used to overstain all components. The red dye is then displaced from the collagen by use of a polyacid. The polyacid in turn is displaced by the second acid dye (light green) which results in staining of collagen. Staining of erythrocytes occurs by stabilisation of the yellow/orange dye (orange G) by addition of phosphomolybdic acid.

Alcian Blue/Sirius Red staining		
stain	**tissue/cell type**	**colour**
Haematoxylin	cell nucleus	black
Alcian Blue	proteoglycans	blue/green
Sirius Red	collagen	red
Goldner's Trichrome staining		
stain	**tissue/cell type**	**colour**
Haematoxylin	cell nucleus	black
Ponceau-fuchsin-azophloxin	all components	red
Phosphomolybdic acid/orange G	erythrocytes	red
Light green	collagen	green/blue

The intense Alcian blue staining of the **8 wpc** human foetal femur illustrated the proteoglycans present in the cartilage anlage with (pre-) hypertrophic chondrocytes in the diaphysis (Figure 4.2 A, B, D). A shift in cell morphology from the centre of the diaphysis toward the epiphysis was clearly visible. Cells in the epiphysis were considerably smaller and showed round morphology compared to enlarged hypertrophic chondrocytes in the diaphysis (Figure 4.2 C). Sirius Red staining (non-specific collagen staining) was observed on the outside of the diaphysis indicating the deposition of collagen, thus forming a bone collar (Figure 4.2 D).

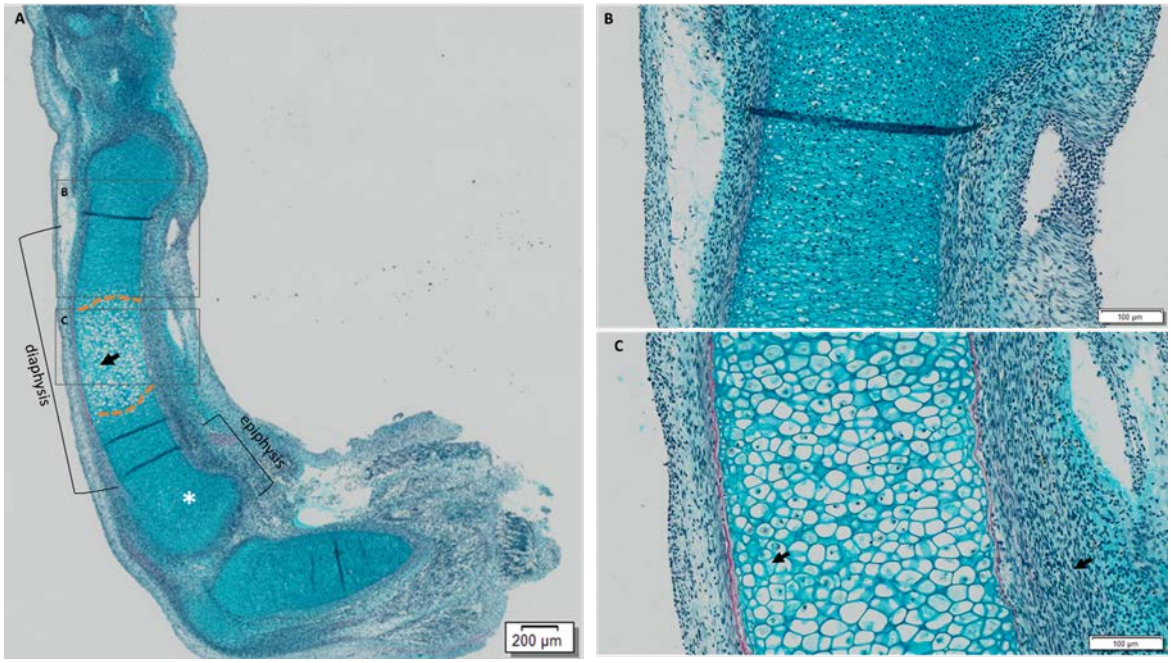

Figure 4.2 Alcian Blue/Sirius Red staining on 6 µm section of human foetal femur (8 wpc). **A:** overview of whole human foetal femur section. Dotted line (orange) marked transition from enlarged hypertrophic chondrocytes (indicated by black arrow) in the diaphysis to chondrocytes (indicated by white asterisk) towards the epiphysis visible. Scale bar: 200µm. **B:** higher magnification of epiphysis. Scale bar: 100 µm. **C:** higher magnification of diaphysis. Bone collar is indicated by arrows. Scale bar: 100 µm.

Figure 4.3 showed Goldner's Trichrome staining of **8 wpc** old human femur cross section illustrating hypertrophic chondrocytes throughout the full length of the diaphysis and chondrocytes characterised by smaller, round morphology toward the epiphysis (Figure 4.3 A). The femur cross section showed very little red staining indicating red blood cells. The biggest amount of red staining was found in the tissue surrounding the femur (Figure 4.3 B-C).

Figure 4.3 Goldner's Trichrome staining on 6 µm section of human foetal femur (8 wpc). A: overview of whole foetal femur section. Dotted line (orange) indicates the transition from enlarged hypertrophic chondrocytes in the diaphysis to chondrocytes towards the epiphysis. Scale bar: 200 µm. **B:** overview of epiphysis and diaphysis. Dotted line (orange) indicates the transition from enlarged hypertrophic chondrocytes (black arrow) in the diaphysis to chondrocytes (black asterisk) towards the epiphysis. Scale bar: 200 µm. **C:** higher magnification of epiphysis. Scale bar: 100 µm. **D:** higher magnification of diaphysis. Scale bar: 100 µm.

Section of **12 wpc** human foetal femur showed intense Sirius Red staining and barely any visible Alcian Blue staining indicating deposition of collagen matrix (Figure 4.4 A). Epiphysis showed less Sirius Red staining and no cavities were visible (Figure 4.4 B). Cavities (indicated by black arrows) were found throughout the femur and the surrounding matrix (Figure 4.4 C).

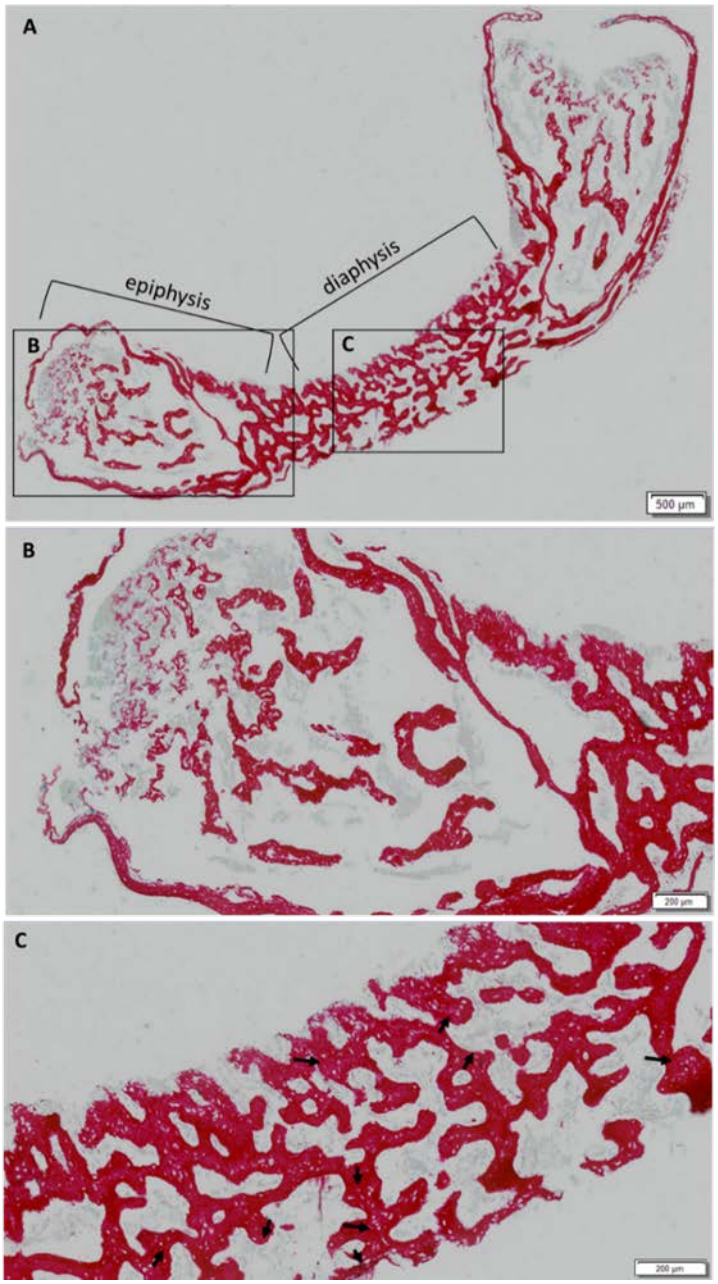

Figure 4.4 Alcian Blue/Sirius Red staining on 6 µm section of human foetal femur (12 wpc). A: overview of whole foetal femur section. Scale bar: 500 µm. **B:** overview of the epiphysis. Scale bar: 200 µm. **C:** overview of the diaphysis. Black arrows indicated cavities within the collagen matrix deposition. Scale bar: 200 µm.

Goldner's Trichrome staining in **12 wpc** femur (Figure 4.5 A) showed intense green staining indicating a collagen matrix with sparse red staining in the diaphysis and intense red staining in epiphysis indicating a high amount of blood vessels (Figure 4.5 B and C). Cavities were found throughout the femur and the surrounding matrix (Figure 4.5). The presence of red stained cells without any nucleus indicated the presence of blood vessels.

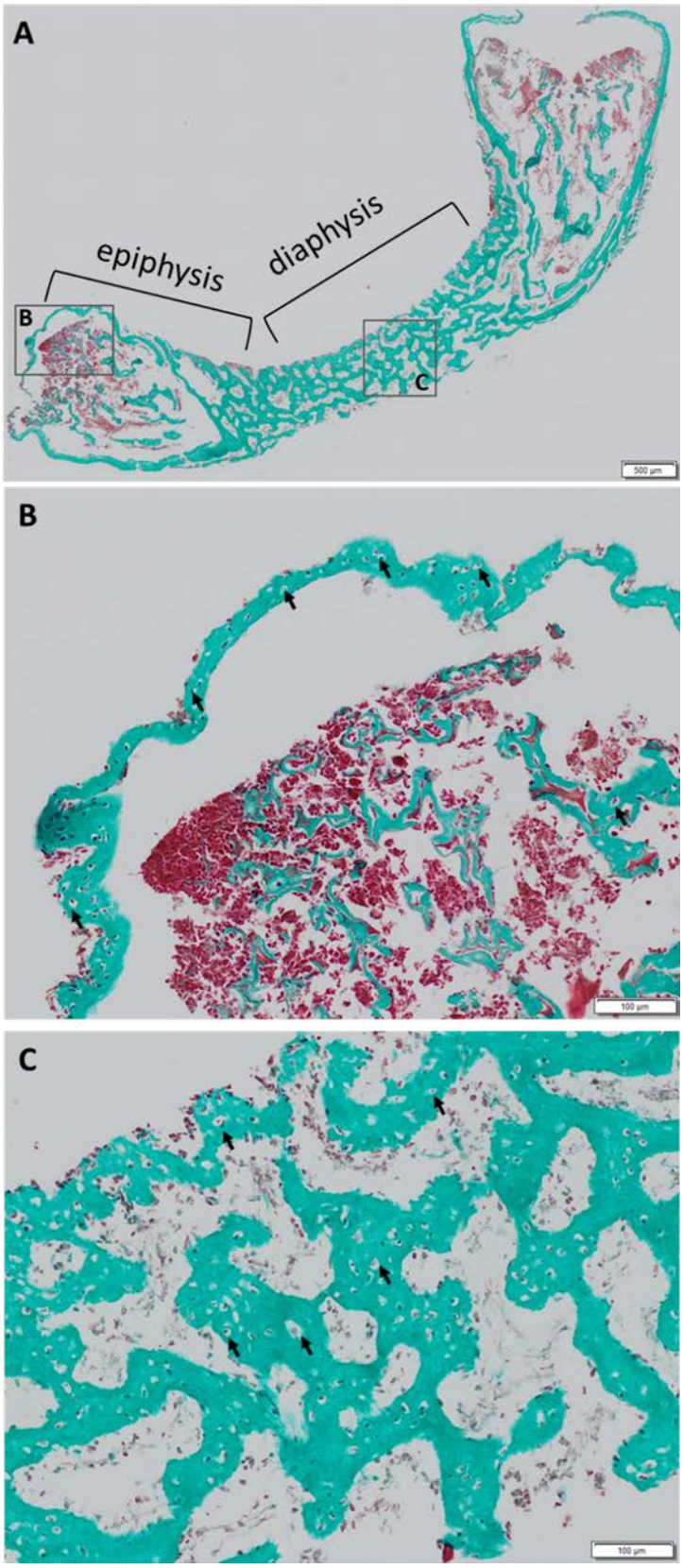

Figure 4.5 Goldner's Trichrome staining on 6 µm section of human foetal femur (12 wpc). A: overview of whole foetal femur section. Scale bar: 500 µm. **B:** overview of epiphysis in higher magnification. Scale bar: 100 µm. **C:** overview of diaphysis in higher magnification. Scale bar: 100 µm. Arrows indicate cavities of blood vessels.

Sections of **15 wpc** human foetal femur showed Sirius Red staining in the diaphysis (Figure 4.6 A and C) indicating deposition of the collagen matrix. Individual cells were not visible, however, discrete cavities were found distributed through the collagen matrix (Figure 4.6 C). Sirius Red staining on the outside of the human foetal femur was found to be closer to the epiphysis as opposed to the centre in 8 wpc human foetal femur section (Figure 4.2). Staining in the epiphysis showed a comparable cell morphology as for epiphysis of 8 wpc human foetal femur, however, differential blue to red shading was detected (Figure 4.6 A and B). Hypertrophic chondrocytes in the distal end of the diaphysis, as well as chondrocytes in the centre of the epiphysis, showed dark blue staining while proliferating chondrocytes in the outer layers of the epiphysis showed red to violet staining (Figure 4.6 B).

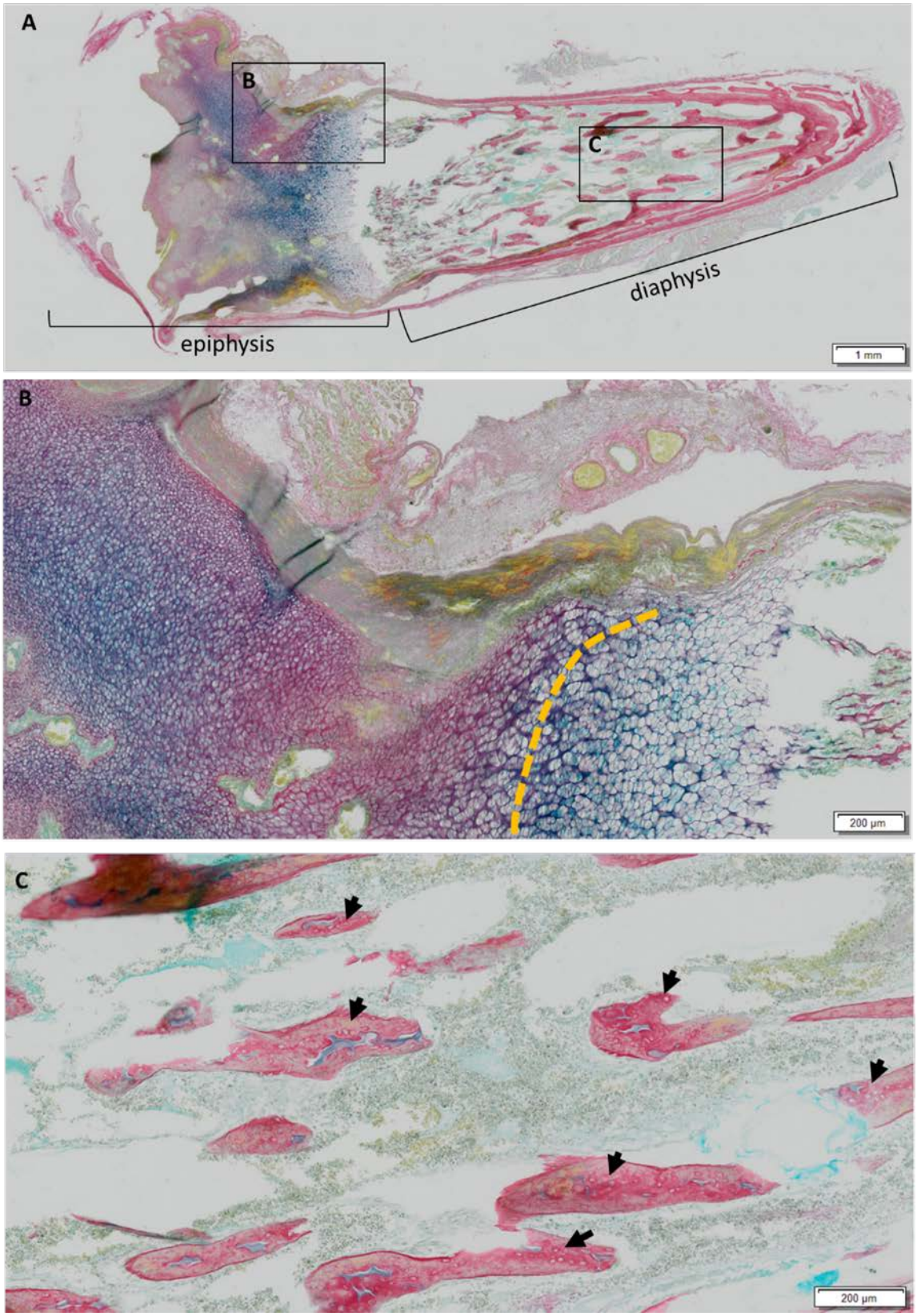

Figure 4.6 Alcian Blue/Sirius Red staining on 6 µm section of human foetal femur (15 wpc). **A:** overview of whole foetal femur section. Scale bar: 1 mm. **B:** higher magnification of epiphysis. Dotted line (orange) indicates the transition from chondrocytes at the epiphyseal end to enlarged hypertrophic chondrocytes near the diaphysis. Scale bar: 200 µm. **C:** higher magnification of

diaphysis. Black arrows indicated cavities within the collagen matrix deposition. Scale bar: 200 μm.

Goldner's Trichrome staining showed overall intense blue/green staining of the **15 wpc** femur section with red stained areas indicating the location of red blood cells, thus allowing for the location of blood vessels (Figure 4.7). An overview of the human foetal femur section showed enhanced red staining spread across the epiphysis (Figure 4.7 A). The epiphysis showed a less intense red staining indicating the reduction of red blood cells. However, the outer border of the epiphysis showed intense red staining as well as round, tube-like areas within the epiphysis (Figure 4.7 B). Figure 4.7 C showed a section of the diaphysis with blue stained areas indicating collagen deposition interspersed with red blood cells (red).

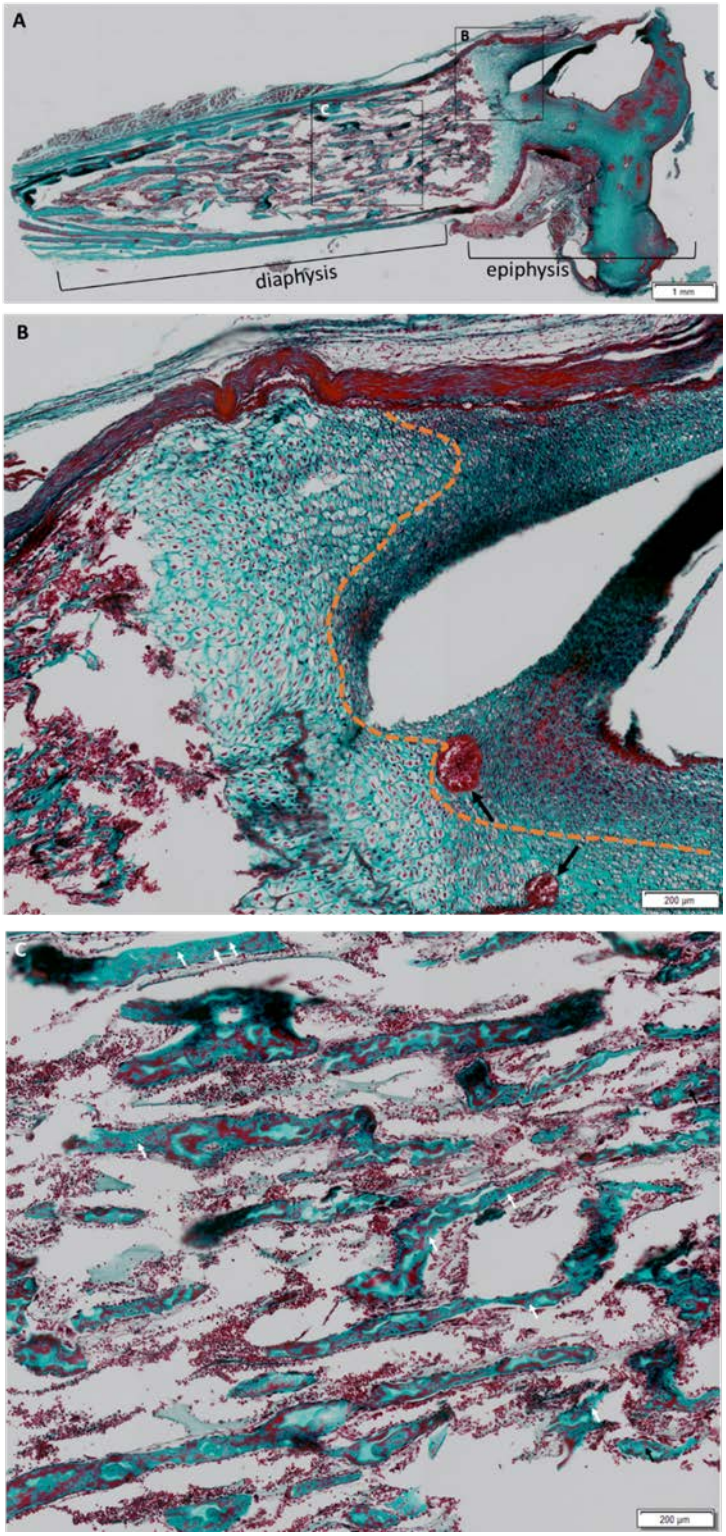

Figure 4.7 Goldner's Trichrome staining on 6 µm section of human foetal femur (15 wpc). **A:** overview of whole foetal femur section. Scale bar: 1 mm. **B:** higher magnification of epiphysis. Dotted line (orange) indicates the transition from chondrocytes at the epiphyseal end to enlarged hypertrophic chondrocytes toward the diaphysis. Scale bar: 200 µm. **C:** higher magnification of diaphysis. Scale bar: 200 µm. Arrows (white) indicate cavities of blood vessels.

A cross section through the diaphysis of the **15 wpc** human foetal femurs showed a single round, a tube-like structure in the centre of the femur which was surrounded by intense blue staining indicating collagen (Figure 4.8 A and B). Cavities in the blue stained collagen suggest the location of blood vessels (Figure 4.8 C).

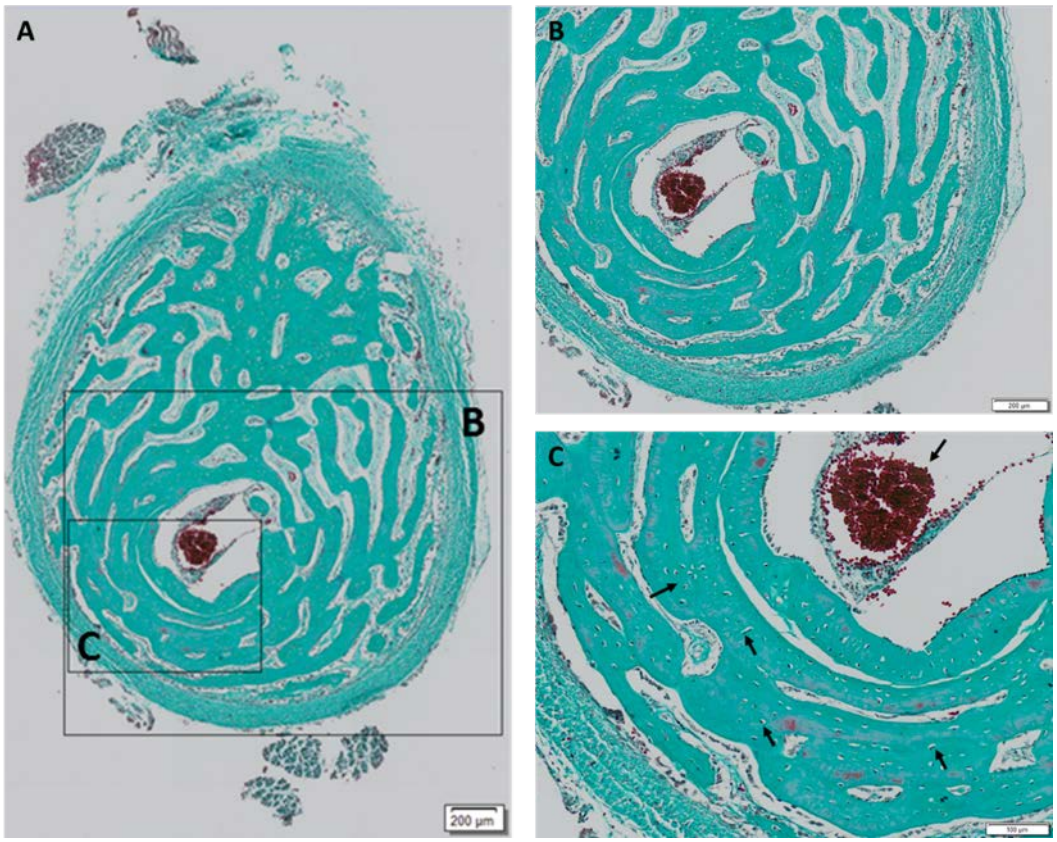

Figure 4.8 Goldner's Trichrome staining on 6 µm section of human foetal femur (15 wpc) through core of diaphysis. A: overview of whole foetal femur section. Scale bar: 200 µm. **B:** higher magnification. Scale bar: 200 µm. **C:** higher magnification. Scale bar: 100 µm. Arrows (black) indicate cavities of blood vessels.

Alcian Blue/Sirius Red staining of a **17 wpc** human foetal femur showed intense Sirius Red staining of the tissue surrounding the femur diaphysis, indicating the location of the bone collar (Figure 4.9 A). The epiphysis was stained blue/purple and showed the characteristic shift in cell morphology from enlarged hypertrophic chondrocytes to small round proliferative chondrocytes (indicated by orange dotted lines), (Figure 4.9 B). Within the diaphysis, red stained areas were identified as deposition of collagen with discrete cavities (indicated by black arrows). Between the red stained collagen in the diaphysis, green stained areas were clearly identified (Figure 4.9 C).

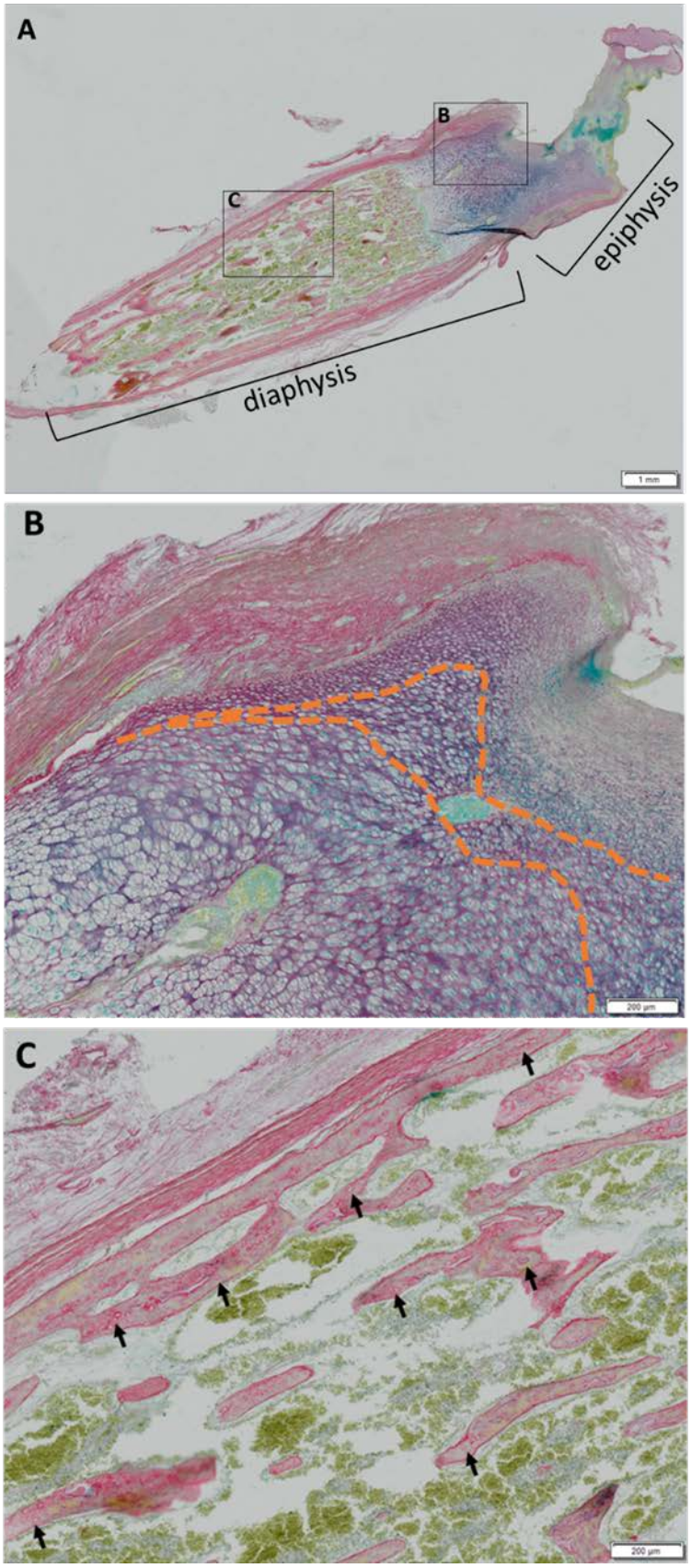

Figure 4.9 Alcian Blue/Sirius Red staining on 6 µm section of human foetal femur (17 wpc). **A:** overview of whole foetal femur section. Scale bar: 1 mm. **B:** higher magnification of epiphysis. Scale bar: 200 µm. Dotted line (orange) indicates a transition from enlarged hypertrophic

chondrocytes to small, round chondrocytes near the epiphysis. **C:** higher magnification of diaphysis. Arrows (black) indicate cavities of blood vessels. Scale bar: 200 μm.

A section of the distal end of the epiphysis of a **17 wpc** human foetal femur provided an overview of the structure of the epiphysis (Figure 4.10 A). Figure 4.10 B showed distinct zones of the different types of chondrogenic cells: chondrocytes at the very far end of the epiphysis characterised by small round morphology, followed by enlarged pre-chondrocytes with deep blue staining further away from the epiphyseal end, and hypertrophic chondrocytes characterised by enlarged cell morphology and less intense blue staining toward the diaphysis. Figure 4.10 C showed a cross section of 17 wpc femur through spongy bone and compact bone surrounding the femur.

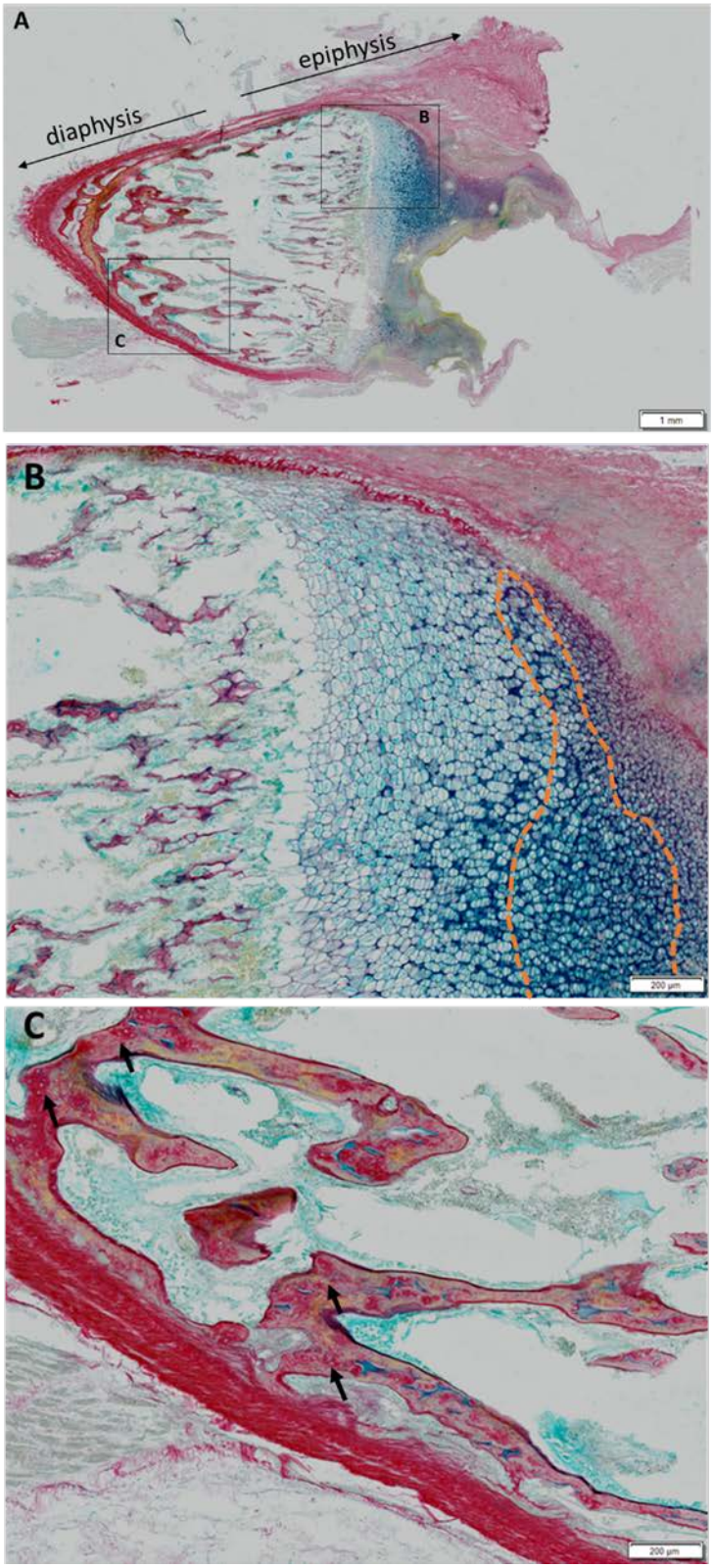

Figure 4.10 Alcian Blue/Sirius Red staining on 6 µm section of human foetal femur (17 wpc) through distal epiphysis. **A:** overview of whole femur section. Scale bar: 1 mm. **B:** higher magnification of epiphysis. Dotted lines (orange) illustrate the different types of chondrocytes present in the epiphysis: enlarged hypertrophic chondrocytes (closest to diaphysis, left), pre-hypertrophic chondrocytes (area between dotted lines) and chondrocytes (closest to epiphysis, right).

Scale bar: 200 µm. **C:** higher magnification of distal end of diaphysis. Arrows (black) indicate cavities of blood vessels. 200 µm.

Alcian Blue/Sirius Red staining of a section through the core of **17 wpc** femur provided an overview of the structure of developing femur (Figure 4.11 A-C). The predominant presence of Sirius Red stain in the section indicated cancellous bone. Figure 4.11 C showed osteons (harbouring the central blood vessels running through the developing bone) in the matrix indicated by black arrows.

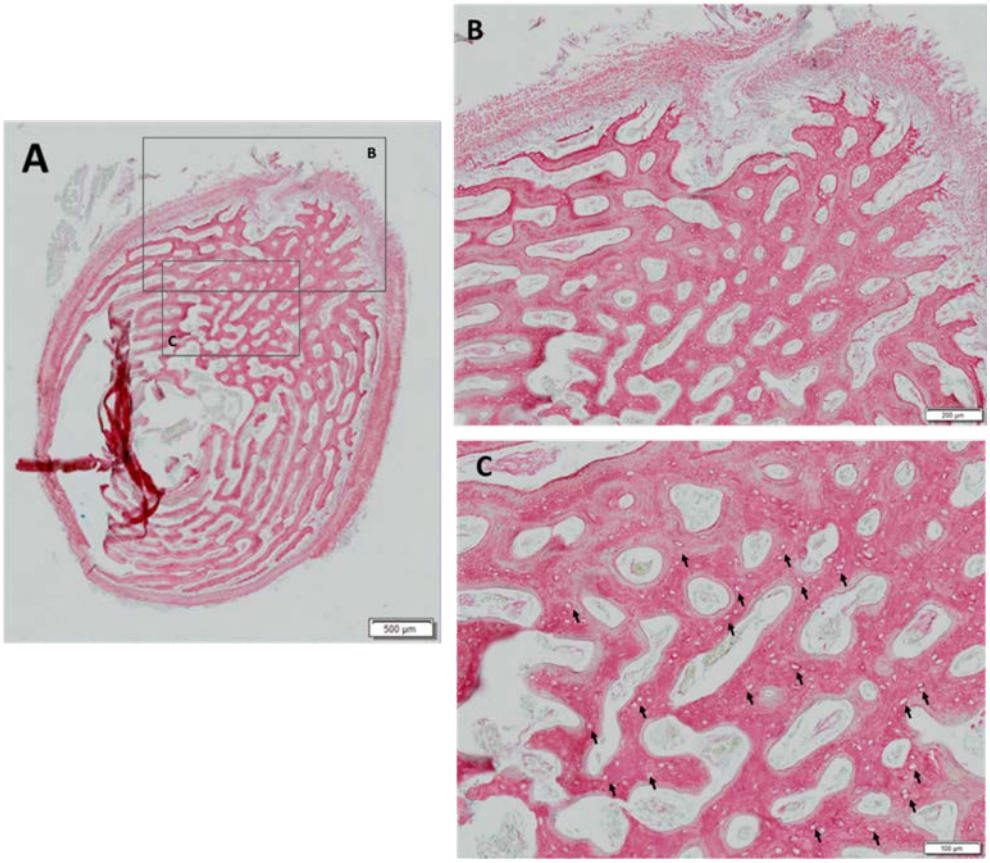

Figure 4.11 Alcian Blue/Sirius Red staining on 6 µm section of human foetal femur (17 wpc) through the core. A: overview of whole foetal femur section. Scale bar: 500 µm. **B and C:** higher magnifications. Arrows (black) indicate cavities of blood vessels. Scale bars: 200 µm.

Goldner's Trichrome staining on the **17 wpc** human foetal femur section was similar to the staining of a 15 wpc human foetal femur, with a slightly higher amount of red stained blood cells in the diaphysis in the 17 wpc human foetal femur section (Figure 4.12 A and C), indicated by white asterisks. As opposed to 15 wpc human foetal femur staining, the borders of the 17 wpc human foetal femur showed less red staining indicating less red blood cells surrounding the foetal femur (Figure 4.12 A-C).

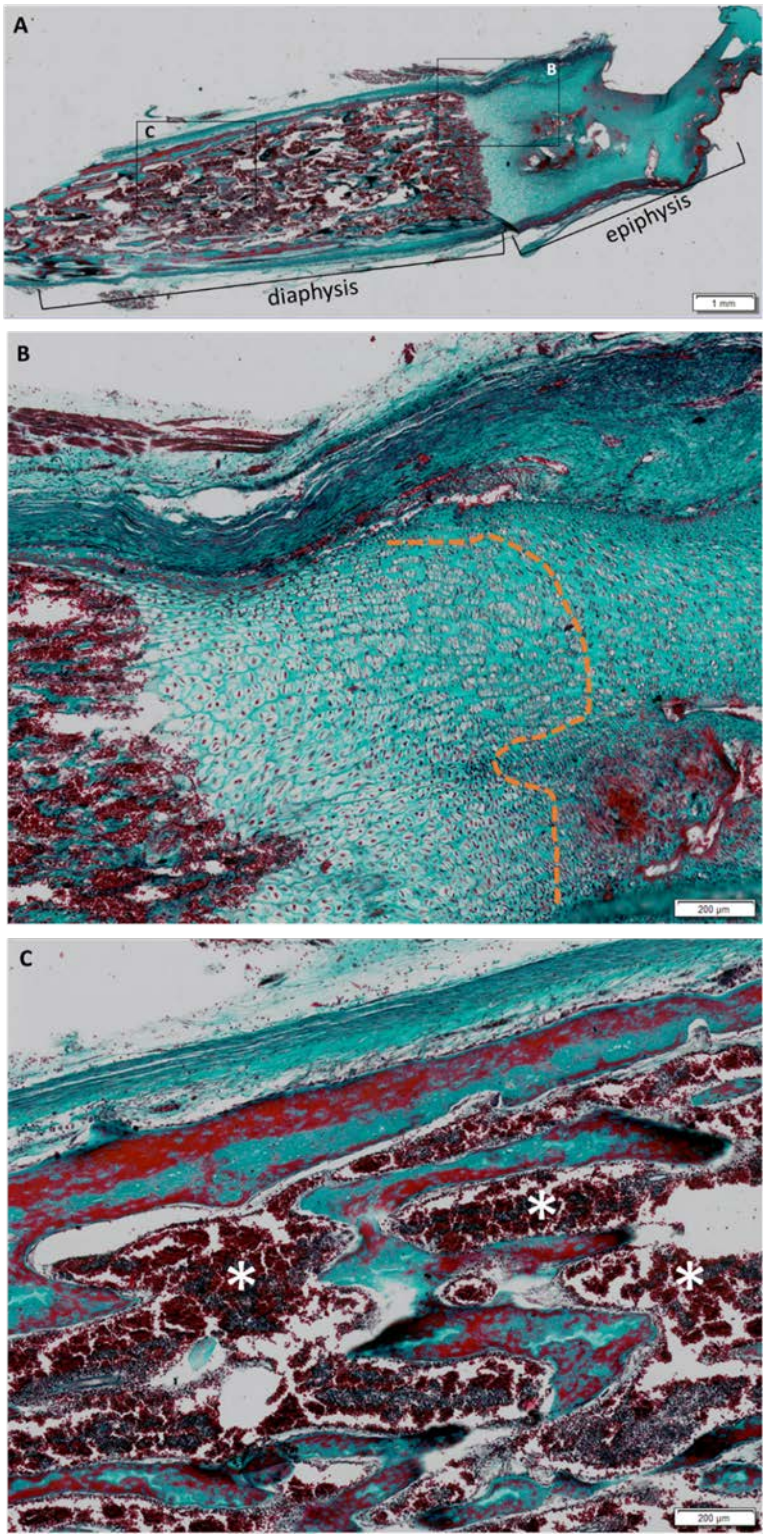

Figure 4.12 Goldner's Trichrome staining on 6 µm section of human foetal femur (17 wpc). A: overview of whole foetal femur section. Scale bar: 1 mm. **B:** higher magnification of epiphysis. Dotted line (orange) indicates the transition from chondrocytes at the epiphyseal end to enlarged hypertrophic chondrocytes toward the diaphysis. Scale bar: 200 µm. **C:** higher magnification of diaphysis. Asterisks (white) indicate accumulation of red blood cells. Scale bar: 200 µm.

Goldner's Trichrome staining of a section through the core of **17 wpc** femur provided an overview of the structure of developing femur (Figure 4.13). The cross section did not display a single round, tube-like structure in the centre of the femur as in the cross section of **15 wpc** femur (Figure 4.13 A). The predominant blue staining indicated the presence of collagen containing cavities, which might indicate the location of blood vessels running through the developing femur (Figure 4.13 B).

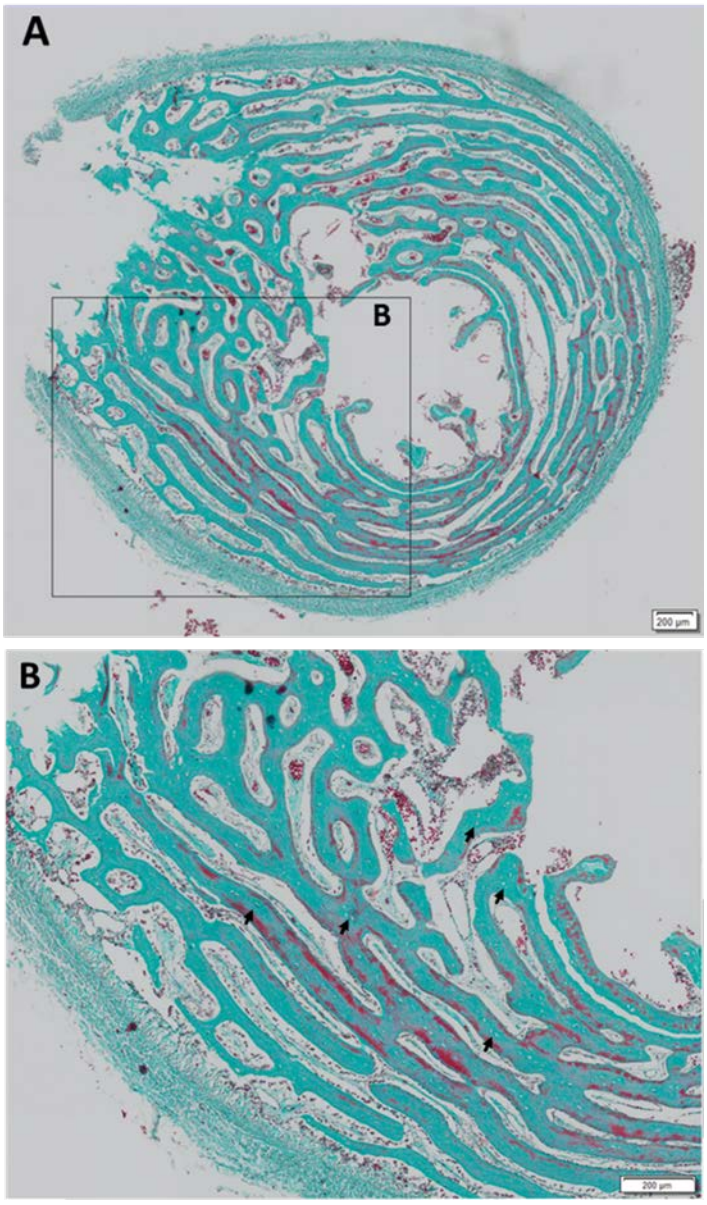

Figure 4.13 Goldner's Trichrome staining on 6 µm section of human foetal femur (17 wpc) through the core. A: overview of whole foetal femur section. Scale bar: 1 mm. **B:** higher magnification of epiphysis. Scale bar: 200 µm. Arrows (black) indicate cavities of blood vessels.

Alican Blue/Sirius Red staining illustrated the different types of chondrocytes in the hyaline cartilage model of the 8 wpc human foetal femur with hypertrophic chondrocytes in the

diaphysis and proliferating chondrocytes both epiphyses. A thin red layer on the outside of the centre of the diaphysis illustrated the developing bone collar. Goldner's Trichrome staining of the 8 wpc human foetal femur demonstrated a high number of erythrocytes in the tissue surrounding the human foetal femur with only few wide spread erythrocytes in the diphysis. Alcian Blue/Sirius Red staining at 12 wpc human foetal femur showed small cavities in the deposited collagen matrix in the diaphysis which resembled the structure of trabecular bone. The cavities were even more visible in the 12 wpc human foetal femur stained with Goldner's Trichrome staining and appear to harbour erythrocytes in the centres of the cavities. However, epiphyses appeared to harbour the majority of erythrocytes. Staining of 15 wpc human foetal femur illustrated the further development of the femur with elongation of the bone collar surrounding the diaphysis as well as the structure difference between cells in diaphysis and epiphysis. The epiphysis still consisted of small, round chondrocytes, although the transition to hypertrophic chondrocytes at the growth plate (area between epiphysis and diaphysis) could be observed, while hypertrophic chondrocytes in the diaphysis observed in 8 wpc human foetal femur have died by 15 wpc of development. Goldner's Trichrome staining of the 15 wpc human foetal femur demonstrated the presence of erythrocytes between areas with collagen deposition. A cross section of the 15 wpc human foetal femur demonstrated a cluster of erythrocytes resembling a round, tube-like structure in the centre of the diaphysis surrounded by areas of collagen deposition resembling the structure of trabecular bone surrounding the developing bone marrow cavity. Small cavities distribute throughout the collagen suggest the location of small blood vessels running through the collagen matrix of the developing femur transporting osteochondral precursors into the femur, thus initiating the mineralisation process. Alcian Blue/Sirius Red as well as Goldner's Trichrome staining of a 17 wpc human foetal femur resembles the structure found in the 15 wpc human foetal femur with more erythrocytes present in the diaphysis of the 17 wpc human foetal femur. Cross sections through the 17 wpc human foetal femur demonstrated the structure of trabecular bone surrounding the bone marrow cavity as well as a thin layer resembling compact bone surrounding the trabecular bone structure.

4.3.2 Morphology and proliferative capacity of HFBCs isolated from 7 – 17 wpc human foetal femurs

HFBCs could potentially serve as alternative cell source for bone tissue engineering and facture repair. Therefore, characterisation of HFBCs isolated from 7 - 17 wpc human foetal femurs is regarded as necessary in order to understand the properties of HFBCs isolated from different stages during foetal femur development. Eleven human foetal femur samples (7 to 17 wpc) were dissected to isolate HFBCs. HFBCs isolated from human foetal femurs were cultured *in vitro* and the cells were lysed after each passage for further analysis i) morphology, ii) proliferation capacity and iii) gene expression using qRT-PCR (see section 2.3.4). Table 4.3 details the human foetal femur samples.

Table 4.3 Foetal samples used for global DNA methylation profiling. wpc: weeks post conception.

Sample ID	Age [wpc]
13986	7
13975	8
13723	8 (late)
13706	9
14007	10
13893	12
13796	13
13901	14
13976	14
14008	16
13766	17

Figure 4.14 and Figure 4.15 display cell morphology of HFBCs isolated from human foetal femurs between 8 wpc and 16 wpc at passage 0 (after isolation from femur), and after one passage *in vitro* culture. No differences were observed in HFBCs morphology isolated from the different human foetal femurs at varying developmental stages in either of the two analysed *in vitro* passages. Overall, HFBCs appeared smaller and less elongated at passage 0 compared to passage 1. However, this could be a consequence of adaptation to *in vitro* culture conditions after one passage.

Cell growth was investigated by using alamarBlue® cell viability assay (see section 2.2.1) (Figure 4.16). Comparison of the cell viability of HFBCs isolated from human foetal femur samples showed a significant reduction in HFBCs isolated from 12 wpc human foetal femur sample compared to 7 wpc human foetal femur sample at passage 1 ($p < 0.05$). HFBCs at passages 1 and 3, isolated from 8, 10, 12, 14 and 16 wpc human foetal femur samples, showed variable cell viability with no clear developmental trend (Figure 4.16 A, Table 4.4). Direct comparison between HFBCs at passages 1 and 3 by individual human foetal femur sample, showed significantly increased cell viability at passage 3 in HFBCs isolated from 12 wpc and 16 wpc human foetal femur samples ($p < 0.01$) (Figure 4.16 B, Table 4.4).

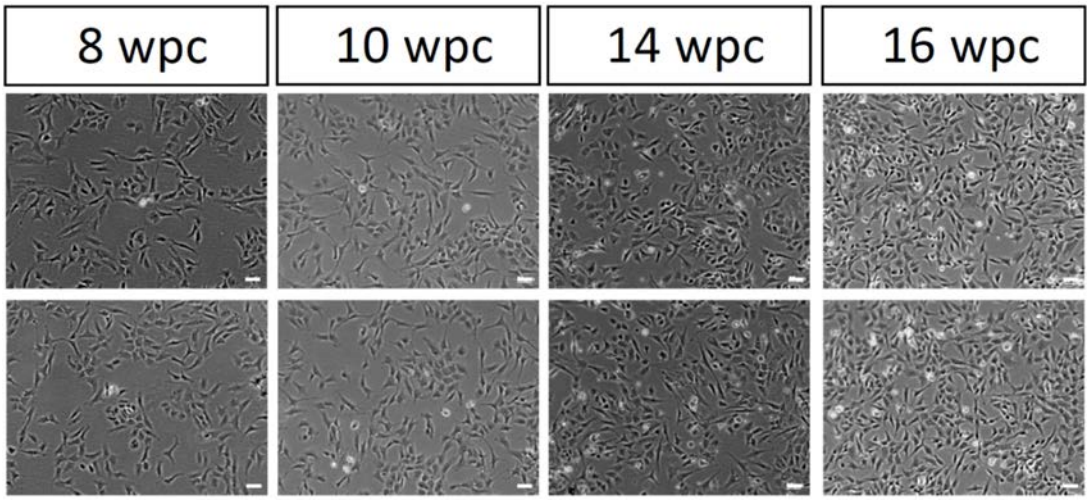

Figure 4.14 Morphology of human foetal bone cells (HFBCs) isolated from 8, 10, 14, 16 wpc human foetal femurs at passage 0. HFBCs were isolated, cultured *in vitro* and morphology was captured using bright field microscopy at passage 0. Morphology of HFBCs isolated from femurs at 8, 10, 14 and 16 wpc are displayed here to give a representative overview. Scale bar: 50 μm. wpc: weeks post conception.

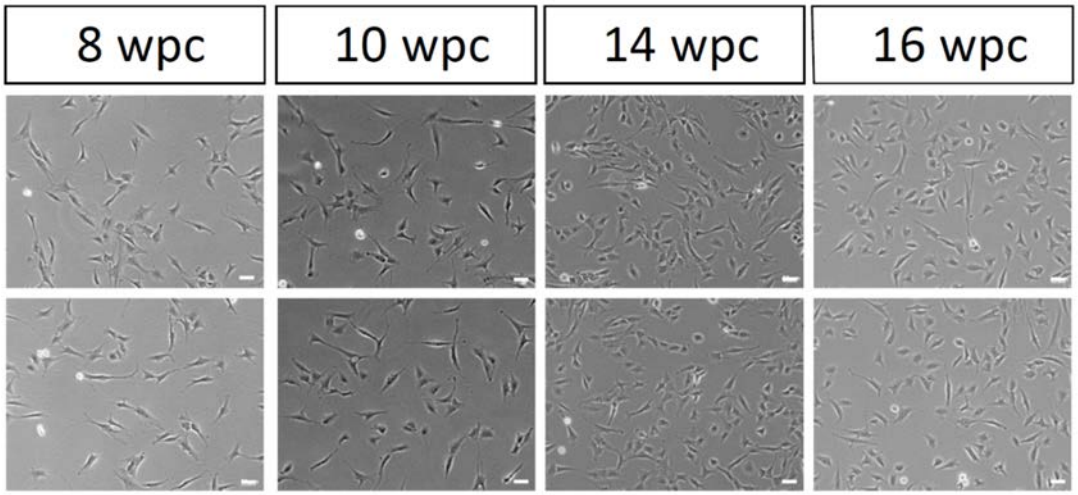

Figure 4.15 Morphology of human foetal bone cells (HFBCs) isolated from 8, 10, 14, 16 wpc human foetal femurs at passage 1. HFBCs were isolated, cultured *in vitro* and morphology was captured using bright field microscopy at passage 1. Morphology of HFBCs isolated from femurs at 8, 10, 14 and 16 wpc are displayed here to provide a representative overview. Scale bar: 50 μm. wpc: weeks post conception.

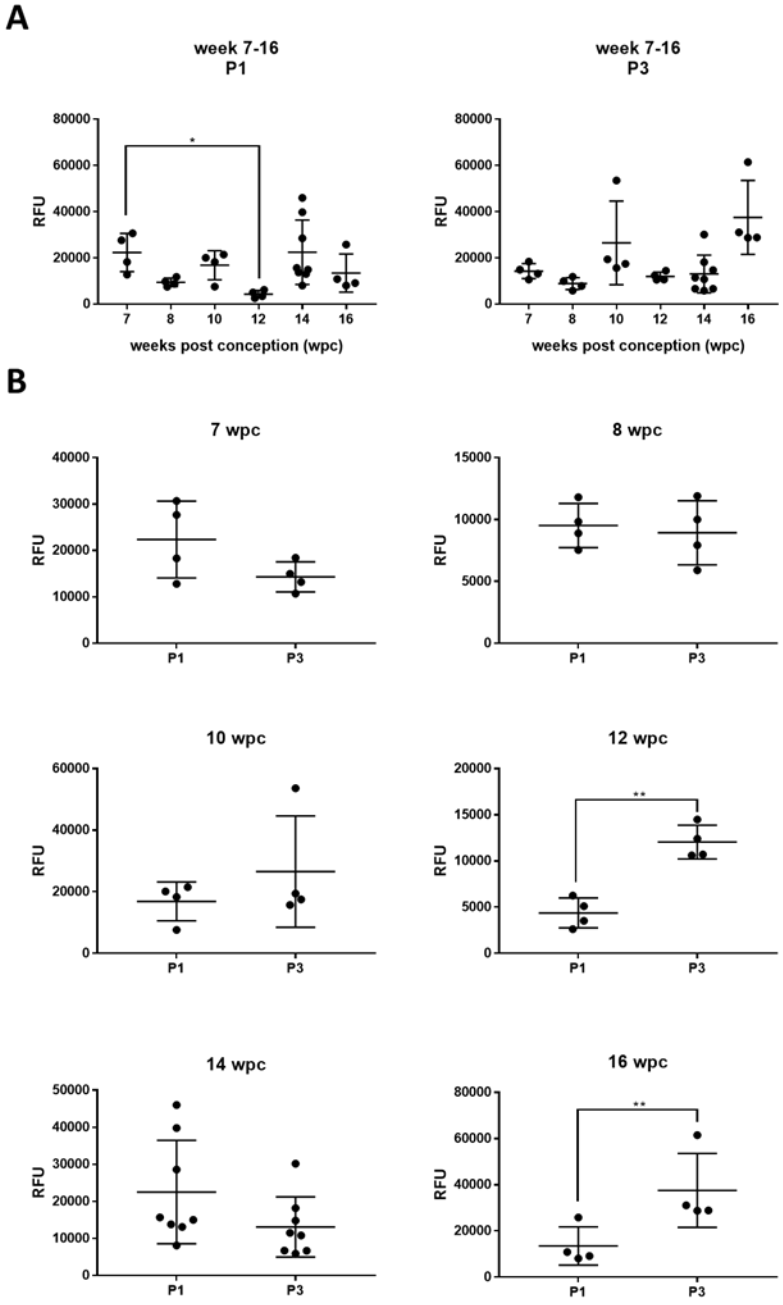

Figure 4.16 Analysis of cell viability and proliferation in human foetal bone cells (HFBCs) following *in vitro* culture determined using the alamarBlue® cell viability assay. Cells were seeded in 96-wells (20,000 cells/cm^2) as four replicates and cultured in MSC medium for 24 h. MSC medium was mixed with 1:10 of alamarBlue® reagent, incubated for four hours at 37°C and fluorescence emission measured at 580-610 nm (peak emission 585 nm) in a plate reader. Measured fluorescence of cells without cells was subtracted from values obtained from wells with seeded cells. Fluorescence was measured as relative fluorescence units (RFU). Mean +/- SD displayed from 4 replicates (N = 4) from n = 1 human foetal femur sample for each developmental week. **A:** Kruskal-Wallis test with Dunn's post-hoc test for multiple comparisons was used to compare statistical significance between HFBCs isolated from human foetal femur samples of different developmental ages at passage 1 (left) and passage 3 (right). **B:** Mann-

Whitney U test was performed to compare passages 1 and 3 of HFBCs within individual human foetal femur samples. * $p < 0.05$; ** $p < 0.01$.

Table 4.4 Summary of cell viability and proliferation in HFBCs following *in vitro* culture determined using the alamarBlue® cell viability assay. Cells were seeded in 96-wells (20,000 cells/cm^2) as four replicates and cultured in MSC medium for 24h. MSC medium was mixed with 1:10 of alamarBlue® reagent, incubated for four hours at 37°C and fluorescence emission measured at 580-610 nm (peak emission 585 nm) in a plate reader. Measured fluorescence of cells without cells was subtracted from values obtained from wells with seeded cells. Mean +/- SD displayed. HFBCs: human foetal bone cells.

7	8	10	12	14	16	
22375 +/- 8285	9515 +/- 1790	16885 +/- 6301	4377.5 +/- 1618	22515 +/- 13949	13490 +/- 8288	**passage 1**
14325 +/- 3239	8935 +/- 2588	26550 +/- 18097	12050 +/- 1830	13101.25 +/- 8131	37575 +/- 15985	**passage 3**

No differences were observed in regards to morphology and proliferative capacity between HFBCs isolated from human foetal femurs from different developmental stages (7 – 17 wpc).

4.3.3 Expression of genes implicated during human skeletal development

Investigation of gene expression was performed in order to aid the understanding of the molecular identity of HFBCs isolated from 7 – 17 wpc. Cells isolated from human foetal femurs were cultured on TCP and expression of genes implicated in skeletal development analysed using qRT-PCR at passage 0 and 1 and normalised to housekeeping gene *RN18S* at 7 wpc.

SOX9, a key regulator of chondrogenesis, and ***COL2A1***, a target of SOX9 and a key component protein in the cartilage model of the foetal femur, did not show an increase in expression in HFBCs isolated from 7-17 wpc human foetal femurs (*SOX9*: $R^2 = 0.1063$; *COL2A1*: $R^2 = 0.3553$). Both genes showed variation in expression (Figure 4.17 A and B, see Table 7.7 in Appendix H).

COL9A1 was equally highly expressed in all analysed femur samples, as observed for *COL2A1*, and showed significantly increased expression between 7 and 17 wpc in analysed

sample cohort at passage 0 (R^2 = 0.7159, $p < 0.001$, Figure 4.17 C) (see Table 7.7 in Appendix H). The proteoglycan aggrecan, encoded by ***ACAN***, was overall less expressed in the femurs, however, increase in gene expression was comparable to *COL9A1* (R^2 = 0.6969, $p < 0.001$) (Figure 4.17 D) (Table 7.7 in Appendix H). Collagen type X, encoded by ***COL10A1*** was reportedly expressed exclusively by hypertrophic chondrocytes [358, 359] in foetal femurs, however, in our samples could not be detected before 10 wpc Gene expression varied in the analysed samples during foetal femur development (R^2 = 0.1436) (Figure 4.17 E, Table 7.7 in Appendix H).

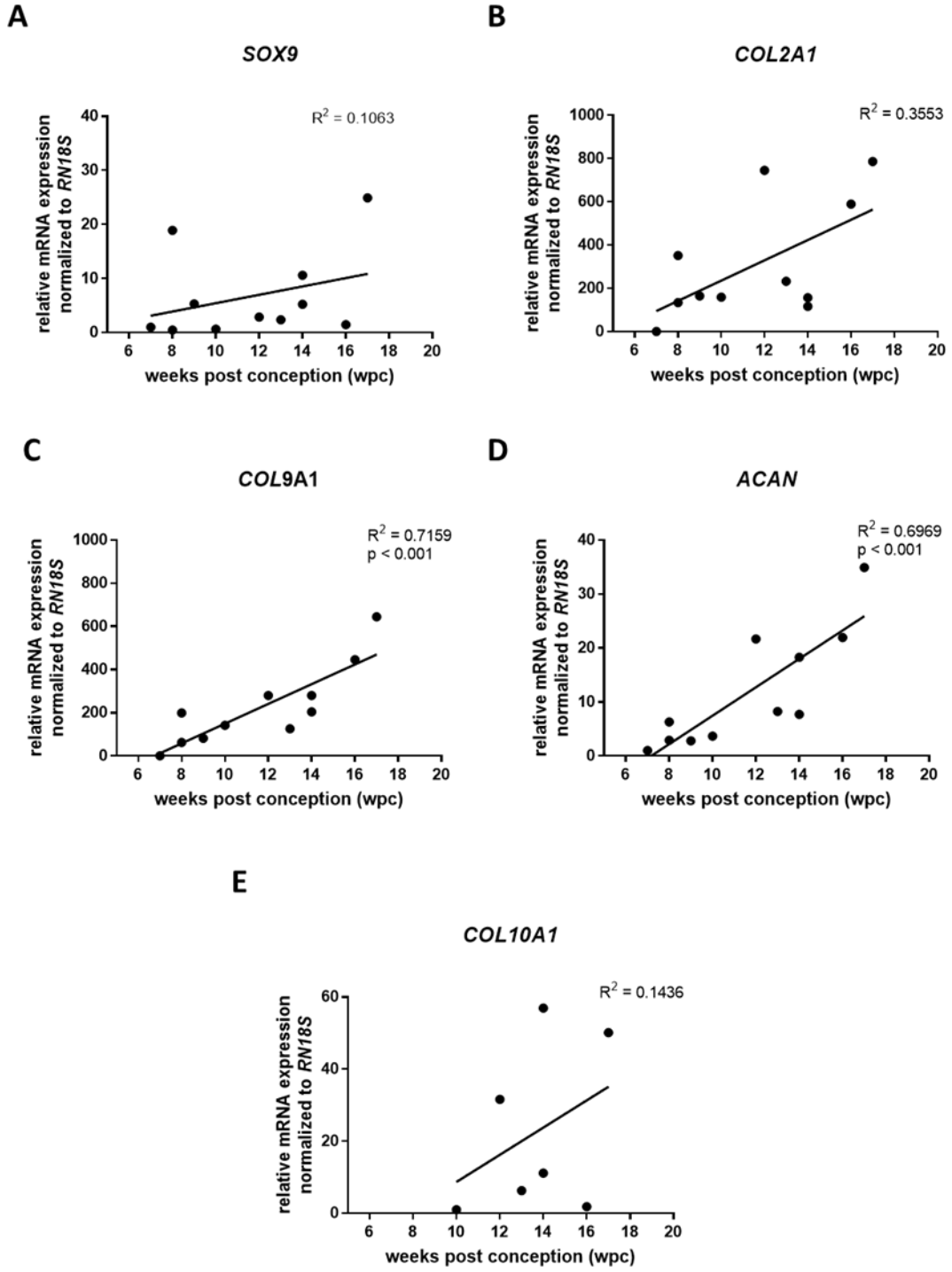

Figure 4.17 Expression of genes characteristic for chondrogenic differentiation in HFBCs) at passage 0.

Gene expression was normalised to *RN18S* (subunit 18S ribosomal RNA) at 7 weeks post conception (wpc). Values represent HFBCs isolated from individual human foetal femurs (n = 1) for each developmental week except 8 and 14 wpc (n = 2). Significance was determined by use of linear regression test. SOX9: SRY-box 9; COL2A1: type II collagen; COL9A1: type IX collagen; ACAN: aggrecan; COL10A1: type X collagen; R^2: Spearman's correlation coefficient.

Osteogenic master regulator ***RUNX2*** did not show any change in expression between 7 and 17 wpc (R^2 = 0.0065), (Figure 4.18 A, see Table 7.7 in Appendix H). ***COL1A1*** expression demonstrated no significant decrease between 7 and 17 wpc (R^2 = 0.2377, Figure 4.18 B, see Table 7.7 in Appendix H). ***OCN*** and ***OPN*** expression levels showed great variation in the individual samples but no significant increase or decrease in gene expression between 7 and 17 wpc (*OCN*: R^2= 0.0603; *OPN*: R^2 = 0.0537) (Figure 4.18 C and D, see Table 7.7 in Appendix H). Expression of ***ALPL*** (Figure 4.18 E, see Table 7.7 in Appendix H) were observed to be similar to *COL1A1* expression (R^2 = 0.3315).

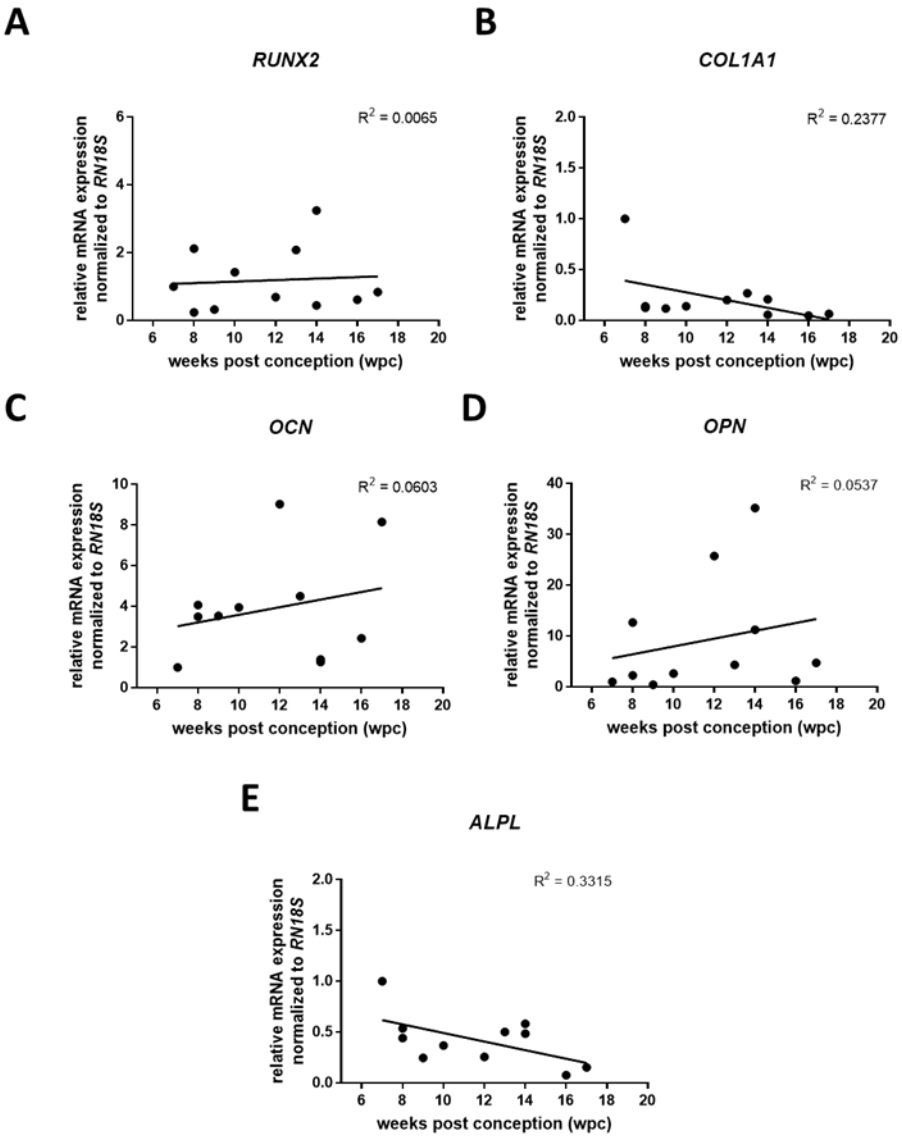

Figure 4.18 Expression of genes characteristic for osteogenic differentiation in human foetal bone cells (HFBCs) at passage 0. Gene expression was normalised to *RN18S* (subunit 18S ribosomal RNA) at 7 weeks post conception (wpc). Values represent HFBCs isolated from individual human foetal femurs (n =1) for each developmental week except 8 and 14 wpc (n = 2).

Significance was determined by use of linear regression test. RUNX2: runt-related transcription factor 2; COL1A1: type I collagen; ALPL: alkaline phosphatase; OCN: osteocalcin; OPN: osteopontin; R^2: Spearman's correlation coefficient.

In summary, only *COL9A1* and *ACAN* demonstrated a significant increase in HFBCs between 7 and 17 wpc. All other analysed genes characteristic for chondrogenesis (*SOX9*, *COL2A1*, *COL10A1*) as well as osteogenesis (*RUNX2*, *COL1A1*, *OCN*, *OPN*, *ALPL*) showed varied expression in HFBCs at the different developmental weeks the cells were isolated from. However, no significant increase or decrease with age of human foetal femurs (7 – 17 wpc) in those genes were observed. Furthermore, *COL10A1* expression was not detected in HFBCs ealier than 10 wpc.. In conclusion, these findings support the predominantly cartilaginous identity of human foetal femur at an earlier stage of development with slow onset of mineralisation during development.

After an additional passage following *in vitro* culture (passage 1), analysis of gene expression for chondrogenic genes in HFBCs isolated from human foetal femur samples, with an age range between 7 and 17 wpc, showed greater variation and wider range from the trend line compared to gene expression measured at passage 0.

SOX9 and ***COL2A1***, encoding for the main proteins in the cartilage template of the foetal femur, showed variation in gene expression (Figure 4.19 A and B), between 7 and 17 wpc (*SOX9*: $R^2 = 0.1214$; *COL2A1*: $R^2 = 0.04868$) (see Table 7.8 in Appendix H). ***COL9A1*** has been suggested to form a bridge between different types of collagens [360]. *COL9A1* expression did not show an increasing or decreasing trend between 7 and 17 wpc ($R^2 = 0.2731$) (Figure 4.19 C, see Table 7.8 in Appendix H). Aggrecan, encoded by ***ACAN***, displayed negligible changes with developmental age ($R^2 = 0.01666$, Figure 4.19 D) (see Table 7.8 in Appendix H). ***COL10A1***, expressed exclusively by hypertrophic chondrocytes, could not be detected in HFBCs at passage 1.

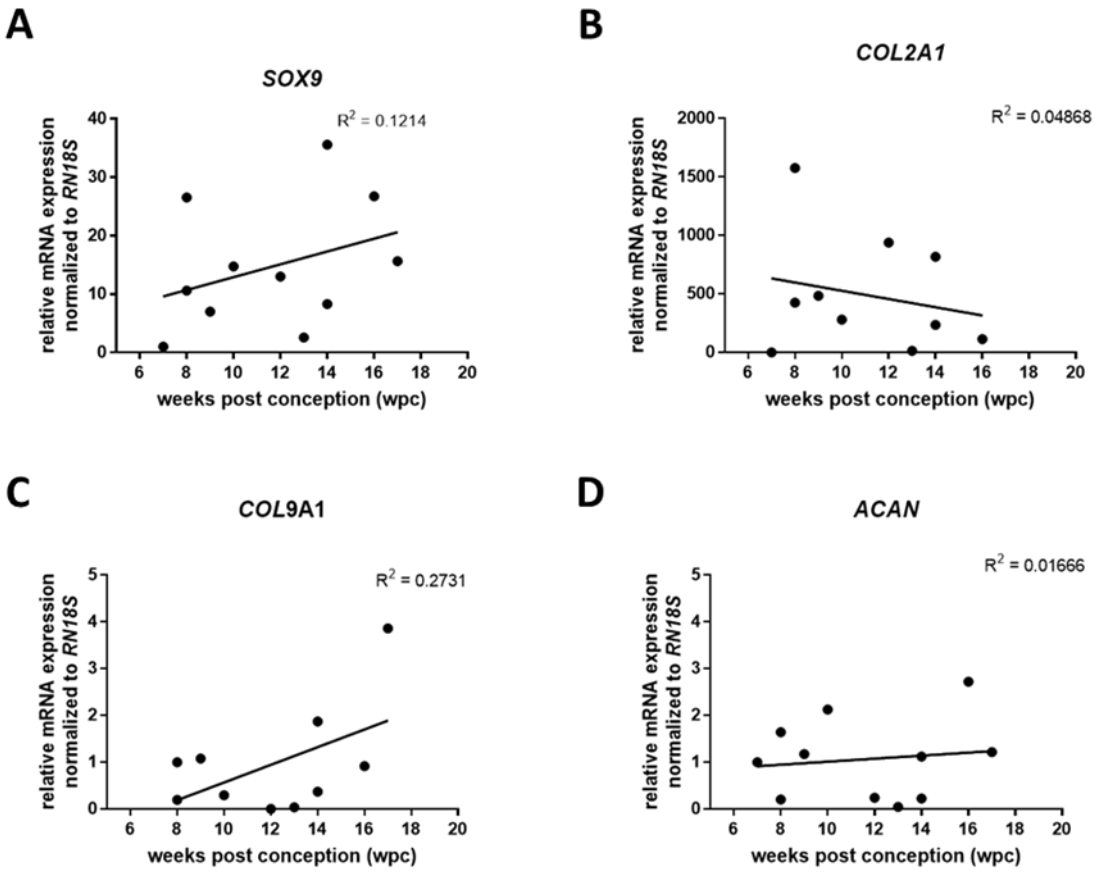

Figure 4.19 Expression of genes characteristic for chondrogenic differentiation in human foetal bone cells (HFBCs) at passage 1. Gene expression was normalised to *RN18S* (subunit 18S ribosomal RNA) at 7 weeks post conception (wpc). Values represent HFBCs isolated from individual human foetal femurs (n =1) for each developmental week except 8 and 14 wpc (n =2). Significance was determined by use of linear regression test. SOX9: SRY-box 9; COL2A1: type II collagen; COL9A1: type IX collagen; ACAN: aggrecan; R^2: Spearman's correlation coefficient.

Expression of osteogenic genes such as *RUNX2*, *OCN*, *OPN*, *ALPL* and *COL1A1* displayed, overall, varied expression in all analysed samples (Figure 4.20, Table 7.8 in Appendix H). ***RUNX2*** did not display any changes (R^2 = 0.02481) in expression between 7 and 17 wpc (Figure 4.20 A, see Table 7.8 in Appendix H) similar to *RUNX2* expression observed in HFBCs at passage 0. ***COL1A1*** mRNA expression demonstrated varied expression in HFBCs isolated from individual human foetal femurs between 7 and 17 wpc and no significant increase or decrease with developmental age (R^2 = 0.1997) in HFBCs at passage 1, (Figure 4.20 B, see Table 7.8 in Appendix H). ***OCN*** expression in HFBCs at passage 1 showed no clear increase (R^2 = 0.008635, Figure 4.20 C, see Table 7.8 in Appendix H). ***OPN*** mRNA expression could not be detected in HFBCs isolated from human foetal femur samples before 12 wpc. *OPN* expression varied in HFBCs isolated from human foetal femurs between 12

and 17 wpc (R^2 = 0.6553, Figure 4.20 D, see Table 7.8 in Appendix H). ***ALPL*** expression in HFBCs at passage 1 displayed great variation between 7 and 17 wpc (R^2 = 0.1607) (Figure 4.20 E, see Table 7.8 in Appendix H).

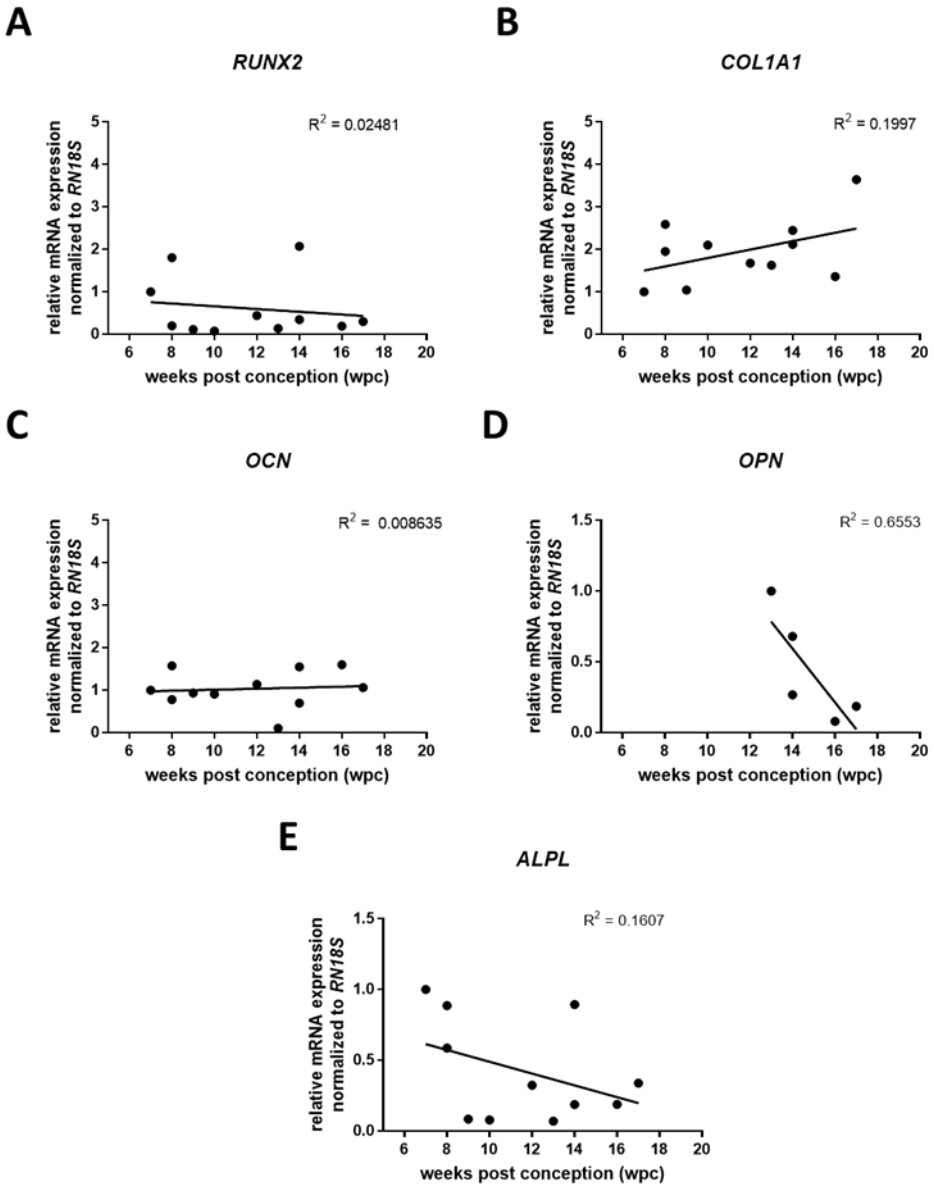

Figure 4.20 Expression of genes characteristic for osteogenic differentiation in human foetal bone cells (HFBCs) at passage 1. Gene expression was normalised to *RN18S* (subunit 18S ribosomal RNA) at 7 weeks post conception (wpc). Values represent HFBCs isolated from individual human foetal femurs (n =1) for each developmental week except 8 and 14 wpc (n = 2). Significance was determined by use of linear regression test. RUNX2: runt-related transcription factor 2; COL1A1: type I collagen; ALPL: alkaline phosphatase; OCN: osteocalcin; OPN: osteopontin; R^2: Spearman's correlation coefficient.

In summary, none of the analysed genes characteristic for chondrogenesis and osteogenesis demonstrated significant increase or decrease in HFBCs between 7 and 17 wpc at P1 with a wider spread of expression at the different developmental stages compared to P0.

4.3.4 Osteogenic differentiation of HFBCs isolated from 8 wpc human foetal femurs

Previous studies have shown osteogenic differentiation of HFBCs isolated from human foetal femurs at an early stage of development [62], or a developmentally more advanced stage [62, 361]. The differentiation potential of cells isolated from the diaphysis or epiphysis of the early and late developmental samples has been investigated [63, 307], however, direct comparison of HFBCs isolated from human foetal femurs at an early and at an advanced developmental stage had not been examined. Experiments in this subchapter will focus on treatment of HFBCs isolated from three 8 wpc human foetal femurs; standard osteogenic differentiation medium (from here on referred to as osteogenic background medium (oBG)) supplemented with a small molecule cocktail containing helioxanthin-derivate TH (4-(4-methoxyphenyl)pyrido[4′,3′:4,5]thieno[2,3-b]pyridine-2-carboxamide) [216] and hedgehog (HH)-pathway activator smoothened agonist (SAG) (see section 2.1.5 for more details on the osteogenic differentiation protocol). This differentiation medium was published before as part of a study looking to generate osteogenic cells from iPSCs with a mesenchymal cell intermediate step [183].

HFBCs isolated from 8 wpc human foetal femurs were treated with a combination of 1 μM TH and 1 μM SAG, each supplemented with osteogenic background medium (oBG) consisting of 10 nM dexamethasone, 10 nM 1,25-$(OH)_2$-vitamin D_3 and 100 μM ascorbic-2-phosphate for 19 days as monolayer culture (see section 2.1.5 for more details). Cells were analysed using histological methods (alkaline phosphatase (ALP) staining, alcian blue staining, alizarin red staining) and expression of genes characteristic for osteogenesis (*RUNX2*, *ALPL*, *COL1A1*, *OCN*, *OPN*) as well as chondrogenesis (*COL2A1*, *ACAN*) was compared between the different media combinations using qRT-PCR.

4.3.4.1 Histological staining

ALP staining showed an increase in intensity over the time course of differentiation in the examined osteogenic and basal medium conditions in HFBCs isolated from three individual

8 wpc human foetal femur samples (Figure 1.21). ALP staining in experiments 1 and 3 was equally weak under both osteogenic conditions (Figure 4.21 A and C), while HFBCs in experiment 2 demonstrated overall intense ALP staining (Figure 4.21 B). oBG and oBG supplemented with TH and SAG (oBG + TH + SAG) showed staining at both time points. The negative control (HFBCs cultured under basal medium in absence of osteogenic differentiation components) showed negligible staining at both time points in HFBCs in experiments 1 and 3 (Figure 4.21 A and C) with only weak staining in experiment 2 (Figure 4.21 B).

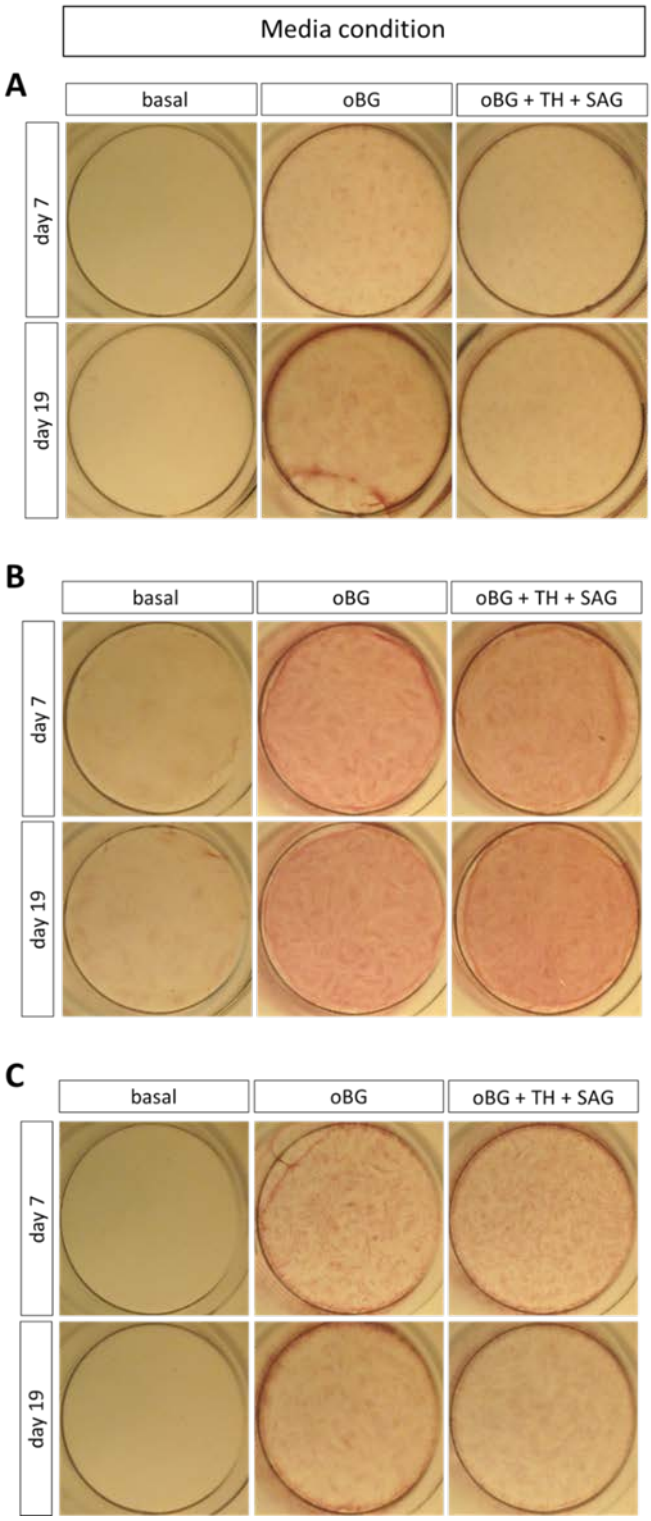

Figure 4.21 Alkaline phosphatase (ALP) staining in HFBCs isolated from 8 wpc human foetal femurs treated with basal medium, osteogenic background medium (oBG, 10 nM dexamethasone, 10 nM 1,25-$(OH)_2$-vitamin D_3 and 100 µM ascorbic-2-phosphate) and osteo background (oBG) medium supplemented with small molecules SAG (smoothened agonist) and TH (4-(4-methoxyphenyl)pyrido[4′,3′:4,5]thieno[2,3-b]pyridine-2-carboxamide). Results of three individual differentiation experiments in 24-wells are displayed in **A - C.** HFBCs: human foetal bone cells.

Alcian blue staining showed a temporal continuous increase in intensity over the time course of differentiation in HFBCS isolated from all samples treated with both osteogenic media. Overall, the most intense staining was detected under oBG + TH + SAG culture conditions after 19 days in all three experiments (Figure 4.22). HFBCs in experiment 2 demonstrated weak staining under basal culture conditions at both time points (Figure 4.22 B), whereas in experiments 1 and 3, no staining was detected under basal culture conditions (Figure 4.22 A and C).

To determine the efficiency of mineralisation, alizarin red staining was performed (Figure 4.23). Alizarin red staining was widely distributed in the HFBC monolayer cultures as opposed to the demonstration of compact nodule-like structures [345]. Treatment with basal or osteogenic medium did not result in measurable differences in alizarin red staining and detection of mineralised nodules (orange colour) after 7 and 19 days.

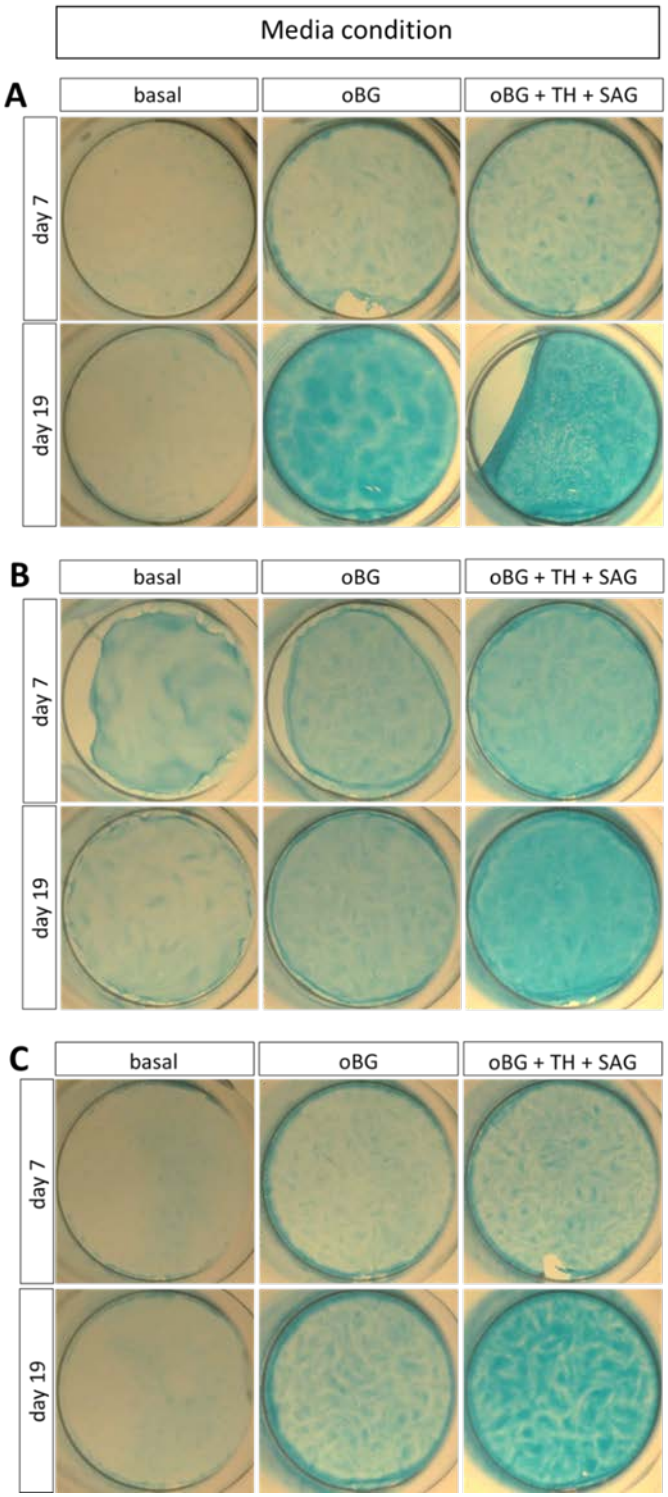

Figure 4.22 Alcian Blue staining in HFBCs isolated from 8 wpc human foetal femurs treated with basal medium, osteogenic background medium (oBG, 10 nM dexamethasone, 10 nM 1,25-$(OH)_2$-vitamin D_3 and 100 µM ascorbic-2-phosphate) and osteo background (oBG) medium supplemented with small molecules SAG (smoothened agonist) and TH (4-(4-methoxyphenyl)pyrido[4′,3′:4,5]thieno[2,3-b]pyridine-2-carboxamide). Results of three individual differentiation experiments in 24-wells are displayed in **A - C.** HFBCs: human foetal bone cells.

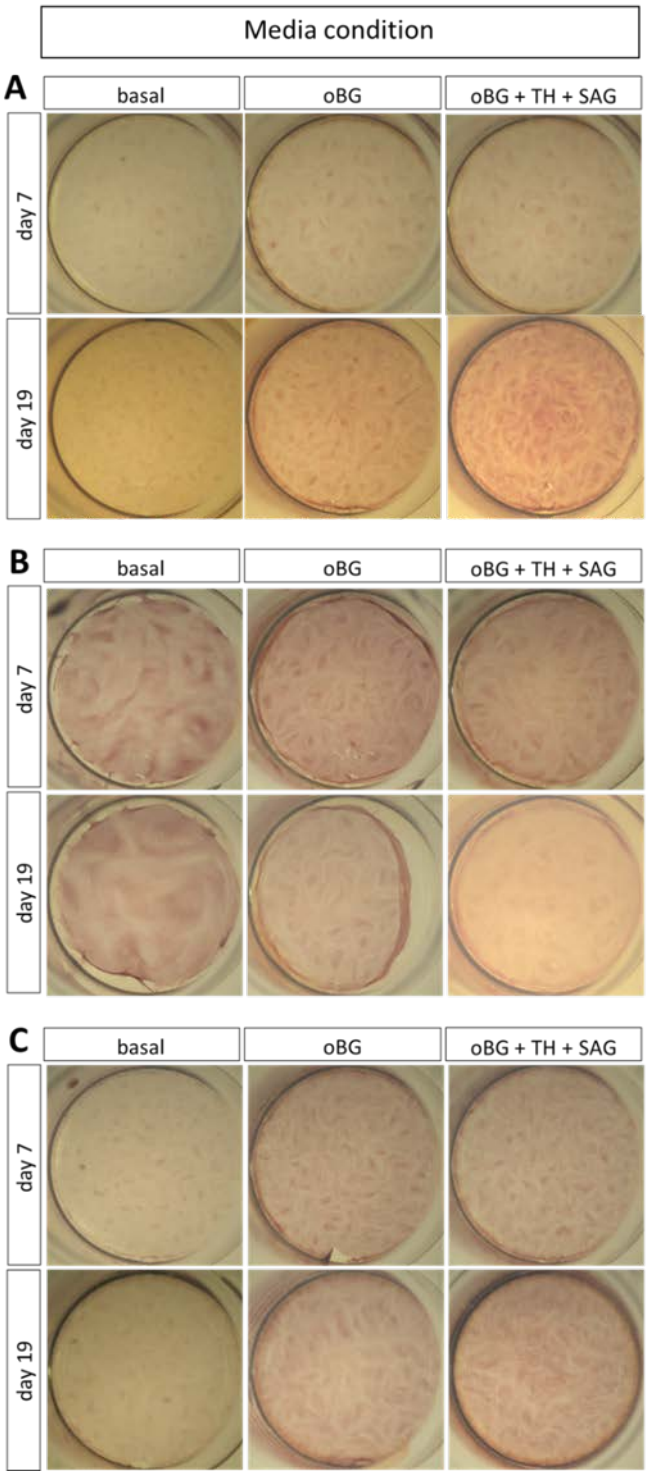

Figure 4.23 Alizarin Red staining in HFBCs isolated from 8 wpc human foetal femurs treated with basal medium, osteogenic background medium (oBG, 10 nM dexamethasone, 10 nM 1,25-$(OH)_2$-vitamin D_3 and 100 µM ascorbic-2-phosphate) and osteo background (oBG) medium supplemented with small molecules SAG (smoothened agonist) and TH (4-(4-methoxyphenyl)pyrido[4′,3′:4,5]thieno[2,3-b]pyridine-2-carboxamide). Results of three individual differentiation experiments in 24-wells are displayed in **A - C.** HFBCs: human foetal bone cells.

ALP staining showed similar staining intensity for both tested osteogenic media after 19 days while Alizarin Red staining was shown to be equally wide spread throughout the monolayer and no mineralised nodules were found for both tested osteogenic media after 19 days. The presence of ALP in differentiated HFBCs in both tested osteogenic media after 19 days indicated the formation of osteoblasts and the presence of Alizarin Red stained cells suggest the success of osteogenic differentiation. However, HFBCs cultered in oBG + TH + SAG demonstrated more intense Alcian Blue staining after 19 days compared to standard osteogenic medium (oBG), in turn suggesting an increased matrix production. Despite the oBG + TH + SAG medium having been previously used for osteogenic differentiation, the higher production of matrix compared to the standard osteogenic medium has never been reported before. It is possible that the starting cell population of HFBCs isolated from 8 wpc human foetal femur had an influence on the higher matrix production after 19 days under oBG + TH + SAG culture conditions.

4.3.4.2 Gene expression analysis

Gene expression for genes characteristic for osteogenesis (*RUNX*2, *ALPL*, *OCN*, *OPN*, *COL1A1*) and chondrogenesis (*COL2A1*, *ACAN*) were analysed using qRT-PCR in order to investigate the success of the osteogenic differentiaton of HFBCs isolated from 8 wpc human foetal femurs.

Key regulator for osteogenesis, ***RUNX2***, demonstrated no significant difference between day 7 and day 19 in all three conditions compared to day 0 (Figure 4.24 A, Table 4.5, Appendix J). *RUNX2* expression showed 0.06-fold change expression after 7 days and 0.32-fold change expression after 19 days under basal culture conditions. Culture in oBG medium resulted in 0.06-fold change expression after 7 days and 0.22-fold change expression after 19 days of culture. NIBSC-8 MSCs cultured in oBG + TH + SAG for 7 days showed 0.10-fold change expression with 1.31-fold change expression after 19 days of culture.

ALPL showed no significant difference between day 7 and day 19 in all three conditions compared to day 0 (Figure 4.24 B, Table 4.5, Appendix J). Basal culture medium resulted in 0.19-fold change *ALPL* expression after 7 days and 0.39-fold change expression after 19 days. Treatment with oBG culture medium demonstrated 2.06-fold change expression after 7 days and 2.15-fold change expression after 19 days. oBG + TH + SAG osteogenic medium

resulted 1.94-fold change expression after 7 days of culture and 5.03-fold change expression after 19 days.

Overall ***COL1A1*** mRNA expression was downregulated in all investigated media compositions at all time points compared to day 0, with *COL1A1* mRNA also similarly expressed in all three tested culture conditions after 7 days (basal: mean 0.18-fold change, $p < 0.0001$; oBG: mean 0.14-fold change, $p < 0.0001$; oBG + TH + SAG: mean 0.20-fold change, $p < 0.0001$) as well as 19 days (basal: mean 0.29-fold change, $p < 0.001$; oBG: mean 0.06-fold change, $p < 0.0001$; oBG + TH + SAG: mean 0.39-fold change, $p < 0.001$). mRNA expression was lowest after 19 days under oBG culture conditions and highest after 19 days under oBG + TH + SAG culture conditions. Expression levels were similar in HFBCs cultured in any of the three tested conditions (Figure 4.24 C, Table 4.5, Appendix J).

OCN mRNA expression levels showed no significant difference between day 7 and day 19 in all three conditions compared to day 0 (Figure 4.24 D, Table 4.5, Appendix J). Under basal culture conditions demonstrated 0.43-fold change expression after 7 days and 0.79-fold change expression after 19 days. Culture of HFBCs isolated from 8 wpc human foetal femur in oBG medium for 7 days resulted in 0.89-fold change expression and 0.50-fold change expression after 19 days. *OCN* expression in HFBCs isolated from 8 wpc human foetal femurs treated with oBG + TH + SAG osteogenic medium for 7 days demonstrated 0.57-fold change and after 19 days 0.87-fold change.

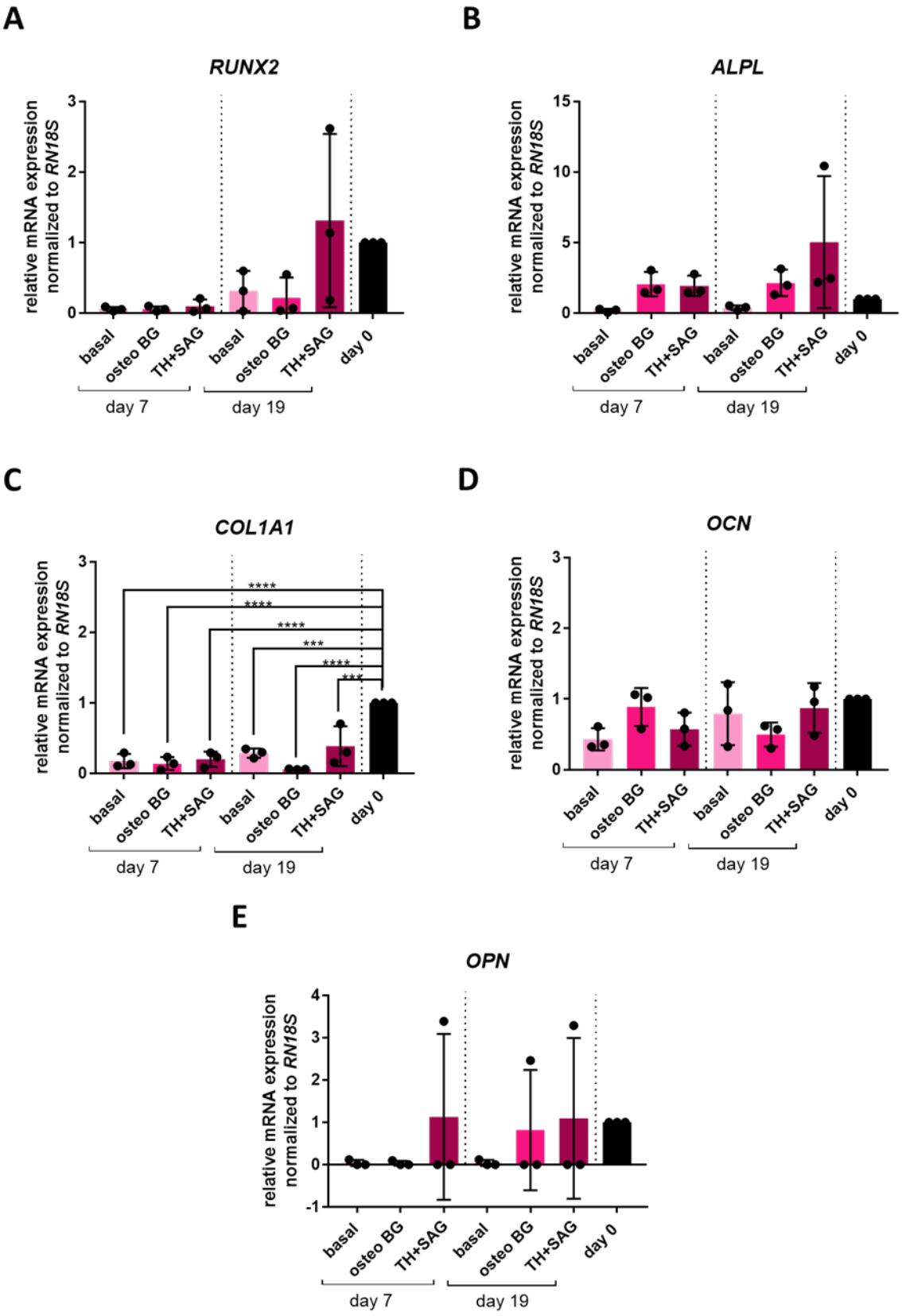

Figure 4.24 Expression of genes characteristic for osteogenesis in HFBCs isolated from 8 wpc old foetal femur samples treated with basal medium, osteogenic background medium (oBG, 10 nM dexamethasone, 10 nM 1,25-$(OH)_2$-vitamin D_3 and 100 µM ascorbic-2-phosphate) and

osteo background (oBG) medium supplemented with small molecules SAG (smoothened agonist) and TH (4-(4-methoxyphenyl)pyrido[4′,3′:4,5]thieno[2,3-b]pyridine-2-carboxamide). Gene expression displayed as mean +/- SD and was normalised to *RN18S* at day 0 in basal medium. Two-way ANOVA with Dunnett's post-hoc test for multiple comparisons was performed to compare different culture conditions of n = 3 differentiation experiments. *** $p < 0.001$; **** $p < 0.0001$. RUNX2: runt-related transcription factor 2; ALPL: alkaline phosphatase; COL1A1: collagen type 1; OCN: osteocalcin; OPN: osteopontin, RN18S: subunit 18S ribosomal RNA; HFBCs: human foetal bone cells; wpc: weeks post conception.

Table 4.5 Summary of respective gene expression characteristic for osteogenesis in HFBCs isolated from 8 wpc human foetal femurs treated with basal medium, osteogenic background medium (oBG, 10 nM dexamethasone, 10 nM 1,25-$(OH)_2$-vitamin D_3 and 100 µM ascorbic-2-phosphate) and oBG supplemented with small molecules SAG (smoothened agonist) and TH (4-(4-methoxyphenyl)pyrido[4′,3′:4,5]thieno[2,3-b]pyridine-2-carboxamide). Gene expression was normalised to *RN18S* (subunit of 18S ribosomal RNA) at day 0. Osteogenic differentiation was performed three times (n = 3). Mean +/- SD displayed. HFBCs: human foetal bone cells**.**

	condition	***RUNX2***	***ALPL***	***COL1A1***	***OCN***	***OPN***
Day 7	basal	0.06 +/- 0.03	0.19 +/- 0.13	0.18 +/- 0.10	0.43 +/- 0.16	0.04 +/- 0.07
	oBG	0.06 +/- 0.04	2.06 +/- 0.86	0.14 +/- 0.09	0.89 +/- 0.27	0.03 +/- 0.06
	oBG + TH + SAG	0.10 +/- 0.09	1.94 +/- 0.71	0.20 +/- 0.11	0.57 +/- 0.24	1.13 +/- 1.96
Day 19	basal	0.32 +/- 0.28	0.39 +/- 0.17	0.29 +/-0.07	0.79 +/- 0.44	0.04 +/- 0.07
	oBG	0.22 +/- 0.28	2.15 +/- 0.93	0.06 +/- 0.004	0.50 +/- 0.17	0.82+/- 1.42
	oBG + TH + SAG	1.31 +/- 1.22	5.03 +/- 4.68	0.39 +/- 0.28	0.87 +/- 0.35	1.10 +/- 1.89

OPN expression showed no significant difference between day 7 and day 19 in all three conditions compared to day 0 (Figure 4.24 E, Table 4.5, Appendix J). Under basal culture conditions was observed to be 0.04-fold change expression after 7 days and 0.04-fold change expression after 19 days. Culture of HFBCs isolated from 8 wpc human foetal femur in oBG medium resulted in 0.03-fold change expression after 7 days and 0.82-fold change expression after 19 days. HFBCs isolated from 8 wpc human foetal femurs cultured in oBG + TH + SAG osteogenic medium demonstrated 1.13-fold change expression after 7 days and 1.10-fold change expression after 19 days.

COL2A1 was barely detectable in all three media compositions at both time points (except under basal conditions at day 7: mean 0.19-fold change). Low mRNA expression was significant in relation to day 0 (day 7: basal mean 0.19-fold change, $p < 0.0001$; oBG: negligible expression, $p < 0.0001$; oBG + TH + SAG: undetectable, $p < 0.0001$; day 19: basal: mean 1.10-fold change, $p < 0.0001$; oBG: undetectable, $p < 0.0001$; oBG + TH + SAG: 0.004-fold change, $p < 0.0001$) (Figure 4.25 A, Table 4.6, Appendix J).

ACAN showed slightly higher expression than *COL2A1*, however, with a similar trend in mRNA in the tested media compositions at both time points. Measured mRNA expression was significant relative to day 0 (day 7: basal mean 0.34-fold change, $p < 0.05$; oBG: mean 0.21-fold change, $p < 0.01$; oBG + TH + SAG: mean 0.25-fold change, $p < 0.01$; day 19: basal: mean 0.45-fold change, $p < 0.05$; oBG: mean 0.29-fold change, $p < 0.05$; oBG + TH + SAG: mean 0.22-fold change, $p < 0.01$) (Figure 4.25 B, Table 4.6, Appendix J).

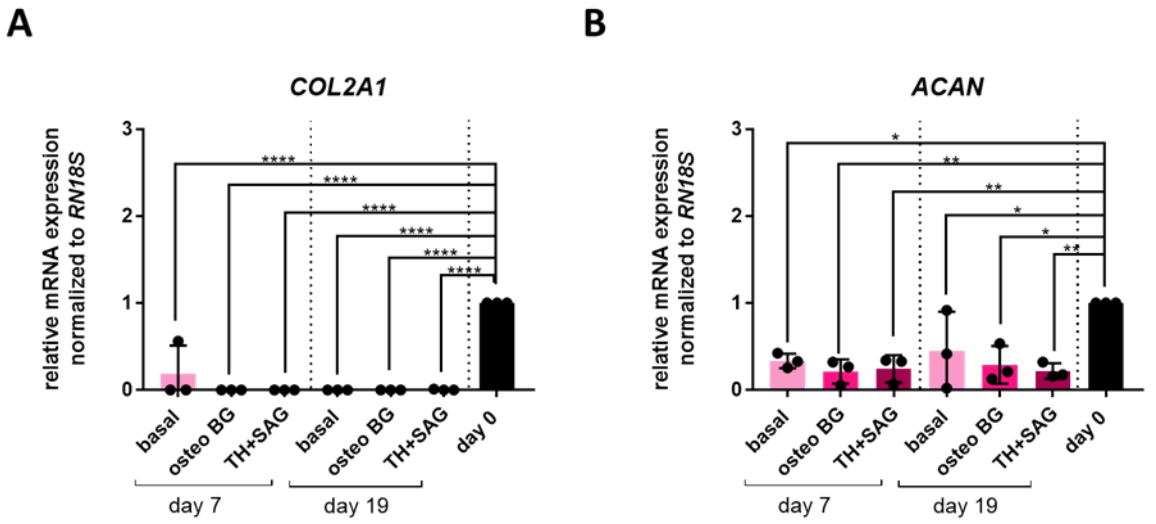

Figure 4.25 Expression of genes characteristic for chondrogenic differentiation in HFBCs isolated from 8 wpc old foetal femur samples treated with basal medium, osteogenic background medium (oBG, 10 nM dexamethasone, 10 nM 1,25-$(OH)_2$-vitamin D_3 and 100 µM ascorbic-2-phosphate) and osteo background (oBG) medium supplemented with small molecules SAG (smoothened agonist) and TH (4-(4-methoxyphenyl)pyrido[4′,3′:4,5]thieno[2,3-b]pyridine-2-carboxamide). Gene expression displayed as mean +/- SD and was normalised to *RN18S* at day 0 in basal medium. Two-way ANOVA with Dunnett's post-hoc test for multiple comparisons was performed to compare different culture conditions of n = 3 differentiation experiments. * $p < 0.05$; ** $p < 0.01$; **** $p < 0.0001$. COL2A1: collagen type2; ACAN: aggrecan; RN18S: subunit 18S ribosomal RNA; HFBCs: human foetal bone cells; wpc: weeks post conception.

Table 4.6 Summary of respective gene expression characteristic for chondrogenesis in HFBCs isolated from 8 wpc human foetal femurs treated with basal medium, osteogenic background medium (oBG, 10 nM dexamethasone, 10 nM 1,25-$(OH)_2$-vitamin D_3 and 100 µM ascorbic-2-phosphate) and oBG supplemented with small molecules SAG (smoothened agonist) and TH (4-(4-methoxyphenyl)pyrido[4′,3′:4,5]thieno[2,3-b]pyridine-2-carboxamide). Gene expression was normalised to *RN18S* (subunit of 18S ribosomal RNA) at day 0. Osteogenic differentiation was performed three times (n = 3). Mean +/- SD displayed. HFBCs: human foetal bone cells.

	condition	*COL2A1*	*ACAN*
Day 7	basal	0.19 +/- 0.32	0.34 +/- 0.084
	oBG	0.00	0.21 +/- 0.14
	oBG + TH + SAG	0.00	0.25 +/- 0.15
Day 19	basal	0.00	0.45 +/- 0.44
	oBG	0.00	0.29 +/- 0.21
	oBG + TH + SAG	0.00 +/- 0.007	0.22 +/- 0.09

In summary, *COL1A1* was shown to be downregulated in all tested osteogenic media conditions compared to days 0 after 19 days as well as 7 days of culture. None of the other tested genes associated with osteogenesis were significantly up- or downregulated in any of the two tested osteogenic culture conditions. The observed downregulation of *COL1A1* did not seem to correlate with the more intense Alcian Blue staining shown in Figure 4.22 after 19 days of culture in osteogenic media compared to day 7 or day 0. The intense Alcian Blue staining after 19 days suggested formation of matrix which contains collagens. The presence of collagen type II is an indicator for a more chondrogenic result of the 19 days differentiaton whereas the presence of collagen type I indicates a type of matrix found during endochondral bone formaton. However, analysis of *COL2A1* showed downregulation of this gene in both tested osteogenic media conditons. Based on gene expression alone it couldn't be determined whether the identified formation of matrix was of a more chondrogenic nature.

Culture of HFBCs in osteogenic medium oBG + TH + SAG showed a more intense Alcian Blue staining after 19 days compared to standard osteogenic medium (oBG). ALP staining showed similar staining intensity for both tested osteogenic media after 19 days while Alizarin Red staining was shown to be equally wide spread throughout the monolayer and no mineralised nodules were found for both tested osteogenic media after 19 days. The

presence of ALP in differentiated HFBCs was identified in both tested osteogenic media after 19 days, indicating the formation of osteoblasts, and the presence of Alizarin Red stained cells suggest the success of osteogenic differentiation. However, the supplementation of the standard osteogenic differentiation medium (oBG) with the small molecules TH and SAG resulted in a greater production of matrix compared to the standard osteogenic medium. Depsite the oBG + TH + SAG medium having been previously used for osteogenic differentiation, the higher production of matrix compared to the standard osteogenic medium has never been reported before. It is also possible that the starting cell population ofHFBCs isolated from 8 wpc human foetal femurs had an influence on the higher matrix production after 19 days under oBG + TH + SAG culture conditions.

In order to test whether HFBCs isolated from a developmentally more advanced human foetal femur would demonstrate better osteogenic differentiation efficiency compared to HFBCs isolated from 8 wpc human foetal femurs, HFBCs isolated from 14 wpc human foetal femurs were cultured in both osteogenic differentiation media as used before for 19 days.

4.3.5 Osteogenic differentiation of HFBCs isolated from 14 wpc human foetal femurs

As described in section 4.3.4, the osteogenic differentiation potential of HFBCs isolated from human foetal femurs at an early and slightly more advanced developmental stage will be investigated. Experiments in this subchapter will focus on treatment of HFBCs, isolated from three 14 wpc human foetal femurs, and standard osteogenic differentiation medium (from here on referred to as osteogenic background medium (oBG)) supplemented with a small molecule cocktail containing helioxanthin-derivate TH (4-(4-methoxyphenyl)pyrido[4′,3′:4,5]thieno[2,3-b]pyridine-2-carboxamide) [216], and hedgehog (HH)-pathway activator smoothened agonist (SAG) (see section 2.1.5 for more details on the osteogenic differentiation protocol). This differentiation medium was published before as part of a study looking to generate osteogenic cells from iPSCs with a mesenchymal cell intermediate step [183].

HFBCs isolated from 14 wpc human foetal femurs were treated with a combination of 1 μM TH and 1 μM SAG, each supplemented with osteogenic background medium (oBG) consisting of 10 nM dexamethasone, 10 nM 1,25-$(OH)_2$-vitamin D_3 and 100 μM ascorbic-2-phosphate for 19 days as monolayer culture (see section 2.1.5 for more details). Cells were analysed using histological methods (ALP staining, alcian blue staining, alizarin red

staining) and expression of genes characteristic for osteogenesis (*RUNX*2, *ALPL*, *COL1A1*, *OCN*, *OPN*) as well as chondrogenesis (*COL2A1*, *ACAN*) were compared between the different media combinations using qRT-PCR.

4.3.5.1 Histological analysis

ALP staining showed an increase in intensity over the time course of differentiation in the examined osteogenic conditions (Figure 4.26). Treatment with osteogenic medium oBG + TH + SAG in experiments 1 and 3 resulted in most intense, yet still weak staining after 19 days (Figure 4.26 A and C). HFBCs in experiment 2 showed less intense ALP staining. Treatment of HFBCs with oBG and oBG + TH + SAG in experiment 1 (Figure 4.26 A) and experiment 3 (Figure 4.26 C) showed equally faint ALP staining at 7 and 19 days. The negative control (HFBCs cultured under basal medium in absence of osteogenic differentiation components) showed no staining at both time points in HFBCs in experiment 1 (Figure 4.26 A) and experiment 3 (Figure 4.26 C). HFBCs in experiment 2 showed overall lower staining intensity at both time points compared to experiments 1 and 3 (Figure 4.26 B).

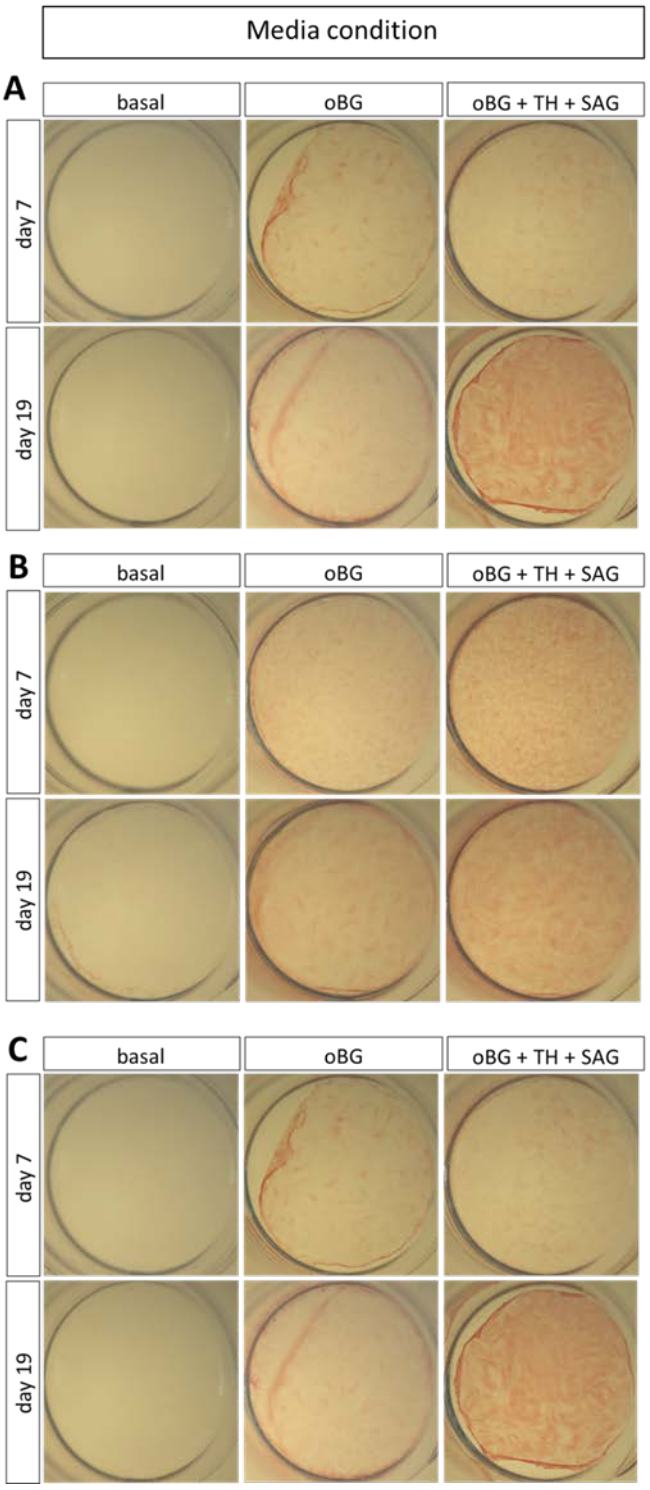

Figure 4.26 Alkaline phosphatase (ALP) staining in HFBCs isolated from 14 wpc human foetal femurs treated with basal medium, osteogenic background medium (oBG, 10 nM dexamethasone, 10 nM 1,25-$(OH)_2$-vitamin D_3 and 100 µM ascorbic-2-phosphate) and osteo background (oBG) medium supplemented with small molecules SAG (smoothened agonist) and TH (4-(4-methoxyphenyl)pyrido[4′,3′:4,5]thieno[2,3-b]pyridine-2-carboxamide). Results of three individual differentiation experiments in 24-wells are displayed in **A - C.** HFBCs: human foetal bone cells.

Alcian blue staining, commonly used to stain polysaccharides (e.g. glycosaminoglycans in cartilage), was widely distributed in all three differentiation experiments using HFBCs (Figure 4.27). Alcian blue staining showed a temporal continuous increase in intensity over the time course of differentiation in HFBCs in all three experiments, treated with both osteogenic media whilst demonstrating negligible staining at days 7 and 19. Overall, HFBCs in experiment 2 (Figure 4.27 B) showed the most intense staining under all culture conditions after 7 and 19 days with oBG + TH + SAG, demonstrating the most intense staining at day 19.

To determine the efficiency of mineralisation, Alizarin red staining was performed (Figure 4.27). Alizarin red staining was widely distributed in the HFBC monolayer cultures as opposed to the demonstration of compact nodule-like structures [345]. Treatment with basal or osteogenic medium did not result in measurable differences in alizarin red staining and, detection of mineralised nodules (orange colour) after 7 and 19 days in all three performed differentiation experiments.

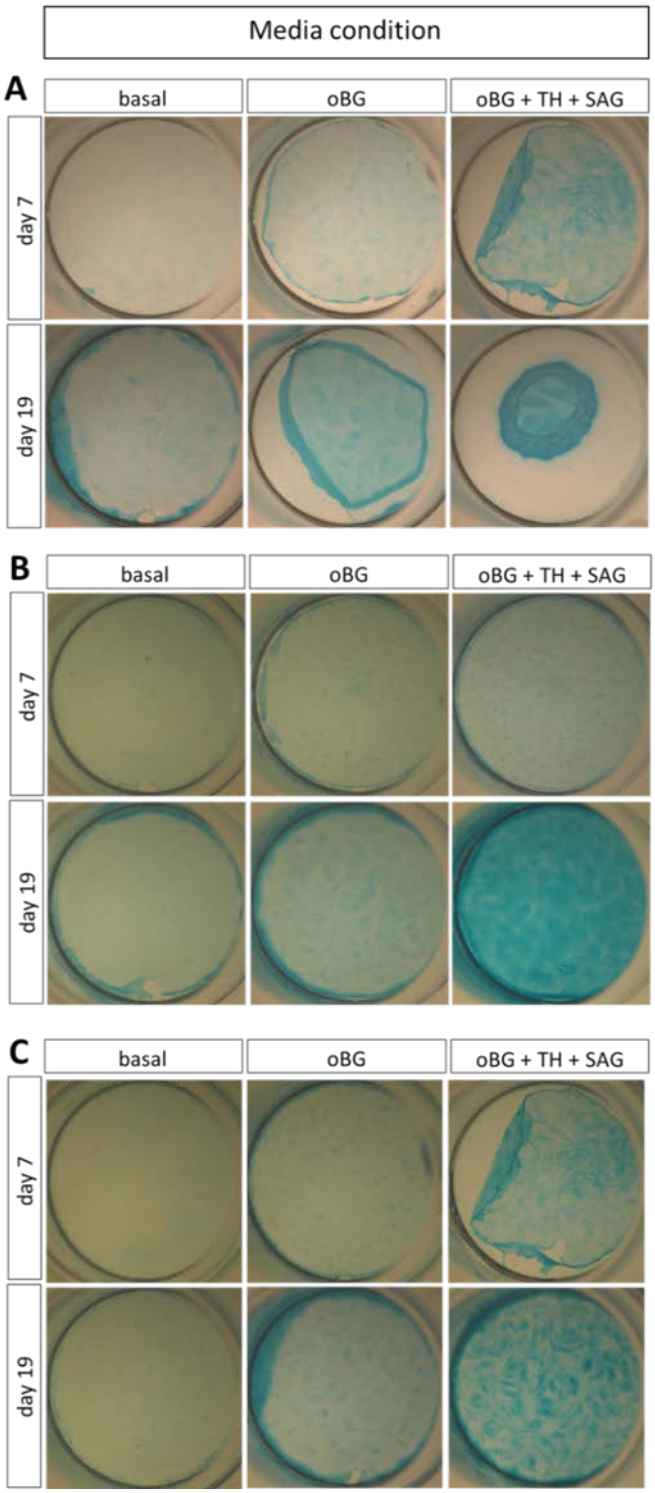

Figure 4.27 Alcian Blue staining in HFBCs isolated from 14 wpc human foetal femurs treated with basal medium, osteogenic background medium (oBG, 10 nM dexamethasone, 10 nM 1,25-$(OH)_2$-vitamin D_3 and 100 µM ascorbic-2-phosphate) and osteo background (oBG) medium supplemented with small molecules SAG (smoothened agonist) and TH (4-(4-methoxyphenyl)pyrido[4′,3′:4,5]thieno[2,3-b]pyridine-2-carboxamide). Results of three individual differentiation experiments in 24-wells are displayed in **A - C.** HFBCs: human foetal bone cells.

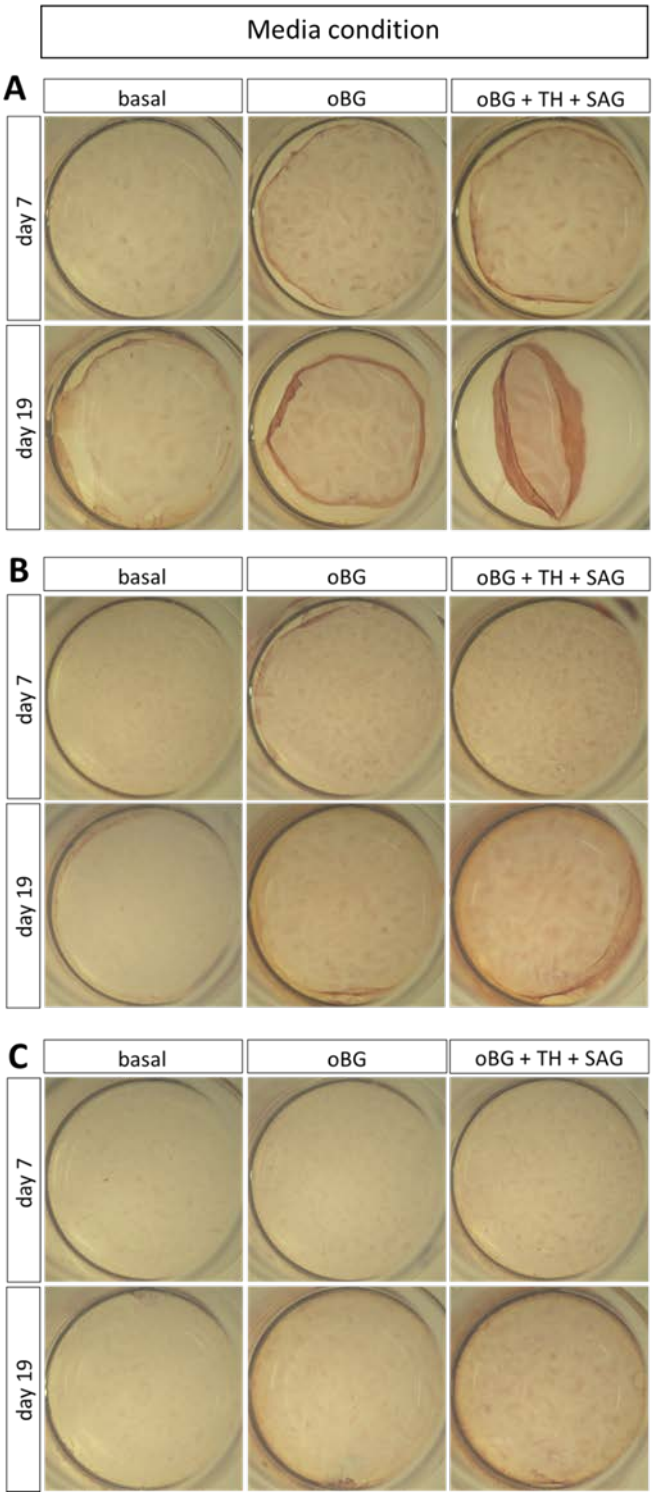

Figure 4.28 Alizarin Red staining in HFBCs isolated from 14 wpc human foetal femurs treated with basal medium, osteogenic background medium (oBG, 10 nM dexamethasone, 10 nM 1,25-$(OH)_2$-vitamin D_3 and 100 µM ascorbic-2-phosphate) and osteo background (oBG) medium supplemented with small molecules SAG (smoothened agonist) and TH (4-(4-methoxyphenyl)pyrido[4′,3′:4,5]thieno[2,3-b]pyridine-2-carboxamide). Results of three individual differentiation experiments in 24-wells are displayed in **A - C.** HFBCs: human foetal bone cells.

In summary, ALP as well as Alizarin Red staining was overall less intense in differentiated HFBCs isolated from 14 wpc human foetal femurs compared to differentiated HFBCs isolated from 8 wpc human foetal femurs. Alican Blue staining demonstrated equal if not more intense staining after 19 days under oBG + TH + SAG media of differentiated HFBCs isolated from 14 wpc human foetal femurs compared to HFBCs isolated from 8 wpc human foetal femurs. Based on these findings suggest that HFBCs isolated from 8 wpc human foetal femurs appeared to be more suitable for a more efficient outcome of osteogenic differentiation compared to differentiated HFBCs isolated from 14 wpc human foetal femurs.

4.3.5.2 Gene expression analysis

Gene expression for genes characteristic for osteogenesis (*RUNX*2, *ALPL*, *OCN*, *OPN*, *COL1A1*) and chondrogenesis (*COL2A1*, *ACAN*) were analysed using qRT-PCR in order to investigate the success of the osteogenic differentiaton of HFBCs isolated from 14 wpc human foetal femurs.

Key regulator for osteogenesis, ***RUNX2***, showed no significant difference between day 7 and day 19 in all three conditions compared to day 0 (Figure 4.29 A, Table 4.7, Appendix K). Under basal culture conditions showed 0.77-fold change expression after 7 days under and 0.73-fold change expression after 19 days. HFBCs isolated from 14 wpc human foetal femurs cultured in oBG medium for 7 days demonstrated 0.76-fold change expression and 0.87-fold change expression after 19 days. oBG + TH + SAG osteogenic culture medium resulted in 0.87-fold change expression in HFBCs isolated from 14 wpc human foetal femurs after 7 days of culture osteogenic medium and 1.35-fold change expression after 19 days.

ALPL mRNA expression analysis resulted in no significant difference between day 7 and day 19 in all three conditions compared to day 0 (Figure 4.29 B, Table 4.7, Appendix K). Under basal culture conditions was observed to be 0.83-fold change expression after 7 days and 0.36-fold change expression after 19 days. Culture of HFBCs isolated from 14 wpc human foetal femurs in oBG culture medium demonstrated 2.15-fold change expression after 7 days and 1.10-fold change expression after 19 days. Gene expression after 7 days of culture in oBG + TH + SAG was significantly increased compared to day 0 (3.71-fold change expression, $p < 0.05$). Expression of *ALPL* after 19 days culture in oBG + TH + SAG was 2.57-fold change expression.

COL1A1 mRNA was similarly expressed in all three tested culture conditions after seven days (basal: mean 0.52-fold change; oBG: mean 0.55-fold change; oBG + TH + SAG: mean 0.60-fold change). mRNA expression was decreased in all three media compositions after 19 days of culture (basal: mean 0.38-fold change; oBG: mean 0.14-fold change; oBG + TH + SAG: mean 0.28-fold change). *COL1A1* mRNA expression in all conditions at both time points was found to be significantly lower in relation to day 0 (day 7 basal $p < 0.01$; oBG $p < 0.05$; oBG + TH + SAG $p < 0.05$; day 19: basal $p < 0.01$; oBG $p < 0.0001$; oBG + TH + SAG $p < 0.001$) (Figure 4.29 C, Table 4.7, Appendix K).

OCN mRNA expression levels were insignificant in all three conditions at both time points compared to day 0 (Figure 4.29 D, Table 4.7, Appendix K). Under basal culture conditions, HFBCs isolated from 14 wpc human foetal femurs gene expression was observed to be 0.84-fold change expression after 7 days and 0.83-fold change expression after 19 days. oBG culture medium resulted in 1.01-fold change expression after 7 days and 0.92-fold change expression after 19 days. oBG + TH + SAG culture medium showed 0.84-fold change expression after 7 days of culture and 0.89-fold change expression after 19 days.

OPN mRNA expression demonstrated similarly low expression in all three tested media compositions after seven days relative to day 0 (basal: mean 0.17-fold change, $p < 0.05$; oBG: mean 0.12-fold change, $p < 0.01$; oBG + TH + SAG: mean 0.13-fold change, $p < 0.01$), whereas mRNA expression increased in all three conditions after 19 days in culture relative to day 0 (basal: 0.11-fold change, $p < 0.01$; oBG: mean 0.31-fold change, $p < 0.05$; oBG + TH + SAG: 0.47-fold change) (Figure 4.29 E, Table 4.7, Appendix K).

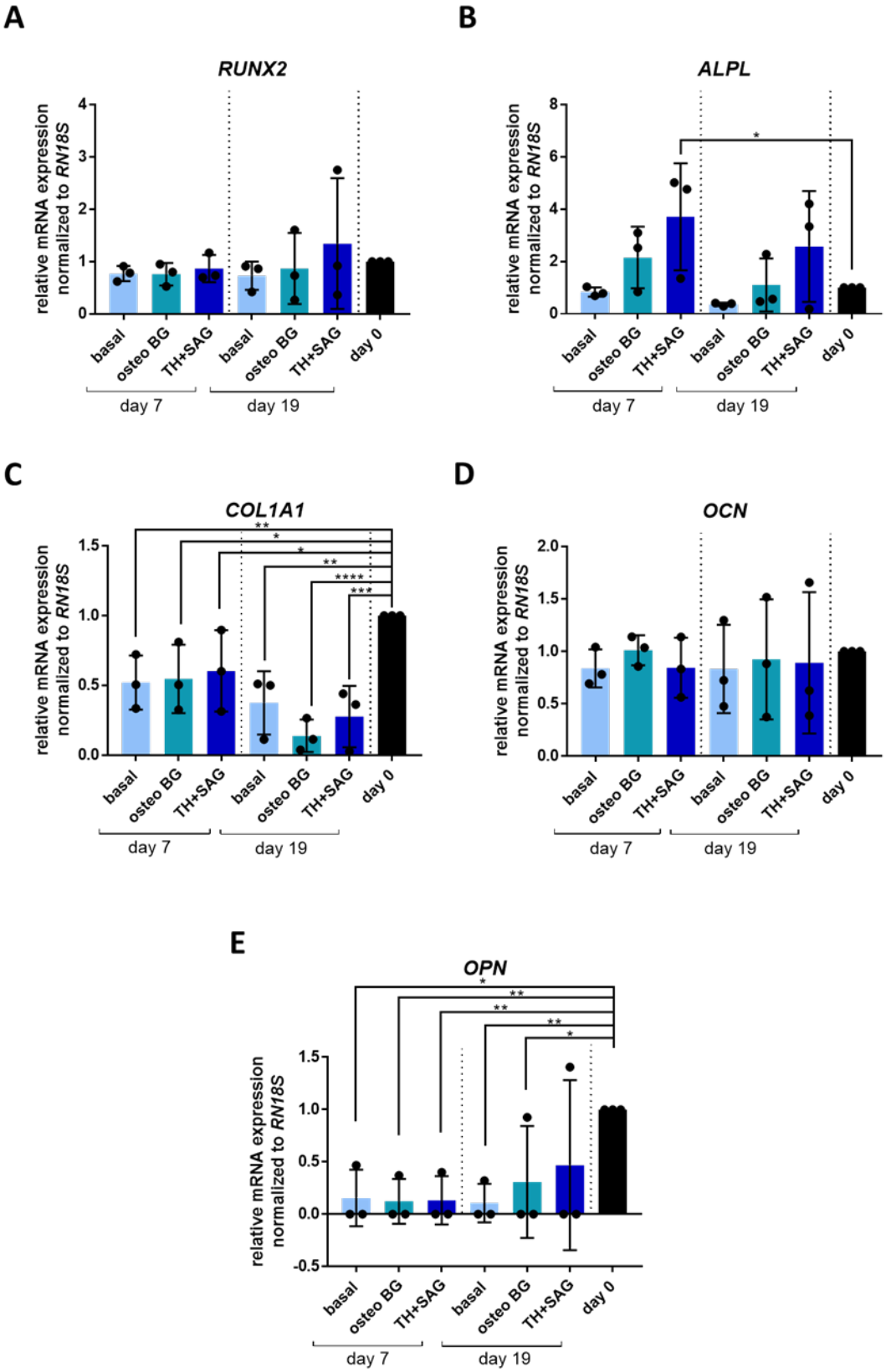

Figure 4.29 Expression of genes characteristic for osteogenic differentiation in HFBCs isolated from 14 wpc old foetal femur samples treated with basal medium, osteogenic background medium (oBG, 10 nM dexamethasone, 10 nM 1,25-$(OH)_2$-vitamin D_3 and 100 µM ascorbic-2-phosphate) and osteo background (oBG) medium supplemented with small molecules

SAG (smoothened agonist) and TH (4-(4-methoxyphenyl)pyrido[4′,3′:4,5]thieno[2,3-b]pyridine-2-carboxamide). Gene expression displayed as mean +/- SD and was normalised to *RN18S* at day 0 in basal medium. Two-way ANOVA with Dunnett's post-hoc test for multiple comparisons was performed to compare different culture conditions of n = 3 differentiation experiments. * $p < 0.05$; ** $p < 0.01$; *** $p < 0.001$; **** $p < 0.0001$. RUNX2: runt-related transcription factor 2; ALPL: alkaline phosphatase; COL1A1: collagen type 1; OCN: osteocalcin; OPN: osteopontin, RN18S: subunit 18S ribosomal RNA; HFBCs: human foetal bone cells. wpc: weeks post conception.

Table 4.7 Summary of respective gene expression characteristic for osteogenesis in HFBCs isolated from 14 wpc human foetal femurs treated with basal medium, osteogenic background medium (oBG, 10 nM dexamethasone, 10 nM 1,25-$(OH)_2$-vitamin D_3 and 100 µM ascorbic-2-phosphate) and oBG supplemented with small molecules SAG (smoothened agonist) and TH (4-(4-methoxyphenyl)pyrido[4′,3′:4,5]thieno[2,3-b]pyridine-2-carboxamide). Gene expression was normalised to *RN18S* (subunit of 18S ribosomal RNA) at day 0. Osteogenic differentiation was performed three times (n = 3). Mean +/- SD displayed. HFBCs: human foetal bone cells**.**

	condition	***RUNX2***	***ALPL***	***COL1A1***	***OCN***	***OPN***
Day 7	basal	0.77 +/- 0.15	0.83 +/-0.18	0.52 +/-0.20	0.84 +/- 0.18	0.16 +/- 0.27
	oBG	0.76 +/- 0.22	2.15 +/-1.17	0.55 +/- 0.25	1.01+/- 0.14	0.12 +/- 0.21
	oBG + TH + SAG	0.87 +/- 0.26	3.71 +/- 2.05	0.60 +/- 0.29	0.84 +/- 0.29	0.13 +/- 0.23
Day 19	basal	0.73 +/-0.27	0.36 +/- 0.07	0.38 +/- 0.23	0.83 +/-0.42	0.11 +/- 0.18
	oBG	0.87 +/- 0.68	1.10 +/- 1.02	0.14 +/- 0.12	0.92 +/- 0.57	0.31 +/- 0.53
	oBG + TH + SAG	1.35 +/- 1.25	2.57 +/- 2.12	0.28 +/- 0.22	0.89 +/- 0.68	0.47 +/- 0.81

COL2A1 was barely detectable in all three media compositions at both time points (except under basal conditions at day 7: mean 0.33-fold change). Low mRNA expression was significant in relation to day 0 (day 7: basal mean 0.33-fold change, $p < 0.01$; oBG: mean 0.02-fold change, $p < 0.001$; oBG + TH + SAG: mean 0.04-fold change, $p < 0.001$; day 19: basal mean 0.02-fold change, $p < 0.001$; oBG: undetected, $p < 0.001$; oBG + TH + SAG: undetected, $p < 0.001$) (Figure 4.30 A, Table 4.8, Appendix K)

ACAN showed overall slightly higher expression than *COL2A1*, however, with a similar trend in mRNA in the tested media compositions at both time points. Measured mRNA

expression was significant relative to day 0 (day 7: basal mean 0.44-fold change, $p < 0.001$; oBG: mean 0.18-fold change, $p < 0.0001$; oBG + TH + SAG: mean 0.19-fold change, $p < 0.0001$; day 19: basal mean 0.18-fold change, $p < 0.0001$; oBG: mean 0.11-fold change, $p < 0.0001$; oBG + TH + SAG: mean 0.19-fold change, $p < 0.0001$) (Figure 4.30 B, Table 4.8, Appendix K).

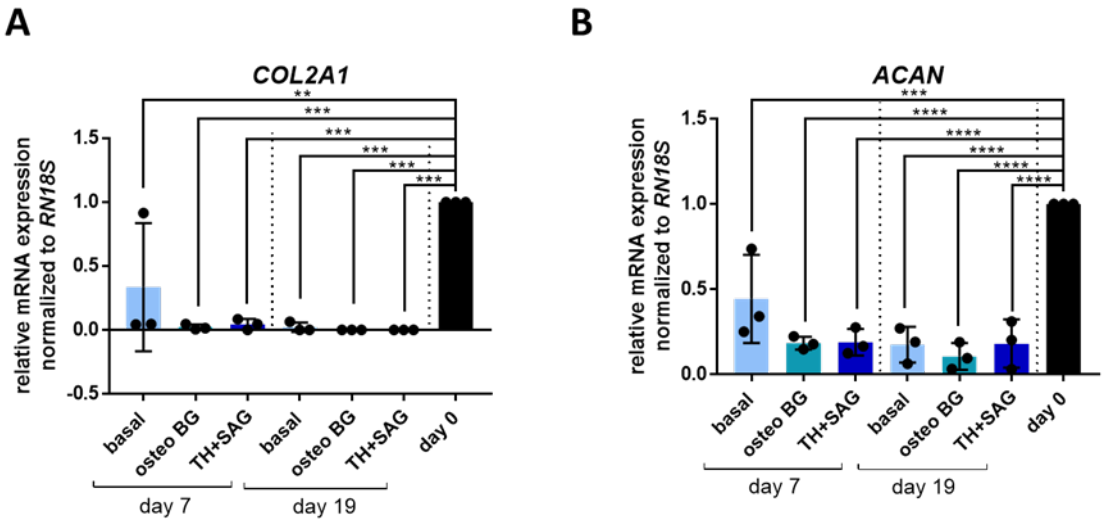

Figure 4.30 Expression of genes characteristic for chondrogenic differentiation in HFBCs isolated from 14 wpc old foetal femur samples treated with basal medium, osteogenic background medium (oBG, 10 nM dexamethasone, 10 nM 1,25-$(OH)_2$-vitamin D_3 and 100 µM ascorbic-2-phosphate) and osteo background (oBG) medium supplemented with small molecules SAG (smoothened agonist) and TH (4-(4-methoxyphenyl)pyrido[4′,3′:4,5]thieno[2,3-b]pyridine-2-carboxamide). Gene expression displayed as mean +/- SD and was normalised to *RN18S* at day 0 in basal medium. Two-way ANOVA with Dunnett's post-hoc test for multiple comparisons was performed to compare different culture conditions of n = 3 differentiation experiments. ** $p < 0.01$; *** $p < 0.001$; **** $p < 0.0001$. COL2A1: collagen type2; ACAN: aggrecan; RN18S: subunit 18S ribosomal RNA; HFBCs: human foetal bone cells; wpc: weeks post conception.

Table 4.8 Summary of respective gene expression characteristic for chondrogenesis in HFBCs isolated from 14 wpc human foetal femurs treated with basal medium, osteogenic background medium (oBG, 10 nM dexamethasone, 10 nM 1,25-$(OH)_2$-vitamin D_3 and 100 µM ascorbic-2-phosphate) and oBG supplemented with small molecules SAG (smoothened agonist) and TH (4-(4-methoxyphenyl)pyrido[4′,3′:4,5]thieno[2,3-b]pyridine-2-carboxamide). Gene expression was normalised to *RN18S* (subunit of 18S ribosomal RNA) at day 0. Osteogenic differentiation was performed three times (n = 3). Mean +/- SD displayed. HFBCs: human foetal bone cells.

	condition	*COL2A1*	*ACAN*
Day 7	basal	0.33 +/- 0.50	0.44 +/- 0.26
	oBG	0.02 +/- 0.02	0.18 +/- 0.04
	oBG + TH + SAG	0.04 +/- 0.04	0.20 +/- 0.08
Day 19	basal	0.02 +/- 0.04	0.18 +/- 0.10
	oBG	0.00	0.11 +/- 0.08
	oBG + TH + SAG	0.000	0.18 +/- 0.14

In summary, *COL1A1* was downregulated in all tested osteogenic media conditions after 7 and 19 days of culture compared to days 0. *OPN*, *COL2A1* and *ACAN* were significantly downregulated compared to day 0. ALP as well as Alizarin Red staining was overall less intense in differentiated HFBCs isolated from 14 wpc human foetal femurs compared to differentiated HFBCs isolated from 8 wpc human foetal femurs. Alican Blue staining demonstrated equal if not more intense staining after 19 days under oBG + TH + SAG media of differentiated HFBCs isolated from 14 wpc human foetal femurs compared to HFBCs isolated from 8 wpc human foetal femurs.

The findings of the histological stainings of the differentiation experiments of both cell sources (HFBCs isolated from 8 or 14 wpc human foetal femurs) suggested HFBCs isolated from 8 wpc human foetal femurs to be more suitable for a more efficient outcome of osteogenic differentiation.

4.4 Discussion

Knowledge of bone development and the activity of differentiation pathways during early foetal development remain poorly understood. A wholesome picture of early foetal femur development covering first and early second trimester with a set of human foetal femurs (7 – 17 wpc) has never been shown before. Literature research of general foetal femur development (as summarised in the introduction to this chapter) enabled an illustration of the events taking place during human foetal femur development and provide knowledge of events on a cellular and molecular level, thus, providing a concise overview of early human foetal femur development (for more details see section 1.2.2).

Previous studies reported the formation of a hyaline cartilage model by the end of 6 wpc of femur development which display of distinct zones of different chondrocyte types [41]. Human foetal femurs at 8 wpc used in this thesis were found to predominantly consist of different types of chondrocytes (proliferation, pre- and hypertrophic chondrocytes), as indicated by the distinct change in morphology during hypertrophy (enlargement of cells) in Alcian Blue/Sirius Red staining at this early developmental stage. The different types of chondrocytes (pre-hypertrophic chondrocytes, hypertrophic chondrocytes) were visible in distinct zones from diaphysis toward epiphysis in human foetal femur at 8 wpc, with cells decreasing in size toward the epiphysis as previously reported [41, 62, 356]. The thin layer of bone collar surrounding the cartilage model at 8 wpc increased in length towards the epiphyses, as well as in thickness with developmental age until 17 wpc. Sirius Red and Goldner's Trichrome staining in the 12 wpc human foetal femur demonstrated the structure of spongy (trabecular) bone. Both stainings illustrated the structure of spongy bone in the diaphysis of the femur at 15 and 17 wpc as well. Spongy bone is mineralised whereas woven bone (primary bone) consists of irregular arranged collegen fibrils with reduced mineral content, thus, providing flexibility to the bone in the embryo. Woven bone is gradually replaced by spongy (trabecular) and compact (cortical) bone during the ossification process [33, 69]. The structure of spongy bone is generated by dying hypertrophic chondrocytes leaving cavities in the deposited extracellular matrix into which blood vessels can invade, guided by pro-angiogenic factors secreted by hypertrophic chondrocytes, the developing femur [43, 60, 362, 363]. Literature reported the formation of primary ossification centres after week 8 or 9 and, becoming visible by week 12 [356]. Osteoprogenitors, essential for ossification, were shown to be transported to the centre of the diaphysis by invading blood vessels after 8 wpc from the surrounding perichondrium [43, 60]. The progenitor cells attach

on the extracellular matrix surrounding dying hypertrophic chondrocytes and begin to produce bone matrix (mainly containing type I collagen [43, 60]. Goldner's Trichrome staining showed only very few blood cells in human foetal femur at 8 wpc. However, in developmentally more advanced analysed human foetal femurs, small cavities within the extracellular matrix were found throughout the diaphysis of the 12, 15 and 17 wpc human foetal femurs. Goldner's Trichrome staining identified the cells within the cavities as erythrocytes. Bone is reportedly highly mineralised and at the same time highly vascularised [363]. Small blood vessels were reported to run through the developing femur and feed into one large vessel located in the centre of the diaphysis within the bone marrow cavity [363]. Literature reports two types of vessels (type L and type H) with type L vessels forming a dense network in the bone marrow cavity [363-365]. This finding in combination with the regular distribution of those cavities throughout the extracellular matrix (especially as observed in the cross section of the 17 wpc human foetal femur) leads to the conclusion that the observed cavities could be small blood vessels running through the extracellular matrix. Mineralisation was reportedly visible using X-ray at around16 weeks of development [356]. Prior to embedding in paraffin the human foetal femurs were decalcified. The need for decalcification prior to embedding presents a limitation as the progress of mineralisation could not be visualised by Alizarin Red or von Kossa staining.

Different imaging modalities of human foetal femurs using 3D imaging tools such as synchrotron X-ray phase contrast-enhanced tomography, contrast-enhanced micro-computed tomography or micro-computed tomography (µCT) could be applied [366-368] in order to visualise ongoing mineralisaton of human foetal femurs as well as invading blood vessels. Imaging techniques that allow the visualization of soft tissue (such as blood vessels) are challenging to apply to the bone. The use of synchrotron X-ray phase contrast-enhanced tomography demonstrated the possibility to visualize blood vessels within the calcified matrix [366]. µCT is a 3D imaging tool for the visualization of bone networks *in vitro* and *in vivo* [369-371]. The use of these two 3D imaging techniques, applied on a subset of human foetal femurs, would provide the community with a detailed atlas of early human foetal development and, in turn, would eliminate any potential bias due to the chosen histological staining method.

The findings in this thesis correspond with the reported literature of human foetal femurs detailing the chondrocyte composition, surrounding perichondrium and, with ongoing development, increasing the number of osteoblasts in the bone collar and the diaphysis [360]. However, it was not possible to provide histological staining for each developmental week

due to lack of human foetal femur samples. Histological staining of additional human foetal femur samples between the provided temporal cross sections of human foetal femur, could deliver a more detailed overview of the structural changes in the human femur during these early stages of foetal development. However, the provided overview with samples from 8 wpc, 12 wpc, 15 wpc and 17 wpc demonstrated the structural changes in the human foetal femur as well as invading blood vessels into the femur as previously reported [43, 275, 362, 363, 372-376]. Multiple samples for each developmental week could reduce gender or environmental differences, however, due to ethical concerns it would be advisable to keep the number of human foetal femurs as low as possible.

Cells isolated from human foetal femurs were termed “human foetal bone cells (HFBCs)” due to the heterogeneous nature of the cell population and, in accordance with previous publications investigating the characteristics of cells from the same sources [62, 63, 307, 332, 379]. Genes upregulated during chondrogenesis were expected to be highly expressed in HFBCs in comparison to genes involved during osteogenesis, due to the chondrogenic nature of the human foetal femurs (especially when isolated from an early developmental stage) [332]. Cartilage is the most prominent tissue during early human foetal femur development with the majority being comprised of type II collagen. This type of collagen forms fibrils entrapping proteoglycans, thus providing the developing femur with flexibility. Type IX collagen is a fibril-associated protein with an interrupted triple-helix (FACIT) and, its main function appears to be as a stabilising bridge between collagens (like types II and XI collagen) and other components of the extracellular matrix (ECM) [360]. HFBCs isolated from human foetal femurs aged 7 – 17 wpc showed an increasing trend of chondrogenic genes, especially for *COL9A1* and *ACAN* as shown before for HFBCs isolated from 7.5 - 9 wpc human foetal femurs [332]. As human foetal femurs consist predominantly of collagen (especially during early stage < 15 wpc), the high presence of collagen type IX can be explained due to interconnecting collagen fibres [360]. Expression of osteogenic genes in human foetal femur samples was not significantly increased or decreased with increasing developmental age. However, osteogenesis (and in turn expression of osteogenic genes) was not expected to increase with developmental age in HFBCs due to chondrogenic nature of human foetal femurs as detected by histological staining. The gene expression findings in concordance with the performed histological staining of human foetal femurs showed that early human foetal femurs predominantly are a cartilage template with ossification being

initiated around 12 - 15 wpc as indicated with the identified cavities for invading blood vessels transporting osteochondro progenitors.
In order for mineralisation to occur, complex remodelling of the ECM is required. This process is driven by matrix metalloproteases (MMPs), zinc-dependent ECM degrading enzymes. ECM degradation occurs by MMPs cleaving components of collagens and gelatins in turn allowing for their degradation. Bone forming/remodelling cells (osteoblasts and osteoclasts), as well as cartilage forming cells, express characteristic sets of MMPs (MMP 2, 9, 13, 14, 16) [380].

Various studies have indicated stem cells isolated from foetal donor tissue offer an exciting approach for bone repair compared to adult tissue [381-383]. This is due to: i) proven multi-lineage differentiation potential of HFBCs [61, 62], ii) the low fraction of cells present in adult tissue (1 in 10,000-100,000 in bone marrow) [18, 19], which further decreases with age and results in impaired functionality/potency [384], and, iii) enhanced proliferation and expansion potential compared to aged cell sources [18-20, 62, 154]. Furthermore, foetal tissue derived stem cells reportedly lack HLA class II and showed lower expression of HLA class I compared to stem cells derived from adult tissue, indicating an immunological advantage of cells isolated from foetal sources compared to cells isolated from adult sources [385]. Previous studies were able to show the different behaviour and differentiation potential of cells isolated from diaphysis and epiphysis of human foetal femurs [62, 63, 307, 332, 379, 386]. However, in order to obtain a wider picture of human foetal femur development, the whole femur was used to isolate HFBCs for experiments in this thesis. HFBCs isolated from human foetal femur samples of different time points during development (7 - 17 wpc) did not show any differences in cell morphology, neither when first isolated/cultured *in vitro* nor when cultured for several passages. Comparison of proliferation by measurement of the cell metabolism using alamarBlue® assay did not show any influence by age of human foetal femur nor *in vitro* culture passage. Previous studies reported a higher proliferation potential of foetal cells compared to cells isolated from aged donor populations [18-20, 62, 154].

Osteogenic differentiation with HFBCs isolated from human foetal femurs was investigated before [61-63, 379, 386, 387]. However, HFBCs were isolated from 8 - 11 wpc [62] as well as 13 – 16 wpc [61] human foetal femurs. Therefore, the question was raised which developmental age would be best suited for HFBCs to be isolated in order to gain HFBCs with greatest osteogenic differentiation potential in order to improve the outcome of bone

repair approaches. HFBCs isolated from 8 and 14 wpc human foetal femur samples were treated with two osteogenic media compositions (oBG and oBG + TH + SAG) in order to compare the capability for bone formation. ALP staining appeared to be more intense in HFBCs isolated from 8 wpc human foetal femurs after 19 days under oBG + TH + SAG culture conditions compared to HFBCs isolated from 14 wpc human foetal femurs. Alizarin Red staining as well as Alcian Blue staining were found to be more intense in HFBCs isolated from 8 wpc human foetal femurs in all tested conditions than in HFBCs isolated from 14 wpc human foetal femurs. These findings suggest that HFBCs isolated from 8 wpc human foetal femurs have a better osteogenic differentiation potential compared to 14 wpc human foetal femurs. HFBCs isolated from human foetal femurs at an ealier developmental stage (e.g. 8 wpc) were hypothesised to possess lower osteogenic differentiation potential compared to HFBCs isolated from developmentally more advanced human foetal femurs (e.g. 14 wpc) due to the predominatly chondrogenic nature of the human foetal femur at this stage in development. Suprisingly, these findings could suggest that HFBCs isolated from 8 wpc human foetal femurs might be better suited for osteogenic differentiation *in vitro*.

In HFBCs isolated from 8 wpc human foetal femurs ALP, Alcian Blue and Alizarin Red stainings were observed to be most intense in oBG + TH + SAG after 19 days of culture suggesting that this osteogenic differentiation medium is more efficient in generation osteoblasts *in vitro*. Suprisingly, Alican Blue staining was observed to be equally intense in oBG + TH + SAG in HFBCs isolated from 8 wpc human foetal femurs as in HFBCs isolated from 14 wpc human foetal femurs compared to HFBCs culture in oBG only. This observation indicates the extent of matrix production to be higher in HFBCs cultured in oBG + TH + SAG medium than in oBG medium. Investigation of the observed more extensive matrix production in oBG + TH + SAG compared to oBG requires further investigation. Immunocytochemistry staining for collagen type I and II would be able to indicate whether the supplementation of standard osteogenic differentiation medium with TH + SAG resulted in an osteogenic outcome with solely osteoblasts after 19 days or with an increased number of chondrocytes compared to the standard osteogenic differentiation medium. Anlysis of *COL1A1* gene expression in HFBCs isolated from 8 and 14 wpc human foetal femurs remained lower in both osteogenic culture conditions at both time points compared to detected expression at day 0. However, *COL1A1* was slightly higher expressed compared to the expression of *COL2A1* as well as *ACAN* (both characteristically expressed in chondrocytes) in HFBCs isolated from 8 and 14 wpc human foetal femurs in both osteogenic

culture conditions after 19 days. This finding in combination with increased intensity of ALP and Alizarin Red staining after 19 days under oBG + TH + SAG culture conditions suggests that the small molecule results in a more efficient osteogenic differentiation outcome compared to oBG. Reason for the improved osteogenic differentiation outcome with small molecule supplemented osteogenic medium could be due to TH reportedly acting in a BMP-dependent manner [216]. However, the recommended concentration of BMP2 (500 ng) [216], in combination with the costs of BMP2, would have resulted in a more expensive and not realistically feasible osteogenic differentiation medium. Previous publications used TH and SAG supplemented with standard osteogenic background medium with and without additional BMP2. In these studies, only markers specific for osteogenesis were investigated with no analysis of chondrogenic or adipogenic outcomes [183, 216].

Gene expression analysis did only show significant changes in few genes and culture conditions, most likely due to the n-number not being high enough. No significance in respective genes in HFBCs isolated from 8 wpc and 14 wpc human foetal femurs was observed which made comparison and determination of advantages of one osteogenic differentiation media and cell source impossible. *OPN* was observed to be sigificanty expressed in HFBCs isolated from 14 wpc human foetal femurs, however lower expressed compared to expression at day 0. *ALPL* expression in HFBCs isolated from 8 wpc human foetal femurs after 19 days in oBG + TH + SAG was observed to be higher expressed compared to day 0. This finding corresponds with intense ALP staining in this condition and time point. However, HFBCs isolated from 8 wpc human foetal femurs cultured in oBG for 19 days showed very similar ALP staining intensity as in oBG + TH + SAG medium after 19 days.

Nonetheless, determination of a clear advantage or disadvantage of oBG + TH + SAG over oBG for the outcome of osteogenic differentiation is hampered in the study due to the lack of quantifiable protein data. Western Blot of flow cytometry analysis would be necessary for a clear statement regarding the more superior osteogenic differentiation medium or source of HFBCs (whether isolated from 8 wpc or 14 wpc human foetal femurs) to be made.

Conclusion

Events up until blastocyst formation have been extensively investigated [377, 378]. Only a few studies have reported the events surrounding early human foetal femur formation and these studies focused on samples ranging between 7 and 11 wpc of development or 13 – 16

wpc [61-63]. Additionally, in these studies the human foetal femur samples were used to isolate HFBCs for *in vitro* multilineage differentiation, not to generate a 'timeline' of human foetal femur development [62, 63]. The uniqueness of the presented study is the inclusion of human foetal femur samples from the second trimester, providing for the first time an overview of bone development up between 7 and 17 wpc.

Histological staining of human foetal femurs illustrated the transition from a cartilage template at 8 wpc to mineralising of proteoglycan matrix 17 wpc. Cavities supposedly harbouring type L blood vessels were found being distributed throughout the extracellular matrix of the diaphysis. A cluster of erthyrocytes in the centre of the cross section of the 17 wpc human foetal femur indicates the location of a central vein running through the bone marrow cavity of the diaphysis. Gene expression analysis of HFBCs also demonstrated the chondrogenic nature of this cell population. However, confirmation of this finding by protein expression analysis with Western Blots or flow cytometry for chondrogenic proteins remains to be elucidated.

HFBCs represent an alternative cell source to adult aged cell populations as the influence of environmental factors and ageing is reduced in HFBCs. Osteogenic differentiation has been performed before using 8 – 11 wpc and 13 – 16 wpc, however, in different research groups. For the first time, HFBCs isolated from human foetal femur from the first (8 wpc) and second (14 wpc) trimester were differentiated toward the osteogenic lineage in parallel in order to determine whether HFBCs isolated from developmentally more advanced human foetal femurs result in a more efficient osteogenic differentiation outcome. HFBCs isolated from 14 wpc human foetal femurs were expected to represent a cell source better suited for osteogenic differentiation outcome compared to HFBCs isolated from 8 wpc human foetal femurs. Surprisingly, gathered data suggested that HFBCs isolated from 8 wpc human foetal femurs resulted in more efficient osteogenic differentiation outcome. Standard osteogenic differentiation medium was used in parallel to standard osteogenic differentiation medium supplemented with small molecules TH + SAG (as published in [183]). The small molecule supplemented osteogenic medium has never before been used for the differentiation of HFBCs. More intense ALP and Alizarin Red staining of HFBCs cultured in both osteogenic media conditons suggest that oBG + TH + SAG after 19 days results in better osteogenic differentiation outcome. However, lack of further quantifiable protein data such as Western Blot or flow cytometry hampers a clear conclusion regarding the more advantageous of the two osteogenic differentiation media. The seclection of isolated HFBCs by surface markers identified to be specific for skeletal stem cells ($PDPN^+$, $CD73^+$, $CD164^+$, $CD146^-$) in [64]

would further improve the outcome of osteogenic differentiation compared to HFBCs as HFBCs are a heterogenous cell population.

Chapter 5 The Epigenetic Landscape in Human Foetal Bone Cells (HFBCs)

5.1 Introduction

The role of epigenetic regulators such as DNA methylation, microRNAs (miRNAs), histone - and chromatin modifications has been widely studied in a variety of cell types with DNA methylation, being the best understood, resulting in a stable permanent change of the chromatin structure without alteration of the DNA sequence itself [241, 388, 389]. DNA methylation is involved in normal development as well as genomic imprinting and X-chromosome inactivation [239, 389, 390]. Regulation of gene expression by DNA de-/methylation is a conserved process during all stages of development and mediated by DNA methyltransferases (DNMTs) by addition of a methyl group to the C-5 position of the pyrimidine ring of a cytosine base in a CpG dinucleotide [239, 391]. There are two types of DNMTs: i) DNMT1 responsible for maintenance of the DNA methylation pattern and, ii) DNMT3A and DNMT3B responsible for the establishment of new DNA methylation patterns (*de novo* DNMTs) [241, 391]. Similarly, as methyl-groups can be attached, they can be removed again by demethylases such as ten-eleven translocation (TET) enzyme oxidising 5-methylcytosine (5mC) to 5-hydroxymethylcytosine (5hmC) and, subsequently to 5-formylcytosine and 5-carboxylcytosine [242, 243]. An increase in DNA methylation level (content of 5mC) is described as hypermethylation, whereas hypomethylation refers to as decrease in the DNA methylation level. For a detailed description of function and effect of the methylation process see section 1.7.1. Early methods for DNA methylation analysis lacked the ability to distinguish between the different methylation states of the nucleotides such as 5mC or 5hmC [392]. Today, high-performance liquid chromatography (HPLC) combined with mass spectrometry have enabled the distinction and quantitation of cytosine (C), 5mC and 5hmC [331], whereas gene promoters can be investigated using techniques such as pyrosequencing [393].

Maternal and paternal genomes undergo DNA demethylation shortly after fertilisation. The process is more rapid in the paternal genome compared to the maternal genome [243]. DNA methylation is erased genome-wide in a major wave until the 2-cell stage with a further, yet, a moderate decrease in DNA methylation levels until the pre-implantation blastocyst [377,

394]. A major wave of *de novo* DNA methylation occurs following implantation of the blastocyst [377, 378, 394] (Figure 5.1). These events and DNA methylation levels have been extensively studied [377, 395-397], however, studies elucidating the DNA methylation dynamics during early human foetal development remain limited with exception of studies on the foetal brain [398].

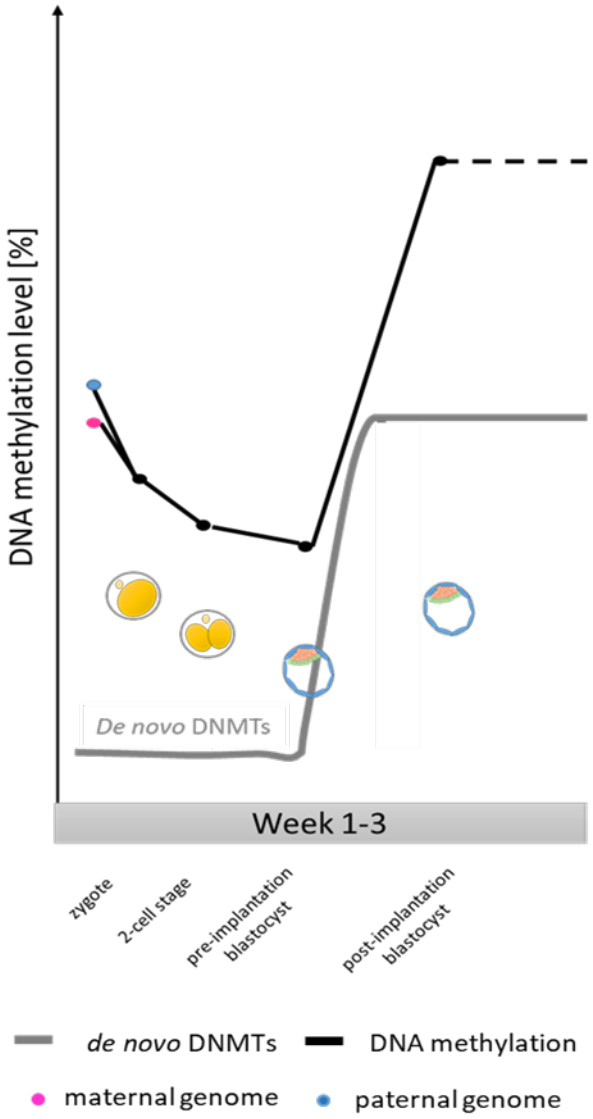

Figure 5.1 DNA methylation of maternal and paternal genomes during early embryonic development. Based on [377, 378, 394].

We obtained a unique sample set of human foetal femur samples from 7 to 17 weeks post conception (wpc), in this chapter we have detailed the DNA methylation status in genes implicated in skeletal development and, the regulatory role of epigenetic mechanisms during the first two trimesters of pregnancy on skeletal development.

miRNAs are also involved during development, providing potential targets for therapeutic approaches. Various miRNAs have been shown to be involved during reprogramming and pluripotency maintenance, as well as during skeletal development and differentiation (see section 1.7.2). miRNA expression profiling during bone development and differentiation could aid our understanding of a second epigenetic mechanism in foetal femur development as well as *in vitro* osteogenic differentiation. Several miRNAs reportedly involved during osteogenic and chondrogenic differentiation (Table 5.1 and Table 5.2) were chosen for analysis in HFBCs isolated from 7 - 17 wpc human foetal femurs as well as during *in vitro* osteogenic differentiation.

Table 5.1. MicroRNAs associated with osteogenesis. FAK: focal adhesion kinase; BMP: bone morphogenetic protein; RUNX2: runt-related transcription factor 2; PPARγ: peroxisome proliferator activator protein gamma; BAMBI: BMP and Activin Membrane Bound Inhibitor; CRIM1: cysteine Rich Transmembrane BMP Regulator 1; SATB2: special AT-rich sequence-binding protein 2; SOST: sclerotin; DKK: dickkopf-related protein; SFRP2: secreted frizzled related protein 2; WNT: wingless; HGS: hepatocyte growth factor-regulated tyrosine kinase substrate.

microRNA	**Effect on osteogenesis**	**Target(s)**	**Function**	**Ref**
miR-138	Inhibition	FAK	Downregulated during osteoblast differentiation *in vitro* in hMSCs; miR-138 has a negative regulatory effect on osteoblast differentiation	[305]
miR-20a,b	Stimulation	BMP antagonists, PPARγ, Bambi and Crim1	Suppression of BMP antagonists, Bambi and Crim1 as well as adipogenic regulator PPARγ; at the same time promotion of osteogenic marker expression	[294, 298]
miR-23a	Inhibition	SATB2 (RUNX2 binding partner)	*RUNX*2 downregulates miR-23a ensuring upregulation of SATB2	[299]
miR-218	Stimulation	Wnt pathway inhibitors SOST, DKK2, SFRP2	Promotion of Wnt pathway through targeting WNT inhibitors	[312]
miR-148b	Stimulation	WNT1	Increase osteogenic activity in SSC	[308, 309]
miR-29a	Stimulation	Wnt inhibitor DKK1	Targeting Wnt inhibitors, resulting in stimulation of Wnt pathway	[301]
miR-133a	Inhibition	RUNX2	Down-regulation of miR-133a allows osteogenesis to progress by prevention of miR-133a mediated inhibition of RUNX2 levels	[300]
let-7f	Stimulation	Axin2	Axin2 is involved in Wnt signalling inhibition; let-7f downregulates	[295]

microRNA	Effect on osteogenesis	Target(s)	Function	Ref
			Axin2, resulting in Wnt pathway inhibition	

Table 5.2 MicroRNAs associated with chondrogenesis. SMAD: SMAD family member; SOX: SRY (Sex-Determining Region Y)-Box; JAG: Jagged; CCND: cyclin D; CDK: cyclin dependent kinase; CDC: cell division cycle.

microRNA	Effect on chondrogenesis	Target(s)	Function	Ref
miR-140-3p	Stimulation	Unknown	Unknown; Upregulated during chondrogenic differentiation	[317, 318]
miR-146a	Stimulation	SMAD2 SMAD3	Downregulated during chondrogenesis enabling de-repression of *SMAD2* and *SMAD3*	[307]
miR-146b	Stimulation	SOX5	Downregulate during chondrogenesis enabling de-repression of SOX5 which is co-expressed with SOX6 and SOX9 resulting in enhanced *COL2A1* expression and binding of SOX9 to *ACAN* enhancer	[323, 324]
miR-34a	Stimulation	JAG1 (ligand of Notch pathway) CCND1 CDK4,6 CDC25a	Downregulation of targets	[302]
miR-145	Stimulation	SOX9 SMAD3	Downregulated during chondrogenic differentiation enabling de-repression of *SOX9* resulting in expression of chondrogenic genes	[319]

5.2 Hypothesis and Aims

Hypothesis

Epigenetic mechanisms are involved in the regulation of gene expression during human foetal femur development and *in vitro* osteogenic differentiation of these cells.

Aims

I. To investigate the influence of DNA methylation as an epigenetic regulatory mechanism in HFBCs isolated from 7- 17 wpc human foetal femur development

Specifically:

a. To determine global DNA methylation profiles in HFBCs isolated from 7 – 17 wpc human foetal femurs at *in vitro* passage (P) 0, 1 and 3 using HPLC-ESI-MS/MS-SRM
b. To use qRT-PCR for quantification of expression of maintenance and *de novo* DNMTs in HFBCs isolated from 7 – 17 wpc human foetal femurs at passage 0
c. To analyse the CpGs in the proximal promoters of *RUNX*2, *COL9A1* and *OCN* genes by bisulfite pyrosequencing methodology in HFBCs isolated from 7 – 17 wpc human foetal femurs at P 0 for analysis of DNA methylation profiles

II. To investigate the influence of miRNA as an epigenetic regulatory mechanism in HFBCs isolated from 7 – 17 wpc human fotal femurs

Specifically:

To undertake miRNA profiling of reported osteogenic and chondrogenic miRNAs in HFBCs isolated from 7 – 17 wpc human foetal femurs at P 0

III. To investigate the regulatory role of miRNAs during osteogenic differentiation of iPSC-MSCs and HFBCs isolated form 8 and 14 wpc human foetal femurs

Specifically:

a. To undertake miRNA profiling of reported osteogenic and chondrogenic miRNAs during *in vitro* osteogenic differentiation of HFBCs isolated from 8 and 14 wpc human foetal femurs
b. To undertake miRNA profiling of reported osteogenic and chondrogenic miRNAs during *in vitro* osteogenic differentiation of NIBSC-8 MSCs

Material and Methods

The methodology used in this chapter can be found in Chapter 2 with the following techniques detailed in respective subchapters: molecular methods in chapter 2.3 with analysis of mRNA expression using qRT-PCR in section 2.3.4, miRNA profiling in section 2.3.5, global DNA methylation in section 2.3.6 and bisulfite pyrosequencing in section 2.3.7.

5.3 Results

5.3.1 Global DNA methylation in HFBCs during early human foetal femur development

DNA methylation has been reported to be strongly involved in the regulation of gene expression during general foetal development as well as tissue specific development. With the availablility of a HFBCs sample set covering the first two trimesters, the regulatory role of DNA methylation during foetal femur development was investigated on a global level as well as on genes implicated in foetal bone development.

In initial experiments, DNA of HFBCs isolated from five human foetal femurs were digested with DNA Degradase Plus™ Kit (Zymo Research, Cambridge Bioscience, UK, Cat. No. E2020) for 2 h at 37°C by Susanne Renz, Bone and Joint Research Group, Southampton General Hospital, Southampton, UK. Samples were then analysed by HPLC-ESI-MS/MS-SRM to determine the ratio of 5mC to total cytosine content (5mC/5mC+C) by Esteban Guitián Fernández, Campus Vida, University of Santiago de Compostela, Spain. The length of the foetal foot can be directly correlated to the age of the foetus (Carnegie stage). Age of human foetal femurs used in initial experiments are displayed in Table 5.3.

Table 5.3 Human foetal femurs used for global DNA methylation profiling. DNA of samples H1415, H1417, H1420, H1421 and 12367 was isolated from isolated HFBCs by María C de Andrés of the Bone and Joint Research Group, Southampton, UK. wpc: weeks post conception; dpc: days post conception; HFBCs: human foetal bone cells.

Sample ID	Foetal foot length [mm]	Age [wpc]
H1415	4.0	7.5
H1417	4.0	7.5
H1420	6.5	8.5
H1421	5.0	7.5
12367	10.0	11

Preliminary data from HFBCs isolated from the five human foetal femurs are depicted in Figure 5.2 and Table 5.4. 5mC percentage varied in samples H1415 (78.10 %), H1417 (30.53 %) and H1420 (11.13 %), all 7.5 wpc. HFBCs isolated from human foetal femur H1420 (8.5 wpc) demonstrated 20.45 % 5mC content while HFBCs isolated from the oldest

human foetal femur sample 12367 (11 wpc) showed 8.86 % 5mC content. The preliminary data showed a trend for a decrease in global 5mC methylation with increasing human foetal femur age although the trend was insignificant due to small sample size ($R^2 = 0.2315$).

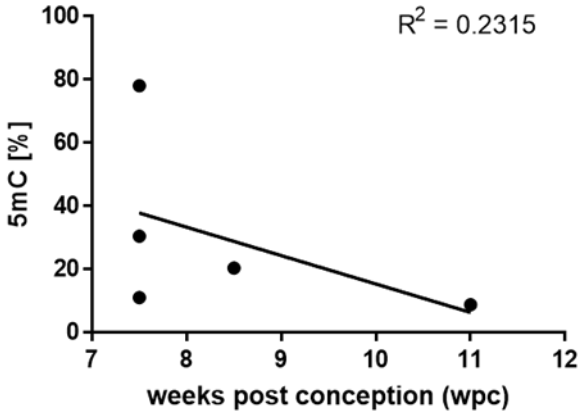

Figure 5.2 Global DNA methylation in HFBCs isolated from 7.5 - 11 wpc human foetal femurs. 500 ng DNA were digested with DNA Degradase Plus™ (Zymo Research) by Susanne Renz, Bone and Joint Research Group, Southampton General Hospital, Southampton, UK and analysed by HPLC-ESI-MS/MS-SRM by Esteban Guitián Fernández, Campus Vida, University of Santiago de Compostela, Spain. Significance was determined by use of non-linear regression test. wpc: weeks post conception; R^2: Spearman's correlation coefficient; 5mC: 5-methylcytosine; HFBCs: human foetal bone cells.

Table 5.4 Global DNA methylation in HFBCs isolated from 7.5-11 wpc human foetal femurs. 500 ng DNA were digested with DNA Degradase Plus™ Kit (Zymo Research) by Susanne Renz, Bone and Joint Research Group, Southampton General Hospital, Southampton, UK and analysed by HPLC-ESI-MS/MS-SRM by Esteban Guitián Fernández, Campus Vida, University of Santiago de Compostela, Spain. wpc: weeks post conception.

Sample ID	Age [wpc]	5mC [%]
H1415	7.50	78.10
H1417	7.50	30.53
H1420	7.50	11.13
H1421	8.50	20.45
12367	11.00	8.86

To strengthen the findings in the preliminary data set and to investigate the influence of global DNA methylation during later stages of early human foetal development, 11 human foetal femurs (age range from 7 to 17 wpc) were dissected to isolate HFBCs. Cells isolated from human foetal femurs were cultured *in vitro* and were lysed after each passage for further

analysis using qRT-PCR for gene expression. Global DNA methylation and DNA methylation in promoter regions in genes implicated in skeletal development were subsequently examined. A full list of human foetal femurs with individual ages detailed (expressed as wpc) for these studies is displayed in Table 5.5.

Table 5.5 Foetal samples used for global DNA methylation profiling. wpc: weeks post conception.

Sample ID	Age [wpc] Carnegie staged
13986	7
13975	8
13723	8 (late)
13706	9
14007	10
13893	12
13796	13
13901	14
13976	14
14008	16
13766	17

DNA from HFBCs was digested using DNA Degradase Plus™ Kit (Zymo Research, Cambridge Bioscience, UK, Cat. No. E2020) for 2h at 37°C by Susanne Renz, Bone and Joint Research Group, Southampton General Hospital, Southampton, UK and sent to colleagues in Spain (Esteban Guitián Fernández, Campus Vida, University of Santiago de Compostela, Spain) for analysis using HPLC-ESI-MS/MS-SRM and determination of the ratio of 5mC to total cytosine content (5mC/5mC+C). 5mC percentage in HFBCs at passage 0 and 1 shown in Figure 5.3 - Figure 5.4. Global 5mC percentage in individual samples depicted in Figure 5.6.

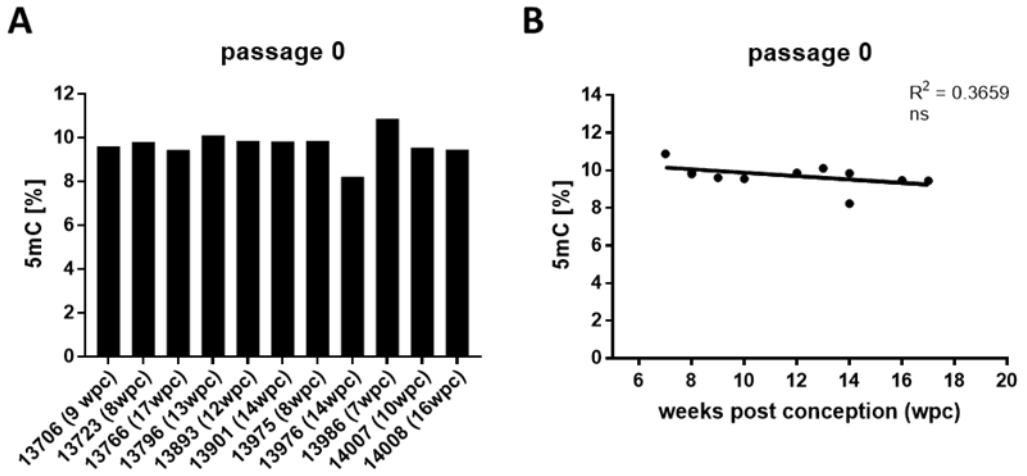

Figure 5.3 Global DNA methylation of HFBCs isolated from 7 – 17 wpc human foetal femurs at passage 0 digested with DNA Degradase Plus™ Kit (Zymo Research). 100 ng DNA were digested with DNA Degradase Plus™ (Zymo Research) by Susanne Renz, Bone and Joint Research Group, Southampton General Hospital, Southampton, UK and analysed by HPLC-ESI-MS/MS-SRM by Esteban Guitián Fernández, Campus Vida, University of Santiago de Compostela, Spain. Values represent HFBCs isolated from individual human foetal femurs (n =1) for each developmental week except 8 and 14 wpc (n =2). **A:** Global DNA methylation displayed for HFBCs from individual human foetal femurs (ID and wpc). **B:** Global DNA methylation for HFBCs displayed by wpc. Significance was determined by use of non-linear regression test. 5mC: 5-methyl cytosine; R^2: Spearman's correlation coefficient; ns: not significant; HFBCs: human foetal bone cells; wpc: weeks post conception.

Global DNA methylation showed no decrease in HFBCs between 7 - 17 wpc at P0 (R^2 = 0.3659, Figure 5.3, Table 5.6) while a modest decrease in global DNA methylation was observed between 7 and 17 wpc in HFBCs at passage 1 (R^2 = 0.504, $p < 0.05$, Figure 5.4, Table 5.6). Further *in vitro* culture of HFBCs did not result in significant change of global DNA methylation levels at passage 3 (R^2 = 0.1657, Figure 5.5, Table 5.6).

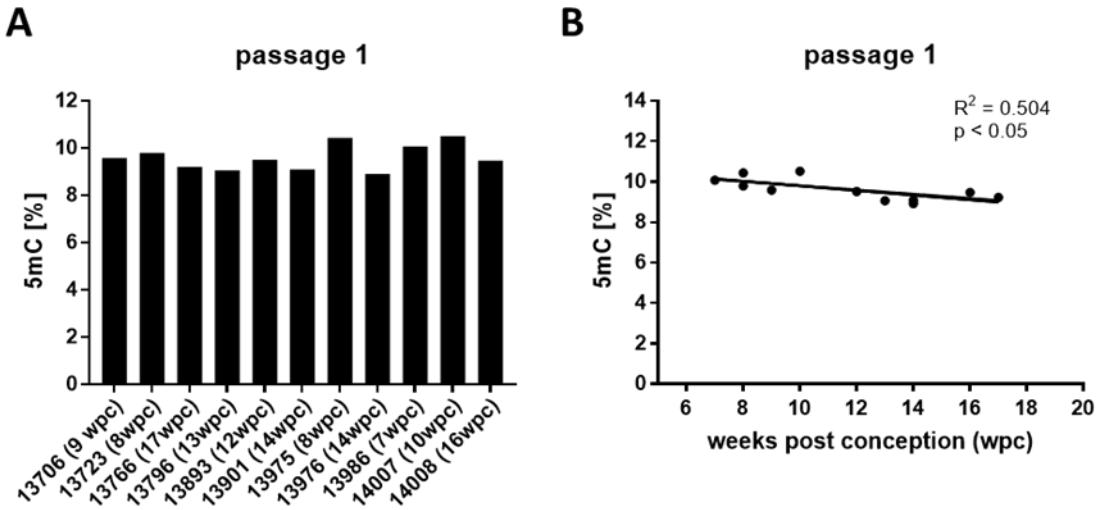

Figure 5.4 Global DNA methylation of HFBCs isolated from 7 - 17 wpc human foetal femurs at passage 1 digested with DNA Degradase Plus™ Kit (Zymo Research). 100 ng DNA were digested with DNA Degradase Plus™ (Zymo Research) by Susanne Renz, Bone and Joint Research Group, Southampton General Hospital, Southampton, UK and analysed by HPLC-ESI-MS/MS-SRM by Esteban Guitián Fernández, Campus Vida, University of Santiago de Compostela, Spain. Values represent HFBCs isolated from individual human foetal femurs (n =1) for each developmental week except 8 and 14 wpc (n =2). **A:** Global DNA methylation displayed for HFBCs from individual human foetal femurs (ID and wpc). **B:** Global DNA methylation for HFBCs displayed by wpc. Significance was determined by use of non-linear regression test. 5mC: 5-methyl cytosine; R^2: Spearman's correlation coefficient; HFBCs: human foetal bone cells; wpc: weeks post conception.

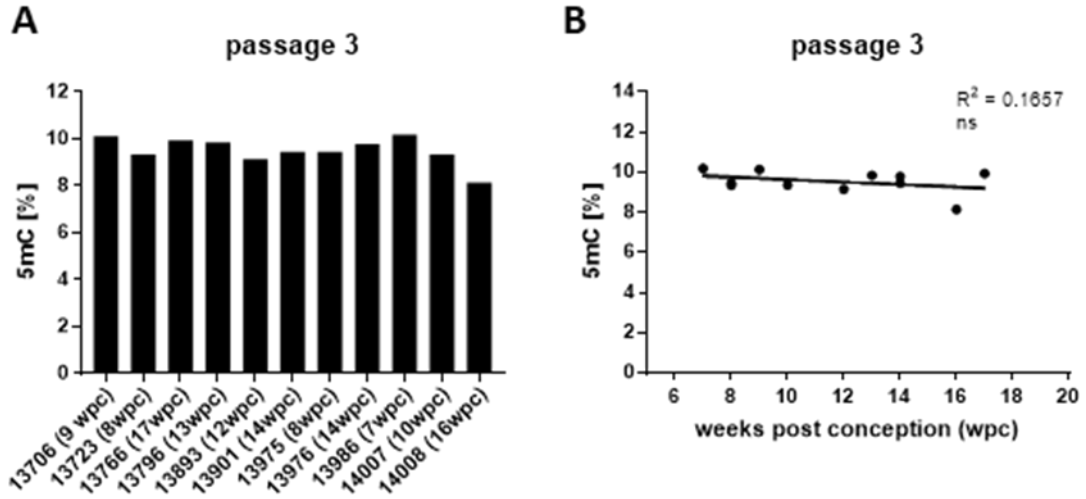

Figure 5.5 Global DNA methylation of HFBCs isolated from 7 – 17 human foetal femurs at passage 3 digested with DNA Degradase Plus™ Kit (Zymo Research). 100 ng DNA were digested with DNA Degradase Plus™ (Zymo Research) by Susanne Renz, Bone and Joint Research Group, Southampton General Hospital, Southampton, UK and analysed by HPLC-ESI-MS/MS-SRM by

Esteban Guitián Fernández, Campus Vida, University of Santiago de Compostela, Spain. Values represent HFBCs isolated from individual human foetal femurs (n =1) for each developmental week except 8 and 14 wpc (n =2). **A:** Global DNA methylation displayed for HFBCs from individual human foetal femurs (ID and wpc). **B:** Global DNA methylation for HFBCs displayed by wpc. Significance was determined by use of non-linear regression test. 5mC: 5-methyl cytosine; R^2: Spearman's correlation coefficient; ns: not significant; HFBCs: human foetal bone cells; wpc: weeks post conception

Global DNA methylation values obtained from passages (P) 0, 1 and 3 were determined for HFBCs isolated from individual human foetal femurs to evaluate any differences between femur samples (Figure 5.6 and Table 5.6).

HFBCs isolated from **7 wpc** human foetal femur showed the 10.87 % 5mC percentages at P0, 10.08 % at P1 10.18 % at P3. The mean 5mC percentage in HFBCs isolated from **8 wpc** human foetal femurs were found to be 9.84 % at P0, 10.11 % at P1 and 9.39 % at P3. DNA methylation levels at P0 and P1 in HFBCs isolated from **9 wpc** human foetal femur were comparable (P0: 9.61 %; P1: 9.58 %) with 10.12 % at P3. 5mC levels in HFBCs isolated from **10 wpc** human foetal femur sample were 9.55 % at P0, 10.51 % at P1, and 9.35 % at P3. HFBCs isolated from **12 wpc** human foetal femur sample demonstrated 9.87 % 5mC content at P0, 9.51 % at P1 and 9.14 % at P3. 5mC levels at P0 in HFBCs isolated from **13 wpc** human foetal femur were 10.11 %, 9.06 % at P1 and 9.83 % at P3. Mean global DNA methylation levels in HFBCs isolated from **14 wpc** human foetal femurs were equally low at P0 and P1 (P0: 9.03 %; P1: 9.00 %) with 9.61 % at P3. 5mC levels in HFBCs isolated from **16 wpc** human foetal femur were similar at P0 and P1 (P0: 9.47 %; P1: 9.47 %) while HFBCs showed 8.14 % DNA methylation at P3. 5mC levels in HFBCs isolated from **17 wpc** human foetal femur showed 9.44 % 5mC methylation at P0, 9.22 % at P1 and 9.92 % at P3.

Given the minimal changes in global DNA methylation in the HFBCs isolated from 7 - 17 wpc human foetal femurs (Figure 5.3 - Figure 5.6), P3 samples were not analysed in subsequent studies with a focus, dependent on sample availability, on P0 and P1 samples.

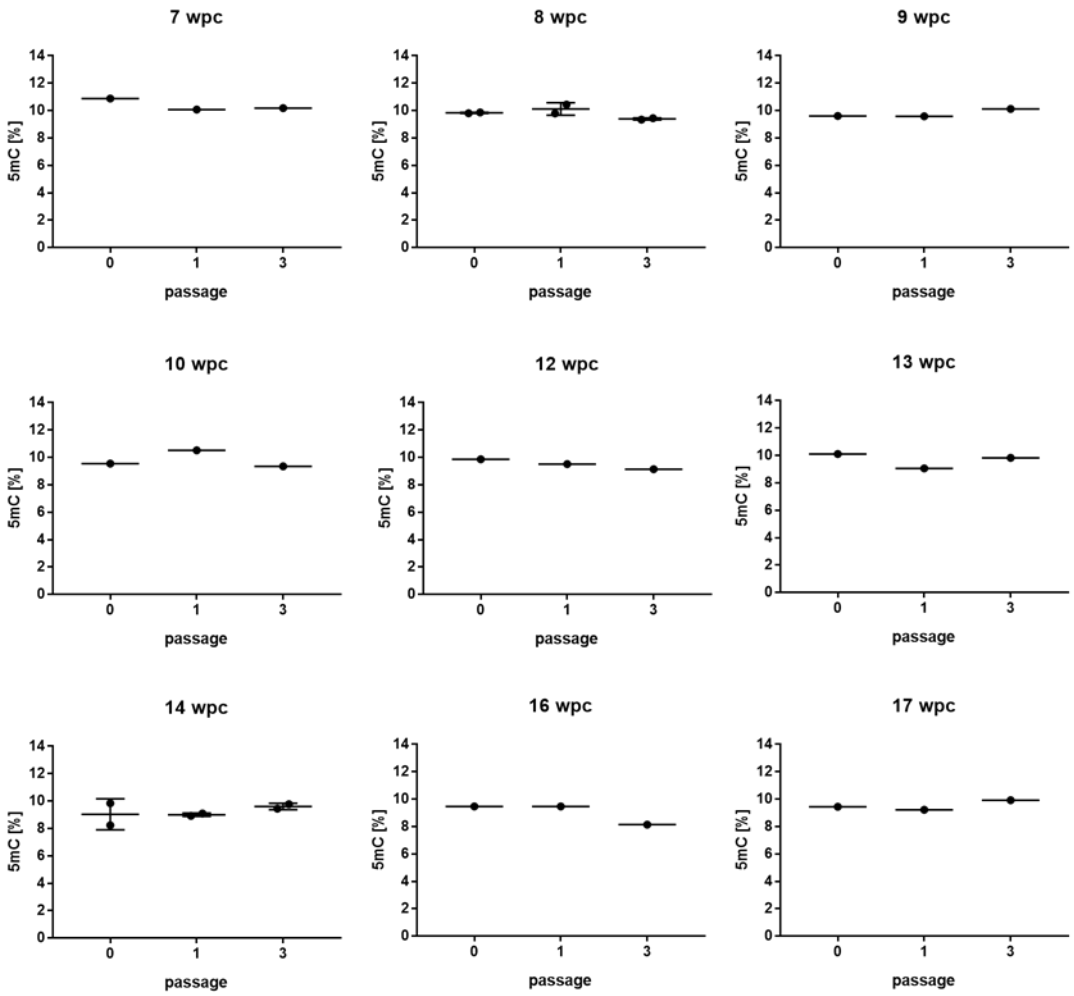

Figure 5.6 Global DNA methylation of HFBCs isolated from 7 -17 wpc human foetal femurs during *in vitro* long term culture in individual human foetal femur samples. 100 ng DNA were digested with DNA Degradase Plus™ (Zymo Research) by Susanne Renz, Bone and Joint Research Group, Southampton General Hospital, Southampton, UK and analysed by HPLC-ESI-MS/MS-SRM by Esteban Guitián Fernández, Campus Vida, University of Santiago de Compostela, Spain. Values represent HFBCs isolated from individual human foetal femurs (n =1) for each developmental week except 8 and 14 wpc (n =2). +/- SD for 8 and 14 wpc. 5mC: 5-methyl cytosine; wpc: weeks post conception; HFBCs: human foetal bone cells.

Table 5.6 Global DNA methylation data in HFBCs isolated from individual 7 - 17 wpc human foetal femurs. 100 ng DNA were digested with DNA Degradase Plus™ Kit (Zymo Research) by Susanne Renz, Bone and Joint Research Group, Southampton General Hospital, Southampton, UK and analysed by HPLC-ESI-MS/MS-SRM by Esteban Guitián Fernández, Campus Vida, University of Santiago de Compostela, Spain. Values in bold represent mean. wpc: weeks post conception; mC: 5-methyl cytosine; HFBCs: human foetal bone cells.

wpc	**5mC passage 0 [%]**	**5mC passage 1 [%]**	**5mC passage 3 [%]**
7	10.873	10.08	10.18
8	9.81 9.87 **9.84**	9.80 10.44 **10.11**	9.34 9.45 **9.39**
9	9.61	9.58	10.12
10	9.55	10.51	9.35
12	9.87	9.51	9.14
13	10.11	9.06	9.83
14	9.84 8.23 **9.03**	9.09 8.92 **9.00**	9.45 9.77 **9.61**
16	9.47	9.47	8.14
17	9.44	9.22	9.92

As only HFBCs at P1 showed a significant, yet, small decrease in DNA methylation between 7 and 17 wpc it could be concluded that major DNA de-/methylation events resulting in a significant change in global DNA methylation levels had already occured prior to 7 wpc of development (see Figure 5.1). Therefore, DNA methylation in promoters of genes implicated in foetal bone development were analysed in order to investigate the role of DNA methylation on gene expression in HFBCs isolated from 7-17 wpc human foetal femurs.

5.3.2 DNA methylation dynamics in genes implicated in foetal bone development

DNA methylation status in proximal promoters of type IX collagen (*COL9A1*), runt-relation transcription factor 2 (*RUNX2*) and osteocalcin (*OCN*) genes were analysed in HFBCs passage 0 cells isolated from 7 - 17 wpc human foetal femurs. Gene expression results for

COL9A1, *RUNX2* and *OCN* from section 4.3.3 were displayed to facilitate comparisons between gene expression and promoter DNA methylation in this chapter.

Type IX collagen (*COL9A1*)

COL9A1 expression in HFBCs at passage 0 isolated from 7 - 17 wpc human foetal femurs was analysed by qRT-PCR in section 4.3.3, Figure 4.17 C and displayed in this section again in order to facilitate the comparison between gene expression and promoter DNA methylation in this chapter. Gene expression levels demonstrated a significant increase in HFBCs isolated from 7 – 17 wpc human foetal femurs ($R^2 = 0.7159$; $p < 0.001$), from 62.93-fold change at 8 wpc to 644.93-fold change at 17 wpc (Figure 5.7 and Table 7.7).

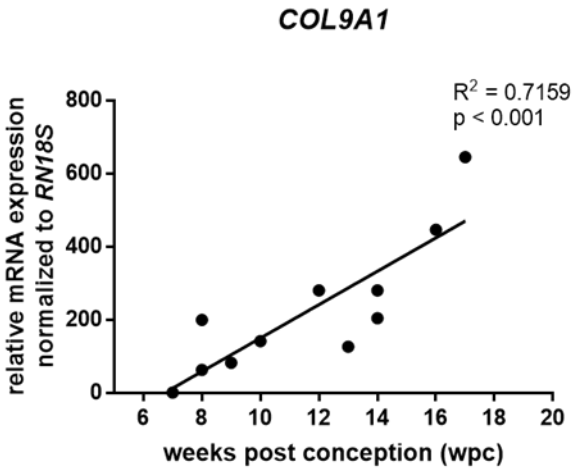

Figure 5.7 *COL9A1* expression in HFBCs isolated from 7 - 17 wpc human foetal femurs. Values represent HFBCs isolated from individual human foetal femurs (n =1) for each developmental week except 8 and 14 wpc (n =2). Significance was determined by non-linear regression test. COL9A1: collagen type IX; R^2: Spearman's correlation coefficient; wpc: weeks post conception.

The human proximal promoter of *COL9A1* contains 8 CpG sites upstream of exon 1 relative to the transcription start site (TSS) (Figure 5.8).

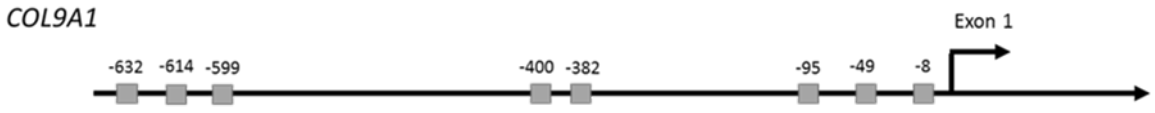

Figure 5.8 Structure of human proximal promoter of *COL9A1*. Arrow represents transcription start site (TSS) and grey squares represent CpG sites within the promoter region. COL9A1: collagen type IX.

DNA methylation levels in the CpG sites were analysed using pyrosequencing technique and, results for proximal promoter of *COL9A1* are displayed in Figure 5.9. CpG sites 632 and 614 upstream of TSS were highly methylated at 7 wpc (mean 74.11 %) with a continuous significant decrease observed to 19.77 % (mean) until 17 wpc (CpG (-632): $R^2 = 0.8001$, $p < 0.001$; CpG (-614): $R^2 = 0.8634$, $p < 0.05$) (Figure 5.9 A and B, Table 5.7).

CpG sites 599, 400 and 382 upstream of TSS could not be analysed due to inefficient primer binding during the pyrosequencing process. CpG sites 95 and 49 upstream of TSS did not show a significant increase or decrease between 7 and 17 wpc (Figure 5.9 D, Table 5.7). In CpG 95 upstream of TSS, 5mC content varied between 7 wpc and 16 wpc with 23.24 % 5mC at 7 wpc and 4.55 % 5mC at 16 wpc. Data for DNA methylation at this CpG site at 17 wpc was not available (Figure 5.9 C, Table 5.7). In CpG 49 upstream of TSS, 5mC content at 7 wpc was similar to 5mC measured at 7 wpc in CpG 95 upstream of TSS (22.87 %). DNA methylation in CpG 49 upstream of TSS varied between 7 wpc and 17 wpc (4.85 %). In Table 5.7, unavailable data refers to samples where no data could be acquired due to technical difficulties or inefficient pyrosequencing assays.

Correlation analysis between *COL9A1* gene expression and DNA methylation was significant in three of the four analysed CpG sites upstream of TSS (CpG -632, -614, -95, -49) in proximal promoter (Figure 5.10). DNA methylation in CpG site 632 upstream of TSS decreased dramatically with increasing *COL9A1* expression ($R^2 = 0.7535$, $p < 0.001$), (Figure 5.10 A). Correlation between *COL9A1* expression and DNA methylation in CpG 614 upstream of TSS was not significant due to insufficient data available (Figure 5.10 B). In CpG sites 95 and 49 upstream of TSS, DNA methylation in relation to increasing gene expression was modest compared to CpG 632 upstream of TSS (CpG (-95): $R^2 = 0.5996$, $p < 0.05$; CpG (-49): $R^2 = 0.4754$, $p < 0.05$), (Figure 5.10 C and D).

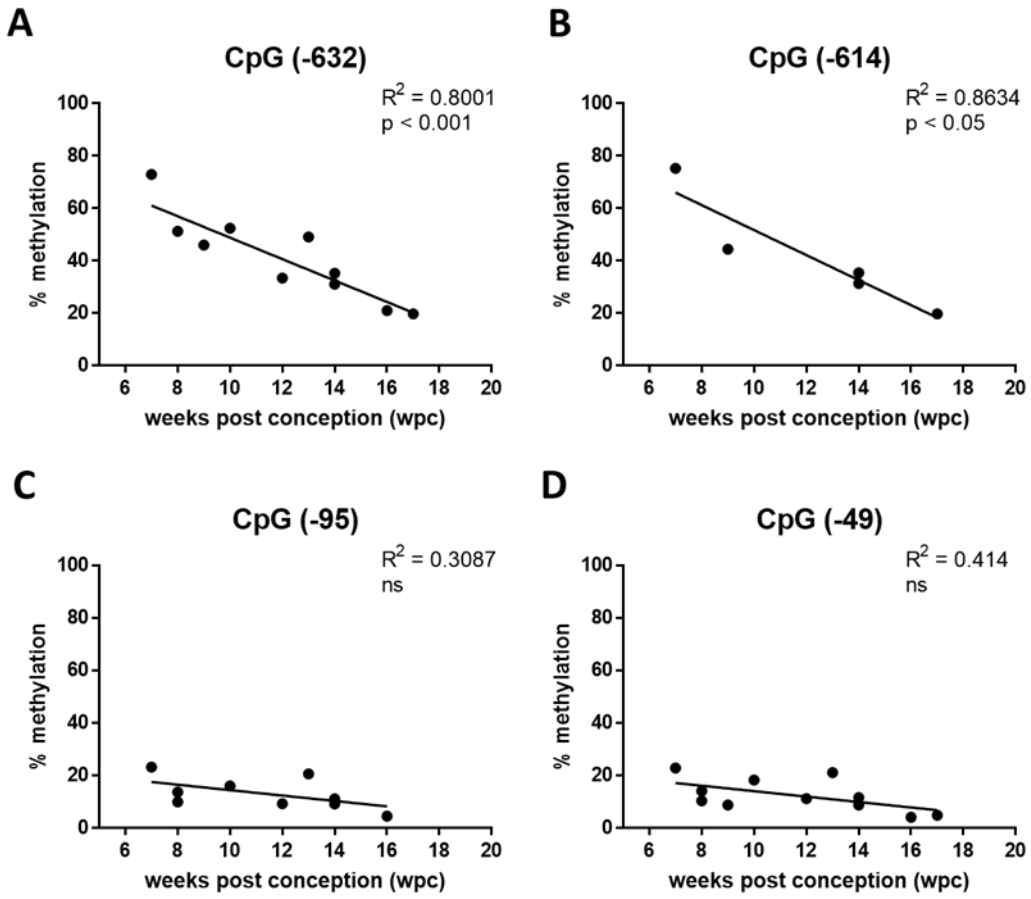

Figure 5.9 DNA methylation in CpG sites in proximal *COL9A1* promoter region in correlation to human foetal femur age (7 - 17 wpc). Values represent HFBCs isolated from individual human foetal femurs (n =1) for each developmental week except 8 and 14 wpc (n =2). Significance was determined by the use of non-linear regression test. COL9A1: collagen type IX; R^2: Spearman's correlation coefficient; ns: not significant; wpc: weeks post conception.

Table 5.7 Summary of DNA methylation at CpG sites within the *COL9A1* proximal promoter region in HFBCs isolated from 7 - 17 wpc human foetal femurs. wpc: weeks post conception; COL9A1: collagen type IX; HFBCs: human foetal bone cells.

wpc	CpG (-632)	CpG (-614)	CpG (-95)	CpG (-49)
7	72.96	75.26	23.24	22.87
8	51.28	No data available	9.96	10.35
8	51.36	No data available	13.74	14.14
9	46.05	44.49	No data available	8.76
10	52.49	No data available	16.01	18.28
12	33.45	No data available	9.33	11.2
13	49.09	No data available	20.64	21.13

wpc	CpG (-632)	CpG (-614)	CpG (-95)	CpG (-49)
14	31.14	31.38	9.22	8.77
14	35.29	35.42	11.15	11.64
16	21.08	No data available	4.55	4.15
17	19.78	19.75	No data available	4.85

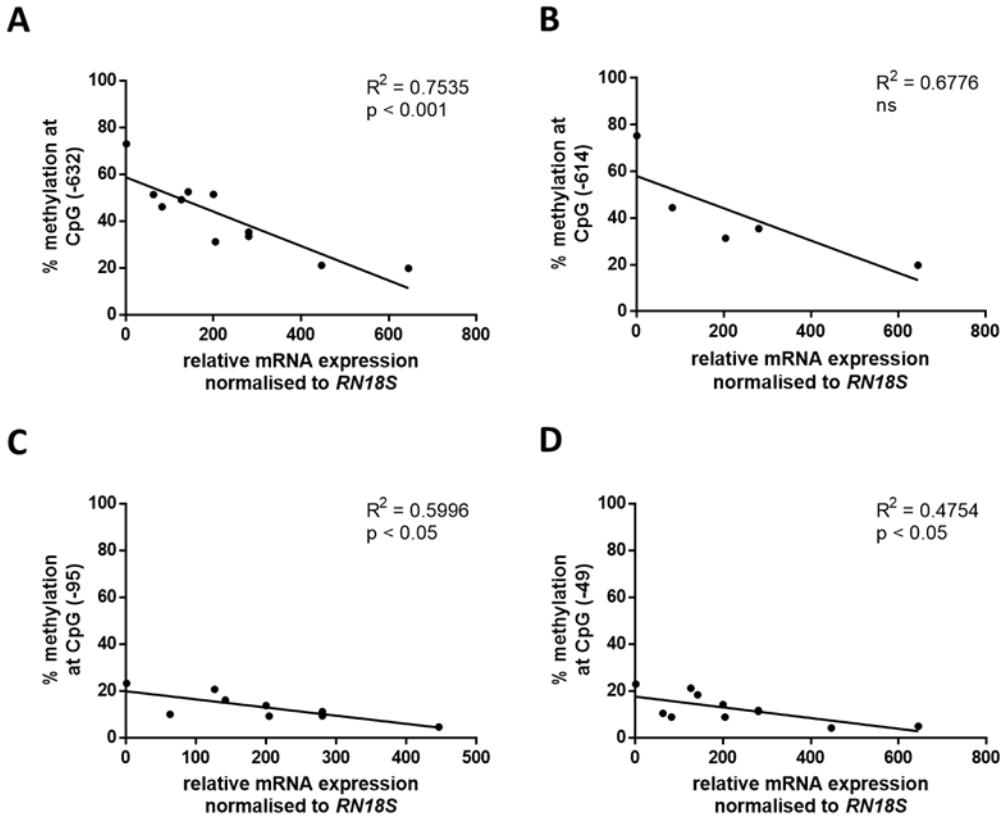

Figure 5.10 Correlation between *COL9A1* expression and DNA methylation in the proximal promoter. Values represent HFBCs isolated from individual human foetal femurs (n = 1) for each developmental week except 8 and 14 wpc (n = 2). Significance was determined by use of non-linear regression test. COL9A1: collagen type IX; R^2: Spearman's correlation coefficient; ns: not significant.

DNA methylation in two of the tested *COL9A1* CpG sites showed significant decrease and this observed decrease correlated significantly with observed significant increase in gene expression. Therefore, this finding demonstrated the regulation of *COL9A1* gene expression by DNA methylation.

Runt-relation transcription factor 2 (*RUNX2*)

Expression of *RUNX2* in HFBCs at passage 0 isolated from 7 - 17 wpc human foetal femurs were analysed including qRT-PCR in section 4.3.3, Figure 4.18 A and displayed in this section again in order to facilitate the comparison between gene expression and promoter DNA methylation in this chapter. *RUNX2* expression demonstrated, overall, low expression levels with unchanged gene expression between 7 – 17 wpc of femur development (R^2 = 0.0008816), see Figure 5.11 and Table 7.7. DNA methylation status of CpGs within the *RUNX2* promoter was performed in order to investigate the contribution of DNA methylation on gene expression.

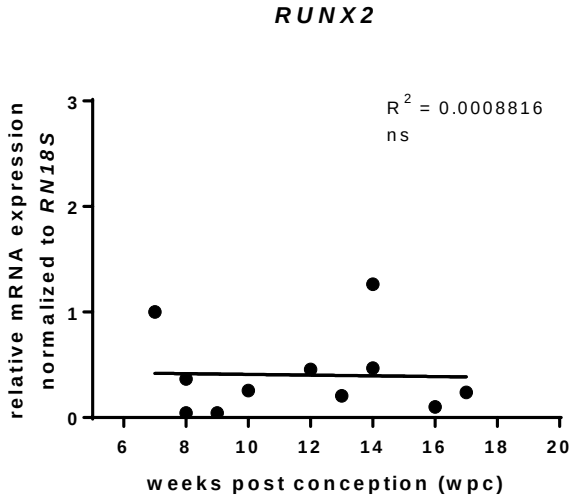

Figure 5.11 *RUNX2* expression in HFBCs isolated from 7 - 17 wpc human foetal femurs. Values represent HFBCs isolated from individual human foetal femurs (n = 1) for each developmental week except 8 and 14 wpc (n = 2). Significance was determined by non-linear regression test. RUNX2: runt-related transcription factor 2; R^2: Spearman's correlation coefficient; wpc: weeks post conception.

The human proximal promoter of *RUNX2* contains 3 CpG sites upstream of exon 1 relative to TSS and 2 CpG sites within exon 1 (Figure 5.12).

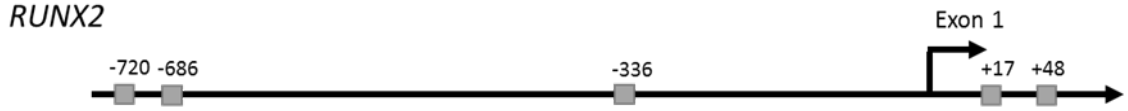

Figure 5.12 Structure of human distal promoter P1 of *RUNX2*. Arrow represents transcription start site (TSS) and grey squares represent CpG sites within the promoter region and exon 1. RUNX2: runt-related transcription factor 2.

DNA methylation level in CpG 720 upstream of TSS was relatively consistent between 7 - 10 wpc (72.76 % at 7wpc; 72.35 % at 17 wpc). A decrease in methylation levels was observed between 12 and 13 wpc (56.66 % at 12 wpc; 63.04 % at 13 wpc) followed by slight increase to 17 wpc (63.11 %). An overall decrease in DNA methylation in CpG 720, upstream of TSS, was significant ($p < 0.05$) (Figure 5.13 A and Table 5.8). DNA methylation in CpG 686 upstream of TSS did not significantly change compared to levels in CpG 720 upstream of TSS (77.81 % at 7 wpc; 77.28 % at 17 wpc), with a slight variation in HFBCs isolated from the different human foetal femurs (Figure 5.13 B and Table 5.8).

DNA methylation in HFBCs isolated from 7 – 17 wpc human foetal femurs in CpG 336 upstream of TSS varied between 7 and 17 wpc and showed overall less DNA methylation compared to CpGs 720 and 686 upstream of TSS and CpG 17 downstream of TSS (CpG(-336): 49.85 % at 7 wpc, 45.81 % at 17 wpc; CpG(-720): 72.76 % at 7 wpc, 63.11 % at 17 wpc; CpG(-686): 77.81 % at 7 wpc, 77.28 % at 17 wpc;). However, decrease in DNA methylation between 7 and 17 wpc was not significant (Figure 5.13 C and Table 5.8).

CpG 17 downstream of TSS demonstrated greater variation between samples compared to CpGs 720, 686, 336 upstream of TSS. DNA methylation showed 62.12 % at 7 wpc and 44.17 % at 17 wpc. DNA methylation at CpG 17 downstream of TSS showed higher DNA methylation than CpG 336 upstream of TSS but less than CpG 720 upstream of TSS. However, decrease in DNA methylation between 7 and 17 wpc was not significant (Figure 5.13 D and Table 5.8).

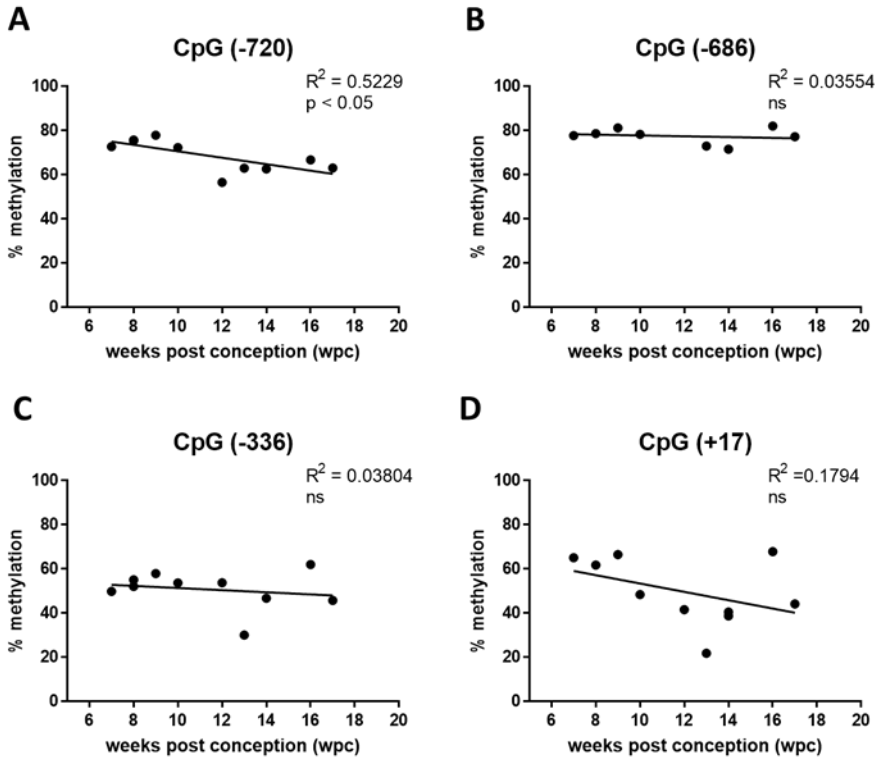

Figure 5.13 DNA methylation in CpG sites in distal *RUNX2* promoter P1 region in correlation to sample age (7 - 17 wpc). Values represent HFBCs isolated from individual human foetal femurs (n = 1) for each developmental week except 8 and 14 wpc (n = 2). Significance was determined by the use of non-linear regression test. RUNX2: runt-related transcription factor 2; R^2: Spearman's correlation coefficient; wpc: weeks post conception; ns: not significant.

Table 5.8 Summary of DNA methylation at CpG sites within *RUNX2* promoter P1 region in HFBCs isolated from 7 - 17 wpc human foetal femurs. wpc: weeks post conception; RUNX2: runt-related transcription factor 2; HFBCs: human foetal bone cells.

wpc	CpG (-720)	CpG (-686)	CpG (-336)	CpG (+17)
7	72.76	77.81	49.85	65.12
8	75.43	78.72	55.12	61.82
8	75.77	No data available	52.09	No data available
9	77.99	81.28	57.97	66.55
10	72.35	78.34	53.74	48.45
12	56.66	No data available	53.79	41.66
13	63.04	73.00	30.13	21.91
14	No data available	No data available	No data available	38.76
14	62.73	71.59	46.79	40.53
16	66.75	82.16	62.05	67.87

wpc	CpG (-720)	CpG (-686)	CpG (-336)	CpG (+17)
17	63.11	77.28	45.81	44.17

RUNX2 CpGs did not show significant change (except CpG (-720)) which in turn did correspond with the observed unchanged *RUNX2* gene expression (Figure 5.11). This finding therefore could also suggest a regulatory role of DNA methylation, as previously observed for *COL9A1*.

Osteocalcin (*OCN*)

Expression of *OCN* in HFBCs at passage 0 isolated from 7 - 17 wpc human foetal femurs was analysed using qRT-PCR in section 4.3.3 (Figure 4.18 C) and displayed in this section again in order to facilitate the comparison between gene expression and promoter DNA methylation in this chapter. *OCN* expression showed varied expression in the HFBCs isolated from the individual human foetal femur samples, however, no significant increase or decrease between 7 and 17 wpc was observed (R^2 = 0.07923, Figure 5.14 and Table 7.7)

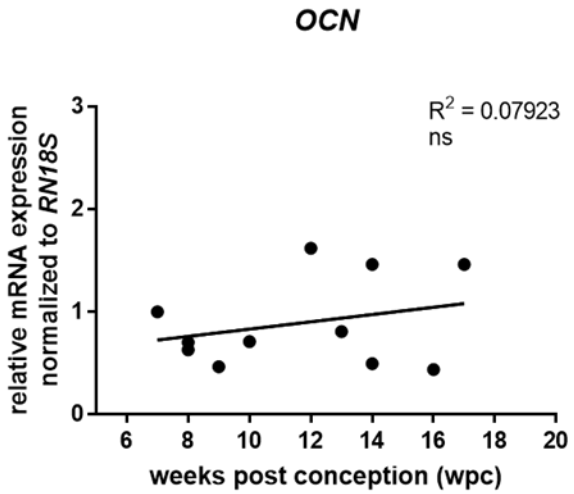

Figure 5.14 *OCN* expression in HFBCs isolated from 7 - 17 wpc human foetal femurs. Values represent HFBCs isolated from individual human foetal femurs (n =1) for each developmental week except 8 and 14 wpc (n =2). Significance was determined by non-linear regression test. OCN: osteocalcin; R^2: Spearman's correlation coefficient; wpc: weeks post conception; ns: not significant.

The human *OCN* promoter contains 10 CpG sites upstream of exon 1, relative to TSS (Figure 5.15).

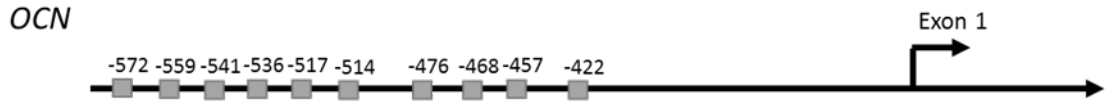

Figure 5.15 Structure of human *OCN* promoter. Arrow represents transcription start site (TSS) and grey squares represent analysed CpG sites within the promoter region. OCN: osteocalcin.

All analysed CpGs within the *OCN* promoter showed similarly high levels of DNA methylation although, the extent of reduction of DNA methylation between 7 and 17 wpc human foetal femurs differed between CpGs. However, all analysed CpGs, with the exception of CpG 541 upstream of TSS, demonstrated a significant decrease in DNA methylation between 7 and 17 wpc (Figure 5.16 and Table 5.9).

DNA methylation in CpG 572 upstream of TSS showed a significant decrease between 7 and 17 wpc ($p < 0.001$). DNA methylation levels were 87.97 % at 7 wpc with only slight decrease until 12 wpc (84.51 %), followed by a more dramatic decrease until 17 wpc (71.97 % at 17 wpc) (Figure 5.16 A and Table 5.9).

DNA methylation levels showed a similar significant decreasing trend in CpG 559 upstream of TSS ($p < 0.05$), as for CpG 572 upstream of TSS with overall lower methylation levels (78.82 % at 7 wpc; 58.76 % at 17 wpc), yet, slightly more dramatic decrease compared to CpG 572 upstream of TSS (Figure 5.16 B and Table 5.9).

CpG 541 upstream of TSS showed similar DNA methylation levels as CpG 572 upstream of TSS, although with greater variation in DNA methylation in HFBCs isolated from the different human foetal femur samples as well as no significant decrease between 7 and 17 wpc (Figure 5.16 C and Table 5.9).

The decrease in DNA methylation in CpG 517 upstream of TSS was similar to CpGs 572 and 559 upstream of TSS with overall DNA methylation levels being similar to the levels found in CpG 559 upstream of TSS (80.23 % at 7 wpc; 62.49 % at 17 wpc) (Figure 5.16 D and Table 5.9).

CpG 514 upstream of TSS showed similar DNA methylation levels as CpGs 517 and 559 upstream of TSS although with a decrease in DNA methylation being greater in CpG 514 than in CpG 559 upstream of TSS (78.64 % at 7 wpc; 53.54 % at 17 wpc) (Figure 5.16 E and Table 5.9).

CpGs 476, 468 and 457 upstream of TSS demonstrated equally high DNA methylation levels and a decrease in DNA methylation levels between 7 and 17 wpc. DNA methylation levels in CpG 476 upstream of TSS were found to be similar to the levels in CpG 572 upstream of TSS (88.49 % at 7 wpc; 78.13 % at 17 wpc) (Figure 5.16 F and Table 5.9).

CpG 468 upstream of TSS showed highest DNA methylation at 7 wpc (92.38 %), which was highest in all analysed CpGs with 70.72 % at 17 wpc and, equally intense decrease as found in CpG 559 upstream of TSS (Figure 5.16 G and Table 5.9).

DNA methylation level at 7 wpc in CpG 457, upstream of TSS, was found to be 90.52 % followed by a dramatic decrease until 14 wpc (79.03 % at 14 wpc). Unfortunately, no data was available for DNA methylation levels in HFBCs isolated from 17 wpc human foetal femurs for this CpG due to technical difficulties or inefficient pyrosequencing assays. No decrease in DNA methylation levels in CpG 457 upstream of TSS was found to be comparable to levels in CpG 468 upstream of TSS (Figure 5.16 H and Table 5.9).

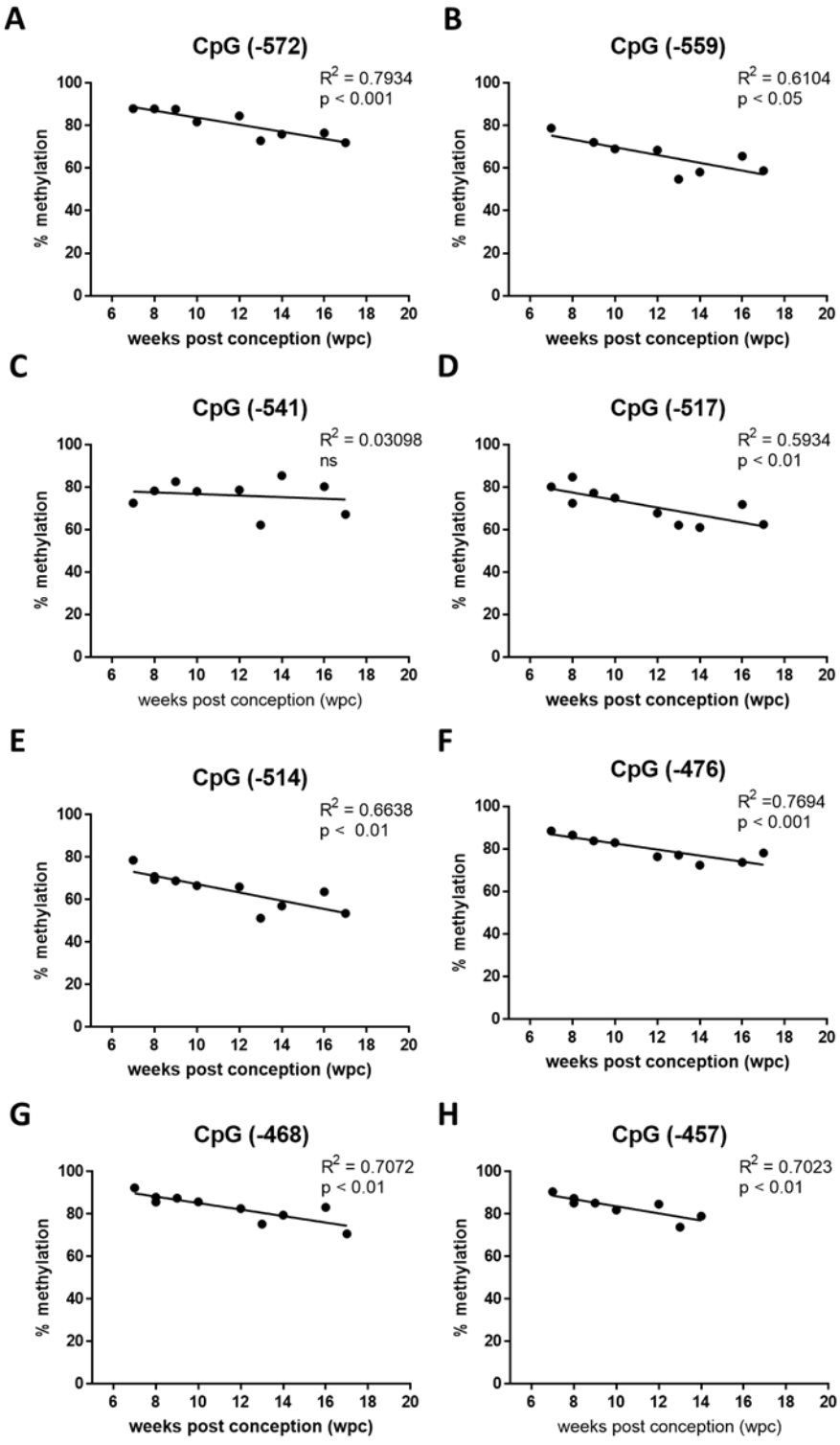

Figure 5.16 DNA methylation in CpG sites in *OCN* promoter region in correlation to sample age (7 - 17wpc). Values represent HFBCs isolated from individual human foetal femurs (n = 1) for each developmental week except 8 and 14 wpc (n = 2). Significance was determined by the use of non-linear regression test. OCN: osteocalcin; R^2: Spearman's correlation coefficient; ns: not significant; wpc: weeks post conception.

Table 5.9 Summary of DNA methylation at CpG sites within the *OCN* promoter region in HFBCs isolated from 7 - 17 wpc human foetal femurs. wpc: weeks post conception; OCN: osteocalcin; HFBCs: human foetal bone cells. Individual samples for each point.

wpc	CpG (-572)	CpG (-559)	CpG (-541)	CpG (-517)	CpG (-514)	CpG (-476)	CpG (-468)	CpG (-547)
7	87.97	78.82	72.56	80.23	78.64	88.49	92.38	90.52
8	87.88	No data available	78.29	72.43	69.48	86.42	85.72	85.23
8	No data available	No data available	No data available	84.81	70.93	86.58	87.97	87.42
9	87.72	72.15	82.59	77.31	68.88	83.76	87.53	85.23
10	81.71	69.02	78.01	74.96	66.60	82.94	85.8	81.98
12	84.51	68.48	78.67	67.79	66.08	76.35	82.60	84.69
13	72.84	54.77	62.17	62.09	51.25	77.10	75.30	73.87
14	No data available	No data available	No data available	No data available	No data available	No data available	No data available	No data available
14	75.99	58.10	85.46	61.02	57.05	72.39	79.51	79.03
16	76.57	65.62	80.33	71.86	63.69	73.72	83.20	No data available
17	71.97	58.76	67.17	62.49	53.54	78.13	70.72	No data available

Significant decrease in DNA methylation was observed in almost all analysed CpGs in the *OCN* promoter. However, no significant increase or decrease in *OCN* gene expression was observed (Figure 5.14). This would suggest that DNA methylation does not regulate the expression of *OCN*. However, as mineralisation is thought of i) occurring later during foetal development and ii) occurring slowly over time, it is possible that in the case of *OCN* certain CpG sites become demethylated before the effect on gene expression can be observed.

In order to assess which type of DNA methylation occurred during foetal femur development between 7 - 17 wpc, expression of *DNMT1* (responsible for maintenance DNA methylation) as well as *DNMT3A* and *DNMT3B* (responsible for *de novo* DNA methylation) was investigated by qRT-PCR.

DNMT1 and *de novo DNMT3A* expression levels remained unchanged (*DNMT1*: R^2 = 0.0644; *DNMT3A*: R^2 = 0.00165) with increasing human foetal femur age (Figure 5.17 A

and B, Table 5.10). *De novo DNMT3B* demonstrated an insignificant change in DNA methylation between 7 and 17 wpc ($R^2 = 0.1572$). Due to the n-number ranging from 1 – 2 samples, this represents insufficient evidence for the influence of *DNMTs* during any stage of human foetal femur development.

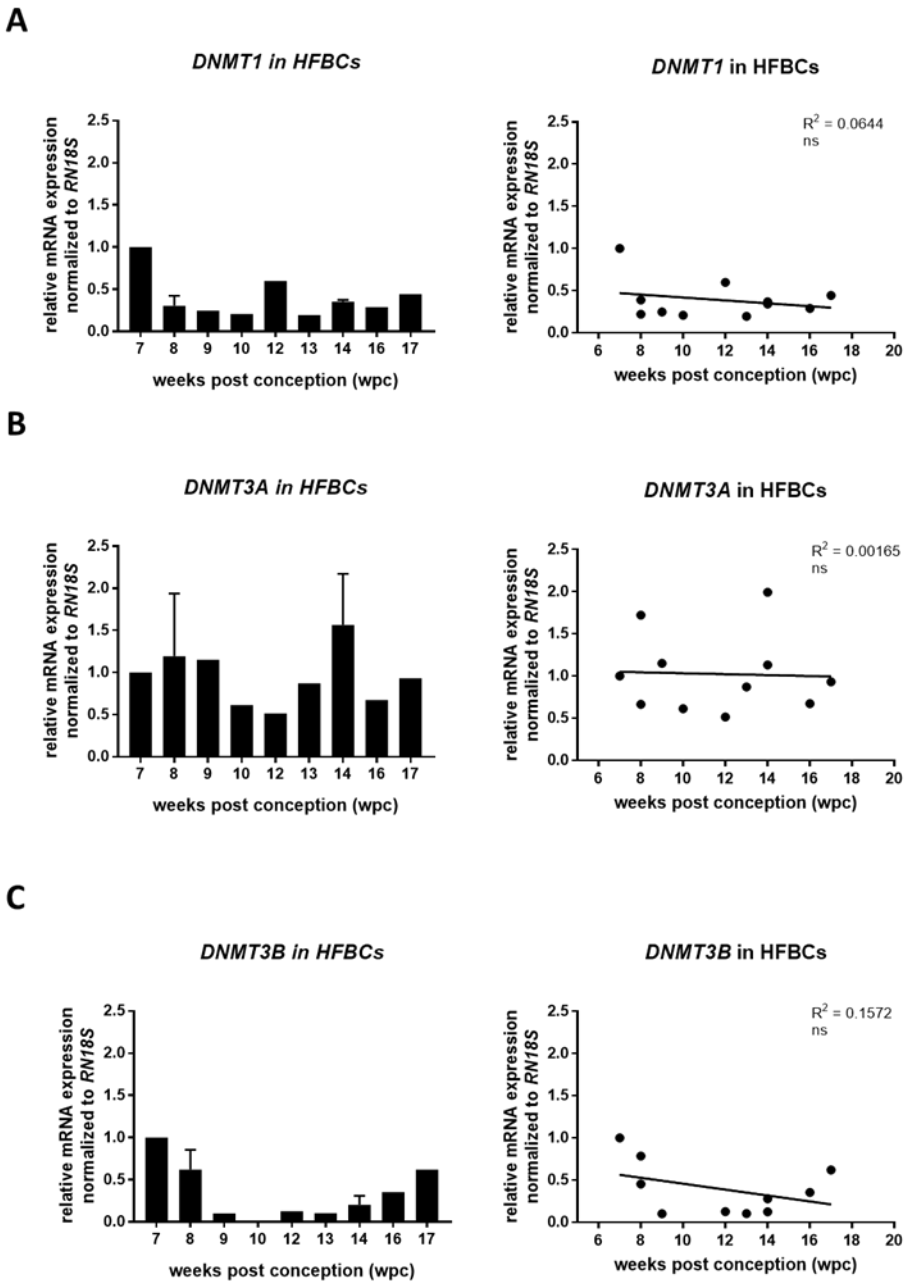

Figure 5.17 DNA methyltransferases (*DNMTs*) in HFBCs isolated from 7 - 17 wpc human foetal femurs.

A: Maintenance *DNMT1*. Expression displayed as mean +/- SD (8 wpc: mean 0.31+/- 0.12; 14 wpc: mean 0.36 +/- 0.02). Individual samples (left) and correlated to foetal femur length (right).

B: *De novo DNMT3A.* Expression is displayed as mean +/- SD (8 wpc: mean 1.19 +/- 0.75; 14 wpc: mean 1.56 +/- 0.61). Individual samples (left) and correlated to foetal femur length (right).

C: *De novo DNMT3B.* Expression is displayed as mean +/- SD (8 wpc: mean 0.62 +/- 0.23; 14

wpc: mean 0.20 +/- 0.11). Individual samples (left) and correlated to foetal femur length (right) represent HFBCs isolated from individual human foetal femurs (n = 1) for each developmental week except 8 and 14 wpc (n = 2). Significance was determined by the use of non-linear regression test. R^2: Spearman's correlation coefficient; wpc: weeks post conception; HFBCs: human foetal bone cells; ns: not significant.

Table 5.10 Summary of gene expression of maintenance and *de novo* DNA methyltransferases (DNMTs) in HFBCs isolated from 7 - 17 wpc human foetal femurs. wpc: weeks post conception; HFBCs: human foetal bone cells.

wpc	***DNMT1***	***DNMT3A***	***DNMT3B***
7	1	1	1
8	0.22	0.67	0.79
8	0.39	1.72	0.46
9	0.25	1.15	0.10
10	0.21	0.61	No data available
12	0.60	0.52	0.13
13	0.20	0.87	0.11
14	0.34	1.99	0.13
14	0.37	1.13	0.28
16	0.29	0.67	0.36
17	0.44	0.93	0.62

5.4 MicroRNAs during human foetal femur development

MiRNAs were shown to regulate protein expression by interfering at the mRNA stage. These small non-coding RNAs can prevent the mRNA from being translated into protein: i) complete binding between miRNA and target mRNA results in the degradation of the mRNA strand into small fragments, and ii) incomplete binding of the miRNA to mRNA results in the inhibition of the translation process [260]. MiRNAs were shown to be involved during the development of several tissues and processes (e.g self-renewal, skeletogenesis) and can target either components of signalling pathways, transcription factors or regulators of matrix production.

MiRNAs involved in regulation of chondrogenesis, miR-140-3p, 146a, 146b and 34a, showed variation in miRNA expression between 7 and 17 wpc with none of the analysed

miRNAs demonstrating a significant increase or decrease in expression between 7 and 17 wpc. **miR-140-3p** demonstrated the overall least variation in expression between samples (R^2 = 0.3002, Figure 5.18 A, Table 5.11). Expression of **miR-146a** showed no significant increase or decrease in expression with increasing developmental age (Figure 5.18 B, Table 5.11). **miR-146b** demonstrated the greatest variation in expression between samples (Figure 5.18 C, Table 5.11) with no signficant increase or decrease with increasing developmental age (R^2 = 0.053). **miR-34a** showed a slight variation in expression between the individual samples (R^2 = 0.2049, Figure 5.18 D, Table 5.11).

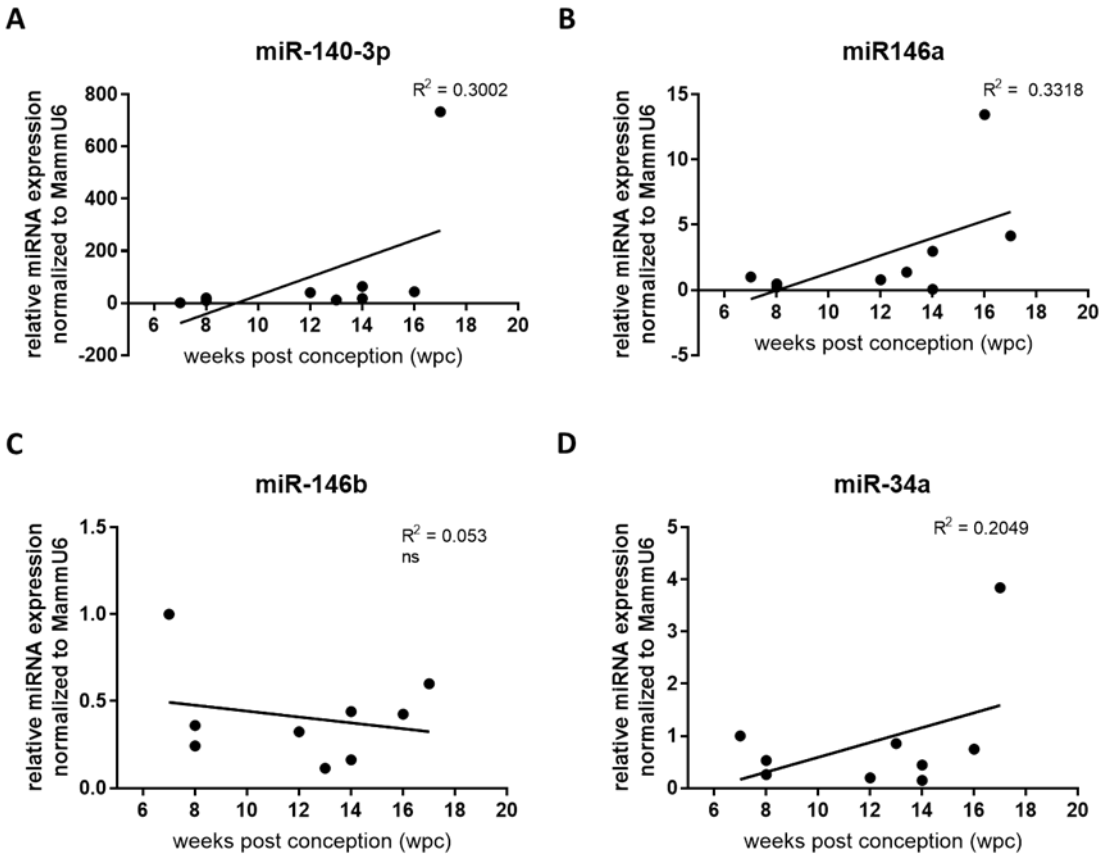

Figure 5.18 Expression of microRNAs (miRNAs) characteristic for chondrogenesis in HFBCs isolated from 7 – 17 wpc human foetal femurs. Values represent HFBCs isolated from individual human foetal femurs (n = 1) for each developmental week except 8 and 14 wpc (n = 2). miRNA expression was normalised to MammU6 in HFBCs isolated from 7 wpc human foetal femurs. Significance was determined by the use of non-linear regression test. R^2: Spearman's correlation coefficient.

Table 5.11 Summary of expression of microRNAs involved in chondrogenesis in HFBCs isolated from 7 - 17 wpc human foetal femurs. No data available due to lack of RNA. Values in blue italic with an asterisk were excluded from statistical analysis due to being outliers. wpc: weeks post conception; HFBCs: human foetal bone cells.

wpc	miR-140-3p	miR-146a	miR-146b	miR-34a
7	1	1	1	1
8	19.95	0.48	0.24	0.53
8	9.44	0.23	0.36	0.26
9	*890.34**	*13.87**	*1.73**	*8.26**
10	No data available	No data available	No data available	No data available
12	40.12	0.80	0.32	0.20
13	11.92	1.37	0.11	0.857
14	63.75	2.98	0.44	0.15
14	17.91	0.06	0.16	0.44
16	44.16	13.46	0.43	0.75
17	733.95	4.16	0.60	3.85

MiRNA expression levels of miRNAs associated with chondrogenesis (see Table 5.11) as well as osteogenesis (see Table 5.12) were checked for potential outliers using the Grubb's test as expression levels detected in HFBCs isolated from 9 wpc human foetal femur sample appeared to be out of range compared to the expression levels in HFBCs isolated from the remaining human foetal femurs. The Grubb's test confirmed that measured expression levels in HFBCs isolated from 9 wpc human foetal femur were outliers compared to expression levels of HFBCs isolated from other human foetal femur samples. There are several reasons for outliers such as air bubbles in the qPCR plate wells, increased concentration of the template due to double pipetting or a calculation error or problems during the qPCR run itself. The detected outliers were excluded from statistical analysis due to not being reliable measurements.

Expression of miRNAs associated with the regulation of osteogenesis varied in most analysed miRNAs, with the exception of miR-20b (Figure 5.19, Table 5.12).

miR-20b demonstrated a decrease in expression with increasing developmental age ($R^2 = 0.5904$, $p < 0.05$) (Figure 5.19 B, Table 5.12). **miR-23a, miR-29a and let7-f** showed

the overall greatest variation in expression between the individual samples and no significant increase or decrease in expression (miR-23a: $R^2 = 0.1463$; miR-29a: $R^2 = 0.138$; let7-f: $R^2 = 0.1082$, Figure 5.19 C, E, F, Table 5.12). Expression patterns for the individual samples were similar for **miR-138** and **miR-148b**, yet did not show a significant increase or decrease with increasing developmental age for neither of these two miRNAs (miR-138: $R^2 = 0.1602$; miR-148b: $R^2 = 0.2724$) (Figure 5.19 A, F, Table 5.12).

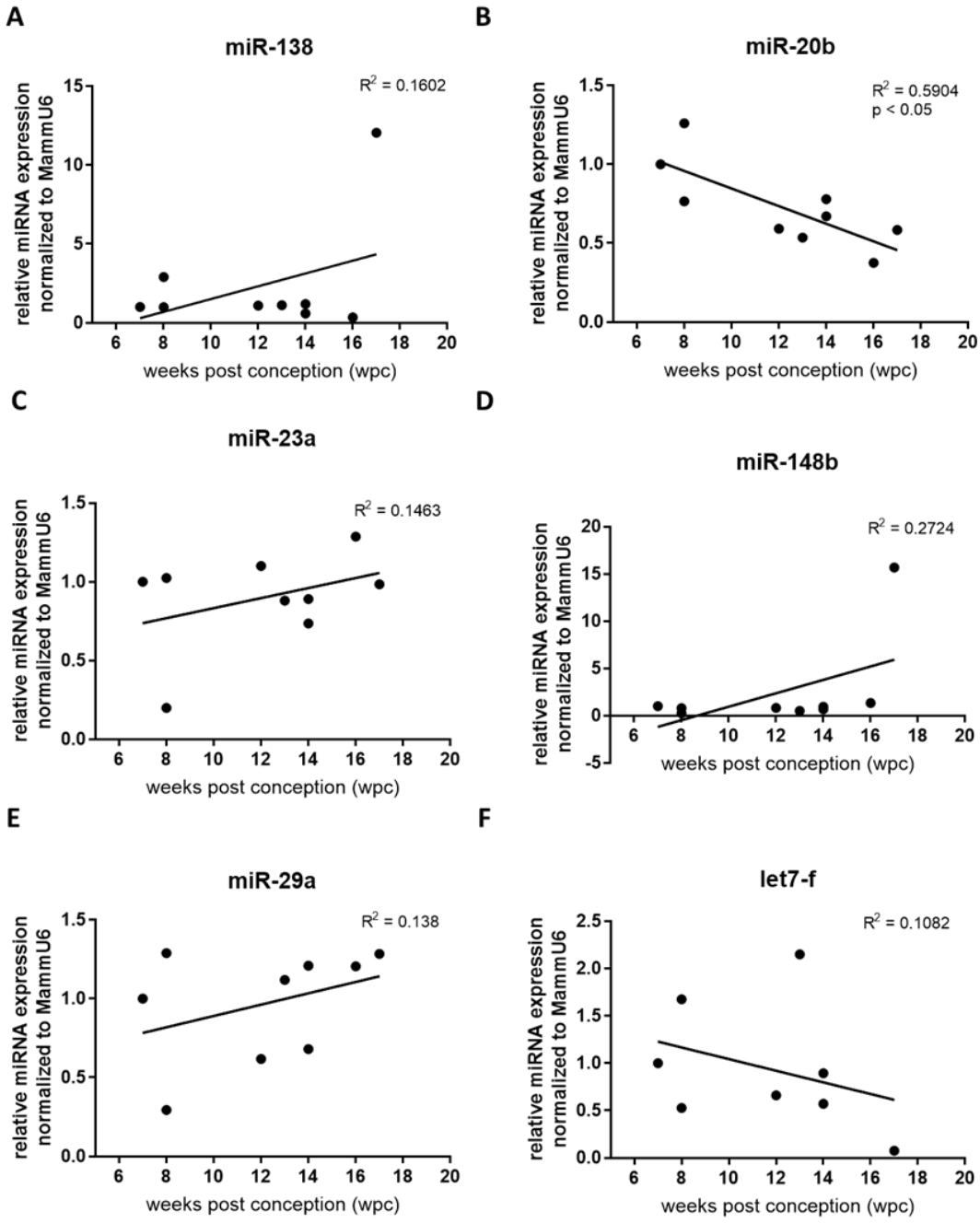

Figure 5.19 Expression of microRNAs (miRNAs) characteristic for osteogenesis in HFBCs isolated from 7 – 17 wpc human foetal femurs. Values represent HFBCs isolated from individual human foetal femurs (n = 1) for each developmental week except 8 and 14 wpc (n = 2). MiRNA

expression was normalised to MammU6 in HFBCs isolated from 7 wpc human foetal femurs. Significance was determined by the use of non-linear regression test. R^2: Spearman's correlation coefficient.

Table 5.12 Summary of expression of microRNAs involved in osteogenesis in HFBCs isolated from 7 - 17 wpc human foetal femurs. No data available due to lack of RNA. Values in blue italic with an asterisk were excluded from statistical analysis due to being outliers. wpc: weeks post conception; HFBCs: human foetal bone cells.

wpc	miR-138	miR-20b	miR-23a	miR-148b	miR-29a	let-7f
7	1.00	1.00	1.00	1.00	1.00	1.00
8	2.90	1.26	0.20	0.26	0.29	1.68
8	1.0	0.77	1.03	0.79	1.29	0.53
9	*85.52**	*14.40**	*19.37**	*2.80**	*5.53**	*1.50**
10	No data available	No data available	No data available	No data available	No data available	No data available
12	1.10	0.59	1.10	0.83	0.62	0.66
13	1.12	0.54	0.88	0.51	1.12	2.15
14	1.19	0.78	0.89	0.96	1.21	0.90
14	0.59	0.67	0.74	0.69	0.68	0.57
16	0.34	0.37	1.29	1.34	1.21	No data available
17	12.05	0.59	0.98	15.68	1.28	0.08

In summary, miRNA expression was observed to be widely spread in the analysed HFBCs isolated from 7 – 17 wpc human foetal femurs. miR-20b showed significant decrease in expression with developmental age. This finding suggests that the target mRNA is most likely upregulated with increasing developmental age due to suppression by miR-20b. MiR-20b was reported to suppress BMP antagonists [294, 298] therefore promoting osteogenesis. As the expression of miR-20b decreased between 7 and 17 wpc, expression of BMP antagonists is most likely increased, resulting in no or impaired osteogenesis. As none of the remaining analysed miRNAs associated with chondrogenesis and osteogenesis showed a significant increase or decrease in HFBCs between 7 and 17 wpc and the observation of variation in expression between HFBCs isolated from the 7-17 wpc human foetal femur

samples, there is no clear evidence for or against the regulatory involvement of the tested miRNAs in HFBCs isolated from 7 – 17 wpc human foetal femurs.

5.5 MicroRNAs expression during *in vitro* osteogenic differentiation of HFBCs isolated from 8 wpc and 14 wpc human foetal femurs

5.5.1 MicroRNAs expression *in vitro* during osteogenic differentiation of HFBCs isolated from 8 wpc human foetal femurs

MiRNAs are involved in several different developmental processes regulating osteo- and chondrogenesis. Therefore, miRNAs associated with chondrogenesis and osteogenesis in HFBCs isolated from 8 wpc human foetal femurs treated with two osteogenic differentiation media (chapter 4) were analysed.

None of the analysed miRNAs (miR-140-3p, miR-146a, miR-146b and miR-34a) demonstrated a significant difference between day 0 and day 19 in either if the three tested culture conditions (basal, oBG, oBG + TH + SAG).

MiR-140-3p expression in HFBCs isolated from 8 wpc human foetal femur was observed to be 0.91-fold change expression after 19 days compared to day 0. Cells cultured in oBG medium and oBG + TH + SAG medium for 19 days showed similar miRNA expression (oBG: 0.08-fold change expression; 0.07-fold change expression) (Figure 5.20 A, Table 5.13, Appendix M).

Culture in basal culture medium resulted in 22.95-fold **miR-146a** expression after 19 days while HFBCs isolated from 8 wpc human foetal femurs culture in oBG medium for 19 days showed 7.03-fold change expression and when cultured in oBG +TH + SAG medium showed 0.48-fold change expression after 19 days (Figure 5.20 B, Table 5.13, Appendix M).

HFBCs isolated from 8 wpc human foetal femurs cultured in basal culture medium demonstrated 6.61-fold change expression for **miR-146b**. Culture in oBG medium resulted in 1.93-fold change expression after 19 days and 0.58-fold change expression in oBG + TH + SAG culture medium (Figure 5.20 C, Table 5.13, Appendix M).

HFBCs isolated from 8 wpc human foetal femurs demonstrated 0.88-fold change expression of **miR-34a** under basal culture conditions. Culture in oBG medium for 19 days resulted in 1.31-fold change expression and culture in oBG + TH + SAG medium demonstrated 0.70-fold change expression (Figure 5.20 D, Table 5.13, Appendix M).

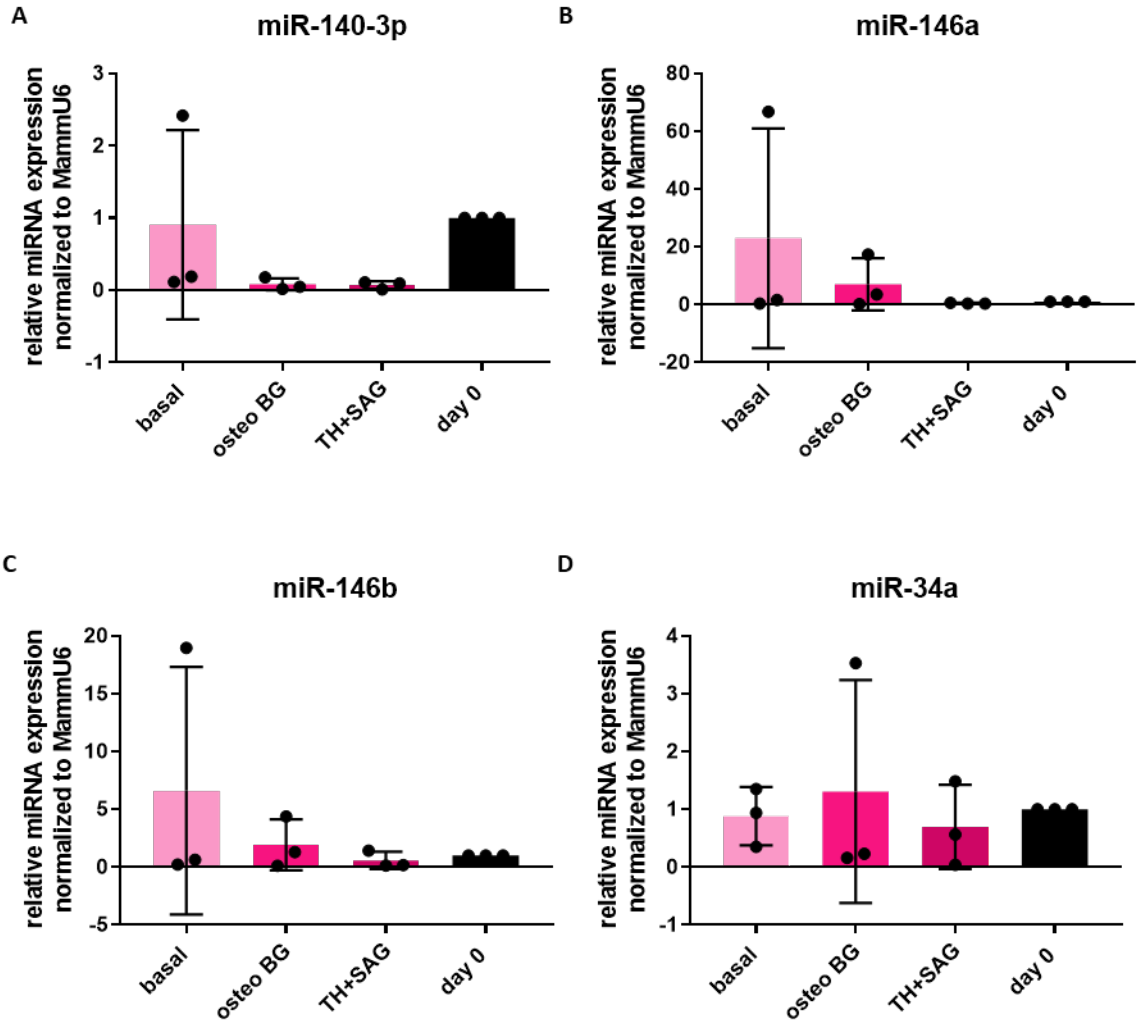

Figure 5.20 Expression of microRNAs (miRNAs) characteristic for chondrogenesis in HFBCs isolated from 8 wpc human foetal femurs treated with basal medium, osteogenic background medium (oBG, 10 nM dexamethasone, 10 nM 1,25-$(OH)_2$-vitamin D_3 and 100 µM ascorbic-2-phosphate) and osteo background (oBG) medium supplemented with small molecules SAG (smoothened agonist) and TH (4-(4-methoxyphenyl)pyrido[4′,3′:4,5]thieno[2,3-b]pyridine-2-carboxamide). MiRNA expression displayed as mean +/- SD and was normalised to MammU6 at day 0 in basal medium. Two-way ANOVA with Dunnett's post-hoc test for multiple comparisons was performed to compare different culture conditions of n = 3 differentiation experiments.

Table 5.13 Summary of respective microRNA expression characteristic for chondrogenesis in HFBCs isolated from 8 wpc human foetal femurs treated with basal medium, osteogenic background medium (oBG, 10 nM dexamethasone, 10 nM 1,25-$(OH)_2$-vitamin D_3 and 100 µM ascorbic-2-phosphate) and oBG supplemented with small molecules SAG (smoothened agonist) and TH (4-(4-methoxyphenyl)pyrido[4′,3′:4,5]thieno[2,3-b]pyridine-2-carboxamide). MiRNA expression displayed as mean +/- SD and was normalised to MammU6 at day 0 in basal medium. Two-way ANOVA with Dunnett's post-hoc test for multiple comparisons was performed to compare different culture conditions of n = 3 differentiation experiments. Mean of three individual experiments +/- SD displayed. HFBCs: human foetal bone cells**.**

condition	miR-140-3p	miR-146a	miR-146b	miR-34a
basal	0.91 +/- 1.31	22.95 +/- 37.99	6.61 +/- 10.71	0.88 +/- 0.50
oBG	0.08 +/- 0.08	7.03 +/- 9.08	1.93 +/- 2.20	1.31 +/- 1.93
oBG + TH + SAG	0.07 +/- 0.05	0.48 +/- 0.13	0.58 +/- 0.74	0.70 +/- 0.73

Overall expression of miRNAs miR-138, 20b, 23a, 148b, 29a and let-7f was lower compared to miRNAs miR-140-3p, 146a, 146b and 34a.

MiR-138, the negative control for osteogenesis, was highest expressed in HFBCs isolated from 8 wpc human foetal femurs under basal conditions (0.17-fold change expression, $p < 0.001$ compared to day 0). MiR-138 expression decreased dramatically following treatment with oBG medium for 19 days to 0.06-fold change expression compared to day 0 ($p < 0.0001$). Culture under oBG + TH + SAG resulted in similar extensive decrease of miRNA expression to 0.04-fold change ($p < 0.0001$), (Table 5.14, Figure 5.21 A, see Table 5.17, Appendix M).

MiR-20b expression demonstrated only slight decrease under basal treatment for 19 days compared to day 0 (0.28-fold change, $p < 0.01$). Treatment with oBG medium for 19 days showed lower expression compared to basal culture conditions (0.11-fold change expression) with reduction being significant compared to day 0 ($p < 0.01$). Expression of miR-20b was lowest after 19 days treatment with oBG + TH + SAG (0.07-fold change expression compared to day 0, $p < 0.05$), (Table 1.14, Figure 5.21 B, Appendix M).

MiR-23a in HFBCs isolated from 8 wpc human foetal femur showed no significant difference in expression after 19 days compared to day 0 in all three culture conditions.

Under basal culture conditions was 0.63-fold change expressed after 19 days. HFBCs cultured in oBG medium demonstrated 0.21-fold expression after 19 days while treatment with oBG + TH + SAG medium resulted in 0.08-fold change expression after 19 days compared to day 0 ($p < 0.05$), (Table 5.14, Figure 5.21 C, Appendix M).

MiR-148b expression was reduced under basal treatment for 19 days compared to day 0 (0.37-fold change, $p < 0.05$). Treatment with oBG medium for 19 days showed slightly lower expression compared to basal culture conditions (0.20-fold change expression compared to day 0, $p < 0.01$). Expression of miR-148b was lowest after 19 days treatment with oBG + TH + SAG (0.12-fold change expression compared to day 0, $p < 0.01$), (Table 5.14, Figure 5.21 D, Appendix M).

HFBCs isolated from 8 wpc human foetal femurs demonstrated no significant difference in **miR-29a** expression after 19 days compared to day 0 in all three analysed culture conditions. MiR-29a showed 1.77-fold change expression under basal culture conditions for 19 days. Culture in oBG medium for 19 days demonstrated 0.57-fold change expression in HFBCs isolated from 8 wpc human foetal femurs while culture in oBG + TH + SAG medium resulted in 0.26-fold change expression (Table 5.14, Figure 5.21 E, Appendix M).

Let-7f did not show a significant difference in expression in HFBCs cultured in either of the three media conditions for 19 days compared to day 0. Expression of let-7f after 19 days of culture in basal medium showed 0.72-fold change expression while culture of HFBCs isolated from 8 wpc human foetal femurs in oBG medium resulted in 1.27-fold change expression and culture in oBG + TH + SAG demonstrated 0.53-fold change expression (Table 5.14, Figure 5.21 F, Appendix M).

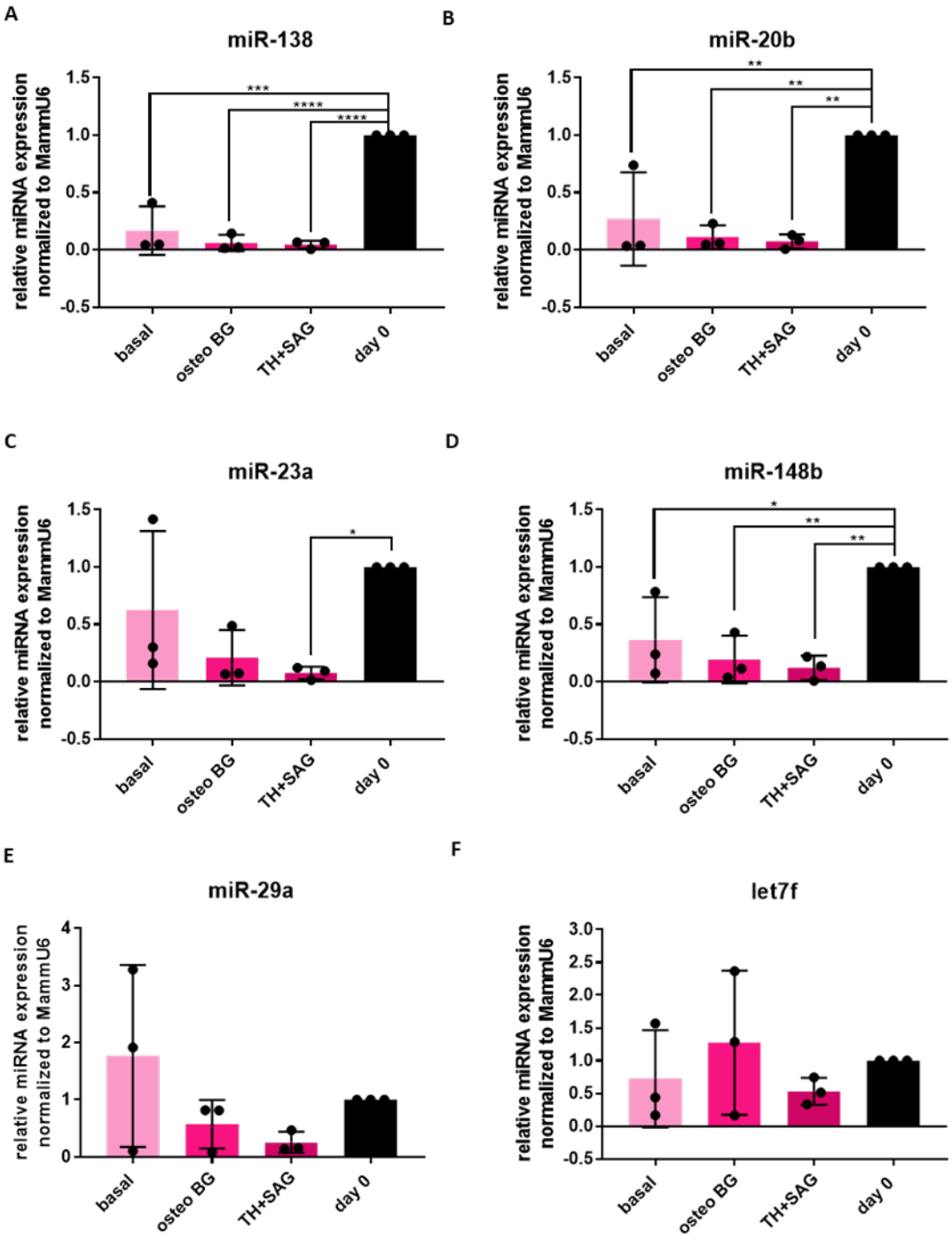

Figure 5.21 Expression of microRNAs (miRNAs) characteristic for osteogenesis in HFBCs isolated from 8 wpc human foetal femurs treated with basal medium, osteogenic background medium (oBG, 10 nM dexamethasone, 10 nM 1,25-(OH)$_2$-vitamin D$_3$ and 100 µM ascorbic-2-phosphate) and osteo background (oBG) medium supplemented with small molecules SAG (smoothened agonist) and TH (4-(4-methoxyphenyl)pyrido[4′,3′:4,5]thieno[2,3-b]pyridine-2-carboxamide). MiRNA expression displayed as mean +/- SD and was normalised to MammU6 at day 0 in basal medium. Two-way ANOVA with Dunnett's post-hoc test for multiple comparisons was performed to compare different culture conditions of n = 3 differentiation experiments. * $p < 0.05$; ** $p < 0.01$; *** $p < 0.001$; **** $p < 0.0001$.

Table 5.14 Summary of respective microRNA expression characteristic for osteogenesis in HFBCs isolated from 8 wpc human foetal femurs treated with basal medium, osteogenic background medium (oBG, 10 nM dexamethasone, 10 nM 1,25-$(OH)_2$-vitamin D_3 and 100 µM ascorbic-2-phosphate) and oBG supplemented with small molecules SAG (smoothened agonist) and TH (4-(4-methoxyphenyl)pyrido[4′,3′:4,5]thieno[2,3-b]pyridine-2-carboxamide). Gene expression was normalised to MammU6 at day 0. Osteogenic differentiation was performed three times (n = 3). Individual values, as well as mean of three individual experiments (in bold), are displayed. HFBCs: human foetal bone cells.

condition	miR-138	miR-20b	miR-23a	miR-148b	miR-29a	let7f
basal	0.17 +/- 0.21	0.27 +/- 0.41	0.63 +/- 0.69	0.37 +/- 0.37	1.77 +/- 1.59	0.72 +/- 0.74
oBG	0.06 +/- 0.07	0.11 +/- 0.10	0.21 +/- 0.24	0.20 +/- 0.21	0.57 +/- 0.42	1.27 +/- 1.10
oBG + TH + SAG	0.05 +/- 0.03	0.07 +/- 0.06	0.08 +/- 0.05	0.12 +/- 0.11	0.26 +/- 0.19	0.53 +/- 0.21

MiRNAs associated with chondrogenesis did not show significant increase or decrease in either of the tested osteogenic differentiation media after 19 days. miR-138, -20b and 148b demonstrated significant downregulation in both tested osteogenic conditions after 19 days of culture compared to day 0. miR-23a was shown to be significantly downregulated in HFBCs treated with oBG + TH + SAG for 19 days. miR-138 was reportedly downregulated during osteogenesis [305], miR-148b was reported to increase the osteogenic activity [308, 309], miR-23a targets SATB2 (a binding partner to RUNX2), resulting in an impaired osteogenesis [299]. miR-20b was reported to suppress BMP anatgonists, resulting in the repression of osteogenesis [294, 298].

The downregulation of miR-138, 23a and 148b in HFBCs treated with osteogenic media for 19 days demonstrates the activity of the osteogenic process. The combination of miR-138 being reportedly downregulated during osteogenesis, the downregulation of miR-148b causing an increase in osteogenic activity and RUNX2 downregulating miR-23a in order to ensure upregulation of RUNX2 binding partner SATB2, results in an increase in osteogenesis. The effect of the downregulation of miR-20b after 19 days of culture in osteogenic media is also decreased osteogenesis due to BMP anatagonists not being repressed by increased levels of miR-20b. This shows the complex interplay between different miRNAs.

5.5.2 MicroRNAs during *in vitro* osteogenic differentiation of HFBCs isolated from 14 wpc human foetal femurs

MiRNA associated with chondrogenesis and osteogenic in HFBCs isolated from 14 wpc human foetal femurs treated with two osteogenic differentiation media (chapter 4) were analysed.Under basal culture conditions, **miR-140-3p** expression showed no significant difference in expression between day 19 compared to day 0 (0.37-fold change expression after 19 days compared to day 0). Expression was decreased under oBG culture conditions (0.14-fold change expression compared to day 0, $p < 0.05$) and, showed significant increase under oBG + TH + SAG compared to treatment with oBG medium (0.28-fold change expression compared to day 0, $p < 0.05$) (Figure 5.22 A, Table 5.15, Appendix N).

Expression of **miR-146a** did not show a significant difference in either of the three tested culture conditions after 19 days compared to day 0. Under both basal and oBG culture conditions showed 0.62-fold change expression after 19 days. Under oBG + TH + SAG culture conditions for 19 days, miR-146a expression in HFBCs isolated from 14 wpc human foetal femurs demonstrated 1.41-fold change expression (Figure 5.22 B, Table 5.15, Appendix N).

MiR-146b did not show a significant difference between day 19 and day 0 in either of the three different culture conditions. . Expression under basal culture conditions was 0.73-fold change after 19 days. Culture in oBG medium resulted in 0.99-fold change expression while culture in oBG + TH + SAG medium demonstrated 0.82-fold change expression in HFBCs isolated from 14 wpc human foetal femurs after 19 days (Figure 5.22 C, Table 5.15, Appendix N).

HFBCs isolated from 14 wpc human foetal femurs did not demonstrate a significant difference in **miR-34a** expression between day 19 and day 0 in either of the three different culture conditions. MiR-34a under basal culture conditions showed a 0.78-fold change expression. Expression under oBG culture conditions resulted in 1.21-fold change while expression under oBG + TH + SAG conditions showed 2.69-fold change expression after 19 days (Figure 5.22 D, Table 5.15, Appendix N).

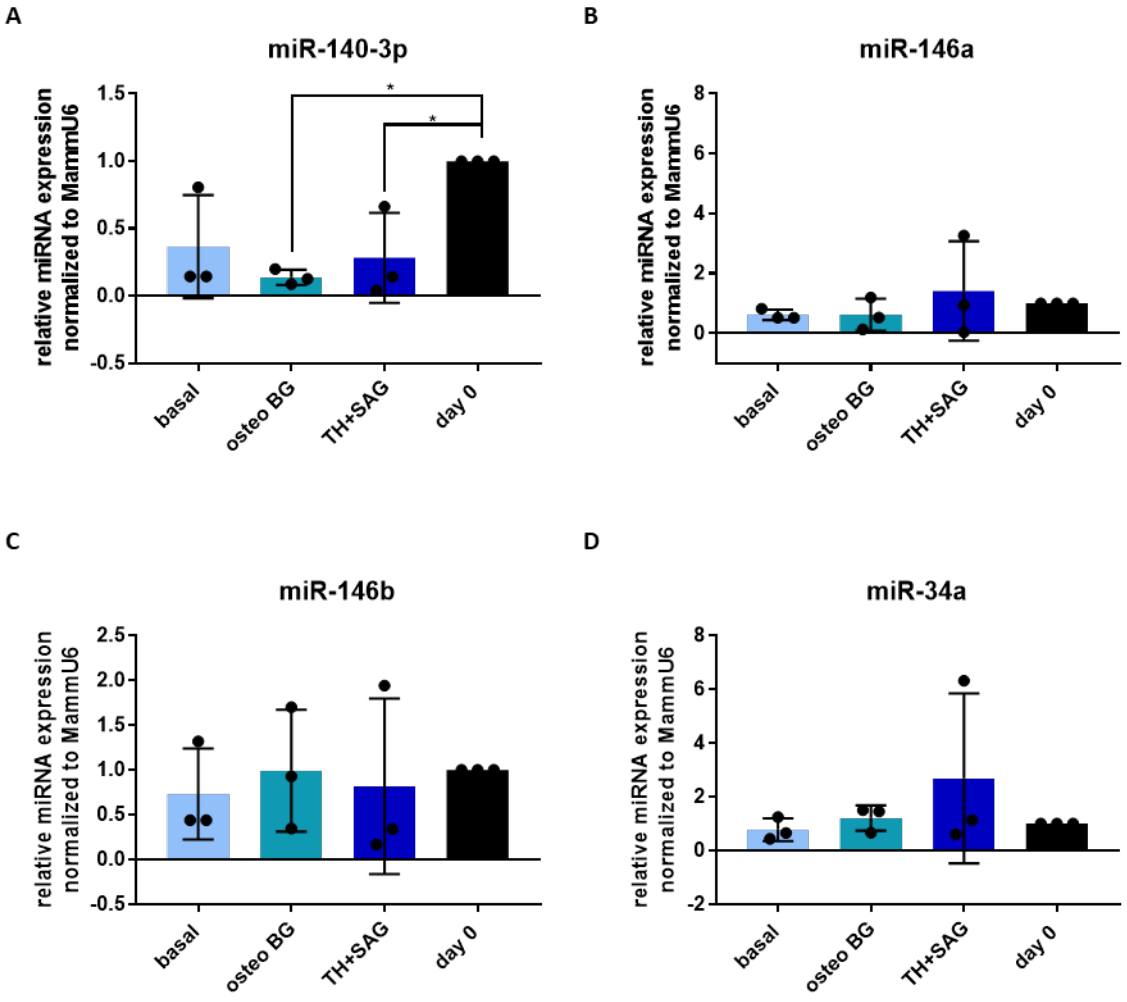

Figure 5.22 Expression of microRNAs (miRNAs) characteristic for chondrogenesis in HFBCs isolated from 14 wpc human foetal femurs treated with basal medium, osteogenic background medium (oBG, 10 nM dexamethasone, 10 nM 1,25-$(OH)_2$-vitamin D_3 and 100 µM ascorbic-2-phosphate) and osteo background (oBG) medium supplemented with small molecules SAG (smoothened agonist) and TH (4-(4-methoxyphenyl)pyrido[4′,3′:4,5]thieno[2,3-b]pyridine-2-carboxamide). MiRNA expression displayed as mean +/- SD and was normalised to MammU6 at day 0 in basal medium. Two-way ANOVA with Dunnett's post-hoc test for multiple comparisons was performed to compare different culture conditions of n = 3 differentiation experiments. * $p < 0.05$.

Table 5.15 Summary of respective microRNA expression characteristic for chondrogenesis in HFBCs isolated from 14 wpc human foetal femurs treated with basal medium, osteogenic background medium (oBG, 10 nM dexamethasone, 10 nM 1,25-$(OH)_2$-vitamin D_3 and 100 µM ascorbic-2-phosphate) and oBG supplemented with small molecules SAG (smoothened agonist) and TH (4-(4-methoxyphenyl)pyrido[4′,3′:4,5]thieno[2,3-b]pyridine-2-carboxamide). Gene expression was normalised to MammU6 at day 0. Osteogenic differentiation was performed three times (n = 3). Mean of three individual experiments +/- SD displayed. HFBCs: human foetal bone cells**.**

condition	miR-140-3p	miR-146a	miR-146b	miR-34a
basal	0.37 +/- 0.38	0.62 +/- 0.17	0.73 +/- 0.51	0.78 +/- 0.42
oBG	0.14 +/- 0.57	0.62 +/- 0.54	0.99 +/- 0.68	1.21 +/- 0.47
oBG + TH + SAG	0.28 +/- 0.33	1.41 +/- 1.66	0.82 +/- 0.98	2.69 +/- 3.16

MiR-138, the negative control for osteogenesis, did not show a significant difference in expression in either of the tested culture conditions after 19 days compared to day 0. Under basal culture conditions miR-138 was 0.31-fold change expressed in HFBCs isolated from 14 wpc human foetal femurs. Expression under oBG culture conditions was 0.18-fold change after 19 days while HFBCs isolated from 14 wpc human foetal femurs demonstrated 0.50-fold change expression (Table 5.16, Figure 5.23 A, Appendix N).

Reduction in **miR-20b** expression after 19 days relative to day 0 was significant in all three tested culture conditions. HFBCs isolated from 14 wpc human foetal femurs demonstrated 0.09-fold change ($p < 0.001$) oBG + TH + SAG culture conditions. Expression under basal culture conditions showed 0.33-fold change ($p < 0.01$) while under oBG culture condition showed 0.20-fold change ($p < 0.05$) (Table 5.16, Figure 5.23 B, Appendix N).

HFBCs isolated from 14 wpc human foetal femurs cultured for 19 days did not show a significant difference in either of the tested culture conditions. **MiR-23a** showed 0.65-fold change expression under basal culture conditions. Expression in cells cultured in oBG medium demonstrated a 0.95-fold change while miR-23a expression under oBG + TH + SAG culture conditions was found to be 0.95-fold change after 19 days (Table 5.16, Figure 5.23 C, Appendix N).

MiR-148b did not show a significant difference in either of the three tested culture conditions after 19 days compared to day 0. MiR-148b was shown to be 0.47-fold change

expressed under basal culture conditions and oBG culture condition 0.37-fold change after 19 days of culture. MiR-148b expression was 1.36-fold change expressed under oBG + TH + SAG culture conditions (Table 5.16, Figure 5.23 D, Appendix N).

Culture of HFBCs isolated from 14 wpc human foetal femurs in basal medium resulted in 0.47-fold change **miR-29a** expression whilst culture in oBG medium demonstrated a 0.31-fold change expression after 19 days. MiR-29a under oBG + TH + SAG culture conditions resulted in 1.07-fold change) expression compared to day 0. However, miR-29a expression in neither of the tested culture conditions was significantly different after 19 days of culture compared to day 0 (Table 5.16, Figure 5.23 E, Appendix N).

Let-7f expression under basal culture conditions resulted in 0.80-fold change after 19 days. Treatment of HFBCs isolated from 14 wpc human foetal femurs with oBG medium for 19 days demonstrated a 0.64-fold change expression in let-7f. Let-7f expression under oBG + TH + SAG culture condition was 1.99-fold change. None of the tested culture conditions resulted in a significant difference after 19 days of culture compared to day 0 (Table 5.16, Figure 5.23 F, Appendix N).

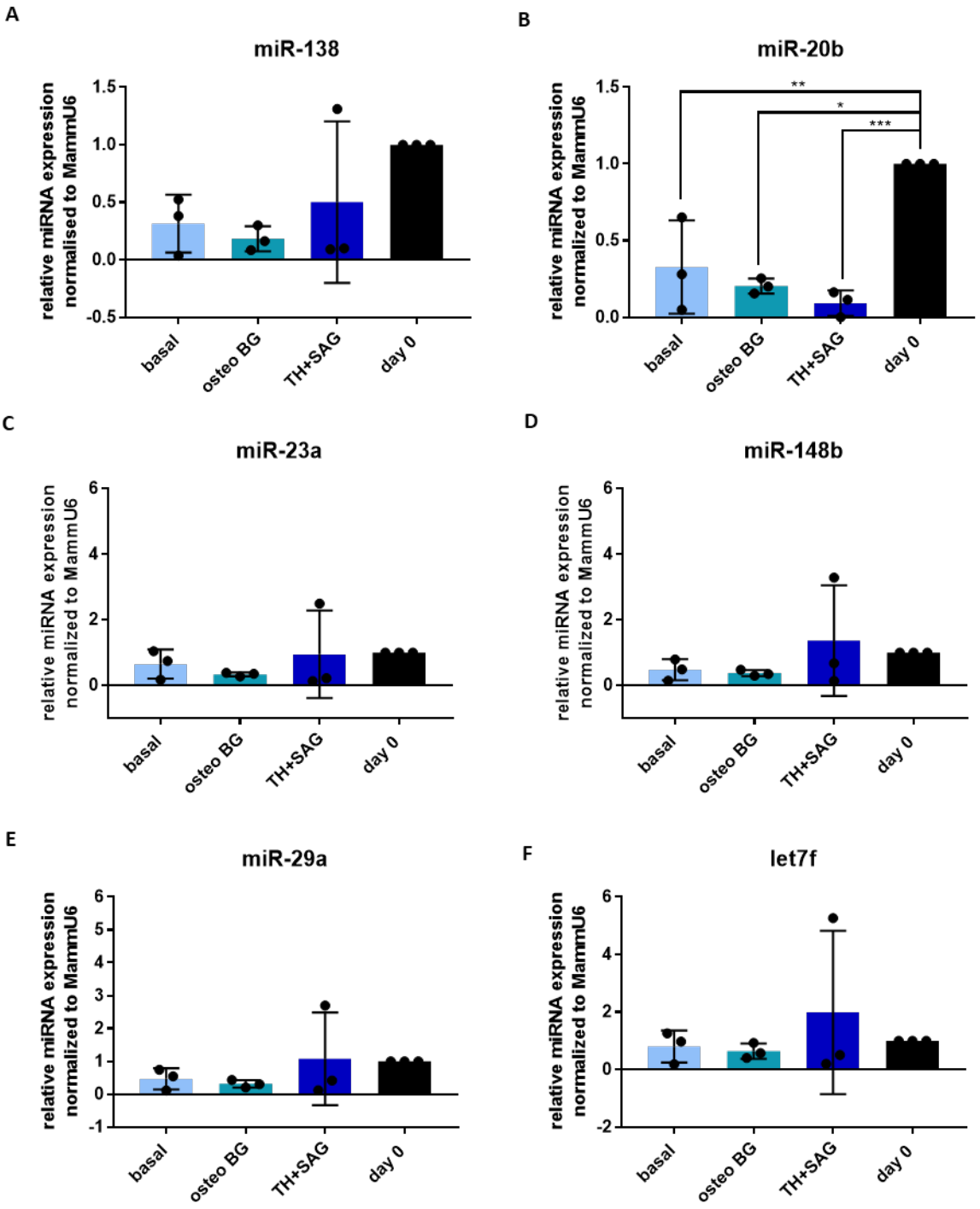

Figure 5.23 Expression of microRNAs (miRNAs) in HFBCs isolated from 14 wpc human foetal femur samples treated with basal medium, osteogenic background medium (oBG, 10 nM dexamethasone, 10 nM 1,25-(OH)$_2$-vitamin D$_3$ and 100 µM ascorbic-2-phosphate) and osteo background (oBG) medium supplemented with small molecules SAG (smoothened agonist) and TH (4-(4-methoxyphenyl)pyrido[4′,3′:4,5]thieno[2,3-b]pyridine-2-carboxamide). MiRNA expression displayed as mean +/- SD and was normalised to MammU6 at day 0 in basal medium. Two-way ANOVA with Dunnett's post-hoc test for multiple comparisons was performed to compare different culture conditions of n = 3 differentiation experiments. * $p < 0.05$; ** $p < 0.01$; *** $p < 0.001$.

Table 5.16 Summary of respective microRNA expression characteristic for osteogenesis in HFBCs isolated from 14 wpc human foetal femurs treated with basal medium, osteogenic background medium (oBG, 10 nM dexamethasone, 10 nM 1,25-$(OH)_2$-vitamin D_3 and 100 µM ascorbic-2-phosphate) and oBG supplemented with small molecules SAG (smoothened agonist) and TH (4-(4-methoxyphenyl)pyrido[4′,3′:4,5]thieno[2,3-b]pyridine-2-carboxamide). Gene expression was normalised to MammU6 at day 0. Osteogenic differentiation was performed three times (n = 3). Mean of three individual experiments +/- SD is displayed. HFBCs: human foetal bone cells**.**

condition	miR-138	miR-20b	miR-23a	miR-148b	miR-29a	let7f
basal	0.31 +/- 0.25	0.33 +/- 0.30	0.65 +/- 0.44	0.47 +/- 0.32	0.47 +/- 0.32	0.80 +/- 0.56
oBG	0.18 +/- 0.11	0.20 +/- 0.05	0.33 +/- 0.06	0.37 +/- 0.09	0.31 +/- 0.11	0.64 +/- 0.27
oBG + TH + SAG	0.50 +/- 0.70	0.09 +/- 0.08	0.95 +/- 1.34	1.36 +/- 1.69	1.07 +/- 1.41	1.99 +/- 2.84

MiR-140-3p was observed to be significantly downregulated in both tested osteogenic differentiation media. This miRNA was reportedly upregulated during chondrogenesis [317, 318], therefore miR-140-3p being downregulated in HFBCs cultured in osteogenic media for 19 days suggested that the chondrogenic process is repressed. miR-20b was also found to be downregulated in oBG + TH + SAG, thus not ensuring BMP antagonists to be repressed, consequently resulting in repression of osteogenesis. Due to only two miRNAs being significantly expressed after osteogenic culture for 19 days compared to day 0 a clear regulatory interaction between the different miRNAs cannot be shown.

5.6 MicroRNAs during osteogenic differentiation of NIBSC-8 MSCs *in vitro*

MiRNAs were reported to regulate the osteogenic differentiation process by promotion or suppression of osteogenic and chondrogenic pathways/regulators. Therefore, miRNAs associated with chondrogenesis and osteogenesis in NIBSC-MSCs treated with two osteogenic differentiation media (chapter 3) were analysed.

Expression of **miR-140-3p** under basal culture condition showed a 0.79-fold change and under oBG culture conditions a 0.53-fold change expression after 19 days. Expression levels for both culture conditions (basal and oBG) after 19 days were not significantly different to miR-140-3p at day 0. Under oBG + TH + SAG culture conditions for 19 days, miR-140-3p expression in NIBSC-8 MSCs demonstrated a significant difference between day 19 and day 0 (0.25-fold change expression) (Figure 5.24 A, Table 5.17, Appendix L).

No significant differences could be detected in the expression of miR-146a as well as miR-146b for either of the three culture conditions after 19 days compared to day 0. Expression of **miR-146a** was 1.52-fold change under basal culture conditions. NIBSC-8 MSCs cultured in oBG medium for 19 days showed 0.83-fold change expression whilst NIBSC-8 MSCs cultured in oBG + TH + SAG medium demonstrated 0.51-fold change expression (Figure 5.24 B, see Table 7.14). Expression of both miR-146a and **miR-146b** was comparable in the different tested osteogenic culture conditions (Figure 5.24 B and C, Table 5.17, Appendix L). Under basal culture conditions, miR-146b demonstrated 1.91-fold change expression (Figure 5.24 C, see Table 7.14, Appendix L).

NIBSC-8 MSCs demonstrated no significantly different **miR-34a** expression after 19 days compared to day 0 in either of the three tested culture conditions.Expression of miR-34a under basal culture conditions showed a 1.34-fold change expression. Culture in oBG medium for 19 days resulted in 0.53-fold change expression and culture in oBG + TH + SAG medium demonstrated 0.37-fold change expression (Figure 5.24 D, Table 5.17, Appendix L).

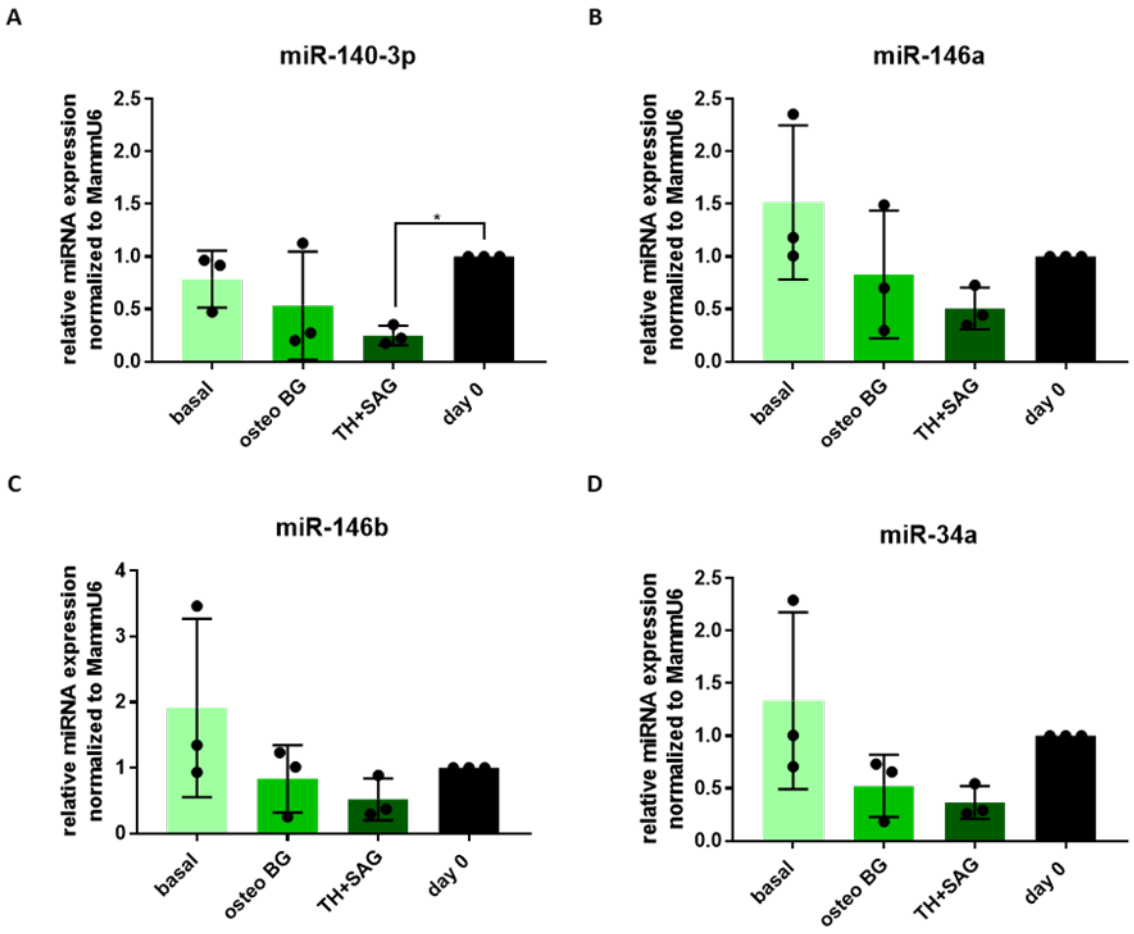

Figure 5.24 Expression of microRNAs (miRNAs) characteristic for chondrogenesis in NIBSC-8 MSCs at day 19 treated with basal medium, osteogenic background medium (oBG, 10 nM dexamethasone, 10 nM 1,25-$(OH)_2$-vitamin D_3 and 100 µM ascorbic-2-phosphate) and osteo background (oBG) medium supplemented with small molecules SAG (smoothened agonist) and TH (4-(4-methoxyphenyl)pyrido[4′,3′:4,5]thieno[2,3-b]pyridine-2-carboxamide). MiRNA expression displayed as mean +/- SD and was normalised to MammU6 at day 0 in basal medium. Two-way ANOVA with Dunnett's post-hoc test for multiple comparisons was performed to compare different culture conditions of n = 3 differentiation experiments. * $p < 0.05$.

Table 5.17 Summary of respective microRNA expression characteristic for chondrogenesis in NIBSC-8 MSCs treated with basal medium, osteogenic background medium (oBG, 10 nM dexamethasone, 10 nM 1,25-$(OH)_2$-vitamin D_3 and 100 µM ascorbic-2-phosphate) and oBG supplemented with small molecules SAG (smoothened agonist) and TH (4-(4-methoxyphenyl)pyrido[4′,3′:4,5]thieno[2,3-b]pyridine-2-carboxamide). Gene expression was normalised to MammU6 at day 0. Osteogenic differentiation was performed three times (n = 3). Mean of three individual experiments +/- SD displayed. HFBCs: human foetal bone cells**.**

condition	miR-140-3p	miR-146a	miR-146b	miR-34a
basal	0.79 +/- 0.27	1.52 +/- 0.73	1.91 +/- 1.36	1.34 +/- 0.84
oBG	0.53 +/-0.52	0.83 +/- 0.61	0.83 +/- 0.51	0.53 +/- 0.29
oBG + TH + SAG	0.25 +/- 0.09	0.51 +/- 0.20	0.52 +/- 0.32	0.37 +/- 0.16

MiR-138, the negative control for osteogenesis, did not show a significant difference after 19 days in either of the three culture conditions compared to day 0. NIBSC-8 MSCs demonstrated a 0.61-fold change under basal culture conditions. Expression under oBG culture conditions was 0.75-fold change after 19 days while NIBSC-8 MSCs demonstrated 0.42-fold change expression (Figure 5.25 A, Table 5.18, Appendix L).

MiR-20b expression in NBSC-MSCs treated with oBG + TH + SAG was three times lower compared to expression under basal conditions (basal: 0.45-fold change; oBG + TH + SAG: 0.13-fold change). Under oBG culture conditions, expression was 50 % lower compared to expression under basal culture conditions (oBG: 0.21-fold change). Decrease in miR-20b expression was statistically significant in all conditions compared to day 0 (basal $p < 0.01$; oBG, oBG + TH + SAG $p < 0.001$), (Figure 5.25 B, Table 5.18, Appendix L).

Neither of the analysed miRNAs miR-23a, miR148b, miR-29a and let-7f showed a significant difference in expression levels in either of the tested culture conditions after 19 days compared to day 0.

NIBSC-8 MSCs cultured in basal medium for 19 days showed 1.03-fold change **miR-23a** expression. Expression in cells cultured in oBG medium was 1.02-fold change. MiR-23a under oBG + TH + SAG culture conditions was 0.43-fold change expressed after 19 days (Figure 5.25 C, Appendix L, Table 5.18).

MiR-148b was shown to be similarly expressed under basal culture conditions (0.99-fold change) and oBG culture condition (0.81-fold change) after 19 days of culture. MiR-148b expression was 0.50-fold change expressed under oBG + TH + SAG culture conditions (Figure 5.25 D, Table 5.18, Appendix L).

Culture of NIBSC-8 MSCs in basal medium resulted in 1.07-fold change **miR-29a** expression whilst culture in oBG medium demonstrated a 0.75-fold change expression after 19 days. MiR-29a under oBG + TH + SAG culture conditions resulted in 0.39-fold change) expression compared to day 0 (Figure 5.25 E, Table 5.18, Appendix L).

Let-7f expression under basal culture conditions resulted in 0.93-fold change after 19 days. Treatment of HFBCs isolated from 14 wpc human foetal femurs with oBG medium for 19 days demonstrated a 0.87-fold change expression in let-7f. Let-7f expression under oBG + TH + SAG culture condition was 0.62-fold change (Figure 5.25 F, Table 5.18, Appendix L).

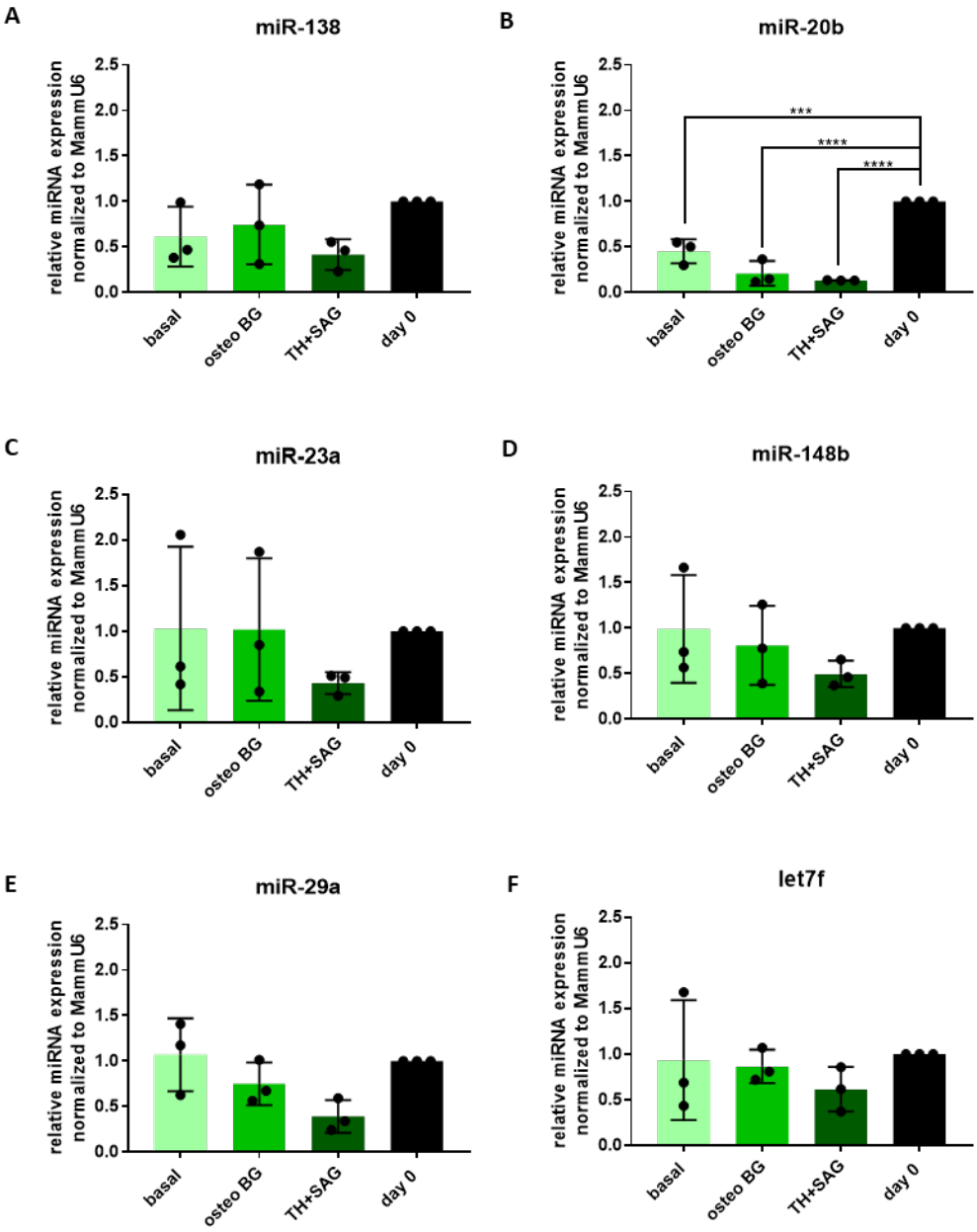

Figure 5.25 Expression of microRNAs (miRNAs) characteristic for osteogenesis in NIBSC-8 MSCs treated with basal medium, osteogenic background medium (oBG, 10 nM dexamethasone, 10 nM 1,25-$(OH)_2$-vitamin D_3 and 100 µM ascorbic-2-phosphate) and osteo background (oBG) medium supplemented with small molecules SAG (smoothened agonist) and TH (4-(4-methoxyphenyl)pyrido[4′,3′:4,5]thieno[2,3-b]pyridine-2-carboxamide). MiRNA expression displayed as mean +/- SD and was normalised to MammU6 at day 0 in basal medium. Two-way ANOVA with Dunnett's post-hoc test for multiple comparisons was performed to compare different culture conditions of n = 3 differentiation experiments. *** $p < 0.001$; **** $p < 0.0001$.

Table 5.18 Summary of respective microRNA expression characteristic for osteogenesis in NIBSC-8 MSCs treated with basal medium, osteogenic background medium (oBG, 10 nM dexamethasone, 10 nM 1,25-$(OH)_2$-vitamin D_3 and 100 µM ascorbic-2-phosphate) and oBG supplemented with small molecules SAG (smoothened agonist) and TH (4-(4-methoxyphenyl)pyrido[4′,3′:4,5]thieno[2,3-b]pyridine-2-carboxamide). Gene expression was normalised to MammU6 at day 0. Osteogenic differentiation was performed three times (n = 3). Mean of three individual experiments +/- SD is displayed. HFBCs: human foetal bone cells**.**

condition	miR-138	miR-20b	miR-23a	miR-148b	miR-29a	let7f
basal	0.61 +/- 0.33	0.45 +/- 0.13	1.03 +/- 0.90	0.99 +/-0.60	1.07 +/- 0.40	0.93 +/- 0.66
oBG	0.75 +/- 0.44	0.21 +/- 0.14	1.02 +/- 0.78	0.81 +/- 0.43	0.75 +/-0.23	0.87 +/- 0.18
oBG + TH + SAG	0.42 +/- 0.17	0.13 +/- 0.00	0.43 +/- 0.12	0.50 +/- 0.15	0.39 +/- 0.18	0.62 +/- 0.24

MiR-140-3p showed downregulation in oBG + TH + SAG after 19 days compared to day 0. This miRNA was reportedly upregulated during chondrogenesis [317, 318], therefore miR-140-3p being downregulated in HFBCs cultured in osteogenic media for 19 days suggested that the chondrogenic process is repressed. miR-20b was also found to be downregulated in both tested osteogenic media, thus not ensuring BMP antagonists to be repressed, consequently resulting in repression of osteogenesis [294, 298].

5.7 Discussion

An understanding of developmental events is key in order to utilise HFBCs for therapeutic bone repair approaches in the future. Previous studies on human foetal tissues reported a decrease in DNA methylation in genes implicated in tissue development and an increase in development associated genes between weeks 9 - 22 [399, 400]. A DNA methylation atlas covering 21 human foetal organs provides a unique overview of DNA methylation patterns during foetal development in various foetal tissues [400]. However, bone or cartilage tissue were, surprisingly, not included in this analysis.

HPLC-ESI-MS/MS-SRM was used to analyse 5mC levels on a global scale in HFBCs isolated from 7.5 – 11 wpc human foetal femurs and later in a larger sample cohort (7 – 17 wpc). Conversely, the overall low percentage in global DNA methylation in the larger sample cohort (7 – 17 wpc) differed from the 7.5 – 11 wpc cohort. In the literature, global DNA methylation levels were reported ~80% at the blastocyst stage due to the fact of only a small subset of genes being required at this developmental stage [377]. Later on in development, transcription of tissue-specific genes becomes necessary, thus, requiring demethylation prior to transcription. However, this demethylation would only occur in the genes required for the formation of the respective tissue and would unlikely result in a significant change in global DNA methylation. The findings in the 7 – 17 wpc cohort showed almost no differences in DNA methylation with age possibly due to only very few additional genes required. It is possible that the chosen technique to analyse global DNA methylation is not sensitive enough to deliver reliable results when lower DNA concentrations are used, possibly due to the reduced responsiveness of the detector. Therefore, in the future, the use of higher DNA concentrations (~500ng) would be recommended in order to provide an accurate overview of global DNA methylation in HFBCs isolated from human foetal femurs during early human foetal development. A further disadvantage of the chosen HPLC-ESI-MS/MS-SRM method is that only measurements of 5mC or 5-hydroxymethyl cytosine percentages can be acquired, however, no additional follow-up investigation of genes affected by DNA methylation by bioinformatics is possible.

Little change was observed in global DNA methylation suggesting that DNA methylation changes during human foetal femur development occured rather on specific genes required for the formation of the specific tissue. However, higher n-number of HFBCs isolated from human foetal femur for each developmental week was reasoned to having been beneficial in

aiding a clearer outcome of the global DNA methylation status in HFBCs. Thus, the low n-number of human foetal femurs for each developmental week (n = 1 or n = 2) is regarded as the greatest limitation in this study. However, the extent of DNA methylation changes in individual genes was supposedly not reflected in global DNA methylation changes. Hence, DNA methylation levels in genes implicated in skeletal development were investigated. More specifically in promoters of those genes as changes in DNA methylation levels in the promoter regions were reported before [332] and the CpG content being higher.

Bisulfite pyrosequencing analysis was used to investigate the DNA methylation status in the gene promoter regions. The pyrosequencing assay primers used here were designed and tested as in previous studies [332, 333]. However, the recommended number of cycles and melting temperature still required optimisation for HFBCs. *COL9A1* pyrosequencing primer Py2 did not deliver any results, possibly due to lack of specificity of the primers.

Increase in *COL9A1* expression correlated with observed loss in DNA methylation in three of the four analysed CpG sites. Significant DNA demethylation in reported SOX/Sry-binding sites at CpG sites 632 and 614 upstream of TSS [401] was observed. Although no significant decrease in CpG sites 95 and 49 upstream of TSS was found overall DNA methylation levels in these CpG sites were observed to be lower compared to overall DNA methylation levels in CpG sites 632 and 614 upstream of TSS. These findings correlated with previous studies [43, 332], reporting the predominant presence of chondrogenic cells within the human foetal femur evidenced by histology of human foetal femurs and the molecular characterisation of HFBCs (chapter 4). The observed overall lower methylation in CpG sites 95 and 49 upstream of TSS compared to CpGs 632 and 614 upstream of TSS could be due to the close proximity of these CpGs to TSS. The significant correlation between *COL9A1* expression and DNA demethylation in CpG sites 632, 614 and 95 upstream of TSS illustrates the regulatory function of DNA methylation in HFBCs.

The distal promoter *RUNX2* P1 was reported to be expressed in osseous as well as mature chondrocytes [196, 402]. As the femur is composed of different types of chondrocytes during early foetal development, with ossification centres being visible at 16 wpc [356], observed unchanged *RUNX*2 mRNA expression is consistent with this developmental process. CpG 720 upstream of TSS demonstrated significant reduction in DNA methylation with 5mC levels varying in CpG sites 686, 336 upstream of TSS and CpG 17 downstream of TSS.

With ongoing development, osteoblasts invading through the blood vessels from the surrounding perichondrium are incorporated into the organic matrix consisting of dense parallel and orthogonal collagen layers. OCN is secreted by osteoblasts invading the

cartilage model with the ingrowing blood vessels and by binding to of calcium, OCN is anchored to hydroxyapatite crystals embedded in the collagen mesh of the bone matrix [403, 404]. Elevated levels of this protein have been correlated with increased bone turnover. OCN along with osteopontin (OPN) are secreted during the late phase of the mineralisation process and control bone mass, mineral size and coordination of matrix-mineral-cell interactions [405]. *OCN* transcription is under the direct control of the 1,25-$(OH)_2$-vitamin D_3. The vitamin D3 response element (VDRE) is located within the human *OCN* promoter between 510 and 483 bp upstream of TSS [406, 407]. This locus is flanked by five CpG sites at the distal and proximal end upstream of TSS. Although demethylation in analysed CpG sites was observed, no correlation with gene expression was observed. *OCN* expression did not show a significant change with foetal femur age. However, it is possible that the observed decrease in DNA demethylation holds a regulatory function on gene expression with a potentially delayed effect. It remains unclear to what extent maintenance DNMTs and *de novo* DNMTs were involved in the observed DNA demethylation in *COL9A1* and *OCN* promoter CpG sites as only n = 1 or n = 2 for each developmental age was used. *DNMT1* is reportedly responsible for the addition of a methyl group after DNA replication whereas *de novo* DNMTs (*DNMT3A*, *DNMT3B*) attach the methyl group to unmethylated CpGs [242, 243]. TET enyzmes are responsible for removing methyl groups from CpGs [242, 243]. It is possible that TET enzymes have removed methyl groups from CpGs in analysed genes in order to allow expression of the respective gene essential during bone development while *de novo* DNMTs added a methyl group to CpGs in genes not or no longer required during skeletal development.

MiRNAs are a second epigenetic regulatory mechanism involved in the post-transcriptional regulation of different processes during differentiation and human development. By degradation of the target mRNA of positive/negative regulators of osteogenesis or chondrogenesis, miRNAs contribute to cell fate decision. Epiphyseal and diaphyseal cells isolated from human foetal femurs were observed to display a distinct pattern of gene expression characteristic for each region of the femur (osteogenic genes upregulated in diaphysis and chondrogenic genes upregulate in epiphysis) [307]. The use of HFBCs isolated from the whole human foetal femur resulted in a mixed population of epiphyseal and diaphyseal cells. Human foetal femurs reportedly consist predominatly of different types of chondrocytes and, with ongoing development, were reasoned to slowly become mineralised [43, 332].

MiRNAs targeting inhbitors of chondrogenesis were expected to be higher expressed in HFBCs isolated from human foetal femurs, thus promoting chondrogenesis. MiRNAs targeting positive regulators of chondrogenesis were expected to become increasingly expressed in HFBCs isolated from human foetal femurs with ongoing age.

miR-140-3p was expected to be upregulated during chondrogenesis, in turn promoting chondrogenic differentiation. This suggests that the target of this miRNA (although unknown) is potentially a positive regulator of osteogenesis which in turn is degarded by upregulation of miR-140-3p [317, 318]. MiR-146a reportedly acts by targeting SMAD2,3 in the TGFβ-pathway [307]. During chondrogenic differentiation, miR-146a was expected to be downregulated resulting in the derepression of SMAD2,3 and subsequently in the increase in SOX9, the key regulator of chondrogenesis, expression and chondrogenic differentiation [307]. Low expression of miR-146b reportedly resulted in upregulation of SOX5 and in turn SOX9, thus resulting in chondrogenic differentiation by binding of SOX9 to ACAN enhancer and enhanced COL2A1 expression [323, 324]. MiR-34a was found to be upregulated during osteogenesis, however, reportedly acts in a negative manner on osteogenic differentiation [302]. Therefore, miR-34a levels were expected to be decreased during chondrogenic differentiation and expression was only expected in presence of osteogenesis.

miR-138, targeting focal adhesion kinase (FAK), was reported to be downregulated during osteogenesis, resulting in expression of FAK which in turn results in the activation of genes associated with osteogenesis [305]. miR-138 is regarded as a negative regulator of osteogenesis, thus increased expression levels of miR-138 would indicate chondrogenic differentiation. MiR-23a is part of a miRNA cluster (miR-23a/27a/24-2) targeting *RUNX2*, *SATB2* (a binding partner to RUNX2) as well as LRP5 [299, 301]. MiR-23a indirectly regulates the osteogenic master regulator RUNX2 by targeting a binding factor SATB2. Increased miR-23a expression (expected during chondrogenic differentiation) would result in decreased expression of SATB2, in turn repressing RUNX2, and decreased expression of LPR5, in turn repressing WNT signalling. During chondrogenic differentiation, miR-20b was expected to be decreased, resulting in repression of BMP anatagonists [294], thus repressing osteogenesis. MiR-29a, 148b and let7f are involved in regulation of the WNT-pathway [295, 301, 308, 309]. miR-29a targets WNT inhibitor Dkk1 resulting in stimulation of the WNT pathway when miR-29a is expressed. let7f targets Axin2, an essential component of the degradation complex for β-catenin, which in turn results in the inhibition of the WNT pathway when let7f in decreased. The target of miR-148b is WNT1 which in

turn results in the negative regulation of the WNT pathway and osteogenesis when miR-148b is expressed [300, 301, 308, 309]. MiRNAs associated with the regulation of chondrogenesis (miR-140-3p, 146a, 146b, 34a) did not show significant increase or decrease in HFBCs with increasing age of human foetal femurs. Of analysed miRNAs associated with osteogenesis (miR-138, 20b, 23a, 148b, 29a, let7f) only miR-20b demonstrated a significant decrease in expression with increasing age of human foetal femurs. The observed decrease in miR-20b expression with age, therefore, suggested increase in chondrogenic differentiation. This finding corresponds with the observed increase in chondrogenic gene expression (*COL9A1* and *ACAN*) with increasing human foetal femur age. The limitation of this study is the low n-number (n = 1 or n = 2 for each developmental week) which in combination with the complex regulatory function of miRNAs hindered the identification of clear results regarding the regulatory function of miRNAs in HFBCs isolated from human foetal femurs during development.

HFBCs isolated from 8 wpc human foetal femurs were shown to possess enhanced osteogenic potential during *in vitro* osteogenic differentiation compared to HFBCs isolated from 14 wpc human foetal femurs (see sections 4.3.4 and 4.3.5). Gathered data from these differentiations also suggested that supplementation of standard osteogenic differentiation medium (oBG) with small molecules TH and SAG resulted in better osteogenic differentiation outcome after 19 days. MiR-138 is regarded as a negative regulator of osteogenesis and acts by repression of focal adhesion kinase which in turn results in the blockage of osteogenesis [305]. MiR-138 was overall low expressed in both osteogenic media conditions in HFBCs isolated from 8 wpc human foetal femurs. This suggests the presence of osteogenesis as the repression of miR-138 reportedly results in the upregulation of FAK, in turn activating osteogenesis related genes. . miR-20b as well as miR-148b also demonstrated decreased expression levels in the tested osteogenic media conditions relative to day 0 in HFBCs isolated from 8 wpc human foetal femurs. miR-20b repression results in the derepression of BMP anatagonists, in turn, impairing osteogenesis [294, 301]. MiR-148b repression results in increased expression of WNT1, a component of the WNT pathway, thus contributing to increases osteogenesis [308, 309]. HFBCs isolated from 14 wpc human foetal femurs demonstrated similar decrease in miR-20b expression in the two tested osteogenic conditions after 19 days under oBG + TH + SAG conditions. These findings suggest the regulatory effect and interaction of miRNAs on osteogenesis as decrease of miR-138 and miR-148b resulted in upregulation of osteogenesis while decrease of miR-20b resulted in repression of osteogenesis

Due to the supposedly unsuccessful generation of mature NIBSC-8 MSCs after culture on TCP the outcome of the osteogenic differentiation of NIBSC-8 MSCs is unclear. *ALPL* was observed to be upregulated in oBG + TH +SAG after 19 days compared to day 0, *COL1A1* demonstrated upregulation in oBG after 7 days compared to day 0 and *ACAN* expression was increased in oBG + TH + SAG after 7 days compared to day 0. Overall faint histological staining (ALP, Alcian Blue, Alizarin Red) indicated either unsuccessful or very low extent of osteogenic differentiation. Based on this unclear outcome of osteogenic differentiation of NIBSC-8 MSCs, the insignificant outcome of miRNA analysis at day 0 and aday 19 of osteogenic differentiation of NIBSC-8 MSCs can be expected. Only miR-20b demonstrated significant downregulation in all tested osteogenic conditions after 19 days of differentiation compared to day 0. Additionally, the low expression of miR-20b and the associated negative effect on osteogenic differentiation could be an additional indication for the unsuccessfulness of the osteogenic differentiation of NIBSC-8 MSCs.

MiRNAs interact with each other in order to provide the required regulatory function by targeting either inhibitors or activators of a gene or a pathway. This makes it difficult to dissect the influence of one miRNA expression on mRNA expression and which miRNAs are key in gene regulation. Upregulation of positive control for chondrogenesis (miR-140-3p) reportedly stimulates chondrogenesis [317, 318]. The low expression of miR-140-3p in the tested osteogenic media in all tested cell types could be an indication for a low extent of chondrogenesis. The negative control for osteogenesis (miR-138) acts by repression of FAK which in turn results in the blockage of osteogenesis [305]. The overall observed low expression of miR-138 in all tested cell types in both tested media might be an indication for the activity of osteogenesis. However, a clear indication of the reported regulatory function of miRNAs is not possible due to only a small number of the tested miRNAs being significantly expressed and possibly due to the low n-number for each developmental week. Inclusion of several more human foetal femur samples at each developmental week would potentially allow the identification of a regulatory interaction of miRNAs and effect on mRNA expression. A major limitation of miRNA analysis of osteogenic differentiations in this chapter is that miRNA expression levels at only one timepoint (day 19) was analysed and compared to day 0. The analysis of only one time point during osteogenic differentiation with different signalling pathways involved at different timepoints provided only a ‘snapshot’ of miRNA expression at one specific point during the differentiation process. Analysis of more timepoints during the osteogenic differentiation would have enabled the investigation of a potential regulatory effect during the differentiation process.

Conclusion

Global DNA methylation as well as DNA methylation in promoters of genes implicated in skeletal development were investigated in HFBCs isolated from 7 - 17 wpc human foetal femurs, thus providing for the first time an overview of DNA methylation in human foetal femure development covering the first two trimesters.

Major DNA demethylation in the *COL9A1* promoter was found to correspond with increased gene expression with ongoing development, thus demonstrating the regulatory function of DNA methylation on gene expression. Decrease in several CpG sites within the *OCN* promoter was observed, with a potential delay in effect on gene expression. In the future, the availability of a DNA methylation atlas covering the whole genome of HFBCs isolated from human foetal femurs from different developmental stages might be of advantage to investigate early foetal development more in-depth.

The regulatory function of miRNAs during femur developmet and osteogenic differentiation could not be clearly demonstrated as only one of the analysed miRNAs (miR-20b) demonstrated significant expression in HFBCs with increasing human foetal femur age which is most likely due to the low n-number (n = 1 or n = 2) of human foetal femurs for each developmental week. miRNAs during osteogenic differentiation were only analysed for one time point during differentiation (day 19) and compared to day 0. Therefore the regulatory role during osteogenic differentiation could not be shown clearly as miRNA expression at the end point of the osteogenic differentiation (day 19) was analysed but not at an earlier time point (day 7). MiRNAs might have been differently expressed at day 7 due to the different activity of signalling pathways at this time point compared to miRNA expression at day 19.

Chapter 6 Discussion and Future Studies

The combination of higher life expectancy and an increase in population dynamics has resulted in an increased frequency of age related diseases, representing a growing socio-economic burden for healthcare systems and in turn, the need for improved treatments for the repair/replacement of tissue for age related degenerative diseases (e.g. OP, OA) [1, 2]. Stem cell based therapies to promote bone fracture healing offer a promising approach to address the above mentioned clinical issues. Nonetheless, the most significant limitation of SSCs in clinical application still remains the paucity of this cell population as well as the decrease in number and functionality/potency with age and in age related diseases [18-20].

SSCs/MSCs are poorly defined by fibroblast-like plastic adherent growth, a panel of non-specific surface markers and the ability to form bone, cartilage and fat [77]. However, a surface marker combination ($PDPN^+$, $CD73^+$, $CD164^+$, $CD146^-$) characteristic for SSCs has recently been identified [64]. In addition, application of SSCs is patient-specific. Thus, there is a need for a cell population that is applicable to more patients, demonstrates high levels of proliferation and differentiation along the osteogenic, chondrogenic and adipogenic lineage and, ideally, is available in large numbers. Foetal-derived cells demonstrate enhanced proliferation capacity and yet, the cell number accessible for tissue repair is still limited. The generation of iPSC-MSCs has been demonstrated and heralded as a promising and efficient approach to supply an almost unlimited pool of generated cells, which, importantly, are under no ethical restrictions as the case for primary foetal cell sources.

The original proposal for this project hypothesised that iPSC-MSCs are comparable in phenotype, molecular and epigenetic identity to HFBCs isolated from human foetal femurs. In collaboration with James Adjaye's research group at Heinrich Heine University in Dusseldorf, Germany, a multidisciplinary strategy encompassing DNA methylation profiling and microRNA profiling, as well as skeletal tissue formation and differentiation *in vitro*, *ex vivo* and *in vivo* was outlined for this thesis.

As shown in **chapter 3**, the generation of iPSC-MSC in Southampton using the same published protocol as our collaboration partners in Dusseldorf [182] was not successful on a standardised control line obtained from the National Institute of Biological Standards and Control (NIBSC) in the UK. Culture in SB431542 supplemented differentiation medium for 10 days resulted in a shift in cell morphology from tightly packed iPSC colonies toward a

monolayer with areas of elongated cells. Positive markers for EMT, N-Cadherin (*CDH2*) and vimentin (*VIM*) were increased, yet not in all passages on TCP (at MP1- MP6 for *CDH2*; MP3 for *VIM*) while the negative marker for EMT, E-Cadherin (*CDH1*), was decreased in all passages on TCP. The subsequent culture on TCP aimed at aiding the maturation and expansion of iPSC-MSCs. However, iPSC-MSCs demonstrated a decrease in proliferation between passages 1 – 6 and cell morphology demonstrated wide spread cells rather than elongated fibroblast-like cells. Therefore, it appears that the process of EMT is successfully induced during 10 days of culture in SB431542 supplemented medium but that the prolonged culture on TCP for maturation has hampered the successful generation of NIBSC-8 MSCs. Osteogenic differentiation of NIBSC-8 MSCs was not effective and did not result in mineralised nodules.

Critically, this work showed that the applied iPSC-MSC generation protocol was not successful. Instead the application of a differentiation protocol for iPSC-MSCs already being tested in clinical trials [179] would be advisable in order to ensure the successful generation of an iPSC-MSCs population use for bone formation *in vitro*. The investigation of the original hypothesis was modified given: i) the iPSC-MSCs derived from HFBCs (55 days post conception, dpc), previously derived by our collaboration partners in Dusseldorf did not show the morphology or proliferative capacity demonstrated by HFBCs and as described in [408], ii) competitive interests from our collaboration partners in Dusseldorf due to the submission of a manuscript comparing iPSCs to iPSC-MSCs [408] and, iii) generation of iPSC-MSCs in Southampton using the same differentiation protocol as in [408] was unsuccessful when tested in two iPSC lines (as shown in chapter 3 and Appendix F). MSCs was more Therefore, this thesis therefore examined the characteristics of HFBCs in order to provide a basis for further future comparison with iPSC-MSCs.

As shown in **chapter 4,** HFBCs were isolated from 7 – 17 wpc human foetal femurs, a rare and unique sample cohort, and characterised for cell morphology, proliferation, gene expression, DNA methylation and miRNA profiling. Histological staining showed the transition from a cartilage template at 8 wpc towards mineralisation of the proteoglycan matrix by 17 wpc. Chondrogenic genes *COL9A1* and *ACAN* were found to be significantly upregulated with increasing developmental age. Osteogenic genes did neither show an increase or decrease in HFBCs isolated from 7 – 17 wpc human foetal femurs, indicating that HFBCs isolated from 7 -17 wpc human foetal femurs represented a rather cartilaginous phenotype with different types of chondrocytes present as previously reported [62].

Supplementation of standard osteogenic medium (Dex, A2P and β-GP) with small molecules or other additives has become more common in recent years (see Table 1.9 and Table 1.10 in section 1.6.2). In **chapters 4**, the comparison of oBG with oBG + TH + SAG tested on HFBCs isolated from 8 and 14 wpc human foetal femurs showed an advantage of oBG + TH + SAG on both tested cell types with HFBCs isolated from 8 wpc human foetal femurs demonstrating a slight advantage during osteogenic differentiation. Publications using TH as supplementation of standard osteogenic differentiation medium showed increased *ALPL* expression compared to standard osteogenic differentiation medium alone [183, 216]. Evidence suggests the mechanism of action of TH could be by targeting the BMP2/SMAD-signalling pathway [216]. The addition of BMP2 to the TH and SAG supplemented osteogenic background medium would most likely have improved the efficiency of the osteogenic differentiation further, as previously demonstrated [216]. However, the cost of BMP2 and the required concentration of BMP2 do not aid the finding of a cost-effective small molecule supplemented osteogenic differentiation medium. Mineralised nodules were not detected in either osteogenic medium condition examined in any of the differentiation experiments. This observation is most likely due to a lack of sufficient phosphate supply. In the standard osteogenic medium, β-GP serves as external phosphate source in addition to the low concentration of phosphate in the basal medium. The impact of the source of phosphate (inorganic or organic) and, the concentration in the differentiation medium, was shown to be crucial on gene expression in composition of the mineral [409]. The use of inorganic phosphate sources could replace β-GP (hydrolysable substitute of inorganic phosphate) given the non-physiological fluctuations in the availability of free phosphate caused by β-GP and the hydrolysation of β-GP under cell free conditions [409]. Vitamin D_3 has been shown to enhance osteogenic differentiation and to increase osteogenic gene expression [202, 410]. β-GP has been a component of all differentiation media containing vitamin D3, thus replacement of β-GP would require an alternative phosphate source for mineralisation to take place. Calcium phosphate ceramics (CaPs) such as tricalcium phosphate, hydroxyapatite and biphasic calcium phosphates could serves as phosphate source [411].

As shown in **chapter 5**, DNA methylation showed a moderate decrease in HFBCs between 7 and 17 wpc at a global level at passage 1. In depth analysis of DNA methylation in gene promoters of *RUNX2*, *OCN* and *COL9A1* demonstrated significant demethylation in proximal *COL9A1* and *OCN* promoters, correlating with significantly increased gene

expression. Therefore, the regulatory function of DNA methylation has been demonstrated for *COL9A1*. HFBCs isolated from 8 – 11 wpc human foetal femurs, covering the first trimester of pregnancy, were analysed for gene expression and DNA methylation by de Andres et al. before [332]. Slieker et al. used different types of tissues with an age range from 9 – 22 wpc, however, only investigated DNA methylation using a 450k array, however, neither bone nor cartilage was included [399]. Transcriptome and methylome analysis, although expensive, offer significant advantages enabling in depth characterisation of HFBCs and iPSC-MSCs. These techniques would allow to investigate the regulatory function of DNA methylation during osteogenesis/foetal femur development further.

A review of the results from **chapters 4 and 5** and comparison with available literature provides an overview of key events of endochondral ossification during early human foetal development at the cellular, molecular and epigenetic level (Figure 6.1). Paternal DNA becomes demethylated more rapidly compared to the maternal genome and DNA methylation is lowest in the pre-blastocyst [377, 394], followed by a rapid increase in DNA methylation in the post-implantation blastocyst [394, 412]. Endochondral bone formation begins with condensation of MSCs in the limb bud (~ week 4) in parallel with increased cell proliferation. With outgrowth of the limb bud, the mesenchymal cells in the centre form hyaline cartilage, providing a template for the future bone. With ongoing development, chondrocytes in the diaphysis become hypertrophic and eventually undergo apoptosis, forming the template for future trabecular bone. At the same time, a bone collar (perichondrium) forms around the diaphysis and elongates toward the epiphyses. Blood vessels invading the femur through the bone collar at the diaphysis transport MSCs and osteoblasts into the diaphysis, thus giving rise to the primary ossification centre. The osteoblasts begin to mineralise the ECM. Secondary ossification centres at both epiphyses become visible around week 16 [41, 356]. With onset of formation of the bone collar and later mineralisation, expression of osteogenic genes become necessary.

DNA methylation levels at the blastocyst stage were reported before as ~80 % [377, 394]. As shown in chapter 5, *COL9A1* and *OCN* promoter DNA methylation reduced from ~80 % to ~20 % in HFBCs isolated from human foetal femurs between 7 and 17 wpc.

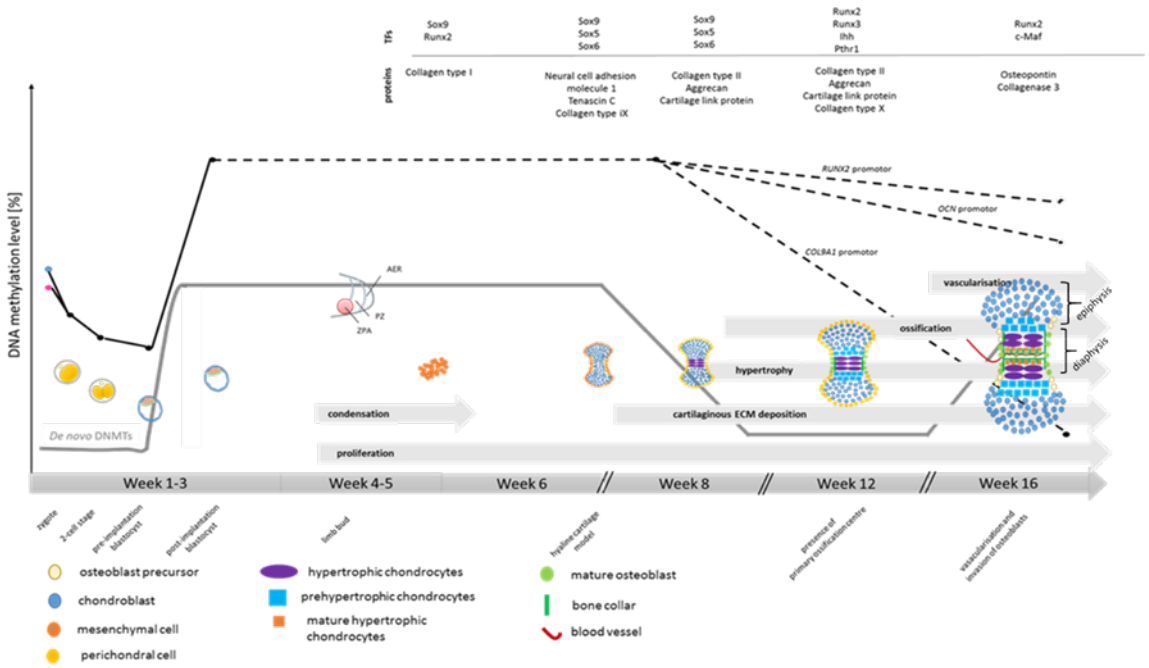

Figure 6.1 Schematic time line of long bone development during early human foetal development. Human development is divided into embryonic (until week 8) and foetal period (week 9 until birth). DNA is rapidly demethylated until the pre-implantation blastocyst stage. Rapid *de novo* DNA methylation occurs post-implantation. Mesenchymal cells in the core of the limb bud (visible at week 4) show increased proliferation resulting in elongation and formation of fingers/toes. Proliferation of mesenchymal cells is accompanied by chondrification, resulting in a hyaline cartilage model at the end of week 6. Endochondral ossification starts at week 8, with peripheral cells surrounding the hyaline cartilage model differentiating into cells of the perichondrium (expressing type I collagen), while cells in the centre (the future primary ossification centre, diaphysis) secrete extracellular matrix (ECM) proteins, e.g. type II, IX, XI collagens and aggrecan. With ongoing development, chondrocytes in the diaphysis increase in size (a process referred to as hypertrophy), expressing type X collagen. Hypertrophic chondrocytes eventually undergo apoptosis, creating cavities within the cartilaginous shaft. Bone length increases rapidly between weeks 8 – 12. Due to Indian hedgehog (IHH) signalling from hypertrophic chondrocytes, the perichondrium is transformed into a bone collar. Osteoblasts from the bone collar are transported into the centre by ingrowing blood vessels, ultimately resulting in the mineralisation of the matrix and formation of woven bone. Adapted from [41, 43, 243, 356, 377, 378, 394].

Future studies

Future work could utilise the characterisation of HFBCs isolated from 7 – 17 wpc human foetal femurs from this study as a comparison control to iPSC-MSCs. Comparison of global DNA methylation in iPSC-MSCs with respective iPSCs and primary donor cells (HFBCs, 55 dpc) demonstrated higher DNA methylation in iPSC-MSCs at a global level compared to the primary donor cells, yet, DNA methylation was lower compared to iPSCs (see Appendix I). HFBCs are a heterogenous cell population, therefore the characterisation of HFBCs using the recently identified surface marker combination $PDPN^{+}$, $CD73^{+}$, $CD164^{+}$, $CD146^{-}$ could aid in the identification of an epigenetic profile which could be used in addition to the above mentioned surface marker combination to identifiy iPSC-MSCs resembling a foetal SSCs phenotype capable of giving rise to bone and cartilage tissue. Published work [339] has shown that iPSCs generated from MSCs isolated from the bone marrow of elderly patients (mean age 56 years) i) maintained donor-specific epigenetic differences in DNA methylation profiles and further maintenance in iPSC-MSCs, ii) tissue-specific differences were erased during reprogramming and not re-established in iPSC-MSCs and, iii) age-related DNA methylation profiles remained reset in iPSC-MSCs [339]. These findings were the first evidence illustrating the foetal phenotype of iPSC-MSCs.

The use of DNA methylation patterns could aid in the classification of iPSC-MSCs. Two sets of CpG sites were identified by de Almeida and colleagues, using pyrosequencing, providing a clear characterisation of MSCs and fibroblasts (referred to as Epi-MSC-Score) and, distinguishing tissue of origin of analysed MSCs (referred to as Epi-Tissue-Score) [413], use of more CpG sites would improve classification. Techniques such as proteomics or transcriptomics are costly and require subsequent complex computational analysis. However, these techniques would be of advantage for depth characterisation of iPSC-MSCs. The advantages of DNA methylation profiling are: i) DNA methylation patterns are relatively stable compared to e.g. gene expression or proteins, ii) the profiling is quantitative, and iii) DNA methylation is directly coupled to cellular differentiation [413]. In order to utilise the finding of the Epi-MSC-Score, HFBCs isolated from 7 – 17 wpc human foetal femurs as well as HBMCs from aged donors need to be screened for DNA methylation levels at the two CpG sites and, compared to the DNA methylation pattern at these CpGs in iPSC-MSC. This direct comparison with a limited number of CpG sites could provide information on: i) if iPSC-MSCs are fibroblasts or not, and ii) if the DNA

methylation in the analysed CpGs resembles either the profile of HMBCs from aged donors or HFBCs isolated from 7 – 17 wpc human foetal femurs.

Characterisation of HBMSCs isolated from elderly patients using the same assays as for the characterisation of HFBCs would enable this cell source to be used as negative control for iPSC-MSCs, given it has been shown that iPSC-MSCs undergo rejuvenation [339]. Several differentiation protocols for the generation of iPSC-MSCs have been published (see Table 1.7 in chapter 1.5). However, it would be advisable to choose a method and protocol that is already tested in clinical trials, or at least in animal models, in order to ensure that the generated iPSC-MSCs are functional and, in addition, perform proliferation assays, DNA methylation profiling using pyrosequencing on the two sets of CpG sites identified in [179]. However, caution is recommended in the comparison of iPSC-MSCs to the Epi-MSC-Score as MSCs isolated from aged donors were used to identify a CpG set that distinguishes MSCs from fibroblasts. Despite the associated costs, it would be advisable to analyse the DNA methylation profiles of HFBCs and aged HBMSCs using, for example, an Illumina assay and, subsequently identify if the published Epi-MSC-Score occurs in the HBMSCs and the HFBC cell populations. The DNA methylation at the identified/confirmed CpG sites could then be verified by pyrosequencing.

Ultimately, iPSC-MSCs were shown to be more comparable to HFBCs than aged HBMCs [408]. Characterisation of HFBCs provided, for the first time, an overview of foetal bone development in the first and second trimester, demonstrating the regulatory function of DNA methylation on gene expression. The current work provides a base for the comparison of iPSC-MSCs to HFBCs isolated from 7 – 17 wpc human foetal femurs and offers new strategies in the identification of a cell population that could be of significant use in bone formation studies.

Chapter 7 Appendices

Appendix A High-Performance Liquid Chromatography Electrospray Ionization-Tandem Mass Spectrometry Selected Reaction Monitoring (HPLC-ESI-MS/MS-SRM)

A.1 Choosing the Right Method for DNA Methylation Profiling

The choice of a suitable method for DNA methylation analysis depends on the research question. Figure 7.1 illustrates different methods available to date and potential applications. In this research project, high-performance liquid chromatography electrospray ionization-tandem mass spectrometry selected reaction monitoring (HPLC-ESI-MS/MS-SRM) was used initially to analyse global methylation status of different undifferentiated cell types and, to test whether any changes in global methylation status occurred during the application of the differentiation protocols.

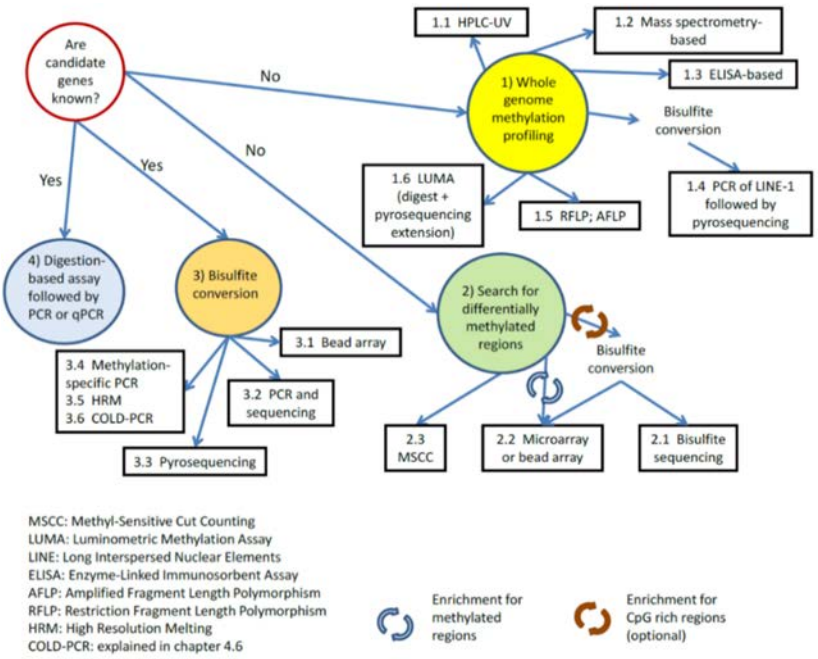

Figure 7.1 Schematic guide for choosing the most suitable method for DNA methylation profiling. Source: [317]

A.2 Principle of HPLC-ESI-MS/MS-SRM

DNA Degradase Plus™ (Figure 7.2) was used to digest DNA samples to their individual nucleotide components. Digested samples were then separated by reversed-phase chromatography using a hydrophobic stationary phase and an aqueous mobile phase. Separated samples were then accelerated by electrospray ionisation. Accelerated nucleotides were deflected by a magnet according to their specific mass and polarity; the heavier and less charged the less deflected. Electrons were detected as a current which was recorded and displayed as a stick diagram (Figure 1.3). Different nucleotides were distinguished by intensity of individual current → fragment ion transitions: 5mC 242.1 m/z → 126.1, C 228.1 m/z → 112.1 [331].

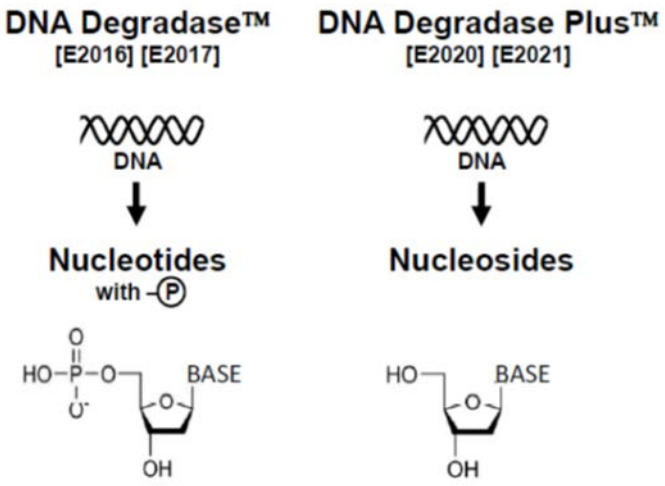

Figure 7.2 DNA Degradase™ and DNA Degradase Plus™ (Zymo Research, Cambridge, UK). Both enzymes efficiently degrade DNA into individual nucleotides. However, DNA Degradase Plus™ additionally cleaves off the phosphate group (PO_3^-) which is necessary for assessment by liquid chromatography/ mass spectrometry (LC/MS). DNA degraded with DNA Degradase™ can be analysed using high performance liquid chromatography (HPLC) but is not suited for analysis in LC/MS. Source: http://www.zymoresearch.com/protein/enzymes/dna-degradase (18052017).

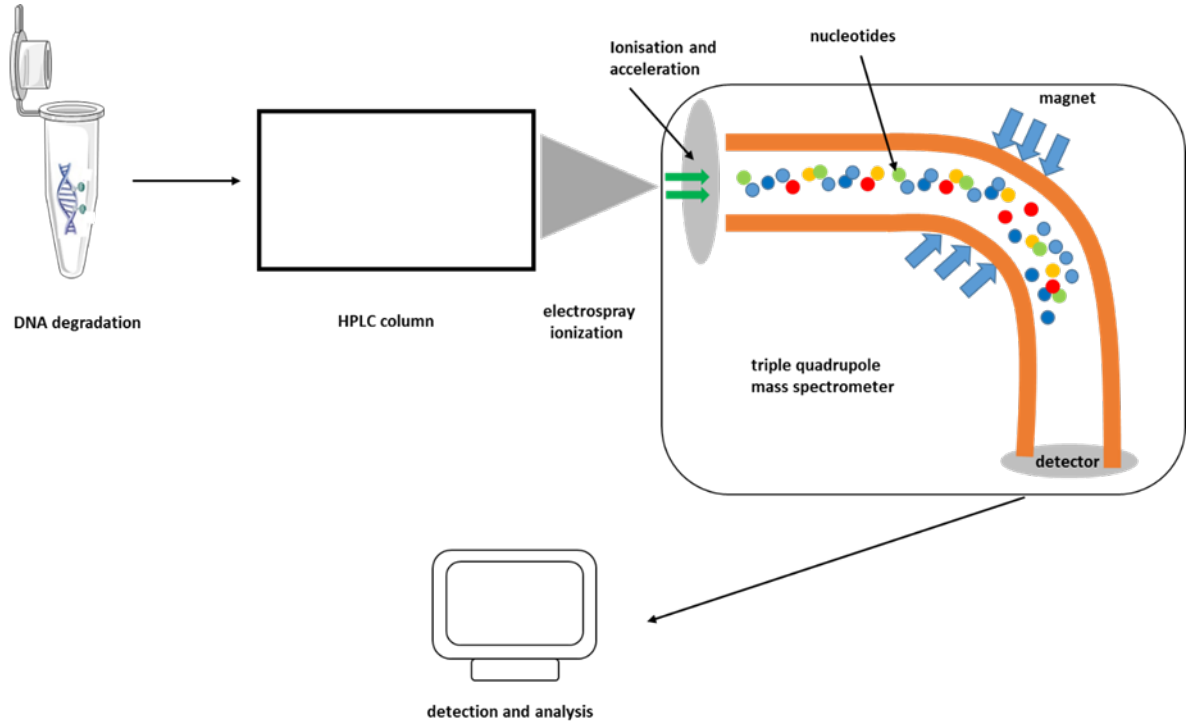

Figure 7.3 Schematic of the principle of high-performance liquid chromatography electrospray ionization-tandem mass spectrometry selected reaction monitoring (HPLC-ESI-MS/MS-SRM). Following digestion of DNA with DNA Degradase Plus™, sample is then separated by a HPLC column containing the sample as a mobile phase and a hydrophobic stationary phase. Nucleotides are then accelerated and deflected by a magnet according to their masses; the heavier the nucleotides are the less deflection. This range is detected and displayed as a stick diagram displaying relative current produced by nucleotides of varying mass/charge ratio.

A.3 Cytosine/5-Methylcytosine Standard Curve for DNA Methylation Profiling

1 µg of 5-methylcytosine (5mC) and 1 µg of cytosine (C) DNA standards (ZymoResearch, Cambridge Bioscience, UK, Cat. No. D5405-2, D5405-1) were digested with DNA Degradase Plus Kit (ZymoResearch, Cambridge Bioscience, UK, Cat. No. E2020) for 2 h at 37°C (Table 7.1). The enzymatic reaction was stopped with 175 µl 0.1 % formic acid (Sigma-Aldrich, Gillingham, UK, Cat. No. F6502). DNA standards were prepared as shown in Table 7.2.

Table 7.1 Composition of one reaction for digestion of DNA standards with DNA Degradase™ Plus Kit (ZymoResearch, Cambridge Bioscience, UK, Cat. No. E2020).

Component	Volume [µl] for one reaction
DNA (1 µg)	20
DNA Degradase™ Reaction Buffer 10x	2.5
DNA Degradase Plus™ (5 units/µl)	1
dH_2O	1.5
Total volume	25

Table 7.2 Preparation of DNA Degradase™ Plus Kit (ZymoResearch, Cambridge Bioscience, UK, Cat. No. E2020) digested cytosine (C) and 5-methylcytosine (5mC) standards for global DNA methylation profiling. Standard samples were comprised of an increasing amount of 5mC (0 – 10 %) and C (0 - 2 %).

% C	% 5mC	Volume C [µl]	Volume 5mC [µl]	1:10 5mC [µl]	1:100 5mC [µl]	0.1 % (w/v) Formic acid [µl]
100	0	20	0			20
99.5	05	19.9	0.1		10	10.1
99	1	19.8	0.2	2		18.2
95	5	19	1	10		11
90	10	18	2			20

Digested and prepared standards were separated using HPLC-ESI-MS/MS-SRM as previously described and, methylation quantified as ratio of 5mC to total cytosine content (5mC/5mC+C) [330, 331] (Figure 7.4).

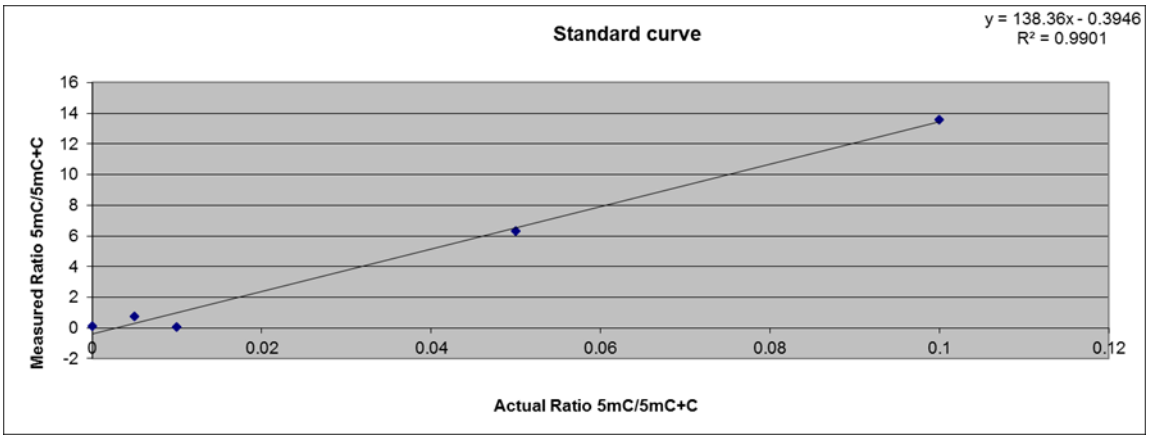

Figure 7.4 Standard curve for analysis of DNA methylation using HPLC-ESI-MS/MS-SRM. Standard samples were comprised of an increasing amount of 5mC (0 – 10 %) and C (0 - 2 %). Standard calibration curve was obtained by plotting obtained data of measured 5mC area to total C content (5mC/5mC+C) against actual percentage of 5mC/5mC+C.

Appendix B Measurement of RNA and DNA concentrations using a Nanodrop

Concentration of isolated RNA and gDNA was measured with a Nanodrop using software NanoDrop® ND 1000 V3.8.1 from Thermo Scientific (spectrometric method with a full spectrum (220 - 750 nm)). Nanodrop was blanked with 1 µl RNase-free dH_2O and 1 µl sample was loaded onto the lower pedestal and the upper pedestal closed. The nanodrop exploits the surface tension of the sample by forming a column, adjusting the pedestals for path length of 0.05 - 1 mm and light is directed through the sample column. Concentration (expressed in ng/µl) is automatically calculated from absorbance measurements and spectrum graph (Figure 7.5). Purity was measured by the 260 nm/280 nm ratio: a ratio of ~ 1.8 for DNA and ~ 2.0 for RNA are accepted as "pure" DNA or RNA. Organic contamination was measured by the 260 nm/230 nm ratio.

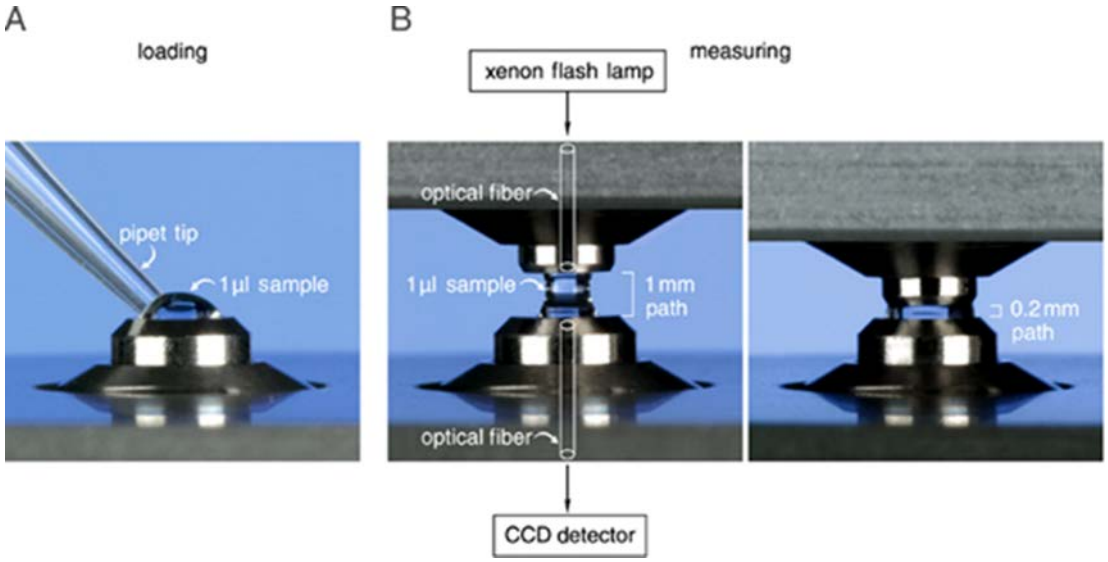

Figure 7.5 Principle of measurement of nucleic acid concentrations using NanoDrop® ND-1000 V3.8.1 from Thermo Scientfic. A: 1 µl RNA or DNA sample was loaded to the lower pedestal. **B:** Upper pedestal was closed and concentration was measured exploiting surface tension of sample. Source:http://www.news-medical.net/whitepaper/20141204/Comparison-of-DNA-Quantification-and-Characterization-Techniques.aspx

Appendix C Housekeeping Genes for HBMSCs, HFBCs and IPSCs

Consistent housekeeping gene expression is key for the reliable quantification of the expression of a gene of interest. Such reference genes are used as internal standards in quantitative gene expression analysis and, were considered to be uniformly expressed during developmental stages in various cell types. However, variation in expression of standard housekeeping genes was reported to vary in different cell types [414], therefore, ideal cell type specific housekeeping gene was first determined.

During quantitative real-time PCR (qRT-PCR), the cDNA sample is denaturated followed by annealing and subsequent extension of the primers to the two singe strands (one cycle). This amplification of the initial cDNA sample is monitored after each cycle. Fluorescence intensity of the amplified sample is too low to be detected during the first cycles (below baseline), but increases exponentially and results in a plateau phase at the end of the process as sample and reagent availability decreases. The threshold cycle (C_t value) indicates the number of cycles required to detect the amount of fluorescence above a set fluorescence threshold level. The threshold is generally set at the exponential phase and 0.2 was used for all performed qRT-PCR experiments in this study. A low C_t value indicates a high amount of the target template while high C_t values indicate a low amount of the amplified template. C_t values > 30 are considered to indicate minimal or even no gene expression. Figure 7.6 A illustrates the components of a typical qRT-PCR amplification curve and Figure 7.6 B shows the amplification plot of *RN18S* and its negative (H_2O) control in viPSCs.

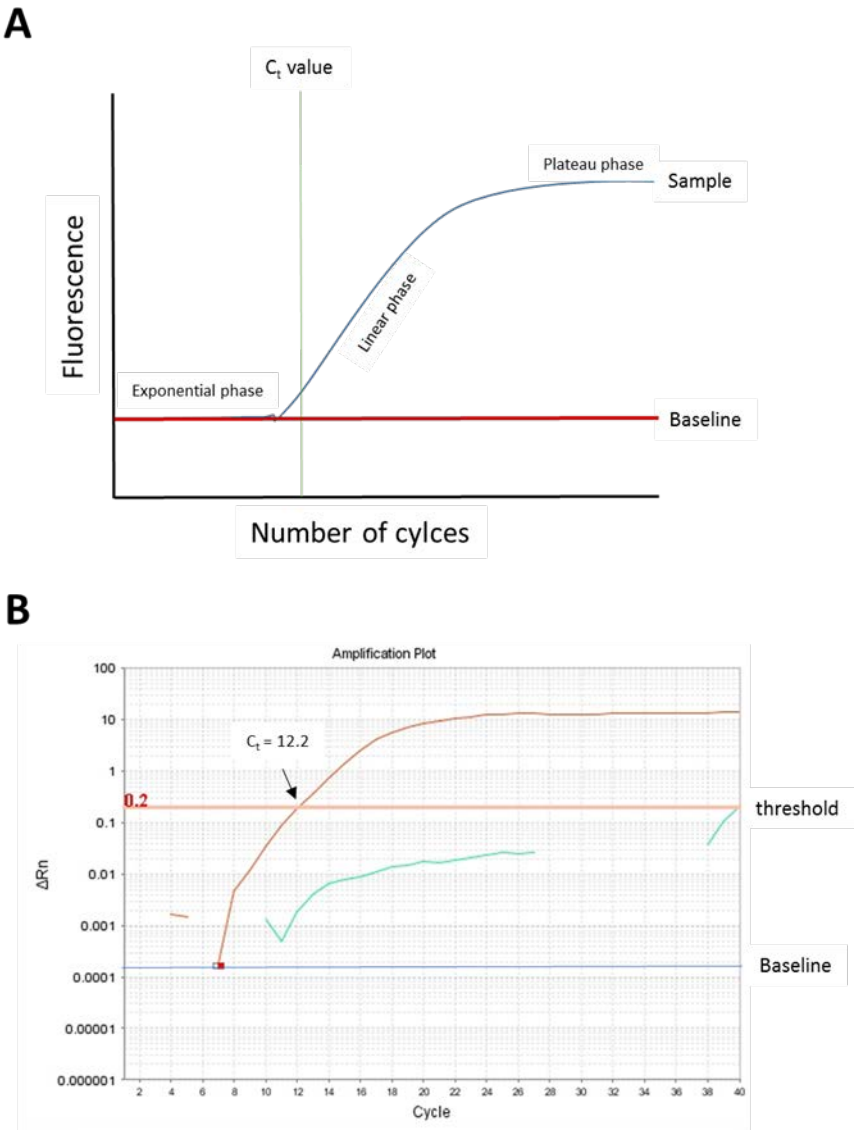

Figure 7.6 Amplification plot of cDNA sample using qRT-PCR. A: Schematic illustration of amplification curve. Reaction is comprised of three phases: i) exponential phase with sufficient amount of all required reagents, ii) linear phase with continuous amplification of sample, iii) plateau phase in which required reagents and template become more and more limited, creating high possibility of variation. **B:** Amplification plot for 18S ribosomal RNA (*RN18S*) for viPSCs (red) and negative control (H_2O, green) in an Applied Biosystems 7500 System SDS Software, version 2.0.5 programme. Baseline (blue) was automatically set by software while threshold (orange) was manually adjusted to 0.2.

The most suitable housekeeping gene for the individual cell types (primary HFBCs, aged primary HBMSCs and iPSCs) used in the performed experiments was validated by comparing the mean C_t values of the following reference genes: glyceraldehyde-3-phosphate dehydrogenase (*GAPDH*), β-actin (*ACTB*), TATA-box binding protein (*TBP*) and 18S ribosomal RNA (*RN18S1*) Figure 7.7.

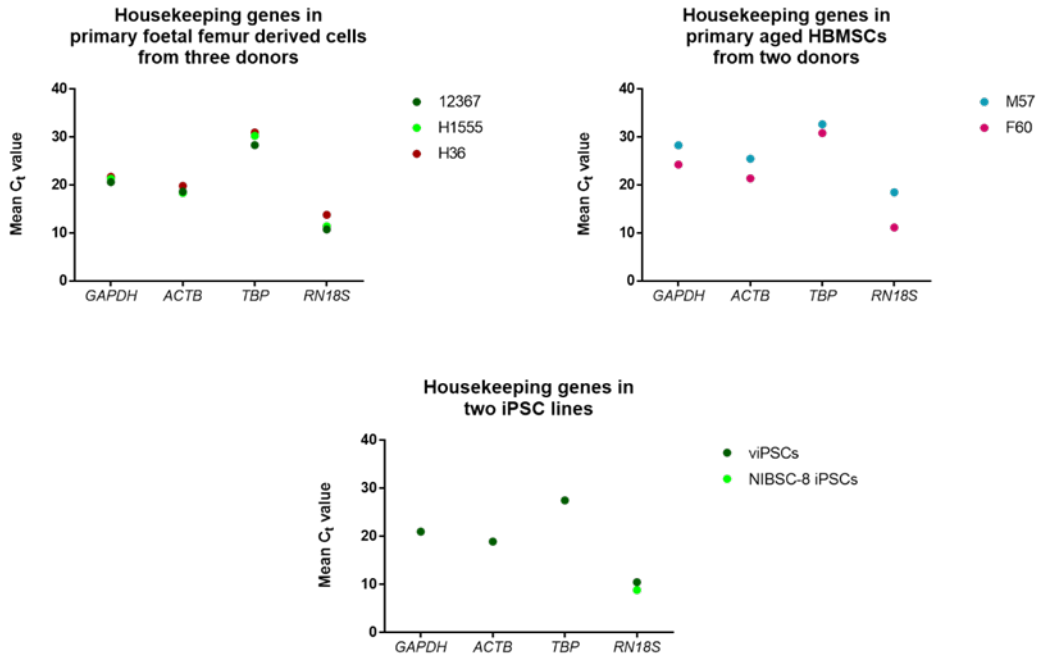

Figure 7.7 C_t values of housekeeping genes 3-phosphate dehydrogenase (*GAPDH*), β-actin (*ACTB*), TATA-box binding protein (*TBP*) and 18S ribosomal RNA (*RN18S*) in different cell types (primary HFBCs, primary aged HBMSCs, viPSCs, NIBSC-8 iPSCs). qRT-PCR was performed as previously described in triplicates using different undifferentiated cell types.

The mean C_t values of *TBP* were highest in the three tested cell types (~ 30 in HFBCs, HBMSCs and iPSCs), a value considered to represent minimal or no gene expression. Therefore, *TBP* was not considered as a suitable housekeeping gene for any of the performed experiments.

The analysed HBMSC samples from two patients in total showed slight variation in the mean C_t values of the tested housekeeping genes. *RN18S1* showed the greatest variation while *GAPDH* and *ACTB* varied to a similar extent. *ACTB* was chosen as standard housekeeping gene for all experiments with HBMSCs from aged donors due to the lower overall mean C_t values and, already published studies applying *ACTB* as housekeeping gene in HBMSCs from the Bone and Joint Research Group [415, 416].

In viPSCs and NIBSC-8 iPSCs, *RN18S* showed the lowest mean C_t values compared to other tested housekeeping genes. The cells to be analysed were undergoing large cellular and metabolic changes, therefore the use of *GADPH,* involved in the cell metabolism and *ACTB,* which is involved in changes in the cytoskeleton, were not viewed as favourable. Instead, *RN18S* was chosen as housekeeping gene as the expression of this gene proved reliably stable. Table 7.3 shows the Ct values for the individual experiments of the osteogenic

differentiation of HFBCs isolated from 14 wpc human foetal femurs as well as the mean Ct value.

Table 7.3 Ct values for housekeeping gene *RN18S* for HFBCs isolated from 14 wpc human foetal femurs during osteogenic differentiation. Exp: experiment; oBG: osteogenic background medium; SAG: smoothened agonist; TH: TH (4-(4-methoxyphenyl)pyrido[4′,3′:4,5]thieno[2,3-b]pyridine-2-carboxamide).

		Day 7			Day 19		
	D0	**basal**	**oBG**	**TH +SAG**	**basal**	**oBG**	**TH +SAG**
exp 1	8.8871259	8.9826192	8.8978481	8.6293220	8.1808271	8.2042760	7.65275717
	9.1180791	9.2499027	8.5568933	8.2289953	8.0016393	8.1792745	7.02597904
exp 2	8.1404676	8.8810195	8.8400011	7.9494810	8.4576206	8.4072198	8.1360178
	8.8647813	8.8045787	8.4304418	8.4715461	8.3969478	8.3356161	8.92201614
exp 3	9.3963022	8.9641332	8.2686882	8.4767055	8.3386755	9.1180791	9.24990273
	8.9453582	8.4968204	8.2648782	8.5849504	7.8179698	8.908909	9.34411049
mean Ct	**8.8920191**	**8.8965123**	**8.5431251**	**8.3901667**	**8.1989467**	**8.525562**	**8.38846389**

Appendix D Bisulfite Pyrosequencing

Pyrosequencing is based on the sequencing-by-synthesis approach as well as on the detection of released pyrophosphate during DNA synthesis [417-419]. Two different approaches have been identified to remove excess nucleotides: i) solid phase pyrosequencing and ii) liquid phase pyrosequencing. Using solid phase pyrosequencing, single stranded (ss) DNA strands with the biotin labelled sequencing primer can be immobilised onto magnetic streptavidin beads. DNA polymerase, ATP sulfurylase and luciferin are added to the magnetic beads with the primed ssDNA. Excess or unincorporated nucleotides are removed using washing steps [420]. During liquid-phase pyrosequencing, the enzyme apyrase is responsible for removing excess nucleotides after each reaction round [418, 421]. The addition of this enzyme eliminated the need for washing steps and reduced fluctuations in the sequencing procedure [418].

During DNA elongation, nucleotides are added to the reaction mix in a predefined order one after another. If a nucleotide is incorporated into the new DNA strand by DNA polymerase, pyrophosphate is released. ATP sulfurylase converts pyrophosphate into ATP using adensoine5’phosphosulfate (APS) as substrate. In turn, ATP catalyses the oxidation of luciferin to oxiluciferin, thus generating a light signal that is recorded as a peak in a

pyrogram. The light signal is proportional to the amount incorporated nucleotides. Apyrase removes all unincorporated nucleotides and enzymes at the end of the reaction or when no nucleotides were incorporated into the DNA strand. If no nucleotides are incorporated no pyrophosphate is generated, hence, no peak appears on pyrogram (Figure 7.8) [418]. Due to the bisulfite step proceeding the pyrosequencing, all methylated cytosines will be detected as C while unmethylated cytocines will be detected as thymine, allowing the distinction between methylated and unmethylated cytosines.

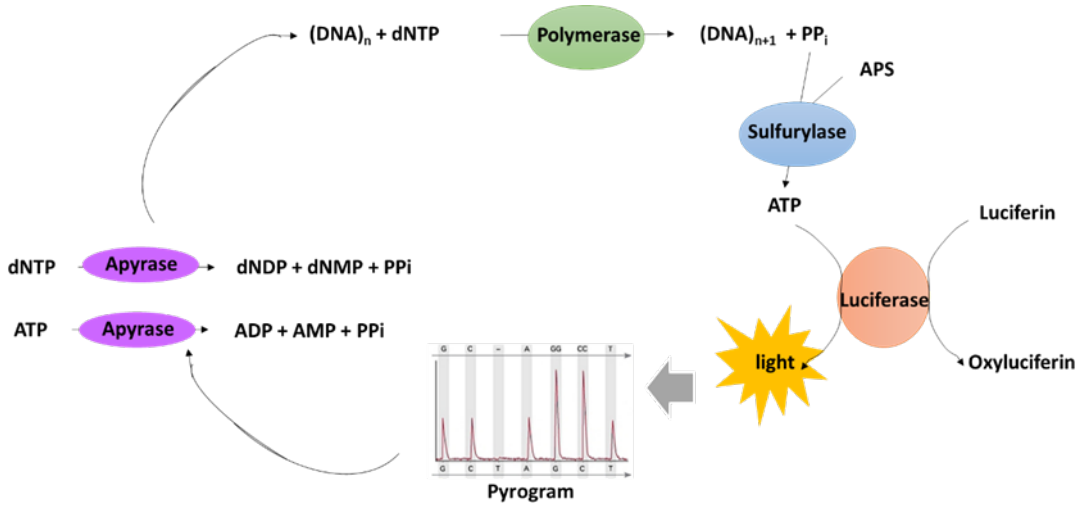

Figure 7.8 Principle of pyrosequencing. dNTPs: nucleotides; PPi: pyrophosphate; ATP: adenosinetrophosphate; ADP: adenosinediphophate; APS: adenosine 5′ phosphosulfate.

Appendix E Standard osteogenic medium composition testing

Aged primary HBMSCs derived from two patients were differentiated as a monolayer, fixed at day 7, 14 and 21 of differentiation and stained for alkaline phosphatase (ALP) (Figure 7.9) and Alizarin Red (Figure 7.10) to determine the efficiency of osteoblast formation under 2D culture conditions.

ALP staining (Figure 7.9) showed an increase in intensity over the time course of differentiation in the examined osteogenic medium compositions with intense staining observed at day 21 in both culture conditions. Medium containing 50 nM dexamethasone, 10 nM 1,25-$(OH)_2$-vitamin D_3 and 100 μM ascorbate-2-phosphate resulted in the strongest staining for ALP after 21 days. The negative control (basal medium in the absence of osteogenic differentiation components) showed negligible staining at any of the three time points examined.

To determine the efficiency of mineralization, alizarin red staining (Figure 7.10) was performed. Alizarin red staining was widely distributed in the monolayer cultures as opposed to the demonstration of compact nodule-like structures. Following 21 days treatment with 50 nM dexamethasone, 10 nM 1,25-$(OH)_2$-vitamin D_3 and 100 μM ascorbate-2-phosphate supplemented medium, enhanced and intensified staining of the cells relative to the cells treated with 10 nM dexamethasone, 25 nM 1,25-$(OH)_2$-vitamin D_3 and 100 μM ascorbate-2-phosphate and basal medium was observed.

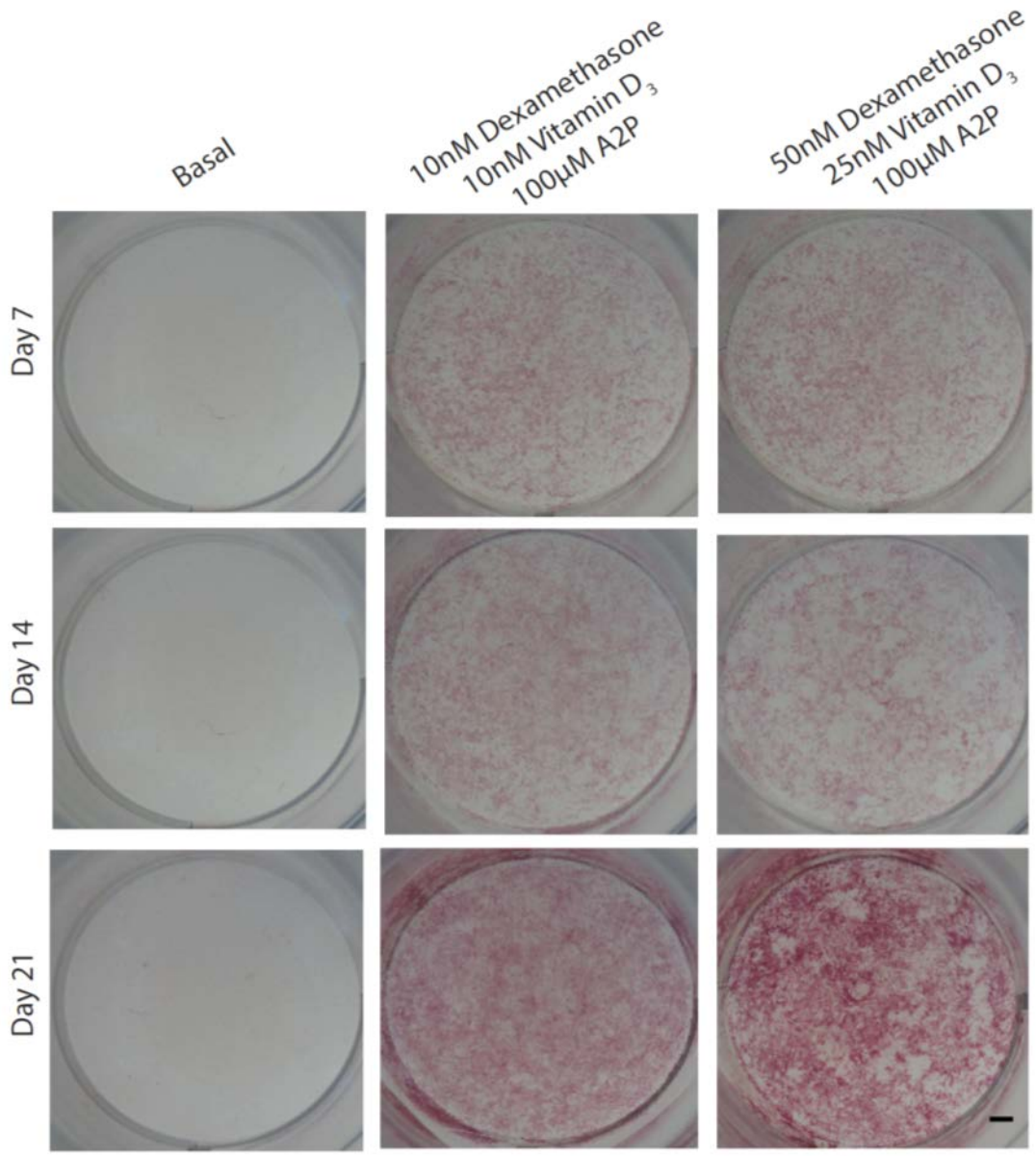

Figure 7.9 Alkaline Phosphatase (ALP) staining of aged primary HBMSCs treated with basal (αMEM supplemented with FBS and P/S) and osteogenic (basal medium supplemented with different concentrations of dexamethasone, ascorbate-2-phosphate (A2P) and 1,25-$(OH)_2$-vitamin D_3 (Vitamin D3)) media in monolayer conditions for 21 days. Images are representative for n = 2 experiments. Scale bar: 1 mm.

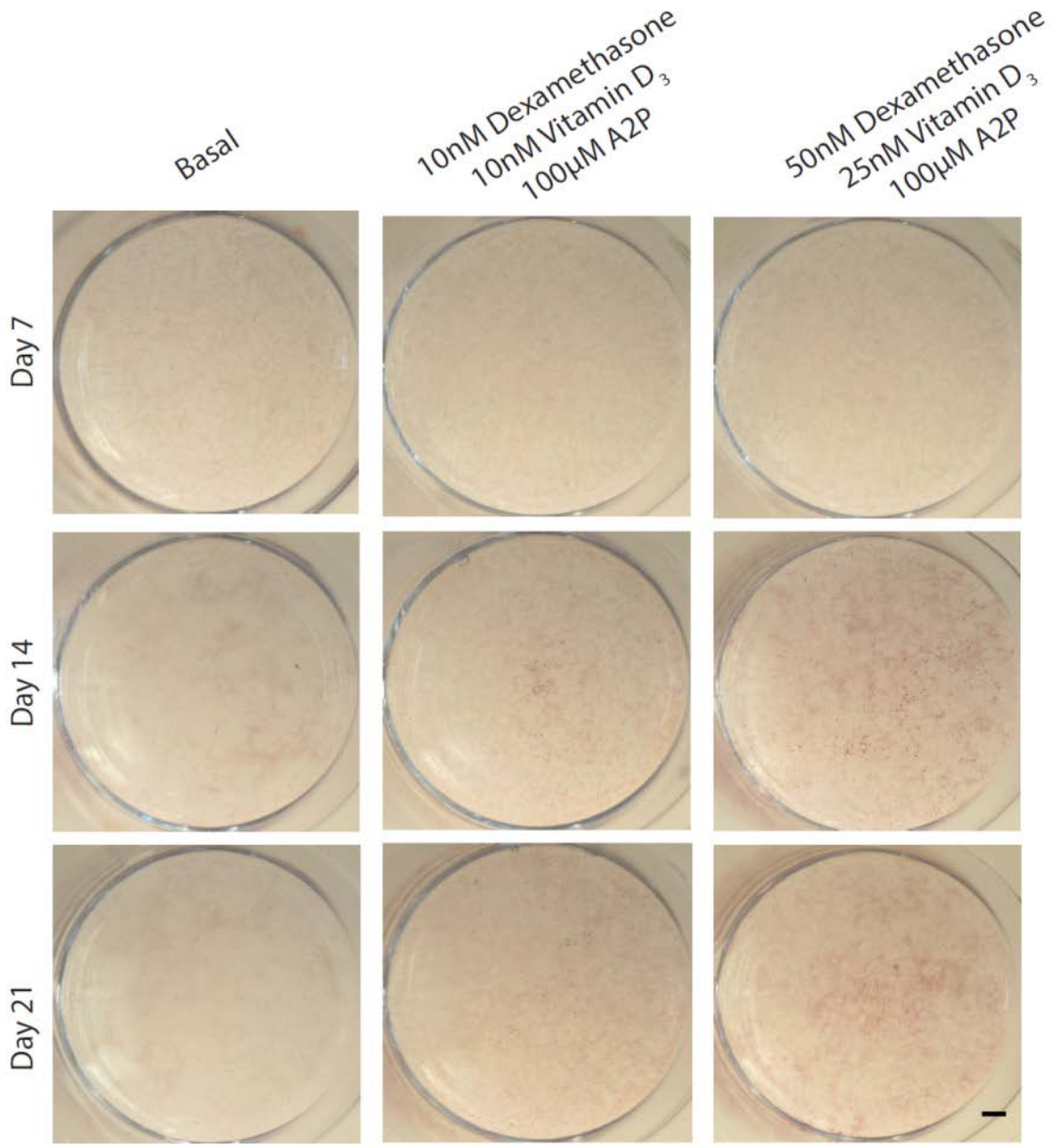

Figure 7.10 Alizarin Red staining of aged primary HBMSCs treated with basal (αMEM supplemented with FBS and P/S) and osteogenic (basal medium supplemented with different concentrations of dexamethasone, ascrobate-2-phosphate (A2P) and 1,25-$(OH)_2$-vitamin D_3 (Vitaminin D3 (Vitamin D3)) media in monolayer conditions for 21 days. Images are representative for n = 2 experiments. Scale bar: 1 mm.

Quantitative real-time PCR (qRT-PCR) was undertaken to determine the expression levels of the osteogenic (*ALPL*, *RUNX*2, *COL1A1*) and adipogenic (*PPARG*) genes during the time course of osteogenic differentiation with either 10 nM dexamethasone, 10 nM 1,25-$(OH)_2$-vitamin D_3 and 100 µM ascorbate-2-phosphate or 50 nM dexamethasone, 25 nM 1,25-$(OH)_2$-vitamin D_3 and 100 µM ascorbate-2-phosphate supplemented medium (Figure 7.11 to Figure 7.18).

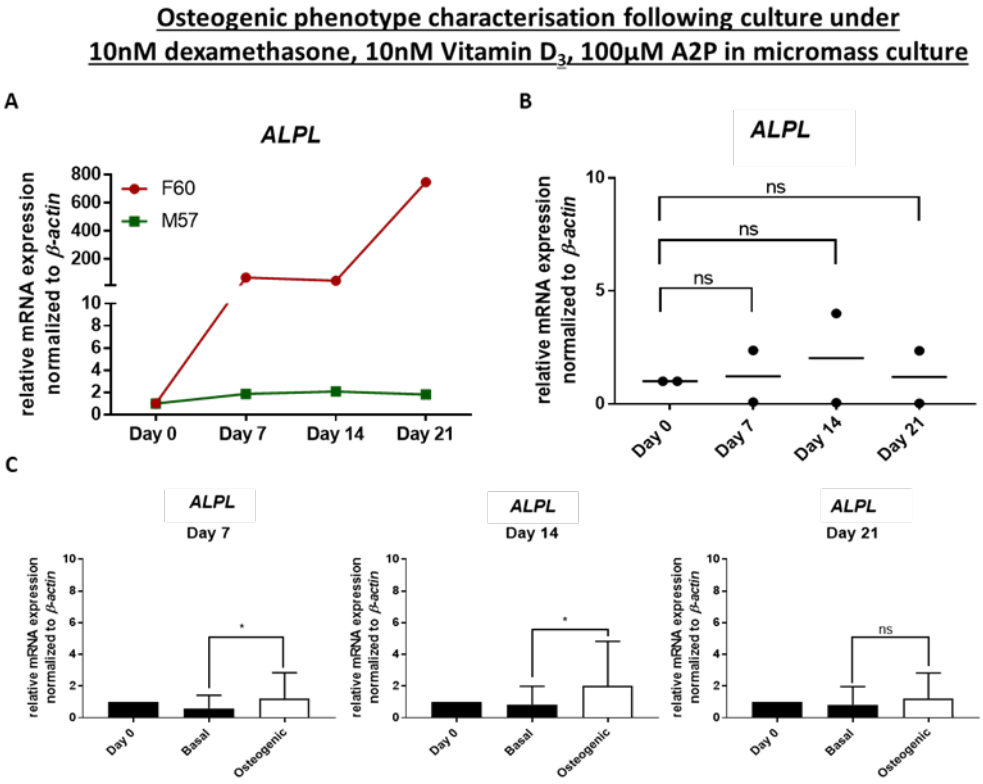

Figure 7.11 Expression of *ALPL* in aged primary HBMSCs from two patients cultured in monolayer treated with 10 nM dexamethasone, 10 nM 1,25-(OH)$_2$-vitamin D$_3$ (Vitamin D3) and 100 µM ascorbate-2-phosphate (A2P) supplementation. **A:** *ALPL* expression of the two different patients F60 and M57 treated with osteogenic medium for 21 days (basal condition not shown). **B:** Mean and individual *ALPL* expression values of the osteogenic medium treated HBMSCs. Two-way ANOVA was performed to compare correlation of *ALPL* expression at day 0 and day 21. **C:** A*LPL* expression (mean +/- SD) in basal and osteogenic condition on the individual time points relative to day 0. Paired t-test was performed to compare gene expression between control and osteogenic condition. F: female; M: male; ns: not significant; n = 2; * $p < 0.05$.

The two patients showed a significant variation in their expression of *ALPL* over the 21 day differentiation period following incubation with 10 nM dexamethasone, 10 nM 1,25-(OH)$_2$-vitamin D$_3$ and 100 µM ascorbate-2-phosphate supplemented medium, with F60 yielding a 600-fold increase in *ALPL* expression in comparison to M57 that displayed a less than two-fold increase at day 21 (Figure 7.11 A). Treatment with 50 nM dexamethasone, 25 nM 1,25-(OH)$_2$-vitamin D$_3$ and 100 µM ascorbate-2-phosphate supplementation resulted in a comparable temporal increase in *ALPL* expression levels until day 14 in both patients (~ 6-fold increase). Gene expression was observed to vary at day 21 in both patients (M57 > 40-fold increase *ALPL* expression and F60 a 5-fold enhancement in expression) (Figure 7.12 A). No significant correlation between day 0 and time points of day 7, 14 or 21

could be identified in either of the two osteogenic conditions (Figure 7.11 B and Figure 7.12 B). Osteogenic media, as expected, demonstrated a temporal enhancement of gene expression compared to basal control (Figure 7.11 C and Figure 7.12 C). Supplementation with 10 nM dexamethasone, 10 nM 1,25-$(OH)_2$-vitamin D_3 and 100 µM ascorbate-2-phosphate yielded higher *ALPL* expression levels (~ 400-fold increase) than medium supplemented with 50 nM dexamethasone, 25 nM 1,25-$(OH)_2$-vitamin D_3 and 100 µM ascorbate-2-phosphate (~ 20-fold increase) at day 21.

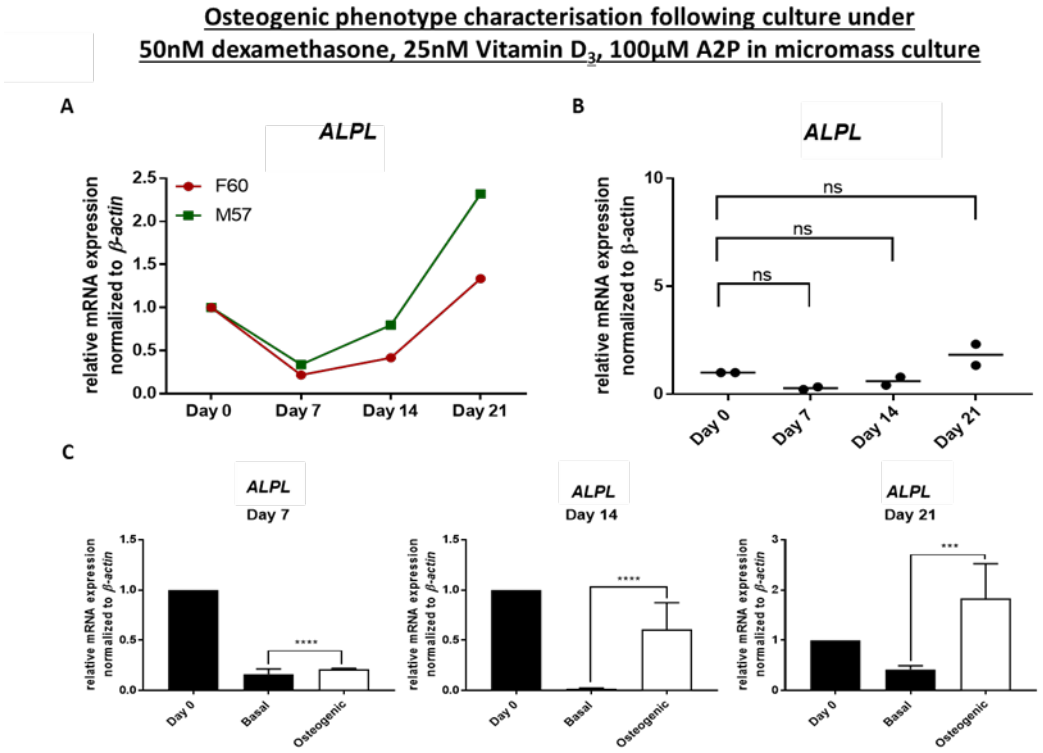

Figure 7.12 Expression of *ALPL* in aged primary HBMSCs from two patients cultured in monolayer treated with 50 nM dexamethasone, 25 nM 1,25-$(OH)_2$-vitamin D_3 (Vitamin D3) and 100 µM ascorbate-2-phosphate (A2P) supplementation. A: *ALPL* expression of the two different patients F60 and M57 treated with osteogenic medium for 21 days (basal condition not shown). **B:** Mean and individual *ALPL* expression values of the osteogenic medium treated HBMSCs. Two-way ANOVA was performed to compare correlation of *ALPL* expression at day 0 and day 21. **C:** A*LPL* expression (mean +/- SD) in basal and osteogenic condition on the individual time points relative to day 0. Paired t-test was performed to compare gene expression between control and osteogenic condition. F: female; M: male; ns: not significant; n = 2; *** $p < 0.001$; **** $p < 0.0001$.

The two patients varied in their expression of *RUNX2* over the first 14 days but were comparable at day 21 of differentiation under 50 nM dexamethasone, 25 nM 1,25-$(OH)_2$-vitamin D_3 and 100 µM ascorbate-2-phosphate supplementation Figure 7.14 A), while in the

presence of 10 nM dexamethasone, 10 nM 1,25-$(OH)_2$-vitamin D_3 and 100 μM ascorbate-2-phosphate supplemented medium, *RUNX2* expression levels were comparable at days 7 and 14 in both patients (2-fold increase at day 7 and 3-fold increase at day 14) with a temporal increase over 14 days (Figure 7.13 A). Gene expression in the 10 nM dexamethasone, 10 nM 1,25-$(OH)_2$-vitamin D_3 and 100 μM ascorbate-2-phosphate treatment group at day 21 varied between the two patients. The F60 sample displayed higher *RUNX2* expression (28-fold increase) than M57 (3-fold increase) (Figure 7.13 A). No significant correlation between day 0 and the time points of day 7, 14 or 21 could be identified in either of the two osteogenic conditions (Figure 7.13 B and Figure 7.14 B). Gene expression was significantly higher following culture in osteogenic media over time compared to basal control (Figure 7.13 C and Figure 7.14C). 10 nM dexamethasone, 10 nM 1,25-$(OH)_2$-vitamin D_3 and 100 μM ascorbate-2-phosphate supplemented medium produced a significantly higher expression of *RUNX2* (~ 15-fold increase) than 50 nM dexamethasone, 25 nM 1,25-$(OH)_2$-vitamin D_3 and 100 μM ascorbate-2-phosphate supplemented medium (~ 2-fold increase) at day 21.

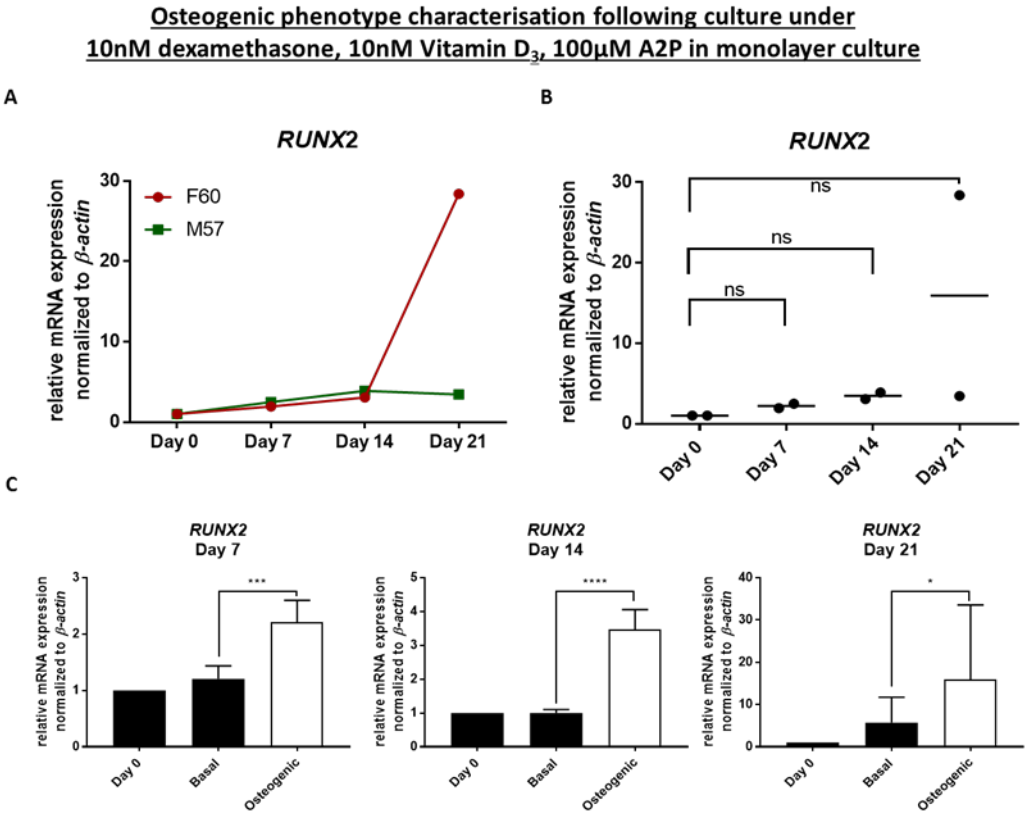

Figure 7.13 Expression of *RUNX2* in aged primary HBMSCs from two patients cultured in monolayer treated with 10 nM dexamethasone, 10 nM 1,25-(OH)$_2$-vitamin D$_3$ (Vitamin D3) and 100 µM ascorbate-2-phosphate (A2P) supplementation. A: *RUNX2* expression of the two different patients F60 and M57 treated with osteogenic medium for 21 days (basal condition not shown). **B:** Mean and individual *RUNX2* expression values of the osteogenic medium treated HBMSCs. Two-way ANOVA was performed to compare correlation of *RUNX2* expression at day 0 and day 21. **C:** *RUNX2* expression (mean +/- SD) in basal and osteogenic condition on the individual time points relative to day 0. Paired t-test was performed to compare gene expression between control and osteogenic condition. F: female; M: male; ns: not significant; n = 2; * $p < 0.05$; *** $p < 0.001$; **** $p < 0.0001$.

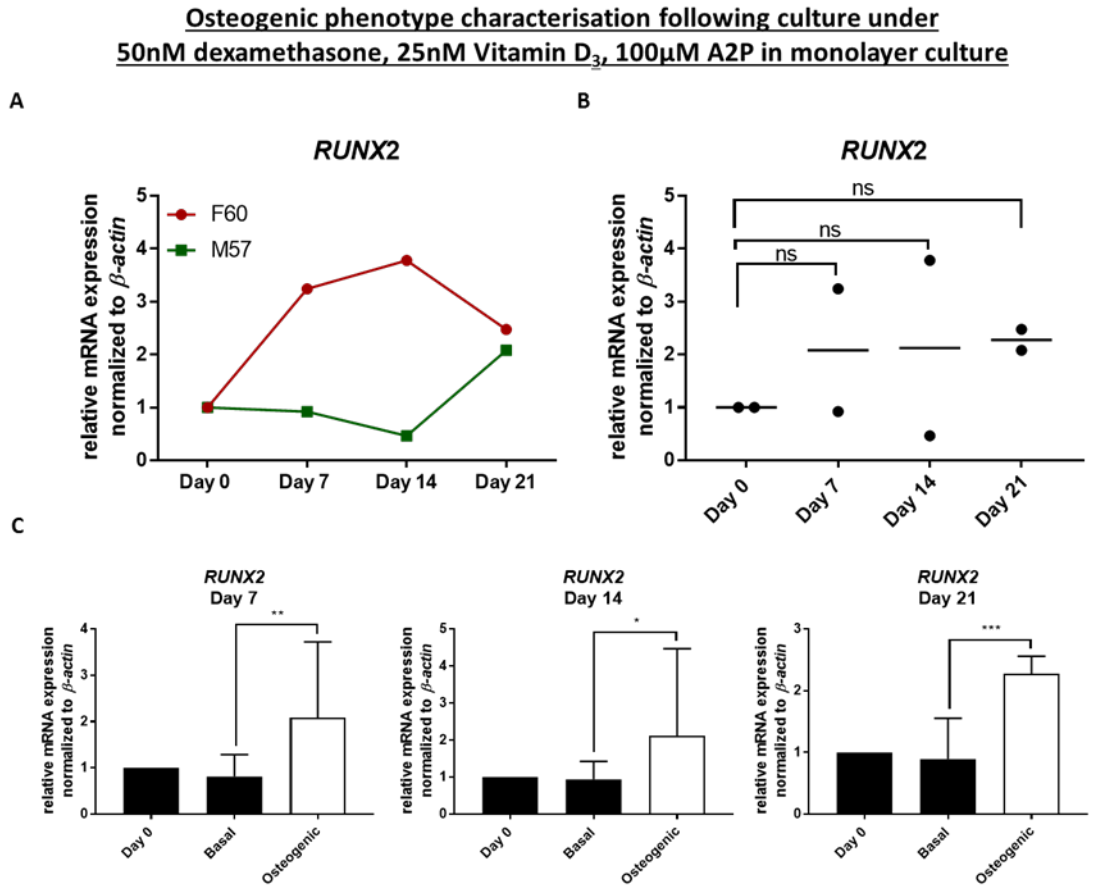

Figure 7.14 Expression of *RUNX2* in aged primary HBMSCs from two patients cultured in monolayer treated with 50 nM dexamethasone, 25 nM 1,25-$(OH)_2$-vitamin D_3 (Vitamin D3) and 100 µM ascorbate-2-phosphate (A2P) supplementation. A: *RUNX2* expression of the two different patients F60 and M57 treated with osteogenic medium for 21 days (basal condition not shown). **B:** Mean and individual *RUNX2* expression values of the osteogenic medium treated HBMSCs. Two-way ANOVA was performed to compare correlation of *RUNX2* expression at day 0 and day 21. **C:** *RUNX2* expression (mean +/- SD) in basal and osteogenic condition on the individual time points relative to day 0. Paired t-test was performed to compare gene expression between control and osteogenic condition. F: female; M: male; ns: not significant; n = 2; * $p < 0.05$; *** $p < 0.001$; **** $p < 0.0001$.

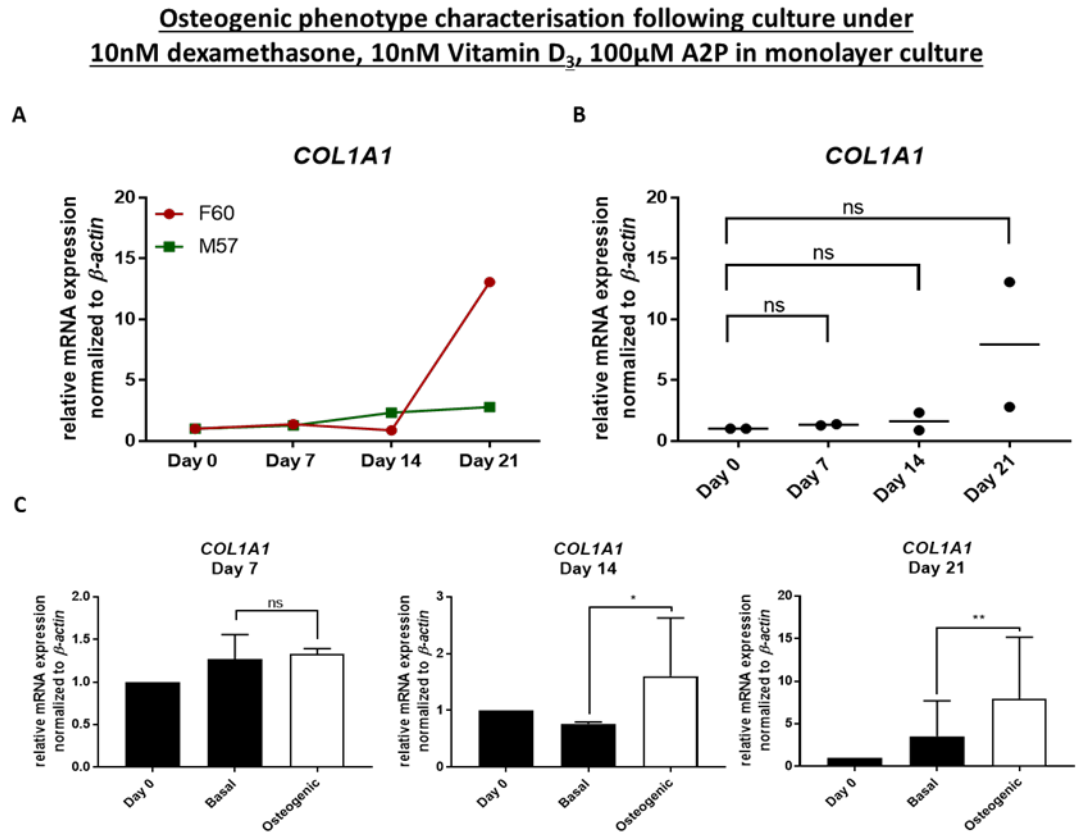

Figure 7.15 Expression of C*OL1A1* in aged primary HBMSCs from two patients cultured in monolayer treated with 10 nM dexamethasone, 10 nM 1,25-(OH)$_2$-vitamin D$_3$ (Vitamin D3) and 100 µM ascorbate-2-phosphate (A2P) supplementation. A: *COL1A1* expression of the two different patients F60 and M57 treated with osteogenic medium for 21 days (basal condition not shown). **B:** Mean and individual *COL1A1* expression values of the osteogenic medium treated HBMSCs. Two-way ANOVA was performed to compare correlation of *COL1A1* expression at day 0 and day 21. **C:** *COL1A1* expression (mean +/- SD) in basal and osteogenic condition on the individual time points relative to day 0. Paired t-test was performed to compare gene expression between control and osteogenic condition. F: female; M: male; ns: not significant; n = 2; * $p < 0.05$; ** $p < 0.01$.

With 10 nM dexamethasone, 10 nM 1,25-(OH)$_2$-vitamin D$_3$ and 100 µM ascorbate-2-phosphate supplementation, *COL1A1* expression was shown to be comparable in both patients over 7 days (1.3-fold increase in F60 and 1.3-fold increase in M57) followed by a decrease in patient F60 (0.9-fold decrease) at day 14 while *COL1A1* continued to increase in patient M57 (2.3-fold increase) (Figure 7.15 A). In the presence of 50 nM dexamethasone, 25 nM 1,25-(OH)$_2$-vitamin D$_3$ and 100 µM ascorbate-2-phosphate gene expression varied amongst the two patients but did not increase significantly over the differentiation period (Figure 7.16 A). No significant differences were observed across the time points examined in both osteogenic culture conditions (Figure 7.15 B and Figure 7.16 B). Higher expression

of *COL1A1* in osteogenic condition at both day 14 and 21 was significant but not in day 7 for 10 nM dexamethasone, 10 nM 1,25-$(OH)_2$-vitamin D_3 and 100 µM ascorbate-2-phosphate supplemented medium, whereas higher *COL1A1* expression was significantly higher at all three time points for 50 nM dexamethasone, 25 nM 1,25-$(OH)_2$-vitamin D_3 and 100 µM ascorbate-2-phosphate supplemented medium (Figure 7.15 C and Figure 7.16 C). 10 nM dexamethasone, 10 nM 1,25-$(OH)_2$-vitamin D_3 and 100 µM ascorbate-2-phosphate supplemented medium resulted in higher expression of *COL1A1* (~ 7.8-fold increase) compared to the other tested osteogenic medium supplementation (~ 1.5-fold increase) at day 21.

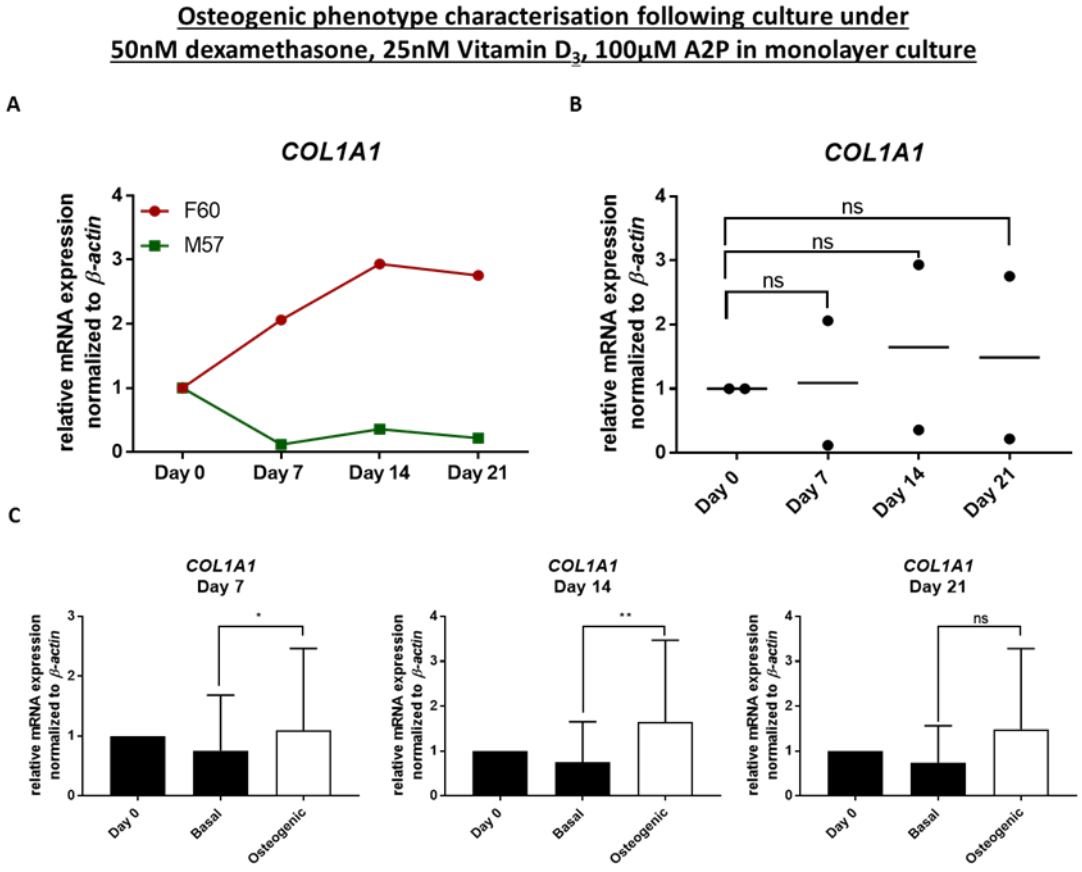

Figure 7.16 Expression of COL1A1 in aged primary HBMSCs from two patients cultured in monolayer treated with 50 nM dexamethasone, 25 nM 1,25-$(OH)_2$-vitamin D_3 (Vitamin D3) and 100 µM ascorbate-2-phosphate (A2P) supplementation. A: *COL1A1* expression of the two different patients F60 and M57 treated with osteogenic medium for 21 days (basal condition not shown). **B:** Mean and individual *COL1A1* expression values of the osteogenic medium treated HBMSCs. Two-way ANOVA was performed to compare correlation of *COL1A1* expression at day 0 and day 21. **C:** *COL1A1* expression (mean +/- SD) in basal and osteogenic condition on the individual time points relative to day 0. Paired t-test was performed to compare gene

expression between control and osteogenic condition. F: female; M: male; ns: not significant; n = 2; * p < 0.05; ** p < 0.01.

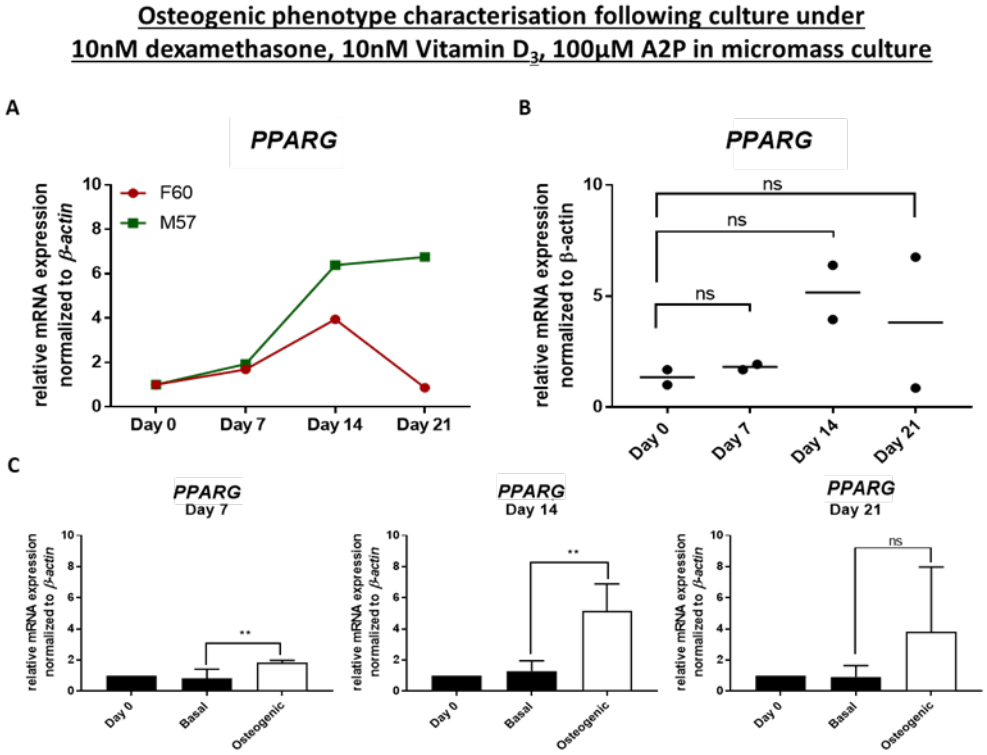

Figure 7.17 Expression of PPARG in aged primary HBMSCs from two patients cultured in monolayer treated with 10 nM dexamethasone, 10 nM 1,25-$(OH)_2$-vitamin D_3 (Vitamin D3) and 100 µM ascorbate-2-phosphate (A2P) supplementation. **A:** *PPARG* expression of the two different patients F60 and M57 treated with osteogenic medium for 21 days (basal condition not shown). **B:** Mean and individual *PPARG* expression values of the osteogenic medium treated HBMSCs. Two-way ANOVA was performed to compare correlation of *PPARG* expression at day 0 and day 21. **C:** *PPARG* expression (mean +/- SD) in basal and osteogenic condition on the individual time points relative to day 0. Paired t-test was performed to compare gene expression between control and osteogenic condition. F: female; M: male; ns: not significant; n = 2; ** p < 0.01; *** p < 0.001.

The two patients varied in the expression of *PPARG* over the 21 day differentiation period following incubation with 10 nM dexamethasone, 10 nM 1,25-$(OH)_2$-vitamin D_3 and 100 µM ascorbate-2-phosphate supplementation. Expression of *PPARG* in F60 yielded a 4.4-fold enhancement at day 7, increased further (22-fold increase at day 14) but was reduced by approximately 50 % by day 21. Similar behaviour was observed in the second patient M57 (3.5-fold increase at day 7, 14-fold increase at day 14, 8-fold increase at day 21) although overall *PPARG* expression levels were reduced compared to F60 (Figure 7.17 A). Treatment with 50 nM dexamethasone, 25 nM 1,25-$(OH)_2$-vitamin D_3 and

100 µM ascorbate-2-phosphate supplemented medium resulted in a temporal increase of *PPARG* expression in F60 (8.5-fold increase at day 7, 12.8-fold increase at day 14, 11.8-fold increase at day 21) and M57 (0.5-fold increase at day 7, 1.5-fold increase at day 14, 0.9-fold increase at day 21) (Figure 7.18 A). Different expression levels between day 0 and the three time points (day 7, 14 and 21) were not statistically significant in either of the osteogenic conditions examined (Figure 7.17 B and Figure 7.18 B). A temporal increase in *PPARG* expression was significant at all three time points in both osteogenic media supplementations compared to basal control. Overall, expression of *PPARG* yielded a similar increase at day 21 (~ 11-fold) and day 14 (~ 14-fold) in the two examined osteogenic media supplementations (Figure 7.17 C and Figure 7.18 C).

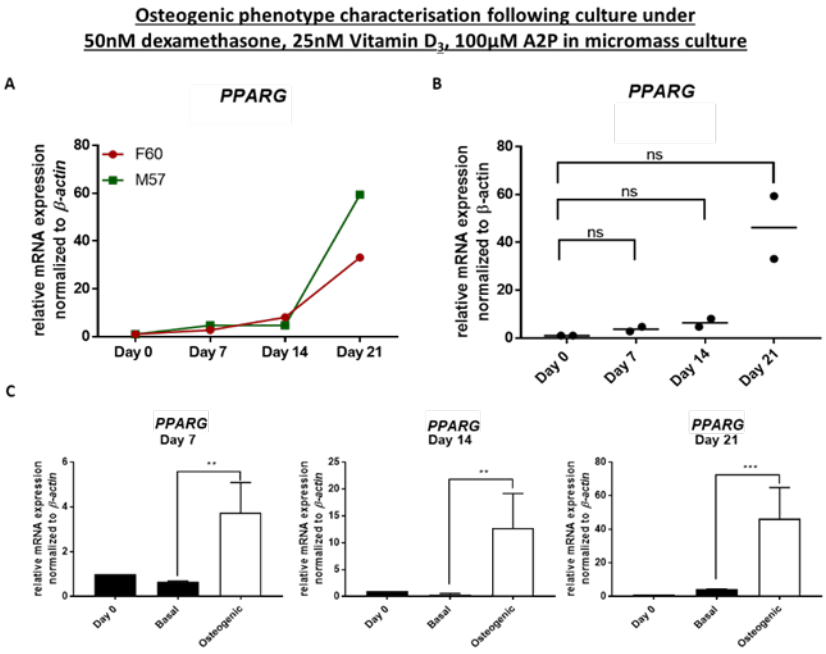

Figure 7.18 Expression of PPARG in aged primary HBMSCs from two patients cultured in monolayer treated with 50 nM dexamethasone, 25 nM 1,25-$(OH)_2$-vitamin D_3 (Vitamin D3) and 100 µM ascorbate-2-phosphate (A2P) supplementation. A: *PPARG* expression of the two different patients F60 and M57 treated with osteogenic medium for 21 days (basal condition not shown). **B:** Mean and individual *PPARG* expression values of the osteogenic medium treated HBMSCs. Two-way ANOVA was performed to compare correlation of *PPARG* expression at day 0 and day 21. **C:** *PPARG* expression (mean +/- SD) in basal and osteogenic condition on the individual time points relative to day 0. Paired t-test was performed to compare gene expression between control and osteogenic condition. F: female; M: male; ns: not significant; n = 2; * $p<0.05$.

Summary

Lower concentrations of the osteogenic media yielded higher expression levels of the tested genes, therefore were viewed as sufficient and considered efficacious compared to higher concentrations of osteogenic media components. Changes in expression levels of the tested genes are summarised in Table 7.4 to ease direct comparison of the two different osteogenic media compositions under 2D culture conditions over time.

Table 7.4 Summary of respective gene expression characteristic for osteogenesis (*ALPL, RUNX2, COL1A1*) and adipogenesis (*PPARG*) levels under treatment with the two osteogenic media compositions under monolayer conditions. Expression levels measured as fold-change compared to day 0. ALPL: alkaline phosphatase; RUNX2: runt-related transcription factor 2; COL1A!: collagen type I; PPARG: peroxisome proliferator activated receptor gamma.

	Day 7		**Day 14**		**Day 21**	
Gene expression levels as fold-change compared to day 0	**10 nM Dex, 10 nM $VitD_3$, 100 µM A2P**	**50 nM Dex, 25 nM $VitD_3$, 100 µM A2P**	**10 nM Dex, 10 nM $VitD_3$, 100 µM A2P**	**50 nM Dex, 25 nM $VitD_3$, 100 µM A2P**	**10 nM Dex, 10 nM $VitD_3$, 100 µM A2P**	**50 nM Dex, 25 nM $VitD_3$, 100 µM A2P**
ALPL	35.10	3.40	23.80	6.20	373.00	22.50
*RUNX*2	2.20	2.10	3.50	2.10	16.00	2.30
COL1A1	1.30	1.10	1.60	1.60	8.00	1.50
PPARG	3.70	4.50	14.20	7.20	8.00	6.30

Appendix F Generation of viPSC-MSCs

To generate viPSC-MSCs, viPSCs (passage 61) were seeded as large fragments onto matrigel coated 12-wells and cultured in StemMACS XF Brew iPSC medium (Miltenyi Biotec) until 85 % confluency. Subsequently, colonies were cultured in differentiation medium containing the TGFβ-pathway inhibitor SB431542 for 10 days with daily medium change (for composition of differentiation medium see section 2.1.4). Changes in cell morphology were captured using bright field microscopy after 10 days (Figure 7.19). After 10 days of SB431542 treatment, cells showed enlarged cytoplasm resembling a 'fried egg'-like morphology (Figure 7.19 A) and in approximately 5 % of the monolayer elongated fibroblast-like looking cells (Figure 7.19 B). Few three dimensional structures were observed as well (Figure 7.19 C). After 10 days, cells were passaged into MSC medium onto TCP (15000 cells/cm^2) (referred to as MSC passage 0 (MP0)). Figure 7.20 shows change in cell morphology over several passages in MSC medium on tissue culture plastic.

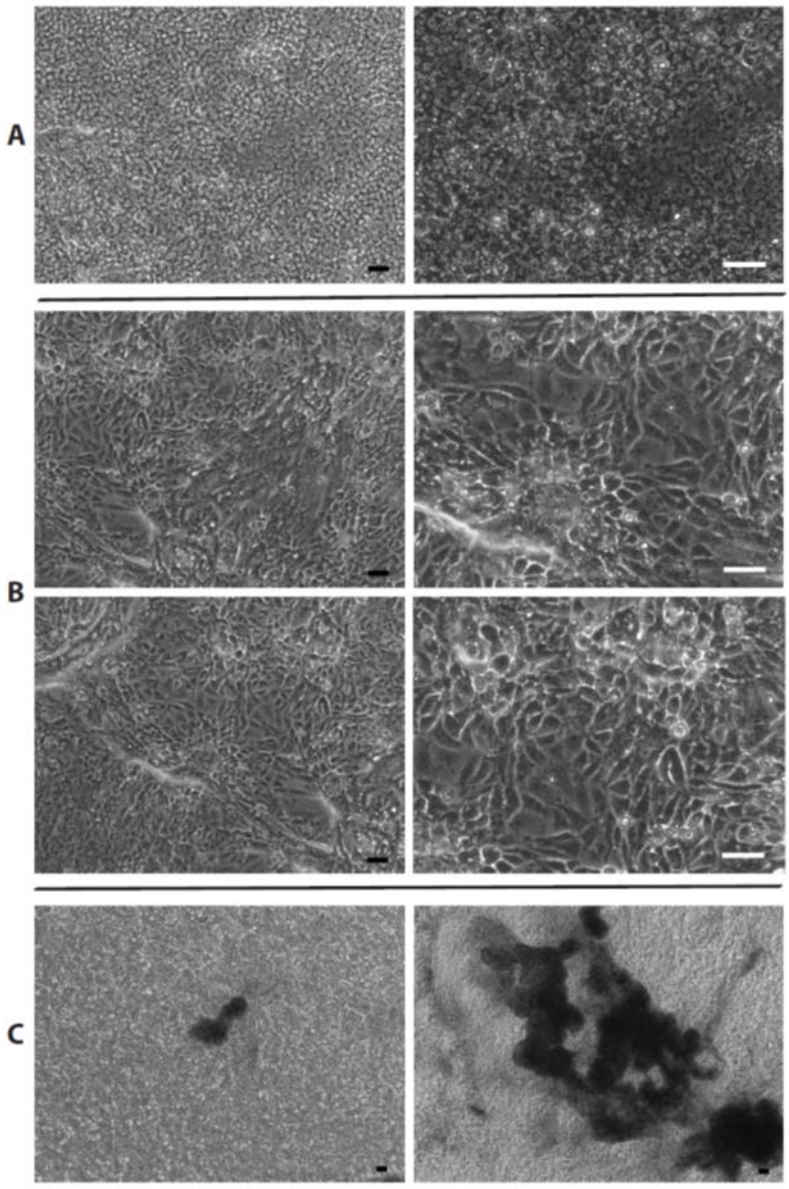

Figure 7.19 viPSCs after 10 days of incubation with differentiation medium supplemented with the TGFβ -pathway inhibitor SB431542. A: Cells with enlarged cytoplasm (‘fried egg-like morphology’); **B:** fibroblast-like morphology; **C:** three dimensional structures. Scale bars: 50 μm.

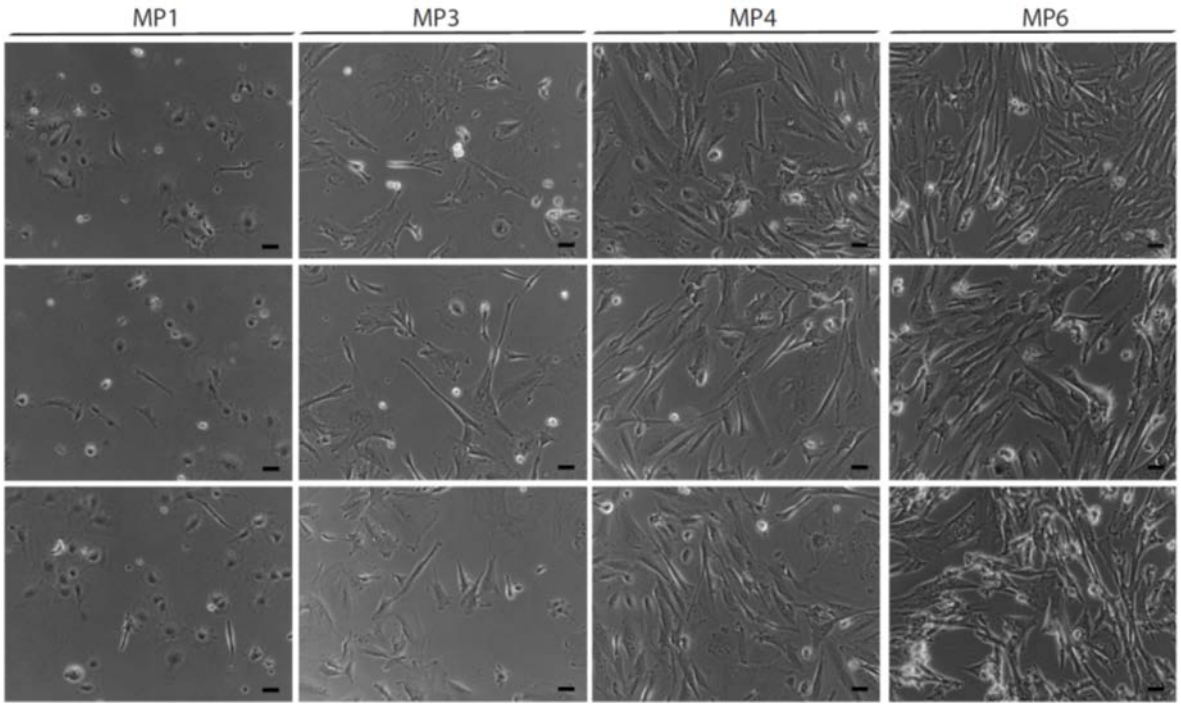

Figure 7.20 Change of morphology of viPSCs treated with SB431542 supplemented medium for 10 days after several passaged in MSC medium on cell culture plastic. At MP1 few cells attached to the plastic surface resembling fibroblast-like morphology whereas the majority of attached cells showed the 'fried-egg' morphology. Further passaging (MP3, MP4 and MP6) showed increase in number and size cells displaying a fibroblast-like morphology and a reduction in cells displaying a 'fried-egg' morphology. MP: mesenchymal passage. Scale bar: 50 μm.

As viPSCs treated with SB431542 supplemented medium showed only a few cells displaying an elongated fibroblast-like morphology at day 10 (Figure 7.19), the experiment was repeated. Starting colony density was further reduced to 50 %. As described above, viPSCs were treated with SB431542 supplemented medium for 10 days and cell morphology captured using bright field microscopy. In contrast to the first attempt, 80-90 % of the monolayer resembled the fibroblast-like morphology already observed in a small fraction during the first attempt (Figure 7.21).

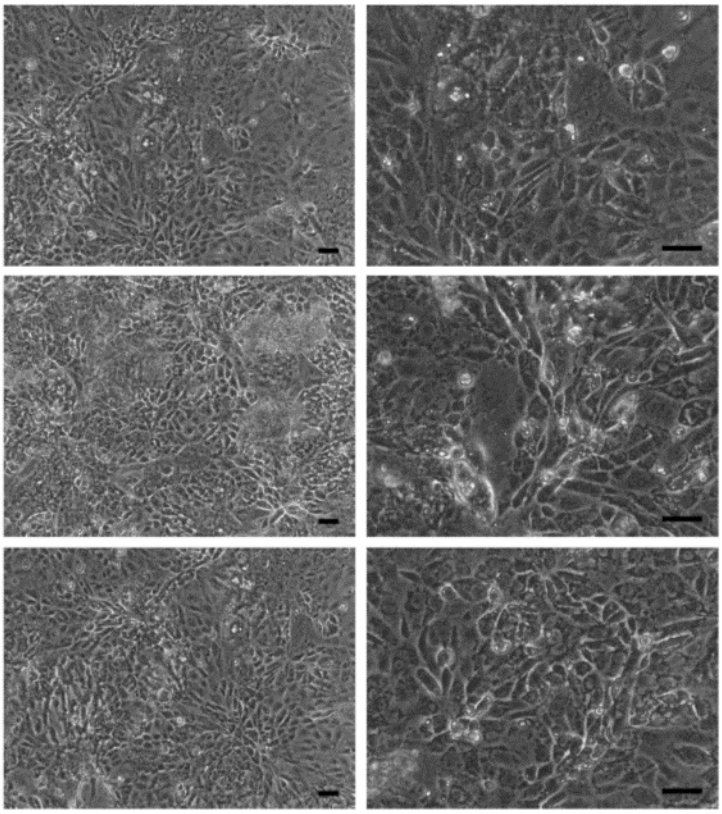

Figure 7.21 viPSCs (passage 63) after 10 days incubation with iPSC-MSC differentiation medium containing the TGFβ-pathway inhibitor SB431542. Flat morphology with big cytoplasm as well as fibroblast-like morphology and few three dimensional structures were observed in the culture. Cytoplasm as well as fibroblast-like morphology and few three dimensional structures were observed in the culture. Scale bars: 50 μm.

viPSCs were transferred on to TCP and cultured MSC medium (MP0), this time with a higher cell number (40000 cells/cm^2) to aid adaption and proliferation of the cells through cell-cell contacts. Morphology was monitored (Figure 7.22) and within one passage number of fibroblast-like looking cells increased.

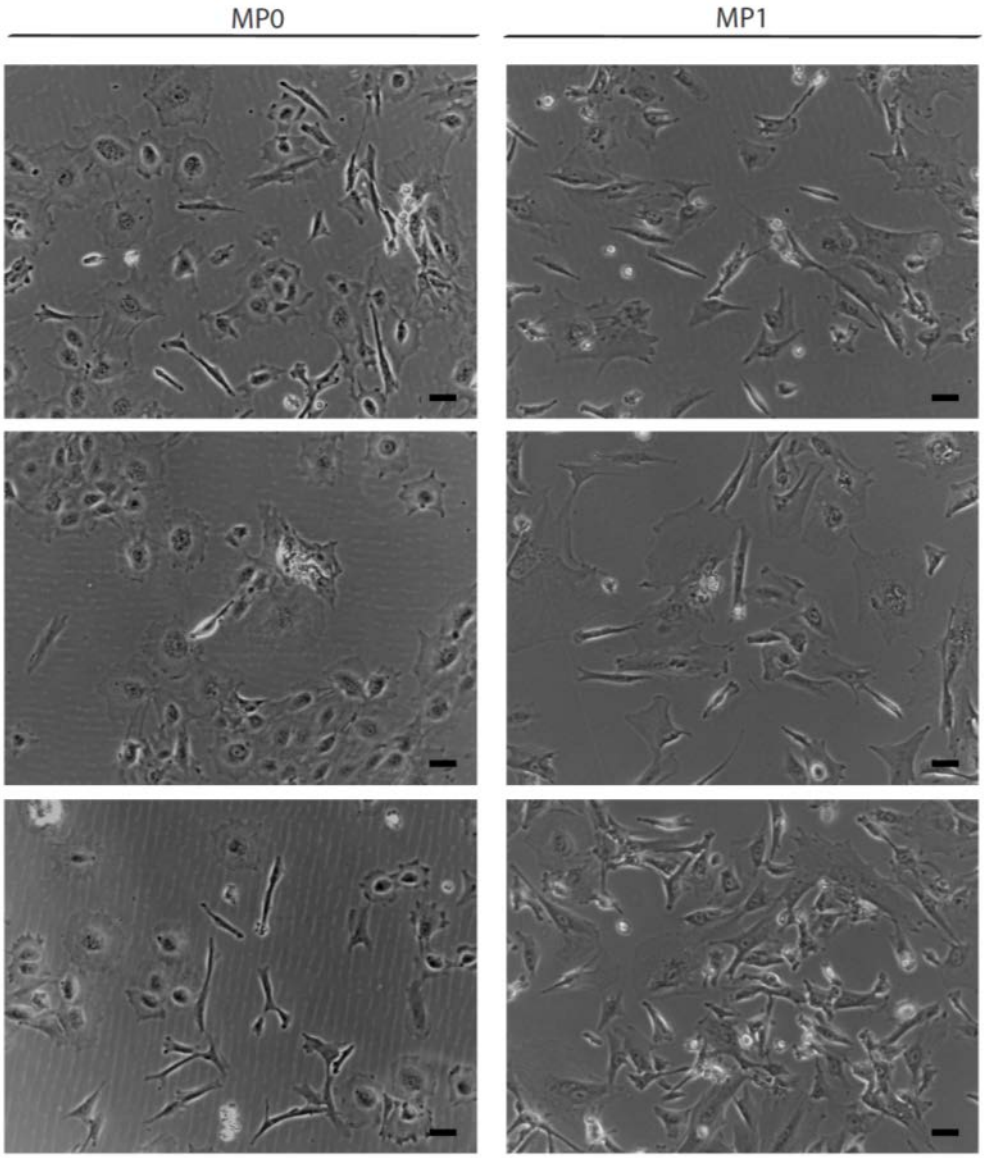

Figure 7.22 Change in morphology of viPSCs treated with SB431542 supplemented medium for 10 days (50 % confluent at day 0 of differentiation media treatment) after several passages in MSC medium on cell culture plastic. MP: mesenchymal passage. Scale bars: 50 μm.

Appendix G Osteogenic differentiation of NIBSC-8 MSCs

Expression of **osteogenic genes** (*RUNX2*, *ALPL*, *COL1A1*, *OCN*, *OPN*) during osteogenic differentiation of NIBSC-8 MSCs displayed in Table 7.5 with mean of the three differentiation experiments (bold) displayed as well as the gene expression of the individual differentiation experiments.

Table 7.5 Summary of respective gene expression characteristic for osteogenesis in NIBSC-8 MSCs treated with basal medium, osteogenic background medium (oBG, 10 nM dexamethasone, 10 nM 1,25-$(OH)_2$-vitamin D_3 and 100 µM ascorbic-2-phosphate) and osteo background (oBG) medium supplemented with small molecules SAG (smoothened agonist) and TH TH (4-(4-methoxyphenyl)pyrido[4′,3′:4,5]thieno[2,3-b]pyridine-2-carboxamide). Gene expression was normalised to *RN18S* (subunit of 18S normalised RNA) at day 0. Osteogenic differentiation was performed three times (n = 3). Individual values as well as mean of three individual experiments (in bold) are displayed.

	condition	*RUNX2*	*ALPL*	*COL1A1*	*OCN*	*OPN*
Day 7	basal	0.53 0.48 0.72 **0.58**	1.85 1.15 1.63 **1.54**	1.59 0.66 0.87 **1.04**	1.42 0.72 0.26 **0.80**	0.82 0.64 1.63 **1.03**
	oBG	1.27 0.57 1.65 **1.16**	7.24 2.21 4.68 **4.71**	3.44 1.40 1.46 **2.10**	5.73 1.45 0.71 **2.63**	0.34 0.20 1.50 **0.68**
	oBG + TH + SAG	0.95 0.70 0.85 **0.83**	5.74 4.11 4.10 **4.65**	2.17 0.98 0.75 **1.30**	3.35 0.99 0.87 **1.74**	0.27 0.27 1.61 **0.72**
Day 19	basal	0.45 0.30 1.16 **0.63**	2.87 0.84 0.71 **1.47**	1.69 0.27 0.41 **0.79**	2.59 0.41 0.77 **1.26**	0.65 0.61 0.94 **0.73**
	oBG	0.94 0.58 1.59 **1.04**	7.94 2.93 1.71 **4.19**	1.59 0.43 0.48 **0.83**	5.34 1.31 2.15 **2.94**	0.29 0.12 0.36 **0.2**
	oBG + TH + SAG	0.85 0.55 1.42 **0.94**	13.00 5.06 1.72 **6.58**	1.38 0.49 0.41 **0.76**	2.53 0.94 1.08 **1.52**	0.31 0.16 0.35 **0.28**

Expression of **chondrogenic genes** (*COL2A1, ACAN*) during osteogenic differentiation of NIBSC-8 MSCs displayed in Table 7.6 with mean of the three differentiation experiments (bold) displayed as well as the gene expression of the individual differentiation experiments.

Table 7.6 Summary of respective gene expression characteristic for chondrogenesis in NIBSC-8 MSCs treated with basal medium, osteogenic background medium (oBG, 10 nM dexamethasone, 10 nM 1,25-$(OH)_2$-vitamin D_3 and 100 µM ascorbic-2-phosphate) and osteo background (oBG) medium supplemented with small molecules SAG (smoothened agonist) and TH (4-(4-methoxyphenyl)pyrido[4′,3′:4,5]thieno[2,3-b]pyridine-2-carboxamide). Gene expression was normalised to *RN18S* (subunit of 18S ribosomal RNA) at day 0. Osteogenic differentiation was performed three times (n = 3). Individual values as well as mean of three individual experiments (in bold) are displayed.

	condition	***COL2A1***	***ACAN***
Day 7	basal	1.78 0.56 0.00 **0.78**	1.33 0.58 0.96 **0.95**
	oBG	0.95 0.61 0.00 **0.52**	2.53 0.91 1.91 **1.79**
	oBG + TH + SAG	2.16 0.08 0.00 **0.75**	3.58 1.03 1.78 **2.13**
Day 19	basal	2.28 0.15 0.00 **0.81**	1.15 0.11 0.29 **0.52**
	oBG	2.32 0.11 0.00 **0.81**	0.97 0.09 0.15 **0.40**
	oBG + TH + SAG	4.20 0.00 0.00 **1.40**	1.25 0.16 0.20 **0.54**

Appendix H Gene expression HFBCs at passage 0 and passage 1

Table 7.7 - Table 7.8 provide an overview of osteogenic and chondrogenic gene expression in HFBCs at passage 0 (Table 7.7) and passage 1 (Table 7.8).

Table 7.7 Chondrogenic and osteogenic gene expression at passage 0 in HFBCs isolated from 7-17 wpc human foetal femurs.

	chondrogenic genes				
Foetal sample	***SOX9***	***COL2A1***	***COL9A1***	***ACAN***	***COL10A1***
13986 (7 wpc)	1.00	1.00	1.00	1.00	0.00
13723 (8 wpc)	18.91	134.98	62.94	2.93	0.00
13975 (8 wpc)	0.49	351.89	199.86	6.32	0.00
13706 (9 wpc)	5.30	165.65	82.46	2.80	0.00
14007 (10 wpc)	0.66	159.28	141.90	3.68	1.00
13893 (12 wpc)	2.87	745.08	280.30	21.68	31.60
13796 (13 wpc)	2.40	233.33	126.66	8.26	6.31
13901 (14 wpc)	10.61	156.69	204.35	7.73	56.92
13976 (14 wpc)	5.24	117.17	280.36	18.27	11.17
14008 (16 wpc)	1.50	589.65	446.63	21.95	1.87
13766 (17 wpc)	24.92	785.93	644.93	34.91	50.13
	osteogenic genes				
Foetal sample	***RUNX2***	***COL1A1***	***OCN***	***OPN***	***ALPL***
13986 (7 wpc)	1.00	1.00	1.00	1.00	1.00
13723 (8 wpc)	0.24	0.14	3.49	2.28	2.93
13975 (8 wpc)	2.12	0.13	4.07	12.67	2.57
13706 (9 wpc)	0.33	0.12	3.54	0.46	1.89
14007 (10 wpc)	1.43	0.14	3.96	2.66	2.46
13893 (12 wpc)	0.69	0.20	9.03	25.75	0.39

13796 (13 wpc)	2.08	0.27	4.50	4.34	5.06
13901 (14 wpc)	0.45	0.21	1.40	35.17	0.56
13976 (14 wpc)	3.25	0.06	1.27	11.25	1.25
14008 (16 wpc)	0.62	0.05	2.44	1.19	0.48
13766 (17 wpc)	0.84	0.07	8.15	4.76	0.54

Table 7.8 Chondrogenic and osteogenic gene expression at passage 1 in HFBCs isolated from 7-17 wpc human foetal femurs.

	chondrogenic genes				
Foetal sample	***SOX9***	***COL2A1***	***COL9A1***	***ACAN***	***COL10A1***
13986 (7 wpc)	1.00	1.00	0.00	1.00	0.00
13723 (8 wpc)	10.62	1576.60	1.00	0.21	0.00
13975 (8 wpc)	26.57	425.68	62.94	1.64	0.00
13706 (9 wpc)	7.01	484.49	199.86	1.18	0.00
14007 (10 wpc)	14.74	281.66	82.46	2.13	0.00
13893 (12 wpc)	13.00	939.22	141.90	0.24	0.00
13796 (13 wpc)	2.57	13.68	280.30	0.05	0.00
13901 (14 wpc)	8.32	817.56	126.66	0.23	0.00
13976 (14 wpc)	35.58	235.55	204.35	1.12	0.00
14008 (16 wpc)	26.74	113.43	280.36	2.72	0.00
13766 (17 wpc)	15.65	15441.15	446.63	1.22	0.00
	osteogenic genes				
Foetal sample	***RUNX2***	***COL1A1***	***OCN***	***OPN***	***ALPL***
13986 (7 wpc)	1.00	1.00	1.00	0.00	1.00
13723 (8 wpc)	0.20	1.95	0.78	0.00	0.59
13975 (8 wpc)	1.81	2.59	1.58	0.00	0.89
13706 (9 wpc)	0.11	1.05	0.94	0.00	0.09
14007 (10 wpc)	0.08	2.10	0.91	0.00	0.08
13893 (12 wpc)	0.44	1.68	1.14	0.00	0.33

13796 (13 wpc)	0.14	1.63	0.11	1.00	0.07
13901 (14 wpc)	0.35	2.45	0.70	0.27	0.19
13976 (14 wpc)	2.07	2.12	1.55	0.68	0.89
14008 (16 wpc)	0.19	1.36	1.60	0.08	0.19
13766 (17 wpc)	0.30	3.64	1.06	0.19	0.34

Appendix I Global DNA methylation comparison iPSCs vs iPSC-MSCs

E1C1 iPSC line was generated by direct reprogramming with an episomal plasmid combination (pEP4EO2SCK2MEN2L and pEP4EO2SET2K, Addgene, Cat. No. 20924, 20927) from foetal cells H1536 by collaboration partners in Dusseldorf. iPSC-MSCs were derived from E1C1 iPSC line using a published protocol [182]. Global DNA methylation profiling was performed on HFBCs H1536 (parental), corresponding iPSC line E1C1 as wells as derived iPSC-MSCs (Figure 7.23 and Table 7.9). E1C1 iPSCs showed higher global methylation than parental foetal cells (2.71 %) and derived iPSC-MSCs (0.72 %). iPSC-MSCs shower higher methylation than parental cells at same passage number (1.99 %).

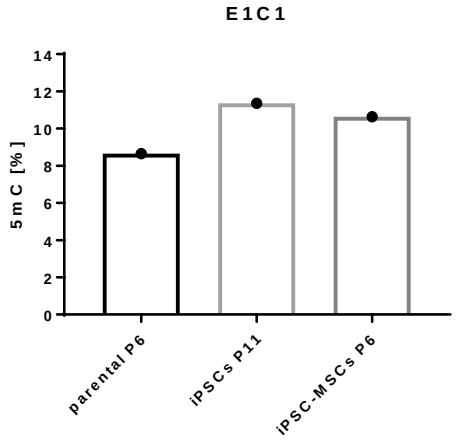

Figure 7.23 Global DNA methylation of HFBCs H1536 (parental), corresponding E1C1 iPSCs and derived iPSC-MSCs. Foetal cells H1536 were reprogrammed using an episomal plasmid combination. Derived iPSC line was renamed E1C1 to avoid confusion with parental line. Protocol for generation of iPSC-MSCs was applied to E1C1 iPSCs [182]. 5mC: 5-methylcytosine: P: passage. n = 1.

Table 7.9 Global DNA methylation of HFBCs H1536 (parental), corresponding E1C1 iPSCs and derived iPSC-MSCs.

Cell type	5mC [%]	Difference between parental cells and iPSC-MSCs [%]	Difference between parental cells and iPSCs [%]	Difference between iPSCs and iPSC-MSCs [%]
parental	8.648339061	0.72 resulting in ↑	2.71 resulting in ↑	1.99 resulting in ↓
iPSCs	11.36044881			
iPSC-MSCs	10.63829787			

Appendix J Osteogenic differentiation of HFBCs isolated from 8 wpc human foetal femurs

Expression of **osteogenic genes** (*RUNX2*, *ALPL*, *COL9A1*, *OCN*, *OPN*) during osteogenic differentiation of HFBCs isolated from 8 wpc human foetal femurs displayed in Table 7.10 with mean of the three differentiation experiments (bold) displayed as well as the gene expression of the individual differentiation experiments.

Table 7.10 Summary of respective gene expression characteristics for osteogenesis in HFBCs isolated from 8 wpc human foetal femurs treated with basal medium, osteogenic background medium (oBG, 10 nM dexamethasone, 10 nM 1,25-$(OH)_2$-vitamin D_3 and 100 µM ascorbic-2-phosphate) and osteo background (oBG) medium supplemented with small molecules SAG (smoothened agonist) and TH (4-(4-methoxyphenyl)pyrido[4′,3′:4,5]thieno[2,3-b]pyridine-2-carboxamide). Gene expression was normalised to *RN18S* (subunit of 18S ribosomal RNA) at day 0. Osteogenic differentiation was performed three times (n = 3). Individual values as well as mean of three individual experiments (in bold) are displayed. HFBCs: human foetal bone cells; RUNX2: runt-related transcription factor 2; ALPL: alkaline phosphatase; COL1A1: collagen type I; OCN: osteocalcin; OPN: osteopontin.

	condition	***RUNX2***	***ALPL***	***COL1A1***	***OCN***	***OPN***
Day 7	basal	0.09 0.05 0.03 **0.06**	0.23 0.05 0.30 **0.19**	0.13 0.11 0.30 **0.18**	0.61 0.33 0.36 **0.43**	0.12 0.00 0.00 **0.04**
	oBG	0.03 0.10 0.06 **0.06**	3.04 1.67 1.47 **2.06**	0.23 0.05 0.14 **0.14**	1.02 1.06 0.58 **0.89**	0.10 0.00 0.00 **0.03**
	oBG + TH + SAG	0.03 0.21 0.07 **0.10**	2.76 1.47 1.59 **1.94**	0.293 0.08 0.23 **0.20**	0.81 0.34 0.58 **0.57**	3.39 0.00 0.00 **1.13**
Day 19	basal	0.03 0.60 0.32 **0.32**	0.42 0.54 0.20 **0.39**	0.22 0.30 0.35 **0.29**	1.21 0.84 0.33 **0.79**	0.12 0.00 0.00 **0.04**
	oBG	0.04 0.55 0.07 **0.22**	3.15 1.98 1.32 **2.15**	0.07 0.06 0.06 **0.06**	0.62 0.57 0.30 **0.50**	2.46 0.00 0.00 **0.82**

	condition	*RUNX2*	*ALPL*	*COL1A1*	*OCN*	*OPN*
	oBG + TH + SAG	1.14 2.62 0.19 **1.31**	2.47 10.44 2.20 **5.03**	0.16 0.70 0.30 **0.39**	0.49 1.18 1.00 **0.87**	3.29 0.00 0.00 1.10

Expression of **chondrogenic genes** (*COL2A1, ACAN*) during osteogenic differentiation of HFBCs isolated from 8 wpc human foetal femurs displayed in Table 7.11 with mean of the three differentiation experiments (bold) displayed as well as the gene expression of the individual differentiation experiments.

Table 7.11 Summary of respective gene expression characteristic for chondrogenesis in HFBCs isolated from 8 wpc human foetal femurs treated with basal medium, osteogenic background medium (oBG, 10 nM dexamethasone, 10 nM 1,25-$(OH)_2$-vitamin D_3 and 100 µM ascorbic-2-phosphate) and osteo background (oBG) medium supplemented with small molecules SAG (smoothened agonist) and TH (4-(4-methoxyphenyl)pyrido[4′,3′:4,5]thieno[2,3-b]pyridine-2-carboxamide). Gene expression was normalised to *RN18S* (subunit of 18S ribosomal RNA) at day 0. Osteogenic differentiation was performed three times (n = 3). Individual values as well as mean of three individual experiments (in bold) are displayed. HFBCs: human foetal bone cells; COL2A1: collagen type II; ACAN: aggrecan.

	condition	*COL2A1*	*ACAN*
Day 7	basal	0.00 0.56 0.00 **0.1**	0.42 0.26 0.33 **0.34**
	oBG	0.00 0.00 0.00 **0.00**	0.27 0.05 0.32 **0.21**
	oBG + TH + SAG	0.00 0.00 0.00 **0.00**	0.34 0.07 0.33 **0.25**
Day 19	basal	3.29 0.00 0.00 **1.10**	0.02 0.92 0.42 **0.45**
	oBG	0.00 0.00 0.00	0.53 0.13 0.21

	condition	*COL2A1*	*ACAN*
		0.00	**0.29**
	oBG + TH + SAG	0.00 0.01 0.00 **0.00**	0.16 0.18 0.32 **0.22**

Appendix K Osteogenic differentiation of HFBCs isolated from 14 wpc human foetal femurs

Expression of **osteogenic genes** (*RUNX2*, *ALPL*, *COL1A1*, *OCN*, *OPN*) during osteogenic differentiation of HFBCs isolated from 14 wpc human foetal femurs displayed in Table 7.12 with mean of the three differentiation experiments (bold) displayed as well as the gene expression of the individual differentiation experiments.

Table 7.12 Summary of respective gene expression characteristic for osteogenesis in HFBCs isolated from 14 wpc human foetal femur samples treated with basal medium, osteogenic background medium (oBG, 10 nM dexamethasone, 10 nM 1,25-$(OH)_2$-vitamin D_3 and 100 µM ascorbic-2-phosphate) and osteo background (oBG) medium supplemented with small molecules SAG (smoothened agonist) and TH (4-(4-methoxyphenyl)pyrido[4′,3′:4,5]thieno[2,3-b]pyridine-2-carboxamide). Gene expression was normalised to *RN18S* (subunit of 18S ribosomal RNA) at day 0. Osteogenic differentiation was performed three times (n = 3). Individual values as well as mean of three individual experiments (in bold) are displayed. HFBCs: human foetal bone cells; RUNX2: runt-related transcription factor 2; ALPL: alkaline phosphatase; COL1A1: collagen type I; OCN: osteocalcin; OPN: osteopontin.

	condition	*RUNX2*	*ALPL*	*COL1A1*	*OCN*	*OPN*
Day 7	basal	0.91	1.03	0.51	0.69	0.00
		0.79	0.78	0.72	1.04	0.47
		0.62	0.69	0.34	0.78	0.00
		0.77	**0.83**	**0.52**	**0.84**	**0.16**
	oBG	0.80	0.84	0.33	1.04	0.00
		0.95	3.10	0.81	1.14	0.37
		0.53	2.53	0.50	0.86	0.00
		0.76	**2.15**	**0.55**	**1.01**	**0.12**
	oBG + TH + SAG	0.70	1.35	0.31	0.56	0.00
		1.17	4.76	0.90	0.83	0.40
		0.74	5.02	0.60	1.14	0.00
		0.87	**3.71**	**0.60**	**0.84**	**0.13**
Day 19	basal	0.42	0.39	0.11	0.48	0.00
		0.91	0.41	0.51	1.30	0.3
		0.86	0.29	0.50	0.72	0.00
		0.73	**0.36**	**0.38**	**0.83**	**0.11**
	oBG	0.27	0.47	0.04	0.37	0.00
		0.74	0.57	0.11	0.88	0.93
		1.60	2.28	0.27	1.52	0.00
		0.87	**1.10**	**0.14**	**0.92**	**0.31**

	condition	*RUNX2*	*ALPL*	*COL1A1*	*OCN*	*OPN*
	oBG + TH + SAG	0.37 0.92 2.75 **1.35**	0.18 3.34 4.20 **2.57**	0.03 0.36 0.44 **0.28**	0.39 0.63 1.66 **0.89**	0.00 1.41 0.00 **0.47**

Expression of **chondrogenic genes** (*COL2A1*, *ACAN*) during osteogenic differentiation of HFBCs isolated from 14 wpc human foetal femur displayed in Table 7.13 with mean of the three differentiation experiments (bold) displayed as well as the gene expression of the individual differentiation experiments.

Table 7.13 Summary of respective gene expression characteristic for chondrogenesis in HFBCs isolated from 14 wpc human foetal femur samples treated with basal medium, osteogenic background medium (oBG, 10 nM dexamethasone, 10 nM 1,25-$(OH)_2$-vitamin D_3 and 100 µM ascorbic-2-phosphate) and osteo background (oBG) medium supplemented with small molecules SAG (smoothened agonist) and TH (4-(4-methoxyphenyl)pyrido[4′,3′:4,5]thieno[2,3-b]pyridine-2-carboxamide). Gene expression was normalised to *RN18S* (subunit of 18S ribosomal RNA) at day 0. Osteogenic differentiation was performed three times (n = 3). Individual values as well as mean of three individual experiments (in bold) are displayed. HFBCs: human foetal bone cells; COL2A1: collagen type II; ACAN: aggrecan.

	condition	*COL2A1*	*ACAN*
Day 7	basal	0.04 0.91 0.05 **0.33**	0.34 0.74 0.25 **0.44**
	oBG	0.01 0.05 0.01 **0.02**	0.22 0.18 0.15 **0.18**
	oBG + TH + SAG	0.05 0.08 0.00 **0.04**	0.12 0.28 0.17 **0.19**
Day 19	basal	0.00 0.06 0.00 **0.02**	0.06 0.27 0.19 **0.18**
	oBG	0.00 0.00 0.00	0.03 0.10 0.19

	condition	*COL2A1*	*ACAN*
		0.00	**0.11**
	oBG + TH + SAG	0.00 0.00 0.00 **0.00**	0.03 0.20 0.31 **0.18**

Appendix L miRNA expression after osteogenic differentiation of NIBSC-8 MSCs

Expression of **miRNAs associated with chondrogenesis** (miR-140-3p, miR-146a, miR-146b, miR-34a), typically associated with chondrogenesis during osteogenic differentiation of NIBSC-8 MSCs are displayed in Table 7.14 with mean of the three differentiation experiments (bold) displayed as well as the gene expression of the individual differentiation experiments.

Table 7.14 Summary of respective microRNA expression characteristic for chondrogenesis in NIBSC-MSCs treated with basal medium, osteogenic background medium (oBG, 10 nM dexamethasone, 10 nM 1,25-$(OH)_2$-vitamin D_3 and 100 µM ascorbic-2-phosphate) and osteo background (oBG) medium supplemented with small molecules SAG (smoothened agonist) and TH (4-(4-methoxyphenyl)pyrido[4′,3′:4,5]thieno[2,3-b]pyridine-2-carboxamide). Gene expression was normalised to MammU6 at day 0. Osteogenic differentiation was performed three times (n = 3). Idividual values as well as mean of three individual experiments (in bold) are displayed.

condition	miR-140-3p	miR-146a	miR-146b	miR-34a
basal	0.92 0.48 0.97 **0.79**	1.01 1.18 2.36 **1.52**	0.93 1.35 3.47 **1.91**	0.71 1.01 2.29 **1.34**
oBG	1.13 0.27 0.20 **0.53**	1.49 0.30 0.70 **0.83**	1.23 0.25 1.01 **0.83**	0.66 0.18 0.73 **0.53**
oBG + TH + SAG	0.35 0.22 0.18 **0.25**	0.44 0.35 0.73 **0.51**	0.37 0.30 0.89 **0.52**	0.29 0.26 0.55 **0.37**

Expression of **miRNAs associated with osteogenesis** (miR-138, miR-20b, miR-23a, miR-148b, miR-29a, let7-f) during osteogenic differentiation of NIBSC-8 MSCs are displayed in Table 7.15 with mean of the three differentiation experiments (bold) displayed as well as the gene expression of the individual differentiation experiments.

Table 7.15 Summary of respective microRNA expression characteristic for chondrogenesis in NIBSC-MSCs treated with basal medium, osteogenic background medium (oBG, 10 nM dexamethasone, 10 nM 1,25-$(OH)_2$-vitamin D_3 and 100 µM ascorbic-2-phosphate) and osteo background (oBG) medium supplemented with small molecules SAG (smoothened agonist) and TH (4-(4-methoxyphenyl)pyrido[4′,3′:4,5]thieno[2,3-b]pyridine-2-carboxamide). Gene expression was nomralised to MammU6 at day 0. Osteogenic differentiaton was performed three times (n = 3). Individual values as well as mean of three individual experiments (in bold) are displayed.

condition	miR-138	miR-20b	miR-23a	miR-148b	miR-29a	let7f
basal	0.47	0.55	0.62	0.74	0.63	0.44
	0.38	0.30	0.42	0.57	1.17	0.69
	0.99	0.50	2.06	1.67	1.41	1.68
	0.61	**0.45**	**1.03**	**0.99**	**1.07**	**0.93**
oBG	1.19	0.37	1.87	1.26	1.01	1.07
	0.31	0.12	0.34	0.39	0.67	0.72
	0.74	0.15	0.85	0.78	0.56	0.81
	0.75	**0.21**	**1.02**	**0.81**	**0.75**	**0.87**
oBG + TH + SAG	0.56	0.13	0.51	0.66	0.24	0.37
	0.23	0.14	0.30	0.37	0.59	0.62
	0.46	0.13	0.49	0.46	0.34	0.86
	0.42	**0.13**	**0.43**	**0.50**	**0.39**	**0.62**

Appendix M miRNA expression after osteogenic differentiation of HFBCs isolated from 8 wpc human foetal femurs

Expression of **miRNAs associated with chondrogenesis** (miR-140-3p, miR-146a, miR-146b, miR-34a) during osteogenic differentiation of HFBCs isolated from 8 wpc human foetal femurs are displayed in Table 7.16 with mean of the three differentiation experiments (bold) displayed as well as the gene expression of the individual differentiation experiments.

Table 7.16 Summary of respective microRNA expression characteristic for chondrogenesis in HFBCs isolated from 8 wpc human foetal femurs treated with basal medium, osteogenic background medium (oBG, 10 nM dexamethasone, 10 nM 1,25-$(OH)_2$-vitamin D_3 and 100 µM ascorbic-2-phosphate) and oBG supplemented with small molecules SAG (smoothened agonist) and TH (4-(4-methoxyphenyl)pyrido[4′,3′:4,5]thieno[2,3-b]pyridine-2-carboxamide). Gene expression was normalised to MammU6 at day 0. Osteogenic differentiation was performed three times (n = 3). Individual values as well as mean of three individual experiments (in bold) are displayed. HFBCs: human foetal bone cells.

condition	miR-140-3p	miR-146a	miR-146b	miR-34a
basal	2.42 0.19 0.11 **0.91**	1.63 66.81 0.41 **22.95**	0.63 18.97 0.23 **6.61**	1.35 0.94 0.35 **0.88**
oBG	0.18 0.05 0.02 **0.08**	17.34 3.51 0.24 **7.03**	4.38 1.29 0.12 **1.93**	3.53 0.23 0.16 **1.31**
oBG + TH + SAG	0.10 0.01 0.12 **0.07**	0.39 0.41 0.63 **0.48**	1.43 0.13 0.174 **0.58**	1.49 0.04 0.56 **0.10**

Expression of **miRNAs associated with osteogenesis** (miR-138, miR-20b, miR-23a, miR-148b, miR-29a, let7-f) during osteogenic differentiation of HFBCs isolated from 8 wpc human foetal femurs are displayed in Table 7.17 with mean of the three differentiation experiments (bold) displayed as well as the gene expression of the individual differentiation experiments.

Table 7.17 Summary of respective microRNA expression characteristic for osteogenesis in HFBCs isolated from 8 wpc human foetal femurs treated with basal medium, osteogenic background medium (oBG, 10 nM dexamethasone, 10 nM 1,25-$(OH)_2$-vitamin D_3 and 100 µM ascorbic-2-phosphate) and oBG supplemented with small molecules SAG (smoothened agonist) and TH (4-(4-methoxyphenyl)pyrido[4′,3′:4,5]thieno[2,3-b]pyridine-2-carboxamide). Gene expression was normalised to MammU6 at day 0. Osteogenic differentiation was performed three times (n = 3). Individual values as well as mean of three individual experiments (in bold) are displayed. HFBCs: human foetal bone cells.

condition	miR-138	miR-20b	miR-23a	miR-148b	miR-29a	let7f
basal	0.41	0.74	1.42	0.78	1.91	1.57
	0.04	0.04	0.16	0.07	0.11	0.44
	0.05	0.03	0.30	0.24	3.28	0.17
	0.17	**0.27**	**0.63**	**0.37**	**1.77**	**0.72**
oBG	0.14	0.2	0.49	0.43	0.82	1.29
	0.02	0.05	0.07	0.04	0.82	2.37
	0.02	0.06	0.07	0.11	0.08	0.16
	0.06	**0.11**	**0.21**	**0.19**	**0.57**	**1.27**
oBG + TH + SAG	0.07	0.08	0.09	0.14	0.14	0.33
	0.001	0.01	0.01	0.001	0.16	0.75
	0.06	0.13	0.12	0.22	0.47	0.51
	0.05	**0.07**	**0.08**	**0.12**	**0.26**	**0.53**

Appendix N miRNA expression after osteogenic differentiation of HFBCs isolated from 14 wpc human foetal femurs

Expression of **miRNAs associated with chondrogenesis** (miR-140-3p, miR-146a, miR-146b, miR-34a) during osteogenic differentiation of HFBCs isolated from 14 wpc human foetal femurs are displayed in Table 7.18 with mean of the three differentiation experiments (bold) displayed as well as the gene expression of the individual differentiation experiments.

Table 7.18 Summary of respective microRNA expression characteristic for chondrogenesis in HFBCs isolated from 8 wpc human foetal femurs treated with basal medium, osteogenic background medium (oBG, 10 nM dexamethasone, 10 nM 1,25-$(OH)_2$-vitamin D_3 and 100 µM ascorbic-2-phosphate) and oBG supplemented with small molecules SAG (smoothened agonist) and TH (4-(4-methoxyphenyl)pyrido[4′,3′:4,5]thieno[2,3-b]pyridine-2-carboxamide). Gene expression was normalised to MammU6 at day 0. Osteogenic differentiation was performed three times (n = 3). Individual values as well as mean of three individual experiments (in bold) are displayed. HFBCs: human foetal bone cells.

condition	miR-140-3p	miR-146a	miR-146b	miR-34a
basal	0.14 0.81 0.14 **0.37**	0.52 0.82 0.52 **0.62**	0.44 1.32 0.44 **0.73**	0.44 1.24 0.65 **0.78**
oBG	0.09 0.13 0.20 **0.14**	0.53 0.13 120 **0.62**	0.93 1.70 0.35 **0.99**	0.67 1.46 1.50 **1.21**
oBG + TH + SAG	0.14 0.04 0.66 **0.28**	0.94 0.04 3.27 **1.41**	0.34 0.17 1.94 **0.82**	1.13 0.60 6.32 **2.69**

Expression of **miRNAs associated with osteogenesis** (miR-138, miR-20b, miR-23a, miR-148b, miR-29a, let7-f) during osteogenic differentiation of HFBCs isolated from 14 wpc human foetal femurs are displayed in Table 7.19 with mean of the three differentiation experiments (bold) displayed as well as the gene expression of the individual differentiation experiments.

Table 7.19 Summary of respective microRNA expression characteristic for osteogenesis in HFBCs isolated from 14 wpc human foetal femurs treated with basal medium, osteogenic background medium (oBG, 10 nM dexamethasone, 10 nM 1,25-$(OH)_2$-vitamin D_3 and 100 µM ascorbic-2-phosphate) and oBG supplemented with small molecules SAG (smoothened agonist) and TH (4-(4-methoxyphenyl)pyrido[4′,3′:4,5]thieno[2,3-b]pyridine-2-carboxamide). Gene expression was normalised to MammU6 at day 0. Osteogenic differentiation was performed three times (n = 3). Individual values as well as mean of three individual experiments (in bold) are displayed. HFBCs: human foetal bone cells.

condition	miR-138	miR-20b	miR-23a	miR-148b	miR-29a	let7f
basal	0.53	0.65	1.04	0.79	0.54	0.97
	0.38	0.28	0.74	0.49	0.74	1.26
	0.04	0.05	0.17	0.14	0.11	0.18
	0.31	**0.33**	**0.65**	**0.47**	**0.47**	**0.80**
oBG	0.16	0.20	0.27	0.30	0.20	0.41
	0.30	0.25	0.38	0.47	0.43	0.93
	0.09	0.16	0.35	0.35	0.31	0.57
	0.18	**0.20**	**0.33**	**0.37**	**0.31**	**0.64**
oBG + TH + SAG	0.09	0.16	0.22	0.67	0.41	0.50
	0.10	0.11	0.13	0.13	0.12	0.19
	1.31	0.00	2.49	3.29	2.69	5.26
	0.50	**0.09**	**0.95**	**1.36**	**1.07**	**1.99**

Bibliography

1. Hernlund, E., et al., *Osteoporosis in the European Union: medical management, epidemiology and economic burden: A report prepared in collaboration with the International Osteoporosis Foundation (IOF) and the European Federation of Pharmaceutical Industry Associations (EFPIA).* Archives of Osteoporosis, 2013. **8**(1-2): p. 136.

2. Flegal, K.M., et al., *Prevalence of obesity and trends in the distribution of body mass index among us adults, 1999-2010.* Journal of the American Medical Association, 2012. **307**(5): p. 491-497.

3. Cooper, C., G. Campion, and L.J. Melton, *Hip fractures in the elderly: A world-wide projection.* Osteoporosis International, 1992. **2**(6): p. 285-289.

4. Holroyd, C., C. Cooper, and E. Dennison, *Epidemiology of osteoporosis.* Best Practice & Research Clinical Endocrinology & Metabolism, 2008. **22**(5): p. 671-685.

5. Popkin, B.M., L.S. Adair, and S.W. Ng, *NOW AND THEN: The Global Nutrition Transition: The Pandemic of Obesity in Developing Countries.* Nutrition Reviews, 2012. **70**(1): p. 3-21.

6. Kastorini, C.-M., et al., *Adherence to the Mediterranean diet in relation to acute coronary syndrome or stroke nonfatal events: A comparative analysis of a case/case-control study.* American Heart Journal, 2011. **162**(4): p. 717-724.

7. Stunkard, A.J., T.T. Foch, and Z. Hrubec, *A twin study of human obesity.* Journal of the Amercian Medical Association, 1986. **256**(1): p. 51-54.

8. Gluckman, P.D., et al., *Losing the War Against Obesity: The Need for a Developmental Perspective.* Science Translational Medicine, 2011. **3**(93): p. 93cm19.

9. Silva, H.G.V.d., et al., *Influence of obesity on bone density in postmenopausal women.* Arquivos Brasileiros de Endocrinologia & Metabologia, 2007. **51**: p. 943-949.

10. Compston, J.E., et al., *Obesity is Not Protective Against Fracture in Postmenopausal Women: GLOW.* The American Journal of Medicine, 2011. **124**(11): p. 1043-1050.

11. Kawai, M. and C.J. Rosen, *Insulin-like growth factor-I and bone: lessons from mice and men.* Pediatric Nephrology, 2009. **24**(7): p. 1277-1285.

12. Akune, T., et al., *PPARγ insufficiency enhances osteogenesis through osteoblast formation from bone marrow progenitors.* The Journal of Clinical Investigation, 2004. **113**(6): p. 846-855.

13. Rosen, C.J. and M.L. Bouxsein, *Mechanisms of Disease: is osteoporosis the obesity of bone?* Nature Clinical Practice Rheumatology, 2006. **2**(1): p. 35-43.

14. Ishimi, Y., *Osteoporosis and Lifestyle.* Journal of Nutritional Science and Vitaminology, 2015. **61**(Supplement): p. S139-S141.

15. Riggs, B.L., *The mechanisms of estrogen regulation of bone resorption.* Journal of Clinical Investigation, 2000. **106**(10): p. 1203-1204.

16. Cawthon, P.M., *Gender Differences in Osteoporosis and Fractures.* Clinical Orthopaedics and Related Research, 2011. **469**(7): p. 1900-1905.

17. McGee, M.A., et al., *Implant retrieval studies of the wear and loosening of prosthetic joints: a review.* Wear, 2000. **241**(2): p. 158-165.

18. Pittenger, M.F., et al., *Multilineage potential of adult human mesenchymal stem cells.* Science, 1999. **284**(5411): p. 143-7.

19. Jiang, Y., et al., *Pluripotency of mesenchymal stem cells derived from adult marrow.* Nature, 2002. **418**(6893): p. 41-49.

20. Oreffo, R.O.C., S. Bord, and J.T. Triffitt, *Skeletal Progenitor Cells and Ageing Human Populations.* Clinical Science, 1998. **94**(5): p. 549.

21. Leitch, Harry G., et al., *Rebuilding Pluripotency from Primordial Germ Cells.* Stem Cell Reports, 2013. **1**(1): p. 66-78.

22. Jiang, W., et al., *WNT3 Is a Biomarker Capable of Predicting the Definitive Endoderm Differentiation Potential of hESCs.* Stem Cell Reports, 2013. **1**(1): p. 46-52.

23. Klingenstein, M., et al., *TBX3 Knockdown Decreases Reprogramming Efficiency of Human Cells.* Stem Cells International, 2016. **2016**: p. 6759343.

24. Maehr, R., et al., *Generation of pluripotent stem cells from patients with type 1 diabetes.* Proceedings of the National Academy of Sciences of the United States of America, 2009. **106**(37): p. 15768-15773.

25. Rashid, S.T., et al., *Modeling inherited metabolic disorders of the liver using human induced pluripotent stem cells.* The Journal of Clinical Investigation, 2010. **120**(9): p. 3127-3136.

26. Brennand, K., et al., *Modeling schizophrenia using hiPSC neurons.* Nature, 2011. **473**(7346): p. 221-225.

27. Yang, Y.M., et al., *A Small Molecule Screen in Stem Cell-derived Motor Neurons Identifies a Kinase Inhibitor as a Candidate Therapeutic for ALS.* Cell Stem Cell, 2013. **12**(6): p. 713-726.

28. Hannan, Nicholas R., et al., *Generation of Multipotent Foregut Stem Cells from Human Pluripotent Stem Cells.* Stem Cell Reports, 2013. **1**(4): p. 293-306.

29. Neofytou, E., et al., *Hurdles to clinical translation of human induced pluripotent stem cells.* The Journal of Clinical Investigation, 2015. **125**(7): p. 2551-2557.

30. Mandai, M., et al., *Autologous Induced Stem-Cell–Derived Retinal Cells for Macular Degeneration.* New England Journal of Medicine, 2017. **376**(11): p. 1038-1046.

31. Taylor, C.J., E.M. Bolton, and J.A. Bradley, *Immunological considerations for embryonic and induced pluripotent stem cell banking.* Philosophical Transactions of the Royal Society B: Biological Sciences, 2011. **366**(1575): p. 2312-2322.

32. Sadler, T.W. and J. Langman, Medical mebryology, *Langman's medical embryology*. Vol. 12. 2012: Philadelphia: Wolters Kluwer Health/Lippincott Williams & Wilkins, c2012.

33. Buck, D.W.I. and G.A. Dumanian, *Bone Biology and Physiology: Part I. The Fundamentals.* Plastic and Reconstructive Surgery, 2012. **129**(6): p. 1314-1320.

34. Hanna, J.H., K. Saha, and R. Jaenisch, *Somatic cell reprogramming and transitions between pluripotent states: facts, hypotheses, unresolved issues.* Cell, 2010. **143**(4): p. 508-525.

35. Nichols, J. and A. Smith, *The origin and identity of embryonic stem cells.* Development, 2010. **138**(1): p. 3-8.

36. Condic, M.L., *Totipotency: What It Is and What It Is Not.* Stem Cells and Development, 2014. **23**(8): p. 796-812.

37. Paul, S. and J.G. Knott, *Epigenetic control of cell-fate in mouse blastocysts: role of covalent histone modifications and chromatin remodeling.* Molecular reproduction and development, 2014. **81**(2): p. 171-182.

38. Shyamala, K., et al., *Neural crest: The fourth germ layer.* Journal of Oral and Maxillofacial Pathology : JOMFP, 2015. **19**(2): p. 221-229.

39. Hall, B.K., *The neural crest as a fourth germ layer and vertebrates as quadroblastic not triploblastic.* Evolution & Development, 2000. **2**(1): p. 3-5.

40. Hall, B.K., *The neural crest and neural crest cells: discovery and significance for theories of embryonic organization.* Journal of Biosciences, 2008. **33**(5): p. 781.

41. Barham, G. and N.M.P. Clarke, *Genetic Regulation of Embryological Limb Development with Relation to Congenital Limb Deformity in Humans.* Journal of Children's Orthopaedics, 2008. **2**(1): p. 1-9.

42. Vogel, A., C. Rodriguez, and J.C. Izpisua-Belmonte, *Involvement of FGF-8 in initiation, outgrowth and patterning of the vertebrate limb.* Development, 1996. **122**(6): p. 1737.

43. Egawa, S., et al., *Growth and differentiation of a long bone in limb development, repair and regeneration.* Development, Growth & Differentiation, 2014. **56**(5): p. 410-424.

44. Widelitz, R.B., et al., *Adhesion molecules in skeletogenesis: II. Neural cell adhesion molecules mediate precartilaginous mesenchymal condensations and enhance chondrogenesis.* Journal of Cellular Physiology, 1993. **156**(2): p. 399-411.

45. Oberlender, S.A. and R.S. Tuan, *Expression and functional involvement of N-cadherin in embryonic limb chondrogenesis.* Development, 1994. **120**(1): p. 177.

46. Haas, A.R. and R.S. Tuan, *Chondrogenic differentiation of murine C3H10T1/2 multipotential mesenchymal cells: II. Stimulation by bone morphogenetic protein-2 requires modulation of N-cadherin expression and function.* Differentiation, 1999. **64**(2): p. 77-89.

47. DeLise, A.M., L. Fischer, and R.S. Tuan, *Cellular interactions and signaling in cartilage development.* Osteoarthritis and Cartilage, 2000. **8**(5): p. 309-334.

48. Toole, B.P., G. Jackson, and J. Gross, *Hyaluronate in morphogenesis: inhibition of chondrogenesis in vitro.* Proceedings of the National Academy of Sciences of the United States of America, 1972. **69**(6): p. 1384-1386.

49. Kosher, R.A., M.P. Savage, and K.H. Walker, *A gradation of hyaluronate accumulation along the proximodistal axis of the embryonic chick limb bud.* Journal of Embryology and Experimental Morphology, 1981. **63**(1): p. 85.

50. Knudson, C.B. and B.P. Toole, *Changes in the pericellular matrix during differentiation of limb bud mesoderm.* Developmental Biology, 1985. **112**(2): p. 308-318.

51. Li, Y., et al., *Hyaluronan in limb morphogenesis.* Developmental Biology, 2007. **305**(2): p. 411-420.

52. Swalla, B.J. and M. Solursh, *Inhibition of limb chondrogenesis by fibronectin.* Differentiation, 1984. **26**(1): p. 42-48.

53. Zanetti, N.C., V.M. Dress, and M. Solursh, *Comparison between ectoderm-conditioned medium and fibronectin in their effects on chondrogenesis by limb bud mesenchymal cells.* Developmental Biology, 1990. **139**(2): p. 383-395.

54. Gehris, A.L., et al., *The Region Encoded by the Alternatively Spliced Exon IIIA in Mesenchymal Fibronectin Appears Essential for Chondrogenesis at the Level of Cellular Condensation.* Developmental Biology, 1997. **190**(2): p. 191-205.

55. Mallein-Gerin, F., et al., *Temporal and spatial analysis of cartilage proteoglycan core protein gene expression during limb development by in situ hybridization.* Developmental Biology, 1988. **126**(2): p. 337-345.

56. Imamura, Y., I.C. Scott, and D.S. Greenspan, *The Pro-α3(V) Collagen Chain: Complete primary structure, expression domains in adult and developing tissues, and comparison to the structures and expression domains of the other types V and XI procollagen chains.* Journal of Biological Chemistry, 2000. **275**(12): p. 8749-8759.

57. Elefteriou, F., et al., *Leptin regulation of bone resorption by the sympathetic nervous system and CART.* Nature, 2005. **434**(7032): p. 514-520.

58. Smits, P., et al., *Sox5 and Sox6 are needed to develop and maintain source, columnar, and hypertrophic chondrocytes in the cartilage growth plate.* The Journal of Cell Biology, 2004. **164**(5): p. 747-758.

59. Gwatkin, R., *Developmental biology by Scott F. Gilbert, Sinauer Associates, Inc., Sunderland, MA, 4th ed., 1994, 894 pp, $57.95.* Molecular Reproduction and Development, 1995. **41**(3): p. 398-398.

60. Erlebacher, A., et al., *Toward a molecular understanding of skeletal development.* Cell, 1995. **80**(3): p. 371-378.

61. Montjovent, M.-O., et al., *Fetal bone cells for tissue engineering.* Bone, 2004. **35**(6): p. 1323-1333.

62. Mirmalek-Sani, S.-H., et al., *Characterization and Multipotentiality of Human Fetal Femur–Derived Cells: Implications for Skeletal Tissue Regeneration.* Stem Cells, 2006. **24**(4): p. 1042-1053.

63. Gothard, D., et al., *Regionally-derived cell populations and skeletal stem cells from human foetal femora exhibit specific osteochondral and multi-lineage differentiation capacity in vitro and ex vivo.* Stem Cell Research & Therapy, 2015. **6**: p. 251-251.

64. Chan, C.K.F., et al., *Identification of the Human Skeletal Stem Cell.* Cell, 2018. **175**(1): p. 43-56.e21.

65. Lange, A., et al., *Marrow Cells Cultured in MSC Medium Expand to CD73, CD90 and CD105 Cells of Fibroblast-Like Morphology.* Blood, 2005. **106**(11): p. 4319-4319.

66. Lv, F.-J., et al., *Concise Review: The Surface Markers and Identity of Human Mesenchymal Stem Cells.* Stem Cells, 2014. **32**(6): p. 1408-1419.

67. Quirici, N., et al., *Isolation of bone marrow mesenchymal stem cells by anti-nerve growth factor receptor antibodies.* Experimental Hematology, 2002. **30**(7): p. 783-791.

68. Sorrentino, A., et al., *Isolation and characterization of CD146+ multipotent mesenchymal stromal cells.* Experimental Hematology, 2008. **36**(8): p. 1035-1046.

69. Buck, D.W., II and G.A. Dumanian, *Bone Biology and Physiology: Part II. Clinical Correlates.* Plastic and Reconstructive Surgery, 2012. **129**(6).

70. Clarke, B., *Normal Bone Anatomy and Physiology.* Clinical Journal of the American Society of Nephrology : Clinical Journal of the American Society of Nephrology, 2008. **3**(Suppl 3): p. S131-S139.

71. Rucci, N., *Molecular biology of bone remodelling.* Clinical Cases in Mineral and Bone Metabolism, 2008. **5**(1): p. 49-56.

72. Gupta, S., et al., *Osteoporosis and Multiple Sclerosis: Risk Factors, Pathophysiology, and Therapeutic Interventions.* CNS Drugs, 2014. **28**(8): p. 731-742.

73. Sims, N.A. and T.J. Martin, *Coupling the activities of bone formation and resorption: a multitude of signals within the basic multicellular unit.* BoneKEy Reports, 2014. **3**.

74. Bianco, P., *Minireview: The Stem Cell Next Door: Skeletal and Hematopoietic Stem Cell "Niches" in Bone.* Endocrinology, 2011. **152**(8): p. 2957-2962.

75. Bianco, P., P.G. Robey, and P.J. Simmons, *Mesenchymal stem cells: revisiting history, concepts, and assays.* Cell Stem Cell, 2008. **2**(4): p. 313-9.

76. Caplan, A.I., *Mesenchymal stem cells.* Journal of Orthopaedic Research, 1991. **9**(5): p. 641-650.

77. Dominici, M., et al., *Minimal criteria for defining multipotent mesenchymal stromal cells. The International Society for Cellular Therapy position statement.* Cytotherapy, 2006. **8**(4): p. 315-7.

78. Sacchetti, B., et al., *No Identical "Mesenchymal Stem Cells" at Different Times and Sites: Human Committed Progenitors of Distinct Origin and Differentiation Potential Are Incorporated as Adventitial Cells in Microvessels.* Stem Cell Reports, 2016. **6**(6): p. 897-913.

79. Mosher, J.T., et al., *Lack of Population Diversity in Commonly Used Human Embryonic Stem-Cell Lines.* New England Journal of Medicine, 2010. **362**(2): p. 183-185.

80. Swijnenburg, R.-J., et al., *In Vivo Imaging of Embryonic Stem Cells Reveals Patterns of Survival and Immune Rejection Following Transplantation.* Stem Cells and Development, 2008. **17**(6): p. 1023-1029.

81. Gurdon, J.B. and I. Wilmut, *Nuclear Transfer to Eggs and Oocytes.* Cold Spring Harbor Perspectives in Biology, 2011. **3**(6): p. a002659.

82. Gurdon, J.B., *The transplantation of nuclei between two species of Xenopus.* Developmental Biology, 1962. **5**(1): p. 68-83.

83. Matsumura, H. and T. Tada, *Cell fusion-mediated nuclear reprogramming of somatic cells.* Reproductive BioMedicine Online, 2008. **16**(1): p. 51-56.

84. Takahashi, K., et al., *Induction of Pluripotent Stem Cells from Adult Human Fibroblasts by Defined Factors.* Cell, 2007. **131**(5): p. 861-872.

85. Bhattacharya, S., Q. Zhang, and M.E. Andersen, *A deterministic map of Waddington's epigenetic landscape for cell fate specification.* BioMed Central Systems Biology, 2011. **5**: p. 85-85.

86. Nichols, J., et al., *Formation of Pluripotent Stem Cells in the Mammalian Embryo Depends on the POU Transcription Factor Oct4.* Cell, 1998. **95**(3): p. 379-391.

87. Chambers, I., et al., *Functional Expression Cloning of Nanog, a Pluripotency Sustaining Factor in Embryonic Stem Cells.* Cell, 2003. **113**(5): p. 643-655.

88. Takahashi, K. and S. Yamanaka, *Induction of Pluripotent Stem Cells from Mouse Embryonic and Adult Fibroblast Cultures by Defined Factors.* Cell, 2006. **126**(4): p. 663-676.

89. Cartwright, P., et al., *LIF/STAT3 controls ES cell self-renewal and pluripotency by a Myc-dependent mechanism.* Development, 2005. **132**(5): p. 885-896.

90. Matsuda, T., et al., *STAT3 activation is sufficient to maintain an undifferentiated state of mouse embryonic stem cells.* The European Medical Biology Organisation Journal, 1999. **18**(15): p. 4261-4269.

91. Mitsui, K., et al., *The Homeoprotein Nanog Is Required for Maintenance of Pluripotency in Mouse Epiblast and ES Cells.* Cell, 2003. **113**(5): p. 631-642.

92. Li, R., et al., *A Mesenchymal-to-Epithelial Transition Initiates and Is Required for the Nuclear Reprogramming of Mouse Fibroblasts.* Cell Stem Cell. **7**(1): p. 51-63.

93. Yu, J., et al., *Induced pluripotent stem cell lines derived from human somatic cells.* Science, 2007. **318**(5858): p. 1917-20.

94. Stadtfeld, M., K. Brennand, and K. Hochedlinger, *Reprogramming of Pancreatic β Cells into Induced Pluripotent Stem Cells.* Current Biology, 2008. **18**(12): p. 890-894.

95. Kim, J.B., et al., *Pluripotent stem cells induced from adult neural stem cells by reprogramming with two factors.* Nature, 2008. **454**(7204): p. 646-650.

96. Hanna, J., et al., *Direct Reprogramming of Terminally Differentiated Mature B Lymphocytes to Pluripotency.* Cell, 2008. **133**(2): p. 250-264.

97. Guo, C.-W., et al., *Culture under low physiological oxygen conditions improves the stemness and quality of induced pluripotent stem cells.* Journal of Cellular Physiology, 2013. **228**(11): p. 2159-2166.

98. Malik, N. and M.S. Rao, *A Review of the Methods for Human iPSC Derivation.* Methods in Molecular Biology, 2013. **997**: p. 23-33.

99. Kawamura, T., et al., *Linking the p53 tumor suppressor pathway to somatic cell reprogramming.* Nature, 2009. **460**(7259): p. 1140-1144.

100. Ebrahimi, B., *Reprogramming barriers and enhancers: strategies to enhance the efficiency and kinetics of induced pluripotency.* Cell Regeneration, 2015. **4**: p. 10.

101. Vidal, S.E., et al., *Combinatorial modulation of signaling pathways reveals cell-type-specific requirements for highly efficient and synchronous iPSC reprogramming.* Stem Cell Reports, 2014. **3**(4): p. 574-584.

102. Lluis, F., et al., *Periodic Activation of Wnt/β-Catenin Signaling Enhances Somatic Cell Reprogramming Mediated by Cell Fusion.* Cell Stem Cell, 2008. **3**(5): p. 493-507.

103. Zhang, P., et al., *Regulation of induced pluripotent stem (iPS) cell induction by Wnt/β-catenin signaling.* The Journal of Biological Chemistry, 2014. **289**(13): p. 9221-9232.

104. Guo, S., et al., *Nonstochastic reprogramming from a privileged somatic cell state.* Cell, 2014. **156**(4): p. 649-662.

105. Banito, A., et al., *Senescence impairs successful reprogramming to pluripotent stem cells.* Genes & Development, 2009. **23**(18): p. 2134-2139.

106. Bhutani, K., et al., *Whole-genome mutational burden analysis of three pluripotency induction methods.* Nature Communications, 2016. **7**: p. 10536.

107. Buganim, Y., D.A. Faddah, and R. Jaenisch, *Mechanisms and models of somatic cell reprogramming.* Nature Reviews Genetics, 2013. **14**(6): p. 427-439.

108. Saha, K. and R. Jaenisch, *Technical challenges in using human induced pluripotent stem cells to model disease.* Cell Stem Cell, 2009. **5**(6): p. 584-595.

109. Theunissen, T.W. and R. Jaenisch, *Molecular Control of Induced Pluripotency.* Cell Stem Cell, 2014. **14**(6): p. 720-734.

110. Guha, P., et al., *Lack of Immune Response to Differentiated Cells Derived from Syngeneic Induced Pluripotent Stem Cells.* Cell Stem Cell, 2013. **12**(4): p. 407-412.

111. Scheiner, Z.S., S. Talib, and E.G. Feigal, *The Potential for Immunogenicity of Autologous Induced Pluripotent Stem Cell-derived Therapies.* The Journal of Biological Chemistry, 2014. **289**(8): p. 4571-4577.

112. Hotta, A. and J. Ellis, *Retroviral vector silencing during iPS cell induction: An epigenetic beacon that signals distinct pluripotent states.* Journal of Cellular Biochemistry, 2008. **105**(4): p. 940-948.

113. Park, I.-H., et al., *Reprogramming of human somatic cells to pluripotency with defined factors.* Nature, 2008. **451**(7175): p. 141-146.

114. Stadtfeld, M., et al., *Induced pluripotent stem cells generated without viral integration.* Science, 2008. **322**(5903): p. 945-949.

115. Zhou, W. and C.R. Freed, *Adenoviral Gene Delivery Can Reprogram Human Fibroblasts to Induced Pluripotent Stem Cells.* Stem Cells, 2009. **27**(11): p. 2667-2674.

116. Seki, T., et al., *Generation of Induced Pluripotent Stem Cells from Human Terminally Differentiated Circulating T Cells.* Cell Stem Cell, 2010. **7**(1): p. 11-14.

117. Ban, H., et al., *Efficient generation of transgene-free human induced pluripotent stem cells (iPSCs) by temperature-sensitive Sendai virus vectors.* Proceedings of the National Academy of Sciences of the United States of America, 2011. **108**(34): p. 14234-14239.

118. Fusaki, N., et al., *Efficient induction of transgene-free human pluripotent stem cells using a vector based on Sendai virus, an RNA virus that does not integrate into the host genome.* Proceedings of the Japan Academy. Series B, Physical and Biological Sciences, 2009. **85**(8): p. 348-362.

119. Schlaeger, T.M., et al., *A comparison of non-integrating reprogramming methods.* Nature Biotechnology, 2015. **33**(1): p. 58-63.

120. Griesenbach, U., et al., *Assessment of F/HN-Pseudotyped Lentivirus as a Clinically Relevant Vector for Lung Gene Therapy.* American Journal of Respiratory and Critical Care Medicine, 2012. **186**(9): p. 846-856.

121. Hu, K., et al., *Efficient generation of transgene-free induced pluripotent stem cells from normal and neoplastic bone marrow and cord blood mononuclear cells.* Blood, 2011. **117**(14): p. e109-19.

122. Kim, D., et al., *Generation of Human Induced Pluripotent Stem Cells by Direct Delivery of Reprogramming Proteins.* Cell Stem Cell, 2009. **4**(6): p. 472-476.

123. Tavernier, G., et al., *Current Methods for Inducing Pluripotency in Somatic Cells.* Advanced Materials, 2013. **25**(20): p. 2765-2771.

124. Warren, L., et al., *Highly Efficient Reprogramming to Pluripotency and Directed Differentiation of Human Cells with Synthetic Modified mRNA.* Cell Stem Cell, 2010. **7**(5): p. 618-630.

125. Anokye-Danso, F., et al., *Highly efficient miRNA-mediated reprogramming of mouse and human somatic cells to pluripotency.* Cell Stem Cell, 2011. **8**(4): p. 376-388.

126. Ma, T., et al., *Progress in the Reprogramming of Somatic Cells.* Circulation Research, 2013. **112**(3): p. 562-574.

127. Zhu, S., et al., *Reprogramming of Human Primary Somatic Cells by OCT4 and Chemical Compounds.* Cell Stem Cell, 2010. **7**(6): p. 651-655.

128. Mikkelsen, T.S., et al., *Dissecting direct reprogramming through integrative genomic analysis.* Nature, 2008. **454**(7200): p. 49-55.

129. Huangfu, D., et al., *Induction of pluripotent stem cells by defined factors is greatly improved by small-molecule compounds.* Nature Biotechnology, 2008. **26**(7): p. 795-797.

130. Ichida, J.K., et al., *A Small-Molecule Inhibitor of Tgf-β Signaling Replaces Sox2 in Reprogramming by Inducing Nanog.* Cell Stem Cell, 2009. **5**(5): p. 491-503.

131. Esteban, M.A., et al., *Vitamin C Enhances the Generation of Mouse and Human Induced Pluripotent Stem Cells.* Cell Stem Cell, 2010. **6**(1): p. 71-79.

132. Xu, Y., et al., *Revealing a core signaling regulatory mechanism for pluripotent stem cell survival and self-renewal by small molecules.* Proceedings of the National Academy of Sciences of the United States of America, 2010. **107**(18): p. 8129-8134.

133. Wang, Y. and J. Adjaye, *A cyclic AMP analog, 8-Br-cAMP, enhances the induction of pluripotency in human fibroblast cells.* Stem Cell Reviews, 2011. **7**(2): p. 331-41.

134. Zhang, H., et al., *MLL1 Inhibition Reprograms Epiblast Stem Cells to Naive Pluripotency.* Cell Stem Cell, 2016. **18**(4): p. 481-484.

135. Maherali, N. and K. Hochedlinger, *Tgfβ Signal Inhibition Cooperates in the Induction of iPSCs and Replaces Sox2 and cMyc.* Current Biology, 2009. **19**(20): p. 1718-1723.

136. Chandra, A., et al., *Epidermal Growth Factor Receptor (EGFR) Signaling Promotes Proliferation and Survival in Osteoprogenitors by Increasing Early Growth Response 2 (EGR2) Expression.* The Journal of Biological Chemistry, 2013. **288**(28): p. 20488-20498.

137. Li, W., et al., *Generation of Human Induced Pluripotent Stem Cells in the Absence of Exogenous Sox2.* Stem Cells, 2009. **27**(12): p. 2992-3000.

138. Nichols, J. and A. Smith, *Naive and Primed Pluripotent States.* Cell Stem Cell, 2009. **4**(6): p. 487-492.

139. Evans, M.J. and M.H. Kaufman, *Establishment in culture of pluripotential cells from mouse embryos.* Nature, 1981. **292**(5819): p. 154-156.

140. Brons, I.G.M., et al., *Derivation of pluripotent epiblast stem cells from mammalian embryos.* Nature, 2007. **448**(7150): p. 191-195.

141. Tesar, P.J., et al., *New cell lines from mouse epiblast share defining features with human embryonic stem cells.* Nature, 2007. **448**(7150): p. 196-199.

142. Nichols, J. and A. Smith, *The origin and identity of embryonic stem cells.* Development, 2011. **138**(1): p. 3.

143. Theunissen, Thorold W., et al., *Systematic Identification of Culture Conditions for Induction and Maintenance of Naive Human Pluripotency.* Cell Stem Cell, 2014. **15**(4): p. 471-487.

144. Wu, G. and H.R. Schöler, *Role of Oct4 in the early embryo development.* Cell Regeneration, 2014. **3**(1): p. 7.

145. O'Leary, T., et al., *Tracking the progression of the human inner cell mass during embryonic stem cell derivation.* Nature Biotechnology, 2012. **30**(3): p. 278-282.

146. Chantzoura, E., et al., *Reprogramming Roadblocks Are System Dependent.* Stem Cell Reports, 2015. **5**(3): p. 350-364.

147. Kim, K., et al., *Epigenetic memory in induced pluripotent stem cells.* Nature, 2010. **467**(7313): p. 285-290.

148. Polo, J.M., et al., *Cell type of origin influences the molecular and functional properties of mouse induced pluripotent stem cells.* Nature Biotechnology, 2010. **28**(8): p. 848-855.

149. Yamanaka, S., *Induced Pluripotent Stem Cells: Past, Present, and Future.* Cell Stem Cell. **10**(6): p. 678-684.

150. Kim, K., et al., *Donor cell type can influence the epigenome and differentiation potential of human induced pluripotent stem cells.* Nature Biotechnology, 2011. **29**(12): p. 1117-1119.

151. Fernandez, T.d.S., et al., *Human Induced Pluripotent Stem Cells from Basic Research to Potential Clinical Applications in Cancer.* BioMed Research International, 2013. **2013**: p. 11.

152. Pappas, J. and P. Yang, *Human ESC vs. iPSC—pros and cons.* Journal of Cardiovascular Translational Research, 2008. **1**: p. 96-99.

153. Medvedev, S.P., A.I. Shevchenko, and S.M. Zakian, *Induced Pluripotent Stem Cells: Problems and Advantages when Applying them in Regenerative Medicine.* Acta naturae, 2010. **2**(2): p. 18-28.

154. Guillot, P.V., et al., *Human First-Trimester Fetal MSC Express Pluripotency Markers and Grow Faster and Have Longer Telomeres Than Adult MSC.* Stem Cells, 2007. **25**(3): p. 646-654.

155. Minguell, J.J., A. Erices, and P. Conget, *Mesenchymal Stem Cells.* Experimental Biology and Medicine, 2001. **226**(6): p. 507-520.

156. Thomson, J.A., et al., *Embryonic Stem Cell Lines Derived from Human Blastocysts.* Science, 1998. **282**(5391): p. 1145.

157. Huang, Y., et al., *Telomere regulation in pluripotent stem cells.* Protein & Cell, 2014. **5**(3): p. 194-202.

158. Lian, Q., et al., *Functional Mesenchymal Stem Cells Derived From Human Induced Pluripotent Stem Cells Attenuate Limb Ischemia in Mice.* Circulation, 2010. **121**(9): p. 1113-1123.

159. Kang, R., et al., *Mesenchymal stem cells derived from human induced pluripotent stem cells retain adequate osteogenicity and chondrogenicity but less adipogenicity.* Stem Cell Research & Therapy, 2015. **6**(1): p. 144.

160. Huang, R.Y.-J., P. Guilford, and J.P. Thiery, *Early events in cell adhesion and polarity during epithelial-mesenchymal transition.* Journal of Cell Science, 2012. **125**(19): p. 4417.

161. Yilmaz, M. and G. Christofori, *EMT, the cytoskeleton, and cancer cell invasion.* Cancer and Metastasis Reviews, 2009. **28**(1): p. 15-33.

162. Niehrs, C., *The complex world of WNT receptor signalling.* Nature Reviews Molecular Cell Biology, 2012. **13**(12): p. 767-779.

163. Thiery, J.P. and J.P. Sleeman, *Complex networks orchestrate epithelial–mesenchymal transitions.* Nature Reviews Molecular Cell Biology, 2006. **7**: p. 131-142.

164. Yilmaz, M. and G. Christofori, *Mechanisms of Motility in Metastasizing Cells.* Molecular Cancer Research, 2010. **8**(5): p. 629.

165. Ridley, Anne J., *Life at the Leading Edge.* Cell, 2011. **145**(7): p. 1012-1022.

166. McNiven, M.A., *Breaking away: matrix remodeling from the leading edge.* Trends in Cell Biology, 2013. **23**(1): p. 16-21.

167. Lamouille, S., J. Xu, and R. Derynck, *Molecular mechanisms of epithelial–mesenchymal transition.* Nature Reviews Molcular Cell Biology, 2014. **15**(3): p. 178-196.

168. Wheelock, M.J., et al., *Cadherin switching.* Journal of Cell Science, 2008. **121**(6): p. 727.

169. Xu, J., S. Lamouille, and R. Derynck, *TGF-beta-induced epithelial to mesenchymal transition.* Cell Research, 2009. **19**(2): p. 156-172.

170. Zhou, B.P., et al., *Dual regulation of Snail by GSK-3β-mediated phosphorylation in control of epithelial–mesenchymal transition.* Nature Cell Biology, 2004. **6**(10): p. 931-940.

171. Yook, J.I., et al., *A Wnt–Axin2–GSK3β cascade regulates Snail1 activity in breast cancer cells.* Nature Cell Biology, 2006. **8**(12): p. 1398-1406.

172. Ivaska, J., *Vimentin: Central hub in EMT induction?* Small GTPases, 2011. **2**(1): p. 51-53.

173. Mendez, M.G., S.-I. Kojima, and R.D. Goldman, *Vimentin induces changes in cell shape, motility, and adhesion during the epithelial to mesenchymal transition.* The Federation of American Societies for Experimental Biology, 2010. **24**(6): p. 1838-1851.

174. Sánchez-Tilló, E., et al., *ZEB1 represses E-cadherin and induces an EMT by recruiting the SWI/SNF chromatin-remodeling protein BRG1.* Oncogene, 2010. **29**(24): p. 3490-3500.

175. Postigo, A.A., et al., *Regulation of Smad signaling through a differential recruitment of coactivators and corepressors by ZEB proteins.* The The European Medical Biology Organisation Journal, 2003. **22**(10): p. 2453-2462.

176. Edgar, R., et al., *LifeMap Discovery™: The Embryonic Development, Stem Cells, and Regenerative Medicine Research Portal.* PLoS ONE, 2013. **8**(7): p. e66629.

177. Granéli, C., et al., *Novel markers of osteogenic and adipogenic differentiation of human bone marrow stromal cells identified using a quantitative proteomics approach.* Stem Cell Research, 2014. **12**(1): p. 153-165.

178. Boregowda, S.V., et al., *A Clinical Indications Prediction Scale Based on TWIST1 for Human Mesenchymal Stem Cells.* EBioMedicine, 2016. **4**: p. 62-73.

179. Vodyanik, M.A., et al., *A Mesoderm-Derived Precursor for Mesenchymal Stem and Endothelial Cells.* Cell Stem Cell, 2010. **7**(6): p. 718-729.

180. Koch, J.M., et al., *Mesenchymoangioblast-derived mesenchymal stromal cells inhibit cell damage, tissue damage and improve peripheral blood flow following hindlimb ischemic injury in mice.* Cytotherapy, 2016. **18**(2): p. 219-228.

181. Tran, N.-T., et al., *Efficient Differentiation of Human Pluripotent Stem Cells into Mesenchymal Stem Cells by Modulating Intracellular Signaling Pathways in a Feeder/Serum-Free System.* Stem Cells and Development, 2012. **21**(7): p. 1165-1175.

182. Chen, Y.S., et al., *Small molecule mesengenic induction of human induced pluripotent stem cells to generate mesenchymal stem/stromal cells.* Stem Cells Translational Medicine, 2012. **1**(2): p. 83-95.

183. Kanke, K., et al., *Stepwise Differentiation of Pluripotent Stem Cells into Osteoblasts Using Four Small Molecules under Serum-free and Feeder-free Conditions.* Stem Cell Reports, 2014. **2**(6): p. 751-760.

184. Deng, P., et al., *Inhibition of IKK/NF-κB Signaling Enhances Differentiation of Mesenchymal Stromal Cells from Human Embryonic Stem Cells.* Stem Cell Reports, 2016. **6**(4): p. 456-465.

185. Sánchez, L., et al., *Enrichment of Human ESC-Derived Multipotent Mesenchymal Stem Cells with Immunosuppressive and Anti-Inflammatory Properties Capable to Protect Against Experimental Inflammatory Bowel Disease.* Stem Cells, 2011. **29**(2): p. 251-262.

186. Yamaguchi, Y., et al., *Mesenchymal stem cell spheroids exhibit enhanced in-vitro and in-vivo osteoregenerative potential.* BMC Biotechnology. **14**: p. 105.

187. Handschel, J.G.K., et al., *Prospects of micromass culture technology in tissue engineering.* Head & Face Medicine, 2007. **3**: p. 4.

188. Shekaran, A., et al., *Enhanced in vitro osteogenic differentiation of human fetal MSCs attached to 3D microcarriers versus harvested from 2D monolayers.* BMC Biotechnology, 2015. **15**: p. 102.

189. Yang, J., et al., *Bone morphogenetic proteins: Relationship between molecular structure and their osteogenic activity.* Food Science and Human Wellness, 2014. **3**(3–4): p. 127-135.

190. Jaiswal, N., et al., *Osteogenic differentiation of purified, culture-expanded human mesenchymal stem cells in vitro.* Journal of Cellular Biochemistry, 1997. **64**(2): p. 295-312.

191. Westhrin, M., et al., *Osteogenic Differentiation of Human Mesenchymal Stem Cells in Mineralized Alginate Matrices.* PLoS ONE, 2015. **10**(3): p. e0120374.

192. Taylor, S.E.B., M. Shah, and I.R. Orriss, *Generation of rodent and human osteoblasts.* BoneKEy Reports, 2014. **3**: p. 585.

193. Costa-Pinto, A.R., et al., *Osteogenic Differentiation of Human Bone Marrow Mesenchymal Stem Cells Seeded on Melt Based Chitosan Scaffolds for Bone Tissue Engineering Applications.* Biomacromolecules, 2009. **10**(8): p. 2067-2073.

194. Gronthos, S., et al., *The STRO-1+ fraction of adult human bone marrow contains the osteogenic precursors.* Blood, 1994. **84**(12): p. 4164-4173.

195. Abzhanov, A., et al., *Regulation of skeletogenic differentiation in cranial dermal bone.* Development, 2007. **134**(17): p. 3133.

196. Harada, H., et al., *Cbfa1 isoforms exert functional differences in osteoblast differentiation.* Journal of Biological Chemistry, 1999. **274**(11): p. 6972-8.

197. Dalle Carbonare, L., G. Innamorati, and M.T. Valenti, *Transcription factor Runx2 and its application to bone tissue engineering.* Stem Cell Reviews, 2012. **8**(3): p. 891-7.

198. Sinha, K.M. and X. Zhou, *Genetic and molecular control of osterix in skeletal formation.* Journal of Cellular Biochemistry, 2013. **114**(5): p. 975-84.

199. Otto, F., et al., *Cbfa1, a candidate gene for cleidocranial dysplasia syndrome, is essential for osteoblast differentiation and bone development.* Cell, 1997. **89**(5): p. 765-71.

200. Muraglia, A., R. Cancedda, and R. Quarto, *Clonal mesenchymal progenitors from human bone marrow differentiate in vitro according to a hierarchical model.* Journal of Cell Science, 2000. **113**(Pt 7): p. 1161-6.

201. Coelho, M.J. and M.H. Fernandes, *Human bone cell cultures in biocompatibility testing. Part II: effect of ascorbic acid, β-glycerophosphate and dexamethasone on osteoblastic differentiation.* Biomaterials, 2000. **21**(11): p. 1095-1102.

202. Kato, H., et al., *Promoting effect of 1,25(OH)(2) vitamin D(3) in osteogenic differentiation from induced pluripotent stem cells to osteocyte-like cells.* Open Biology, 2015. **5**(2): p. 140-201.

203. Spence, J.R., et al., *Directed differentiation of human pluripotent stem cells into intestinal tissue in vitro.* Nature, 2011. **470**(7332): p. 105-109.

204. Zhong, X., et al., *Generation of three dimensional retinal tissue with functional photoreceptors from human iPSCs.* Nature Communications, 2014. **5**: p. 4047.

205. Pagliuca, F.W., et al., *Generation of functional human pancreatic β cells in vitro.* Cell, 2014. **159**(2): p. 428-439.

206. Shimoyama, A., et al., *Ihh/Gli2 Signaling Promotes Osteoblast Differentiation by Regulating Runx2 Expression and Function.* Molecular Biology of the Cell, 2007. **18**(7): p. 2411-2418.

207. McCarthy, T.L. and M. Centrella, *Novel Links among Wnt and TGF-β Signaling and Runx2.* Molecular Endocrinology, 2010. **24**(3): p. 587-597.

208. Xian, L., et al., *Matrix IGF-1 maintains bone mass by activation of mTOR in mesenchymal stem cells.* Nature Medicine. **18**(7): p. 1095-101.

209. Yokota, J.U.N., et al., *PDGF-induced PI3K-mediated signaling enhances the TGF-β-induced osteogenic differentiation of human mesenchymal stem cells in a TGF-β-activated MEK-dependent manner.* International Journal of Molecular Medicine, 2014. **33**(3): p. 534-542.

210. Dani, C., et al., *Differentiation of embryonic stem cells into adipocytes in vitro.* Journal of Cell Science, 1997. **110**(Pt 11): p. 1279-85.

211. Bain, G., et al., *Embryonic Stem Cells Express Neuronal Properties in Vitro.* Developmental Biology, 1995. **168**(2): p. 342-357.

212. Dani, C., *Embryonic stem cell-derived adipogenesis.* Cells Tissues Organs, 1999. **165**(3-4): p. 173-80.

213. Lind, T., et al., *Vitamin A Is a Negative Regulator of Osteoblast Mineralization.* PLoS ONE, 2013. **8**(12): p. e82388.

214. Murry, C.E. and G. Keller, *Differentiation of Embryonic Stem Cells to Clinically Relevant Populations: Lessons from Embryonic Development.* Cell, 2008. **132**(4): p. 661-680.

215. Latinkic, B.V., et al., *The Xenopus Brachyury promoter is activated by FGF and low concentrations ofactivinandsuppressed by high concentrationsof activin and by paired-type homeodomain proteins.* Genes & Development, 1997. **11**(23): p. 3265-3276.

216. Ohba, S., et al., *A novel osteogenic helioxanthin-derivative acts in a BMP-dependent manner.* Biochemical & Biophysical Research Communications, 2007. **357**(4): p. 854-60.

217. Liu, X., et al., *Cross-talk between EGF and BMP9 signalling pathways regulates the osteogenic differentiation of mesenchymal stem cells.* Journal of Cellular and Molecular Medicine, 2013. **17**(9): p. 1160-1172.

218. Hojo, H., et al., *Hedgehog-Gli Activators Direct Osteo-chondrogenic Function of Bone Morphogenetic Protein toward Osteogenesis in the Perichondrium.* The Journal of Biological Chemistry, 2013. **288**(14): p. 9924-9932.

219. Zaragosi, L.-E., et al., *Effects of GSK3 inhibitors on in vitro expansion and differentiation of human adipose-derived stem cells into adipocytes.* BMC Cell Biology, 2008. **9**: p. 11.

220. Hojo, H., et al., *Gli1 Protein Participates in Hedgehog-mediated Specification of Osteoblast Lineage during Endochondral Ossification.* The Journal of Biological Chemistry, 2012. **287**(21): p. 17860-17869.

221. Kao, C.L., et al., *Resveratrol promotes osteogenic differentiation and protects against dexamethasone damage in murine induced pluripotent stem cells.* Stem Cells & Development. **19**(2): p. 247-58.

222. Kawaguchi, J., P.J. Mee, and A.G. Smith, *Osteogenic and chondrogenic differentiation of embryonic stem cells in response to specific growth factors.* Bone, 2005. **36**(5): p. 758-769.

223. Tang, Q.-Q., T.C. Otto, and M.D. Lane, *Commitment of C3H10T1/2 pluripotent stem cells to the adipocyte lineage.* Proceedings of the National Academy of Sciences of the United States of America, 2004. **101**(26): p. 9607-9611.

224. Tsai, K.-S., et al., *Type I collagen promotes proliferation and osteogenesis of human mesenchymal stem cells via activation of ERK and Akt pathways.* Journal of Biomedical Materials Research Part A, 2010. **94A**(3): p. 673-682.

225. Phillips, B.W., et al., *Compactin Enhances Osteogenesis in Murine Embryonic Stem Cells.* Biochemical and Biophysical Research Communications, 2001. **284**(2): p. 478-484.

226. Chen, J. and F. Long, *mTORC1 Signaling Promotes Osteoblast Differentiation from Preosteoblasts.* PLoS ONE, 2015. **10**(6): p. e0130627.

227. Guntur, A.R. and C.J. Rosen, *New Insights into Osteoblasts and Their Role in Bone Formation: The Central Role of PI3Kinase.* The Journal of Endocrinology, 2011. **211**(2): p. 123-130.

228. Thouverey, C. and J. Caverzasio, *Sclerostin inhibits osteoblast differentiation without affecting BMP2/SMAD1/5 or Wnt3a/β-catenin signaling but through activation of platelet-derived growth factor receptor signaling in vitro.* BoneKEyReports, 2015. **4**: p. 757.

229. Constam, D.B. and E.J. Robertson, *Regulation of Bone Morphogenetic Protein Activity by Pro Domains and Proprotein Convertases.* The Journal of Cell Biology, 1999. **144**(1): p. 139-149.

230. Wang, Y.-K., et al., *Bone Morphogenetic Protein-2-Induced Signaling and Osteogenesis Is Regulated by Cell Shape, RhoA/ROCK, and Cytoskeletal Tension.* Stem Cells and Development, 2012. **21**(7): p. 1176-1186.

231. zur Nieden, N.I., et al., *Induction of chondro-, osteo- and adipogenesis in embryonic stem cells by bone morphogenetic protein-2: Effect of cofactors on differentiating lineages.* BMC Developmental Biology, 2005. **5**: p. 1.

232. Kim, B.S., et al., *Fucoidan promotes osteoblast differentiation via JNK- and ERK-dependent BMP2–Smad 1/5/8 signaling in human mesenchymal stem cells.* Experimental & Molecular Medicine, 2015. **47**(1): p. e128.

233. Lin, F.-x., et al., *Naringin promotes osteogenic differentiation of bone marrow stromal cells by up-regulating Foxc2 expression via the IHH signaling pathway.* American Journal of Translational Research, 2016. **8**(11): p. 5098-5107.

234. Jeon, O.H., et al., *Human iPSC-derived osteoblasts and osteoclasts together promote bone regeneration in 3D biomaterials.* Scientific Reports, 2016. **6**: p. 26761.

235. Bilousova, G., et al., *Osteoblasts derived from Induced Pluripotent Stem Cells form Calcified Structures in Scaffolds both in vitro and in vivo.* Stem Cells, 2011. **29**(2): p. 206-216.

236. Katsuhisa, T., et al., *Efficient Adipocyte and Osteoblast Differentiation from Mouse Induced Pluripotent Stem Cells by Adenoviral Transduction.* Stem Cells, 2009. **27**(8): p. 1802-1811.

237. Heng, B.C., et al., *An autologous cell lysate extract from human embryonic stem cell (hESC) derived osteoblasts can enhance osteogenesis of hESC.* Tissue and Cell, 2008. **40**(3): p. 219-228.

238. Gibney, E.R. and C.M. Nolan, *Epigenetics and gene expression.* Heredity, 2010. **105**(1): p. 4-13.

239. Robertson, K.D., *DNA methylation and human disease.* Nature Review Genetics, 2005. **6**(8): p. 597-610.

240. Lister, R., et al., *Human DNA methylomes at base resolution show widespread epigenomic differences.* Nature, 2009. **462**(7271): p. 315-322.

241. Bird, A., *DNA methylation patterns and epigenetic memory.* Genes & Development, 2002. **16**(1): p. 6-21.

242. Jin, B., Y. Li, and K.D. Robertson, *DNA Methylation: Superior or Subordinate in the Epigenetic Hierarchy?* Genes & Cancer, 2011. **2**(6): p. 607-617.

243. Kohli, R.M. and Y. Zhang, *TET enzymes, TDG and the dynamics of DNA demethylation.* Nature, 2013. **502**(7472): p. 472-479.

244. Bannister, A.J. and T. Kouzarides, *Regulation of chromatin by histone modifications.* Cell Research, 2011. **21**(3): p. 381-395.

245. Apostolou, E. and K. Hochedlinger, *Chromatin Dynamics during Cellular Reprogramming.* Nature, 2013. **502**(7472): p. 462-471.

246. David, L. and J.M. Polo, *Phases of reprogramming.* Stem Cell Research, 2014. **12**(3): p. 754-761.

247. Ho, R., C. Chronis, and K. Plath, *Mechanistic Insights into Reprogramming to Induced Pluripotency.* Journal of Cellular Physiology, 2011. **226**(4): p. 868-878.

248. Mah, N., et al., *Molecular Insights into Reprogramming-Initiation Events Mediated by the OSKM Gene Regulatory Network.* PLoS ONE, 2011. **6**(8): p. e24351.

249. Muraro, M.J., H. Kempe, and P.J. Verschure, *Concise Review: The Dynamics of Induced Pluripotency and Its Behavior Captured in Gene Network Motifs.* Stem Cells, 2013. **31**(5): p. 838-848.

250. Lister, R., et al., *Hotspots of aberrant epigenomic reprogramming in human induced pluripotent stem cells.* Nature, 2011. **471**(7336): p. 68-73.

251. Nishino, K. and A. Umezawa, *DNA methylation dynamics in human induced pluripotent stem cells.* Human Cell, 2016. **29**(3): p. 97-100.

252. Teven, C.M., et al., *Epigenetic Regulation of Mesenchymal Stem Cells: A Focus on Osteogenic and Adipogenic Differentiation.* Stem Cells International, 2011. **2011:** p. 201371.

253. Pérez-Campo, F.M. and J.A. Riancho, *Epigenetic Mechanisms Regulating Mesenchymal Stem Cell Differentiation.* Current Genomics, 2015. **16**(6): p. 368-383.

254. Collas, P., *Programming differentiation potential in mesenchymal stem cells.* Epigenetics, 2010. **5**(6): p. 476-482.

255. Sørensen, A.L., et al., *Promoter DNA Methylation Patterns of Differentiated Cells Are Largely Programmed at the Progenitor Stage.* Molecular Biology of the Cell, 2010. **21**(12): p. 2066-2077.

256. Aranda, P., et al., *Epigenetic Signatures Associated with Different Levels of Differentiation Potential in Human Stem Cells.* PLoS ONE, 2009. **4**(11): p. e7809.

257. Eslaminejad, M.B., N. Fani, and M. Shahhoseini, *Epigenetic Regulation of Osteogenic and Chondrogenic Differentiation of Mesenchymal Stem Cells in Culture.* Cell Journal , 2013. **15**(1): p. 1-10.

258. Reppe, S., H. Datta, and K.M. Gautvik, *The Influence of DNA Methylation on Bone Cells.* Current Genomics, 2015. **16**(6): p. 384-392.

259. Du, T. and P.D. Zamore, *microPrimer: the biogenesis and function of microRNA.* Development, 2005. **132**(21): p. 4645-4652.

260. Ha, M. and V.N. Kim, *Regulation of microRNA biogenesis.* Nature Reviews Molecular Cell Biology, 2014. **15**(8): p. 509-524.

261. Leonardo, T.R., et al., *The functions of microRNAs in pluripotency and reprogramming.* Nature Cell Biology, 2012. **14**(11): p. 1114-1121.

262. Bar, M., et al., *MicroRNA discovery and profiling in human embryonic stem cells by deep sequencing of small RNA libraries.* Stem Cells, 2008. **26**(10): p. 2496-2505.

263. Laurent, L.C., et al., *Comprehensive MicroRNA Profiling Reveals a Unique Human Embryonic Stem Cell Signature Dominated by a Single Seed Sequence.* Stem Cells, 2008. **26**(6): p. 1506-1516.

264. Morin, R.D., et al., *Application of massively parallel sequencing to microRNA profiling and discovery in human embryonic stem cells.* Genome research, 2008. **18**(4): p. 610-621.

265. Greer Card, D.A., et al., *Oct4/Sox2-Regulated miR-302 Targets Cyclin D1 in Human Embryonic Stem Cells.* Molecular and Cellular Biology, 2008. **28**(20): p. 6426-6438.

266. Craig, V.J., et al., *Myc-mediated repression of microRNA-34a promotes high-grade transformation of B-cell lymphoma by dysregulation of FoxP1.* Blood, 2011. **117**(23): p. 6227-6236.

267. O'Donnell, K.A., et al., *c-Myc-regulated microRNAs modulate E2F1 expression.* Nature, 2005. **435**(7043): p. 839-843.

268. Mott, J.L., et al., *Transcriptional Suppression of mir-29b-1/mir-29a Promoter by c-Myc, Hedgehog, and NF-kappaB.* Journal of Cellular Biochemistry, 2010. **110**(5): p. 1155-1164.

269. Lee, Y.J., et al., *Dissecting microRNA-mediated regulation of stemness, reprogramming, and pluripotency.* Cell Regeneration, 2016. **5**(1): p. 2.

270. Becker, K.A., et al., *Self-renewal of human embryonic stem cells is supported by a shortened G1 cell cycle phase.* Journal of Cellular Physiology, 2006. **209**(3): p. 883-893.

271. Subramanyam, D., et al., *Multiple targets of miR-302 and miR-372 promote reprogramming of human fibroblasts to induced pluripotent stem cells.* Nature Biotechnology, 2011. **29**(5): p. 443-448.

272. Vallier, L., M. Alexander, and R.A. Pedersen, *Activin/Nodal and FGF pathways cooperate to maintain pluripotency of human embryonic stem cells.* Journal of Cell Science, 2005. **118**(19): p. 4495.

273. Barroso-delJesus, A., et al., *The Nodal inhibitor Lefty is negatively modulated by the microRNA miR-302 in human embryonic stem cells.* The Federation of American Societies of Experimental Biology Journal, 2011. **25**(5): p. 1497-1508.

274. Hong, H., et al., *Suppression of Indued Pluripotent Stem Cell Generation by the p53-p21 Pathway.* Nature, 2009. **460**(7259): p. 1132-1135.

275. Marión, R.M., et al., *A p53-mediated DNA damage response limits reprogramming to ensure iPS cell genomic integrity.* Nature, 2009. **460**(7259): p. 1149-1153.

276. Guo, X., et al., *microRNA-29b is a novel mediator of Sox2 function in the regulation of somatic cell reprogramming.* Cell Research, 2013. **23**(1): p. 142-156.

277. Yang, C.-S., Z. Li, and T.M. Rana, *microRNAs modulate iPS cell generation.* RNA, 2011. **17**(8): p. 1451-1460.

278. Ye, D., et al., *MiR-138 Promotes Induced Pluripotent Stem Cell Generation Through the Regulation of the p53 Signaling.* Stem Cells, 2012. **30**(8): p. 1645-1654.

279. Neveu, P., et al., *MicroRNA Profiling Reveals Two Distinct p53-Related Human Pluripotent Stem Cell States.* Cell Stem Cell. **7**(6): p. 671-681.

280. Choi, Y.J., et al., *miR-34 miRNAs provide a barrier for somatic cell reprogramming.* Nature Cell Biology, 2011. **13**(11): p. 1353-1360.

281. Gregory, P.A., et al., *The miR-200 family and miR-205 regulate epithelial to mesenchymal transition by targeting ZEB1 and SIP1.* Nature Cell Biology, 2008. **10**(5): p. 593-601.

282. Wang, G., et al., *Critical regulation of miR-200/ZEB2 pathway in Oct4/Sox2-induced mesenchymal-to-epithelial transition and induced pluripotent stem cell generation.* Proceedings of the National Academy of Sciences of the United States of America, 2013. **110**(8): p. 2858-2863.

283. Lim, Y.-Y., et al., *Epigenetic modulation of the miR-200 family is associated with transition to a breast cancer stem-cell-like state.* Journal of Cell Science, 2013. **126**(10): p. 2256.

284. Li, Z., et al., *Small RNA-mediated regulation of iPS cell generation.* The European Medical Biology Organisation Journal, 2011. **30**(5): p. 823-834.

285. Liao, B., et al., *MicroRNA cluster 302-367 enhances somatic cell reprogramming by accelerating a mesenchymal-to-epithelial transition.* The Journal of Biological Chemistry, 2011. **286**(19): p. 17359-17364.

286. Lin, S.-L., et al., *Regulation of somatic cell reprogramming through inducible mir-302 expression.* Nucleic Acids Research, 2011. **39**(3): p. 1054-1065.

287. Lee, M.R., et al., *Epigenetic regulation of NANOG by miR-302 cluster-MBD2 completes induced pluripotent stem cell reprogramming.* Stem Cells, 2013. **31**(4): p. 666-681.

288. Zhang, Z., et al., *Dissecting the roles of miR-302/367 cluster in cellular reprogramming using TALE-based repressor and TALEN.* Stem Cell Reports, 2013. **1**(3): p. 218-225.

289. Yu, J., et al., *Induced Pluripotent Stem Cell Lines Derived from Human Somatic Cells.* Science, 2007. **318**(5858): p. 1917.

290. Sharma, A., et al., *The role of SIRT6 protein in aging and reprogramming of human induced pluripotent stem cells.* The Journal of Biological Chemistry, 2013. **288**(25): p. 18439-18447.

291. Mackie, E.J., et al., *Endochondral ossification: How cartilage is converted into bone in the developing skeleton.* The International Journal of Biochemistry & Cell Biology, 2008. **40**(1): p. 46-62.

292. Alečković, M. and Y. Kang, *Bone marrow stroma-derived miRNAs as regulators, biomarkers and therapeutic targets of bone metastasis.* BoneKEyReports, 2015. **4**: p. 671.

293. Jing, D., et al., *The role of microRNAs in bone remodeling.* International Journal of Oral Science, 2015. **7**(3): p. 131-143.

294. Papaioannou, G., F. Mirzamohammadi, and T. Kobayashi, *MicroRNAs involved in bone formation.* Cellular and molecular life sciences : Cellular and Molecular Life Sciences, 2014. **71**(24): p. 4747-4761.

295. Egea, V., et al., *Tissue inhibitor of metalloproteinase-1 (TIMP-1) regulates mesenchymal stem cells through let-7f microRNA and Wnt/β-catenin signaling.* Proceedings of the National Academy of Sciences, 2012. **109**(6): p. E309-E316.

296. Vimalraj, S., N.C. Partridge, and N. Selvamurugan, *A positive role of microRNA-15b on regulation of osteoblast differentiation.* Journal of Cellular Physiology, 2014. **229**(9): p. 1236-1244.

297. Zhou, M., et al., *MicroRNA-17-92 cluster regulates osteoblast proliferation and differentiation.* Endocrine, 2014. **45**(2): p. 302-310.

298. Zhang, J.-f., et al., *MiRNA-20a promotes osteogenic differentiation of human mesenchymal stem cells by co-regulating BMP signaling.* RNA Biology, 2011. **8**(5): p. 829-838.

299. Hassan, M.Q., et al., *A network connecting Runx2, SATB2, and the miR-23a~27a~24-2 cluster regulates the osteoblast differentiation program.* Proceedings of the National Academy of Sciences of the United States of America, 2010. **107**(46): p. 19879-19884.

300. Zhang, Y., et al., *A program of microRNAs controls osteogenic lineage progression by targeting transcription factor Runx2.* Proceedings of the National Academy of Sciences, 2011. **108**(24): p. 9863-9868.

301. Kapinas, K., et al., *miR-29 Modulates Wnt Signaling in Human Osteoblasts through a Positive Feedback Loop.* The Journal of Biological Chemistry, 2010. **285**(33): p. 25221-25231.

302. Chen, L., et al., *MicroRNA-34a Inhibits Osteoblast Differentiation and In Vivo Bone Formation of Human Stromal Stem Cells.* Stem Cells, 2014. **32**(4): p. 902-912.

303. Bae, Y., et al., *miRNA-34c regulates Notch signaling during bone development.* Human Molecular Genetics, 2012. **21**(13): p. 2991-3000.

304. Engin, F., et al., *Dimorphic effects of Notch signaling in bone homeostasis.* Nature Medicine, 2008. **14**(3): p. 299-305.

305. Eskildsen, T., et al., *MicroRNA-138 regulates osteogenic differentiation of human stromal (mesenchymal) stem cells in vivo.* Proceedings of the National Academy of Sciences of the United States of America, 2011. **108**(15): p. 6139-6144.

306. Itoh, T., Y. Nozawa, and Y. Akao, *MicroRNA-141 and -200a Are Involved in Bone Morphogenetic Protein-2-induced Mouse Pre-osteoblast Differentiation by Targeting Distal-less Homeobox 5.* Journal of Biological Chemistry, 2009. **284**(29): p. 19272-19279.

307. Cheung, K.S.C., et al., *MicroRNA-146a Regulates Human Foetal Femur Derived Skeletal Stem Cell Differentiation by Down-Regulating SMAD2 and SMAD3.* PLoS ONE, 2014. **9**(6): p. e98063.

308. Schoolmeesters, A., et al., *Functional Profiling Reveals Critical Role for miRNA in Differentiation of Human Mesenchymal Stem Cells.* PLOS ONE, 2009. **4**(5): p. e5605.

309. Liao, Y.-H., et al., *Osteogenic differentiation of adipose-derived stem cells and calvarial defect repair using baculovirus-mediated co-expression of BMP-2 and miR-148b.* Biomaterials, 2014. **35**(18): p. 4901-4910.

310. Bhushan, R., et al., *miR-181a promotes osteoblastic differentiation through repression of TGF-β signaling molecules.* The International Journal of Biochemistry & Cell Biology, 2013. **45**(3): p. 696-705.

311. Kim, K.M., et al., *miR-182 is a negative regulator of osteoblast proliferation, differentiation, and skeletogenesis through targeting FoxO1.* Journal of Bone and Mineral Research, 2012. **27**(8): p. 1669-1679.

312. Hassan, M.Q., et al., *miR-218 Directs a Wnt Signaling Circuit to Promote Differentiation of Osteoblasts and Osteomimicry of Metastatic Cancer Cells.* The Journal of Biological Chemistry, 2012. **287**(50): p. 42084-42092.

313. Gámez, B., et al., *MicroRNA-322 (miR-322) and its target protein Tob2 modulate Osterix (Osx) mRNA stability.* The Journal of Biological Chemistry, 2013. **288**(20): p. 14264-14275.

314. Zhang, J., et al., *Effects of miR-335-5p in modulating osteogenic differentiation by specifically downregulating Wnt antagonist DKK1.* Journal of Bone and Mineral

research : the official journal of the American Society for Bone and Mineral Research, 2011. **26**(8): p. 1953-1963.

315. Zhang, J.-f., et al., *MiR-637 maintains the balance between adipocytes and osteoblasts by directly targeting Osterix.* Molecular Biology of the Cell, 2011. **22**(21): p. 3955-3961.

316. Lisse, T.S., et al., *Vitamin D activation of functionally distinct regulatory miRNAs in primary human osteoblasts.* Journal of bone and mineral research : the official journal of the American Society for Bone and Mineral Research, 2013. **28**(6): p. 1478-1488.

317. Budd, E., et al., *The Potential of microRNAs for Stem Cell-based Therapy for Degenerative Skeletal Diseases.* Current Molecular Biology Reports, 2017. **3**(4): p. 263-275.

318. Buechli, M.E., J. LaMarre, and T.G. Koch, *MicroRNA-140 Expression During Chondrogenic Differentiation of Equine Cord Blood-Derived Mesenchymal Stromal Cells.* Stem Cells and Development, 2013. **22**(8): p. 1288-1296.

319. Yang, B., et al., *MicroRNA-145 regulates chondrogenic differentiation of mesenchymal stem cells by targeting Sox9.* PloS ONE, 2011. **6**(7): p. e21679-e21679.

320. Kim, D., J. Song, and E.-J. Jin, *MicroRNA-221 regulates chondrogenic differentiation through promoting proteosomal degradation of slug by targeting Mdm2.* The Journal of Biological Chemistry, 2010. **285**(35): p. 26900-26907.

321. Karlsen, T.A., et al., *microRNA-140 Targets RALA and Regulates Chondrogenic Differentiation of Human Mesenchymal Stem Cells by Translational Enhancement of SOX9 and ACAN.* Stem Cells and Development, 2013. **23**(3): p. 290-304.

322. Miyaki, S., et al., *MicroRNA-140 is expressed in differentiated human articular chondrocytes and modulates interleukin-1 responses.* Arthritis and Rheumatism, 2009. **60**(9): p. 2723-2730.

323. Aszódi, A., et al., *Normal skeletal development of mice lacking matrilin 1: redundant function of matrilins in cartilage?* Molecular and Cellular Biology, 1999. **19**(11): p. 7841-7845.

324. Budd, E., et al., *MiR-146b is down-regulated during the chondrogenic differentiation of human bone marrow derived skeletal stem cells and up-regulated in osteoarthritis.* Scientific Reports, 2017. **7**: p. 46704.

325. Hou, C., et al., *MiR-193b regulates early chondrogenesis by inhibiting the TGF-beta2 signaling pathway.* Federation of European Biochemical Societies Letters, 2015. **589**(9): p. 1040-1047.

326. Zhang, Z., et al., *Expression of microRNAs during chondrogenesis of human adipose-derived stem cells.* Osteoarthritis and Cartilage, 2012. **20**(12): p. 1638-1646.

327. Xu, J., et al., *MiR-194 regulates chondrogenic differentiation of human adipose-derived stem cells by targeting Sox5.* PloS ONE, 2012. **7**(3): p. e31861-e31861.

328. Lee, S., et al., *microRNA-495 inhibits chondrogenic differentiation in human mesenchymal stem cells by targeting Sox9.* Stem Cells and Development, 2014. **23**(15): p. 1798-1808

329. Megges, M., et al., *Generation of an iPS cell line from bone marrow derived mesenchymal stromal cells from an elderly patient.* Stem Cell Research, 2015. **15**(3): p. 565-568.

330. de Andres, M.C., et al., *Assessment of global DNA methylation in peripheral blood cell subpopulations of early rheumatoid arthritis before and after methotrexate.* Arthritis Research & Therapy, 2015. **17**(1): p. 233.

331. Le, T., et al., *A sensitive mass-spectrometry method for simultaneous quantification of DNA methylation and hydroxymethylation levels in biological samples.* Analytical Biochemistry, 2011. **412**(2): p. 203-209.

332. de Andrés, M.C., et al., *Epigenetic Regulation during Fetal Femur Development: DNA Methylation Matters.* PLoS ONE, 2013. **8**(1): p. e54957.

333. Takahashi, A., et al., *DNA methylation of the RUNX2 P1 promoter mediates MMP13 transcription in chondrocytes.* Scientific Reports, 2017. **7**(1): p. 7771.

334. Zhang, J., et al., *The challenges and promises of allogeneic mesenchymal stem cells for use as a cell-based therapy.* Stem Cell Research & Therapy, 2015. **6**(1): p. 234.

335. Qin, Y., J. Guan, and C. Zhang, *Mesenchymal stem cells: mechanisms and role in bone regeneration.* Postgraduate Medical Journal, 2014. **90**(1069): p. 643.

336. Lin, W., et al., *Mesenchymal stem cells homing to improve bone healing.* Journal of Orthopaedic Translation, 2017. **9**: p. 19-27.

337. Chen, G., et al., *Chemically defined conditions for human iPSC derivation and culture.* Nature Methods, 2011. **8**(5): p. 424-429.

338. Squillaro, T., G. Peluso, and U. Galderisi, *Clinical Trials With Mesenchymal Stem Cells: An Update.* Cell Transplantation, 2016. **25**(5): p. 829-848.

339. Frobel, J., et al., *Epigenetic Rejuvenation of Mesenchymal Stromal Cells Derived from Induced Pluripotent Stem Cells.* Stem Cell Reports, 2014. **3**(3): p. 414-422.

340. Kalluri, R. and R.A. Weinberg, *The basics of epithelial-mesenchymal transition.* The Journal of Clinical Investigation, 2009. **119**(6): p. 1420-1428.

341. Vallier, L. and R.A. Pedersen, *Human embryonic stem cells.* Stem Cell Reviews, 2005. **1**(2): p. 119-130.

342. Vallier, L., et al., *Signaling Pathways Controlling Pluripotency and Early Cell Fate Decisions of Human Induced Pluripotent Stem Cells.* Stem Cells, 2009. **27**(11): p. 2655-2666.

343. Xu, R.-H., et al., *NANOG is a Direct Target of TGFβ/Activin Mediated SMAD Signaling in Human ES Cells.* Cell Stem Cell, 2008. **3**(2): p. 196-206.

344. Hannan, N.R.F., et al., *BMP-11 and Myostatin Support Undifferentiated Growth of Human Embryonic Stem Cells in Feeder-Free Cultures.* Cloning and Stem Cells, 2009. **11**(3): p. 427-435.

345. Gough, J.E., J.R. Jones, and L.L. Hench, *Nodule formation and mineralisation of human primary osteoblasts cultured on a porous bioactive glass scaffold.* Biomaterials, 2004. **25**(11): p. 2039-2046.

346. Golub, E.E. and K. Boesze-Battaglia, *The role of alkaline phosphatase in mineralization.* Current Opinion in Orthopaedics, 2007. **18**(5): p. 444-448

347. Brown, S.E., W. Tong, and P.H. Krebsbach, *The Derivation of Mesenchymal Stem Cells from Human Embryonic Stem Cells.* Cells Tissues Organs, 2009. **189**(1-4): p. 256-260.

348. Hwang, N.S., et al., *In vivo commitment and functional tissue regeneration using human embryonic stem cell-derived mesenchymal cells.* Proceedings of the National Academy of Sciences of the United States of America, 2008. **105**(52): p. 20641-20646.

349. Barberi, T., et al., *Derivation of Multipotent Mesenchymal Precursors from Human Embryonic Stem Cells.* PLoS Medicine, 2005. **2**(6): p. e161.

350. Mahmood, A., et al., *Enhanced differentiation of human embryonic stem cells to mesenchymal progenitors by inhibition of TGF-β/activin/nodal signaling using SB-431542.* Journal of Bone and Mineral Research, 2010. **25**(6): p. 1216-1233.

351. Olivier Emmanuel, N., C. Rybicki Anne, and E. Bouhassira Eric, *Differentiation of Human Embryonic Stem Cells into Bipotent Mesenchymal Stem Cells.* Stem Cells, 2009. **24**(8): p. 1914-1922.

352. Trivedi, P. and P. Hematti, *Simultaneous generation of CD34$^+$ primitive hematopoietic cells and CD73$^+$ mesenchymal stem cells from human embryonic stem cells cocultured with murine OP9 stromal cells.* Experimental Hematology, 2007. **35**(1): p. 146-154.

353. Rampersad, S.N., *Multiple Applications of Alamar Blue as an Indicator of Metabolic Function and Cellular Health in Cell Viability Bioassays.* Sensors , 2012. **12**(9): p. 12347-12360.

354. Diederichs, S. and R.S. Tuan, *Functional comparison of human-induced pluripotent stem cell-derived mesenchymal cells and bone marrow-derived mesenchymal stromal cells from the same donor.* Stem Cells and Development, 2014. **23**(14): p. 1594-1610.

355. Krattinger, N., et al., *Regulation of proliferation and differentiation of human fetal bone cells.* eCells & Materials, 2011. **21**: p. 46-58.

356. Pansky, B., *Review of Medical Embryology*. New York:Macmillan. 1982.

357. Gentili, P., A. Trasimeni, and C. Giorlandino, *Fetal ossification centers as predictors of gestational age in normal and abnormal pregnancies.* Journal of Ultrasound in Medicine, 1984. **3**(5): p. 193-197.

358. Shen, G., *The role of type X collagen in facilitating and regulating endochondral ossification of articular cartilage.* Orthodontics & Craniofacial Research, 2005. **8**(1): p. 11-17.

359. Kielty, C.M., et al., *Type X collagen, a product of hypertrophic chondrocytes.* The Biochemical Journal, 1985. **227**(2): p. 545-554.

360. Hagg, R., et al., *Absence of the α1(IX) Chain Leads to a Functional Knock-out of the Entire Collagen IX Protein in Mice.* Journal of Biological Chemistry, 1997. **272**(33): p. 20650-20654.

361. Mirmalek-Sadi, S.-H., *Characterisation of Human Foetal Femur-Derived Cells and Their Potential for Bone Tissue Regeneration*, in *Faculty of Medicine*. 2006, University of Southampton

362. Kronenberg, H.M., *Developmental regulation of the growth plate.* Nature, 2003. **423**(6937): p. 332-336.

363. Sivaraj, K.K. and R.H. Adams, *Blood vessel formation and function in bone.* Development, 2016. **143**(15): p. 2706-2715.

364. Kopp, H.-G., et al., *The Bone Marrow Vascular Niche: Home of HSC Differentiation and Mobilization.* Physiology, 2005. **20**(5): p. 349-356.

365. Aird, W.C., *Phenotypic Heterogeneity of the Endothelium.* Circulation Research, 2007. **100**(2): p. 174-190.

366. Núñez, J.A., et al., *Simultaneous visualisation of calcified bone microstructure and intracortical vasculature using synchrotron X-ray phase contrast-enhanced tomography.* Scientific Reports, 2017. **7**(1): p. 13289.

367. Bribiesca-Contreras, F. and W.I. Sellers, *Three-dimensional visualisation of the internal anatomy of the sparrowhawk (Accipiter nisus) forelimb using contrast-enhanced micro-computed tomography.* PeerJ - the Jurnal of Life and Environmental Sciences, 2017. **5**: p. e3039.

368. Räth, C., et al., *Strength through structure: visualization and local assessment of the trabecular bone structure.* New Journal of Physics, 2008. **10**(12): p. 125010.

369. Chung, H.-W., et al., *Three-dimensional nuclear magnetic resonance microimaging of trabecular bone.* Journal of Bone and Mineral Research, 1995. **10**(10): p. 1452-1461.

370. Hildebrand, T., et al., *Direct Three-Dimensional Morphometric Analysis of Human Cancellous Bone: Microstructural Data from Spine, Femur, Iliac Crest, and Calcaneus.* Journal of Bone and Mineral Research, 1999. **14**(7): p. 1167-1174.

371. Mueller, D., et al., *The 3D-based scaling index algorithm: a new structure measure to analyze trabecular bone architecture in high-resolution MR images in vivo.* Osteoporosis International, 2006. **17**(10): p. 1483-1493.

372. Risau, W. and I. Flamme, *Vasculogenesis.* Annual Review of Cell and Developmental Biology, 1995. **11**(1): p. 73-91.

373. Kusumbe, A.P., S.K. Ramasamy, and R.H. Adams, *Coupling of angiogenesis and osteogenesis by a specific vessel subtype in bone.* Nature, 2014. **507**: p. 323-328.

374. Trueta, J. and J.D. Morgan, *The vascular contribution to osteogenesis.* The Journal of Bone and Joint Surgery, 1960. **42-B**(1): p. 97-109.

375. Ortega, N., D.J. Behonick, and Z. Werb, *Matrix remodeling during endochondral ossification.* Trends in Cell Biology, 2004. **14**(2): p. 86-93.

376. Vu, T.H., et al., *MMP-9/Gelatinase B Is a Key Regulator of Growth Plate Angiogenesis and Apoptosis of Hypertrophic Chondrocytes.* Cell, 1998. **93**(3): p. 411-422.

377. Smith, Z.D., et al., *DNA methylation dynamics of the human preimplantation embryo.* Nature, 2014. **511**: p. 611-615.

378. Zhu, P., et al., *Single-cell DNA methylome sequencing of human preimplantation embryos.* Nature Genetics, 2018. **50**(1): p. 12-19.

379. El-Serafi, A., et al., *Developmental plasticity of human foetal femur-derived cells in pellet culture: Self assembly of an osteoid shell around a cartilaginous core.* European Cells & Materials, 2011. **21**: p. 558-67.

380. Liang, H., et al., *Matrix metalloproteinases in bone development and pathology: current knowledge and potential clinical utility*. Metalloproteases in Medicine. . 2016. **3**: p. 93-102.

381. Chang, P.-L., et al., *Comparison of Fetal and Adult Marrow Stromal Cells in Osteogenesis with and without Glucocorticoids.* Connective Tissue Research, 2006. **47**(2): p. 67-76.

382. Zhi-Yong, Z., et al., *Superior Osteogenic Capacity for Bone Tissue Engineering of Fetal Compared with Perinatal and Adult Mesenchymal Stem Cells.* Stem Cells, 2009. **27**(1): p. 126-137.

383. Brady, K., et al., *Human Fetal and Adult Bone Marrow-Derived Mesenchymal Stem Cells Use Different Signaling Pathways for the Initiation of Chondrogenesis.* Stem Cells and Development, 2014. **23**(5): p. 541-554.

384. D'Ippolito, G., et al., *Age-Related Osteogenic Potential of Mesenchymal Stromal Stem Cells from Human Vertebral Bone Marrow.* Journal of Bone and Mineral Research, 1999. **14**(7): p. 1115-1122.

385. Gotherstrom, C., et al., *Difference in gene expression between human fetal liver and adult bone marrow mesenchymal stem cells.* Haematologica, 2005. **90**(8): p. 1017-1026.

386. Inglis, S., et al., *Human endothelial and foetal femur-derived stem cell co-cultures modulate osteogenesis and angiogenesis.* Stem Cell Research & Therapy, 2016. **7**(1): p. 13.

387. El-Serafi, A.T., R.O.C. Oreffo, and H.I. Roach, *Epigenetic modifiers influence lineage commitment of human bone marrow stromal cells: Differential effects of 5-aza-deoxycytidine and trichostatin A.* Differentiation, 2011. **81**(1): p. 35-41.

388. Berger, S.L., *The complex language of chromatin regulation during transcription.* Nature, 2007. **447**: p. 407-412.

389. Reik, W., *Stability and flexibility of epigenetic gene regulation in mammalian development.* Nature, 2007. **447**: p. 425-432.

390. Gopalakrishnan, S., B.O.V. Emburgh, and K.D. Robertson, *DNA methylation in development and human disease.* Mutation research, 2008. **647**(1-2): p. 30-38.

391. Moore, L.D., T. Le, and G. Fan, *DNA Methylation and Its Basic Function.* Neuropsychopharmacology, 2013. **38**(1): p. 23-38.

392. Parle-Mcdermott, A. and A. Harrison, *DNA Methylation: A Timeline of Methods and Applications.* Frontiers in Genetics, 2011. **2**: p. 74.

393. Delaney, C., S.K. Garg, and R. Yung, *Analysis of DNA Methylation by Pyrosequencing.* Methods in Molecular Biology, 2015. **1343**: p. 249-264.

394. Guo, H., et al., *The DNA methylation landscape of human early embryos.* Nature, 2014. **511**: p. 606-610.

395. Fulka, H., et al., *DNA methylation pattern in human zygotes and developing embryos.* Reproduction, 2004. **128**(6): p. 703-708.

396. Okae, H., et al., *Genome-Wide Analysis of DNA Methylation Dynamics during Early Human Development.* PLoS Genetics, 2014. **10**(12): p. e1004868.

397. Smith, Z.D., et al., *A unique regulatory phase of DNA methylation in the early mammalian embryo.* Nature, 2012. **484**: p. 339-344.

398. Spiers, H., et al., *Methylomic trajectories across human fetal brain development.* Genome Research, 2015. **25**(3): p. 338-352.

399. Slieker, R.C., et al., *DNA Methylation Landscapes of Human Fetal Development.* PLoS Genetics, 2015. **11**(10): p. e1005583.

400. Roost, M.S., et al., *DNA methylation and transcriptional trajectories during human development and reprogramming of isogenic pluripotent stem cells.* Nature Communications, 2017. **8**: p. 908.

401. Zhang, P., S.A. Jimenez, and D.G. Stokes, *Regulation of Human COL9A1 gene expression: activation of the proximal promoter region by SOX9.* Journal of Biological Chemistry, 2003. **278**(1): p. 117-123.

402. Michael, S. and O. Florian, *Control of RUNX2 isoform expression: The role of promoters and enhancers.* Journal of Cellular Biochemistry, 2005. **95**(3): p. 506-517.

403. Blair, H.C., et al., *Osteoblast Differentiation and Bone Matrix Formation In Vivo and In Vitro.* Tissue Engineering. Part B, Reviews, 2017. **23**(3): p. 268-280.

404. Dorota, P.J. and Z. Danuta, *Osteocalcin as a biochemical marker of bone turnover.* Nephrology, 1998. **4**(5-6): p. 339-346.

405. Stacyann, B., et al., *Osteocalcin and osteopontin influence bone morphology and mechanical properties.* Annals of the New York Academy of Sciences, 2017. **1409**(1): p. 79-84.

406. Kerner, S.A., R.A. Scott, and J.W. Pike, *Sequence elements in the human osteocalcin gene confer basal activation and inducible response to hormonal vitamin D3.* Proceedings of the National Academy of Sciences of the United States of America, 1989. **86**(12): p. 4455-4459.

407. Ozono, K., et al., *The vitamin D-responsive element in the human osteocalcin gene. Association with a nuclear proto-oncogene enhancer.* Journal of Biological Chemistry, 1990. **265**(35): p. 21881-8.

408. Spitzhorn, L.-S., et al., *Human iPSC-derived MSCs (iMSCs) from aged individuals acquire a rejuvenation signature.* Stem Cell Research & Therapy, 2019. **10**(1): p. 100.

409. Schäck, L.M., et al., *The Phosphate Source Influences Gene Expression and Quality of Mineralization during In Vitro Osteogenic Differentiation of Human Mesenchymal Stem Cells.* PLoS ONE, 2013. **8**(6): p. e65943.

410. Lou, Y.-R., et al., *25-Hydroxyvitamin D(3) induces osteogenic differentiation of human mesenchymal stem cells.* Scientific Reports, 2017. **7**: p. 42816-42816.

411. Li, Y., et al., *Osteogenic differentiation of mesenchymal stem cells (MSCs) induced by three calcium phosphate ceramic (CaP) powders: A comparative study.* Materials Science and Engineering: C, 2017. **80**: p. 296-300.

412. Smith, Z.D., et al., *DNA methylation dynamics of the human preimplantation embryo.* Nature, 2014. **511**(7511): p. 611-615.

413. de Almeida, Danilo C., et al., *Epigenetic Classification of Human Mesenchymal Stromal Cells.* Stem Cell Reports, 2016. **6**(2): p. 168-175.

414. Rebouças, E.d.L., et al., *Real time PCR and importance of housekeepings genes for normalization and quantification of mRNA expression in different tissues.* Brazilian Archives of Biology and Technology, 2013. **56**: p. 143-154.

415. Li, S., et al., *Chondrogenic potential of human articular chondrocytes and skeletal stem cells: A comparative study.* Journal of Biomaterials Applications, 2015. **29**(6): p. 824-836.

416. Janeczek, A.A., et al., *Transient Canonical Wnt Stimulation Enriches Human Bone Marrow Mononuclear Cell Isolates for Osteoprogenitors.* Stem Cells, 2016. **34**(2): p. 418-430.

417. Ronaghi, M., *Pyrosequencing Sheds Light on DNA Sequencing.* Genome Research, 2001. **11**(1): p. 3-11.

418. Fakruddin, M., et al., *Pyrosequcening - Principles and Applications.* International Journal of Life Science adn Pharma Research, 2012. **2**(2): p. 65-76.

419. Hyman, E.D., *A new method of sequencing DNA.* Analytical Biochemistry, 1988. **174**(2): p. 423-436.

420. Gharizadeh, B., et al., *Multiple group-specific sequencing primers for reliable and rapid DNA sequencing.* Molecular and Cellular Probes, 2003. **17**(4): p. 203-210.

421. Nyrén, P., *Apyrase immobilized on paramagnetic beads used to improve detection limits in bioluminometric ATP monitoring.* Journal of Bioluminescence and Chemiluminescence, 1994. **9**(1): p. 29-34.